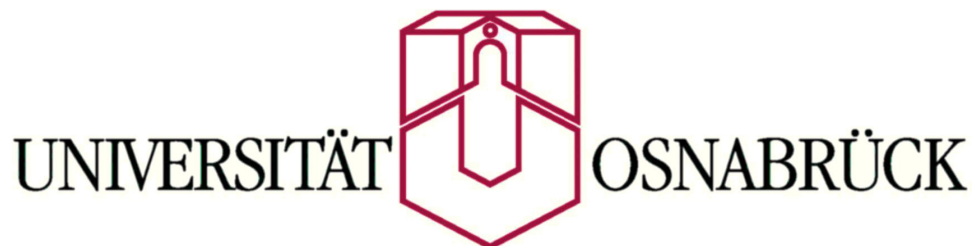


Preparation of novel bitumen nanocomposites out of polymer- modified montmorillonite nanoparticles



Inaugural Dissertation

zur Erlangung der Doktorwürde
der
Universität Osnabrück
Fachbereich Biologie/Chemie

vorgelegt von
Eduard Belke

Osnabrück 2017

1. Gutachter:

Prof. Dr. Uwe Beginn,

Universität Osnabrück,

Organic Materials Chemistry and Bio-Organic Chemistry

2. Gutachter:

Prof. Dr. Lorenz Walder,

Universität Osnabrück,

Organic Chemistry and Molecular Electrochemistry

Erklärung

Hiermit erkläre ich an Eides Statt, dass ich die vorliegende Arbeit selbständig angefertigt und keine anderen Hilfsmittel als die angegebenen verwendet habe. Diejenigen Stellen der Arbeit, die anderen Werken oder dem Sinn nach entnommen wurden, sind in jedem einzelnen Fall unter Angabe der Quelle kenntlich gemacht.

Ein früherer Promotionsversuch an einer deutschen Hochschule hat nicht stattgefunden.

.....
(Ort, Datum)

.....
(Unterschrift)

Danksagung

An dieser Stelle möchte ich mich bei denjenigen Menschen bedanken, die mich während meiner Promotionszeit unterstützt haben.

Herrn Prof. Dr. Uwe Beginn danke ich dafür, dass er es mir ermöglicht hat auf einem sehr interessanten Gebiet zu forschen, sowie für seine hilfreichen Anregungen und Verbesserungsvorschläge. Ich danke Herrn Prof. Dr. Lorenz Walder dafür, dass er sich als Zweitgutachter zur Verfügung gestellt hat. Für ihre Teilnahme an der Prüfungskommission bedanke ich mich bei Herrn Prof. Dr. Markus Haase und Herrn Dr. Ulrich Wahlbrink.

Für ihre Hilfe bei der Erstellung von Unterlagen und ihre Unterstützung bei Fragen rund um den verwaltungstechnischen Ablauf bedanke ich mich bei Frau Gertraud Strunk, Frau Monika Dubiel und Frau Anna Hodge. Frau Petra Bösel danke ich für die durchgeführten GPC, DSC und NMR Messungen, sowie für ihre Unterstützung im Labor. Für die IR Messungen und für ihre Arbeit im Chemikalienlager danke ich Frau Iris Helms. Frau Elisabeth Michalek danke ich für die MALDI-TOF Messungen und die Bestellungen der Chemikalien. Frau Eva Becker danke ich für ihre Arbeit im Labor. Für ihre zahlreichen NMR und XRF Messungen bedanke ich mich herzlich bei Frau Marianne Gather. Frau Anja Schuster danke ich für die Elementaranalysen und IR Messungen. Bei Frau Kerstin Rücker bedanke ich mich für die TGA und bei der gesamten Arbeitsgruppe Funktionale Nanomaterialien, im besonderen bei Herrn Dr. Karsten Kömpe, für die XRD Messungen.

Mein besonderer Dank für ihre Unterstützung im Laboralltag und die freundliche Atmosphäre gilt den jetzigen und ehemaligen Mitarbeitern der Arbeitsgruppe Organic Materials Chemistry and Bio-Organic Chemistry: Nadine Diek, Martin Frosinn, Xihomara Lizzet Casallas Cruz, Adrian Dragulelei, Dr. Ralf Beckmann, Dr. Enfeng Song, Dr. Sandra Schwitke, Dr. Marina Zorn, Dr. Marius Ciobanu, Dr. Ana-Maria Lepadatu und Dr. Miriam Brandt.

Abstract

To extend the time of service of asphalt roads modified montmorillonite nanoparticles were incorporated into bitumen with the aim of creating a gas barrier inside the bitumen which slows down the diffusion of oxygen through the bitumen. For this purpose [montmorillonite/alkyl-quat-primer] adducts ($[\text{MMT}/\text{PEI}(\text{nkD})_{\text{xQ}}^{\text{yR}}]$) were fabricated in which single-montmorillonite platelets were coated by a ultrathin polymer film by reacting montmorillonite particles with poly(ethylenimine) based polycations. The alkyl-quat-primer polymers were synthesised by adding ammonium groups and alkyl chains to hyperbranched poly(ethylenimine)s in a solvent-free reaction. Adducts with fully intercalated polymers were obtained when the polymers were reacted with an aqueous solution of [MMT/CTAB] or by mixing the polymers with montmorillonite and CTAB in an aqueous solution. The polymers replaced the CTAB in an intermediate formed [MMT/CTAB] adduct and adhered strongly to the montmorillonite due to a cooperative electrostatic interaction between the positively charged ammonium moieties of the macromolecules and the negatively charged montmorillonite surface. [MMT/alkyl-quat-primer] and [MMT/CTAB] adducts were incorporated via a single screw extruder into polymer- and non-polymer-modified bitumina to create bitumen-nanocomposites. Composites prepared under optimised conditions exhibited an adduct network inside the bitumen at adduct concentrations larger 5 wt.% and when non-polymer modified bitumina were modified. The aspect ratio of the incorporated montmorillonite platelets depended strongly on the adduct composition and the used bitumen, and was with $[\text{MMT}/\text{PEI}(10\text{kD})_{10\text{Q}}^{80\text{R}10}]$ adducts were very high ($\sim 300 - 1000$) but with $[\text{MMT}/\text{PEI}(10\text{kD})_{10\text{Q}}^{60\text{R}14}]$ and [MMT/CTAB] adducts considerably lower ($\sim 30 - 90$).

Table of contents

1	Introduction.....	1
2	Literature review.....	4
2.1	Asphalt roads.....	5
2.2	Bitumen and bitumen-nanocomposites.....	6
2.2.1	Bitumen.....	6
2.2.2	Chemical composition of bitumen.....	6
2.2.3	Physical properties of bitumen.....	7
2.2.4	Bitumen ageing.....	8
2.2.5	Polymer and wax modified bitumen.....	11
2.2.6	Bitumen-nanocomposites.....	13
2.3	Montmorillonite.....	14
2.3.1	Structure and properties of montmorillonite.....	14
2.3.2	Organically modified montmorillonite.....	18
2.4	Hyperbranched polymers.....	24
2.4.1	Branched and hyperbranched polymers.....	24
2.4.2	Hyperbranched poly(ethylenimine).....	26
2.5	Methods.....	27
2.5.1	X-ray diffraction (XRD).....	27
2.5.2	Light scattering.....	28
2.5.3	Size-exclusion chromatography (SEC).....	30
2.5.4	“Polarised light” and “dark field” microscopy.....	31
2.5.5	Rheology.....	32
	References.....	35
3	Synthesis of PEI(nkD)xQyR polymers.....	48
3.1	Introduction.....	49

Table of contents

3.2	Experimental part.....	50
3.2.1	Materials.....	50
3.2.2	Techniques.....	50
3.2.3	Synthesis of poly[ethylenimine-co-(ethylenimine-N-(2-hydroxypropyl-3-(N,N,N-trimethylammonium chloride)))].....	53
3.2.4	Synthesis of hyperbranched poly[ethylenimine-co-(N-(2-hydroxydodecyl)-ethylenimine)].....	54
3.2.5	Synthesis of hyperbranched poly[ethylenimine-co-(ethylenimine-N-(2-hydroxypropyl-3-(N,N,N-trimethylammonium chloride)))-co-(N-(2-hydroxydodecyl)-ethylenimine)].....	55
3.2.6	Synthesis of hyperbranched poly[ethylenimine-co-(ethylenimine-N-(2-hydroxypropyl-3-(N,N,N-trimethylammonium chloride)))-co-(N-(2-hydroxyhexadecyl)-ethylenimine)].....	58
3.2.7	Synthesis of poly[ethylenimine-co-(ethylenimine-(undecan-2-ylidene))}].....	60
3.3	Results and discussion.....	61
	Discussion.....	90
3.4	Conclusion.....	94
	References.....	95
4	Preparation of [montmorillonite/PEI_xQyR] adducts.....	97
4.1	Introduction.....	98
4.2	Experimental part.....	100
4.2.1	Materials.....	100
4.2.2	Techniques.....	100
4.2.3	Reaction of PEI(nkD) _x Q with Na-MMT.....	102
4.2.4	Reaction of PEI(nkD) _x QyR10 with Na-MMT.....	103
4.2.5	Reaction of CTAB with Na-MMT.....	104
4.2.6	Reaction of PEI(nkD) _x QyR10 with [MMT/CTAB].....	106
4.2.8	Reaction of PEI(nkD) _x QyR with Na-MMT in the presence of CTAB or 1-hexadecylamine.....	108

4.3	Results and Discussion.....	113
4.3.1	Characterization of the Na-bentonites B1 and B2.....	113
4.3.3	“Direct addition” of PEI(nkD)xQyR polymers to Na-MMT.....	119
	Discussion.....	132
	Summary.....	133
4.3.4	Characterisation of [MMT/CTAB] adducts.....	134
	Summary.....	141
4.3.5	“Replacement” of CTAB by addition of PEI(nkD)xQyR polymers to [MMT/CTAB] adducts.....	142
	Discussion.....	156
	Summary.....	157
4.3.6	[MMT/PEI(nkD)xQyR] adducts prepared by the “indirect replacement” method.....	158
	Discussion.....	178
	Summary.....	180
4.4	Conclusion.....	182
	References.....	183
5	Preparation of bitumen- [montmorillonite/PEI(nkD)xQyR] composites.....	188
5.1	Introduction.....	189
5.2	Experimental part.....	191
5.2.1	Materials.....	191
5.2.2	Techniques.....	191
5.2.3	Preparation of Total Azalt 50/70-[MMT/CTAB] composites.....	193
5.2.4	Preparation of 70/100-[MMT/PEI(10kD)5Q67R10] composites using adduct E2.....	193
5.2.5	Preparation of bitumen-[MMT/PEI(10kD)10Q80R10] and bitumen-[MMT/PEI(10kD)10Q60R14] composites with the adducts prepared by the “indirect replacement” method.....	194

5.3	Results and Discussion.....	200
5.3.1	Microscopical investigation of bitumen-[MMT/PEI(nkD)xQyR] and bitumen-[MMT/CTAB] composites.....	208
	Discussion.....	221
	Summary.....	224
5.3.2	Rheological investigation of bitumen-[MMT/PEI(nkD)xQyR] and bitumen-[MMT/CTAB] composites.....	224
	Discussion.....	255
	Summary.....	259
5.4	Conclusion.....	262
	References.....	263
6	Preparation of [montmorillonite/PEI(nkD)xQyPS(nkD)].....	264
6.1	Introduction.....	265
6.2	Experimental Part.....	266
6.2.1	Materials.....	266
6.2.2	Techniques.....	267
6.2.3	Synthesis of 2-bromo-2-methyl-propionic acid 2,5- dioxopyrrolidin-1-yl ester.....	269
6.2.4	Synthesis of polystyrenes with active ester chain ends.....	270
6.2.5	Synthesis of polystyrene-quat-primer polymers bearing ammonium moieties and polystyrene groups.....	272
6.2.6	Preparation of [MMTB2/PEI(10kD)10Q2.2PS(6.4kD)].....	273
6.3	Results and Discussion.....	275
6.3.1	Preparation of polystyrenes with active ester chain ends.....	276
	Discussion.....	289
6.3.2	Preparation of “polystyrene-quat-primer” polymers bearing ammonium moieties and polystyrene groups (= PEI(nkD)xQyPS(nkD)).....	291
	Discussion.....	302

Table of contents

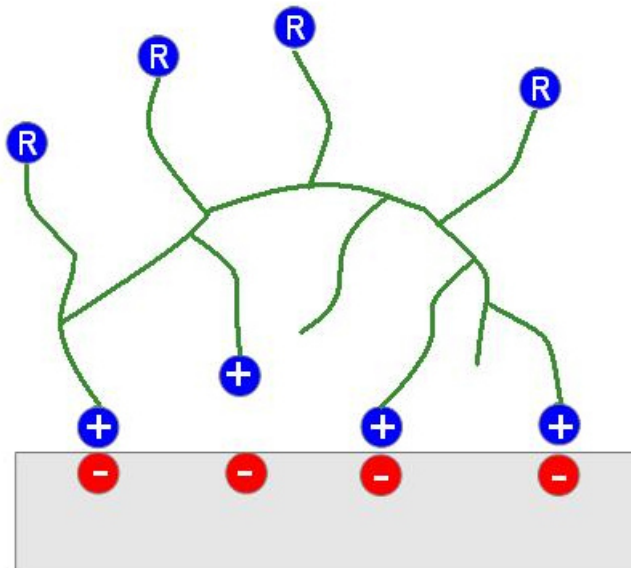
6.3.3 Preparation of the [MMTB2/PEI(10kD)10Q2.2PS(6.4kD)] adduct EP1.....	303
Discussion.....	310
Summary.....	311
6.4 Conclusion.....	314
References.....	315
7 Summary.....	319

1 Introduction

1 Introduction

Montmorillonite (MMT) modified with organic compounds (= [MMT/organo]) is of interest for a wide range of applications due to its unique chemical and physical properties. These materials can be used for the modification of bitumen since the large surface of the montmorillonite platelets creates a gas barrier which slows down the diffusion of oxygen through the bitumen and extends the time of service. The compatibility between the montmorillonite and the bitumen is ensured by the organic fraction of the [MMT/organo] compounds.

Since [MMT/organo] compounds consisting of montmorillonite and non-charged polymers segregate when exposed to an environment that is able to dissolve the organic fraction this work focuses on the preparation of [MMT/organo] adducts consisting of montmorillonite and macromolecular polycations. By using polycations [MMT/organo] adducts are created with the polymers strongly attached to the MMT due to the high number of positively charged groups which undergo cooperative electrostatic interaction with the negatively charged montmorillonite surface.



Concept of the interaction of an polycation with montmorillonite

Natural occurring MMT consists of montmorillonite stacks build up of several montmorillonite platelets. These agglomerates exhibit a low aspect ratio A_f (length/thickness) and their use as a gas barrier is only limited. In this work a method is described which enables the preparation of adducts with completely intercalated polymers which are able to exfoliate in bitumen into MMT-single layer platelets coated by a

polymer film.

The compatibility of [MMT/organo] adducts with bitumen depend strongly on the composition of the polycations. Since bitumen is soluble in semi-polar to non-polar only polymers can be used which exhibits similar solubility properties. In this study hyper-branched poly(ethylenimine) (PEI) was used as the scaffold for the preparation of “alkyl-quat-primer” polymers” which bears ammonium groups and alkyl chain moieties.

In Chapter **2** an overview of the studies performed on bitumen-nanocomposites, [MMT/organo] compounds, and modified poly(ethylenimine)s is given.

Within Chapter **3** the synthesis of alkyl-quat-primer polymers is described. The polymers were prepared by reacting poly(ethylenimine) with (i) glycidyltrimethylammonium chloride (= “quat”) with the aim to add positively charged ammonium groups to the polymer and with either (ii) 1,2-epoxydodecane or (iii) 1,2-epoxyhexadecane with the purpose of adjusting the solubility of the polymer.

In Chapter **4** pathways for the preparation of [MMT/alkyl-quat-primer] adducts are shown. Three different methods termed as “direct addition”, “replacement”, and “indirect replacement” were evaluated to determine the conditions necessary for the preparation of adducts with fully intercalated polymers.

In Chapter **5** the morphology and viscoelastic properties of bitumen-[MMT/alkyl-quat-primer] composites are evaluated with the aim to determine the influence of (i) the used bitumen, (ii) the adduct composition, (iii) the preparation method of a respective adduct, (iv) the applied compounding procedure, and (v) the targeted weight concentration of the adduct in the bitumen matrix.

The preparation of polystyrene-quat-primer polymers and an [MMT/polystyrene-quat-primer] adduct is described in Chapter **6**. The polystyrene-quat-primer polymers were prepared by adding simultaneous glycidyltrimethylammonium chloride and polystyrene active esters, prepared by an ATRP polymerization, to poly(ethylenimine). The [MMT/polystyrene-quat-primer polymer] adduct was fabricated by mixing a polystyrene-quat-primer polymer with an aqueous solution of CTAB and montmorillonite.

2 Literature review

2.1 Asphalt roads

The use of bitumen for road construction was recorded during the reigns of King Nabopolassar and his son, King Nebuchadnezzar for the first time. The roads were constructed with stone slabs which were set in a bituminous mortar. The interstices were very narrow at the surface and widened towards the base of the stones. The foundation consisted of three or more layers of bricks, connected by a bituminous mortar. The first modern road was laid 1858 in Paris. The bitumen was composed of a foundation of concrete with a rock asphalt mastic on the surface [1]. A modern asphalt road consists primary of three components. The surfacing which consists of the surface course and the binder course, the base, and the foundation which is made up of the capping and the sub-base [2]. The cross section of an asphalt road is shown in Figure 2.1. The surface course is the uppermost layer and is build up of fine aggregates mixed with bitumen. The surface course must be durable and resist weather effects, traffic loading and protect the lower layers. The thickness of the surface course is in the region of 1 to 4 cm. Due to abrasion on the road surface by weathering and traffic, the surface course has to be replaced after 10 to 15 years [2 - 7].

The binder course is made up of bitumen and chippings, sand, and crushed rock. The layer distributes the stresses of the surface course to the base. The binder course exhibits a thickness of 4 – 8 cm. The base layer consists of a coarse-grained rock mix which ensures the uniform distribution of the stress. It gives also a solid base for the upper layers. The base layer has a service life up to 50 years when maintained properly. The thickness of this layer is in the range of 8 to 22 cm. The sub-base course consists of unbound gravel, sand or chippings. Due to the composition, the layer is resistant to weathering and allow water to be drained quickly. This prevents damage by frost in the upper layers of asphalt. The capping is the boundary region between the sub-base and the sub-soil. The capping consists of sub-soil reinforced with asphalt, cement or lime [2 - 7].

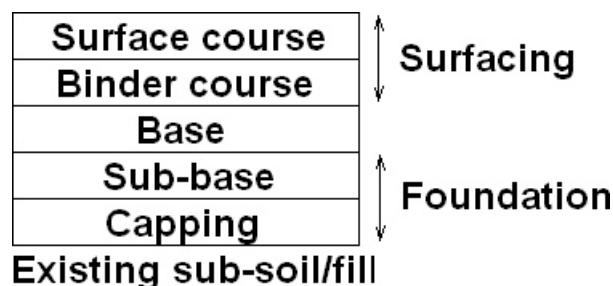


Figure 2.1: Cross section of an asphalt road [2]

The service life of an asphalt road is determined by the volume of traffic and weather

conditions due to the abrasion of the road surface. This leads to lane grooves and the formation of cracks. Also, the bitumen loses its properties during the construction of the road and the service life due to oxidative ageing by oxygen [2]. Many attempts were tried to improve the properties and persistence of roads by varying the composition and type of the filler materials and by modification of bitumen as illustrated in the following paragraphs.

2.2 Bitumen and bitumen-nanocomposites

2.2.1 Bitumen

Bitumen is used in many applications because of its unique properties. The discovery of trees and skeletons embedded in bitumen from 25,000 years ago proof the preservation properties of bitumen. Examples of the use of bitumen for building purposes were found at Khafaje. The floors were composed of an asphalt mastic with a thickness of 3 to 6 cm. The composition has been identified as bitumen, vegetable fibres (straw) and mineral fillers (loam, limestone, and marl) [1]. Besides from bitumen lakes, bitumen is produced from the fractional distillation of crude oil in industrial refineries. To separate the bitumen fraction from the crude oil, a distillation at atmospheric pressure followed by a vacuum distillation is carried out [2]. Bitumen is a generic class of dark-brown to black coloured, cement-like semi-solid, solid or viscous liquid, depending on composition and temperature. It is composed of high molecular mass hydrocarbons which are soluble in carbon disulphide, chloroform, ether, and acetone. It is insoluble in water at 20°C and partially soluble in aliphatic organic solvents [8].

2.2.2 Chemical composition of bitumen

The general concept approved today states that bitumen is a colloidal system of an oily phase and colloids (asphaltenes, resins), with the oily phase acting as the dispersion medium for the colloids. The asphaltenes in these colloids are surrounded by resins [9]. Bitumen consists generally of four fractions which are termed “saturates”, “aromatics”, “resins”, and “asphaltenes” (= SARA-model, cf. Figure 2.2) [10]. Asphaltenes are amorphous solids with dark brown or black colour, they exhibit no definite melting point and are insoluble in n-heptane. When heated above a certain temperature, they usually swell up and decompose. The decomposition products are carbonaceous residues. Asphaltenes contain polycyclic structures of naphthenes and aromatics with attached paraffine. Asphaltenes contain also sulphur, oxygen, and ni-

trogen derivatives. The molecular weight of asphaltenes was determined to be in the range of 1,000 g/mol (obtained by viscosity measurements) to 300,000 g/mol (obtained by ultracentrifugation). Asphaltenes constitute 5 to 25 wt.% of the total mass of bitumen [2].



Figure 2.2: SARA-model of bitumen [10]

Aromatics consist of multi-ring structures of naphthenes and aromatics with attached carbon chains. Sulphur, oxygen, and nitrogen derivatives, as well as traces of metals, are also present in the polar aromatics fraction. The molecular weight of polar aromatics was found to be in the region of 300 to 2,000 g/mol. Of the total mass of bitumen, aromatics constitute 40 to 65 wt.% [2]. Saturates are composed of linear and branched aliphatic hydrocarbon chains as well as alkyl-naphthenes and alkyl-aromatics. The molecular weight of saturates was similar to those of aromatics. Saturates contribute 5 to 20 wt.% of the total mass [2]. Resins are soluble in n-heptane and are composed largely of hydrogen and carbon and contain small amounts of sulphur, oxygen, and nitrogen. The molecular weight of resins was measured to be ranging from 500 to 50,000 g/mol. The proportions of resins to asphaltenes determine whether the bitumen is more the solution (sol) or gelatinous (gel) type [2].

Although bitumen from different sources were not chemically identical, the elemental analysis of several bitumens showed that most bitumens contain 79 - 88 wt.% carbon, 7 - 13 wt.% hydrogen, up to 8 wt.% sulphur, 2 - 8 wt.% oxygen and up to 3 wt.% nitrogen. Also, the elemental analysis of bitumen from different crude sources showed that some bitumen contained traces of vanadium and nickel in different quantities. The quantity of these metals in the bitumen serve like a fingerprint to distinguish bitumen of different sources [2, 11 - 14].

2.2.3 Physical properties of bitumen

The characteristics of bitumen are described by its physical properties. The characterisation methods are described in ASTM and DIN publications [15 - 18]. The measuring of the softening point is carried out with a steel ball of 9.5 mm diameter and a mass of 3.50 ± 0.05 g which is placed over a disk-shaped sample. The softening point is reached when the ball sinks 25.4 mm into the sample while the ball, the bath,

and the sample are heated up at a specific rate. Although bitumen does not have a definite melting point but changes with increasing temperature gradually from solid like to liquid, this method deliver an approximation when the transition of solid like to liquid take place [19]. The glass transition temperature can be determined more precisely by means of calorimetry or rheological tests. Bitumen types are classified by their penetration number. The penetration number is measured by penetrating the bituminous sample with a needle under specific conditions of time, load and temperature. The unit of penetration is 0.1 mm and ranges from 0 to 300. The harder the bitumen, the lower its penetration number [20].

The determination of the viscosity of bitumen at 60°C is carried out by means of vacuum capillary viscometers. From the data, the resistance to flow (the internal friction) of bitumen at this specific temperature is determined [2, 21]. Measuring the flash point gives an information about the presence of volatile and flammable substances in non-volatile or non-flammable materials such as bitumen. The flash point is defined as the lowest temperature at which a material evolve sufficient vapour to form flammable vapour-air mixtures which flash when ignited [22]. The ductility of a bitumen is given by the distance at which the material elongates before breaking (in cm). It is carried out by pulling apart a briquette sample at a given temperature and pulling rate [23]. The measure of the Fraass breaking point provides information on which temperature a layer of bitumen (0.5 mm) breaks when bent under specific conditions. It can be used to estimate the low-temperature elastic behaviour of a bitumen [24]. Bitumen is a viscoelastic material and can be much better characterised by its rheological behaviour. The test method described in ASTM D7175 – 08 covers the determination of the dynamic shear modulus and phase angle of bitumen binders when tested by dynamic (oscillatory) shear rheology equipped with a parallel plate geometry [25].

2.2.4 Bitumen ageing

During the time of service of bitumen in asphalt roads, many types of failures like rutting, fatigue cracking and thermal cracking occur, which reduces the quality and performance of roads over the time. Ageing of bitumen is one of the main causes for bitumen hardening and reduction of the time of service [26]. Ageing of bitumen can be divided into oxidative ageing [16, 27], evaporation ageing [28] and structural ageing [29]. Ageing of bitumen occurs when air diffuses through the bitumen and oxidises the organic compounds. Oxidative ageing is initiated by oxygen and UV-light. Carbon-hydrogen bonds or carbon-carbon bonds are attacked and form hydroperoxides. In a chain reaction, the hydroperoxides react with other organic compounds

based on a radical mechanism [30]. Intermediates such as ketones, alcohols, aldehydes and carbonic acids are formed during the oxidative ageing. These compounds form asphaltene-like structures which lead to an enrichment of the asphaltene fraction in the bitumen. Due to oxidative ageing, the bitumen hardens which lead to a lower penetration point and a higher softening point. Structural ageing of the bitumen is characterised by an increase in the size of the colloidal dispersed asphaltenes and resins molecules [31]. The dispersed micelles coagulate and grow to large aggregates. This changes the characteristics of a bitumen from a liquid sol to a solid gel (cf. Figure 2.3).

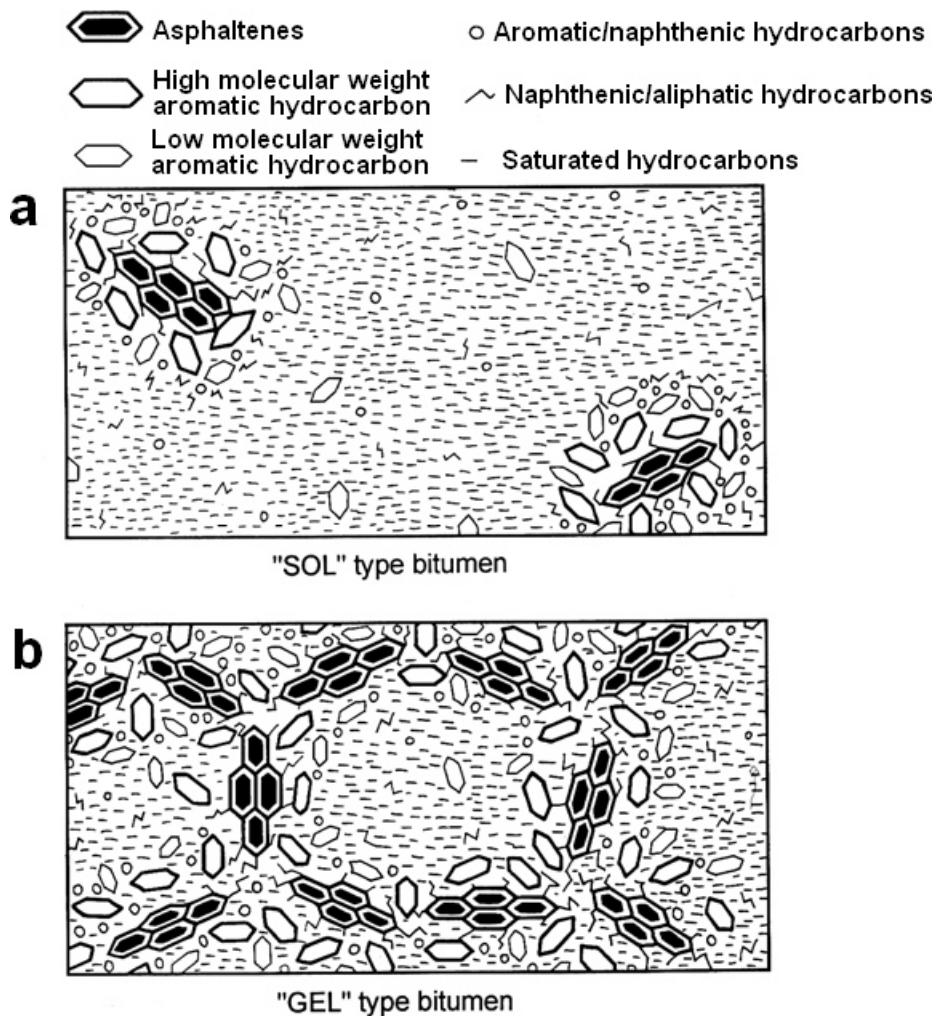


Figure 2.3: Models of a) sol type and b) gel type bitumen [2]

A sol doesn't show an elasticity by deformation. With increasing concentration of colloids, more interactions between the colloid micelles take place. This is shown by the formation of anisometric aggregates. The aggregates displace the oily phase which leads to a reduction of the bitumen volume. A hardening through more interaction

between the aggregates takes place which leads in the gel form to a brittle bitumen [31]. As a way to reduce or delay the failures, blends of bitumen and one or more polymers are used [32, 33].

During the test termed as the “thin-film oven test” (TFOT), a bitumen is exposed to air and heat. Differences in the properties of the bitumen before and after the test are determined by viscosity, penetration, mass, rheological and ductility measurements. The test has the aim to simulate the short-term ageing of bitumen. The oven used for this test has a hinged door with a window and a ventilation system. Openings for the entrance of air and exit of heat and vapours are present. Furthermore, the oven contains a thermometric device and a rotating shelf. The measurement is carried out by pouring the sample into a cylindrical container. The container is placed into an oven and stored at 163°C for 5 hours [2, 34]. The test called the “rolling thin-film oven test” (RTFOT) simulates also the short-term ageing of a bitumen. Additionally, the loss of volatiles during the test can be quantified. The samples are placed into a vessel, which is placed into a rotation carriage within an oven. The carriage rotates within the oven at a certain temperature and time (usually 163°C for 75 minutes). Differences in the properties before and after the test are determined analogously to the methods used with the thin-film oven test [2, 35]. The long-term ageing of bitumen is simulated with “pressure ageing vessel” test (PAV). Example devices for an RTFOT and a PAV test are shown in Figure 2.4.

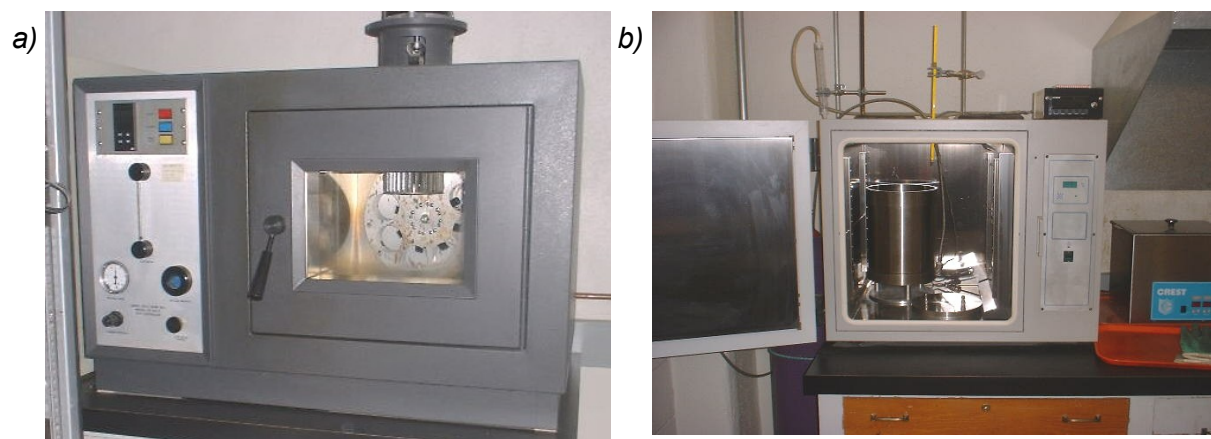


Figure 2.4: Devices for a) the rolling thin-film oven test (RTFOT) [37], and b) the pressure ageing vessel test (PAV) [38]

The test is carried out by performing firstly an RTFOT test as an initial ageing, followed by the ageing of the bitumen for 20 hours at 90 – 110°C and an air pressure of 2070 kPa in a pressure ageing vessel [2, 36].

2.2.5 Polymer and wax modified bitumen

To counteract the increasing stress on the asphalt of roads bitumen are blended with polymers. The main categories of polymers used to modify bitumen are thermoplastic elastomers (e. g. styrene-butadiene-styrene triblock copolymers), plastomers (e. g. ethylene-vinyl acetate copolymer) and reactive polymers (e. g. ethylene-butyl acrylate-glycidylmethacrylate terpolymer). Thermoplastic elastomers enhance the elastic properties of the bitumen and thus its elastic recovery capacity. This lead to a better resistance to permanent deformations of the bitumen. Polymer modified bitumen exhibit typically a two-phase morphology which depends on the structure of the polymer and the composition of the base bitumen [39]. Figure 2.5 shows the fluorescence microscopy images of four polymer-modified bitumen, namely: a) ASBS1, b) BEVA1, c) BEVA2 and d) BEVA3.

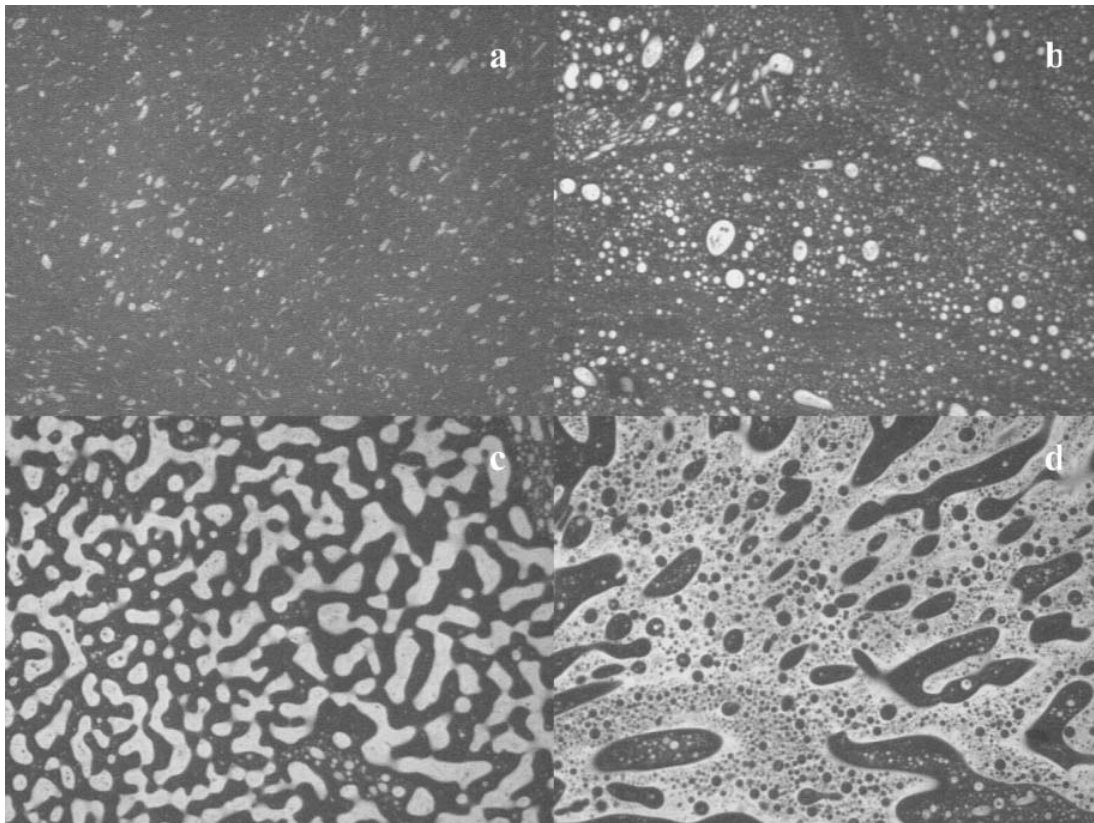


Figure 2.5: Fluorescence microscopy images of a) ASBS1, b) BEVA1, c) BEVA2 and d) BEVA3 [39]

According to the authors, the light-coloured fraction consisted of polymer and low-molecular-weight aromatic components and the dark-coloured fraction of asphaltenes. A scale bar was not given by the authors, the size of the polymer particles could, therefore, not be surely determined. ASBS1 consisted of 70/100 pen grade

bitumen modified with 4 wt.% styrene-butadiene-styrene (SBS). BEVA1, BEVA2, and BEVA3 consisted of 200/300 pen grade bitumen modified with 4, 6, and 8 wt.% ethylene vinyl acetate (EVA), respectively. With all four samples, the polymers segregated from the bitumen and formed micelles which indicate that the polymers exhibited a low compatibility with the used bitumen.

Some polymers swell in bitumen and form, through the overlap of the swollen strands, a three-dimensional network. Plastomers and reactive polymers confer a high rigidity and reduce conformation under load [39, 40]. Styrene-butadiene-styrene triblock copolymer (SBS) is a thermoplastic rubber and forms a two-phase morphology when blended with bitumen. The polystyrene terminal blocks exhibit a glass transition at about 100°C and the butadiene central block at around -80°C. The polymer behaves in the temperature region of -80°C to 100°C like a physically cross-linked elastomer. The polybutadiene fragments adsorb on molecules of the maltene fraction of the bitumen. Then, they swell up and reach a volume which is up to nine times larger the initial value. The typical concentration of SBS in the bitumen lies between 3 and 5 wt.%. The modified bitumen is more elastic and exhibits a higher viscosity on increased temperature. Because of the incompatibility of SBS and the bitumen, the polymer segregates from the bitumen during storage [41].

It was also tried to improve the performance of bitumen by blending bitumen with tire rubber. It was found that the addition of rubber led to a bitumen with a higher resistance against loading due to the elastic nature of the rubber [42]. When a wax was added to bitumen, a softening of the bitumen took place at high service temperatures. When the wax crystallised, an increase of the stiffness of the bitumen was observed. This behaviour leads to a higher possibility of thermal cracking at a lower temperature which is not desired. Blends of wax and bitumen have an application in warm mix asphalts. The wax lowers the viscosity of the bitumen and enable lower mixing and laying temperatures. This allows cold weather paving and longer hauls [43, 44]. Further, to enhance the adhesion between the bitumen in an asphalt, organically modified silanes were added to bitumen [45].

To sum up, the mechanisms why polymers and additives enhance some of the properties of the bitumen are not fully understood. Also, the addition of polymers or other additives leads to higher production costs due to the necessity to produce the polymers. Since polymer modified bitumen often exhibit a two-phase morphology, the addition of a compatibilizer is also necessary. In conclusion, although the addition of polymers or other additives to bitumen enhances some of the properties of the bitumen, the steadily increasing traffic load demand other approaches to increase the service time of the bitumen.

2.2.6 Bitumen-nanocomposites

Mineral fillers have strong effects on the properties and performance of bitumen. The effects are attributed to a bitumen layer which is formed around the filler particles [46 - 48]. They have the ability to enhance the resistance against “stripping” of asphalt films. Stripping is called the breaking of the adhesive bonds between the bitumen and the components in an asphalt [49, 50]. The modification of bitumen with mineral fillers of diameters in the μm region showed that the addition of limestone [51] or quartz [52] increased the anti-stripping properties of the bitumen. In the next step, the influence of the addition of a kaolinite clay/styrene-butadiene-styrene nanocomposite to bitumen was investigated [53]. It was found that the modified bitumen was very stable at high temperatures when the ratio SBS to kaolinite was around three. On the other hand, the kaolinite had only little influence on the mechanical properties of the bitumen and improved the rheological properties only to some extent.

To investigate to which extend the addition of montmorillonite nanoparticles can enhance the properties of bitumen, organic modified bentonites and montmorillonites (organic = quaternary ammonium salt bearing an alkyl chain) were added to a polymer or non-polymer modified bitumen. The addition of a benzyldimethylhexadecylammonium chloride modified montmorillonite to bitumen enhanced the ageing resistance of the bitumen which was shown by comparing the properties of modified and non-modified bitumen after a thin film oven tests [54, 55]. It was found, that the addition of alkylammonium modified montmorillonite to bitumen increased the viscosity and complex shear modulus of the bitumen at a given temperature. The increase of the complex shear modulus shows that the bitumen became stiffer after addition of the additive and, therefore, more resistant to deformation under load [56].

Encouraged by the good result of the addition of quaternary ammonium salt modified bentonites and montmorillonites to bitumen, mixtures of this adduct type and polymers were added to bitumen. The addition of an alkylammonium-bentonite/styrene-butadiene-styrene mixture to bitumen led to a composite with improved high-temperature storage stability. Furthermore, the resistance against ageing increased as shown through rheological investigations [33, 57, 58]. The composite was prepared by mixing the additive with the bitumen in a high shear mixer at 180°C and 4,000 rpm for 1 hour [33, 58]. Other investigated combinations were alkylammonium modified bentonite/ethylene-vinyl acetate [59], alkylammonium modified montmorillonite/crumb rubber [60], and alkylammonium modified montmorillonite/epoxy resin [61]. A bitumen/alkylammonium modified montmorillonite/poly(vinyl chloride) composite was obtained by mixing the additive with the bitumen in a high shear emulsifier at 150°C and 3,750 rpm for 1 hour [62]. Although the used additives led to better thermal oxidative

ageing properties and a higher thermal storage stability of the bitumen, only a limited amount of the adducts could be added because of agglomeration of the modified montmorillonite particles. Neat bentonite was also mixed with bitumen and used to create an asphalt. It was found that the addition of the bentonite led to a decrease of the penetration and ductility, and an increase of the softening point. The best result was obtained when the bentonite concentration was set to 20 wt.% [63].

In conclusion, the addition of organically modified montmorillonites to bitumen was found to increase the complex shear modulus, the bitumen became more resistant to deformation under load [18]. Furthermore, the ageing resistance and the storage stability of the bitumen increased. On the other hand, when the adduct concentration exceeded a certain limit large montmorillonite agglomerates were formed. Since the polymers and the quaternary ammonium salts didn't adhere strongly to the montmorillonite they could be washed out by solvents which dissolve these materials. This leads, as with polymer modified bitumen, to phase separated structures which consist of the polymer, the bitumen, and the montmorillonite. The addition of neat bentonite to bitumen increase, due to the swelling properties of the montmorillonite in water, the risk of damage by frost. Since the bitumen nanocomposites were typically prepared by mixing the modified montmorillonites with bitumen in a high shear mixer at 150 – 180°C and 3,750 – 4,000 rpm for 1 hour it is concluded that the preparation of the investigated composites [33, 58, 62] was very difficult.

2.3 Montmorillonite

2.3.1 Structure and properties of montmorillonite

Montmorillonite, as well as beidellite and nontronite, are clay minerals from the class of smectites (Figure 2.6) [69]. Smectites are layered silicates which are able to adsorb cations and water. Montmorillonite is the product of hydrothermal decomposition of volcanic rock or by alteration of volcanic ash. In nature, montmorillonite is found alongside other smectites, illite, cristobalite, zeolites and calcite. Mixtures of clay minerals which contain high amounts of montmorillonite are called bentonites. Commercially available bentonites contain 60 – 80 wt.% montmorillonite [64 - 69].

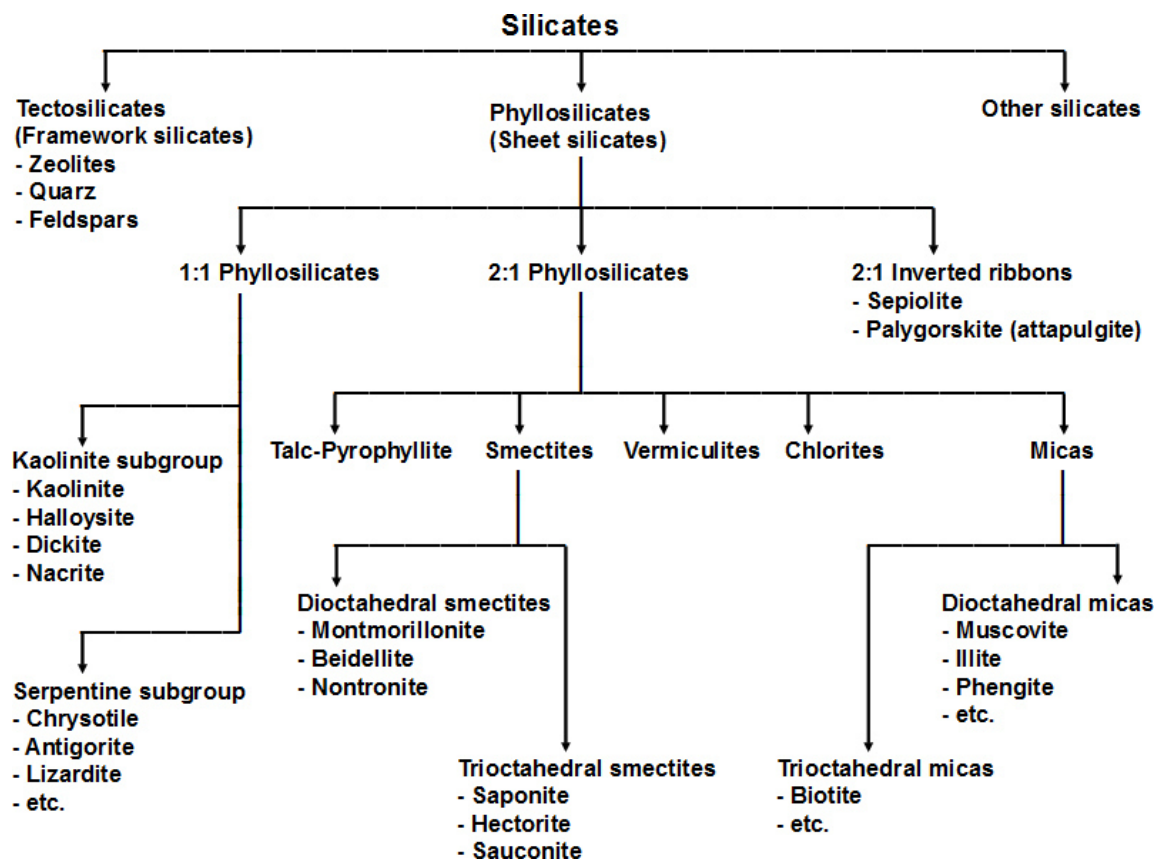


Figure 2.6: Classification of silicates [69]

Structure of montmorillonite

The space group of montmorillonite was found to be $C2/m$, montmorillonite exhibits a monoclinic crystal system. The elementary cell dimensions of montmorillonite were calculated from X-ray diffraction data. The cell dimensions are $a = 5.17 \pm 0.02 \text{ \AA}$, $b = 8.94 \pm 0.02 \text{ \AA}$, $c = 9.95 \pm 0.06 \text{ \AA}$, and $\beta = 99^\circ 54' \pm 30'$ [74]. Montmorillonite is composed of units in which two silica tetrahedral sheets sandwich a central alumina octahedral sheet [70]. Figure 2.7 shows the arrangement of the silica tetrahedral sheets and the alumina octahedral sheet in the montmorillonite [64]. One set of two silica tetrahedral sheets and one alumina octahedral sheet is called a montmorillonite layer or montmorillonite platelet ($d_s \approx 0.66 \text{ nm}$). The layers are continuous in the a and b directions (the length and the width), but are stacked along the c direction (the height). Between two montmorillonite layers, cations like sodium or calcium as well as water molecules are located. The cations have the purpose of compensating the negative charge of the montmorillonite silicate layers. The distance between two montmorillonite layers is defined as the interlayer distance d_L and is measured by X-ray diffraction (XRD). The interlayer distance of neat montmorillonite is about 0.96 nm . The interlayer distance is the sum of the thickness of one layer ($\approx 0.66 \text{ nm}$) and the space occupied by cations and water molecules ($\approx 0.30 \text{ nm}$) [71].

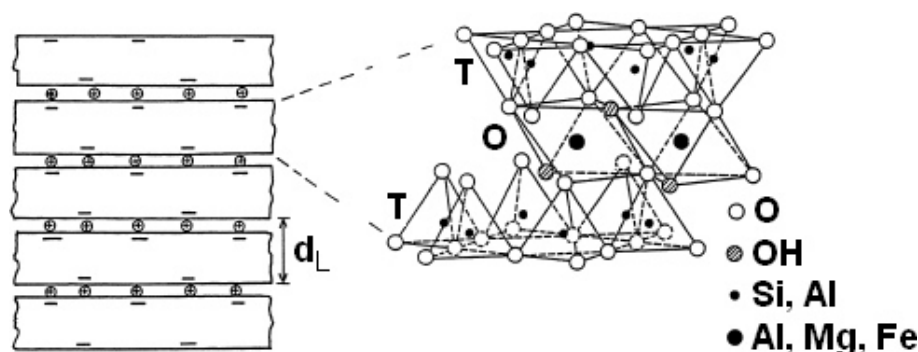


Figure 2.7: Structure and arrangement of montmorillonite [64], T = tetrahedral sheet, O = octahedral sheet, d_L = interlayer distance

Size of montmorillonite platelets

The size of montmorillonite platelets has been investigated by electro-optical birefringence, electron microscopy, and atomic force microscopy. From electro-optical birefringence studies, the lateral extension of the platelets was measured to be ranging from 245 to 1230 nm. The thickness of the platelets, calculated from birefringence and viscosity data, was determined to be 0.9 – 7.3 nm. Measurements of the length of the platelets by electron microscopy resulted in smaller values of 135 to 690 nm [72]. Atomic force microscopy (AFM) studies showed that the average thickness of the platelets was 0.97 nm with a standard deviation of ± 0.25 nm. The length of the platelets was in the range of 10 - 1000 nm. From the data obtained by the AFM studies, the average aspect ratio A_f (the length to the height of the platelets) was calculated to range from 60 to 500, with most of the platelets having aspect ratios in the range of 80 – 300. From this data, the mean aspect ratio was calculated to be $A_f = 166 \pm 86$ with a median A_f of 147 [73].

Adsorption properties of montmorillonite

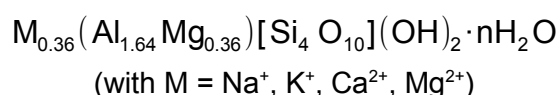
Montmorillonite is able to adsorb cations and water molecules. The factors which control the adsorption capacity are the total number of charge on the clay mineral surface and the charge density, the acidity and the number of hydroxyl groups and oxygen atoms on the clay mineral surface, and the specific surface area of the mineral. The total surface area of montmorillonite was found to be in the region of 346 - 780 m^2/g [75 - 77]. Studies on the adsorption of water molecules on montmorillonite revealed that for this molecules about 90 % of the total area was accessible. The large surface area accessible to water molecules was attributed to the fact that water molecules can diffuse into the space between the montmorillonite layers. With non-polar gases, such as nitrogen and oxygen, only the external surface was accessible and the degree of adsorption was about fifty times lower [78, 79].

Swelling behaviour of montmorillonite

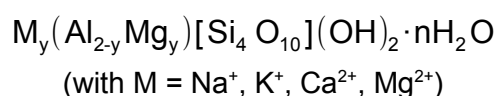
Montmorillonite has the ability to swell which is caused by water molecules which diffuse into the space between the layers and widen the interlayer gaps. The degree of swelling can be measured by X-ray diffraction. Studies on the swelling behaviour of montmorillonite have shown that the d_{001} interlayer spacing increased from about 1.0 nm to values around 14 nm after water was added to the montmorillonite [70, 80]. The mechanism behind the swelling is that at a certain concentration the water forms a complete film around the montmorillonite layers. At this concentration, the attraction between the platelets is reduced and smaller platelets are able to reorientate themselves into a condition of closer packing. This leads to a thickening of the water film between the aggregates [81 - 85]. Swelling is accompanied by a loss of elasticity, i. e. the swollen MMT turns into a soft, smeary paste.

Charge of montmorillonite

Investigations on the charge of montmorillonite have shown that this mineral exhibits a non-uniform charge distribution across the surface of the platelets [86, 87]. The total charge of a platelet is defined as layer charge ξ per formula unit. The total charge of one montmorillonite platelet can be divided into two parts: the interlayer charge and the charge on the edges of the platelet. The interlayer charge is attributed to the substitution of Al^{3+} ions by Mg^{2+} ions in the octahedral sheets and is, therefore, negative. The edges, on the other hand, are positively charged due to broken Al-O-OH octahedral sheets [84]. Analysis of 19 montmorillonites from different locations have shown that the number of interlayer cations per formula unit was in the region of 0.33 – 0.39 [88, 89]. Based on this results, the sum formula of montmorillonite can be written as:



The general sum formula can be written as:



Cation exchange capacity (CEC) of montmorillonite

Montmorillonite either contains naturally or artificially added cations such as sodium or calcium between the layers. Those cations can be replaced by either other cations like barium, lithium, and hydrogen [78] or ammonium moieties [90]. The number of

cations which can be replaced are expressed as the cation exchange capacity. After exchanging the montmorillonite cations by alkylammonium cations, the cationic exchange capacity can be calculated from X-ray diffraction data. The interlayer spacing can be correlated with the cation density which enables the calculation of the cation exchange capacity (CEC). The CEC is expressed as equivalents of exchanged cations per formula unit of montmorillonite as shown in Equation 2.1.

$$\text{CEC} = \frac{\bar{\xi}}{M} \quad \text{Eq. 2.1}$$

(with CEC = cation exchange capacity [eq/gram], $\bar{\xi}$ = number of exchanged cations [eq], M = molecular mass of one formula unit of montmorillonite [≈ 370 g])

The CEC measured by the cation exchange method gives the total exchange capacity. It exceeds the interlayer CEC by the number of cations attached to the crystal edges (Figure 2.8). The interlayer CEC contributes about 80% to the total CEC and 20% of the total CEC originates from cations attached to the edges [88]. At a pH larger than 4 - 5, the edges develop a negative charge and carry exchangeable cations. Depending on the pH the ratio interlayer CEC: total CEC ranges from 0.6 to 0.9 [91].

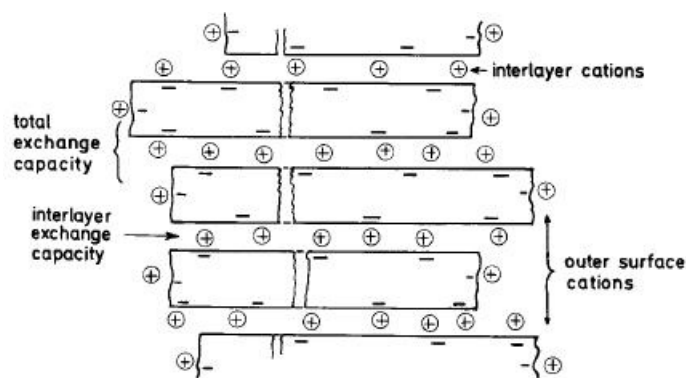


Figure 2.8: Exchangeable cations in montmorillonite [91]

2.3.2 Organically modified montmorillonite

Reactions of low molecular organic molecules with montmorillonite

The cations between the montmorillonite platelets can be replaced by ammonium groups. When alkylammonium compounds are intercalated into montmorillonite they arrange themselves and form mono-, bi-, or pseudo trimolecular layers (Figure 2.9). N-alkylammonium compounds with different chain lengths were intercalated into montmorillonite and the influence of the chain length with regard to the interlayer distance was investigated. The replacement of the cations by the N-alkylammonium

compounds was quantitative and the measured interlayer distances reproducible [92]. Different from observations of the intercalation of N-alkylammonium compounds into mica [93] and vermiculite [94], where the N-alkylammonium arranged themselves perpendicular between the platelets, the compounds were lying flat between the montmorillonite platelets.

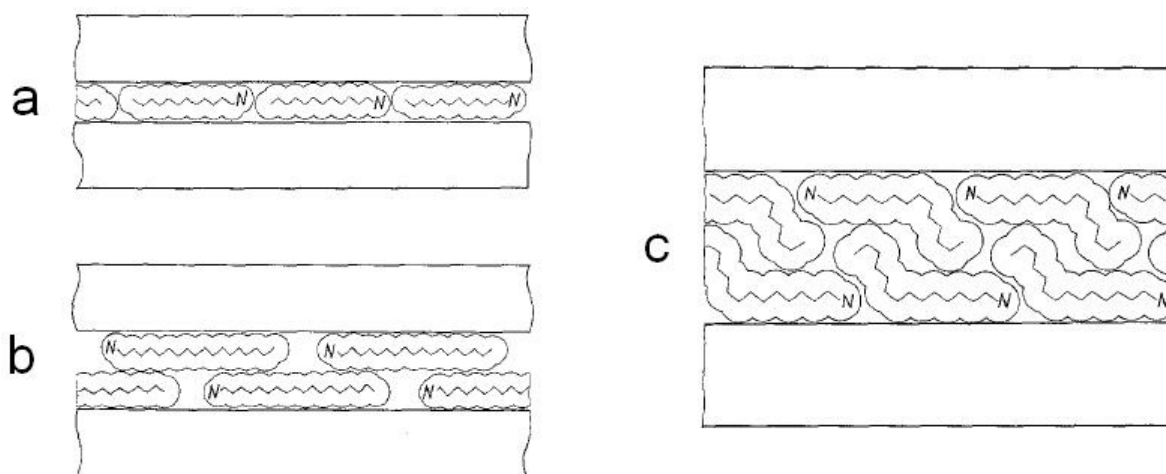


Figure 2.9: Arrangement of alkyl chains in montmorillonite: monolayers (a), bilayers (b), and pseudo trimolecular layers (c) [90]

The arrangement of the molecules was verified by intercalating several organic compounds into montmorillonite and measuring the interlayer distances. It was found that the spacings were less than the sum of the van der Waals cross-section of the molecules plus the thickness of the montmorillonite layer [95]. N-alkylammonium compounds with chain lengths between 4 and 9 carbon atoms formed monolayers as shown by the similar interlayer distances obtained with the investigated compounds. The interlayer distances were found to be in the region of 13.3 to 13.6 Å, a continuous increase of 1.26 Å per C-atom was not observed. With chain lengths between 10 and 13 carbon atoms monolayers as well as bilayers were formed and the interlayer distances increased monotonously from 13.6 Å up to 17.6 Å. With 14 – 17 carbon atoms in the alkyl chain, the interlayer distances showed a plateau at 17.6 Å which was attributed to the formation of bilayers. When the alkyl chains exceeded 18 carbon atoms, pseudo trimolecular layers were formed and another increase in the interlayer distances up to 18.0 Å took place [90, 96].

Reactions of polymers with montmorillonite

To enhance the mechanical properties, charged and non-charged polymers were reacted with montmorillonite to give montmorillonite/polymer hybrid materials which are called “nanocomposites” [97]. Polymer/montmorillonite composites were prepared by

mixing polymer monomers with montmorillonite which were subsequent polymerised [77, 98 - 102]. Composites were also obtained by addition of polymers to the montmorillonite at temperatures above the melting point of the polymers [103, 104] or by mixing polymers with montmorillonite in an aqueous solution followed by the removal of the solvent under reduced pressure afterwards [105 - 108]. In some cases, the cations attached to the montmorillonite were replaced by N-alkylammonium compounds with the aim to enlarge the interlayer distances priorly to the addition of the polymers. With all composites, all organic compounds used during the preparation remained in the final product.

Linear polymers are able to adsorb on the montmorillonite surface when water molecules are desorbed. The gained entropy provides the driving force for adsorption of this kind of polymers [109 - 111]. Positively charged polymers (polycations), on the other hand, are adsorbed through electrostatic (coulomb) interactions between the cationic groups of the polymer and the negatively charged montmorillonite [112, 113]. Also, after a certain number of polymer molecules are adsorbed, a charge reversal can occur and the montmorillonite/polycation system behaves like an anion exchanger [109]. Polyanions don't enter the interlayer space of expanding layer silicates [114] but intercalation can occur at a low pH when the polyanion behaves and adsorbs like an uncharged polymer [115, 116].

Mixtures of poly(ethylenimine), montmorillonite and other materials have been used for several applications. Poly(ethylenimine) was used as a glue in foundry moulding compositions in combination with bentonite, sand, and water [117]. Multilayer films of positively and negatively charged proteins were assembled by alternate electrostatic adsorption on positively charged poly(ethylenimine) or negatively charged poly(styrene sulfonate) which were attached to montmorillonite [118]. Montmorillonite/poly(ethylenimine) composites were also used for the removal of Cr(VI) [119], Co(II) and Ni(II) [120] ions in water. Gas barrier films were prepared by assembling poly(ethylenimine) and poly(acrylic acid) on montmorillonite. The obtained composites showed low oxygen permeability when the thickness of the film was above 51 nm [121]. Poly(ethylenimine)s with weight average molecular masses of 800 and 25,000 g/mol were reacted with montmorillonite to create a base for UV-curable nanocomposites with antimicrobial activity. With both polymers, an increase of the interlayer distance from about 1.0 nm to about 1.45 nm was observed [122].

Gas barrier properties of polymer films filled with inorganic fillers

The diffusion of gas molecules through a polymer film filled with inorganic fillers can be described by the "tortuous path" model. The model states that the gas molecules must diffuse around the filler particles if the filler particles are impenetrable to the dif-

fusing molecules. This leads to a tortuous path for the gas molecules through the polymer film [123]. Figure 2.10 shows the diffusion paths of gas molecules in filled polymers. The model is valid for filler particles that are circular or rectangular plates which are uniformly and completely dispersed in the polymer film. In the model, the particles are oriented parallel to the polymer film surface.

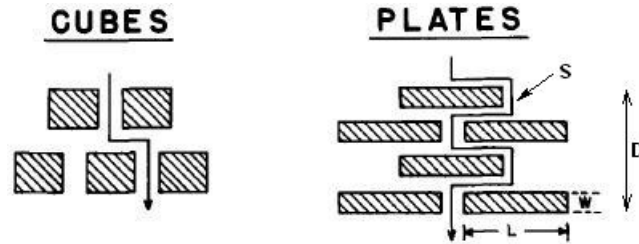


Figure 2.10: Model for the path of a diffusing molecule through a polymer filled with circular or square plates [123]

Under this conditions, the distance which a diffusing molecule travel is maximised and the maximum possible tortuosity factor τ can be written as shown in Equation 2.2 [123]. The tortuosity factor is defined as the ratio of actual to the shortest distance which a gas molecule have to travel in a filled material [124].

$$\tau = 1 + \left(\frac{L}{2} \cdot W\right) \cdot \Phi_F = \frac{S}{D} \quad \text{Eq. 2.2}$$

(with τ = tortuosity factor, L = length of a face of the filler particle [nm], W = thickness of the filler particle [nm], Φ_F = volume fraction of the filler particle, S = diffusion way a gas molecule have to take [nm], D = thickness of the material [nm])

With the tortuosity factor, the permeability ratio of gaseous molecules in filled and un-filled polymers can be calculated using Equation 2.3 [123].

$$\frac{P_F}{P_U} = \frac{\Phi_P}{\tau} = \frac{\Phi_P}{1 + \left(\frac{L}{2} \cdot W\right) \cdot \Phi_F} \quad \text{Eq. 2.3}$$

(with P_F and P_U = permeability of the filled and unfilled polymer, Φ_P = volume fraction of the polymer, Φ_F = volume fraction of the filler, τ = tortuosity factor, L = length of a face of a filler particle [nm], W = thickness of the filler particle [nm])

When the plates are oriented perpendicular to the surface, the definition of the tortuosity factor is rewritten to the form shown in Equation 2.4 [123]. For the calculation of the tortuosity factor, the inverse aspect ratio ($1/A_f$) is then used instead of the aspect

ratio (A_f = a measure of particle asymmetry = length of the major axis to the length of the minor axis).

$$\tau = 1 + \left(\frac{W}{2} \cdot L\right) \cdot \Phi_F \quad \text{Eq. 2.4}$$

(with τ = tortuosity factor, L = length of a face of a filler particle [nm], W = thickness of the filler particle [nm], Φ_F = volume fraction of the filler)

Further calculations and simulations on the diffusion of gaseous molecules through a space filled with disc-shaped fillers have shown that the decrease of the permeability depends on several factors. The calculations were improved taking the factors aspect ratio, concentration and orientation of the particles into account [124 - 126]. With randomly orientated disc-shaped fillers, fillers with high aspect ratios and high length exhibit a higher barrier property than fillers with low aspect ratios at a given particle orientation. With an aspect ratio $A_f > 500$, the gas barrier property of a system with randomly orientated fillers was reported to be similar to that of a system with particles aligned parallel to the diffusion path [124].

Studies on the gas barrier properties of films which consisted of polystyrene and dimethyl ditallow modified montmorillonite were performed. The polymer/filler films were prepared by mixing the polymer with the organo-modified montmorillonite in toluene. Films with a thickness of 0.06 to 0.27 mm were prepared by spray casting and subsequent drying. The diffusion of oxygen was studied with films having montmorillonite concentrations in the range of 3.8 to 37.9 vol.%. It was found that the oxygen permeation rate decreased consistently with increasing montmorillonite concentration. Comparing different models of the diffusion of gas molecules, the importance of the orientation of the platelets in polymer/montmorillonite nanocomposites became clear. Since the experimental and theoretical permeations differed quite largely, a correction factor was applied which took into account the orientation of the platelets [127].

Viscosity of disc-shaped particle dispersions

Since the aspect ratio and the volume fraction Φ of particles in a dispersion influences the dynamic viscosity η_{dyn} of a material [128 - 130], Bicerano, Douglas and Brune developed a model which correlates the viscosity of a dispersion with the aspect ratio of the incorporated particles [131]. The theory was based on the percolation theory [132, 133] and divided particle dispersion into three regimes which are called the dilute regime, the semidilute regime, and the concentrated regime (Figure 2.11).

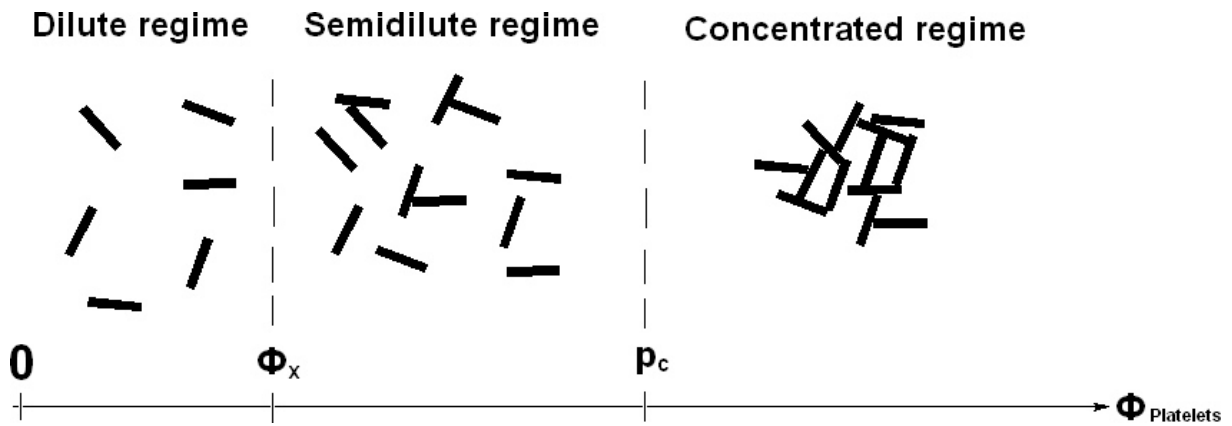


Figure 2.11: Arrangement of disc-shaped particles in dispersions [131]

In the dilute regime, the relative viscosity η_{relative} (cf. Equation 2.5) is proportional to the intrinsic viscosity $[\eta]$ and the volume fraction Φ of particles as shown in Equation 2.6 [131]. No interparticle interactions occur in the dilute regime.

$$\eta(\text{relative}) = \frac{\eta(\text{dispersion})}{\eta(\text{dispersing fluid})} \quad \text{Eq. 2.5}$$

(with η = viscosity [Pa·s])

$$\eta(\text{relative}) \approx 1 + [\eta]\Phi \quad \text{Eq. 2.6}$$

(with η = viscosity [Pa·s], Φ = volume fraction of the dispersed particles)

The boundary between the dilute and the semidilute regime is given by the crossover volume fraction Φ_x at which interparticle interactions occur for the first time, i. e. the rotational volumes of the particles starts to overlap. The semidilute regime ranges from the crossover volume fraction Φ_x up to the geometrical percolation threshold p_c . At the percolation threshold, the volume of the particles overlaps and span the region they are placed into [131]. At the percolation threshold, the interparticle interactions begin to be predominant. The concentrated regime is located above the value of p_c . With increasing volume fraction of the particles, the particles form large network-clusters until they reach a critical volume fraction Φ^* at which the viscosity of the dispersion approaches infinity. Above Φ^* the dispersion behaves like a solid [131].

With the relative viscosity η and the volume fraction of the dispersed particles Φ , the critical volume fraction Φ^* of the dispersed particles can be calculated by means of Equation 2.7 [131]. At the critical volume fraction Φ^* the collective motions become strong enough to cause a transition from a highly viscous fluid to a solid for which $\eta \rightarrow \infty$ is valid. Equation 2.7 is valid for volume fractions in the range of $0 < \Phi < \Phi^*$ [131].

$$\eta(\text{relative}) \approx \left(1 - \frac{\Phi}{\Phi^*}\right)^{-2} \cdot \left[1 - 0.4 \cdot \left(\frac{\Phi}{\Phi^*}\right) + 0.34 \cdot \left(\frac{\Phi}{\Phi^*}\right)^2\right] \quad \text{Eq. 2.7}$$

(with η = viscosity [Pa·s], Φ = volume fraction of the dispersed particles, Φ^* = critical volume fraction of the dispersed particles)

To determine the critical volume fraction Φ^* , the authors have shown that Φ^* correlates also with the intrinsic viscosity $[\eta]$ of the dispersion as described in Equation 2.8 [131].

$$\Phi^* \approx \frac{1.7}{[\eta]} \quad \text{Eq. 2.8}$$

(with Φ^* = critical volume fraction, $[\eta]$ = intrinsic viscosity of the dispersion [Pa·s])

They found empirically a correlation between the intrinsic viscosity $[\eta]$ and the aspect ratio (A_f) of the dispersed particles (cf. Equation 2.9) [131]. For disc-shaped particles, the inverted aspect ratio (= $1/A_f$) is valid instead of the aspect ratio.

$$[\eta] \approx \frac{1012 + 2904A_f - 1855A_f^{1.5} + 1604A_f^2 + 80.44A_f^3}{1497A_f + A_f^2} \quad \text{Eq. 2.9}$$

(with $[\eta]$ = intrinsic viscosity of the dispersion [Pa·s], A_f = aspect ratio of the particles (diameter/thickness))

Although the model correlates the increase of the viscosity in a particle filled system well with the aspect ratio of the incorporated particles, the value of the percolation threshold and the critical volume fraction Φ^* can be reached at lower volume fractions than expected when strong attractive interactions occur between the particles. Also, the model doesn't take interactions between the medium and the particles into account. In conclusion, up to date, no theory is available which enables the calculation of the aspect ratio of platelets in a real system which takes all factors into account. Nonetheless, the described model and calculations can be used to get a hunch of the aspect ratio of montmorillonite platelets in bitumen-nanocomposites.

2.4 Hyperbranched polymers

2.4.1 Branched and hyperbranched polymers

The term “branched polymers” describes a class of polymers in which polymer chains exhibit branch points that connect three or more chain segments to build up non-linear structures [134]. Branched polymers are divided into three classes which are cas-

cadanes, dendrimers, and hyperbranched polymers [135]. Cascadanes are monodisperse molecules with regular branching and defect-free structures. They exhibit a degree of branching DB (Equation 2.10, [136]) of 100 %.

$$DB = \frac{2D}{2D+L} \quad \text{Eq. 2.10}$$

(with DB = degree of branching, D = number of dendritic units, L = number of linear units)

Dendrimers are almost monodisperse molecules with only a low number of linear units. The degree of branching of dendrimers is found close to 100 % [135]. Hyperbranched polymers are polydisperse molecules with strongly imperfect branching structures. The degree of branching of these polymers is found between 50 and 85 %, depending on the used monomer [135]. Hyperbranched polymers don't exhibit the well-defined structures of dendrimers, but they exhibit also a large number of functional groups and similar physical properties [137, 138]. In an early approach, branched polymers were obtained by condensation polymerisation of a mixture of A_3 , A_2 and B_2 monomers [139, 134]. Although highly branched polymers with linear segments were obtained, gelation occurred when the degree of polymerization approached a critical limit [134]. Polymers which are branched and soluble were obtained from the condensation polymerization of AB_n (with $n \geq 2$) monomers [136, 140 - 143]. A model for the condensation of AB_2 monomers in which the monomer contains one functional group A and two functional groups B, which can react with the functional group A, is shown in Figure 2.12.

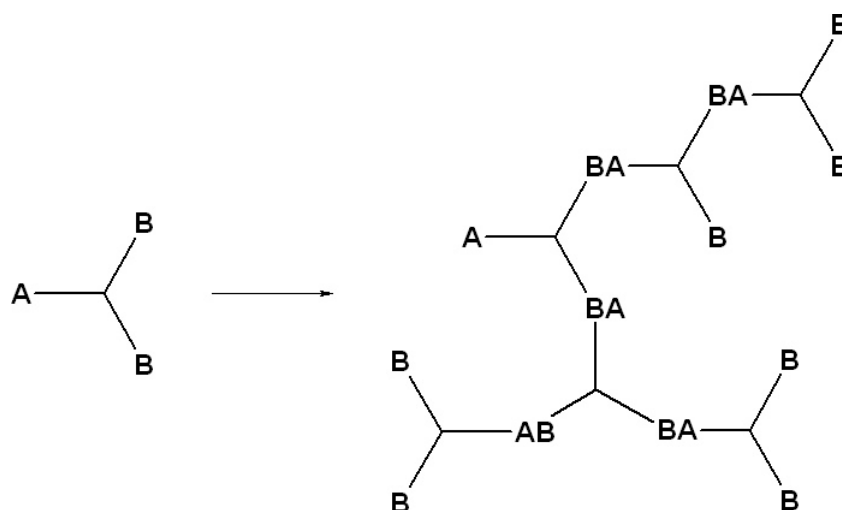


Figure 2.12: Model of branched polymers prepared by condensation of AB_2 -type monomers [140]

Hyperbranched polymers are also obtained by ring-opening polymerization of cyclic

carbamates [144], 3-ethyl-3-(hydroxymethyl)oxetanes [145], glycidols [146, 147] and ethylenimines [148]. With proton-transfer polymerization, epoxy or hydroxyl functionalized hyperbranched polymers are obtained [149]. Branching can also occur during free radical polymerization of vinyl monomers when the monomer perform the function of a chain transfer agent [150 - 152].

2.4.2 Hyperbranched poly(ethylenimine)

Technical hyperbranched poly(ethylenimine) (PEI) is synthesised by cationic ring-opening polymerization of aziridine. Hyperbranched poly(ethylenimine) exhibits terminal, linear and dendritic units in a ratio of 30:39:31 (Figure 2.13) [153, 154]. Hyperbranched poly(ethylenimine) can be used as an additive for printing ink [155], as chelating agent for metal ions [156 - 158], in the paper industry for flocculation of negatively charged fibres [159], as a sorbent for carbon dioxide [160], in anion-exchange resins [161], as an additive in foundry molding compositions [117] and as an antistatic agent for propellant powder [162].

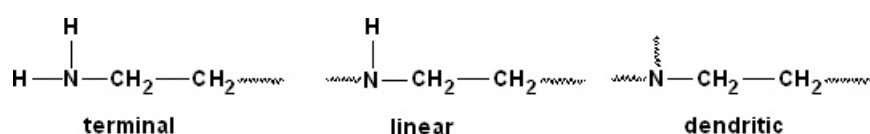


Figure 2.13: Structure units of hyperbranched poly(ethylenimine)

Depending on the desired applications, several modifications on poly(ethylenimine)s were performed. Hyperbranched poly(ethylenimine)s had been reacted with a palmitic acid, as well as a palmitic acid active ester, to obtain amphiphilic polymers with a hydrophilic core and a hydrophobic shell. The modification had the aim to create a polymer which can adhere simultaneously to silver nanoparticles and a polar substrate to create an antimicrobial coating [163, 164]. Poly(ethylenimine)-*g*-poly(ϵ -caprolactone) and poly(ethylenimine)-*g*-polystyrene polymers were synthesised and the potential of those polymers on the encapsulation of dyes was investigated. [165 - 167]. Poly(ethylenimine)-*g*-poly(ethylene glycol) polymers were synthesised to investigate, how structural modifications of poly(ethylenimine)s affect the condensation of nucleic acids and the biological activity of PEI/DNA complexes [168].

The neat poly(ethylenimine) exhibits a good adhesion on negatively charged surfaces due to coulomb binding, Stern layer binding, hydrophobic binding or adsorption, hydrolytic binding and ligand binding [169]. But due to the amino groups, the polymer is only a weak electrolyte and its adhesion properties on negatively charged surfaces are strongly pH dependent [170]. To increase the adhesion properties, qua-

ternary ammonium groups are linked to poly(ethylenimine)s via carboxyl, epoxy, isocyanate and carbonate groups, which leads to strong permanently positive charged polyelectrolytes [171 - 173]. The obtained polymers are called “quat-primer” polymers and are used as dispersants for terbium doped lanthanide phosphate nanorods [174]. Grafting of poly(methylmethacrylate) onto a poly(ethylenimine) “quat-primer” polymer gave a core-shell polymer, which can be used as a dispersant to prepare PM-MA-nanocomposites [175, 176].

2.5 Methods

2.5.1 X-ray diffraction (XRD)

In this study the interlayer distances of the montmorillonite in the [MMT/PEI(nkD)_{xQ}^{yR}] adducts (cf. Chapters **4** and **6**) were calculated from wide- and small-angle X-ray diffraction (XRD) data. When the conditions satisfy Bragg's Law (Equation 2.11), a constructive interference from the interaction of the incident rays with the sample occurs. Bragg's Law establishes a relationship between the wavelength of the reflected electromagnetic radiation λ with the lattice spacing d and the “reflection” angle θ in a sample [177].

$$n \cdot \lambda = 2 \cdot d \cdot \sin(\theta) \quad \text{Eq. 2.11}$$

(with n = positive integer, λ = wavelength [Å], d = interplanar spacing [Å], θ = scattering angle [°])

Equation 2.12 shows the relation between the Miller indices parameters d_{hkl} and the lattice constants of a monoclinic crystalline system [177].

$$\frac{1}{d_{hkl}^2} = \frac{h^2}{a^2 \cdot \sin^2 \beta} + \frac{k^2}{b^2} + \frac{l^2}{c^2 \cdot \sin^2 \beta} - \frac{2 \cdot h \cdot l \cdot \cos \beta}{a \cdot c \cdot \sin^2 \beta} \quad \text{Eq. 2.12}$$

(with d_{hkl} = interplanar spacings [Å], h , k , and l = integer of the lattice spacings, a , b , and c = lattice constants [Å], β = angle [°])

For d_{00l} spacings Equation 2.12 simplifies to:

$$d_{00l} = \frac{c \cdot \sin \beta}{l} \quad \text{Eq. 2.13}$$

(with d_{00l} = interplanar spacing [Å], l = integer of the lattice spacing, c = lattice constant c [Å], β = angle [°])

In this work wide-angle measurements were performed of the region $2\theta = 5 - 79^\circ$. Interlayer distances d_{001} which would appear at angles smaller $2\theta = 5^\circ$ had to be calculated by minimising the sum of squared errors of prediction (SSE, Eq. 2.14) of the experimentally and simulated d_{001} spacings and extrapolated to d_{001} . The calculated d_{001} spacings are approximations due to the asymmetric bands of the montmorillonite in the diffractograms of the [MMT/PEI(nkD)_{xQ}^{YR}] adducts which are caused by the disordered layer sequences of the montmorillonite [178].

$$SSE = \sum_{i=1}^n (d_{001,exp} - d_{001,sim})^2 \quad \text{Eq. 2.14}$$

(with d_{001} = interplanar spacing [Å], $d_{001,exp}$ = experimentally obtained interplanar spacing [Å], $d_{001,sim}$ = simulated interplanar spacing [Å])

With the d_{001} spacing the lattice constant c was calculated by means of Equation 2.15.

$$c = \frac{d_{001} \cdot l}{\sin\beta} \quad \text{Eq. 2.15}$$

(with d_{001} = interplanar spacing [Å], l = integer of the lattice spacing, c = lattice constant [Å], β = angle [°])

The gap between the montmorillonite platelets was calculated by subtracting the thickness of the platelets (= 0.66 nm [71]) from the lattice constant c .

2.5.2 Light scattering

The scattering of light by particles was described first by Strutt [179 - 182]. He found that light waves coming through the atmosphere are diverted from their original course when they strike particles. The scattering of the incident light by particles smaller than the wavelength of the incident wave ($d < \lambda/20$) is called Rayleigh scattering. Small particles scatter light preferably perpendicular to the incident wave. For particles with diameters larger or equal to the wavelength of the incident wave, Mie scattering predominates which means the particles scatter the light in the direction of the incident wave. The ratio of the intensity of the scattered light to the intensity of the incident light is expressed by the Rayleigh ratio given in Equation 2.16. With small particles ($d < \lambda/20$), the Rayleigh ratio is independent of the angle.

2 Literature review

$$R_{\Theta} = \frac{r^2}{f \cdot V} \cdot \frac{I(r, \Theta)}{I_0} \quad \text{Eq. 2.16}$$

(with R_{Θ} = Rayleigh ratio at the measurement angle Θ [nm^{-1}], r = distance between the volume of the scatterer and the detector [nm], f = correction factor for the polarisation of the incident light ($= 1 + \cos^2(\Theta)$ for non-polarized), V = volume of the scatterer [nm^3], $I_{\text{excess}}(r, \Theta)$ = intensity measured at a distance r and an angle Θ [s^{-1}], I_0 = intensity of the incident light [s^{-1}])

To determine the intensity of the light which is scattered by macromolecules, the light scattered by the solvent is subtracted from the light scattered by the solution (Equation 2.17).

$$I(r, \Theta) = I_{\text{excess}}(r, \Theta) = I_{\text{solution}}(r, \Theta) - I_{\text{solvent}}(r, \Theta) \quad \text{Eq. 2.17}$$

(with $I_{\text{excess}}(r, \Theta)$ = excess scattered light intensity [s^{-1}], $I_{\text{solution}}(r, \Theta)$ = scattered light intensity of the solution [s^{-1}], $I_{\text{solvent}}(r, \Theta)$ = scattered light intensity of the solvent [s^{-1}], (r, Θ) = distance r and angle Θ to the incident wave)

Debye derived a relationship between the weight average molecular weight, the second virial coefficient A_2 , and the Rayleigh ratio [183 - 185] as shown in Equation 2.18.

$$\frac{K \cdot C_0}{R_{\Theta}} = \frac{1}{M_w \cdot P(\Theta)} + 2 \cdot A_2 \cdot C_0 \quad \text{Eq. 2.18}$$

(with K = optical constant [$\text{nm}^2 \text{ mol g}^{-2}$], C_0 = sample concentration [g/nm^3], R_{Θ} = Rayleigh ratio [nm^{-1}], M_w = weight average molecular weight [g/mol], A_2 = second virial coefficient [nm^3/g], $P(\Theta)$ = particle scattering function, Θ = scattering angle)

The optical constant K is defined as shown in Equation 2.19. The refractive index increment dn/dc characterises the change of the refractive index n of the solution with the concentration c .

$$K = \frac{2 \cdot \pi^2 \cdot n_0^2}{N_A} \cdot \frac{1}{\lambda^4} \cdot \left(\frac{dn}{dc} \right)^2 \quad \text{Eq. 2.19}$$

(with K = optical constant [$\text{nm}^2 \cdot \text{mol}/\text{g}^2$], n_0 = refractive index of the solvent, N_A = Avogadro constant [$6.02214086 \cdot 10^{23} \text{ mol}^{-1}$], λ = wavelength of the incident light [nm], dn/dc = refractive index increment of the sample [nm^3/g])

The particle scattering function $P(\Theta)$ enables the calculation of the radius of gyration of polymers as shown in Equation 2.20.

$$\frac{1}{P(\Theta)} = 1 + \frac{16 \cdot \pi^2}{3 \cdot \lambda^2} \cdot R_G^2 \cdot \sin^2\left(\frac{\Theta}{2}\right) \quad \text{Eq. 2.20}$$

(with $P(\Theta)$ = particle scattering function, λ = wavelength of the incident wave [nm], R_G = radius of gyration [nm], Θ = scattering angle)

To determine the weight average molecular weight and the radius of gyration of polymers with unknown molecular weight, measurements are made at many different angles and concentrations. The plotting of $K \cdot C/R\Theta$ versus $\sin^2(\Theta/2) + C$ is called the Zimm method [186, 187]. From this plot, the molecular weight is obtained by double extrapolation to the angle of zero and the concentration of zero. The intercept at $\Theta = 0$ gives $1/M_w$, the radius of gyration R_G is obtained from the slope of the $c = 0$ line, extrapolated from different values of Θ . The slope of the $\Theta = 0$ line, extrapolated from different values of the concentration, yields the second virial coefficient A_2 [188, 189] as shown in Figure 2.14.

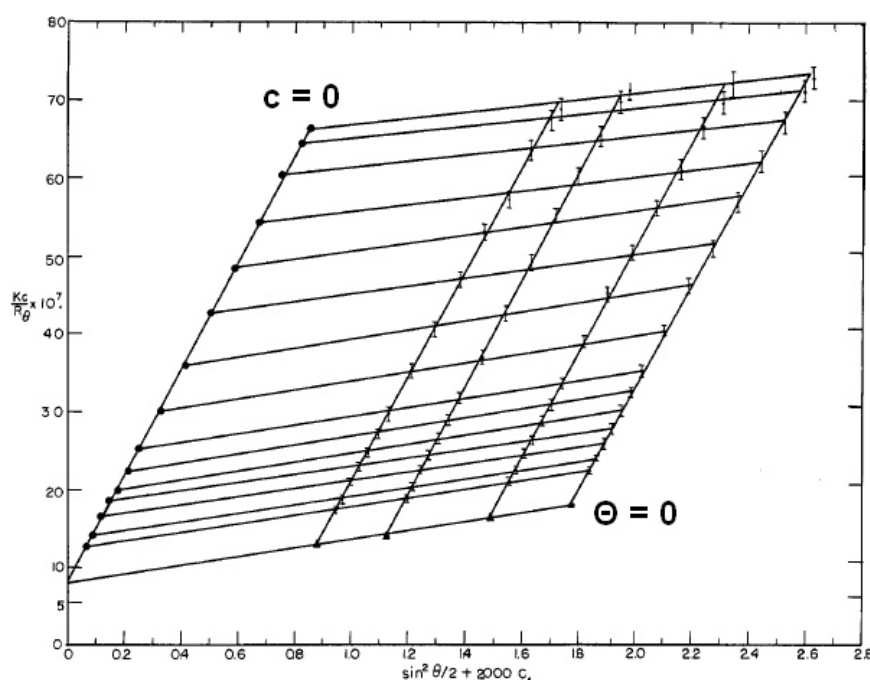


Figure 2.14: Experimental Zimm plot for cellulose nitrate obtained from [188] indexed as shown in [189]

2.5.3 Size-exclusion chromatography (SEC)

The molecular weight of polymers can be determined by size-exclusion chromatography (SEC). Size-exclusion chromatography works in that way that a diluted polymer solution is pumped through a column filled with macroporous gels. The polymers

are separated by their hydrodynamic volume and the fractions are detected by light scattering and refractive index detectors [190].

2.5.4 “Polarised light” and “dark field” microscopy

In this study, the microscopic methods used to investigate the size and distribution of organically modified bentonite particles in bitumen matrices were “polarised light” and “dark field” microscopy. Figure 2.15 shows the setup for a dark field and a polarised light measurement. The polarisation of the light in polarised light microscopy is used to confine the direction of the wave oscillation of the light. A polariser is used to allow only light oscillating in one orientation to pass. All crystals without cubic symmetry have the property of birefringence (= the difference between the highest and lowest refractive indices in crystals [191]) which causes the incoming light to split into two beams. Each beam travels at a different speed hence a phase-shift between both the beams emerges. The beams become recombined by a second polariser called the “analyser”, which polarisation direction is oriented perpendicular to that of the polariser. The light beams interfere constructively and destructively with each other and a visual interferogram is formed at the back focal plane of the objective [191].

Generally, the investigation of a sample by polarised light microscopy reveals the presence of crystalline materials. With montmorillonite/bitumen composites, the polarisation discloses the presence of the montmorillonite since the mineral exhibits a monoclinic crystal system. The limit of resolution is described by the diffraction theory (Ernst Abbe, 1873) which states that particles can't be distinguished when the particles are closer to each other than half the wavelength of the incident light wave due to the overlap of the diffracted waves [191]. The resolution of a microscope is determined by the numerical aperture of the objective and the wavelength of the light as shown in Equation 2.21 [191].

$$d_r = \frac{0.61\lambda}{NA} \quad \text{Eq. 2.21}$$

(with d_r = resolution [nm], λ = wavelength of the light [nm], NA = numerical aperture of the objective)

In a dark field microscopy setup, the central light beams along the optical axis of the microscope are blocked and only light rays at large angles are able to strike the sample. Hence, no direct light from the sample reaches the objective. The light is scattered by particles present in the sample and can be detected. Furthermore, self-luminous objects are also visible [192]. The resolution depends on the numerical aperture (NA) of the objective and the brightness upon the square of the aperture

(NA^2) [192]. Furthermore, particles which are smaller than the resolution of the microscope can be detected as points of light in the form of so-called diffraction discs. When the distance between two particles is larger than $\lambda/2$ two separate particles can be distinguished. When the distance is smaller than $\lambda/2$ the deflected light of the two particles merge and the two particles appear as one particle with increased brightness [192]. With montmorillonite/bitumen composites, dark field microscopy reveals the presence of the montmorillonite particles in the amorphous bitumen matrix.

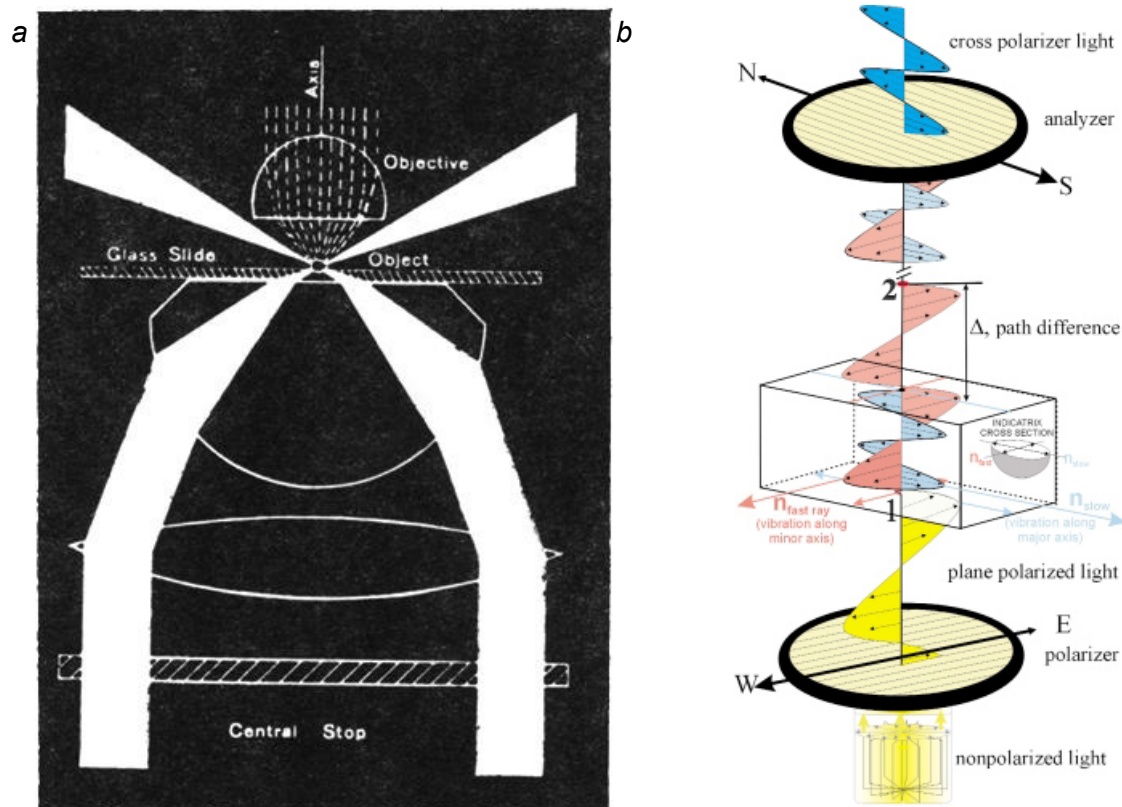


Figure 2.15: Setup for a) dark field [192] and b) polarised light [193] measurements

2.5.5 Rheology

In this work rheological investigations on bitumen nanocomposites were performed to investigate the changes of the viscoelastic properties of bitumen after addition of montmorillonite nanoparticles. Rheology is defined as the science of deformation and flow and is applied to investigate the properties and behaviour of different materials such as bitumen and polymers under an applied force. A viscoelastic material exhibits viscous and elastic properties simultaneously. To determine the properties of a viscoelastic material, the response of the material to an oscillatory shear is measured [194 - 196]. When a sinusoidal shear stress is applied on a material, the shear stress

defined as:

$$\sigma(t) = \sigma_0 \cdot \sin(\omega \cdot t) \quad \text{Eq. 2.22}$$

(with $\sigma(t)$ = shear stress [Pa], σ_0 = shear stress amplitude [Pa], ω = frequency [rad/s], t = time [s])

The resulting shear strain can be calculated with Equation 2.23. The resulting strain sinus curve is shifted from the stress sinus curve by the phase angle δ . The phase angle δ exhibit values between 0 and 90°. Materials which show an ideal elastic behaviour exhibit a phase angle δ of 0°. Materials which show an ideal viscous behaviour exhibit a phase angle δ of 90°. Viscoelastic materials exhibit a phase angle between 0 and 90°.

$$\gamma(t) = \gamma_0 \cdot \sin(\omega \cdot t + \delta) \quad \text{Eq. 2.23}$$

(with $\gamma(t)$ = shear strain [%], γ_0 = shear strain amplitude [%], ω = frequency [rad/s], t = time [s], δ = phase angle [°])

The complex shear modulus G^* , which is a measure of the stiffness of a material, is connected with the shear stress $\sigma(t)$ and the shear strain $\gamma(t)$ by:

$$G^* = \frac{\sigma(t)}{\gamma(t)} \quad \text{Eq. 2.24}$$

(with G^* = complex shear modulus [Pa], $\sigma(t)$ = shear stress [Pa], $\gamma(t)$ = shear strain [%])

The complex shear modulus G^* can be divided into the storage modulus G' and the loss modulus G'' as shown in Equation 2.25.

$$|G^*| = \sqrt{G'^2 + G''^2} \quad \text{Eq. 2.25}$$

(with G^* = complex shear modulus [Pa], G' = storage modulus [Pa], G'' = loss modulus [Pa])

The storage modulus G' is a measure of the stored deformation energy during the shearing process. After the stress is removed the energy is available again and compensates the previous deformation completely or partially. Materials which store the deformation energy completely show a reversible deformation behaviour. The storage modulus G' represents hence the elastic behaviour of the material and is also called the dynamic rigidity. The storage modulus G' is connected with the shear stress $\sigma(t)$ and the shear strain $\gamma(t)$ by:

2 Literature review

$$G' = \frac{\sigma(t)}{\gamma(t)} \cdot \cos \delta \quad \text{Eq. 2.26}$$

(with G' = storage modulus [Pa], $\sigma(t)$ = shear stress [Pa], $\gamma(t)$ = shear strain [%])

The loss modulus G'' is a measure of the deformation energy consumed during the shearing process. This energy is lost due to structural changes of the material or released to the environment. The loss modulus G'' is connected with the shear stress $\sigma(t)$ and the strain $\gamma(t)$ by:

$$G'' = \frac{\sigma(t)}{\gamma(t)} \cdot \sin \delta \quad \text{Eq. 2.27}$$

(with G'' = loss modulus [Pa], $\sigma(t)$ = shear stress [Pa], $\gamma(t)$ = shear strain [%])

The loss factor $\tan \delta$ is defined as the ratio G''/G' and is a measure of the damping in a viscoelastic system. A material exhibiting a high $\tan \delta$ behaves like a viscous liquid and a material showing a low $\tan \delta$ like an elastic solid [197 - 199].

$$\tan \delta = \frac{G''}{G'} \quad \text{Eq. 2.28}$$

(with δ = phase angle δ [°], G'' = loss modulus [Pa], G' = storage modulus [Pa])

The complex viscosity η^* is defined as the rate shear stress $\sigma(t)$ to strain rate $\dot{\gamma}(t)$ as shown in Equation 2.29.

$$\eta^* = \frac{\sigma(t)}{\dot{\gamma}(t)} \cdot \sin \delta \quad \text{Eq. 2.29}$$

(with η^* = complex viscosity [Pa·s], $\sigma(t)$ = shear stress [Pa], $\dot{\gamma}(t)$ = strain rate [s⁻¹])

The strain rate $\dot{\gamma}(t)$ is defined as:

$$\dot{\gamma}(t) = \frac{d\gamma}{dt} \quad \text{q. 2.30}$$

(with $\dot{\gamma}(t)$ = strain rate [s⁻¹], $\gamma(t)$ = shear strain, t = time [s])

The dynamic viscosity η' provides information about the resistance of a material to shearing and is defined as:

$$\eta' = \frac{G''}{\omega} \quad \text{Eq. 2.31}$$

(with η' = dynamic viscosity [Pa·s], G'' = loss modulus [Pa], ω = frequency [rad/s])

References

- 1 Herbert A.; Asphalts and Allied Substances 4th Edition (1938) 2 - 50
- 2 Read J., Whiteoak D.; The Shell Bitumen Handbook 5th (2003)
- 3 Forschungsgesellschaft für Straßen- und Verkehrswesen e. V.; Arbeitsgruppe Asphaltbauweisen; ZTV Asphalt-StB 07/13, TL Asphalt-StB 07/13, TL Bitumen-StB 07/13 (2013)
- 4 Deutscher Asphaltverband (DAV) e.V.; <http://www.asphalt.de/site/startseite/gestaltung/grundregeln/schichtenaufbau/> (05.09.2016)
- 5 Westdeutsche Grauwacke-Union GmbH; <http://www.grauwacke-union.de/produkte/asphaltnischgut/die-asphaltstrasse/> (05.09.2016)
- 6 <Http://www.aboutcivil.org/road-structure-cross-section.html> (05.09.2016)
- 7 Forschungsgesellschaft für Straßen- und Verkehrswesen; Arbeitsgruppe Infrastrukturmanagement; Richtlinien für die Standardisierung des Oberbaues von Verkehrsflächen RStO 12 (2012)
- 8 Irving S. N.; Hawley Gessner Goodrich; Haxley's condensed chemical dictionary 11th Edition (1987) 102 - 103, 290, 320
- 9 Jovanović J. A.; Models of an asphaltene aggregate and a micelle of the petroleum colloid system; Chemical Industry & Chemical Engineering Quarterly 6 (2000) 270 – 275
- 10 Eberhardsteiner L., Füssl J., Hofko B., Handle F., Hospodka M., Blab R., Grothe H.; Influence of asphaltene content on mechanical bitumen behavior: experimental investigation and micromechanical modeling; Materials and Structures 48 (2015) 3099 – 3112
- 11 ASTM D4124 - 09 Standard Test Method for Separation of Asphalt into Four Fractions
- 12 Ullmann's Encyclopedia of Industrial Chemistry, Volume A3 (1985) 169 - 188
- 13 Speight J. G., Moschopedis S. E.; On the Molecular Nature of Petroleum Asphaltenes; Chemistry of Asphaltenes (1982) 1 - 15
- 14 Wess J. A., Olsen L. D.; Asphalt (Bitumen) (Concise International Chemical Assessment Document) 59 (2005) 4, 9
- 15 Petersen J.C., Robertson R. E., Branthaver J. F., Harnsberger P. M., Duvall J. J., Kim S. S., Anderson D. A., Christiansen D. W., Bahia H. U., Dongre R., Antle C. E., Sharma M. G., Button J., Glover J. C.; SHRP-A-367 Binder Characterization and Evaluation 1 (1994)
- 16 Branthaver J. F., Petersen J.C., Robertson R. E., Duvall J. J., Kim S. S., Harnsberger P. M., Mill T., Ensley E. K., Barbour F. A., Schabron J. F.; SHRP-A-368 Binder Characterization and Evaluation 2 (1993)

2 Literature review

- 17 Anderson D. A., Christiansen D. W., Bahia H. U., Dongre R., Sharma M. G., Antle C. E., Button J., Glover J. C.; SHRP-A-369 Binder Characterization and Evaluation 3 (1994)
- 18 Petersen J.C., Robertson R. E., Branthaver J. F., Harnsberger P. M., Duvall J. J., Kim S. S., Anderson D. A., Christiansen D. W., Bahia H. U., Dongre R., Antle C. E., Sharma M. G., Button J., Glover J. C.; SHRP-A-370 Binder Characterization and Evaluation 4 (1994)
- 19 ASTM D 36 – 95; Standard Test Method for Softening Point of Bitumen (Ring-and-Ball Apparatus)
- 20 ASTM D5 - 06e1 Standard Test Method for Penetration of Bituminous Materials
- 21 ASTM D2171 / D2171M - 10 Standard Test Method for Viscosity of Asphalts by Vacuum Capillary Viscometer
- 22 ASTM D92 - 12 Standard Test Method for Flash and Fire Points by Cleveland Open Cup Tester
- 23 ASTM D113 - 07 Standard Test Method for Ductility of Bituminous Materials
- 24 ÖNORM EN 12593 Bitumen and bituminous binders - Determination of the Fraass breaking point
- 25 ASTM D7175 - 08 Standard Test Method for Determining the Rheological Properties of Asphalt Binder Using a Dynamic Shear Rheometer
- 26 Bell C. A.; Summary Report on Aging of Asphalt Aggregate systems; SR-OSU-A-003A-89-2 (1989)
- 27 Robertson R. E.; Chemical Properties of Asphalts and Their Relationship to Pavement Performance; SHRP-A/UWP-91-510 (1991)
- 28 Kuszewski J. R., Gorman W. B., Kane E. G.; Characterization of Asphalt Volatility Using TGA and Iatroscan Analyses; Proceedings of the International Symposium on Roofing Technology (1997) 285 - 291
- 29 Neumann H.-J., Rahimian I., Paczynska-Lahme B.; Zur Strukturalterung von Bitumen; Bitumen 54 (1992) 54 - 56
- 30 Rieche A.; Die Oxydation organischer Verbindungen mit Luft-Sauerstoff; Angewandte Chemie 50 (1937) 520 - 524
- 31 Neumann H. J.; Was ist Bitumen?; Bitumen 4 (1995) 146 - 151
- 32 Polacco G., Stastna J., Biondi D., Zanzotto L.; Relation Between Polymer Architecture and Nonlinear Viscoelastic Behavior of Modified Asphalts; Current Opinion in Colloid & Interface Science 11 (2006) 230 - 245
- 33 Polacco G., Kříž P., Filippi S., Stastna J., Biondi D., Zanzotto L.; Rheological properties of asphalt/SBS/clay blends; European Polymer Journal 44 (2008) 3512 - 3521
- 34 ASTM D1754 / D1754M - 09 Standard Test Method for Effect of Heat and Air on

- Asphaltic Materials (Thin-Film Oven Test)
- 35 ASTM D2872 - 04 Standard Test Method for Effect of Heat and Air on a Moving Film of Asphalt (Rolling Thin-Film Oven Test)
 - 36 ASTM D6521 – 13 Standard Practice for Accelerated Aging of Asphalt Binder Using a Pressurized Aging Vessel (PAV)
 - 37 <http://home.cc.umanitoba.ca/~shalabya/images/rtfo.jpg> (07.09.2016)
 - 38 <http://home.cc.umanitoba.ca/~shalabya/images/PAV.jpg> (07.09.2016)
 - 39 Polacco G., Stastna J., Vlachovicova Z., Biondi D., Zanzotto L.; Temporary networks in polymer-modified asphalts; *Polymer Engineering & Science* 44 (2004) 2185 - 2193
 - 40 Zainab H. N., Ibrahim K., Madzalan N., Tan I. M.; Rheological Properties of Polyethylene and Polypropylene Modified Bitumen; *International Journal of Civil and Environmental Engineering* 3 (2011) 96 - 100
 - 41 Santos Fernandes M. R., Camargo Forte M. M., Mathias Leite L. F.; Rheological evaluation of polymer-modified asphalt binders; *Material Research* 11 (2008) 381 - 386
 - 42 Zaman A. A., Fricke A. L., Beatty C. L.; Rheological properties of rubber-modified asphalt; *Journal of Transportation Engineering* 121 (1995) 461 - 467
 - 43 Filippo M., Felice G.; Rheological characterization of wax-modified asphalt binders at high service temperatures; *Materials and Structures* 44 (2011) 1809 - 1820
 - 44 Edwards Y., Redelius P.; Rheological Effects of Waxes in Bitumen; *Energy Fuels* 17 (2003) 511 - 520
 - 45 Zydex Industries; Zycotherm; http://www.zydexindustries.com/webfiles/Products/14322015033221ZycoThern_19th_Sept,_2015.pdf (05.09.2016)
 - 46 Watanabe T., Abe Y.; Special Characteristics of Thin Asphalt Films in Filler-Asphalt and Sand-Filler-Asphalt Mixes; *Preprints - American Chemical Society, Division of Petroleum Chemistry* 16 (1971) 74 - 88
 - 47 Petersen J. C., Ensley E. K., Barbour F. A.; Molecular interactions of asphalt in the asphalt-aggregate interface region; *Transportation Research Record* 515 (1974) 67 - 78
 - 48 Petersen J. C., Dorrence S. M., Paving asphalts: chemical composition, oxidative weathering, and asphalt-aggregate interactions. Part II; FHWA-RD-74-71 (1974)
 - 49 Cause and Prevention of Stripping in Asphalt Pavements; Educational Series No. 10, Asphalt Institute, College Park, MD (1981)
 - 50 Tarrer A. R., Wagh V.; The Effect of the Physical and Chemical Characteristics of the Aggregate on Bonding; SHRP-A/UIR-91-507 (1991)
 - 51 Majidzadeh K., Brovold F. N.; State of the Art: Effect of Water on Bitumen-

- Aggregate Mixtures; Highway Research Board Special Report 98 (1968)
- 52 Thelen E.; Surface Energy and Adhesion Properties in Asphalt-Aggregate Systems; Highway Research Board Bulletin 192 (1958)
- 53 Ouyang C., Wang S., Zhang Y., Zhang Y.; Preparation and properties of styrene-butadiene-styrene copolymer/kaolinite clay compound and asphalt modified with the compound; *Polymer Degradation and Stability* 87 (2005) 309 - 317
- 54 Zhang H.L., Yu J. Y., Xue L. H., Li Z. C.; Effect of montmorillonite organic modification on microstructures and ultraviolet aging properties of bitumen; *Journal of Microscopy* 244 (2011) 85 - 92
- 55 Mahdi L. M. J., Muniandy R., Yunus R. B., Hasham S., Aburkaba E.; Effect of Short Term Aging on Organic Montmorillonite Nanoclay Modified Asphalt; *Indian Journal of Science and Technology* 6 (2013) 5434 - 5442
- 56 You Z., Mills-Beale J., Foley J. M., Roy S., Odegard G. M., Dai Q., Goh S. W.; Nanoclay-modified asphalt materials: Preparation and characterization; *Construction and Building Materials* 25 (2011) 1072 - 1078
- 57 Wang Y.-P., Liu D.-J., Li Y.-F., Wang Y.-P., Gao J.-M.; Preparation and properties of asphalt modified with SBS/organobentonite blends; *Polymers & Polymer composites* 14 (2006) 403 - 411
- 58 Merusi F., Giuliani F., Polacco G.; Linear viscoelastic behaviour of asphalt binders modified with polymer/clay nanocomposites; *Procedia - Social and Behavioral Sciences* 53 (2012) 335 - 345
- 59 Markanday S. S., Stastna J., Polacco G., Filippi S., Kazatchkov I., Zanzotto L.; Rheology of Bitumen Modified by EVA-Organoclay Nanocomposites; *Journal of Applied Polymer Science* 118 (2010) 557 – 565
- 60 Xiao X.-Y., Yang Z.-Q.; Properties of organic montmorillonite/crumb rubber compound modified asphalt; *Journal of South China University of Technology (Natural Science Edition)* 6 (2013) 116 - 120
- 61 Xiao X.-Y., Zhang D.-K., Yan Y., Zhu W.-Q.; Properties of Asphalt Modified with Organic Montmorillonite/Epoxy Resin; *Journal of South China University of Technology (Natural Science Edition)* 2 (2015) 139 - 143, 150
- 62 Fang C., Liu X., Yu R., Liu P., Lei W.; Preparation and Properties of Asphalt Modified with a Composite Composed of Waste Package Poly(vinyl chloride) and Organic Montmorillonite; *Journal of Materials Science & Technology* 30 (2014) 1304 – 1310
- 63 Hassan Z., Hassan D., Rezvan B., Ali A.; Influence of Bentonite Additive in Bitumen and Asphalt Mixture Properties; *World Academy of Science, Engineering and Technology; International Journal of Civil, Environmental, Structural, Construction and Architectural Engineering* 6 (2012) 629 – 634

- 64 Lagaly G., Jasmund K.; Tonminerale und Tone (1993)
- 65 Bergaya F., Theng B. K. G., Lagaly G.; Handbook of Clay Science (2006)
- 66 Grim R. E.; Clay Mineralogy (1953)
- 67 Bailey S. W.; Summary of recommendations of AIPEA nomenclature committee on clay minerals; American Mineralogist 65 (1980) 1 - 7
- 68 Rieder M., Cavazzini G., D'Yakonov Y. S., Frank-Kamenetsii V. A., Gottardi G., Guggenheim S., Koval P. W., Müller G., Neiva A. M. R., Radoslovich E. W., Robert J.-L., Sassi F. P., Takeda H., Weiss Z., Wones D. R.; Nomenclature of the micas; Clays and Clay Minerals 46 (1998) 586 - 595
- 69 Adamis Z., Fodor J., Williams, R. B., Bentonite, Kaolin, and selected clay minerals; Environmental Health Criteria 231 (2005)
- 70 Hofmann U., Endell K., Wilm D.; Kristallstruktur und Quellung von Montmorillonit; Zeitschrift für Kristallographie - Crystalline Materials 86 (1933) 340 - 348
- 71 Hendricks S. B.; Base Exchange of the Clay Mineral Montmorillonite for Organic Cations and its Dependence upon Adsorption due to van der Waals Forces; The Journal of Physical Chemistry 45 (1941) 65 - 81
- 72 Kahn A.; Studies on the size and shape of clay particles in aqueous suspension; Clays and Clay Minerals, Prec. 6th Conf., Pergamon Press, New York, (1959) 220 - 236
- 73 Ploehn H. J., Liu C.; Quantitative Analysis of Montmorillonite Platelet Size by Atomic Force Microscopy; Industrial Engineering Chemistry Research 45 (2006) 7025 - 7034
- 74 Zvyagin B. B., Pinsker Z. G.; An Electron-diffraction study of the structure of montmorillonite; Doklady Akademii Nauk SSSR 68 (1949)
- 75 Greenland D. J., Quirk J. P.; Determination of the total specific surface area of soils by adsorption of cetyl pyridinium bromide; Journal of Soil Science 15 (1964) 178 - 191
- 76 Macht F., Eusterhues K., Pronk G. J., Totsche K. U.; Specific surface area of clay minerals: Comparison between atomic force microscopy measurements and bulk-gas (N₂) and -liquid (EGME) adsorption methods; Applied Clay Science 53 (2011) 20 - 26
- 77 Blumstein A.; Polymerization of adsorbed monolayers. I. Preparation of the clay-polymer complex; Journal of Polymer Science. A: Polymer Chemistry 3 (1965) 2653 - 2664
- 78 Hendricks S. B., Nelson R. A., Alexander L. T.; Hydration Mechanism of the Clay Mineral Montmorillonite Saturated with Various Cations; Journal of the American Chemical Society 62 (1940) 1457 - 1464
- 79 Ammann L.; Cation exchange and adsorption on clays and clay minerals (2003)

2 Literature review

- 80 Norrish K.; Crystalline Swelling of Montmorillonite: Manner of Swelling of Montmorillonite; *Nature* 173 (1954) 256 - 257
- 81 Norton F. H., Hodgson P. B.; Some notes on the nature of clay; *Journal of the American Ceramic Society* 15 (1932) 191 - 205
- 82 Mering J.; On the hydration of montmorillonite; *Transactions of the Faraday Society* 42 (1946) B205 - B219
- 83 Van Olphen H.; Stabilisation of montmorillonite sols by chemical treatment; *Recueil des Travaux Chimiques des Pays-Bas* 69 (1950) 1308 - 1322
- 84 Van Olphen H.; Rheological phenomena of clay sols in connection with the charge distribution of the micelles; *Discussions of the Faraday Society* 11 (1951) 82 - 84
- 85 Hofmann U., Fahn R., Weiss A.; Thixotropie bei Kaolinit und innerkristalline Quellung bei Montmorillonit; *Kolloid-Zeitschrift* 151 (1957) 97 - 115
- 86 Stul M. S., Mortier W. J.; The heterogeneity of the charge density in montmorillonite; *Clays and Clay Minerals* 22 (1974) 391 - 396
- 87 Peigneur P., Maes A., Cremers A.; Heterogeneity of charge density distribution in montmorillonite as inferred from cobalt adsorption; *Clays and Clay Minerals* 23 (1975) 71 - 75
- 88 Vogt K., Köster H. M.; Zur Mineralogie, Kristallchemie und Geochemie einiger Montmorillonite aus Bentoniten; *Clay Minerals* 13 (1978) 25 - 43
- 89 Lagaly G., Weiss A.; Neue Methoden zur Charakterisierung und Identifizierung quellungsfähiger Dreischichttonminerale; *Zeitschrift für Pflanzenernährung und Bodenkunde* 130 (1971) 9 - 24
- 90 Lagaly G., Weiss A.; Anordnung und Orientierung kationischer Tenside auf Silicatoberflächen IV; *Kolloid-Zeitschrift und Zeitschrift für Polymere* 243 (1971) 48 - 55
- 91 Lagaly G.; Characterization of clays by organic compounds; *Clay Minerals* 16 (1981) 1 - 21
- 92 Lagaly G., Weiss A.; Anordnung und Orientierung kationischer Tenside auf ebenen Silicatoberflächen I; *Kolloid-Zeitschrift und Zeitschrift für Polymere* 237 (1970) 266 - 273
- 93 Lagaly G., Weiss A.; Anordnung und Orientierung kationischer Tenside auf ebenen Silicatoberflächen II; *Kolloid-Zeitschrift und Zeitschrift für Polymere* 237 (1970) 364 - 368
- 94 Lagaly G., Weiss A.; Anordnung und Orientierung kationischer Tenside auf ebenen Silicatoberflächen III; *Kolloid-Zeitschrift und Zeitschrift für Polymere* 238 (1970) 485 - 493
- 95 Brindley G. W., Hoffmann R. W.; Orientation and packing of aliphatic chain

- molecules on montmorillonite: Clay-Organic studies-VI; Clays and Clay Minerals (1962) 546 - 556
- 96 Jordan J. W.; Organophilic Bentonites. I. Swelling in Organic Liquids; The Journal of Physical Chemistry 53 (1949) 294 – 306
- 97 Ray S. S., Okamoto M.; Polymer/layered silicate nanocomposites: a review from preparation to processing; Progress in Polymer Science 28 (2003) 1539 – 1641
- 98 Blumstein A.; Polymerization of adsorbed monolayers. II. Thermal degradation of the inserted polymer; Journal of Polymer Science. A: Polymer Chemistry 3 (1965) 2665 - 2672
- 99 Usuki A., Mizutani T., Fukushima Y., Fujimoto M., Fukumori K., Kojima Y., Sato N., Kurauchi T., Kamigaito O.; Composite material containing a layered silicate; Patent US4889885 A (1989)
- 100 Usuki A., Kojima Y., Kawasumi M., Okada A., Fukushima Y., Kurauchi T., Kamigaito O.; Synthesis of nylon 6-clay hybrid; Journal of Materials Research 8 (1993) 1179 - 1182
- 101 Kojima Y., Usuki A., Kawasumi M., Okada A., Fukushima Y., Kurauchi T., Kamigaito O.; Mechanical properties of nylon 6-clay hybrid; Journal of Materials Research 8 (1993) 1185 - 1189
- 102 Lan T., Pinnavaia T. J.; Clay-Reinforced Epoxy Nanocomposites; Chemistry of Materials 6 (1994) 2216 - 2219
- 103 Vaia R. A., Ishii H., Giannelis E. P.; Synthesis and properties of two-dimensional nanostructures by direct intercalation of polymer melts in layered silicates; Chemistry of Materials 5 (1993) 1694 - 1696
- 104 Vaia R. A., Vasudevan S., Krawiec W., Scanlon L. G., Giannelis E. P.; New polymer electrolyte nanocomposites: Melt intercalation of poly(ethylene oxide) in mica-type silicates; Advanced Materials 7 (1995) 154 - 156
- 105 Plummer C. J. G., Garamszegi L., Leterrier Y., Rodlert M., Månson J.-A. E.; Hyperbranched polymer layered silicate nanocomposites; Chemistry of Materials 14 (2002) 486 - 488
- 106 Amin A., Taha A. S., M. El-Ghaffar M. A. A.; Aliphatic polyamidoamine hyperbranched polymers/layered silicate nanocomposites; Journal of Applied Polymer Science 118 (2010) 525 - 537
- 107 Fotiadou S., Karageorgaki C., Chrissopoulou K., Karatasos K., Tanis I., Tragoudaras D., Frick B., Anastasiadis S. H.; Structure and Dynamics of Hyperbranched Polymer/Layered Silicate Nanocomposites; Macromolecules 46 (2013) 2842 - 2855
- 108 Chrissopoulou K., Fotiadou S., Frick B., Anastasiadis S. H.; Structure and Dynamics in Hydrophilic Polymer/Layered Silicate Nanocomposites;

- Macromolecular Symposia 331 - 332 (2013) 50 - 57
- 109 Theng B. K. G.; Clay-polymer interactions: summary and perspectives; *Clays and Clay Minerals* 30 (1982) 1 - 10
- 110 Parfitt R. L., Greenland D. J.; The adsorption of poly(ethylene glycols) on clay minerals; *Clay Minerals* 8 (1970) 305 - 315
- 111 Greenland D. J.; Adsorption of polyvinyl alcohols by montmorillonite; *Journal of Colloid Science* 18 1963 647 - 664
- 112 Hesslink F. Th.; On the theory of polyelectrolyte adsorption. The effect on adsorption behavior of the electrostatic contribution to the adsorption free energy; *Journal of Colloid and Interface Science* 60 (1977) 448 - 466
- 113 Ueda T., Harada S.; Adsorption of Cationic Polysulfone on Bentonite; *Journal of Applied Polymer Science* 12 (1968) 2395 - 2401
- 114 Ruehrwein R. A.; Ward D. W.; Mechanism of clay aggregation by polyelectrolytes; *Soil Science* 73 (1952) 485 - 492
- 115 Schnitzer M., Kodama H.; Montmorillonite: effect of pH on its adsorption of a soil humic compound; *Science* 153 (1966) 70 - 71
- 116 Mortensen J. L.; Adsorption of Hydrolyzed Polyacrylonitrile on Kaolinite; *Clays and Clay Minerals* 9 (1960) 530 - 545
- 117 Dewey J. L., West J. T.; Foundry molding composition containing a polyalkylenimine; US 3042641 A (1959)
- 118 Lvov Y., Ariga K., Ichinose I., Kunitake T.; Assembly of Multicomponent Protein Films by Means of Electrostatic Layer-by-Layer Adsorption; *Journal of the American Chemical Society* 117 (1995) 6117 - 6123
- 119 Larraza I., López-González M., Corrales T., Marcelo G.; Hybrid materials: Magnetite–Polyethylenimine–Montmorillonite, as magnetic adsorbents for Cr(VI) water treatment; *Journal of Colloid and Interface Science* 385 (2012) 24 - 33
- 120 Goncharuk V. V., Puzyrnaya L. N., Pshinko G. N., Bogolepov A. A., Demchenko V. Y.; The Removal of Heavy Metals from Aqueous Solutions by Montmorillonite Modified with Polyethylenimine; *Journal of Water Chemistry and Technology* 32 (2010) 67 - 72
- 121 Priolo M. A., Gamboa D., Holder K. M., Grunlan J. C.; Super Gas Barrier of Transparent Polymer–Clay Multilayer Ultrathin Films; *Nano Letters* 10 (2010) 4970 - 4974
- 122 Larraza I., Peinado C., Abrusci C., Catalina F., Corrales T.; Hyperbranched polymers as clay surface modifiers for UV-cured nanocomposites with antimicrobial activity; *Journal of photochemistry and photobiology A-chemistry* 224 (2011) 46 - 54
- 123 Nielsen, L.; Models for the Permeability of Filled Polymer Systems; *Journal of*

- Macromolecular Science: Part A – Chemistry 1 (1967) 929 - 942
- 124 Bharadwaj R. K.; Modeling the Barrier Properties of Polymer-Layered Silicate Nanocomposites; *Macromolecules* 34 (2001) 9189 - 9192
- 125 Fredrickson G. H., Bicerano J.; Barrier properties of oriented disk composites; *The Journal of Chemical Physics* 110 (1999) 2181 - 2188
- 126 Gusev A. A., Lusti H. R.; Rational Design of Nanocomposites for Barrier Applications; *Advanced Materials* 13 (2001) 1641 - 1643
- 127 Dunkerley E., Schmidt D.; Effects of Composition, Orientation and Temperature on the O₂ Permeability of Model Polymer/Clay Nanocomposites; *Macromolecules* 43 (2010) 10536 – 10544
- 128 Metzner A. B.; Rheology of suspensions in polymeric liquids; *Journal of Rheology* 29 (1985) 739 – 775
- 129 Russel W. B.; Review of the role of colloidal forces in the rheology of suspensions; *Journal of Rheology* 24 (1980) 287 – 317
- 130 Brenner H.; Rheology of a dilute suspension of axisymmetric Brownian particles; *International Journal of Multiphase Flow* 1 (1974) 195 – 341
- 131 Bicerano J., Douglas J. F., Brune D. A.; Model for the Viscosity of Particle Dispersions; *Journal of Macromolecular Science, Part C* 39 (1999) 561 – 642
- 132 Shante V. K. S., Kirkpatrick S.; An introduction to percolation theory; *Advances in Physics* 20 (1971) 325 – 357
- 133 Basta M., Picciarelli V., Stella R.; An introduction to percolation; *European Journal of Physics* 15 (1994) 97 - 101
- 134 Flory P. J.; Constitution of Three-dimensional Polymers and the Theory of Gelation; *The Journal of Physical Chemistry* 46 (1942) 132 - 140
- 135 Vögtle F., Richardt G., Werner N.; *Dendrimer Chemistry: Concepts, Syntheses, Properties, Applications* (2009)
- 136 Hölter D., Burgath A., Frey H.; Degree of branching in hyperbranched polymers; *Acta Polymerica* 48 (1997) 30 – 35
- 137 Gao C., Yan D.; Hyperbranched polymers: from synthesis to applications; *Progress in Polymer Science* 29 (2004) 183 - 275
- 138 Seiler M.; Hyperbranched polymers: Phase behavior and new applications; *Fluid Phase Equilibria* 241 (2006) 155 - 174
- 139 Flory P. J.; Molecular Size Distribution in Three Dimensional Polymers. I. Gelation; *Journal of the American Chemical Society* 63 (1941) 3083 - 3090
- 140 Flory P. J.; Molecular Size Distribution in Three Dimensional Polymers. VI. Branched Polymers Containing A-R-B_{f-1} Type Units; *Journal of the American Chemical Society* 74 (1952) 2718 - 2723
- 141 Kim Y. H., Webster O. W.; Water-Soluble Hyperbranched Polyphenylene: “A

2 Literature review

- Unimolecular Micelle"?; *Journal of the American Chemical Society* 112 (1990) 4593 - 4594
- 142 Kim Y. H., Webster O. W.; Hyperbranched Polyphenylenes; *Macromolecules* 25 (1992) 5561 - 5572
- 143 Uhrich K. E., Hawker C. J., Fréchet J. M. J., Turner S. R.; One-Pot Synthesis of Hyperbranched Polyethers; *Macromolecules* 25 (1992) 4583 - 4587
- 144 Suzuki M., Li A., Saegusa T.; Multibranching polymerization: palladium-catalyzed ring-opening polymerization of cyclic carbamate to produce hyperbranched dendritic polyamine; *Macromolecules* 25 (1992) 7071 - 7072
- 145 Magnusson H., Malmström E., Hult A.; Synthesis of hyperbranched aliphatic polyethers via cationic ring-opening polymerization of 3-ethyl-3-(hydroxymethyl)oxetane; *Macromolecular Rapid Communications* 20 (1999) 453 - 457
- 146 Tokar B., Kubisa P., Penczek S., Dworak A.; Cationic polymerization of glycidol: coexistence of the activated monomer and active chain end mechanism; *Macromolecules* 27 (1994) 320 - 322
- 147 Dworak A., Walach W., Trzebicka B.; Cationic polymerization of glycidol. Polymer structure and polymerization mechanism; *Macromolecular Chemistry and Physics* 196 (1995) 1963 - 1970
- 148 Jones G. D., Langsjoen A., Neumann M. M. C., Zomlefer J.; The polymerization of ethylenimine; *The Journal of Organic Chemistry* 9 (1944) 125 - 147
- 149 Chang H.-T., Fréchet J. M. J.; Proton-transfer polymerization: a new approach to hyperbranched polymers; *Journal of the American Chemical Society* 121 (1999) 2313 - 2314
- 150 Flory P. J.; The Mechanism of Vinyl Polymerizations; *Journal of the American Chemical Society* 59 (1937) 241 - 253
- 151 Flory P. J.; *Principles of Polymer Chemistry*; Cornell University Press: Ithaca, NY (1953)
- 152 Fréchet J. M. J., Henmi M., Gitsov I., Aoshima S., Leduc M. R., Grubbs B.; Self-Condensing Vinyl Polymerization: An Approach to Dendritic Materials; *Science* 269 (1995) 1080 - 1083
- 153 Zhuk D. S., Gembitskii P. A., Kargin V. A.; Advances in the chemistry of polyethyleneimine (polyaziridine); *Russian Chemical Reviews* 34 (1965) 515 - 527
- 154 Von Harpe A., Petersen H., Li Y., Kissel T.; Characterization of commercially available and synthesized polyethylenimines for gene delivery; *Journal of Controlled Release* 69 (2000) 309 - 322
- 155 Siddiqui J. A.; Polyester film coating with polyamido-polyethyleneimine; US

- 5453326 A (1995)
- 156 Kobayashi S., Hiroishi K., Tokunoh M., Saegusa T.; Chelating properties of linear and branched poly(ethylenimines); *Macromolecules* 20 (1978) 1496 - 1500
- 157 Korus I., Bobik M., Nowak E.; Selective separation of Ni(II) and Cr(VI) ions by polymer enhanced ultrafiltration; *Membranes and Membrane Processes in Environmental Protection* 119 (2014) 37 - 48
- 158 Mishra H., Yu C., Chen D. P., Goddard W. A., Dalleska N. F., Hoffmann M. R., Diallo M. S.; Branched Polymeric Media: Boron-Chelating Resins from Hyperbranched Polyethylenimine; *Environmental Science & Technology* 46 (2012) 8998 - 9004
- 159 Petzold G., Schwarz S.; Polyelectrolyte Complexes in Flocculation Applications; *Advances in Polymer Science* 256 (2014) 25 - 66
- 160 Satyapal S., Filburn T., Trela J., Strange J.; Performance and Properties of a Solid Amine Sorbent for Carbon Dioxide Removal in Space Life Support Applications; *Energy & Fuels* 15 (2001) 250 - 255.
- 161 Manecke G., Heller H.; Amphotere Ionenaustauscherharze (Teil II); *Die Makromolekulare Chemie* 59 (1963) 106 - 122
- 162 Barr C. J.; Propellant powder; US 2960393 A (1958)
- 163 Aymonier C., Schlotterbeck U., Antonietti L., Zacharias P., Thomann R., Tiller J. C., Mecking S.; Hybrids of silver nanoparticles with amphiphilic hyperbranched macromolecules exhibiting antimicrobial properties; *Chemical Communications* 24 (2002) 3018 - 3019
- 164 Antonietti L., Aymonier C., Schlotterbeck U., Garamus V. M., Maksimova T., Richtering W., Mecking S.; Core-Shell-Structured Highly Branched Poly(ethylenimine amide)s: Synthesis and Structure; *Macromolecules* 38 (2005) 5914 - 5920
- 165 Kowalski A., Libiszowski J., Biela T., Cypryk M., Duda A., Penczek S.; Kinetics and Mechanism of Cyclic Esters Polymerization Initiated with Tin(II) Octoate. Polymerization of ϵ -Caprolactone and L,L-Lactide Co-initiated with Primary Amines; *Macromolecules* 38 (2005) 8170 - 8176
- 166 Liu H., Shen Z., Stiriba S.-E., Chen Y., Zhang W., Wei L.; Core-Shell-Type Multiarm Star Polyethylenimine-block-Poly(ϵ -caprolactone): Synthesis and Guest Encapsulation Potential; *Journal of Polymer Science Part A: Polymer Chemistry* 44 (2006) 4165 - 4173
- 167 Jin M., Liu H., Pu H., Wan D.; Kinetic Topology-Selective Encapsulation and Mixture Separation by a Nanocapsule with Hyperbranched Polyethylenimine as Core and Polystyrene as Shell; *Journal of Polymer Science Part B: Polymer Physics* 51 (2013) 1273 - 1281

- 168 Petersen H.; Structurally Modified Polyethylenimines and their Interpolyelectrolyte Complexes with DNA as Non-Viral Gene Delivery Systems; Dissertation (2002)
- 169 Sélégny E., Mandel M., Strauss U. P. Gregor H. P.; The Modes of Specific Binding of Ions to Polyelectrolytes; Polyelectrolytes (1974) 87 - 95
- 170 Rembaum A., Sélégny E., Anderson R. E.; On the Pickup of Hydrochloric and Sulfuric Acids on a Polyamine Resin; Polyelectrolytes and their Applications (1975) 263 - 274
- 171 Möller M., Beginn U., Keul H., Thomas H.; EP 1710283A1 (2006)
- 172 Goel V., Beginn U., Mourran A., Möller M.; 'Quat-Primer' Polymers Bearing Cationic and Reactive Groups: Synthesis, Characterization, and Application; Macromolecules 41 (2008) 8187 - 8197
- 173 Goel V.; "Quat-Primer" polymers based on b-PEI and their application in composites; Dissertation (2010)
- 174 Komban R., Beckmann R., Sebastian Rode S., Ichilmann S., Kühnle A., Beginn U., Haase M.; Surface Modification of Luminescent Lanthanide Phosphate Nanorods with Cationic "Quat-primer" Polymers; Langmuir 27 (2011) 10174 - 10183
- 175 Beckmann R.; "Quat – Primer" Polymers as Dispersants for Nanoparticles; Dissertation (2012)
- 176 Beckmann R., Beginn U.; Synthesis and Characterization of New Poly(ethyleneimine)-g-Poly(methylmethacrylate) Star-Block Copolymers with Hyperbranched Cationic Core; Journal of Polymer Science Part A: Polymer Chemistry 51 (2013) 3700 - 3715
- 177 Spieß L., Teichert G., Schwarzer R., Behnken H., Genzel C.; Moderne Röntgenbeugung (2009)
- 178 Brindley G.W.; Identification of clay minerals by x-ray diffraction analysis; Clays and Clay Technology 169 (1955) 119 - 129
- 179 Strutt J. W.; On the scattering of light by small particles; Philosophical Magazine 4 (1871) 447 – 454
- 180 Strutt J. W.; On the light from the sky its polarization and colour; Philosophical Magazine 4 (1871) 107 – 120
- 181 Lord Rayleigh F. R. S.; X. On the electromagnetic theory of light; Philosophical Magazine 12 (1881) 81 - 101
- 182 Lord Rayleigh F. R. S.; XXXIV. On the transmission of light through an atmosphere containing small particles in suspension, and on the origin of the blue of the sky; Philosophical Magazine 47 (1899) 375 - 384
- 183 Debye P.; Light Scattering in Solutions; Journal of Applied Physics 15 (1944) 338

- 342

- 184 Debye P.; Molecular-weight Determination by Light Scattering; The Journal of Physical and Colloid Chemistry 51 (1947) 18 – 32
- 185 Lechner M. D., Gehrke K., Nordmeier E. H.; Makromolekulare Chemie Third Edition (2003)
- 186 Zimm B. H.; The Scattering of Light and the Radial Distribution Function of High Polymer Solutions; The Journal of Chemical Physics 16 (1948) 1093 – 1099
- 187 Zimm B. H.; Apparatus and Methods for Measurement and Interpretation of the Angular Variation of Light Scattering; Preliminary Results on Polystyrene Solutions; The Journal of Chemical Physics 16 (1948) 1099 – 1116
- 188 Benoit H., Holtzer A. M., Doty P.; An Experimental Study of Polydispersity by Light Scattering; The Journal of Physical Chemistry 58 (1954) 635 – 640
- 189 Hiemenz P. C., Rajagopalan R.; Principles of Colloid and Surface Chemistry Third Edition, Revised and Expanded (1997)
- 190 Wu C.; Handbook of Size Exclusion Chromatography 69 (1995)
- 191 Carlton R. A.; Pharmaceutical Microscopy (2011), Chapter 2 Polarized Light Microscopy
- 192 Gage S. H.; Modern Dark-Field Microscopy and the History of Its Development; Transactions of the American Microscopical Society 39 (1920) 95 – 141
- 193 Weaver R.; Rediscovering Polarized Light Microscopy; American Laboratory (2003) 55 - 61
- 194 Barnes H. A., Hutton J. F., Walters K.; An Introduction to Rheology (1989)
- 195 Mezger T. G.; Das Rheologie Handbuch (2000).
- 196 Collyer A. A., Clegg D. W.; Rheological Measurement Second Edition (1998)
- 197 ISO 6721-1:2011
- 198 Macosko C. W.; Rheology: principles, measurements and applications (1994)
- 199 Mezger T. G.; The rheology handbook: for users of rotational and oscillatory rheometers 2nd Edition (2006)

3 Synthesis of PEI(nkD)_{xQ}^{yR} polymers

3.1 Introduction

Within this Chapter the preparations and characterisations of quarternized and alkylated hyperbranched poly(ethylenimine)s, so-called “alkyl-quat-primer” polymers (= PEI(nkD)_xQ^{YR}), are described. The modification of the poly(ethylenimine) was necessary since for the purpose of this investigation polymers with priorly chosen qualities were required. Firstly, the polymers had to be permanent positive charged to enable a pH independent electrostatic interaction with montmorillonite. Secondly, the polymers had to be soluble in a priorly chosen fraction of bitumen. In this work, glycidyltrimethylammonium chloride was added to the poly(ethylenimine)s to add permanent positive charge to the polymers which served as a linkage between the polymers and the montmorillonite. In this study, poly(ethylenimine)s modified by glycidyltrimethylammonium chloride are marked with the letter Q (= Quat). To enable the polymers to be soluble in the oily phase (maltenes and resins) of bitumen, epoxides bearing alkyl chains with 10 or 14 carbon atoms were added to the poly(ethylenimine). In this work, poly(ethylenimine)s modified by 1,2-epoxydodecane are marked with the abbreviation R10 (= 10 carbon atoms in the alkyl chain), the presence of 1,2-epoxyhexadecane is marked with the addition of the abbreviation R14 (= 14 carbon atoms in the alkyl chain). Alternatively to the epoxide chemistry, the addition of 2-undecanone to poly(ethylenimine) was tried.

Technical hyperbranched poly(ethylenimine) is synthesised by cationic ring-opening polymerization of aziridine, more information about hyperbranched polymers can be found in Chapter 2. Hyperbranched poly(ethylenimine) exhibits terminal, linear and dendritic units in a ratio of 30:39:31 [1, 2]. Hyperbranched poly(ethylenimine) is used in the paper industry for flocculation of negatively charged fibres [3], another application of poly(ethylenimine) is the use in polymer enhanced ultrafiltration to remove metal ions [4]. Grafting of poly(methylmethacrylate) onto poly(ethylenimine) gave a core-shell polymer, which can be used as dispersants to prepare PMMA-nanocomposites [5]. Poly(ethylenimine) is due to the amine groups a highly polar polymer and the solubility is limited to water, polar and semipolar solvents. To generate amphiphilic polymers, poly(ethylenimine) has been reacted with palmitic acid and carbonyldiimidazole [6]. Poly(ethylenimine)s bearing cationic groups for the purpose of electrostatic interactions with carbon fibres were synthesised by reacting the polymer with ammonium reagents bearing either epoxide or cyclocarbonate units [7].

3.2 Experimental part

3.2.1 Materials

Table 3.1: Used solvents

Solvent	Purity	Supplier
Methanol	99.8 %	Sigma Aldrich
Methanol	Technical	Stockmeiner Chemie GmbH
Chloroform	Technical	VWR Chemicals
Dimethylformamide (DMF)	99.9 %	VWR Chemicals
Water	Deionized	

Table 3.2: Used chemicals

Reagent	Purity	Supplier
Calcium chloride	Water-free	Grüssing GmbH
1,2-Epoxydodecane	95 %	Sigma-Aldrich
1,2-Epoxydodecane	98 %	Chemos GmbH
1,2-Epoxyhexadecane	83.5 %	Chemos GmbH
Glycidyltrimethylammonium chloride	90 wt.% (calc. based on dry substance), containing 20 – 25 wt. % water; calculated purity 67 wt.%	Sigma-Aldrich
Hydrochloric acid	37 %	Sigma Aldrich
Poly(ethylenimine), branched	Average Mn ~ 10,000 g/mol by GPC, average Mw ~ 25,000 g/mol by LS	Sigma-Aldrich
Poly(ethylenimine), solution	Average Mn ~ 1,200 g/mol by GPC, average Mw ~ 1,300 g/mol by LS, 50 wt. % solution in water	Sigma-Aldrich
Sodium sulfate	Water-free	Sigma Aldrich
2-Undecanone	99 %	Sigma-Aldrich

3.2.2 Techniques

¹H-NMR (500 MHz), ¹H-DOSY-NMR (500 MHz), and ¹³C-NMR (125 MHz) experi-

ments were recorded on a Bruker Avance III 500 spectrometer at 30°C. The concentration was set to be 20 mg/mL with ^1H measurements and to be 200 mg/mL with ^{13}C measurements. The chemical shifts were given in parts per million (ppm). ^1H -DOSY-NMR measurements were performed using a Bruker 5 mm PABBO BB-1H/D Z-GRD z110902/0001 probe. The software used to acquire the data was called Bruker Topspin 2.1.

ATR-FT-IR investigations were performed using a Perkin Elmer Spectrum Two spectrometer equipped with a Perkin Elmer Spectrum Two universal diamond/ZnSe-ATR crystal. The samples were pressed on the ATR unit and measured in reflection. The scan resolution was set to be 4 cm^{-1} , each sample was scanned four times and an average spectrum was created.

Differential scanning calorimetry (DSC) measurements were performed with a Netzsch 204 F1 Phoenix thermal analyzer, equipped with a T-sensor and a Netzsch Intracooler. The DSC was calibrated against Bi, Hg, In, Sn and Zn standards. 5 to 15 mg samples were weighed in 25 μL aluminium pans. The pans were sealed with a perforated lid. The samples were measured under an N_2 stream over a temperature range of -80 to 180°C and at a heating and cooling rate of 10 K/minute .

Elemental analysis was performed with an Elementar vario MICRO cube to determine the carbon, hydrogen, and nitrogen content. 2.5 mg of a sample was measured and the experiment was performed three times to get an average.

GC/MS measurements were performed with a Shimadzu GCMS-QPB1010 SE device equipped with a Restek Rxi-5ms column. The column was filled with a crosslinked diphenyl dimethyl polysiloxane which consisted of 5% diphenyl and 95% dimethyl polysiloxane. 10 mg of a sample was weighed into a 22 mL glass phial and sealed afterwards. The phial was then heated to either 150 or 220°C for 1 minute with a heat gun. 1 μL of the gas in the upper part of the phial was then removed with a syringe and used for the headspace analysis. The sample was injected into the gas chromatograph, the injection temperature was set to 250°C . The column oven was heated from 40 to 300°C . The heating rate was set to 5°C/minute with a hold time of one minute after 40 and 300° . The flow rate was set to 1 mL/minute under a He stream. The measured mass-to-charge (m/z) ratios ranged from 35 to 400.

Rheology investigations were performed using a TA Instruments AR 2000ex dynamic shear rheometer. The measurement setup consisted of a parallel plate geometry us-

ing a TA Instruments Peltier plate assembly AR2000 plate which consisted of copper and was coated with chrome. The plate exhibited a diameter of 40 mm and could be operated in the temperature region of $-20 - 200^{\circ}\text{C}$ and at a heating rate up to $20^{\circ}\text{C}/\text{minute}$. The plate exhibited a temperature accuracy of $\pm 0.1^{\circ}\text{C}$. The samples were measured in the temperature range of 20 to 90°C , with a frequency $\omega = 6.28 \text{ rad/s}$, and a stress $\delta = 5 \text{ Pa}$. The gap was typically set to be $h = 900 \text{ }\mu\text{m}$. The samples were poured onto the lower plate of the rheometer after heating the samples at 60°C for 1 minute with a heat gun. During the measurements, an environmental chamber was not used and the upper plate was not heated.

The size-exclusion chromatography (SEC) setup consisted of four main devices. The pumping device was a Waters 2695 alliance autosampler. The column was a styrene-divinylbenzene copolymer (SDV) network, received from PSS Polymer Standards Service GmbH. The diameter of the particles were $5 \text{ }\mu\text{m}$ and the nominal pore sizes were 10^3 , 10^5 and $10^6 \text{ }\text{\AA}$, respectively. For low molecular samples, the particles with the pore size of $10^3 \text{ }\text{\AA}$ were replaced by particles with a pore size of $10^2 \text{ }\text{\AA}$. Light scattering was measured with a multi-angle light scattering (MALS) Wyatt Dawn Heleos II detector and the refractive index (RI) with a Wyatt Optilab rEX detector. The wavelength of the laser of both detectors was 658 nm . Tetrahydrofuran was used as the eluent. Typically, the samples were measured at a concentration of 4 mg/mL . The molecular weight of the polymers was calculated using linear polystyrene standards with weight average molecular weights ranging from $1,920$ to $524,000 \text{ g/mol}$.

The solubility of the polymers was tested by weighing 5 mg of the sample into a glass vial, adding 0.5 mL of the respective solvent, closing the lid and allowing the mixture to stand for half an hour at 20°C . When the substance didn't dissolve, the vial was shaken for 2 minutes. The solubility was qualitative judged by optical inspection, distinguishing between soluble, dispersion, and insoluble.

Thermogravimetric (TGA) measurements were performed with an NETZSCH STA 449 C Jupiter Thermo-microbalance in the temperature region of $30 - 530^{\circ}\text{C}$ at a heating rate of 10 K/minute and under a He stream. $25 \text{ }\mu\text{L}$ aluminium pans were used in which 8 to 16 mg of a sample was weighed. The pans weren't covered by a lid.

3.2.3 Synthesis of poly[ethylenimine-co-(ethylenimine-N-(2-hydroxypropyl-3-(N,N,N-trimethylammonium chloride)))]

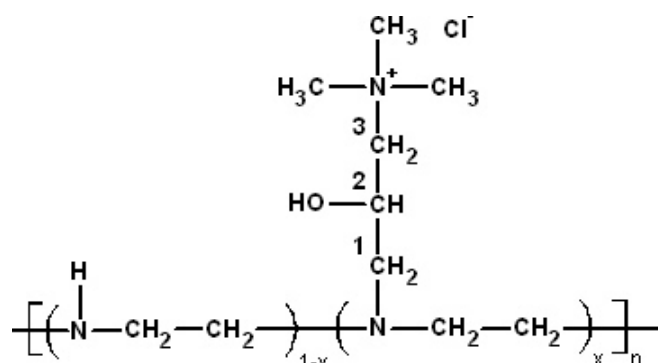


Figure 3.1: Structure of hyperbranched poly[ethylenimine-co-(ethylenimine-N-(2-hydroxypropyl-3-(N,N,N-trimethylammonium chloride)))] (PEI(nkD)_{xQ})

(PA1) Synthesis of PEI(1.2kD)_{13Q}

20.0 g (0.465 mol) poly(ethylenimine) was diluted in 30 mL deionized water and 9.5 g (0.062 mol) glycidyltrimethylammonium chloride was added. The solution was then stirred for 24 h at 60°C. Afterwards, the solvent was removed under reduced pressure and the polymer was dried in vacuum at 70°C for 48 h. The resulting polymer was a thick and sticky liquid with a yellow colour. The yield was not determined.

¹H-NMR (D₂O, δ [ppm]): 4.40 (1H_Q, -CH₂-CHOH-CH₂-), 3.50 – 3.40 (2H_Q, -CH-CH₂-N(CH₃)₃), 3.35 – 3.15 (9H_Q, N(CH₃)₃), 2.90 – 2.50 (4H_{PEI}, 2H_Q, D-CH₂-CH₂-D, D-CH₂-CH₂-L, D-CH₂-CH₂-T, L-CH₂-CH₂-L, L-CH₂-CH₂-T, PEI-NH-CH₂-CHOH-, PEI-N-CH₂-CHOH-); ¹H-DOSY-NMR log D (in D₂O): -9.62; ¹³C-NMR (D₂O, δ [ppm]): 69.4 (-CH₂-N(CH₃)₃), 65.1 (-CH₂-CHOH-CH₂-N(CH₃)₃), 56.0 (T-CH₂-CH₂-D), 54.7 (-N(CH₃)₃), 53.3 (D-CH₂-CH₂-L), 52.7 (PEI-CH₂-CHOH-, D-CH₂-CH₂-L), 51.3 (D-CH₂-CH₂-D, L-CH₂-CH₂-T), 50.7 (L-CH₂-CH₂-D), 47.8 (L-CH₂-CH₂-L), 45.8 (L-CH₂-CH₂-D), 40.0 (L-CH₂-CH₂-T), 38.0 (T-CH₂-CH₂-D); DSC: T_G = -10.6°C; Elemental analysis, found (calculated for [C₂H₄N]_{1-x}[C₆H₁₅NO]_x, x = 0.13): C: 40.87 (44.71), H: 10.51 (7.99), N: 19.38 (19.38); IR (ATR; ν [cm⁻¹]): 3271, 2938, 2828, 1646, 1601, 1474, 1355, 1300, 1102, 1051, 963, 917, 543

3.2.4 Synthesis of hyperbranched poly[ethylenimine-co-(N-(2-hydroxydodecyl)-ethylenimine)]

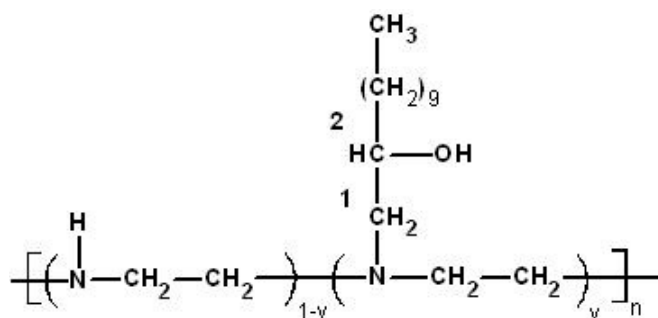


Figure 3.2: Structure of hyperbranched poly[ethylenimine-co-(N-(2-hydroxydodecyl)-ethylenimine)] (PEI(nkD)^{yR10})

(PB1) Synthesis of PEI(10kD)^{65R10}

30.2 g (0.702 mol) poly(ethylenimine) was dissolved in 200 mL methanol (99.8 %) and 84.1 g (0.456 mol) 1,2-epoxydodecane in 160 mL chloroform was added. The solution was stirred for 48 h at 60°C. Afterwards, the solvent was removed under reduced pressure and the polymer was dried in vacuum at 70°C for 48 h. After drying, 56.5 g (= 49.0 % of theory) of a thick and sticky liquid with a yellow colour was obtained.

¹H-NMR (CDCl₃, δ [ppm]): 5.20 – 4.20 (4H_{PEI}, D-CH₂-CH₂-D, D-CH₂-CH₂-L, D-CH₂-CH₂-T, L-CH₂-CH₂-L, L-CH₂-CH₂-T, PEI-NH-CH₂-CHOH-, PEI-N-CH₂-CHOH-), 3.70 – 3.50 (1H_{R10}, -CH₂-CHOH-CH₂-), 2.90 – 2.20 (4H_{PEI}, 2H_{R10}, D-CH₂-CH₂-D, D-CH₂-CH₂-L, D-CH₂-CH₂-T, L-CH₂-CH₂-D, L-CH₂-CH₂-L, L-CH₂-CH₂-T, T-CH₂-CH₂-D, T-CH₂-CH₂-L, PEI-NH-CH₂-CHOH-, PEI-N-CH₂-CHOH-), 1.60 – 1.20 (18H_{R10}, -CHOH-(CH₂)₉-CH₃-), 1.00 – 0.80 (3H_{R10}, -(CH₂)₉-CH₃); ¹H-DOSY-NMR log D (in CDCl₃): -9.43; ¹³C-NMR (CDCl₃, δ [ppm]): 71.0 – 67.0 (-N-CH₂-CHOH-CH₂-CH₂-), 66.0 – 61.0 (-N-CH₂-CHOH-), 54.0 – 51.0 (-N-CH₂-CH₂-N-), 35.4 (-CHOH-CH₂-CH₂-), 32.1 (-CH₂-CH₂-CH₂-CH₃), 29.8 (-CH₂-(CH₂)₅-CH₂-), 26.0 (-CH₂-CH₂-(CH₂)₅-), 22.8 (-CH₂-CH₂-CH₃), 14.2 (-CH₂-CH₃); DSC: T_G = -23.4°C; Elemental analysis, found (calculated for [C₂H₄N]_{1-y}[C₁₂H₂₅O]_y, y = 0.65): C: 69.81 (37.54), H: 10.67 (6.47), N: 7.67 (7.67); IR (ATR; ν [cm⁻¹]): 3370, 2953, 2921, 2851, 1651, 1463, 1376, 1338, 1293, 1092, 1042, 960, 867, 754, 720, 494

3.2.5 Synthesis of hyperbranched poly[ethylenimine-co-(ethylenimine-N-(2-hydroxypropyl-3-(N,N,N-trimethylammonium chloride)))-co-(N-(2-hydroxydodecyl)-ethylenimine)]

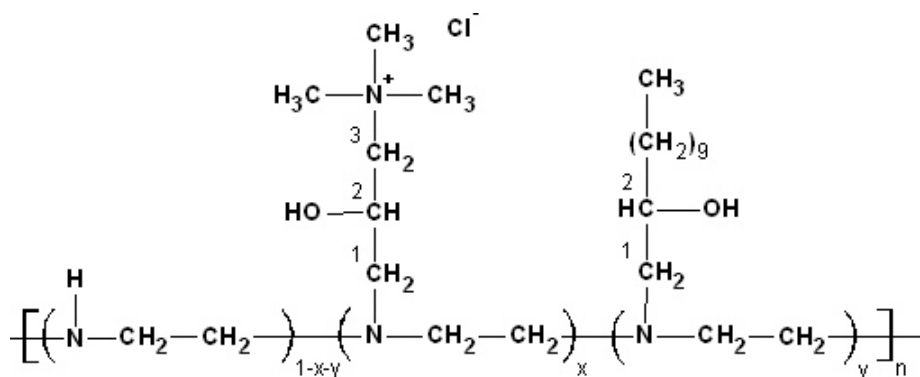


Figure 3.3: Structure of hyperbranched poly[ethylenimine-co-(ethylenimine-N-(2-hydroxypropyl-3-(N,N,N-trimethylammonium chloride)))-co-(N-(2-hydroxydodecyl)-ethylenimine)] (PEI(nkD)_{xQ}^{yR10})

(PB2) Synthesis of PEI(10kD)_{10Q}^{80R10}

26.0 g (0.609 mol) poly(ethylenimine) was dissolved in 313 mL chloroform and 89.8 g (0.487 mol) 1,2-epoxydodecane was added. The solution was stirred for 96 h at 60°C. Afterwards, a solution of 9.3 g (0.061 mol) glycidyltrimethylammonium chloride, diluted in 84 mL methanol (99.8 %), was added. The solution was stirred for another 48 h at 60°C. After the reaction was finished, the solvents were removed under reduced and the polymer was re-dissolved in 150 mL chloroform. The polymer was then precipitated in 1.5 L dimethylformamide. The polymer was collected, dissolved in another 50 mL chloroform and precipitated in 0.5 L dimethylformamide. The polymer was collected, dissolved in 50 mL chloroform and precipitated in 500 mL methanol. The last step was repeated for another five times, the solvents were removed afterwards under reduced pressure and the polymer was dried in vacuum at 70°C for 48 h. The yield after drying was 38.4 g (30.4 % of theory), the polymer was a clear, thick and sticky liquid with a yellow colour.

¹H-NMR (CDCl₃, δ [ppm]): 5.20 – 4.20 (4 H_{PEI}, D-CH₂-CH₂-D, D-CH₂-CH₂-L, D-CH₂-CH₂-T, L-CH₂-CH₂-D, L-CH₂-CH₂-L, L-CH₂-CH₂-T, T-CH₂-CH₂-D, T-CH₂-CH₂-L, PEI-NH-CH₂-CHOH-, PEI-N-CH₂-CHOH-), 4.50 – 4.20 (1H_Q, -CH₂-CHOH-CH₂-), 3.70 – 3.55 (1H_{R10}, -CH₂-CHOH-CH₂-), 3.55 – 3.40 (11H_Q, -CH-CH₂-N(CH₃)₃, -N(CH₃)₃), 2.90 – 2.20 (4H_{PEI}, 2H_Q, 2H_{R10}, D-CH₂-CH₂-D, D-CH₂-CH₂-L, D-CH₂-CH₂-T, L-CH₂-CH₂-L, L-CH₂-CH₂-T, PEI-NH-CH₂-CHOH-, PEI-N-CH₂-CHOH-), 1.55 – 1.20 (18H_{R10}, -CHOH-(CH₂)₉-CH₃-), 1.00 – 0.80 (3H_{R10}, -(CH₂)₉-CH₃); ¹H-DOSY-NMR log D (in CDCl₃): -9.25;

3 Synthesis of PEI(nkD)_xQyR polymers

¹³C-NMR (CDCl₃, δ [ppm]): 71.0 – 67.0 (-N-CH₂-CHOH-CH₂-CH₂-), 66.0 – 61.0 (-N-CH₂-CHOH-), 54.8 (CH₂-N(CH₃)₃), 54.7 – 51.0 (-N-CH₂-CH₂-N-), 35.4 (-CHOH-CH₂-CH₂-), 32.0 (-CH₂-CH₂-CH₂-CH₃), 29.8 (-CH₂-(CH₂)₅-CH₂-), 26.0 (-CH₂-CH₂-(CH₂)₅-), 22.8 (-CH₂-CH₂-CH₃), 14.2 (-CH₂-CH₃); DSC: T_G = -25.8°C; Elemental analysis, found (calculated for [C₂H₄N]_{1-x-y}[C₆H₁₅NO]_x[C₁₂H₂₅O]_y, x = 0.1, y = 0.8): C: 65.43 (71.2), H: 11.40 (12.51), N: 8.65 (8.65); IR (ATR; ν [cm⁻¹]): 3369, 2953, 2921, 2851, 1656, 1555, 1464, 1376, 1338, 1293, 1092, 1066, 963, 868, 720, 564

One additional PEI(10kD)_{5Q}^{67R10} polymer (= **PB3**) was synthesised analogously to the procedure described with polymer **PB2** by a co-worker of the institute [9].

(PB4.3) Synthesis of PEI(10kD)_{10Q}^{80R10}

359.2 g (1.949 mol) 1,2-epoxydodecane was added to 104.0 g (2.436 mol) poly(ethylenimine). The mixture was then stirred with a mechanical stirrer at 80°C for 48 h. Afterwards, 36.9 g (0.244 mol) glycidyltrimethylammonium chloride was added. The mixture was then stirred for another 24 h at 80°C. A thick and sticky liquid with a colourless to yellow colour was obtained in quantitative yield.

¹H-NMR (CDCl₃, δ [ppm]): 5.20 – 4.20 (4 H_{PEI}, D-CH₂-CH₂-D, D-CH₂-CH₂-L, D-CH₂-CH₂-T, L-CH₂-CH₂-D, L-CH₂-CH₂-L, L-CH₂-CH₂-T, T-CH₂-CH₂-D, T-CH₂-CH₂-L, PEI-NH-CH₂-CHOH-, PEI-N-CH₂-CHOH-), 4.40 – 4.30 (1H_Q, -CH₂-CHOH-CH₂-), 3.70 – 3.50 (1H_{R10}, -CH₂-CHOH-CH₂-), 3.50 – 3.30 (11H_Q, -CH-CH₂-N(CH₃)₃, -N(CH₃)₃), 2.90 – 2.20 (4H_{PEI}, 2H_Q, 2H_{R10}, D-CH₂-CH₂-D, D-CH₂-CH₂-L, D-CH₂-CH₂-T, L-CH₂-CH₂-L, L-CH₂-CH₂-T, PEI-NH-CH₂-CHOH-, PEI-N-CH₂-CHOH-), 1.55 – 1.10 (18H_{R10}, -CHOH-(CH₂)₉-CH₃-), 0.95 – 0.80 (3 H_{R10}, -(CH₂)₉-CH₃); ¹H-DOSY-NMR log D (in CDCl₃): -9.30; ¹³C-NMR (CDCl₃, δ [ppm]): 71.0 – 67.0 (-N-CH₂-CHOH-CH₂-CH₂-), 66.0 – 61.0 (-N-CH₂-CHOH-), 54.8 (CH₂-N(CH₃)₃), 54.7 – 51.0 (-N-CH₂-CH₂-N-), 35.4 (-CHOH-CH₂-CH₂-), 32.1 (-CH₂-CH₂-CH₂-CH₃), 29.8 (-CH₂-(CH₂)₅-CH₂-), 26.0 (-CH₂-CH₂-(CH₂)₅-), 22.8 (-CH₂-CH₂-CH₃), 14.2 (-CH₂-CH₃); DSC: T_G = -26.3°C; Elemental analysis, found (calculated for [C₂H₄N]_{1-x-y}[C₆H₁₅NO]_x[C₁₂H₂₅O]_y, x = 0.1, y = 0.8): C: 70.10 (57.32), H: 12.11 (10.07), N: 6.96 (6.96); IR (ATR; ν [cm⁻¹]): 3380, 2953, 2921, 2851, 1647, 1465, 1338, 1295, 1093, 1065, 964, 868, 720, 493

Furthermore, one PEI(1.2kD)_{20Q}^{80R10} polymer (= **PA2**) was synthesised analogously to the procedure described with polymer **PB4.3**.

Table 3.3: Prepared batches of polymer PB4

Entry	Prepared quantity (g)	Yield (%)
<u>PB4.1</u>	501.1	100
<u>PB4.2</u>	501.1	100
<u>PB4.3</u>	500.2	100
<u>PB4.4</u>	500.2	100
<u>PB4.5</u>	301.0	100
<u>PB4.6</u>	99.1	100
<u>PB4.7</u>	47.4	100
<u>PB4.8</u>	200.0	100
<u>PB4.9</u>	200.1	100
<u>PB4.10</u>	820.3	100
<u>PB4.11</u>	820.3	100
<u>PB4.12</u>	433.7	100
<u>PB4.13</u>	717.5	100
<u>PB4.14</u>	717.5	100
<u>PB4.15</u>	717.5	100
<u>PB4.16</u>	717.5	100
<u>PB4.17</u>	717.5	100
<u>PB4.18</u>	14.5	100
<u>PB4.19</u>	195.2	100
<u>PB4.20</u>	718.3	100

3.2.6 Synthesis of hyperbranched poly[ethylenimine-co-(ethylenimine-N-(2-hydroxypropyl-3-(N,N,N-trimethylammonium chloride)))-co-(N-(2-hydroxyhexadecyl)-ethylenimine)]

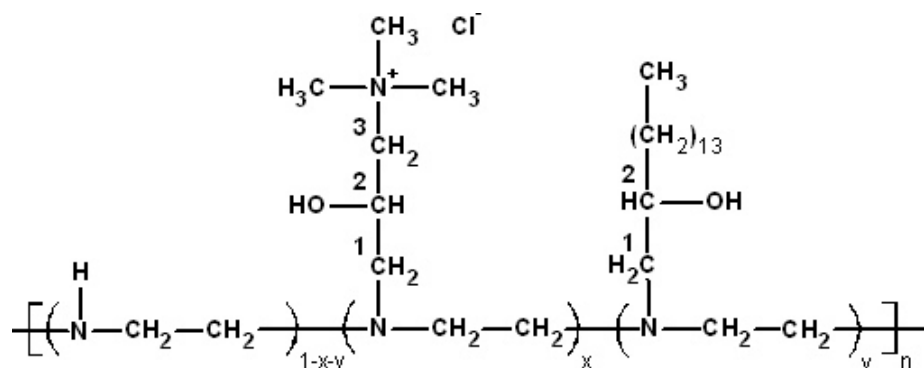


Figure 3.4: Structure of hyperbranched poly[ethylenimine-co-(ethylenimine-N-(2-hydroxypropyl-3-(N,N,N-trimethylammonium chloride)))-co-(N-(2-hydroxyhexadecyl)-ethylenimine)] (PEI(nkD)_{xQ}^{yR14})

(PC1) Synthesis of PEI(10kD)_{10Q}^{60R14}

0.4 g (0.003 mol) glycidyltrimethylammonium chloride was diluted in 0.5 mL methanol and then added to 1.0 g (0.023 mol) poly(ethylenimine), dissolved in 2 mL methanol. The solution was then stirred with a magnetic stirrer at 60°C for 24 h. Afterwards, 3.3 g (0.014 mol) 1,2-epoxyhexadecane, diluted in 5 mL chloroform was added. The solution was then stirred for another 118 h at 60°C. Then, the polymer was diluted in 2.5 mL chloroform and precipitated in 100 mL dimethylformamide. The polymer was collected, 10 mL methanol was added and the solvent was removed under reduced pressure. This step was performed another three times. Then, the polymer was dried in vacuum at 80°C for 48 h. After drying, 2.5 g (= 53.1 % of theory) of a solid wax with a yellow colour was obtained.

¹H-NMR (CDCl₃, δ [ppm]): 4.90 – 4.20 (4 H_{PEI}, D-CH₂-CH₂-D, D-CH₂-CH₂-L, D-CH₂-CH₂-T, L-CH₂-CH₂-D, L-CH₂-CH₂-L, L-CH₂-CH₂-T, T-CH₂-CH₂-D, T-CH₂-CH₂-L, -N-CH₂-CHOH-, PEI-N-CH₂-CHOH-), 4.40 – 4.30 (1 H_Q, -CH₂-CHOH-CH₂-), 3.80 – 3.55 (2 H_{R14(a)}, 1 H_{R14(b)}, -CH₂-CHOH-CH₂-), 3.55 – 3.25 (11 H_Q, -CH-CH₂-N(CH₃)₃, -N(CH₃)₃), 3.20 – 2.20 (4 H_{PEI}, 2 H_Q, 2 H_{R14(b)}, 1 H_{R14(a)}, D-CH₂-CH₂-D, D-CH₂-CH₂-L, D-CH₂-CH₂-T, L-CH₂-CH₂-L, L-CH₂-CH₂-T, PEI-NH-CH₂-CHOH-, PEI-N-CH₂-CHOH-), 1.70 – 1.05 (26 H_{R14}, -CHOH-(CH₂)₁₃-CH₃-), 1.00 – 0.80 (3 H_{R14}, -(CH₂)₁₃-CH₃); ¹H-DOSY-NMR log D (in CDCl₃): -9.33; ¹³C-NMR (C₆D₆, δ [ppm]): 71.0 – 67.0 (-N-CH₂-CHOH-CH₂-CH₂-), 66.0 – 61.0 (-N-CH₂-CHOH-), 54.8 (CH₂-N(CH₃)₃), 54.7 – 51.0 (-N-CH₂-CH₂-N-), 36.1 (-CHOH-CH₂-CH₂-), 33.5 (-CH₂-CH₂-CH₂-CH₃), 29.9 (-CH₂-(CH₂)₉-

3 Synthesis of PEI(nkD)xQyR polymers

CH₂-), 26.1 (-CH₂-CH₂-(CH₂)₉-), 22.8 (-CH₂-CH₂-CH₃), 14.2 (-CH₂-CH₃); DSC: T_M = 21.6°C; Elemental analysis, found (calculated for [C₂H₄N]_{1-x-y}[C₆H₁₅NO]_x[C₁₄H₃₃O]_y, x = 0.1, y = 0.6): C: 69.15 (27.9), H: 11.88 (4.9), N: 6.38 (6.38); IR (ATR; ν [cm⁻¹]): 3362, 2954, 2917, 2849, 1653, 1466, 1376, 1339, 1261, 1081, 965, 860, 720, 569

(PC2.4) Synthesis of PEI(10kD)_{10Q}^{60R14}

8.8 g (0.037 mol) 1,2-epoxyhexadecane was added to 2.6 g (0.061 mol) poly(ethylenimine). The mixture was then stirred with a mechanical stirrer at 80°C for 48 h. Afterwards, 0.9 g (0.006 mol) glycidyltrimethylammonium chloride was added. The mixture was then stirred for another 24 h at 80°C. A solid wax with a yellow colour in quantitative yield was obtained.

Table 3.4: Prepared batches of polymer PC2

Entry	Prepared quantity (g)	Yield (%)
PC2.1	5.7	100
PC2.2	5.3	100
PC2.3	58.4	100
PC2.4	12.3	100
PC2.5	347.7	100
PC2.6	362.4	100
PC2.7	347.3	100
PC2.8	371.2	100
PC2.9	70.0	100
PC2.10	71.2	100
PC2.11	407.1	100
PC2.12	436.9	100

¹H-NMR (CDCl₃, δ [ppm]): 4.90 – 4.20 (4 H_{PEI}, D-CH₂-CH₂-D, D-CH₂-CH₂-L, D-CH₂-CH₂-T, L-CH₂-CH₂-D, L-CH₂-CH₂-L, L-CH₂-CH₂-T, T-CH₂-CH₂-D, T-CH₂-CH₂-L, -N-CH₂-CHOH-, PEI-N-CH₂-CHOH-), 4.40 – 4.30 (1 H_Q, -CH₂-CHOH-CH₂-), 3.80 – 3.55 (2 H_{R14(a)}, 1 H_{R14(b)}, PEI-CH-CH₂OH, -CH₂-CHOH-CH₂-), 3.55 – 3.25 (11 H_Q, -CH-CH₂-N(CH₃)₃, -N(CH₃)₃), 3.20 – 2.20 (4 H_{PEI}, 2 H_Q, 2 H_{R14(b)}, 1 H_{R14(a)}, D-CH₂-CH₂-D, D-CH₂-CH₂-L, D-CH₂-CH₂-T, L-CH₂-CH₂-L, L-CH₂-CH₂-T, PEI-N-CH₂-CHOH-, PEI-N-CH-CH₂OH-), 1.70 – 1.05 (26 H_{R14}, -CHOH-(CH₂)₁₃-CH₃-), 1.00 – 0.80 (3 H_{R14}, -(CH₂)₁₃-CH₃); ¹H-DOSY-NMR log D (in CDCl₃): -9.47; ¹³C-NMR (CDCl₃, δ [ppm]): 71.0 – 67.0 (-N-CH₂-CHOH-CH₂-CH₂-), 66.0 – 61.0 (-N-CH₂-CHOH-), 54.8 (CH₂-N(CH₃)₃), 54.7 – 51.0 (-N-CH₂-CH₂-N-), 35.3 (-CHOH-CH₂-CH₂-), 32.0 (-CH₂-CH₂-CH₂-CH₃), 29.8 (-

3 Synthesis of PEI(nkD)xQyR polymers

CH₂-(CH₂)₉-CH₂-), 26.1 (-CH₂-CH₂-(CH₂)₉-), 22.8 (-CH₂-CH₂-CH₃), 14.2 (-CH₂-CH₃); DSC: T_M = 26.5°C; Elemental analysis, found (calculated for [C₂H₄N]_{1-x}·[C₆H₁₅NO]_x[C₁₄H₃₃O]_y, x = 0.1, y = 0.6): C: 70.43 (28.03), H: 12.10 (4.92), N: 6.41 (6.41); IR (ATR; ν [cm⁻¹]): 3360, 2954, 2917, 2849, 1662, 1466, 1294, 1079, 965, 860, 720

In addition, a PEI(10kD)^{60R14} polymer (= **PC3**) was synthesised analogously to the procedure described with polymer **PC2.4**.

3.2.7 Synthesis of poly[ethylenimine-co-(ethylenimine-(undecan-2-ylidene))]

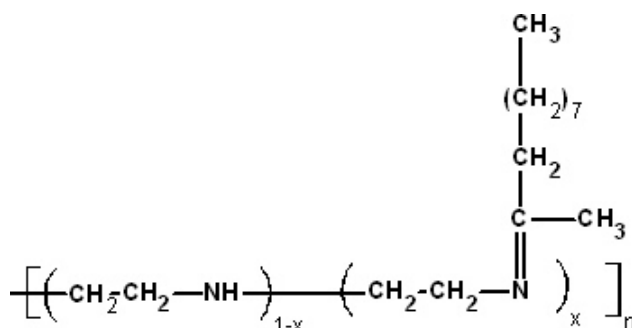


Figure 3.5: Structure of an poly[ethylenimine-co-(ethylenimine-(undecan-2-ylidene))] (PEI(nkD)^{xU11})

(PD1) Synthesis of PEI(10kD)^{52U11}

1.0 g (0.023 mol) poly(ethylenimine) was dissolved in 10 mL methanol (99.8 %) and 1 mL (0.012 mol) hydrochloric acid was added. Afterwards, 2.0 g (0.012 mol) 2-undecanone and 15.1 g (0.106 mol) sodium sulfate were added and the mixture was stirred for 24 h at 60°C. The apparatus was sealed with a drying tube filled with calcium chloride. After the reaction, the substance was filtered and the liquid fraction as well as the residue separately collected. The solvent of the liquid fraction was then removed under reduced pressure. Afterwards, both fractions were dried at 60°C under reduced pressure for 90 h. The residue appeared as an orange solid and the liquid fraction as a yellow liquid. The yield of both fractions was not determined.

3.3 Results and discussion

In this study hyperbranched poly(ethylenimine) was reacted with glycidyltrimethylammonium chloride and either 1,2-epoxydodecane or 1,2-epoxyhexadecane. The investigated polymers were a quat-primer polymer (PEI(1.2kD)_{13Q}), two alkyl-primer polymers (PEI(10kD)^{65R10} and PEI(10kD)^{60R14}), two alkyl-quat-primer polymers with 1,2-epoxydodecane supplying the alkyl function (PEI(10kD)_{10Q}^{80R10}), and two alkyl-quat-primer polymers with 1,2-epoxyhexadecane as the alkyl group (PEI(10kD)_{10Q}^{60R14}). The general synthesis route for the preparation of alkyl-quat-primer polymers is shown in Figure 3.6.

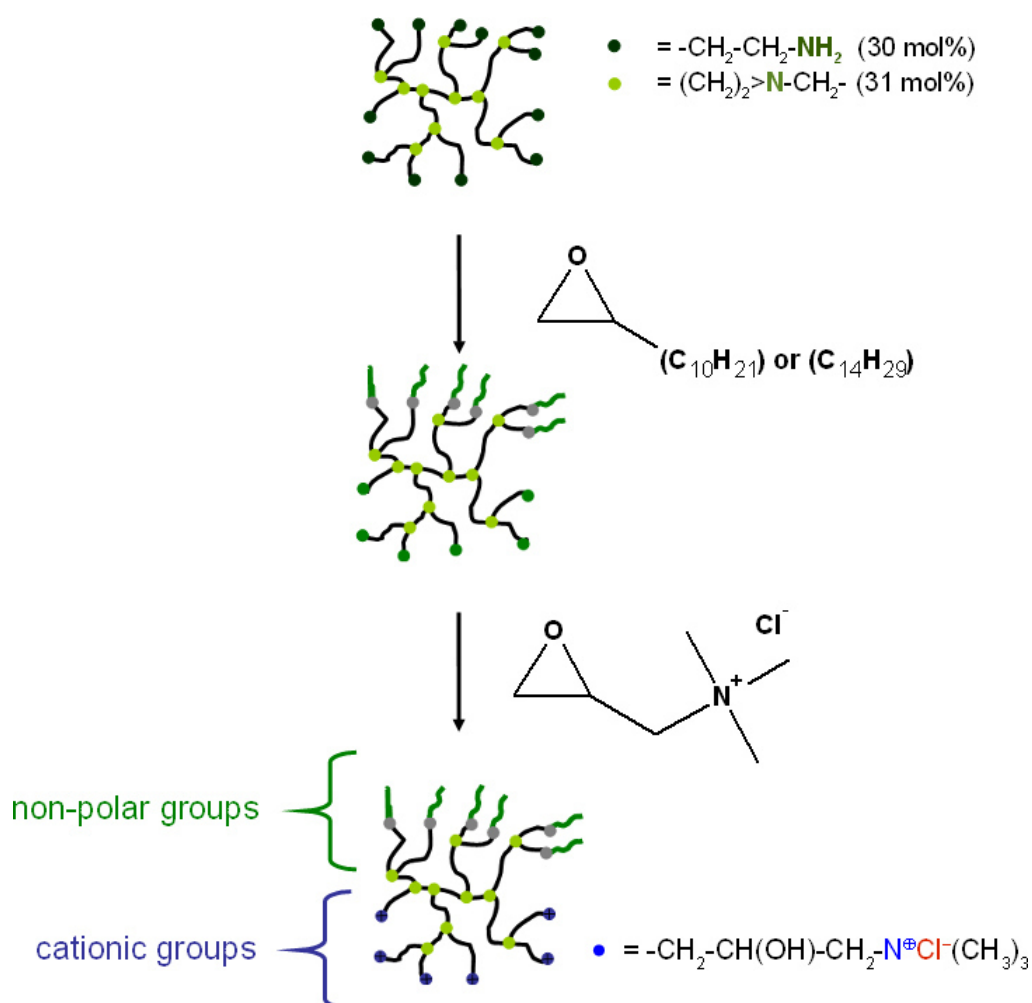


Figure 3.6: Synthesis route for the preparation of alkyl-quat-primer polymers

The polymers were synthesised either in solution (polymers **PA1**, **PB1**, **PB2**, **PB3**, **PC1**) or solvent-free, i. e. in bulk (polymers **PA2**, **PB4.1** – **PB4.20**, **PC2.1** – **PC2.12**, **PC3**). While the reaction condition for the synthesis of the quat-primer polymer

3 Synthesis of PEI(nkD)_xQ_yR polymers

(PEI(nkD)_xQ_y, polymer **PA1**) was researched thoroughly [8], the reaction conditions for the addition of the 1,2-epoxydodecane and the 1,2-epoxyhexadecane to the poly(ethylenimine) had to be determined. A quantitative addition of the reactants to the poly(ethylenimine) was found when the reactions were performed in a methanol/chloroform mixture at a temperature of 60°C for 144 h (polymers **PB1**, **PB2**, **PB3**, **PC1**). The degree of the addition was verified by ¹H-NMR measurements. The drawbacks of this method were the high amounts of solvents needed and the low yield of 30.4 - 53.1 wt.% after purification of the polymers as shown in Table 3.5. Furthermore, intensive drying of the polymers was necessary to remove the solvents.

Table 3.5: Synthesised PEI(nkD)_xQ_yR polymers

Entry	Composition	Synthesis condition	Yield (wt.%)
PA1	PEI(1.2kD) _{13Q}	60°C, 24 h, H ₂ O	-
PA2	PEI(1.2kD) _{20Q} ^{80R10}	70°C, 72 h	100
PB1	PEI(10kD) _{65R10}	60°C, 48 h, CH ₃ OH, CHCl ₃	49.0
PB2	PEI(10kD) _{10Q} ^{80R10}	60°C, 144 h, CH ₃ OH, CHCl ₃	30.4
PB3	PEI(10kD) _{5Q} ^{67R10}	[9]	-
PB4.1 – PB4.20	PEI(10kD) _{10Q} ^{80R10}	80°C, 72 h	100
PC1	PEI(10kD) _{10Q} ^{60R14}	60°C, 142 h, CH ₃ OH, CHCl ₃	53.1
PC2.1 – PC2.12	PEI(10kD) _{10Q} ^{60R14}	80°C, 72 h	100
PC3	PEI(10kD) _{60R14}	80°C, 72 h	100
PD1	PEI(10kD) _{52U11}	60°C, 24 h, CH ₃ OH, HCl (37%)	-

PEI(10kD) = poly(ethylenimine) with M_n = 10,000 g/mol, M_w/M_n = 2.5, PEI(1.2kD) = poly(ethylenimine) with M_n = 1,200 g/mol, M_w/M_n = 1.08, xQ = mol% 2-hydroxypropyl-3-(N,N,N-trimethylammonium chloride, yR10 = mol% 2-hydroxydodecane, yR14 = mol% 2-hydroxyhexadecane, yU = mol% 2-undecanone

To avoid these problems, the reaction of the reactants with the poly(ethylenimine) was performed in a bulk reaction. As verified by taking samples during the reaction and performing ¹H-NMR measurements, the quantitative addition of the 1,2-epoxydodecane and the 1,2-epoxyhexadecane was finished after a reaction time of 48 h when the reaction temperature was set to be 80°C. At this temperature, the addition reaction of the glycidyltrimethylammonium chloride was finished after another 24 h (polymers **PA2**, **PB4.1 – PB4.20**, **PC2.1 – PC2.12**, **PC3**). For further investigations, larger quantities of the polymers **PB4** and **PC2** were prepared. The quantity was ca. 9.4 kg of polymer **PB4** and ca. 2.5 kg of polymer **PC2** in total. To test in which order the reactants should be added to the poly(ethylenimine) to obtain the desired polymers, experiments were performed in which the glycidyltrimethylammonium chloride

3 Synthesis of PEI(nkD)xQyR polymers

was added previously to the 1,2-epoxydodecane. The reaction of glycidyltrimethylammonium chloride with poly(ethylenimine) in a bulk reaction was performed in that way that poly(ethylenimine) was put into a snap cover glass, glycidyltrimethylammonium chloride was then added and the mixture was allowed to stay at 20°C for 24 h without stirring. It was found that the poly(ethylenimine) at the surface exhibited large amounts and the poly(ethylenimine) at the bottom very small amounts of attached glycidyltrimethylammonium chloride. On the other hand, the reaction between 1,2-epoxydodecane and poly(ethylenimine) took place only at an elevated temperature which made it easier to control the reaction.

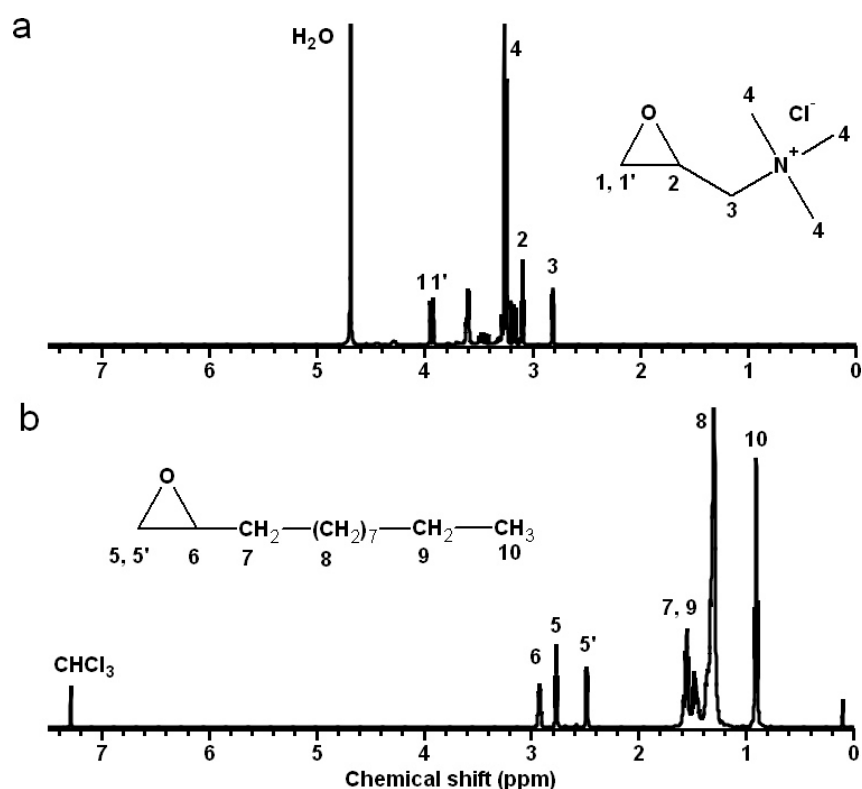


Figure 3.7: ¹H-NMR spectra of a) glycidyltrimethylammonium chloride (D₂O, 30°C), and b) 1,2-epoxydodecane (CDCl₃, 30°C)

The ¹H-NMR spectra of a) glycidyltrimethylammonium chloride and b) 1,2-epoxydodecane are shown in Figure 3.7. The signals of the glycidyltrimethylammonium chloride (Figure 3.7.a) were assigned as reported from previous investigations [8]. The signals of the hydrogen atoms of the epoxide ring were found at 3.10, 3.92 and 3.94 ppm (1, 1', 2). The hydrogen atoms of the methylene group connecting the epoxide and the ammonium moiety gave a signal at 2.8 ppm (3). The signal of the hydrogen atoms of the three methyl groups attached to the nitrogen was detected at 3.2 ppm (4). The ¹H-NMR spectrum of the 1,2-epoxydodecane (Figure 3.7.b) showed signals

3 Synthesis of PEI(nkD)xQyR polymers

corresponding to the hydrogen atoms of the epoxide ring at 2.4, 2.7 and 2.9 ppm (5, 5', 6). Signals of the hydrogen atoms of the alkyl chain showed up at 0.9, 1.2, 1.4 and 1.5 ppm (7 - 10). The signals of the hydrogen atoms of the 1,2-epoxyhexadecane were located at the same position as with the 1,2-epoxydodecane.

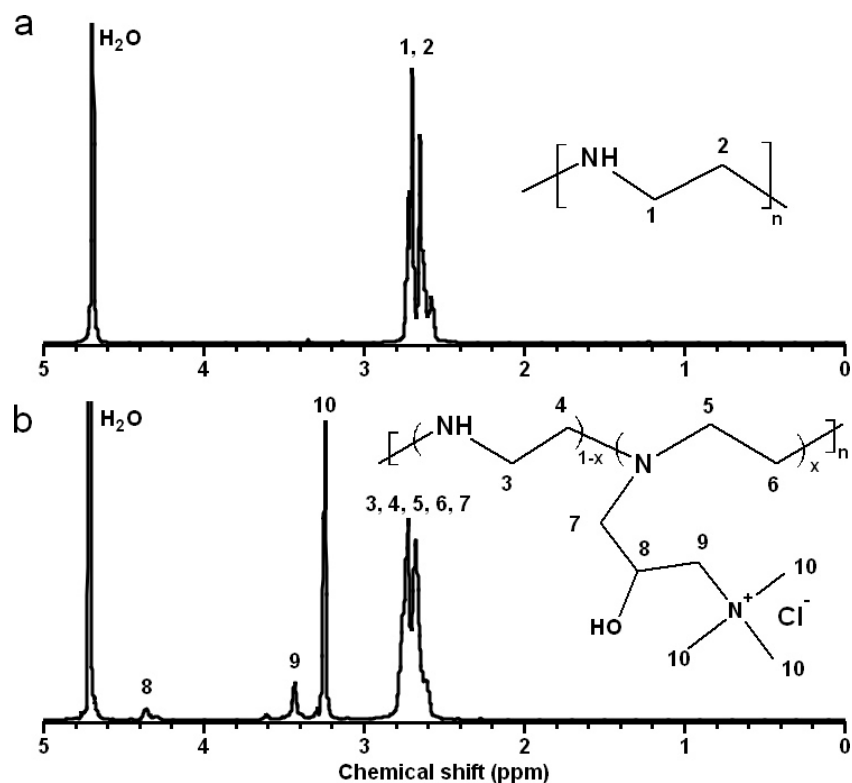


Figure 3.8: ¹H-NMR spectra of a) poly(ethylenimine), and b) polymer **PA1**, D₂O, 30°C

In Figure 3.8 the ¹H-NMR spectra of a) hyperbranched poly(ethylenimine), and b) polymer **PA1** are compared. The signal of the hydrogen atoms of the poly(ethylenimine) was detected with both the neat polymer (Figure 3.8.a) and polymer **PA1** (Figure 3.8.b) between 2.5 and 2.9 ppm (1 - 6). Compared to the neat glycidyltrimethylammonium chloride (cf. Figure 3.7.a), polymer **PA1** exhibited no signals of the epoxide ring. Instead, the signal of the hydrogen atoms of the methylene group connecting the polymer and the 2-hydroxypropyl-3-(N,N,N-trimethylammonium chloride) (7) was found to be overlapping with the signal of the poly(ethylenimine) methylene hydrogen atoms. The signal of the hydrogen atom of the methylene group attached to the hydroxyl moiety showed up at 4.6 ppm (8). The hydrogen atoms of the methylene group connecting the methylene group attached to the hydroxyl group and the nitrogen atom of the ammonium group gave a signal at 3.4 ppm (9). The signal of the hydrogen atoms of the three methyl groups attached to the nitrogen appeared, as with the neat glycidyltrimethylammonium chloride (cf. Figure 3.7.a), at 3.2 ppm (10).

3 Synthesis of PEI(nkD)xQyR polymers

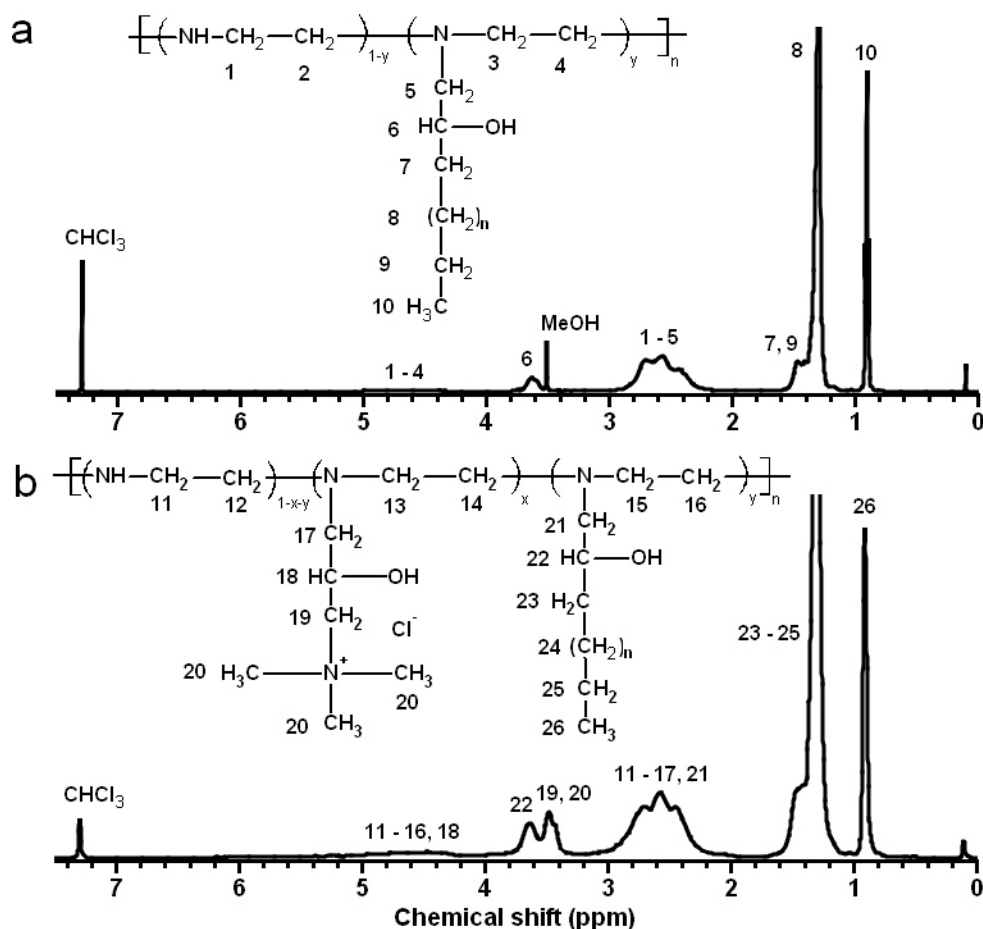


Figure 3.9: $^1\text{H-NMR}$ spectra of a) polymer **PB1**, and b) polymer **PB2**, CDCl_3 , 30°C

Figure 3.9 shows the $^1\text{H-NMR}$ spectra of a) polymer **PB1**, and b) polymer **PB2**. Different to the neat poly(ethylenimine) (cf. Figure 3.8.a), the hydrogen atoms attached to the carbon atoms of the poly(ethylenimine) gave two signals. With both polymers the signals were located at 2.2 - 2.9 ppm and 4.2 - 5.2 ppm (cf. Figure 3.9, 1 - 4, 11 - 16). The reason for the shift of some of the poly(ethylenimine) hydrogen atoms to 4.2 - 5.2 ppm is not yet known but it is possible that some of the hydroxyl and ammonium groups of the reactants formed hydrogen bonds with the amine moieties of the polymer. This would cause a decrease in the electron density around some of the hydrogen atoms attached to the methylene units of the polymer, i. e. they would be deshielded from the external magnetic field, their signal would shift downfield. Signals of the epoxide ring of the 1,2-epoxydodecane at 2.4, 2.7 and 2.9 ppm (cf. Figure 3.7.b) were no longer visible which is a sign of a quantitative reaction between the amine and the epoxide.

With the polymers **PB1** (Figure 3.9.a) and **PB2** (Figure 3.9.b), the signal of the hydrogen atoms of the methylene group connecting the poly(ethylenimine) and the reactants (5, 17, 21) overlapped with the signal of the poly(ethylenimine) methylene hydro-

gen atoms at 2.2 to 2.9 ppm. Also with both polymers, the hydrogen atoms of the methylene group attached to the hydroxyl moiety gave a signal which was located between 3.50 and 3.70 ppm (6, 22). The signal of the alkyl chain hydrogen atoms showed up in the region of 1.20 – 1.60 ppm with both polymers. With polymer **PB2**, the signal of the hydrogen atoms of the 2-hydroxypropyl-3-(N,N,N-trimethylammonium chloride) methylene group attached to the hydroxyl moiety appeared in the region of 4.20 and 4.50 (18).

Different to polymer **PA1**, the hydrogen atoms of the methylene group connecting the methylene group attached to the hydroxyl moiety and the nitrogen atom of the ammonium group of polymer **PB2** could not be distinguished from the hydrogen atoms from the three methyl groups attached to the nitrogen (19 – 20). Instead, one signal is found between 3.40 and 3.55. The comparison of the ¹H-NMR spectra of the polymers **PB2**, **PB4**, **PC1**, and **PC2** showed that the position of the signals was the same with all four polymers.

Calculation of the degree of R10 alkylation as well as the degree of quarternization Q of the polymers **PA1 – **PB4.20** based on ¹H-NMR spectroscopy**

To calculate the degree of R10-alkylation and quarternization Q, the areas below the signals of the hydrogen atoms were used. To determine the correct area corresponding to the hydrogen atoms of the poly(ethylenimine) methylene groups, calculations had to be performed. With the polymers **PB2** to **PC3**, one signal of the hydrogen atoms of the polymer backbone was located between 4.20 - 5.20 ppm (cf. Figure 3.9, 1 – 4, 11 – 16) and overlapped with one hydrogen atom of the methyl group of the ammonium units (cf. Figure 3.9, 18). Between 2.20 and 2.90 ppm, a second overlap occurred between the signal of two hydrogen atoms coming from the alkyl groups, the signal derived from two hydrogen atoms the ammonium units (cf. Figure 3.9, 1 – 5, 9 – 17, 21) and the signal of the polymer methylene hydrogen atoms. Hence, the area of the signal of the polymer hydrogen atoms had to be corrected by means of Equation 3.1.

$$A'_{\text{PEIC}_2\text{H}_4} = A_{\text{PEIC}_2\text{H}_4} - 3 \cdot \frac{A_{\text{QC}_4\text{H}_{11}}}{11} - 2 \cdot \frac{A_{\text{R}_{10}\text{CH}_3}}{3} \quad \text{Eq. 3.1}$$

($A_{\text{PEIC}_2\text{H}_4}$ = integrated ¹H-NMR signal intensity of the poly(ethylenimine) methylene groups from 4.20 - 5.20 and 2.20 - 2.90 ppm, $A_{\text{QC}_4\text{H}_{11}}$ = integrated ¹H-NMR signal intensity of the ammonium methyl and methylene hydrogen atoms from 3.25 - 3.55 ppm, $A_{\text{R}_{10}\text{CH}_3}$ = integrated ¹H-NMR signal intensity of the alkyl-CH₃ group from 0.80 - 1.00 ppm)

The degree of quarternization was defined as the ratio of the number of modified repeating units per macromolecule and the degree of polymerization. The degree of

3 Synthesis of PEI(nkD)xQyR polymers

quarternization was defined as shown in Equation 3.2. The degree of quarternization was calculated using the area below the signal of the ammonium-methyl hydrogen atoms from 3.25 - 3.55 ppm (cf. Figure 3.9, 19, 20), and the corrected area of the polymer hydrogen atoms from 4.20 - 5.20 ppm and 2.20 - 2.90 ppm obtained from Equation 3.1.

$$Q = \frac{N_{\text{QC4H11}}}{X_n} = \frac{A_{\text{QC4H11}}}{A'_{\text{PEIC2H4}}} \cdot \frac{4}{11} \quad \text{Eq. 3.2}$$

(with Q = degree of quarternization, N_{QC4H11} = number of modified repeating units, X_n = degree of polymerization, A_{QC4H11} = integrated $^1\text{H-NMR}$ signal intensity from 3.25 - 3.55 ppm, A'_{PEIC2H4} = corrected area of the $^1\text{H-NMR}$ signal intensity from 4.20 - 5.20 and 2.20 - 2.90 ppm)

The degree of R10-alkylation was calculated using the area below the signal of the methyl hydrogen atoms of the alkyl units from 0.80 - 1.00 ppm (cf. Figure 3.9, 10, 26) and the corrected area below the poly(ethylenimine) hydrogen atoms from 4.20 - 5.20 ppm and 2.20 - 2.90 ppm (cf. Equation 3.1) and is defined as shown in Equation 3.3.

$$R10 = \frac{N_{\text{R10CH3}}}{X_n} = \frac{A_{\text{R10CH3}}}{A'_{\text{PEIC2H4}}} \cdot \frac{4}{3} \quad \text{Eq. 3.3}$$

(with R10 = degree of alkylation, N_{R10CH3} = number of modified repeating units, X_n = degree of polymerization, A_{R10CH3} = integrated $^1\text{H-NMR}$ signal intensity from 0.80 - 1.00 ppm, A'_{PEIC2H4} = corrected area of the $^1\text{H-NMR}$ signal intensity from 4.20 - 5.20 and 2.20 - 2.90 ppm)

Calculation of the degree of R14-alkylation based on $^1\text{H-NMR}$ spectroscopy

The calculation of the degree of R14-alkylation of the polymers **PC1** – **PC3** analogously to the degree of R10-alkylation (cf. Equation 3.3) gave degrees of R14-alkylations larger 1. In water as well as in a methanol/chloroform mixture, both used as reaction environments for the synthesis, poly(ethylenimine) and glycidyltrimethylammonium chloride exhibited an alkaline pH. The solutions of 1,2-epoxydodecane and 1,2-epoxyhexadecane exhibited both an acidic pH of 5. The $^{13}\text{C-NMR}$ spectra of polymer **PC2** showed the presence of a substance bearing a carbon-carbon double bond, probably a precursor for the preparation of the 1,2-epoxyhexadecane. The acidic pH of the 1,2-epoxyhexadecane can be therefore caused either by a precursor or an added acid. The addition of the reactants to the poly(ethylenimine) took place via a ring-opening reaction of the epoxide ring. Epoxides can exhibit an asymmetric structure, thus, the nucleophilic attack of the amine can occur either on the more or the less substituted side of the epoxides. Under neutral or basic conditions, the nucleophilic

attack occurs on the less substituted side while under acidic conditions the more substituted side is preferred [10]. The structure elements which can be formed during the reaction are shown in Figure 3.10.

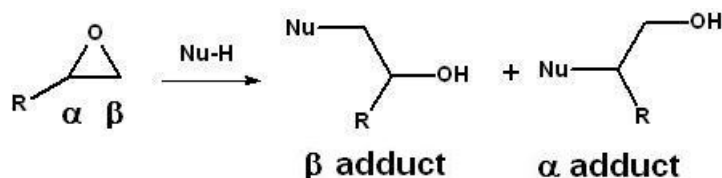


Figure 3.10: Structure elements formed by the reaction of a nucleophile with an asymmetrically substituted epoxide

To examine on which side of the epoxide the nucleophilic attack occurred preferably, the ratio between the area of the signal of the methylene alkyl units at 3.55 - 3.80 ppm (cf. Figure 3.9, 6, 22) and the area of the signal of three hydrogen atoms of the methyl group at the end of the alkyl chain at 0.80 - 1.00 ppm (cf. Figure 3.9, 10, 26) was compared. When only the less substituted side of the epoxide was attacked (= β adduct, cf. Figure 3.10), the area of the signal at 3.55 - 3.80 ppm should be one-third of the area of the signal at 0.80 - 1.00 ppm. On the other hand, when only the more substituted side of the epoxide was attacked (= α adduct, cf. Figure 3.10) the area below the signal at 3.55 - 3.80 ppm is expected to exhibit two-thirds of the area of the signal at 0.80 - 1.00 ppm.

With the polymers **PA2** – **PB4.20**, the ratio between the area of the signal at 3.55 - 3.80 ppm and the area of the signal at 0.80 - 1.00 ppm was determined to be 1:3. The reaction between the poly(ethylenimine), the glycidyltrimethylammonium chloride, and the 1,2-epoxydodecane led to the β adduct. When the poly(ethylenimine) was reacted with 1,2-epoxyhexadecane, on the other hand, the ratio was larger than one-third. When the addition of the glycidyltrimethylammonium chloride was done previous to the addition of the 1,2-epoxyhexadecane (**PC1**), the ratio of areas was determined to be 1.15 to 3. In comparison, when the alkyl reagent was reacted first, the ratios of the areas were measured to be 1.46 to 3 (**PC2.4**) and 1.21 to 3 (**PC3**). This leads to the conclusion that although the poly(ethylenimine) is strongly alkaline and the mixture thereof also the attack of the amine occurred, when 1,2-epoxyhexadecane was used, not only on the less substituted but also on the more substituted side of the epoxide. Furthermore, the examination of several batches of polymer **PC2** showed that the ratios exhibited values between 1.1 and 1.5. Since the polymers **PC2.4** and **PC3** were prepared in a bulk reaction it is not known if the reaction in solution will diminish the formation of the α adduct.

With the aim to calculate to which degree the amine atoms of the poly(ethylenimine)

attacks the more substituted side of the epoxide, the area of the signal at 0.80 - 1.00 ppm was normalised to three. Then the area of the signal at 3.55 - 3.80 ppm was determined, one ratio-unit was subtracted, and the obtained value multiplied with 100. It was found that with polymer **PC1** 15 mol %, with polymer **PC2.4** 46 mol %, and with polymer **PC3** 21 mol% of the amines attacked the more substituted side of the epoxide. To calculate the degree of R14-alkylation, the area below the signals of the poly(ethylenimine) hydrogen atoms had to be corrected by means of Equation 3.4. After the area corresponding to the signals of the poly(ethylenimine) hydrogen atoms was determined, the degree of R14-alkylation was calculated using also Equation 3.3.

$$A'_{\text{PEIC}_2\text{H}_4} = A_{\text{PEIC}_2\text{H}_4} - 2 \cdot A_{\text{R}_{14}\text{CH}_3} \cdot \frac{x}{3} - A_{\text{R}_{14}\text{CH}_3} \cdot \frac{y}{3} - \frac{3 \cdot A_{\text{QC}_4\text{H}_{11}}}{11} \quad \text{Eq. 3.4}$$

($A_{\text{PEIC}_2\text{H}_4}$ = integrated $^1\text{H-NMR}$ signal intensity of the poly(ethylenimine) backbone from 4.20 - 5.20 and 2.20 - 2.90 ppm, $A_{\text{QC}_4\text{H}_{11}}$ = integrated $^1\text{H-NMR}$ signal intensity of the ammonium-trimethyl group from 3.20 - 3.55 ppm, $A_{\text{R}_{14}\text{CH}_3}$ = integrated $^1\text{H-NMR}$ signal intensity of the alkyl- CH_3 group from 0.80 - 1.00 ppm, x = fraction of the addition on the less substituted side of the epoxide, y = fraction of the addition on the more substituted side of the epoxide)

The experimentally obtained degrees of modification obtained from $^1\text{H-NMR}$ measurements and from the elemental analysis are listed in Table 3.6. It was found that the values of $\text{PEI}(\text{nkD})_{\text{xQ}}$ and $\text{PEI}(\text{nkD})_{\text{xQ}}^{\text{yR}10}$ polymers were in good agreement to the theoretical degrees of modification. With $\text{PEI}(\text{nkD})_{\text{xQ}}^{\text{yR}14}$ polymers, the experimentally obtained values differed much more from the theoretical ones. The degrees of modification of $\text{PEI}(\text{nkD})_{\text{xQ}}^{\text{yR}10}$ polymers before and after purification showed no differences. With $\text{PEI}(\text{nkD})_{\text{xQ}}^{\text{yR}14}$ polymers, on the other hand, degrees of alkylation over 100 mol% were obtained when the polymers weren't purified. The differences were most likely caused by impurities present in the used 1,2-epoxyhexadecane solution. The analysis of the data obtained from the elemental analysis of the $\text{PEI}(\text{nkD})_{\text{xQ}}^{\text{yR}14}$ polymers led to the conclusion that the polymers **PC1** and **PC2** contained no 2-hydroxypropyl-3-(N,N,N-trimethylammonium chloride) which was not supported by the $^1\text{H-NMR}$ spectra of the polymers. The wrong values obtained from the elemental analysis were probably caused by matrix effects which led to the detection of lower amounts of nitrogen molecules as it should be. As shown from the results obtained with polymers prepared in solution (**PA1**, **PB1**, **PB2**, **PB3**, **PC1**) and polymers prepared in a bulk reaction (**PA2**, **PB4.1** – **PB4.20**, **PC2.1** – **PC2.12**, **PC3**), with both methods polymers with similar compositions were obtained. Also, the order in which the reactants were added to the poly(ethylenimine) played only a minor role.

3 Synthesis of PEI(nkD)_xQ_yR polymers

Table 3.6: Degree of alkylation and quarternization of the prepared PEI(nkD)_xQ^{yR10} and PEI(nkD)_xQ^{yR14} polymers

Entry	Composition	¹ H-NMR		Elemental analysis	
		R (mol%)	Q (mol%)	R (mol%)	Q (mol%)
PA1	PEI(1.2kD) ₁₃ Q	-	14	-	8
PB1	PEI(10kD) ⁶⁵ R ¹⁰	67	-	81	-
PB2	PEI(10kD) ₁₀ Q ⁸⁰ R ¹⁰	67	9	78	10
PB4.3	PEI(10kD) ₁₀ Q ⁸⁰ R ¹⁰	84	12	84	10
PC1	PEI(10kD) ₁₀ Q ⁶⁰ R ¹⁴	92	16	84	0
PC2.4	PEI(10kD) ₁₀ Q ⁶⁰ R ¹⁴	89	14	84	0

R = degree of alkylation, Q = degree of quarternization, PEI(10kD) = poly(ethylenimine) with M_n = 10,000 g/mol, M_w/M_n = 2.5, PEI(1.2kD) = poly(ethylenimine) with M_n = 1,200 g/mol, M_w/M_n = 1.08, xQ = mol% 2-hydroxypropyl-3-(N,N,N-trimethylammonium chloride), yR10 = mol% 2-hydroxydodecane, yR14 = mol% 2-hydroxyhexadecane

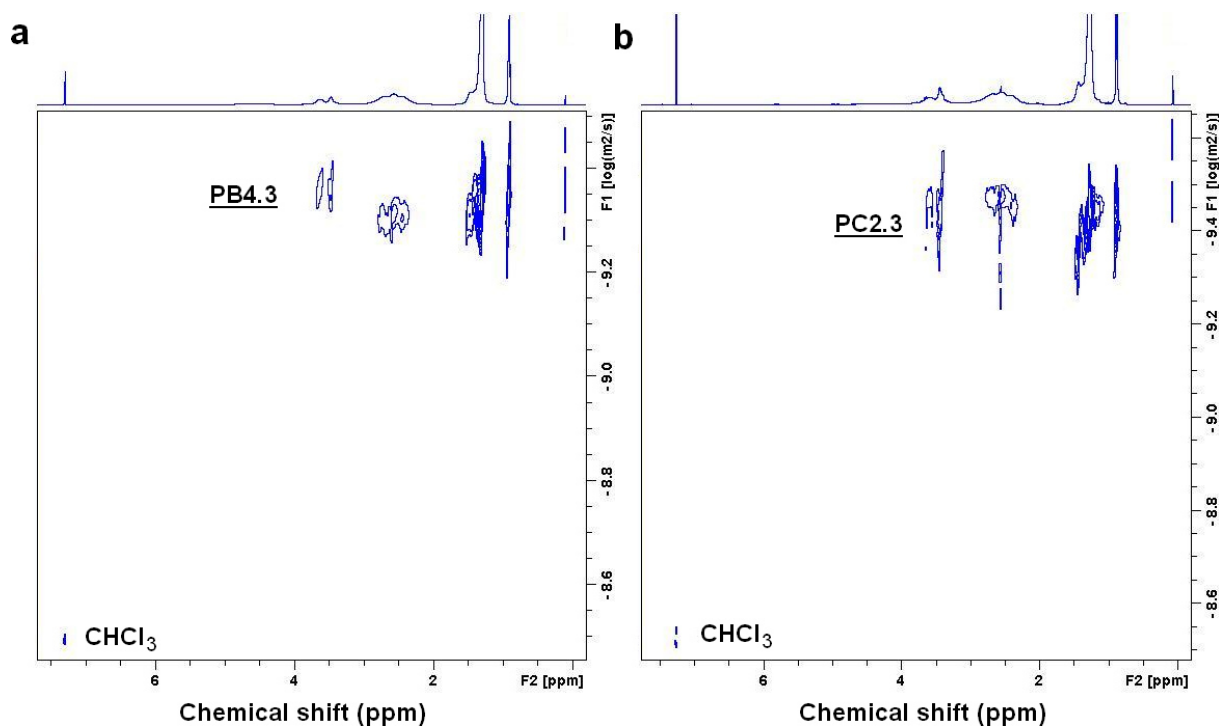


Figure 3.11: ¹H-DOSY NMR spectra of a) polymer **PB4.3**, and b) polymer **PC2.3**, CDCl₃, 30°C

To confirm the covalent attachment of the reactants to the poly(ethylenimine), ¹H-DOSY NMR measurements were performed. Figure 3.11 shows the ¹H-DOSY NMR spectra of a) polymer **PB4.3**, and b) polymer **PC2.3**. Since at high -log D values no signals of low-molecular compounds were detected, the presence of non-reacted ep-

oxides can be ruled out. The diffusion coefficient of dissolved molecules is described by the Stokes-Einstein Equation 3.5, which allows to calculate R_0 , the hydrodynamic radius of the diffusing molecule. With polymer **PB4.3**, a diffusion coefficient of $-\log D = 9.30 \text{ m}^2/\text{s}$ was found which corresponded, calculated with the dynamic viscosity of chloroform at 303.15K of 0.507 mPa·s [11], to a hydrodynamic radius $R_0 = 0.87 \text{ nm}$. Polymer **PC2.3**, on the other hand, exhibited a diffusion coefficient of $-\log D = 9.47 \text{ m}^2/\text{s}$ which corresponded to a hydrodynamic radius $R_0 = 1.29 \text{ nm}$. The neat CHCl_3 exhibited a $-\log D$ value of 8.5 m^2/s which corresponded to a diffusion coefficient of $D = 3.16 \cdot 10^{-9} \text{ m}^2/\text{s}$ and a hydrodynamic radius of 0.14 nm. The mole fraction of the polymer in the solution was calculated to be 0.0079. The measured diffusion coefficient of the neat chloroform was in good agreement to the reported diffusion coefficient of chloroform of $D = 2.56 \cdot 10^{-9} \text{ m}^2/\text{s}$ of a chloroform methyl acrylate solution measured at 30°C and with a mole fraction of methyl acrylate of 0.01 [12]. The slightly higher experimentally measured diffusion coefficient of the chloroform may be attributed to an interaction between the solvent and the polymer [13].

$$R_0 = K_B \cdot \frac{T}{6 \cdot \pi \cdot \eta \cdot D} \quad \text{Eq. 3.5}$$

(with R_0 = hydrodynamic radius of the diffusing molecule [m], K_B = Boltzmann constant [$1.3806485279 \cdot 10^{-23} \text{ kg} \cdot \text{m}^2 \cdot \text{s}^{-2} \cdot \text{K}^{-1}$], T = temperature [K], η = dynamic viscosity of the solvent [$\text{kg} \cdot \text{m}^{-1} \cdot \text{s}^{-1}$], D = diffusion coefficient [$\text{m}^2 \cdot \text{s}^{-1}$])

The measured diffusion coefficients of the used poly(ethylenimine)s, the reactants and the synthesised polymers **PA1**, **PB1**, **PB2**, **PB4.3**, **PC1**, and **PC2.3** are listed in Table 3.7. It was found that the hydrodynamic radii of polymers and reactants which were measured in D_2O were larger than those obtained from measurements performed in CDCl_3 as shown by comparing the hydrodynamic radii of the polymers **PA1** and **PB1**. Although both polymers exhibited similar hydrodynamic radii, polymer **PA1** exhibited only a number average molecular mass of 1,749 g/mol which is much lower than that of polymer **PB1** of 37,829 g/mol. All investigated PEI(10kD)_xQ^{yR} polymers which were soluble in CDCl_3 and measured in this solvent exhibited similar hydrodynamic radii of about 1 nm independent of the degrees of alkylation and quarternization. Comparing the hydrodynamic radii of the polymers **PB4.3** and **PC2.3** (cf. Figure 3.11) with the hydrodynamic radii of neat poly(ethylenimine), glycidyltrimethylammonium chloride, 1,2-epoxydodecane, and 1,2-epoxyhexadecane lead to the conclusion that the reactants were covalently attached to the polymers.

Table 3.7: Diffusion coefficient of the used poly(ethylenimine)s and epoxides, and the polymers PA1, PB1, PB2, PB4.3, PC1, and PC2

Entry	Composition	Solvent	Diffusion coefficient [-log D m ² /s]	R ₀ [nm]
PEI(1.2kD)		D ₂ O	9.57	1.04
PEI(10kD)		D ₂ O	10.20	4.41
PEI(10kD)		CDCl ₃	8.98	0.42
Q		D ₂ O	9.00	0.28
R10		CDCl ₃	8.72	0.23
R14		CDCl ₃	8.82	0.29
<u>PA1</u>	PEI(1.2kD) ₁₃ Q	D ₂ O	9.62	1.16
<u>PB1</u>	PEI(10kD) ₆₅ R10	CDCl ₃	9.43	1.18
<u>PB2</u>	PEI(10kD) ₁₀ Q ₈₀ R10	CDCl ₃	9.25	0.78
<u>PB4.3</u>	PEI(10kD) ₁₀ Q ₈₀ R10	CDCl ₃	9.30	0.87
<u>PC1</u>	PEI(10kD) ₁₀ Q ₆₀ R14	CDCl ₃	9.33	0.94
<u>PC2.3</u>	PEI(10kD) ₁₀ Q ₆₀ R14	CDCl ₃	9.47	1.29

PEI(1.2kD) = poly(ethylenimine) with M_n = 1,200 g/mol, M_w/M_n = 1.08, PEI(10kD) = poly(ethylenimine) with M_n = 10,000 g/mol, M_w/M_n = 2.5, xQ = mol% 2-hydroxypropyl-3-(N,N,N-trimethylammonium chloride, yR10 = mol% 2-hydroxydodecane, yR14 = mol% 2-hydroxyhexadecane, R₀ = hydrodynamic radius [nm]

Figure 3.12 compares the ¹³C-NMR spectra of a) poly(ethylenimine), and b) polymer **PA1**. The neat poly(ethylenimine) (Figure 3.12.a) exhibited signals of the methylene carbon atoms sandwiched by one dendritic and one terminal unit at 38.0 (1) and 56.7 ppm (7). The signals of the methylene carbon atoms sandwiched by one linear and one terminal unit were detected at 40.1 (2) and 51.3 ppm (8), overlapping with the signal of the methylene carbon atoms sandwiched by two dendritic units at 51.3 ppm (5). The signals of the methylene carbon atoms sandwiched by one linear and one dendritic unit appeared at 45.8 (3) and 53.4 ppm (6). The signal of the methylene carbon atoms sandwiched by two linear units showed up at 47.9 ppm (4).

With polymer **PA1** (Figure 3.12.b), the signals corresponding to the poly(ethylenimine) carbon atoms exhibited the same position as with the neat polymer (cf. (Figure 3.12.a). Two additional signals of the poly(ethylenimine) carbon atoms were detected at 50.7 (12) and 52.7 (15) ppm of poly(ethylenimine) units directly attached to the 2-hydroxypropyl-3-(N,N,N-trimethylammonium chloride) units. The signal of the carbon atom of the methylene group connecting the methylene group attached to the hydroxyl moiety and the ammonium group appeared at 69.4 ppm (20). The signal of the carbon atom of the methylene group attached to the hydroxyl moiety showed up at

3 Synthesis of PEI(nkD)xQyR polymers

65.1 ppm (19). The carbon atoms of the three methyl groups attached to the nitrogen gave a signal at 54.7 ppm (17). The signal of the carbon atom of the methylene group connecting the polymer and the 2-hydroxypropyl-3-(N,N,N-trimethylammonium chloride) was located at 52.7 ppm (14).

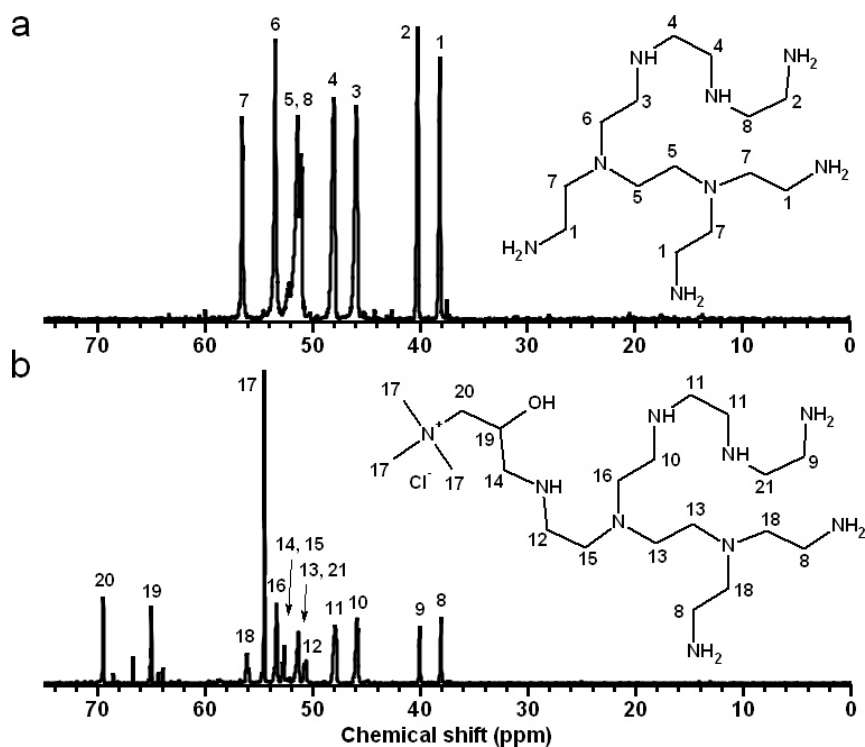


Figure 3.12: ^{13}C -NMR spectra of a) poly(ethylenimine), and b) polymer **PA1**, D_2O , 30°C

Figure 3.13 shows the ^{13}C -NMR spectra of a) polymer **PB1**, and b) polymer **PB2**. Different to the neat poly(ethylenimine) (cf. Figure 3.12.a), the signal intensities of the carbon atoms of the poly(ethylenimine) methylene groups in the polymers **PB1** and **PB2** were very weak. The signals were detected in the region of 51.0 to about 54.7 ppm (1 – 4, 11 – 16).

With polymer **PB1** (Figure 3.13.a), the signal of the carbon atom of the methylene group connecting the polymer and the 2-hydroxydodecane was stretched from 61.0 to 66.0 ppm (5). The signal of the carbon atom of the methylene group attached to the hydroxyl moiety appeared in the region of 67.0 – 71.0 ppm (6). The carbon atoms of the alkyl chains gave signals at 35.4 (7), 32.1 (11), 29.8 (9, 10), 26.0 (8), 22.8 (12), and 14.2 ppm (13).

With polymer **PB2** (Figure 3.13.b), the signals for the alkyl units exhibited the same position as with polymer **PB1**. Different to polymer **PB1**, polymer **PB2** showed at 54.8 ppm (20) an additional signal derived from the carbon atoms of the three methyl groups attached to the nitrogen. Other signals of the 2-hydroxypropyl-3-(N,N,N-tri-

3 Synthesis of PEI(nkD)xQyR polymers

methylammonium chloride) were too weak to be assigned correctly. The comparison of the spectra of the polymers **PB2**, **PB4**, **PC1**, and **PC2** showed that the signals detected with polymer **PB2** appeared also in the spectra of the other polymers. Since the ^{13}C -NMR spectra of the polymers **PB2**, **PB4**, **PC1**, and **PC2** were practically identical, no statement about the type of adduct formed during the reactions (α or β , cf. Figure 3.10) can be made.

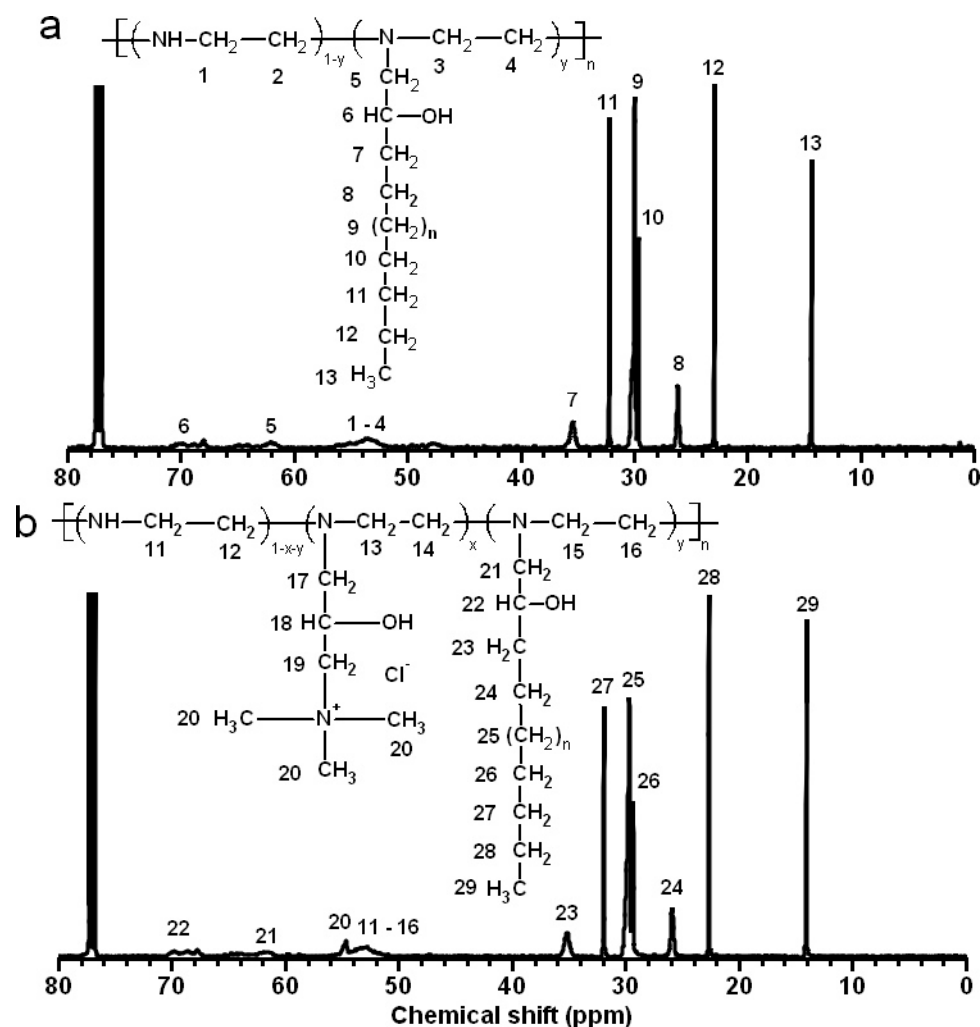


Figure 3.13: ^{13}C -NMR spectra of a) polymer **PB1**, and b) polymer **PB2**, CDCl_3 , 30°C

3 Synthesis of PEI(nkD)xQyR polymers

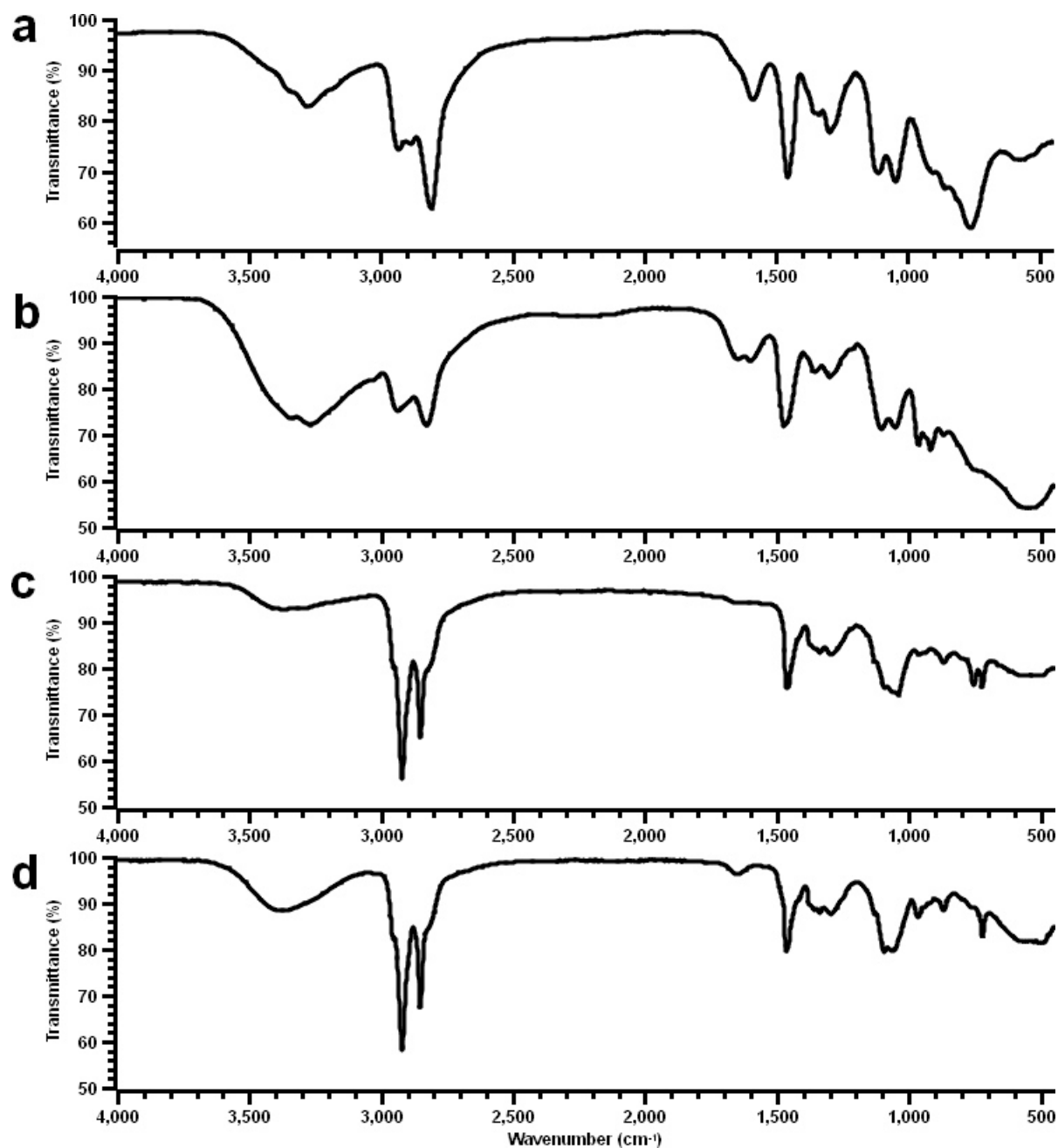


Figure 3.14: ATR-FT infrared spectra of a) poly(ethylenimine), b) polymer **PA1**, c) polymer **PB1**, and d) polymer **PB2**

In Figure 3.14 the infrared spectra of a) hyperbranched poly(ethylenimine), b) polymer **PA1**, c) polymer **PB1**, and d) polymer **PB2** are shown. The neat poly(ethylenimine) (Figure 3.14.a) exhibited an amine N-H stretching band at 3277 cm^{-1} . An amine N-H deformation vibration band appeared at 1587 cm^{-1} . C-N deformation vibration bands were detected at 1333 , 1295 , 1111 , and 1045 cm^{-1} . Alkane C-H stretching bands showed up at 2932 , 2885 , and 2810 cm^{-1} . An alkane C-H deformation vibration band was measured at 1455 cm^{-1} . In the fingerprint region ($= <1000\text{ cm}^{-1}$),

bands were detected at 762 and 575 cm⁻¹. With the PEI(1.2kD)_{13Q} polymer **PA1** (Figure 3.14.b), an overlap of stretching vibration bands corresponding to an amine N-H, an alcohol O-H, and a water O-H group was found at 3271 cm⁻¹. Compared to the neat poly(ethylenimine) (cf. Figure 3.14.a), the alkane C-H stretching bands shifted from 2932 to 2938 cm⁻¹ and from 2810 to 2828 cm⁻¹. The alkane C-H deformation vibration band shifted also from 1455 to 1474 cm⁻¹. A shift of the amine N-H deformation vibration band from 1587 to 1646 cm⁻¹ was also observed. Since the amine C-N deformation vibration bands found with polymer **PA1** were, similar to the neat poly(ethylenimine) (Figure 3.14.a), at 1355, 1300, 1102, and 1051 cm⁻¹, the presence of an alcohol group could not be determined surely. The spectrum showed also a water OH deformation vibration band at 1601 cm⁻¹ which originated most likely from the used glycidyltrimethylammonium chloride solution. In the fingerprint region (= <1000 cm⁻¹), bands were detected at 963, 917, and 543 cm⁻¹. In conclusion, it was found that the disappearance of the alkane C-H stretching band at 2885 cm⁻¹ and the shift of the amine N-H deformation vibration band from 1587 to 1646 cm⁻¹ can be used to distinguish the neat poly(ethylenimine) and PEI(nkD)_{xQ} polymers. Beside the mentioned bands, the bands at 963 and 917 cm⁻¹ in the fingerprint region can be used additionally to differentiate the polymers.

With the PEI(10kD)_{65R10} polymer **PB1** (Figure 3.14.c), an amine N-H stretching band was detected at 3370 cm⁻¹. Alkane C-H stretching bands appeared at 2953, 2921, and 2851 cm⁻¹. An alkane C-H deformation vibration band was located at 1463 cm⁻¹. An amine N-H deformation vibration showed up at 1651 cm⁻¹. Amine C-N deformation vibration bands were measured, similar to the neat poly(ethylenimine) (Figure 3.14.a), at 1338, 1293, 1092, and 1042 cm⁻¹. Because of the similar position of the amine C-N deformation vibration bands, the presence of an alcohol group could not be surely determined. In the fingerprint region (= <1000 cm⁻¹), bands were found at 960, 867, 754, 720, and 494 cm⁻¹. To distinguish the neat poly(ethylenimine), PEI(nkD)_{xQ}, and PEI(nkD)_{yR} polymers, the alkane C-H stretching bands, as well as the bands at 867 and 720 cm⁻¹, can be used.

With polymer **PB2** (Figure 3.14.d), the bands exhibited similar positions as with polymer **PB1** (Figure 3.14.c). Different to polymer **PB1**, the band at 963 cm⁻¹ was, similar to polymer **PA1** (Figure 3.14.b), more prominent. On the other hand, the intensity of the band at 754 cm⁻¹ found with polymer **PB1** was diminished. The polymers **PB4**, **PC1**, and **PC2** exhibited bands at similar positions as with polymer **PB2**. In conclusion, it was found that the non-modified poly(ethylenimine) can be well distinguished from PEI(nkD)_{xQ} and PEI(nkD)_{yR} polymers by the position of the alkane C-H stretching bands. PEI(nkD)_{yR} and PEI(nkD)_{xQ}^{yR} polymers, on the other hand, can only be differentiated by bands appearing in the fingerprint region.

3 Synthesis of PEI(nkD)xQyR polymers

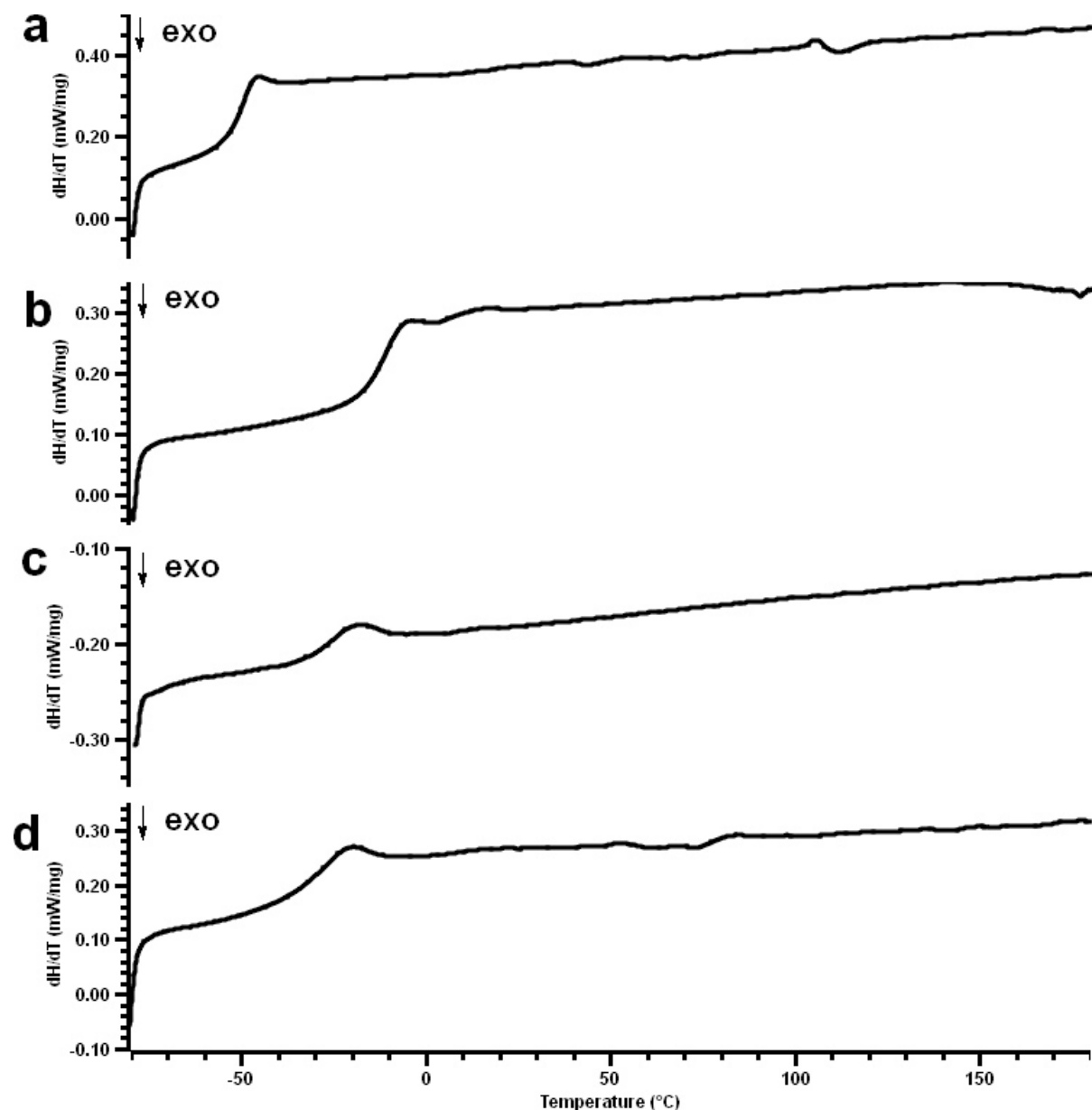


Figure 3.15: Differential scanning calorimetry thermograms of a) poly(ethylenimine), b) polymer **PA1**, c) polymer **PB1**, and d) polymer **PB4.1**, 2. heating run, N₂ atmosphere, dT/dt = 10 K/minute

In the following paragraphs, the differential scanning calorimetry thermograms of the neat poly(ethylenimine) and the polymers **PA1** – **PC2** will be discussed. With the differential scanning calorimetry, the thermal behaviour of the polymers upon heating and cooling are measured. The method shows the temperatures at which melting or glass transitions occur.

In Figure 3.15 the differential scanning calorimetry thermograms of a) poly(ethylenimine), b) polymer **PA1**, c) polymer **PB1** and d) polymer **PB4.1** are shown. While the

neat poly(ethylenimine) (Figure 3.15.a) exhibited a glass transition at -49.5°C , polymer **PA1** (Figure 3.15.b) showed a glass transition at -10.6°C . The heat capacity change was determined to be $\Delta C_p = 0.84 \text{ J}/(\text{g}\cdot\text{K})$ with the neat poly(ethylenimine) and $0.91 \text{ J}/(\text{g}\cdot\text{K})$ with polymer **PA1**. Comparing the glass transition of polymer **PA1** with the data obtained from previous studies [8], the measured glass transition at -10.6°C corresponded to a degree of quarternization of about 16 mol% which is in good agreement with the theoretical degree of quarternization of polymer **PA1** of 13 mol%. The transition was reversible with both polymers.

With the PEI(10kD)^{65R10} polymer **PB1** (Figure 3.15.c), the glass transition shifted from -49.5°C with the neat poly(ethylenimine) to -23.4°C . The heat capacity change was measured to be $\Delta C_p = 0.19 \text{ J}/(\text{g}\cdot\text{K})$. Polymer **PB4.1** (Figure 3.15.d) showed a glass transition at -26.3°C . The transitions of the four polymers were reversible. The heat capacity change was found to be $\Delta C_p = 0.58 \text{ J}/(\text{g}\cdot\text{K})$. With polymer **PB3**, the glass transition was measured to be at -25.8°C . Comparing the glass transition temperature of the PEI(10kD)_{10Q}^{80R10} polymers **PB3** and **PB4.1** of -25.8 and -26.3°C it was found that although the synthesis environment was different, both polymers exhibited similar glass transition temperatures. It is therefore concluded that the synthesis of the polymers in bulk and in solution result in polymers with similar thermal behaviour.

Figure 3.16 compares the differential scanning calorimetry thermograms of a) poly(ethylenimine), b) polymer **PC3**, and c) polymer **PC2.3**. While the neat poly(ethylenimine) (Figure 3.16.a) exhibited a glass transition at -49.5°C with a heat capacity change of $\Delta C_p = 0.84 \text{ J}/(\text{g}\cdot\text{K})$, the PEI(10kD)^{60R14} polymer **PC3** (Figure 3.16.b) didn't show a glass transition. Instead, a melting transition, derived from the melting of the alkyl chains, appeared at 23.6°C . The melt transition enthalpy was measured to be $\Delta H_m = 15.1 \text{ J/g}$. Observing the slope between -80 and 20°C it is indicative that a second transition previous to the melting transition at 23.6°C occurred. The corresponding heat capacity change was determined to be $\Delta C_p = 0.69 \text{ J}/(\text{g}\cdot\text{K})$.

With polymer **PC2.3** (Figure 3.16.c) a melting transition derived from the melting of the alkyl chains was detected at 26.5°C . The enthalpy of the melting transition was found to be $\Delta H_m = 39.6 \text{ J/g}$. Furthermore the slope of the thermogram in the temperature region of -80 to 20°C indicate the presence of a glass transition. The corresponding heat capacity change was measured to be $\Delta C_p = 0.89 \text{ J}/(\text{g}\cdot\text{K})$. The transitions of the three polymers were reversible.

Differential scanning calorimetry Investigations on poly(*t*-butyl acrylate) alkyl side chain comb polymers showed that the modified polymers exhibited different transitions at a polymer-air interface and a polymer-solid interface [15]. While at the polymer-solid interface the melting transition temperatures of the polymers were similar to

3 Synthesis of PEI(nkD)xQyR polymers

those of the bulk polymers, at the polymer-air interface two melting transitions were measured of which one was near the bulk melting temperature and the second one at a 10 to 20°C higher temperature [15]. It was concluded that the alkyl chains formed ordered smectic-like structures which were stable until 10 to 20°C above the bulk melting temperature [14 - 17].

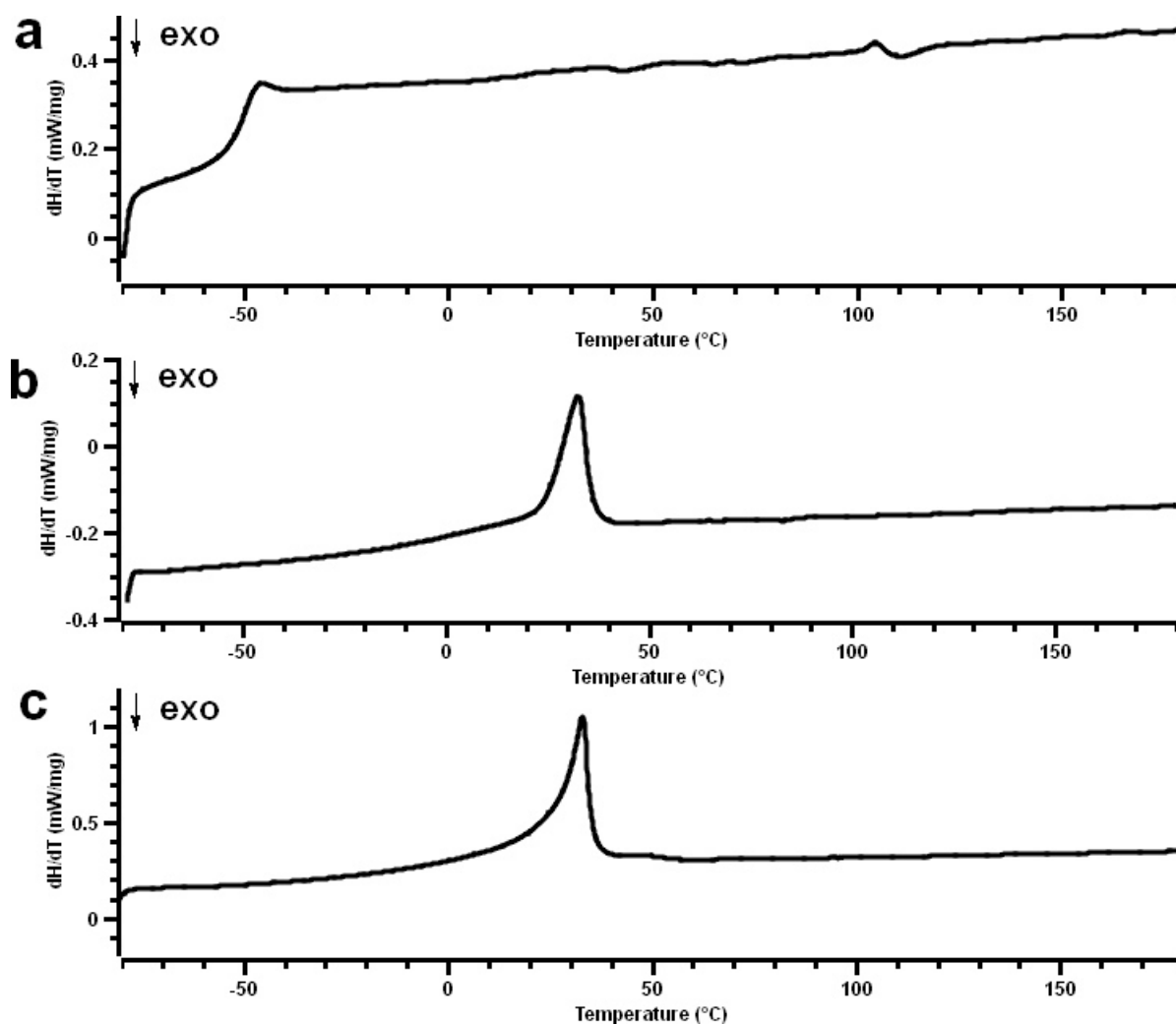


Figure 3.16: Differential scanning calorimetry thermograms of a) poly(ethylenimine), b) polymer **PC3**, and c) polymer **PC2.3**, 2. heating run, N₂ atmosphere, dT/dt = 10 K/minute

In conclusion, it was found that the alkyl chains of PEI(nkD)_xQ^{yR14} polymers arranged themselves into side chain crystals which led to microphase segregations. The alkyl chains of PEI(nkD)_xQ^{yR10} polymers (cf. Figure 3.15), on the other hand, didn't show this behaviour. With polymer **PC1** a melting transition at 21.6°C was observed. Comparing the melting transition temperatures of the PEI(10kD)₁₀Q^{60R14} polymers **PC1** and **PC2.3** of 21.6 and 26.5°C it was, as with the polymers **PB2** and **PB3**, found that although the synthesis environment was different, both polymers exhibited similar melt-

ing transition temperatures. The similar melting transition temperatures of the polymers **PC1** and **PC2.3** show again that the synthesis of the polymers in bulk and in solution lead to polymers with similar thermal behaviours.

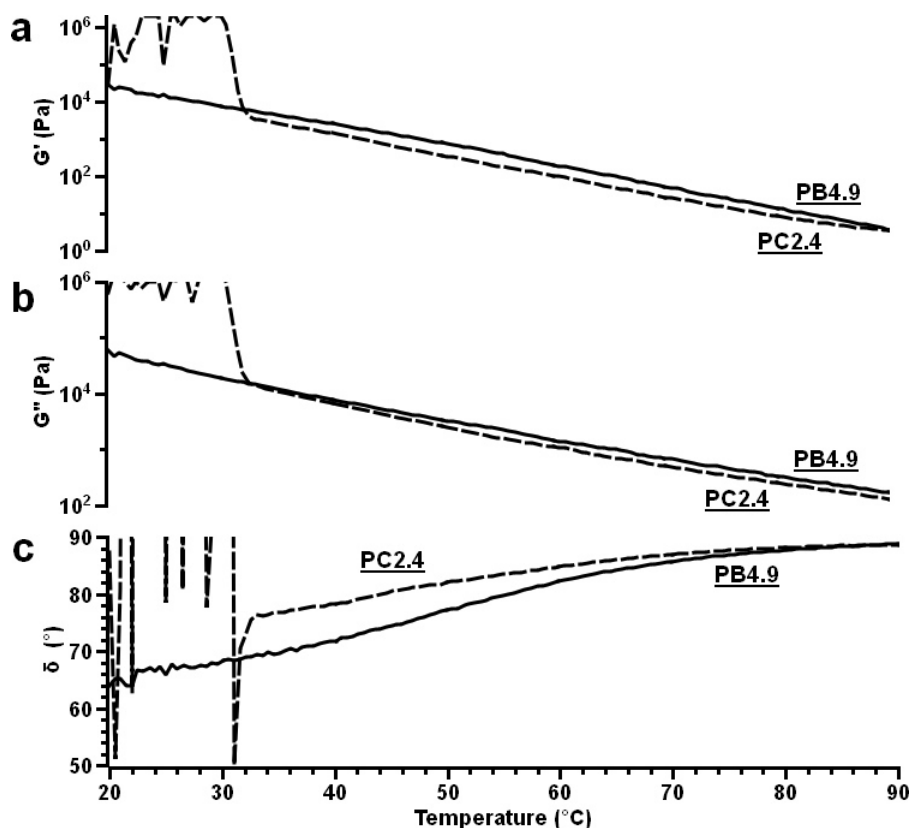


Figure 3.17: Rheology plot of a) the storage modulus G' , b) the loss modulus G'' , and c) the phase angle δ of the polymers **PB4.9** and **PC2.4**, ($\omega = 6.28 \text{ rad/s}$, $\sigma = 5 \text{ Pa}$, $h = 900 \text{ }\mu\text{m}$)

To obtain information about the viscoelastic behaviour of the polymers **PB4.9** and **PC2.4**, rheological investigations were performed. By rheological studies, the temperature dependence of the polymers can be characterised by examining the storage modulus G' , the loss modulus G'' and the phase angle δ .

In Figure 3.17, the storage modulus G' (a), the loss modulus G'' (b), and the phase angle δ (c) in the temperature region of 20 to 90°C of the polymers **PB4.9** and polymer **PC2.4** are shown. Polymer **PB4.9** showed with increasing temperature a monotonous decrease of both the moduli. Polymer **PC2.4**, on the other hand, exhibited between 20 and 32°C a strong scattering of the measuring points which shows that the polymer is solid at temperatures below 32°C. Above 32°C, the storage modulus G' and the loss modulus G'' of polymer **PC2.4** decreased, as with polymer **PB4.9**, steadily with increasing temperature. With both polymers, the storage modulus G' exhibited a lower value than the loss modulus G'' at a given temperature which shows

that the viscous properties of the polymers dominate [18].

The loss factor $\tan \delta$ is defined as the ratio G''/G' and is a measure of the energy lost. A material exhibiting a high $\tan \delta$ behaves like a viscous liquid and a material showing a low $\tan \delta$ like an elastic solid [19 - 21]. $\tan \delta$ increased with polymer **PB4.9** from 2 at 20°C to 47 at 90°C and with polymer **PC2.4** from 3.3 at 32°C to 38 at 90°C which shows that the polymers changed from viscoelastic bodies at lower temperatures to viscous melts at higher temperatures. With both polymers, values of $\tan \delta < 1$, which may be a sign for the formation of gels [22], were not measured in the investigated temperature region. Since polymer **PB4.9** exhibited a $\tan \delta$ value of 10 at 65.5°C and polymer **PC2.4** at 58.4°C it was concluded that above these temperatures the polymers behaved mainly like a viscous liquid.

In the following paragraphs, the results of the thermogravimetric analysis (TGA) of the polymers **PA1**, **PB4.1**, and **PC1** will be discussed. The TGA studies of the polymers gave information about their decomposition temperature and revealed, furthermore, the presence of moisture residues. Figure 3.18 compares the TGA thermograms of a) polymer **PA1**, b) polymer **PB4.1**, and c) polymer **PC1**. The overview over the decomposition temperature of the polymers **PA1**, **PB2**, **PB4.1**, **PC1**, and **PC2.3** is given in Table 3.8.

The decomposition temperature was defined as that point at which the mass of the polymer started to decrease strongly. The extrapolation to the decomposition temperature from the slope (where a strong reduction of the mass takes place) can lead to different values depending on the position of the baseline and the angle of the slope. Therefore, a derivation of the thermogram was performed and the decomposition temperature was defined as the temperature at which the deviated function started to approach the minimum. As reported earlier [8], poly(ethylenimine) which is modified by glycidyltrimethylammonium chloride exhibit a high water content even after drying for prolonged time at elevated temperature. With polymer **PA1** (Figure 3.18.a), the residue water contributed about 20 wt.% of the total mass. The presence of water was shown by the slow decrease of the mass in the temperature region of 30 to 240°C which indicates that during the experiment small molecules were removed by the He-stream. The water originated from the used glycidyltrimethylammonium chloride solution (cf. Table 3.2).

When besides glycidyltrimethylammonium chloride 1,2-epoxyhexadecane was also added to the poly(ethylenimine) and the reaction was performed in a solvent solution (polymer **PC1**, Figure 3.18.c), the residue moisture contributed about 10 wt.% of the total mass which indicates that besides the water of the used glycidyltrimethylammonium chloride solution also small amounts of methanol and chloroform were

3 Synthesis of PEI(nkD)xQyR polymers

present in the polymer. When the preparation of a PEI(10kD)_{10Q}^{60R14} polymer was performed in a bulk reaction (polymer **PB4.1**, Figure 3.18.b), only 3 wt.% of the total mass was contributed by residual water which was originated from the water content of the added glycidyltrimethylammonium chloride solution. It was found by comparing the decomposition temperatures of the polymers **PA1** to **PC2.3**, that the main part of the polymers started to decompose at a temperature between 230 and 240°C.

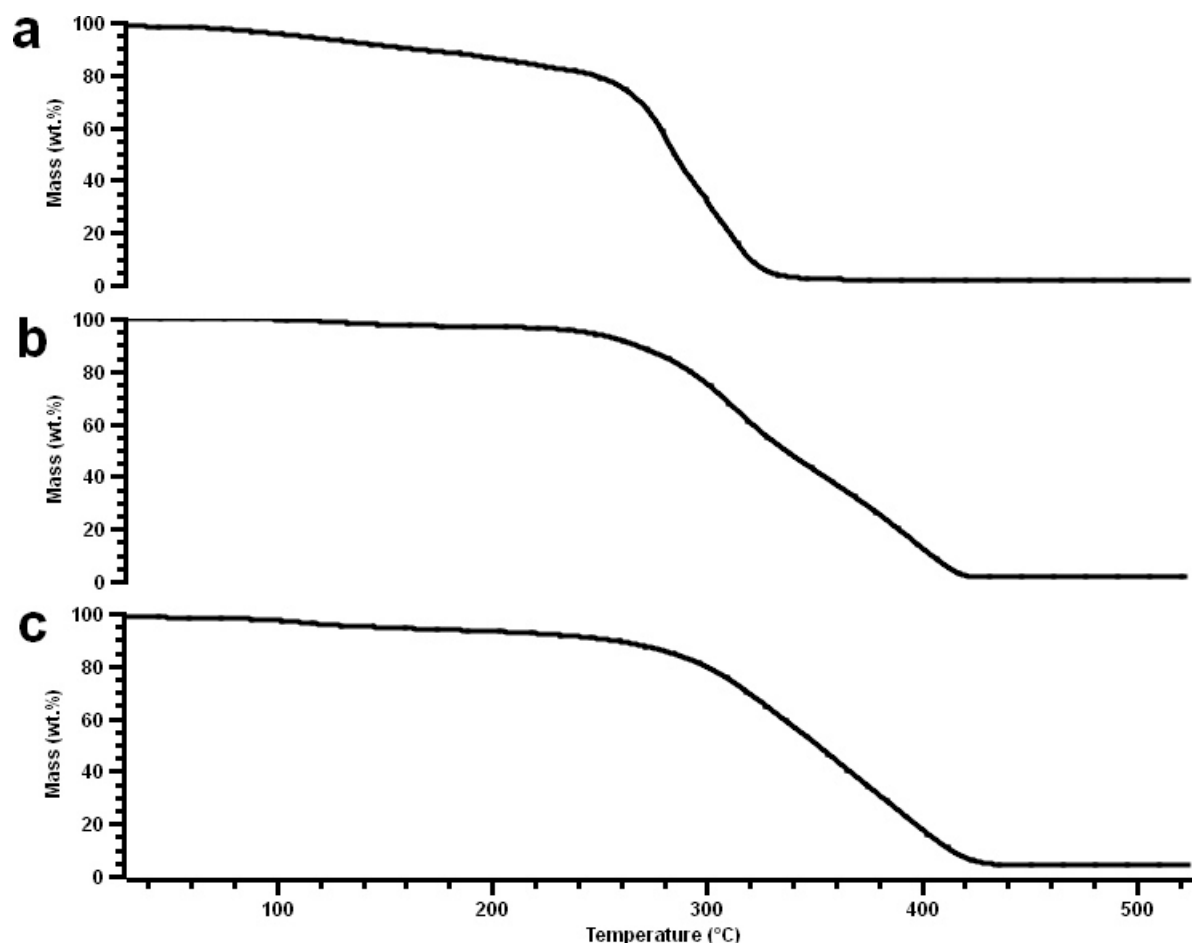


Figure 3.18: TGA thermograms of a) polymer **PA1**, b) polymer **PB4.1**, and c) polymer **PC1**, He atmosphere, $dT/dt = 10$ K/minute

Table 3.8: Decomposition temperature of the polymers PA1, PB2, PB4.1, PC1, and PC2.3

Entry	Composition	Decomposition temperature [°C]	Δm at 500°C [wt.%]
PA1	PEI(1.2kD) _{13Q}	240	96.5
PB2	PEI(10kD) _{10Q} ^{80R10}	240	98.3
PB4.1	PEI(10kD) _{10Q} ^{80R10}	230	98.0
PC1	PEI(10kD) _{10Q} ^{60R14}	230	94.5
PC2.3	PEI(10kD) _{10Q} ^{60R14}	230	99.3

PEI(10kD) = poly(ethylenimine) with $M_n = 10,000$ g/mol, $M_w/M_n = 2.5$, PEI(1.2kD) = poly(ethylenimine) with $M_n = 1,200$ g/mol, $M_w/M_n = 1.08$, xQ = mol% 2-hydroxypropyl-3-(N,N,N-trimethylammonium chloride, yR10 = mol% 2-hydroxydodecane, yR14 = mol% 2-hydroxyhexadecane, wt.% = weight per cent

In the following paragraphs, the GC/MS headspace analysis of the polymers **PA1** and **PB4.9** will be discussed. With this method, the products created during the decomposition of the polymers are collected, separated by the gas chromatograph and detected by the mass spectrometer. The investigation was necessary since when PEI(nkD)_xQ^{yR} polymers were heated to temperatures above 120°C an intense fish-like smell was detected which led to concerns about the type of decomposition products created. In addition, the investigation of [MMT/PEI(nkD)_xQ^{yR}] adducts by a “tube test” revealed that after a standing time of 72 h at 180°C the upper part of the sample exhibited a higher penetration number [23]. In light of this finding, an [MMT/PEI(10kD)_{10Q}^{80R10}] adduct (= **E8.1**) was heated to 180°C for 1 and 70 h, respectively, and the decomposition products were identified by ¹H-NMR. The samples for the GC/MS investigations were prepared by weighing 10 mg of a polymer into a 22 mL glass phial. The phial was sealed afterwards and heated to a chosen temperature for 1 minute with a heat gun. 1 μL of the gas phase was then removed with a syringe and injected into the GC/MS device.

In Figure 3.19 the GC chromatograms of decomposition products of a) polymer **PA1.1** (= **PA1** after heating to 150°C for one minute), b) polymer **PA1.2** (= **PA1** after heating to 220°C for one minute), and c) polymer **PB4.9** (after heating to 220°C for one minute) are shown.

With polymer **PA1.1** (Figure 3.19.a), signals after 11.3 (P_a), 13.9 (P_b), 15.5 (P_c), 23.9 (P_d), and 25.0 (P_e) minutes of elution were detected. Also, signals appeared after 16.5 and 19.1 minutes which corresponded, according to the spectral database of the mass spectrometer, to impurities. The signals P_a and P_d are attributed to 1,2-ethanediamine. The signals P_c and P_e corresponded to 1-(2-aminoethyl)piperazine. Signal P_b was attributed to 1,3-pentanediamine. Besides fragments of the decomposed

poly(ethylenimine), no fragments of the 2-hydroxypropyl-3-(N,N,N-trimethylammonium chloride) were detected. But since the ammonium chloride moiety is able to form salts it can not be excluded that the ammonium units also started to decompose at this temperature.

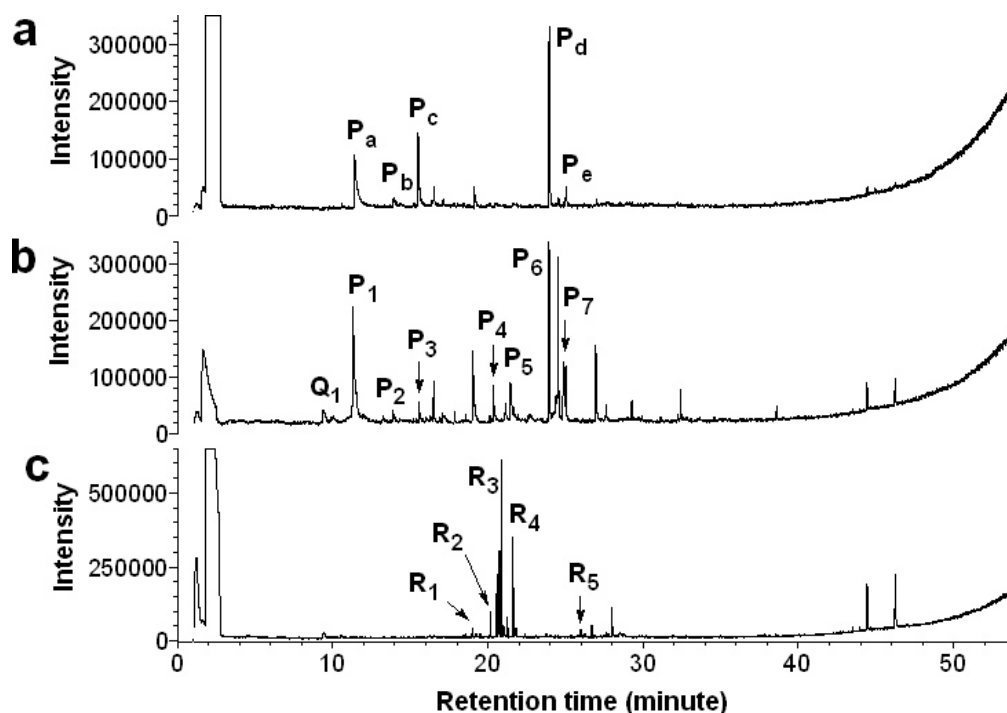


Figure 3.19: GC chromatograms of the headspace analysis of the samples a) polymer **PA1.1**, b) polymer **PA1.2**, and c) polymer **PB4.9**, injection temperature = 250°C, flow = 1 mL/minute, Q = 2-hydroxypropyl-3-(N,N,N-trimethylammonium chloride), P = poly(ethylenimine), R = 2-hydroxydodecane

From the chromatogram of polymer **PA1.2** (Figure 3.19.b) signals which corresponded either to the 2-hydroxypropyl-3-(N,N,N-trimethylammonium chloride) or the poly(ethylenimine) were detected after 9.3 (Q₁), 11.2 (PA₁), 13.8 (PB₁), 15.5 (PB₂), 20.3 (PB₃), 21.5 (PA₂), 23.9 (PB₄), and 25.0 (PC₁) minutes according to the spectral database of the mass spectrometer. The poly(ethylenimine) decomposed into 1,2-ethanediamine (PA₁, PB₁, PA₂, and PB₄), 1-(2-aminoethyl)piperazine (PB₂ and PC₁), and tris(2-aminoethyl)amine (PB₃). In conclusion, it was found that heating the polymer to 220°C for one minute led to a decomposition of the polymer as shown by the presence of fragments corresponding to the poly(ethylenimine) and the 2-hydroxypropyl-3-(N,N,N-trimethylammonium chloride). The detection of 2-hydroxypropyl-3-(N,N,N-trimethylammonium chloride) units shows that when the polymers are heated to higher temperatures evaporable fragments are created.

With polymer **PB4.9** (Figure 3.19.c), according to the spectral database of the mass spectrometer only signals corresponding to the 2-hydroxydodecane moieties were detected. The signals appeared after 18.9 (R_1), 20.1 (R_2), 20.7 (R_3), 21.6 (R_4), and 25.9 (R_5) minutes. The 2-hydroxydodecane decomposed into fragments identified as 3-undecanone (R_1), 1,2-epoxydodecane (R_2 and R_3), 1-dodecanol (R_4), and 2-dodecanol (R_5). Besides fragments of the 1,2-epoxydodecane, no fragments of the poly(ethylenimine) or the 2-hydroxypropyl-3-(N,N,N-trimethylammonium chloride) were detected. From this data, it is assumed that with PEI(nkD)_xQ^{YR10} polymers the alkyl chains decompose earlier than the poly(ethylenimine) backbone. The missing fragments of the 2-hydroxypropyl-3-(N,N,N-trimethylammonium chloride) may be caused by the low amount of substance present in the polymer.

In conclusion, it was found that heating a PEI(1.2kD)_{13Q} polymer (**PA1**) to 150 (for one minute) only fragments of the poly(ethylenimine) backbone were found in the gas phase. When the polymer was heated to 220°C for one minute a fragment of the 2-hydroxypropyl-3-(N,N,N-trimethylammonium chloride) was found which shows that at this temperature evaporable fragments of the 2-hydroxypropyl-3-(N,N,N-trimethylammonium chloride) are created. When a PEI(10kD)_{10Q}^{80R10} polymer (**PB4.9**) was heated to 220°C for one minute only fragments of the alkyl chains were found. On the other hand, the ¹H-NMR spectrum of a [MMT/PEI(10kD)_{10Q}^{80R10}] adduct (**E8.1**) heated to 180°C for 70 h revealed that the polymer decomposition products consisted of N(CH₃)₃, [HN(CH₃)₃Cl, aminopropanol, and alkyl chain compounds. While the removed mass after heating an [MMT/PEI(10kD)_{10Q}^{80R10}] adduct (**E8.1**) to 180°C for 1 h was only 2.5 wt%, the heating to 180°C for 70 h led to a reduction of 39 wt%. In conclusion, the PEI(10kD)_{10Q}^{80R10} polymers can not be stored at high temperatures for extended times.

The solubility of hyperbranched poly(ethylenimine) and the polymers **PA1**, **PB1**, **PB4.9**, **PC2.3**, and **PC3** in common solvents was investigated. The solubility was qualitatively judged by optical inspection of a mixture of 10 mg substance per mL solvent after a standing time of 30 minutes at $T = 20^\circ\text{C}$. The samples were distinguished between soluble (no visible substance particles in the solution), dispersion (visible substance particles in the solution), and insoluble (no dissolved substance). The solubility of the polymers is listed in Table 3.9. The solvents are arranged from the most polar to the most non-polar solvent in descending order using the empirical parameter of the solvent polarity $E_r(30)$ [24, 25].

While the neat poly(ethylenimine) was soluble in water and polar to semi-polar solvents ranging from methanol to chloroform, polymer **PA1** was only soluble in methanol and water. With the polymers **PB1** and **PC3**, which contain large amounts

3 Synthesis of PEI(nkD)_xQyR polymers

of alkyl groups but no ammonium units, a shift of the solubility to semi-polar to non-polar solvents ranging from dichloromethane to heptane was observed. When the poly(ethylenimine) was modified with 80 mol% of alkyl and 10 mol% of ammonium units (polymer **PB4.9**) the solubility of the polymer was similar to that of polymer **PB1**. Although polymer **PC2.3** contained only 60 mol% of the alkyl units, the total number of carbon atoms of the alkyl chains was similar to that of polymer **PB4.9** which explains the identical solubility of the two polymers.

Table 3.9: Solubility of poly(ethylenimine) and the polymers PA1, PB1, PB4.9, PC2, and PC3 in common solvents

	PEI(10kD)	PA1	PB1	PB4.9	PC2.3	PC3
xQ		13	0	10	10	0
yR		0	65 (R10)	80 (R10)	60 (R14)	60 (R14)
Solvent						
Water	o	o	x	x	x	x
Methanol	o	o	x	-	-	x
Dimethylformamide	o	x	x	x	x	x
Acetone	o	x	x	x	x	x
Dichloromethane	o	x	o	o	o	o
Chloroform	o	-	o	o	o	o
Ethyl acetate	-	x	-	x	x	-
Tetrahydrofuran	-	x	o	o	o	o
Diethyl ether	x	x	o	o	o	o
Toluene	x	x	o	o	o	o
Cyclohexane	x	x	o	o	o	o
Heptane	x	x	o	o	o	o

o = soluble, - = dispersion, x = insoluble, PEI(10kD) = poly(ethylenimine) with $M_n = 10,000$ g/mol, $M_w/M_n = 2.5$, xQ = mol% 2-hydroxypropyl-3-(N,N,N-trimethylammonium chloride), yR10 = mol% 2-hydroxydodecane, yR14 = mol% 2-hydroxyhexadecane

Solubility investigations on PEI(nkD)_xQ^{yR10} polymers with degrees of alkylation between 0 and 90 mol% with 1,2-epoxydodecane and degrees of quarternization between 0 and 75 mol% with glycidyltrimethylammonium chloride have shown that only polymers with a certain amount of alkyl groups (> 65 mol %) and ammonium moieties (< 15 mol%) are soluble in non-polar solvents (cf. Figure 3.20) [9]. Based on this study, only polymers bearing ≥ 65 mol% alkyl groups and ≤ 15 mol% ammonium moieties were synthesised for further reactions with montmorillonite.

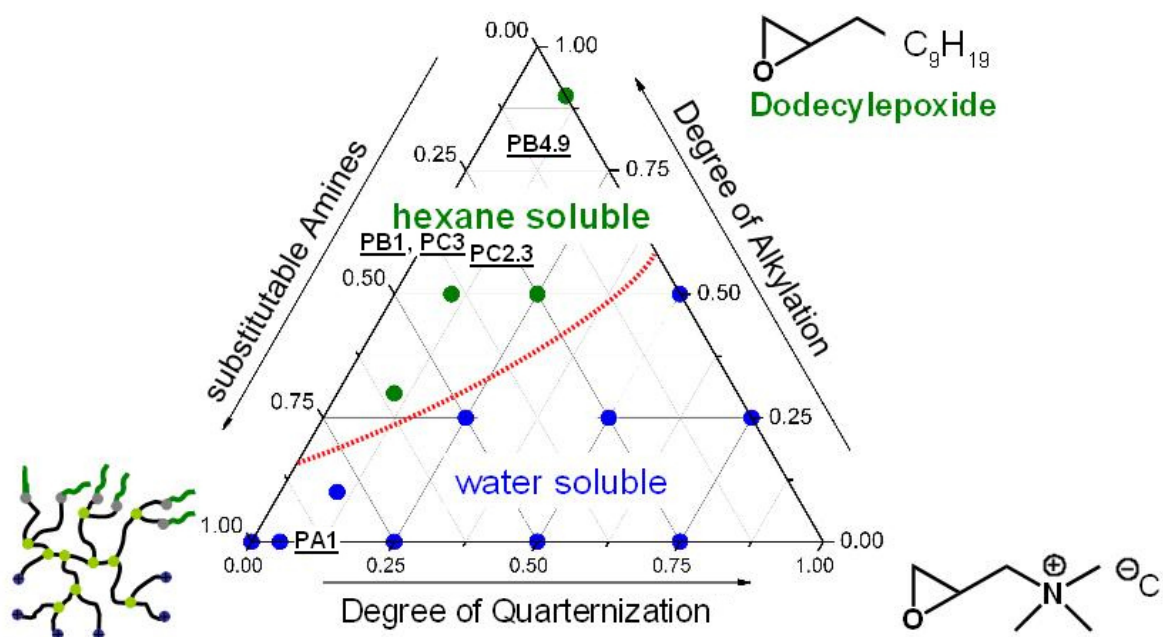


Figure 3.20: Solubility of $PEI(nkD)_{xQ}yR^{10}$ polymers [9] and the polymers **PA1**, **PB1**, **PB4.9**, **PC2.3**, and **PC3** in water and hexane

It was attempted to determine the molecular weights of the polymers **PB1** and **PB4.9** by size-exclusion chromatography (SEC). Although the polymers **PB1** to **PC3** are soluble in the eluent tetrahydrofuran (cf. Table 3.9) the measurements were not successful. It was found that the detectors were not able to detect the polymer of a $PEI(nkD)_{xQ}yR$ /tetrahydrofuran solution. The reason may be that the polymers interacted with the column. To avoid the use of a column, the static light scattering of the polymer solutions was measured. The theoretical background about the determination of the molecular weight of the polymers by light scattering experiments is given in Chapter 2. To determine the weight average molecular weight and the radius of gyration of the alkyl-primer polymer **PB1**, solutions with different concentrations in tetrahydrofuran were prepared. The prepared and measured concentrations are listed in Table 3.10. The refractive index increment of polymer **PB1** was determined to be $dn/dc = 0.083 \text{ mL/g}$. The wavelength of the respective laser was with both detectors 658 nm.

In Figure 3.21, the Zimm plot of polymer **PB1** is shown. It was found that the polymer exhibited a weight average molecular weight of $M_w = 157,300 \text{ g/mol}$ and a radius of gyration of $R_g = 3 \pm 0.5 \text{ nm}$. With the composition of the polymer, the number average molecular weight of the polymer was calculated to be $M_n = 37,829 \text{ g/mol}$. Since the used poly(ethylenimine) (= PEI(10kD)) exhibited a polydispersity of 2.5 (cf. Table 3.2) it was accepted that the weight average molecular weight of polymer **PB1** was equal to the number average molecular weight multiplied by 2.5. Comparing the experi-

3 Synthesis of PEI(nkD)xQyR polymers

mentally obtained weight average molecular mass of polymer **PB1** with the theoretically expected weight average molecular weight of about 94,530 g/mol it was found that the polymer was about 50,000 g/mol larger than expected. On the other hand, the negative slope of the second virial coefficient A_2 indicates a strong interaction between the polymer molecules due to their polyelectrolyte nature [26]. The high measured weight average molecular weight may be, therefore, caused by polymer molecules which interact with each other.

The evaluation of Zimm plots of polymers bearing ammonium moieties was not possible. Due to the polyelectrolyte properties of the polymers, the created Zimm plots showed bent lines which made the double extrapolation to the angle of zero and the concentration of zero unsure. Also, experiments in which different amounts of LiBr was added to the polymer solutions to screen the electrostatic interactions did not result in evaluable plots. Although it was clear that the tried salt concentrations were not sufficient to compensate the positive charge of the polymers an in-depth research of this problem was not performed due to the lack of time.

Table 3.10: Prepared solutions of polymer **PB1 in tetrahydrofuran**

Polymer solution	Polymer concentration [g/mL]
PB1.1	$4.87 \cdot 10^{-4}$
PB1.2	$9.74 \cdot 10^{-4}$
PB1.3	$2.43 \cdot 10^{-3}$
PB1.4	$4.87 \cdot 10^{-3}$

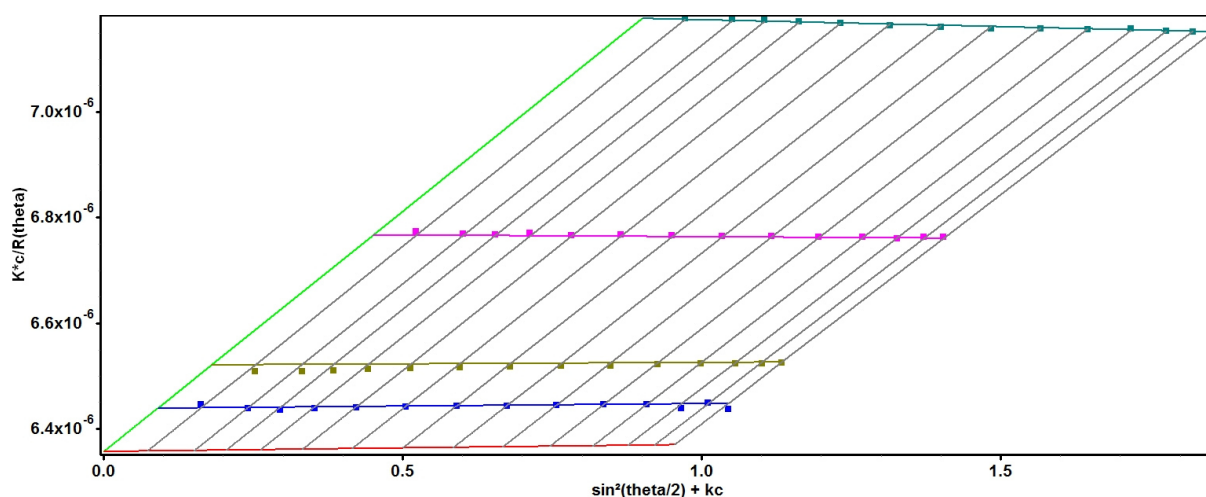


Figure 3.21: Zimm plot of polymer **PB1**

Attempts to synthesise PEI(10kD)^{52U11}

As an alternative to 1,2-epoxydodecane and 1,2-epoxyhexadecane, it was tried to

3 Synthesis of PEI(nkD)xQyR polymers

add 2-undecanone to hyperbranched poly(ethylenimine). The condensation reaction of a primary amine with a ketone leads to imines (Figure 3.22.a), while secondary amines form enamines (Figure 3.22.b).

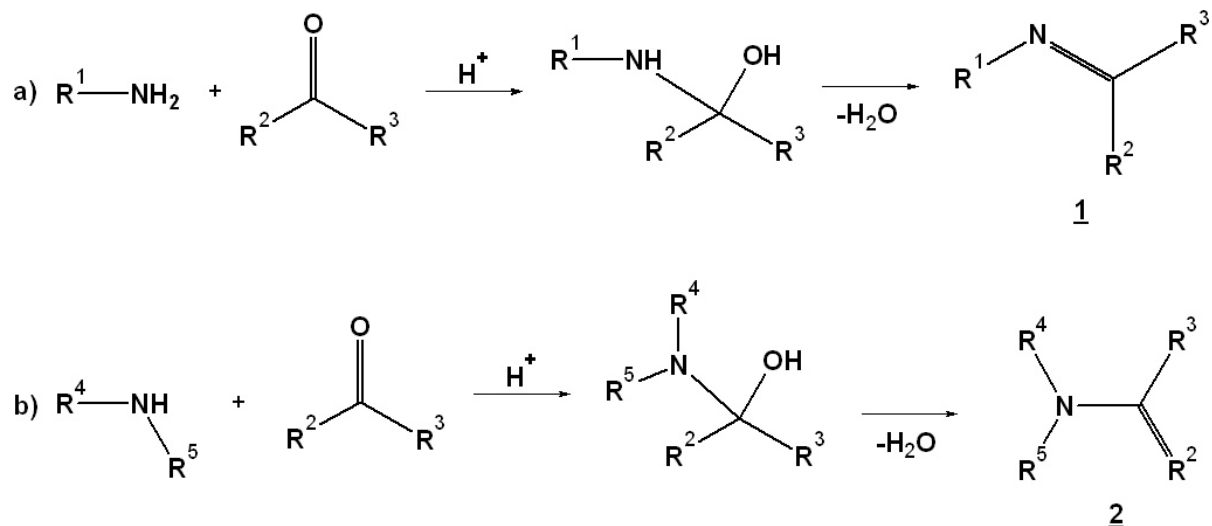


Figure 3.22: Reaction of amines with ketones [27]

The PEI(10kD)^{52U11} polymer **PD1** was prepared by mixing poly(ethylenimine) with 2-undecanone in methanol. The reaction took place in an acidic environment and in the presence of a water absorbing salt. As the acid was added to the poly(ethylenimine)/methanol mixture, the poly(ethylenimine) precipitated and gave a white solid. During the reaction, it was observed that the colour of the liquid 2-undecanone fraction changed from colourless to yellow and the colour of the poly(ethylenimine) changed from white to orange. After 24 hours, the reaction mixture still consisted of a liquid and a solid phase. The mixture was filtered and the solvent in the liquid fraction was removed under reduced pressure. Both fractions were dried afterwards at elevated temperature and under reduced pressure. After drying, the fractions were investigated by ¹H-NMR.

While the residue of the reaction was a mixture of sodium sulphate and neat poly(ethylenimine), the liquid fraction was identified as non-reacted 2-undecanone. The reason may be that the precipitated poly(ethylenimine) was not able to react with the ketone. Another reason why the desired product could not be isolated may be because imines bearing an alkyl or proton rest on the amine are easily hydrolysed and decompose into a ketone and an amine. The hydrolysis of Schiff bases (with an aromatic rest on the amine), on the other hand, is more difficult and requires acid or base catalysis. Another possible route for obtaining the desired product is to react the amine with a ketone and an aldehyde by a Mannich reaction [27] or by a reductive alkylation of the primary and secondary amines [28]. But since priority was given to the

preparation of PEI(nkD)_xQ^{yR} polymers and adducts prepared thereof the alternative routes were not studied in detail.

Discussion

In this chapter the synthesis and characterisation of alkyl-quat-primer polymers (PEI(nkD)_xQ^{yR}), obtained by reacting hyperbranched poly(ethylenimine) with glycidyltrimethylammonium chloride and either 1,2-epoxydodecane or 1,2-epoxyhexadecane, is described. The polymers were either prepared in solution or in a bulk reaction.

¹H-NMR measurements and elemental analysis showed that the experimentally obtained compositions of the polymers were in good agreement to the theoretically expected values with poly(ethylenimine)s bearing 2-hydroxypropyl-3-(N,N,N-trimethylammonium chloride) and 2-hydroxydodecane moieties (polymers **PA1** - **PB4**). On the other hand, with poly(ethylenimine)s bearing 2-hydroxypropyl-3-(N,N,N-trimethylammonium chloride) and 2-hydroxyhexadecane groups (polymers **PC1** - **PC3**), the nitrogen content obtained by elemental analysis was much too low which could lead to the false assumption that no 2-hydroxypropyl-3-(N,N,N-trimethylammonium chloride) was present in the polymers. Also, the degree of 2-hydroxyhexadecane alkylation, as well as the degree of quaternization of the PEI(10kD)_{10Q}^{60R14} polymers **PC1** and **PC2**, obtained from ¹H-NMR measurements, was higher than theoretically expected. To be able to prepare larger quantities of [MMT/polymer] adducts for further studies, larger quantities of the polymers **PB4** (ca. 8.4 kg in total) and **PC2** (ca. 2.5 kg in total) were prepared in batches of different sizes. Comparing the composition of the batches it was found that the composition of the polymers doesn't differ significantly. This led to the conclusion that the polymers **PB4** and **PC2** can be prepared in larger quantities with the desired compositions.

The ¹H-DOSY NMR spectra of the polymers **PA1** to **PC3** showed only one diffusion coefficient at high -log D values which point to that the polymers contained no non-reacted epoxides. These results lead to the conclusion that the reactants are covalently attached to the poly(ethylenimine). Comparing the hydrodynamic radii of the polymer measured in D₂O to those measured in CDCl₃ it was found that the hydrodynamic radii of polymers and reactants measured in D₂O are larger than those obtained from measurements performed in CDCl₃. The hydrodynamic radii of polymers were found in the region of 0.78 to 1.29. A correlation between the degree of modification of the poly(ethylenimine) and the hydrodynamic radius was not obvious.

The comparison of the ¹³C-NMR spectra of the neat poly(ethylenimine), the epoxides, and the polymers **PA1** to **PC3** showed that with neat poly(ethylenimine) and

poly(ethylenimine) bearing 2-hydroxypropyl-3-(N,N,N-trimethylammonium chloride) units the signals corresponding to the expected methyl and methylene groups of both the poly(ethylenimine) and the 2-hydroxypropyl-3-(N,N,N-trimethylammonium chloride) could be assigned accordingly. When 2-hydroxydodecane or 2-hydroxyhexadecane units were attached to the poly(ethylenimine), the spectra became dominated with signals corresponding to the segments of the alkyl reactants with very weak signals of the poly(ethylenimine) and the 2-hydroxypropyl-3-(N,N,N-trimethylammonium chloride).

IR investigations of the neat poly(ethylenimine), PEI(nkD)_xQ, PEI(nkD)_yR¹⁰, and PEI(nkD)_xQ^{yR10} polymers showed that the polymers can be well distinguished from each other by the alkane C-H stretching bands, the amine N-H deformation vibration band and bands in the fingerprint region. A distinction between PEI(10kD)_{10Q}^{80R10} and PEI(10kD)_{10Q}^{60R14} polymers, on the other hand, was not possible.

The thermal behaviour of the neat poly(ethylenimine), and the polymers **PA1** – **PC3** was investigated by DSC. It was found that the addition of glycidyltrimethylammonium chloride and 1,2-epoxydodecane to the poly(ethylenimine) led to an increase of the glass transition temperature of the polymer. When the poly(ethylenimine) was modified by 1,2-epoxyhexadecane instead of the 1,2-epoxydodecane no glass transitions were measured. Instead, melting transitions derived from the alkyl chains were observed. The comparison of polymers prepared in solution and in bulk showed that both preparation procedures led to polymers with similar thermal behaviours. The rheological investigation of the PEI(10kD)_{10Q}^{80R10} polymer **PB4.9** and the PEI(10kD)_{10Q}^{60R14} polymer **PC2.4** showed that at a given temperature the storage modulus G' was lower than the loss modulus G'' which points to that the viscous properties of the polymers dominate. The ratio G''/G' increased steadily with increasing temperature and passed with polymer **PB4.9** the value of 10 at 65.5°C and with polymer **PC2.4** at 58.4°C which shows that the polymers change from a viscoelastic material at lower temperatures to a viscous melt at higher temperatures. The same was also found as the values of phase angles δ in the investigated temperature region were evaluated. The phase angles of the polymers increased steadily and reached values near 90° at a temperature of 90°C. Furthermore, the PEI(10kD)_{10Q}^{60R14} polymer **PC2.4** turned out to be less elastic than polymer **PB4.9** after the alkyl chains were molten.

Thermogravimetric investigations of the polymers **PA1**, **PB2**, **PB4.1**, **PC1**, and **PC2.3** showed that these polymers exhibited decomposition temperatures between 230 and 240°C. GC/MS headspace analysis of the PEI(1.2kD)_{13Q} polymer **PA1**, performed after heating one sample to 150 and one to 220°C for one minute, showed that when the polymer was heated to 150°C only fragments of the poly(ethylenimine) backbone

were found. Since the 2-hydroxypropyl-3-(N,N,N-trimethylammonium chloride) is able to form salts, it may be possible that the 2-hydroxypropyl-3-(N,N,N-trimethylammonium chloride) was also fragmented. When the polymer was heated to 220°C, fragments of the poly(ethylenimine) backbone, as well as fragments of 2-hydroxypropyl-3-(N,N,N-trimethylammonium chloride), were found in the gas phase.

Although the decomposition temperature of the polymer obtained from the thermogravimetric investigation was found to be around 240°C the fragments obtained after heating at lower temperatures lead to the conclusion that the heating rate of the thermogravimetric experiment (= 10 K/minute) was not low enough. From the GC/MS headspace analysis of the PEI(10kD)_{10Q}^{80R10} polymer **PB4.9**, performed after heating the sample to 220°C for one minute, it was found that only the alkyl chains were fragmented from the polymer. On the other hand, heating a [MMT/PEI(10kD)_{10Q}^{80R10}] adduct (**E8.1**) to 180°C for 70 h revealed that the decomposition products of the polymer of the adduct consisted of N(CH₃)₃, [HN(CH₃)₃Cl, aminopropanol, and alkyl chain compounds which show that PEI(10kD)_{10Q}^{80R10} polymers could not be stored at high temperatures.

The determination of the molecular weight of the PEI(10kD)^{65R10} polymer **PB1** and the PEI(10kD)_{10Q}^{80R10} polymer **PB4.9** by size-exclusion chromatography (SEC) failed most likely due to an interaction of the polymers with the column. The determination of the weight average molecular weight by static light scattering was successful with the PEI(10kD)^{65R10} polymer **PB1** and showed that the polymer exhibited a weight average molecular weight of $M_w = 157,300$ g/mol and a radius of gyration R_g of 3 ± 0.5 nm. The measured molecular weight was higher than theoretically expected and point to the formation of associated polymer molecules as indicated by the negative slope of the second virial coefficient A_2 . Due to the polyelectrolyte properties of polymers bearing ammonium moieties, the evaluation of the Zimm plots were not possible. But due to the lack of time, the correct amount of LiBr which should be added to compensate the electrostatic interactions between the polymers was not found.

It was found that while the neat poly(ethylenimine) was soluble in water and polar to semi-polar solvents ranging from methanol to chloroform, the PEI(1.2kD)_{13Q} polymer **PA1** was only soluble in methanol and water. The addition of large amounts of alkyl groups to the poly(ethylenimine) (polymer **PB1**) led to a shift of the solubility of the polymer to semi-polar to non-polar solvents ranging from dichloromethane to heptane. When the poly(ethylenimine) was modified with 80 mol% of the alkyl and 10 mol% of the ammonium moieties (polymer **PB4.9**), the solubility of the polymer was similar to that of the PEI(10kD)^{65R10} polymer **PB1**. The solubility behaviour of the PEI(10kD)_{10Q}^{60R14} polymer **PC2.3** was identical to that of the PEI(10kD)_{10Q}^{80R10} polymer **PB4.9** which could be explained by that although the PEI(10kD)_{10Q}^{60R14} polymers con-

3 Synthesis of PEI(nkD)xQyR polymers

tained only 60 mol% of the alkyl units, the total number of carbon atoms of the alkyl chains was similar to that of the PEI(10kD)_{10Q}^{80R10} polymer.

The attempt of reacting hyperbranched poly(ethylenimine) with 2-undecanone under an acidic condition and in the presence of a water absorbing substance failed probably either due to the fast hydrolysis of imines by water molecules or, since the poly(ethylenimine) precipitated during the reaction, due to the inability of the precipitated polymer to react with the ketone.

3.4 Conclusion

In this chapter the synthesis and characterisation of alkyl-quat-primer polymers (PEI(nkD)_xQ^{yR}), obtained by reacting hyperbranched poly(ethylenimine)s with glycidyltrimethylammonium chloride and either 1,2-epoxydodecane or 1,2-epoxyhexadecane is described. The results from ¹H-NMR, ¹H-DOSY NMR, ¹³C-NMR, IR, and DSC investigations of two alkyl-quat-primer polymers bearing 1,2-epoxydodecane as the alkyl moiety (PEI(10kD)_{10Q}^{80R10}) and two alkyl-quat-primer polymers bearing 1,2-epoxyhexadecane as the alkyl group (PEI(10kD)_{10Q}^{60R14}) showed that polymers prepared in solution and polymers prepared in bulk exhibited comparable chemical and physical characteristics. Nonetheless, bulk synthesis should be preferred because of the more rapid, and simple work-up. From ¹H-NMR measurements and elemental analysis, the composition of PEI(nkD)_xQ and PEI(nkD)_xQ^{yR10} polymers were found to be in good agreement to the theoretically expected values. With PEI(10kD)_{10Q}^{60R14} polymers, the degrees of alkylation and quarternization were higher than expected. The DSC measurement of the neat poly(ethylenimine) showed that the polymer exhibited a glass transition at -49.5°C. The addition of glycidyltrimethylammonium chloride to the poly(ethylenimine) led to an increase of the glass transition temperature. The addition of 1,2-epoxydodecane led also to an increase of the glass transition temperature, but the shift of the transition temperature was not as drastic as with PEI(nkD)_xQ polymers. Different to the PEI(nkD)_xQ^{yR10} polymers, PEI(10kD)^{60R14} and PEI(10kD)_{10Q}^{60R14} polymers didn't exhibit a glass transition but showed instead a melting transition in the region of 21.6 to 26.5°C. It was found, that PEI(nkD)_xQ^{yR} polymers decomposed between 230 and 240°C. The GC/MS headspace analysis of PEI(nkD)_xQ polymers showed that after heating these polymers for one minute at 150°C the side-chains of the poly(ethylenimine) backbone fragmented preferably. The fragments measured after heating a PEI(nkD)_xQ^{yR10} polymer for one minute at 220°C consisted mainly of alkyl chain fractions. On the other hand, the analysis of the fragments obtained after heating an [MMT/PEI(10kD)_{10Q}^{80R10}] adduct to 180°C for 70 h revealed that when heated for a prolonged time, the whole polymer decomposed already at this temperature. While the neat poly(ethylenimine) was soluble in water and polar to semi-polar solvents ranging from methanol to chloroform, the PEI(1.2kD)_{13Q} polymer was only soluble in methanol and water. The addition of large amounts of alkyl groups to the poly(ethylenimine) led to a shift of the solubility to semi-polar to non-polar solvents ranging from dichloromethane to heptane. The solubility behaviour of the PEI(10kD)_{10Q}^{60R14} polymer was found to be identical to that of the PEI(10kD)_{10Q}^{80R10} polymer which can be explained by the similar total number of carbon atoms of the alkyl chains of the polymers. Due to the good solubility of the PEI(10kD)_{10Q}^{80R10} and the PEI(10kD)_{10Q}^{60R14} polymer in non-polar solvents, it was assumed that these polymers should be well soluble in bitumen.

References

- 1 Allen G., Bevington J. C.; *Comprehensive Polymer Science* 3 (1989) 838 - 840
- 2 Von Harpe A., Petersen H., Li Y., Kissel T.; Characterization of commercially available and synthesized polyethylenimines for gene delivery; *Journal of Controlled Release* 69 (2000) 309 - 322
- 3 Petzold G., Schwarz S.; *Polyelectrolyte Complexes in Flocculation Applications; Advances in Polymer Science* 256 (2014) 25 - 66
- 4 Korus I., Bobik M., Nowak E.; Selective separation of Ni(II) and Cr(VI) ions by polymer enhanced ultrafiltration; *Membranes and Membrane Processes in Environmental Protection* 119 (2014) 37 - 48
- 5 Beckmann R., Beginn U.; Synthesis and Characterization of New Poly(ethyleneimine)-g-Poly(methylmethacrylate) Star-Block Copolymers with Hyperbranched Cationic Core; *Journal of Polymer Science Part A: Polymer Chemistry* 51 (2013) 3700 - 3715
- 6 Antonietti L., Aymonier C., Schlotterbeck U., Garamus V. M., Maksimova T., Richtering W., Mecking S.; Core-Shell-Structured Highly Branched Poly(ethylenimine amide)s: Synthesis and Structure; *Macromolecules* 38 (2005) 5914 - 5920
- 7 Goel V., Beginn U., Mourran A., Möller M.; 'Quat-Primer' Polymers Bearing Cationic and Reactive Groups: Synthesis, Characterization, and Application; *Macromolecules* 41 (2008) 8187 - 8197
- 8 Beckmann R.; "Quat - Primer" Polymers as Dispersants for Nanoparticles; *Dissertation* (2012)
- 9 Brandt M.; *New quat-alkyl-primer polymers for use in montmorillonite-nanocomposites* (2012)
- 10 Smith J. G.; Synthetically Useful Reactions of Epoxides; *Synthesis* 8 (1984) 629 - 656
- 11 Oswal S. L., Phalak R. P.; Viscosities of nonelectrolyte liquid mixtures. I. binary mixtures containing p-dioxane; *International Journal of Thermophysics* 13 (1992) 251 - 267
- 12 Haase R., Engels W.; Diffusion in the Liquid System Chloroform + Methyl Acetate; *Zeitschrift für Naturforschung* 41a (1986) 1337 - 1338
- 13 Masaro L., Zhu X. X.; Physical models of diffusion for polymer solutions, gels and solids; *Progress in Polymer Science* 24 (1999) 731 - 775
- 14 Shibaev V. P., Platé N. A., Freidzon Ya. S.; Thermotropic liquid crystalline polymers. I. Cholesterol-containing polymers and copolymers; *Journal of Polymer Science Part A: Polymer Chemistry* 17(1979) 1655 - 1670

- 15 Gautam K. S., Dhinojwala A.; Melting at Alkyl Side Chain Comb Polymer Interfaces; *Physical Review Letters* 88 (2002) 145501
- 16 Prasad S., Hanne L., Dhinojwala A.; Thermodynamic Study of a Novel Surface Ordered Phase above the Bulk Melting Temperature in Alkyl Side Chain Acrylate Polymers; *Macromolecules* 38 (2005) 2541 - 2543
- 17 Gautam K. S., Kumar S., Wermeille D., Robinson D., Dhinojwala A.; Observation of Novel Liquid-Crystalline Phase above the Bulk-Melting Temperature; *Physical Review Letters* 90 (2003) 215501
- 18 Rao M. A.; *Rheology of Fluid and Semisolid Foods: Principles and Applications* (2007)
- 19 ISO 6721-1:2011
- 20 Macosko C. W.; *Rheology: principles, measurements and applications* (1994)
- 21 Mezger T. G.; *The rheology handbook: for users of rotational and oscillatory rheometers* 2nd Edition (2006)
- 22 Ross-Murphy S. B.; Rheological characterization of gels; *Journal of Texture Studies* 26 (1995) 391 – 400
- 23 Beckedahl H., Paffrath T.; Bergischen Universität Wuppertal; *Straßenentwurf- und Straßenbau (SE-SB)*
- 24 Dimroth K., Reichardt C., Siepmann T., Bohlmann F.; Über Pyridinium-N-phenolbetaine und ihre Verwendung zur Charakterisierung der Polarität von Lösungsmitteln; *Justus Liebigs Annalen der Chemie* 661 (1963) 1 - 37
- 25 Reichardt C.; Solvatochromic Dyes as Solvent Polarity Indicators; *Chemical Reviews* 94 (1994) 2319 - 2358
- 26 Bodycomb J., Hara M.; Light Scattering Study of Ionomers in Solution. 4. Angular Measurements of Sulfonated Polystyrene Ionomers in a Polar Solvent (Dimethylformamide); *Macromolecules* 27 (1994) 7369 – 7377
- 27 *March's Advanced Organic Chemistry* 6th Edition (2007)
- 28 Taibakhsh M., Hosseinzadeh R., Alinezhad H., Ghahari S., Heydari A., Khaksar S.; Catalyst-Free One-Pot Reductive Alkylation of Primary and Secondary Amines and N,N-Dimethylation of Amino Acids Using Sodium Borohydride in 2,2,2-Trifluoroethanol; *Synthesis* (2011) 490 - 496

4 Preparation of [montmorillonite/PEI_xQ^{yR}] adducts

4.1 Introduction

The aim of this work is to completely exfoliate montmorillonite (MMT), and to surround the individual MMT-single layer platelets with a monomolecular coat of an alkyl-functionalized polymer, hence generating polymer-modified plate-shaped nanoparticles of high aspect ratio (Figure 4.1). A detailed overview about the work that has been done in the field of the modification of montmorillonite with organic molecules is given in Chapter 2.

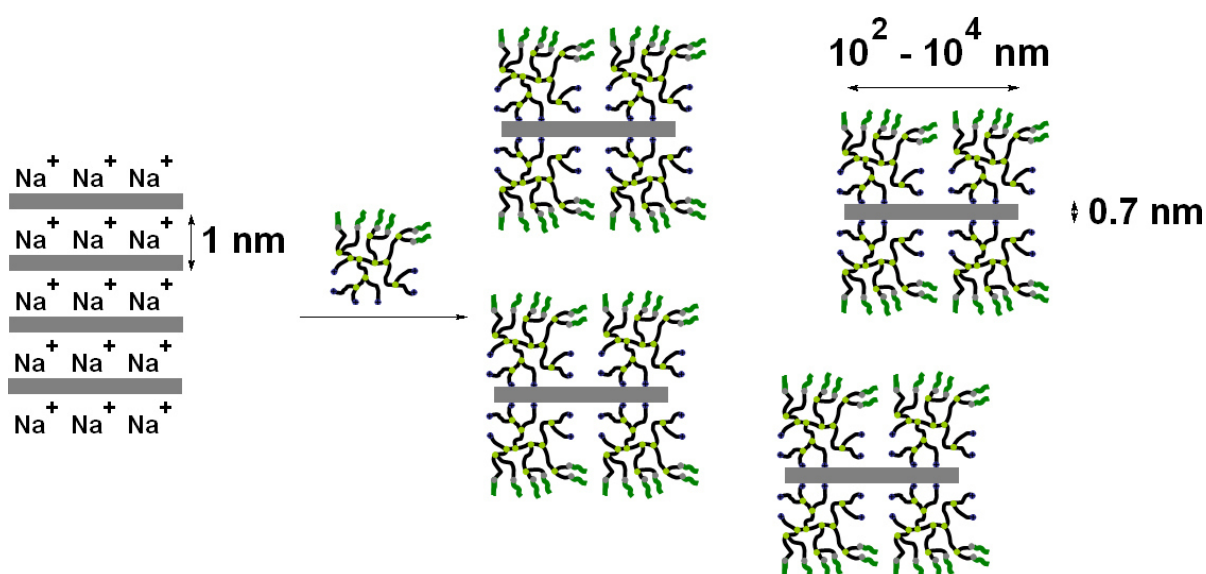


Figure 4.1: Preparation of polymer-coated anisotropic, plate-shaped nanoparticles by exfoliating, and polymer-coating of MMT layers

To allow for strong adsorption of the polymer on the MMT surface, the macromolecules shall be positively charged. This permits the replacement of mobile cations of the MMT against the covalently bound cations of the polymer. To create an alkyl-surface on the modified particles, the coating polymer must simultaneously bear covalently fixed alkyl groups. It was decided to use a hyperbranched polymer backbone, because this architecture provides a large number of terminal groups that are accessible to chemical modification, hence allowing to introduce the required number of cations, and alkyl groups per macromolecule [1, 2].

Hyperbranched poly(ethylenimine) was chosen as the architectural scaffold, because of its commercial availability, and the high reactivity of amine groups that make chemical modification feasible. The preparation and characterization of the used alkyl-quat-primer polymers, PEI(nkD)_{xQ}^{yR}, has been described in Chapter 3.

4 Preparation of [montmorillonite/PEI_xQ_yR] adducts

Within this Chapter the investigated pathways to obtain [MMT/PEI(nkD)_xQ^{yR}] nanoparticles is described. The polymer backbone consisted of poly(ethylenimine)s with two molecular weights, namely: **PEI(1)** (= PEI(1.2kD), with $M_n = 1,200$ g/mol, $M_w/M_n = 1.08$) and **PEI(2)** (= PEI(10kD), with $M_n = 10,000$ g/mol, $M_w/M_n = 2.5$).

Polymer **PEI(1)** was chosen because it exhibited a smaller diameter than polymer **PEI(2)**. Since the montmorillonite is able to swell in water, under enlargement of the gap between two montmorillonite platelets in the process, it was tried if the enlargement of the gap was sufficient to permit an intercalation of the polymer into the montmorillonite.

On the other hand, the high molar weight of polymer **PEI(2)** provides a higher number of primary and secondary amine groups, allowing more glycidyltrimethylammonium chloride molecules per polymer molecule to be added ensuring a strong attraction between the polymer and the montmorillonite.

The poly(ethylenimine)s were grafted with different quantities of glycidyltrimethylammonium chloride (5 – 20 mol%) and either 1,2-epoxydodecane (67 – 80 mol%) or 1,2-epoxyhexadecane (60 mol%) to investigate the influence of the degrees of the modifications on the final adducts.

To obtain [MMT/PEI(nkD)_xQ^{yR}] adducts, PEI(nkD)_xQ^{yR} alkyl-quat-primer polymers were added to Na-bentonite in an aqueous solution. The preparation conditions tried will be described in the following paragraphs.

4.2 Experimental part

4.2.1 Materials

Table 4.1: Used solvents

Solvent	Purity	Supplier
Ethanol	Technical	Berkel
Methanol	Technical	Stockmeier Chemie GmbH
Toluene	Technical	VWR Chemicals
Water	Deionized	

Table 4.2: Used chemicals

Reagent	Purity/Impurities	Supplier
PEI(10kD) _{5Q} ^{67R10}		Miriam Brandt [3]
Na-Bentonite batch <u>1</u> (= B1)	Main impurities: Cristobalite, quartz, iron	Alfa Aesar
Na-Bentonite batch <u>2</u> (= B2)	Main impurities: Quartz, calcite, iron; montmorillonite content \approx 72.0 wt. %	Alfa Aesar
1-Hexadecylamine	95 %	ABCR GmbH
(1-Hexadecyl)trimethylammonium bromide (= CTAB)	98 %	Alfa Aesar
Hydrochloric acid	37 %	Sigma-Aldrich
Sodium hydroxide	97 %	Fluka

4.2.2 Techniques

ATR-FT-IR investigations were performed using a Perkin Elmer Spectrum Two spectrometer equipped with a Perkin Elmer Spectrum Two universal diamond/ZnSe-ATR crystal or a Bruker Vertex 70 spectrometer equipped with a Golden Gate-Diamond-ATR unit. The samples were pressed on the ATR unit and measured in reflection. The scan resolution was set to be 4 cm⁻¹, each sample was scanned four times and an average spectrum was created.

Calcination experiments were performed with a Naber N 11 industrial oven. The samples were heated from 30 to 530°C with a heating rate of 10 K/minute. All experiments were performed in an air atmosphere without a lid. 25 g porcelain crucibles were used in which 100 to 200 mg of a sample was weighed.

Differential scanning calorimetry (DSC) measurements were performed with a Netzsch 204 F1 Phoenix thermal analyzer, equipped with a T-sensor and a Netzsch Intracooler. The DSC was calibrated against Bi, Hg, In, Sn and Zn standards. 5 to 15 mg samples were weighed in 25 μ L aluminium pans. The pans were sealed with a perforated lid. The samples were measured under an N₂ stream over a temperature range of -80 to 180°C and at a heating and cooling rate of 10 K/minute.

Scanning electron microscopy (SEM) was performed with a JEOL JSM-6510 scanning electron microscope. One droplet of a prepared dispersion (0.1 to 2.5 mg/mL solvent) was added onto an aluminium platelet and spin-coated with 2200 rpm for one minute. After spin-coating, the samples were sputtered with gold for twenty seconds with a sputtering current of 8 mA in a JEOL JFC-1200 Fine Coater. The samples were examined at a voltage of 10 kV.

Solid-state magic angle spinning nuclear magnetic resonance spectroscopy (MAS-NMR) ¹H-NMR (500 MHz) and ¹³C-NMR (125 MHz) measurements were recorded on a Bruker Avance III 500 spectrometer. The temperature was set to be 30°C and the samples were rotated at a frequency of 8 kHz at an angle of 54.7° oriented to the applied magnetic field. About 17 mg of the sample was weighed in 50 μ L ZrO₂ holder. 3 to 4 drops CDCl₃ were added to lower the viscosity. The chemical shifts were given in parts per million (ppm). The measurements were performed using a high-resolution magic angle spinning (HR-MAS) probe with the label: 4 mm HRMAS 1H/2H/13C/31P Z-GRD B3175/0476. The software used to acquire the data was called Bruker Topspin 2.1.

The melting point was measured with a Stuart melting point apparatus SMPB2 device under ambient atmosphere with a heating rate of 10°C/minute.

Thermogravimetric (TGA) measurements were performed with an NETZSCH STA 449 C Jupiter Thermo-microbalance in the temperature region of 30 - 530°C at a heating rate of 10 K/minute and under a He stream. 25 μ L aluminium pans were used in which 8 to 16 mg of a sample was weighed. The pans weren't covered by a lid.

X-ray diffraction (XRD) measurements were performed with a Panalytical X'Pert Pro Diffractometer, equipped with a copper cathode and a Bragg-Brentano geometry. Measurements were done with a voltage of 40 kV and a current of 40 mA. About 100 mg of a sample was measured between $2\theta = 5 - 79^\circ$ with a step width of 0.033423°/s. Samples that exhibited a good adhesion with alumina platelets were

4 Preparation of [montmorillonite/PEI_xQ_yR] adducts

measured between $2\theta = 0.15 - 10^\circ$ at a voltage of 40 kV and a current of 40 mA. The samples were positioned perpendicularly and measured with a step width of $0.0005^\circ/\text{s}$.

X-ray fluorescence (XRF) was measured with a PANalytical AXios 1 kW XRF spectrometer at 35°C . 0.4 to 1 g of a powder sample was weighed into a polypropylene holder, and measured under a He stream. The device was equipped with a PANalytical Rh SST tube. The calibration of the device was performed with PANalytical standards containing mixtures of elements. Depending on the element a set containing a specific filter, crystal, voltage, amperage, angle (given on $^\circ 2\theta$), and detector (flow or scintillator) was used. The software used was named Omnian, the element concentration in the sample was calculated with the pulse height analysis and expressed in kcps (kilo counts per second).

4.2.3 Reaction of PEI(nkD)_xQ with Na-MMT

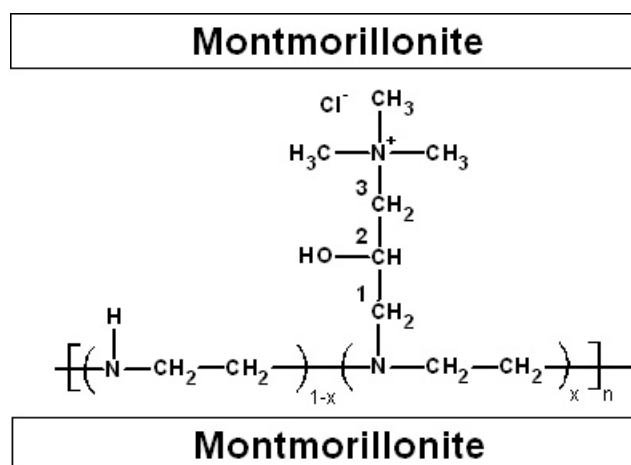


Figure 4.2: Structure of montmorillonite/poly[ethylenimine-co-(ethylenimine-g-{2-hydroxypropyl-3-(N,N,N-trimethylammonium chloride)})] (MMT/PEI(nkD)_xQ)

(E1) Preparation of [MMT_{B1}/PEI(1.2kD)_{13Q}]

5.1 g Na-bentonite **B1** (cf. Table 4.2) was stirred with a mechanical stirrer (KPG, 150 rpm) in 204 mL deionized water for 24 h at 65°C . 1.6 g (0.026 mol) PEI(1.2kD)_{13Q} (= **PA1**, cf. Chapter 3) was dissolved in 10 mL deionized water and added to the bentonite solution. Afterwards, the mixture was stirred for another 48 h at 65°C . The mixture was then centrifuged at 2817 g (2817 times the acceleration due to gravity) for 10 minutes. The sediment was collected, slurried in 30 mL methanol and again centrifuged at 2817 g for 10 minutes. Afterwards, the sediment was collected and dried under vacuum at 80°C for 96 h. The substance appeared grey after drying and

4 Preparation of [montmorillonite/PEI_xQyR] adducts

gave a powder after grinding. The yield was not determined.

DSC: No glass or melting transitions; IR (ATR; ν [cm⁻¹]): 3624, 3361, 2980, 2925, 2854, 1658, 1473, 1111, 998, 913, 843, 514; TGA: Organic material: 14.4 wt.% (theory: 23.9 wt.%), polymer decomposition temperature 230°C; XRD (wide-angle): Lattice constant $c = 1.43 \pm 0.06$ nm; XRF (wt.%): Si (61.8), Al (18.8), Fe (11.8), Mg (2.3), Ca (2.3), Cl (1.4), K (0.8), Na (0.5), S (0.3)

4.2.4 Reaction of PEI(nkD)_xQ^{yR10} with Na-MMT

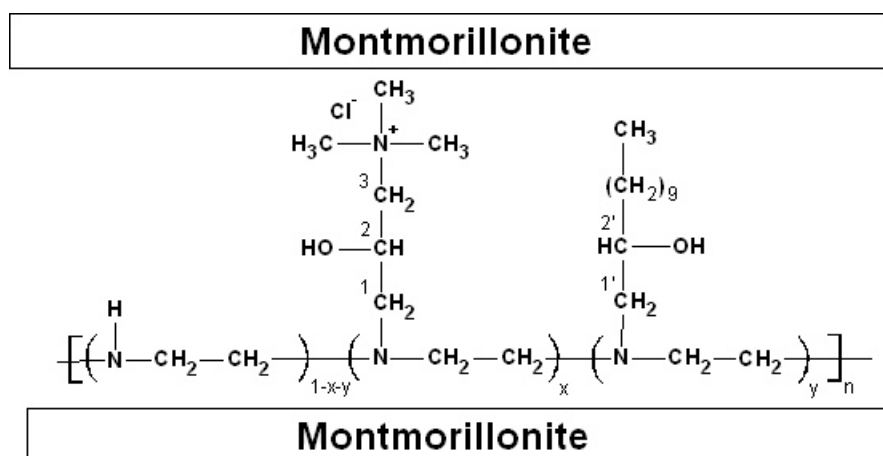


Figure 4.3: Structure of montmorillonite/poly[ethyleneimine-co-(ethyleneimine-g-{2-hydroxydecyl})-co-(ethyleneimine-g-{2-hydroxypropyl-3-(N,N,N-trimethylammonium chloride)})] (MMT/PEI(nkD)_xQ^{yR10})

(E2) Preparation of [MMT_{B1}/PEI(10kD)_{5Q}^{67R10}]

60.0 g Na-bentonite **B1** (cf. Table 4.2) was stirred with a mechanical stirrer (KPG, 300 rpm) in 1.2 L deionized water for 4 h at ambient temperature. 58.1 g (0.334 mol) PEI(10kD)_{5Q}^{67R10} (= **PB3**, cf. Chapter 3) was dispersed in 400 mL ethanol and added to the bentonite solution. Afterwards, the mixture was stirred for another 48 h at 65°C. The mixture was then centrifuged at 2817 g (2817 times the acceleration due to gravity) for 10 minutes. The sediment was collected and dried in a desiccator over 202 g CaCl₂ and under reduced pressure at ambient temperature for 216 h. The substance appeared grey after drying and gave a powder after grinding. The yield was 112.9 g (95.6 % of theory).

DSC: T_G = -46.2°C; IR (ATR; ν [cm⁻¹]): 3627, 3360, 2956, 2923, 2852, 1639, 1463, 1374, 1008, 917, 846, 515; TGA: Organic material: 66.3 wt.% (theory: 49.2 wt.%), polymer decomposition temperature 240°C; XRD (wide-angle): Lattice constant $c = 1.44 \pm 0.14$ nm; XRF (wt.%): Si (59.9), Al (17.2), Fe (9.4), Ca (6.6), Cl (2.2), Mg (2.1),

4 Preparation of [montmorillonite/PEI_xQyR] adducts

K (1.0), S (0.9), Na (0.7)

(E3) Preparation of [MMT_{B1}/PEI(10kD)_{10Q}^{80R10}]

1.5 g Na-bentonite **B1** (cf. Table 4.2) was stirred with a mechanical stirrer (KPG, 150 rpm) in 58 mL deionized water for 24 h at 70°C in the presence of 0.5 mL hydrochloric acid (37 %). 2.0 g (0.010 mol) PEI(10kD)_{10Q}^{80R10} (= **PB4.1**, cf. Chapter 3) was dispersed in 20 mL ethanol and added to the bentonite solution. Afterwards, the mixture was stirred for another 48 h at 70°C. Afterwards, 6.5 mL of a NaOH solution (10 wt.% in water) was added and the mixture was then centrifuged at 2817 g (2817 times the acceleration due to gravity) for 10 minutes. The sediment was collected, slurried in 10 mL ethanol and again centrifuged at 2817 g for 10 minutes. The sediment was collected and dried under vacuum at 70°C for 48 h. The substance appeared brown after drying and gave a powder after grinding. The yield was not determined.

DSC: $T_G = -40.1^\circ\text{C}$; IR (ATR; ν [cm^{-1}]): 3624, 3386, 2955, 2922, 2852, 1655, 1466, 1113, 1011, 914, 515; TGA: Organic material: 50.5 wt.% (theory: 57.1 wt.%), polymer decomposition temperature 220°C; XRD (wide-angle): Lattice constant $c = 2.94 \pm 0.40$ nm; XRF (wt.%): Si (60.5), Al (17.4), Fe (13.6), Cl (3.5), Mg (2.2), Ca (1.3), K (0.9), S (0.5), Na (0.2)

4.2.5 Reaction of CTAB with Na-MMT

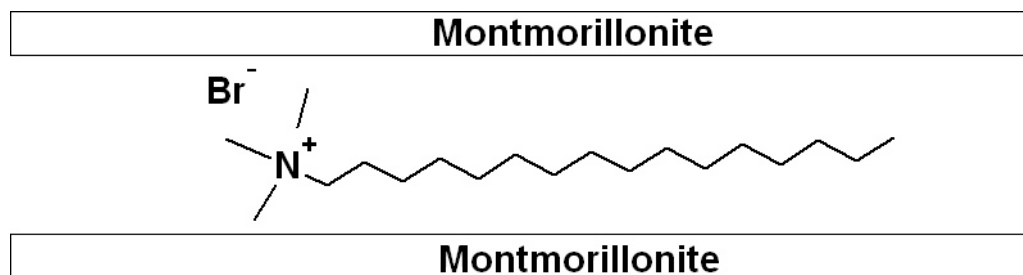


Figure 4.4: Structure of montmorillonite/(1-hexadecyl)trimethylammonium bromide (MMT/CTAB)

(E4.10) Preparation of [MMT_{B1}/CTAB]

40.0 g Na-bentonite **B1** (cf. Table 4.2) was stirred with a mechanical stirrer (KPG, 150 rpm) in 2.0 L deionized water for 4 h at 65°C. 60.0 g (0.1646 mol) CTAB was then added and the mixture was stirred for another 24 h. The mixture was then centrifuged at 4472 g (4472 times the acceleration due to gravity) for 10 minutes. The sediment was collected and dried under vacuum at 80°C for 94 h. After drying, 51.2 g (51.2 wt.% of theory) of a grey substance was obtained.

4 Preparation of [montmorillonite/PEI_xQyR] adducts

¹H-MAS-NMR (CDCl₃, δ [ppm]): 3.59 (2 H, -N-CH₂-CH₂-), 3.35 (9 H, -N-(CH₃)₃), 1.94 (2 H, -N-CH₂-CH₂-CH₂-), 1.54 (2 H, -CH₂-CH₂-CH₃), 1.45 (24 H, CH₃-CH₂-(CH₂)₁₂-CH₂-), 1.03 (3 H, -CH₂-CH₃); ¹³C-MAS-NMR (CDCl₃, δ [ppm]): 66.9 (-N-CH₂-CH₂-), 53.3 (-N-(CH₃)₃), 31.8 (-CH₂-CH₂-CH₂-CH₃), 29.2 (CH₃-CH₂-CH₂-(CH₂)₁₀-CH₂-), 26.1 (-N-CH₂-CH₂-CH₂-), 23.1 (-N-CH₂-CH₂-CH₂-CH₂-), 22.5 (-CH₂-CH₂-CH₃), 13.9 (-CH₂-CH₃); DSC: T_{M1} = 47.7°C, T_{M2} = 98.2°C; IR (ATR; ν [cm⁻¹]): 3627, 3395, 2917, 2849, 1642, 1486, 1472, 1463, 1114, 1007, 911, 515; TGA: Organic content: 45.5 wt.% (theory: 60.0 wt.%), CTAB decomposition temperatures 190°C, 300°C, 390°C; XRD (wide-angle): Lattice constant c₍₁₎ = 1.32 nm (single layer CTAB) and lattice constant c₍₂₎ = 1.96 nm (double/pseudo trimolecular layer CTAB); XRF (wt.%): Si (47.5), Br (30.1), Al (11.7), Fe (7.0), Mg (1.4), Ca (1.1), K (0.6), S (0.3), Na (0.3)

Table 4.3: Prepared batches of adduct E4

Entry	Bitumen batch	Prepared quantity (g)	Yield (wt.% of th.)	CTAB content (wt.% of th.)
<u>E4.1</u>	1	238.2	86.9	53.6 (a)
<u>E4.2</u>	1	224.1	84.6	58.5 (a)
<u>E4.3</u>	1	268.2	not determined	not determined
<u>E4.4</u>	1	268.2	not determined	not determined
<u>E4.5</u>	1	268.2	not determined	not determined
<u>E4.6</u>	1	918.4	82.5	not determined
<u>E4.7</u>	1			
<u>E4.8</u>	1			
<u>E4.9</u>	1			
<u>E4.10</u>	1	51.2	51.2	45.5 (a)
<u>E4.11</u>	1	56.0	56.0	not determined

(a) = TGA, CTAB = (1-hexadecyl)trimethylammonium bromide

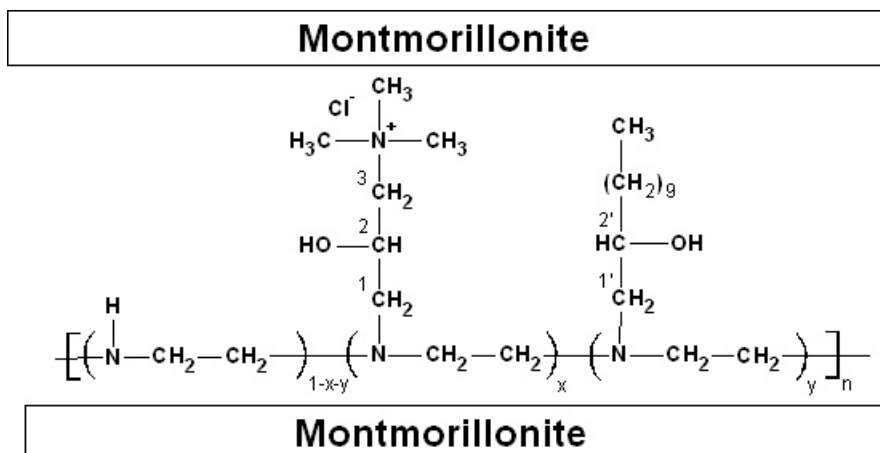
4.2.6 Reaction of PEI(nkD)_xQ^{yR10} with [MMT/CTAB]

Figure 4.5: Structure of montmorillonite/poly[ethylenimine-co-(ethylenimine-g-{2-hydroxydecyl})-co-(ethylenimine-g-{2-hydroxypropyl-3-(N,N,N-trimethylammonium chloride)})] (MMT/PEI(nkD)_xQ^{yR10})

(E5) Preparation of [MMT_{B1}/PEI(1.2kD)_{13Q}]

11.6 g [MMT_{B1}/CTAB] (= mixture of adduct **E4.1** and **E4.2**, averagely 44.0 wt.% bentonite) was stirred with a mechanical stirrer (KPG, 150 rpm) in 204 mL deionized water for 24 h at 65°C. 1.6 g (0.026 mol) PEI(1.2kD)_{13Q} (= **PA1**, cf. Chapter 3) was dissolved in 10 mL deionized water and added to the [MMT_{B1}/CTAB] solution. Afterwards, the mixture was stirred for another 48 h at 65°C. The mixture was then centrifuged at 2817 g (2817 times the acceleration due to gravity) for 10 minutes. The sediment was collected, slurried in 30 mL methanol and again centrifuged at 2817 g for 10 minutes. Afterwards, the sediment was collected and dried under vacuum at 80°C for 96 h. The substance appeared grey after drying and gave a powder after grinding. The yield was not determined.

¹H-MAS-NMR (D₂O, δ [ppm]): 3.27 – 3.40 (11H_Q, -N(CH₃)₃), -CH-CH₂-N(CH₃)₃), 3.00 – 2.50 (4H_{PEI}, 2H_Q, D-CH₂-CH₂-D, D-CH₂-CH₂-L, D-CH₂-CH₂-T, L-CH₂-CH₂-L, L-CH₂-CH₂-T, PEI-NH-CH₂-CHOH-, PEI-N-CH₂-CHOH-); DSC: T_M = 45.9°C; IR (ATR; ν [cm⁻¹]): 3625, 3399, 2918, 2849, 1644, 1468, 1114, 1013, 913, 844, 517; TGA: Organic content: 30.3 wt.% (theory: 23.9 wt.%), polymer decomposition temperatures 198°C, 300°C, 380°C, XRD (wide-angle): Lattice constant c = 2.03 ± 0.20 nm; XRF (wt.%): Si (58.4), Al (15.3), Br (13.2), Fe (8.7), Mg (1.8), Ca (1.1), K (0.8), Cl (0.5), Na (0.2), S (0.02)

(E6) Preparation of [MMT_{B1}/PEI(1.2kD)_{20Q}^{80R10}]

4.6 g [MMT_{B1}/CTAB] (= mixture of adduct **E4.1** and **E4.2**, averagely 44.0 wt.% bentonite) was stirred with a mechanical stirrer (KPG, 150 rpm) in 58 mL deionized water for 24 h at 70°C. Then, 2.0 g (0.009 mol) PEI(1.2kD)_{20Q}^{80R10} (= **PA2**, cf. Chapter **3**) was dispersed in 8 mL ethanol and added to the [MMT_{B1}/CTAB] solution. Afterwards, the mixture was stirred for another 48 h at 65°C. The mixture was then centrifuged at 2817 g (2817 times the acceleration due to gravity) for 10 minutes. The sediment was collected, slurried in 10 mL ethanol and again centrifuged at 2817 g for 10 minutes. Afterwards, the sediment was collected and dried under vacuum at 70°C for 48 h. The substance appeared grey after drying and was amorphous. The yield was not determined.

¹H-MAS-NMR (CDCl₃, δ [ppm]): 5.00 – 4.00 (4 H_{PEI}, D-CH₂-CH₂-D, D-CH₂-CH₂-L, D-CH₂-CH₂-T, L-CH₂-CH₂-D, L-CH₂-CH₂-L, L-CH₂-CH₂-T, T-CH₂-CH₂-D, T-CH₂-CH₂-L, PEI-NH-CH₂-CHOH-, PEI-N-CH₂-CHOH-), 3.90 – 3.45 (1 H_{R10}, -CH₂-CHOH-CH₂-), 3.45 – 3.00 (11 H_Q, -CH-CH₂-N(CH₃)₃, -N(CH₃)₃), 3.00 – 2.00 (4 H_{PEI}, 2 H_Q, 2 H_{R10}, D-CH₂-CH₂-D, D-CH₂-CH₂-L, D-CH₂-CH₂-T, L-CH₂-CH₂-D, L-CH₂-CH₂-L, L-CH₂-CH₂-T, T-CH₂-CH₂-D, T-CH₂-CH₂-L, PEI-NH-CH₂-CHOH-, PEI-N-CH₂-CHOH-), 2.00 – 1.00 (18 H_{R10}, -CHOH-(CH₂)₉-CH₃-), 0.90 – 0.80 (3 H_{R10}, -(CH₂)₉-CH₃); ¹³C-MAS-NMR (CDCl₃, δ [ppm]): 35.4 (-CHOH-CH₂-CH₂-), 32.0 (-CH₂-CH₂-CH₂-CH₃), 29.8 (-CHOH-CH₂-CH₂-(CH₂)₅-CH₂-), 25.9 (-CHOH-CH₂-CH₂-(CH₂)₅-), 22.8 (-CH₂-CH₂-CH₃), 14.2 (-CH₂-CH₃); DSC: T_G = -28.1°C; IR (ATR; ν [cm⁻¹]): 3625, 3394, 2953, 2919, 2850, 1648, 1464, 1377, 1070, 1009, 912, 839, 514; TGA: Organic material: 51.8 wt.% (theory: 50.0 wt.%), polymer decomposition temperature 250°C; XRD: Lattice constant c_(wide-angle) = 4.44 ± 3.08 nm and lattice constant c_(small-angle) = 4.77 ± 0.70 nm; XRF (wt.%): Si (53.2), Br (15.1), Al (13.3), Fe (11.6), Cl (2.3), Mg (1.6), Ca (1.3), Na (0.7), K (0.7), S (0.2)

4.2.8 Reaction of PEI(nkD)_xQ^{yR} with Na-MMT in the presence of CTAB or 1-hexadecylamine

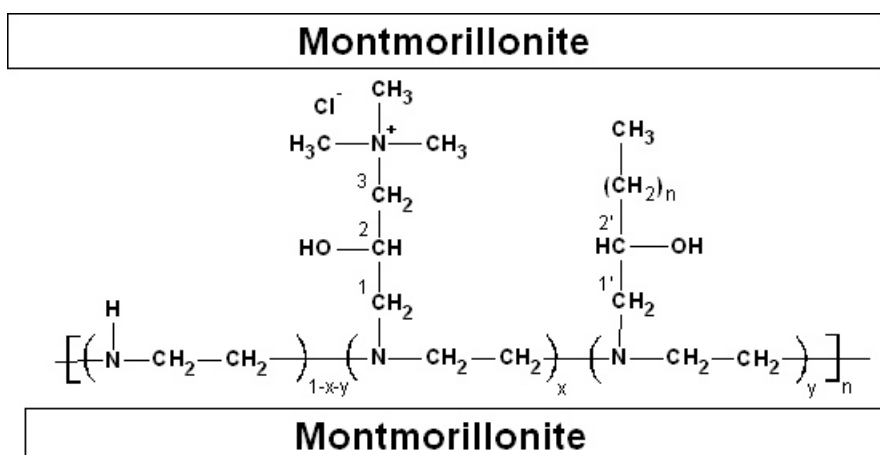


Figure 4.6: Structure of MMT/PEI(nkD)_xQ^{yR}, (R = 2-hydroxydodecane or 2-hydroxyhexadecane)

(E7) Preparation of [MMT_{B1}/PEI(10kD)_{10Q}^{80R10}] by using an acid activated bentonite

36.9 g Na-bentonite **B1** (cf. Table 4.2) was stirred with a mechanical stirrer (KPG, 150 rpm) in 1.7 L deionized water for 24 h at 35°C. Afterwards, 24.8 g (0.103 mol) 1-hexadecylamine was protonated by the addition of 12 mL hydrochloric acid (37 %) in 50 mL deionized water and added to the bentonite solution. The mixture was then stirred for 72 h. 37.6 g (0.183 mol) PEI(10kD)_{10Q}^{80R10} (= **PB2**, cf. Chapter 3) dispersed in 225 mL ethanol and 58 g of a NaOH solution (10 wt.% in water) were then added and the mixture was stirred for another 48 h. Afterwards, the mixture was centrifuged at 2817 g (2817 times the acceleration due to gravity) for 10 minutes. The sediment was collected, slurried 4 times in 100 mL ethanol and centrifuged each time. The sediment was collected and dried under vacuum at 70°C for 79 h. The substance appeared grey after drying and gave a powder after grinding. The yield was 76.3 g (102.3 % of theory).

DSC: T_g = -5°C; IR (ATR; ν [cm⁻¹]): 3624, 3330, 2955, 2917, 2850, 1645, 1566, 1485, 1466, 1392, 1071, 1008, 914, 514; TGA: Organic material: 56.5 wt.% (theory: 50.5 wt.%), polymer decomposition temperature 220°C; XRD: Lattice constant c was not accessible from wide-angle measurements; XRF (wt.%): Si (56.1), Fe (17.8), Al (16.1), Cl (3.6), Ca (2.7), Mg (1.8), K (1.2), Na (0.4), S (0.3)

(E8.2) Preparation of [MMT_{B1}/PEI(10kD)_{10Q}^{80R10}]

91.0 g Na-bentonite **B1** (cf. Table 4.2) was stirred with a mechanical stirrer (KPG, 150 rpm) in 4.6 L deionized water for 4 h at 65 °C. Afterwards, 136.5 g (0.375 mol) CTAB was added and the mixture was stirred further for 70 h. 171.6 g (0.834 mol) PEI(10kD)_{10Q}^{80R10} (**PB4.1**, cf. Chapter 3), dispersed in 0.75 L ethanol was then added and the mixture was stirred for another 48 h. Afterwards, the mixture was centrifuged at 4472 g (4472 times the acceleration due to gravity) for 10 minutes. The sediment was collected, slurried in 300 mL toluene/methanol (V/V) and again centrifuged. The sediment was collected and dried under vacuum at 80 °C for 94 h. The substance appeared brown after drying and was amorphous. The yield was 233.7 g (89.0 % of theory).

¹H-MAS-NMR (CDCl₃, δ [ppm]): 5.20 – 4.10 (4 H_{PEI}, D-CH₂-CH₂-D, D-CH₂-CH₂-L, D-CH₂-CH₂-T, L-CH₂-CH₂-D, L-CH₂-CH₂-L, L-CH₂-CH₂-T, T-CH₂-CH₂-D, T-CH₂-CH₂-L, PEI-NH-CH₂-CHOH-, PEI-N-CH₂-CHOH-), 4.40 (1 H_Q, -CH₂-CHOH-CH₂-), 3.70 – 3.45 (1 H_{R10}, -CH₂-CHOH-CH₂-), 3.45 – 3.25 (11 H_Q, -CH-CH₂-N(CH₃)₃, -N(CH₃)₃), 3.00 – 2.10 (4 H_{PEI}, 2 H_Q, 2 H_{R10}, D-CH₂-CH₂-D, D-CH₂-CH₂-L, D-CH₂-CH₂-T, L-CH₂-CH₂-D, L-CH₂-CH₂-L, L-CH₂-CH₂-T, T-CH₂-CH₂-D, T-CH₂-CH₂-L, PEI-NH-CH₂-CHOH-, PEI-N-CH₂-CHOH-), 1.80 – 0.90 (18 H_{R10}, -CHOH-(CH₂)₉-CH₃-), 0.90 – 0.80 (3 H_{R10}, -(CH₂)₉-CH₃); ¹³C-MAS-NMR (CDCl₃, δ [ppm]): 35.2 (-CHOH-CH₂-CH₂-), 31.9 (-CH₂-CH₂-CH₂-CH₃), 29.7 - 29.3 (-CHOH-CH₂-CH₂-(CH₂)₅-CH₂-), 25.8 (-CHOH-CH₂-CH₂-(CH₂)₅-), 22.6 (-CH₂-CH₂-CH₃), 14.0 (-CH₂-CH₃); DSC: T_G = -23.2 °C; IR (ATR; ν [cm⁻¹]): 3625, 3385, 2953, 2921, 2851, 1658, 1465, 1376, 1071, 1014, 915, 515; TGA: Organic material: 67.9 wt.% (theory: 65.4 wt.%), decomposition temperature polymer 240 °C; XRD: Lattice constant c_(wide-angle) 4.66 ± 1.58 nm and lattice constant c_(small-angle) = 6.89 ± 2.95 nm; XRF (wt.%): Si (50.7), Br (25.7), Al (11.3), Fe (8.5), Mg (1.3), Cl (1.0), Ca (0.7), K (0.6), S (0.3), Na (0.1)

With the preparation procedure described with adduct **E8.2** four additional adducts, **E11** – **E14**, were prepared with a different amount of polymer used with each sample. With adduct **E10**, the concentration of the Na-bentonite in water was lowered from 20 g (as with adduct **E8.2**) to 10 g bentonite per litre water.

Table 4.4: Prepared batches of adduct E8

Entry	Used polymer (cf. Chapter 3)	Bitumen batch	Prepared quantity (g)	Yield (wt.% of theory)
<u>E8.1</u>	<u>PB4.1</u>	1	260.7	66.3
<u>E8.2</u>	<u>PB4.3</u>	1	234.0	89.0
<u>E8.3</u>	<u>PB4.3</u>	1	255.1	97.0
<u>E8.4</u>	<u>PB4.3, PB4.4</u>	1	262.9	99.0
<u>E8.5</u>	<u>PB4.4</u>	1	261.1	99.0
<u>E8.6</u>	<u>PB4.4</u>	1	260.1	99.0
<u>E8.7</u>	<u>PB4.5</u>	1	262.4	99.9
<u>E8.8</u>	<u>PB4.5, PB4.6</u>	1	258.4	98.4
<u>E8.9</u>	<u>PB4.8</u>	1	259.2	96.4
<u>E8.10</u>	<u>PB4.1, PB4.2</u>	1	273.2	103.4
<u>E8.11</u>	<u>PB4.9</u>	1	266.8	101.6
<u>E8.12</u>	<u>PB4.10</u>	1	1254.4	99.7
<u>E8.13</u>	<u>PB4.11</u>	1	1258.0	not determined
<u>E8.14</u>	<u>PB4.12</u>	1	665.2	not determined
<u>E8.15</u>	<u>PB4.13</u>	2	1038.8	94.4
<u>E8.16</u>	<u>PB4.14</u>	2	1052.2	95.7
<u>E8.17</u>	<u>PB4.15</u>	2	1015.1	92.3
<u>E8.18</u>	<u>PB4.16</u>	2	1059.1	96.3
<u>E8.19</u>	<u>PB4.17</u>	2	1029.4	93.4
<u>E8.20</u>	<u>PB4.18</u>	2	14.0	62.9
<u>E8.21</u>	<u>PB4.19</u>	2	161.2	85.1
<u>E8.22</u>	<u>PB4.20</u>	2	1008.0	91.6

(E9) Preparation of an [MMT_{B2}/PEI(10kD)_{10Q}^{80R10}] adduct in a concentrated solution

2.5 g Na-bentonite **B2** (cf. Table 4.2) was slurried in 2.5 mL deionized water. Then, 3.8 g (0.010 mol) CTAB was slurried in 3.9 mL deionized water and added. 4.8 g (0.023 mol) PEI(10kD)_{10Q}^{80R10} (**PB4.17**, cf. Chapter 3), dispersed in 5 mL ethanol was then added and the mixture was stirred with a mechanical stirrer (KPG, 150 rpm) for 66 h at 65 °C. Afterwards, the mixture was centrifuged at 2817 g (2817 times the acceleration due to gravity) for 10 minutes. The sediment was collected, slurried in 7.2 mL toluene/methanol (V/V) and again centrifuged. The sediment was again collected and the cleaning step was performed another two times. Afterwards, the sediment was dried under vacuum at 80 °C for 68 h. The substance appeared green-brown

4 Preparation of [montmorillonite/PEI_xQyR] adducts

after drying and was amorphous. The yield was 3.7 g (50.7 % of theory).

¹H-MAS-NMR (CDCl₃, δ [ppm]): 5.20 – 4.10 (4 H_{PEI}, D-CH₂-CH₂-D, D-CH₂-CH₂-L, D-CH₂-CH₂-T, L-CH₂-CH₂-D, L-CH₂-CH₂-L, L-CH₂-CH₂-T, T-CH₂-CH₂-D, T-CH₂-CH₂-L, PEI-NH-CH₂-CHOH-, PEI-N-CH₂-CHOH-), 4.40 (1 H_Q, -CH₂-CHOH-CH₂-), 3.70 – 3.45 (1 H_{R10}, -CH₂-CHOH-CH₂-), 3.45 – 3.25 (11 H_Q, -CH-CH₂-N(CH₃)₃, -N(CH₃)₃), 3.00 – 2.10 (4 H_{PEI}, 2 H_Q, 2 H_{R10}, D-CH₂-CH₂-D, D-CH₂-CH₂-L, D-CH₂-CH₂-T, L-CH₂-CH₂-D, L-CH₂-CH₂-L, L-CH₂-CH₂-T, T-CH₂-CH₂-D, T-CH₂-CH₂-L, PEI-NH-CH₂-CHOH-, PEI-N-CH₂-CHOH-), 1.80 – 0.90 (18 H_{R10}, -CHOH-(CH₂)₉-CH₃-), 0.90 – 0.80 (3 H_{R10}, -(CH₂)₉-CH₃); ¹³C-MAS-NMR (CDCl₃, δ [ppm]): 35.2 (-CHOH-CH₂-CH₂-), 31.9 (-CH₂-CH₂-CH₂-CH₃), 29.7 - 29.3 (-CHOH-CH₂-CH₂-(CH₂)₅-CH₂-), 25.8 (-CHOH-CH₂-CH₂-(CH₂)₅-), 22.6 (-CH₂-CH₂-CH₃), 14.0 (-CH₂-CH₃); Calcination: Organic material: 65.9 wt.% (theory: 65.8 wt.%); DSC: T_G = -25.0 °C; IR (ATR; ν [cm⁻¹]): 3625, 3381, 2953, 2920, 2851, 1653, 1465, 1377, 1067, 1009, 913, 514; XRD (wide-angle): Lattice constant c = 4.29 ± 0.50 nm; XRF (wt.%): Si (45.0), Br (24.1), Al (10.6), Fe (10.1), Ca (4.8), Mg (2.0), Cl (1.5), K (1.3), S (0.4), Na (0.3)

(E15.8) Preparation of [MMT_{B2}/PEI(10kD)_{10Q}^{60R14}]

301.9 g Na-bentonite **B2** (cf. Table 4.2) was stirred with a mechanical stirrer (KPG, 110 rpm) in 10.7 L deionized water for 4 h at 65 °C. Afterwards, 285.3 g (0.783 mol) CTAB was added and the mixture was stirred further for 24 h. 347.3 g (1.715 mol) PEI(10kD)_{10Q}^{60R14} (= **PC2.7**, cf. Chapter 3), dispersed in 0.65 L isopropanol was then added and the mixture was stirred for another 92 h. Afterwards, the mixture was centrifuged at 4472 g (4472 times the acceleration due to gravity) for 10 minutes. The sediment was collected, slurried in 650 mL toluene/methanol (V/V) and again centrifuged. The sediment was collected, again slurried in 500 mL toluene/methanol (V/V) and centrifuged. The sediment was collected and dried under vacuum at 80 °C for 113 h. The substance appeared green-white after drying and gave a powder after grinding. The yield was 455.1 g (70.1 % of theory).

¹H-MAS-NMR (CDCl₃, δ [ppm]): 5.10 – 4.10 (4 H_{PEI}, D-CH₂-CH₂-D, D-CH₂-CH₂-L, D-CH₂-CH₂-T, L-CH₂-CH₂-D, L-CH₂-CH₂-L, L-CH₂-CH₂-T, T-CH₂-CH₂-D, T-CH₂-CH₂-L, PEI-NH-CH₂-CHOH-, PEI-N-CH₂-CHOH-), 4.30 (1 H_Q, -CH₂-CHOH-CH₂-), 3.90 – 3.50 (2 H_{R14(a)}, 1 H_{R14(b)}, PEI-CH-CH₂OH, -CH₂-CHOH-CH₂-), 3.50 – 3.20 (11 H_Q, -CH-CH₂-N(CH₃)₃), 3.00 – 2.10 (4 H_{PEI}, 2 H_Q, 2 H_{R14(b)}, 1 H_{R14(a)}, D-CH₂-CH₂-D, D-CH₂-CH₂-L, D-CH₂-CH₂-T, L-CH₂-CH₂-D, L-CH₂-CH₂-L, L-CH₂-CH₂-T, T-CH₂-CH₂-D, T-CH₂-CH₂-L, PEI-CH₂-CHOH-, PEI-CH-CH₂OH-), 1.80 – 0.95 (26 H_{R14}, -CHOH-(CH₂)₁₃-CH₃-), 0.90 – 0.40 (3 H_{R14}, -(CH₂)₁₃-CH₃); ¹³C-MAS-NMR (CDCl₃, δ [ppm]): 53.3 (CTAB, -N-

4 Preparation of [montmorillonite/PEIxQyR] adducts

(CH₃)₃), 31.8 (-CH₂-CH₂-CH₂-CH₃), 29.6 - 29.2 (-CHOH-CH₂-CH₂-(CH₂)₉-CH₂-), 25.8 (-CHOH-CH₂-CH₂-(CH₂)₉-), 22.5 (-CH₂-CH₂-CH₃), 13.9 (-CH₂-CH₃); **Calcination:** Organic material: 60.6 wt.% (theory: 53.5 wt.%); **DSC:** T_M = 16.9 °C; **IR (ATR; ν [cm⁻¹]):** 3625, 3370, 2954, 2917, 2849, 1651, 1467, 1069, 1007, 912, 839, 512; **XRD (wide-angle):** Lattice constant c = 4.04 ± 0.40 nm; **XRF (wt.%):** Si (42.0), Br (29.9), Al (10.0), Fe (9.1), Ca (4.0), Mg (1.8), Cl (1.7), K (1.1), S (0.4), Na (0.1)

Table 4.5: Prepared batches of adduct E15

Entry	Bitumen batch	Used polymer (cf. Chapter 3)	Prepared quantity (g)	Yield (wt.% of theory)
E15.1	2	PC2.3 (a)	34.7	106.0
E15.2	2	PC2.3 (b)	3.9	89.3
E15.3	2	PC2.3 (c)	3.5	79.5
E15.4	2	PC2.3 (a)	3.7	85.2
E15.5	2	PC2.3 (d)	4.3	98.2
E15.6	2	PC2.5 (d)	360.0	55.4
E15.7	2	PC2.6 (d)	311.1	45.9
E15.8	2	PC2.7 (d)	942.6	70.1
E15.9	2	PC2.8 (d)		
E15.10	2	PC2.9 (d)	136.4	104.1
E15.11	2	PC2.10 (d)	142.6	107.0
E15.12	2	PC2.11 (d)	619.6	81.4
E15.13	2	PC2.12 (d)	722.4	88.4

(a) = dispersed in ethanol, (b) = dispersed in 1,4-dioxane, (c) = dispersed in methanol, (d) = dispersed in 2-propanol

4.3 Results and Discussion

In this study PEI(nkD)_xQ^{yR} polymers were attempted to intercalate into montmorillonite to form [MMT/PEI(nkD)_xQ^{yR}] adducts. The term “adduct” was chosen instead of the generally used term “nanocomposite” [4] since the alkyl-quat-primer polymers were strongly attached to the montmorillonite due to a cooperative electrostatic interaction. The used polymers are listed in Table 4.6 and were discussed in Chapter 3 in detail.

Table 4.6: PEI(nkD)_xQ^{yR} polymers and alkyl-ammonium reactants of adducts discussed in this Chapter

Entry	Polymer composition	Entry Chapter 3	yR10 or yR14 (¹ H-NMR)	xQ (¹ H-NMR)
E1, E5	PEI(1.2kD) _{13Q}	PA1	-	14
E2	PEI(10kD) _{5Q} ^{67R10} [3]	PB3	73	8
E3, E8.1 - E8.22, E9, E10, E11 - E14	PEI(10kD) _{10Q} ^{80R10}	PB4.1 – PB4.20	84 (PB4.3)	12 (PB4.3)
E4.1 – E4.11	CTAB			
E6	PEI(1.2kD) _{20Q} ^{80R10}	PA2	80	17
E7	PEI(10kD) _{10Q} ^{80R10}	PB2	67	9
E15.1 – E15.13	PEI(10kD) _{10Q} ^{60R14}	PC2.1 – PC2.12	89 (PC2.4)	14 (PC2.4)

CTAB = (1-hexadecyl)trimethylammonium bromide, PEI(10kD) = poly(ethylenimine) with $M_n = 10,000$ g/mol, $M_w/M_n = 2.5$, PEI(1.2kD) = poly(ethylenimine) with $M_n = 1,200$ g/mol, $M_w/M_n = 1.08$, xQ = mol% 2-hydroxypropyl-3-(N,N,N-trimethylammonium chloride), yR10 = mol% 2-hydroxydodecane, yR14 = mol% 2-hydroxyhexadecane

4.3.1 Characterization of the Na-bentonites **B1** and **B2**

Sodium bentonites are natural products, obtained by surface mining of clay layers, followed by some workups (cf. Chapter 2). Commercial MMT contains other minerals and metal ions other than alkali metals. For this reason, the used Na-bentonites were characterised by means of X-ray diffraction, X-ray fluorescence elemental analysis, and infrared spectroscopy. Figure 4.7 compares the wide-angle XRD diffractograms of a) Na-bentonite **B1** (cf. Table 4.2), and b) Na-bentonite **B2** (cf. Table 4.2), with the intensities of the diffractograms normalised to the reflexes at $2\Theta = 19.8^\circ$. The reflexes were assigned using comparative spectra. The reflexes derived from the X-ray diffractograms and their interpretation are listed in Table 4.7.

4 Preparation of [montmorillonite/PEI_xQyR] adducts

Na-bentonite **B1** (Figure 4.7.a) contained montmorillonite [5, 6], cristobalite, and quartz. Different to Na-bentonite **B1**, Na-bentonite **B2** (Figure 4.7.b) contained calcite but no cristobalite, hence both the materials were no pure montmorillonites. Although the purification of montmorillonite has been described in the literature [5, 7], due to the large quantities needed for further experiments the bentonites were used as received. The interlayer distance between the montmorillonite platelets of the bentonites was indicated by the d_{001} reflex. With Na-bentonite **B1**, the d_{001} interlayer distance exhibited a value of 1.18 nm and with Na-bentonite **B2** of 1.26 nm which corresponded to a lattice constant c of 1.20 and 1.28 nm. A quantification of the minerals was not possible since their reflexes were overlapping.

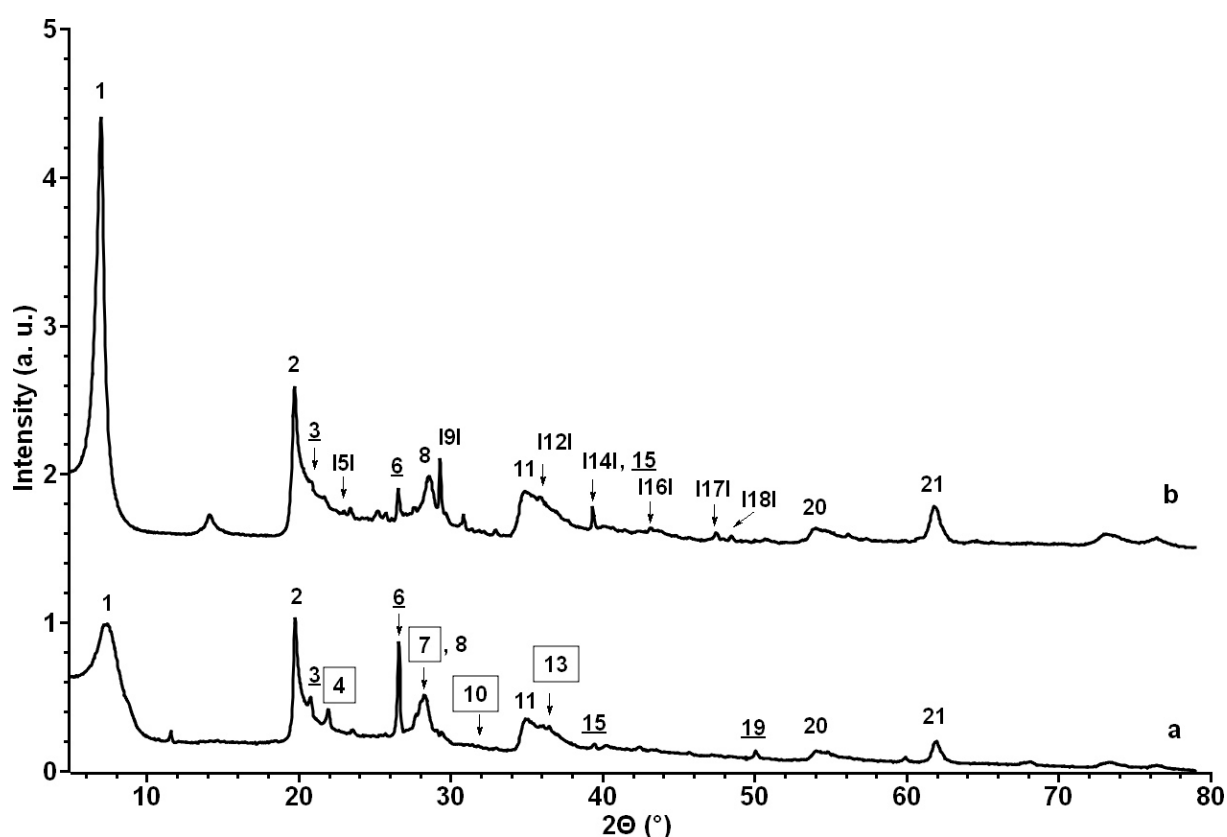


Figure 4.7: Wide-angle X-ray diffractograms of a) Na-bentonite **B1** and b) Na-bentonite **B2**, w = montmorillonite, x = quartz, $l\bar{y}l$ = cristobalite, lzl = calcite

Table 4.7: X-ray diffraction reflexes of Na-bentonite **B1 and Na-bentonite **B2****

Reflex	MMT _{B1}		MMT _{B2}		Compound and Miller index
	2 θ (°)	d (Å)	2 θ (°)	d (Å)	
1	7.52	11.75	7.00	12.57	Montmorillonite (001)
2	19.75	4.49	19.71	4.50	Montmorillonite (110, 020)
3	20.82	4.26	20.86	4.25	Quartz (100)
4	21.96	4.04			Cristobalite (101)
5			23.02	3.86	Calcite (012)
6	26.61	3.34	26.56	3.35	Quartz (011)
7	28.27	3.15			Cristobalite (111)
8	28.27	3.15	28.46	3.13	Montmorillonite (003)
9			29.31	3.04	Calcite (104)
10	31.36	2.85			Cristobalite (102)
11	34.82	2.57	34.61	2.59	Montmorillonite (130, 200)
12			35.93	2.49	Calcite (110)
13	36.51	2.46			Cristobalite (200)
14			39.64	2.28	Calcite (113)
15	40.21	2.24	40.07	2.25	Quartz (111)
16			43.15	2.09	Calcite (202)
17			47.49	1.91	Calcite (018)
18			48.47	1.87	Calcite (116)
19	50.08	1.82			Quartz (112)
20	53.98	1.69	53.91	1.70	Montmorillonite (310, 150, 240)
21	61.80	1.49	61.75	1.50	Montmorillonite (060, 330)

MMT_{B1} = Na-bentonite **B1** (cf. Table 4.2), MMT_{B2} = Na-bentonite **B2** (cf. Table 4.2), d = lattice spacing [Å], d_{hkl} = Miller indices

To investigate whether the elemental composition of Na-bentonite **B2** changes after a pre-treatment, a non-treated Na-bentonite **B2**, a bentonite **B2** treated with hydrochloric acid (= **HM**), and a bentonite **B2** washed with demineralized water (= **WM**) were investigated by X-ray fluorescence spectroscopy. Bentonite **HM** was prepared by heating 1.26 g of the bentonite **B2** in 5 mL of hydrochloric acid (37 %) for one hour at 90°C. Afterwards, the solution was diluted with 50 mL demineralized water, centrifuged and dried at 100°C for 17 h under reduced pressure. The yield after drying was 0.90 g (= 71.0 % of theory). The water-washed bentonite **WM** was prepared by stirring 2.01 g bentonite **B2** in 15 mL demineralized water for 24 h at ambient temperature. Afterwards, the solution was further diluted with 10 mL demineralized water,

4 Preparation of [montmorillonite/PEIxQyR] adducts

centrifuged and dried at 80°C for 46 h under reduced pressure. The yield after drying was 0.73 g (= 36.3 % of theory).

The elemental composition and the sum formula of the montmorillonite of the three samples are listed in Table 4.8. The main elements found with bentonite **B2** and bentonite **WM** were Si, Al, Fe and Ca. Furthermore, both bentonites contained small amounts of Mg, Na, K and S. Different to bentonite **B2** and bentonite **WM**, bentonite **HM** contained less calcium and sodium but showed the presence of chlorine. The chlorine was attributed to hydrochloric acid residues. Bentonite **B2** exhibited a montmorillonite Al/Mg [mol/mol] ratio of 4.31 which was in good agreement to the ratio of previously investigated montmorillonites of 4.56 [8, 9]. The HCl treated bentonite **HM** showed a higher Al/Mg [mol/mol] ratio of 6.33. The lower Mg content shows, that the hydrochloric acid dissolved the Mg ions as described in the literature [10]. The water washed bentonite **WM**, on the other hand, exhibited with an Al/Mg [mol/mol] ratio of 3.93 a similar ratio as the non-treated bentonite.

Table 4.8: Elemental composition of the bentonites **B2, **HM**, and **WM****

Element	B2 (wt.%)	HM (wt.%)	WM (wt.%)
Si	53.07	63.32	45.88
Al	17.14	18.86	14.65
Fe	11.48	11.28	12.41
Ca	8.83	0.79	17.51
Mg	3.58	2.69	3.36
Na	3.12	0.23	2.37
K	1.74	1.87	1.98
S	1.05	0.58	1.84
Cl		0.37	
Sum formula of montmorillonite	$\text{Na}_{0.35}(\text{Al}_{1.62}\text{Mg}_{0.38})(\text{Si}_4\text{O}_{10})(\text{OH})_2$	$\text{Na}_{0.03}(\text{Al}_{1.73}\text{Mg}_{0.27})(\text{Si}_4\text{O}_{10})(\text{OH})_2$	$\text{Na}_{0.30}(\text{Al}_{1.59}\text{Mg}_{0.41})(\text{Si}_4\text{O}_{10})(\text{OH})_2$

B2 = Na-bentonite batch **2** (cf. Table 4.2), **HM** = with HCl treated Na-bentonite **B2**, **WM** = with demineralized water washed Na-bentonite **B2**

Of the elemental composition, the calculation of the montmorillonite, quartz, and calcite content of the bentonite samples was possible. Table 4.9 lists the mineral composition of bentonite **B2**, **HM**, and **WM**. With intercalated sodium, bentonite **B2** consisted of 72.0 wt.% montmorillonite, 9.8 wt.% quartz (SiO₂), 11.1 wt.% calcite (CaCO₃), and 7.2 wt.% of iron, potassium, and sulphur. The water content of bentonite

4 Preparation of [montmorillonite/PEI_xQyR] adducts

B2, determined from experiments in which bentonite samples were dried in vacuum at 80°C for 24 h, was determined to be 6.0 wt.%. Bentonite **HW** consisted of 73.0 montmorillonite, 19.1 wt.% quartz (SiO₂), 1.0 wt.% calcite (CaCO₃), and 7.1 wt.% of iron, potassium, and sulphur. The hydrochloric acid dissolved the CaCO₃ as shown by low calcite content of the bentonite. The higher quartz to montmorillonite ratio of 0.26 of bentonite **HM** compared to the ratio of 0.14 of bentonite **B2** could be explained by that the acid also dissolved the montmorillonite to a certain extent [10]. Compared to the other two bentonites, sample **WM** had a lower montmorillonite content. Since only the residue after the centrifugation of the water/bentonite solution was investigated, it is assumed that the liquid fraction, which was discarded, contained also montmorillonite.

Table 4.9: Mineral composition of the bentonites **B2, **HM**, and **WM****

Entry	Na-Montmorillonite (wt.%)	Quartz (wt.%)	Calcite (wt.%)	Other (wt.%)
B2	72.0	9.8	11.1	7.2
HM	73.0	19.1	1.0	6.9
WM	62.1	8.1	21.8	8.1

B2 = Na-bentonite batch **2** (cf. Table 4.2), **HM** = with HCl treated Na-bentonite **B2**, **WM** = with demineralized water washed Na-bentonite **B2**, Other = potassium, sulphur, iron

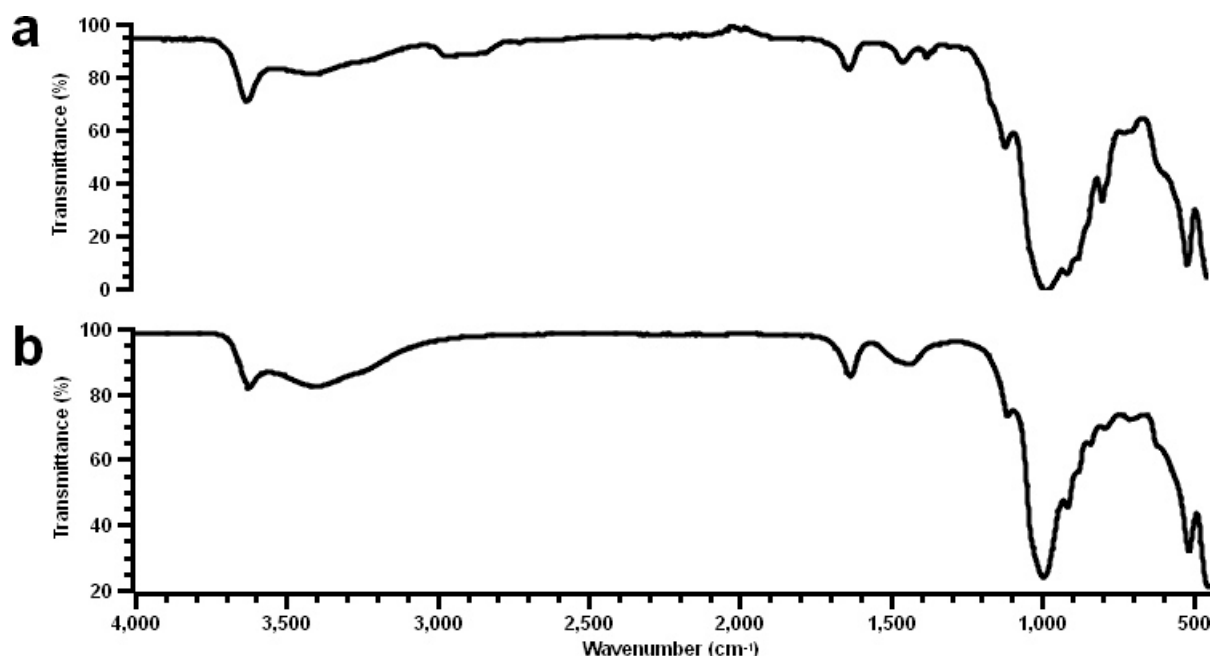


Figure 4.8: ATR-FT Infrared spectra of a) Na-bentonite **B1** and b) Na-bentonite **B2**

Figure 4.8 shows the infrared spectra of a) Na-bentonite **B1** and b) Na-bentonite **B2**. Na-bentonite **B1** (Figure 4.8.a) exhibited an Al-OH stretching vibration band at 3624

cm⁻¹ and Si-O-Si stretching vibration bands at 1117 and 980 cm⁻¹. Studies on hydrogenated silicon oxides showed that the Si-O-Si band at 1117 cm⁻¹ corresponded to a Si-O-Si angle of 180° [11], the band at 980 cm⁻¹ was attributed to a Si-O-Si angle of 120° [11]. An Al-OH-Al deformation vibration band was detected at 912 cm⁻¹, and an Al-O-Si deformation vibration band at 514 cm⁻¹. Bands corresponding to water were measured at 3414 (O-H stretching) and 1633 cm⁻¹ (O-H deformation). With Na-bentonite **B2** (Figure 4.8.b) also one Al-OH stretching vibration band (3623 cm⁻¹) and two Si-O-Si stretching vibration bands (1117 and 980 cm⁻¹) were found. An Al-OH-Al deformation vibration band appeared at 911 cm⁻¹, and an Al-O-Si deformation vibration band at 513 cm⁻¹. Bands of water showed up at 3414 cm⁻¹ (O-H stretching vibration) and 1633 cm⁻¹ (O-H deformation vibration). All bands were assigned according to previous studies [12, 13]. With both bentonites, all bands were found at the same position which indicates that the montmorillonite of both bentonites was the same.

4.3.2 Adduct preparation methods evaluated in this Chapter

With the two Na-bentonites (**B1** and **B2**), [MMT/PEI(nkD)_xQ^{yR}] adducts were prepared. To create [MMT/PEI(nkD)_xQ^{yR}] adducts in which the polymer is completely intercalated into the montmorillonite platelets, three different preparation procedures were evaluated, namely:

- 1) “Direct addition” of PEI(nkD)_xQ^{yR10} polymers to Na-MMT. In this procedure a polymer was dissolved in water or dispersed in ethanol and then added to a water/montmorillonite mixture, containing water-swollen montmorillonite. The mixture was then stirred for a certain time at an elevated temperature. After the reaction was finished, the product was received after separating the adduct from the solution by centrifugation and drying of the adduct at elevated temperature and under reduced pressure.
- 2) “Replacement” of CTAB by the addition of PEI(nkD)_xQ^{yR10} polymers to [MMT/CTAB]. In this procedure, a polymer was dissolved in water or dispersed in ethanol and then added to an aqueous dispersion of CTAB intercalated montmorillonite (= [MMT/CTAB]). The mixture was then stirred for a certain time at an elevated temperature. The adduct was received after centrifugation, purification and drying of the raw material.
- 3) “Indirect replacement” of CTAB by the addition of PEI(nkD)_xQ^{yR} polymers to CTAB and MMT. In this procedure, a polymer was dispersed in ethanol or isopropanol and then added simultaneously with CTAB to an aqueous MMT dispersion. The mixture was then stirred for a certain time at an elevated temperature. The adduct was also received after centrifugation, purification and drying of the raw material.

4.3.3 “Direct addition” of PEI(nkD)_{xQ}^{yR} polymers to Na-MMT

The first preparation procedure evaluated involved the reaction of a PEI(nkD)_{xQ}^{yR} polymer with water-swollen montmorillonite as shown in Figure 4.9. The swelling had the aim to separate the montmorillonite platelets or at least widen the interlayer gap. In a second step, a polymer was added with the goal to intercalate into the separated montmorillonite platelets. The polymer intercalation from solution is mainly entropy driven due to the gain in translational freedom of ions desorbed from the MMT [14]. The mixture was stirred at elevated temperature and the adduct was obtained after centrifugation and drying. The adduct was investigated by wide-angle X-ray diffraction, IR, TGA and DSC. Since the treatment of montmorillonite with hydrochloric acid promoted the intercalation of (1-hexadecyl)trimethylammonium bromide [15], the reaction of an PEI(nkD)_{xQ}^{yR} polymer with an acid activated montmorillonite was also investigated.

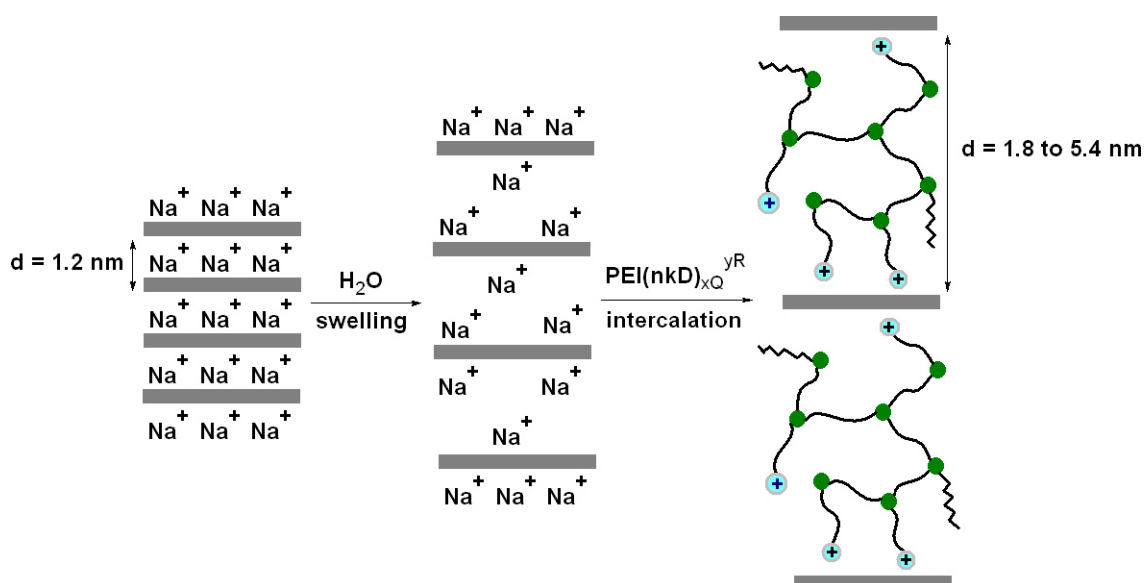


Figure 4.9: Model of the preparation of [MMT/PEI(nkD)_{xQ}^{yR}] adducts by the “direct addition” method

The [MMT/PEI(nkD)_{xQ}^{yR10}] adducts discussed in this paragraph are listed in Table 4.10. While adduct **E1** was prepared using a low molecular weight poly(ethylenimine (= PEI(1.2kD)) based quat-polymer, the adducts **E2** and **E3** were alkyl-quat polymers, based on a high molecular weight PEI(10kD). Furthermore, during the preparation of adduct **E3** hydrochloric acid was added to test whether the addition of the acid could promote the reaction of the polymer with the montmorillonite.

4 Preparation of [montmorillonite/PEI_xQ_yR] adducts

Table 4.10: [MMT/PEI(nkD)_{xQ}^{yR10}] adducts prepared by the “direct addition” method

Entry	Adduct composition	Sol. conc. (g/mL)	Preparation condition
E1	[MMT _{B1} /PEI(1.2kD) _{13Q}]	0.03	65°C, 72 h, 150 rpm, H ₂ O
E2	[MMT _{B1} /PEI(10kD) _{5Q} ^{67R10}]	0.07	65°C, 52 h, 300 rpm, H ₂ O/ ethanol (V/V) = (3/ 1)
E3	[MMT _{B1} /PEI(10kD) _{10Q} ^{80R10}]	0.05	70°C, 72 h, 150 rpm, H ₂ O/ ethanol/ HCl (37%) (V/ V/ V) = (116/ 40/ 1)

HCl = HCl 37 %, MMT_{B1} = Na-bentonite **B1** (cf. Table 4.2), PEI(1.2kD) = poly(ethylenimine) with M_n = 1,200 g/mol, M_w/M_n = 1.08, PEI(10kD) = poly(ethylenimine) with M_n = 10,000 g/mol, M_w/M_n = 2.5, xQ = mol% 2-hydroxypropyl-3-(N,N,N-trimethylammonium chloride), yR10 = mol % 2-hydroxydodecane, Sol. conc. = solid concentration = MMT + polymer

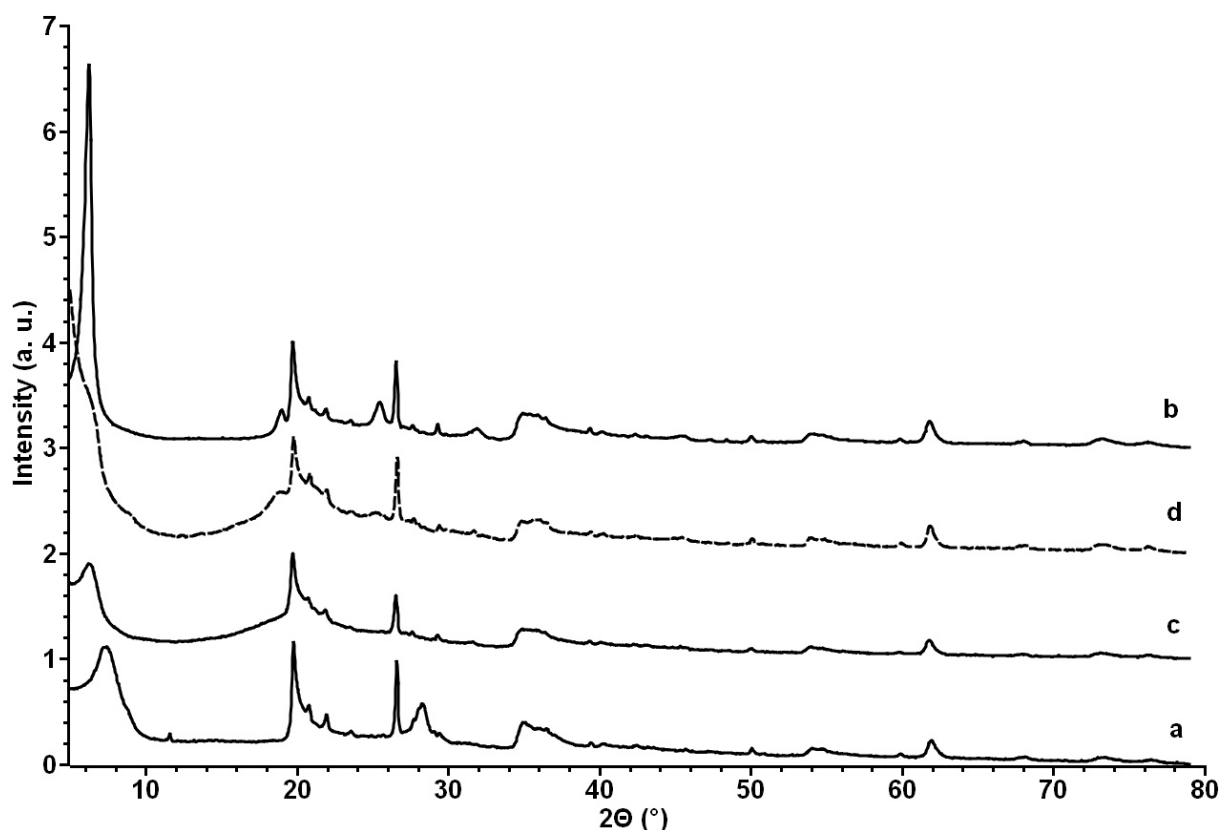


Figure 4.10: Wide-angle X-ray diffractograms of a) Na-bentonite **B1**, b) adduct **E1**, c) adduct **E2**, and d) adduct **E3**

Figure 4.10 compares the wide-angle XRD diffractograms of a) Na-bentonite **B1**, b) adduct **E1**, c) adduct **E2**, and d) adduct **E3**. The intensities of the diffractograms were normalised to the reflexes at $2\Theta = 19.7^\circ$. An overview over the obtained lattice constant *c* of the adducts and the calculated diameter of the used polymers is given in

Table 4.11. The diffractogram of adduct **E1** (Figure 4.10.b) showed a sharp reflex at $2\Theta = 18.9^\circ$ which corresponded to a lattice distance of 0.47 nm. Furthermore, a second reflex was measured at $2\Theta = 6.25^\circ$ with a full width at half maximum of $\Delta\Theta_{1/2} = 0.57^\circ$. Using the formula of a monoclinic crystal system (cf. Chapter 2, Equation 2.12), the reflexes were attributed to the Miller indices d_{003} and d_{001} . Although a reflex corresponding to the Miller index d_{002} was not detected, the reflex at $2\Theta = 6.25^\circ$ was still attributed to the d_{001} interlayer distance which led then to a lattice constant c of 1.43 ± 0.06 nm. From the lattice constant c the thickness of the montmorillonite platelets of 0.66 nm [16] was subtracted, leading to an interlayer distance d_m between the montmorillonite platelets of 0.77 nm.

The “degree of polymer intercalation”, D_i , was calculated using Equation 4.1 using the interlayer distance of an adduct with a completely intercalated polymer (adduct **E5**, $d_i = 1.37$ nm, cf. Figure 4.29). On average it was found that 56 % of the total area of one polymer molecule was “sandwiched” by two montmorillonite platelets while 46 % was located outside as sketched in Figure 4.11.

$$D_i = \frac{d_m}{d_i} \cdot 100 \quad \text{Eq. 4.1}$$

(with D_i = degree of intercalation, d_m = measured interlayer distance [nm], d_i = interlayer distance with a completely intercalated polymer [nm])

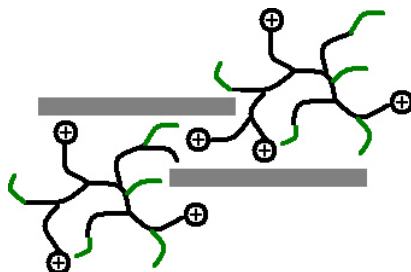


Figure 4.11: Model of partially intercalated polymers

With adduct **E2** (Figure 4.10.c) no sharp reflexes were detected in the region $2\Theta = 15 - 20^\circ$. Between $2\Theta = 5 - 15^\circ$, only one reflex was measured at $2\Theta = 6.24^\circ$ with a full width at half maximum of $\Delta\Theta_{1/2} = 1.19^\circ$. The reflex corresponded to an interlayer distance d_{001} and was used to calculate the lattice constant c to be 1.44 ± 0.14 nm. After subtracting the thickness of the montmorillonite platelets from the lattice constant c the gap d_m between the platelets was determined to be 0.78 nm. Using Equation 4.1 and the interlayer distance of an adduct with a completely intercalated polymer (adduct **E8.2**, $d_i = 6.23$ nm, cf. Figure 4.39), the result from the calculation of the degree of intercalation showed that about 13 % of the polymer was intercalated while about 87 % remained outside. Although the slope of the scattered intensity in the region 2Θ

4 Preparation of [montmorillonite/PEI_xQ_yR] adducts

= 5 - 6° indicated the presence of a second and larger d_{001} interlayer distance, the exact angle of the maximum of the reflex could not be determined.

The diffractogram of adduct **E3** (Figure 4.10.d) showed besides a broad signal between $2\Theta = 15$ and 20° reflexes at $2\Theta = 6.10, 8.70, 16.60$ and 19.00° . The reflexes were assigned to the Miller indices d_{002} to d_{007} , the full width at half maximum of the d_{002} index was determined to $\Delta\Theta_{1/2} = 0.39^\circ$. The value of the lattice constant c of 2.94 ± 0.40 nm was then calculated from the Miller indices. Subtracting the thickness of the montmorillonite platelets led to an interlayer distance d_m of 2.28 nm. Using Equation 4.1 and the interlayer distance of adduct **E8.2** ($d_i = 6.23$ nm, cf. Figure 4.39), the calculation of the degree of intercalation revealed that only 37 % of the polymer was intercalated. The increased amount of intercalated polymer of adduct **E3** compared to adduct **E2** shows, that the addition of hydrochloric acid promoted the intercalation of the polymer analogously to previous experiments of the intercalation of (1-hexadecyl)trimethylammonium bromide into montmorillonite [15]. The disadvantage of the addition of hydrochloric acid to montmorillonite is that the acid partially dissolved the montmorillonite as reported in the literature [10].

Table 4.11: Lattice constant c and diameter of the polymers of the adducts **E1 – **E3****

Entry	Adduct composition	Lattice constant c (nm)	Calc. polymer diameter (nm)	D_i (%)
E1	[MMT _{B1} /PEI(1.2kD) _{13Q}]	1.43 ± 0.06 (w)	1.69	56
E2	[MMT _{B1} /PEI(10kD) _{5Q} ^{67R10}]	1.44 ± 0.14 nm (w)	5.28	13
E3	[MMT _{B1} /PEI(10kD) _{10Q} ^{80R10}]	2.94 ± 0.40 (w)	5.28	37

MMT_{B1} = Na-bentonite **B1** (cf. Table 4.2), PEI(1.2kD) = poly(ethylenimine) with $M_n = 1,200$ g/mol, $M_w/M_n = 1.08$, PEI(10kD) = poly(ethylenimine) with $M_n = 10,000$ g/mol, $M_w/M_n = 2.5$, xQ = mol% 2-hydroxypropyl-3-(N,N,N-trimethylammonium chloride), yR10 = mol% 2-hydroxydecane, D_i = degree of polymer intercalation, w = wide-angle XRD

The used polymers exhibited a certain size distribution due to the ratio of weight average to the number average molecular weight of the used poly(ethylenimine)s ($M_w/M_n = 2.5$ with PEI(10kD) and $M_w/M_n = 1.08$ with PEI(1.2kD)). It was attempted to correlate the size distribution of the polymers with the width of the reflexes obtained from XRF measurements by calculating the full width at half maximum of the reflexes either by a fit with a Lorentzian or a Gaussian function.

The volume of the polymers was calculated with the assumption that the macromolecules exhibited a spherical structure (Equation 4.2). The assumption is valid for an unperturbed molecule since a hyperbranched poly(ethylenimine) was used as the

4 Preparation of [montmorillonite/PEI_xQyR] adducts

base polymer.

$$V = \frac{m}{\rho} = \frac{4 \cdot \pi \cdot r^3}{3} \quad \text{Eq. 4.2}$$

(with V = volume [nm³], m = mass [g], ρ = density [g/nm³], r = radius [nm])

The density of the polymers was determined using the pycnometer and the respective value is listed in Table 4.12. The density of polymer **PB3** was not determined but was assumed to be similar to those of the polymers **PB4** and **PB2** due to the similar composition of the three polymers. For the calculating of the weight of one polymer molecule, the mass m obtained from Equation 4.2 can be written as shown in Equation 4.3.

$$m_p = \frac{M_n}{N_A} \quad \text{Eq. 4.3}$$

(with m_p = mass of one polymer molecule [g], M_n = number average molar mass of the polymer [g/mol], N_A = Avogadro constant [6.02214129·10²³ mol⁻¹])

Table 4.12: Density of the PEI(nkD)_{xQ}^{yR} polymers used

Entry Chapter 3	Polymer composition	ρ (g/cm ³)
A1	PEI(1.2kD) _{13Q}	1.15
PB3	PEI(10kD) _{5Q} ^{67R10} [3]	not determined
PB4.1 – PB4.20	PEI(10kD) _{10Q} ^{80R10}	1.03
PA2	PEI(1.2kD) _{20Q} ^{80R10}	1.14
PB2	PEI(10kD) _{10Q} ^{80R10}	1.03
PC2.1 – PC2.12	PEI(10kD) _{10Q} ^{60R14}	1.17

PEI(10kD) = poly(ethylenimine) with M_n = 10,000 g/mol, M_w/M_n = 2.5, PEI(1.2kD) = poly(ethylenimine) with M_n = 1,200 g/mol, M_w/M_n = 1.08, xQ = mol% 2-hydroxypropyl-3-(N,N,N-trimethylammonium chloride), yR10 = mol% 2-hydroxydodecane, yR14 = mol% 2-hydroxyhexadecane

Combining Equation 4.2 and 4.3 led to Equation 4.4.

$$V = \frac{M_n}{\rho_a \cdot N_A} = \frac{4 \cdot \pi \cdot r^3}{3} \quad \text{Eq. 4.4}$$

(with V = volume [nm³], M_n = number average molar mass of the polymer [g/mol], ρ_a = weighted average density [g/nm³], N_A = Avogadro constant [6.02214129·10²³ mol⁻¹], r = radius [nm])

4 Preparation of [montmorillonite/PEI_xQyR] adducts

To calculate the diameter of one polymer molecule Equation 4.4 was rewritten to:

$$d=2 \cdot r=2 \cdot \left[\left(\frac{3 \cdot M_n}{4 \cdot \pi \cdot \rho_a \cdot N_A} \right)^{1/3} \right] \quad \text{Eq. 4.5}$$

(with d = diameter [nm], r = radius [nm], M_n = number average molar mass of the polymer [g/mol], ρ_a = weighted average density [g/nm³], N_A = Avogadro constant [6.02214129 · 10²³ mol⁻¹])

To investigate whether the attachment of the polymers to the montmorillonite changes the thermal transitions of the polymers, the adducts were investigated by differential scanning calorimetry. In Figure 4.12, the DSC thermograms of a) adduct **E1** and polymer **PA1** and b) adduct **E3** and polymer **PB4.1** are shown.

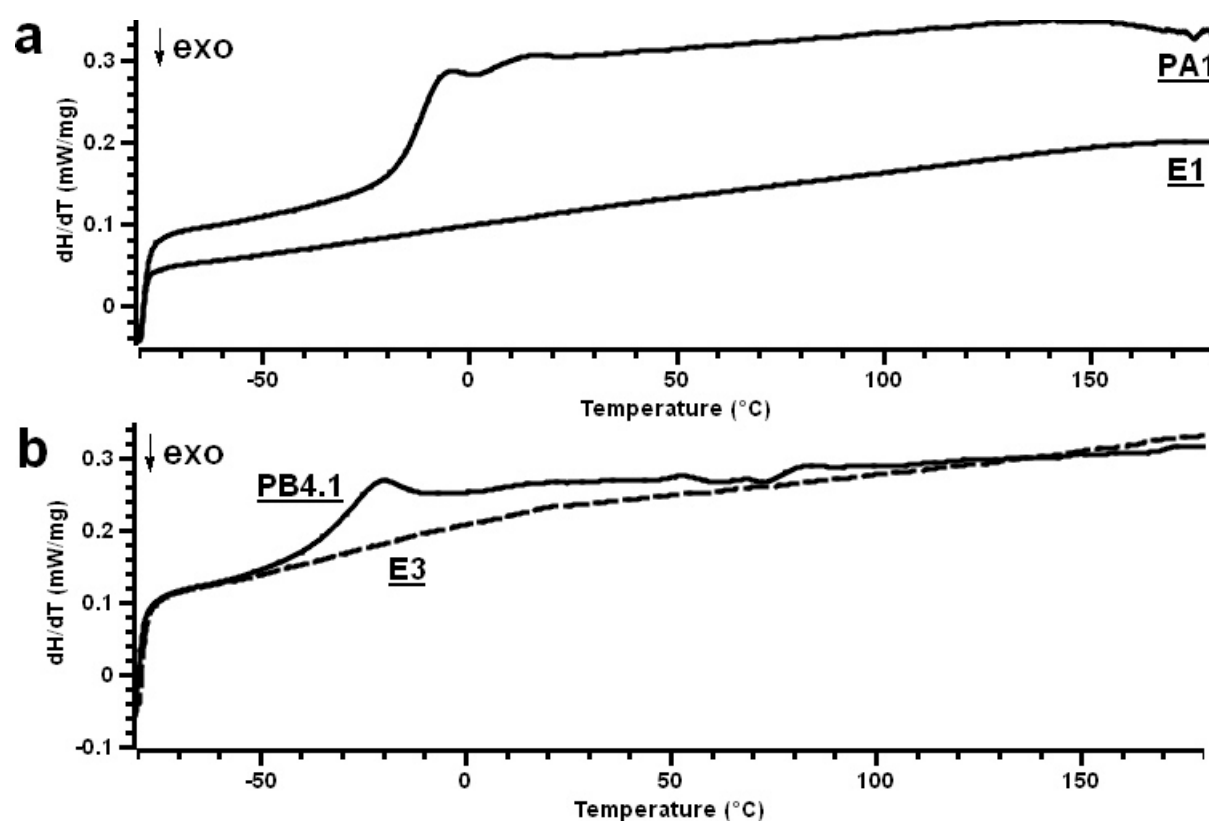


Figure 4.12: DSC thermograms of a) adduct **E1** and polymer **PA1**, and b) adduct **E3** and polymer **PB4.1**, 2. heating run, N₂ atmosphere, dT/dt = 10 K/minute

It was found that while polymer **PA1** (Figure 4.12.a) exhibited a glass transition of $T_G = -10.6^\circ\text{C}$, no transitions were detected with adduct **E1** (Figure 4.12.a). With polymer **PB4.1** (Figure 4.12.b), a glass transition was measured at $T_G = -26.3^\circ\text{C}$. The polymer in adduct **E3** (Figure 4.12.b), on the other hand, gave only a weak signal at -40.1°C . Although previous investigations revealed that the glass transition temperatures of

polymers decreased upon confinement [17 - 24], other studies stated that either an increase or no change of the transition temperatures can also occur. The reasons for changes in the transition temperatures are not clear yet since the configurational entropy theory of the glass transition implies that T_G should increase for supported thin films and for materials confined in nanopores [25, 26]. The reason for a temperature change is that confinement of polymers is to be expected to decrease the entropy of the segments and, therefore, increase the glass transition temperature. In contrast, the free volume [27 - 30] and also the entropy [25, 26] theory of the glass transition predict that a decrease of the density of a confined liquid could cause a decrease of T_G [31]. Due to the unpredictable changes of the glass transitions of polymers in confinement no statements about the extent of the intercalation of polymers in nanopores can be made.

To determine the thermal stability of the adducts, thermogravimetric studies were performed. Figure 4.13 shows the TGA thermograms of a) adduct **E1** and polymer **PA1**, b) adduct **E2** and polymer **PB3**, and c) adduct **E3** and polymer **PB4.1**.

As reported earlier [32], and was also shown in the thermogram of polymer **PA1** (Figure 4.13.a), quarternized poly(ethylenimine)s can not be obtained water-free even after drying for prolonged time at elevated temperature. The decomposition of the neat polymer started at 240°C after losing about 20 wt.% water between 50 and 240°C which was in reasonable agreement to the water content of the used glycidyltrimethylammonium chloride (cf. Chapter 3). Different to the neat polymer, the polymer in adduct **E1** (Figure 4.13.a) exhibited a lower decomposition temperature of 230°C and no water residues. Comparing the decomposition temperatures of different PEI(nkD)_{xQ}^{yR} polymers (cf. Chapter 3), The decomposition temperatures of PEI(nkD)_{xQ}^{yR} polymers were generally in the region around 240°C. The polymer content of the adduct was determined to be 14.4 wt.% which was lower than the theoretically expected value of 23.9 wt.%.

In analogy to polymer **PA1**, polymer **PB3** (Figure 4.13.b) and polymer **PB4.1** (Figure 4.13.c) contained also up to 5 wt.% water which originated from the used glycidyltrimethylammonium chloride solution (cf. Chapter 3). The decomposition of PEI(10kD)_{5Q}^{67R10} and the polymer of adduct **E2** (Figure 4.13.b) started at 250 and 240°C, respectively. Adduct **E2** contained 66.3 wt.% organic material which was 17.1 wt.% higher than theoretically expected.

The decomposition temperature of polymer **PB4.1** (Figure 4.13.c) was with 230°C similar to that of the polymer of adduct **E3** (Figure 4.13.c) of 220°C. The noise of the measuring points in the thermogram of adduct **E3** was caused by a faulty operating valve. The polymer content of adduct **E3** was determined to be 50.5 wt.% which was

4 Preparation of [montmorillonite/PEI_xQyR] adducts

about 6.6 wt.% lower than the theoretical value.

In conclusion, it was found that compared to the neat polymers the adducts **E1** – **E3** contained no water. The missing water indicates that the hydration shell around the 2-hydroxypropyl-3-(N,N,N-trimethylammonium chloride) was broken which enabled the polymers to be completely dried. The lower decomposition temperatures of the adduct polymers compared to the neat polymers may indicate a destabilising effect caused by the montmorillonite but since the differences were only small the reason for this behaviour may be also a measuring error.

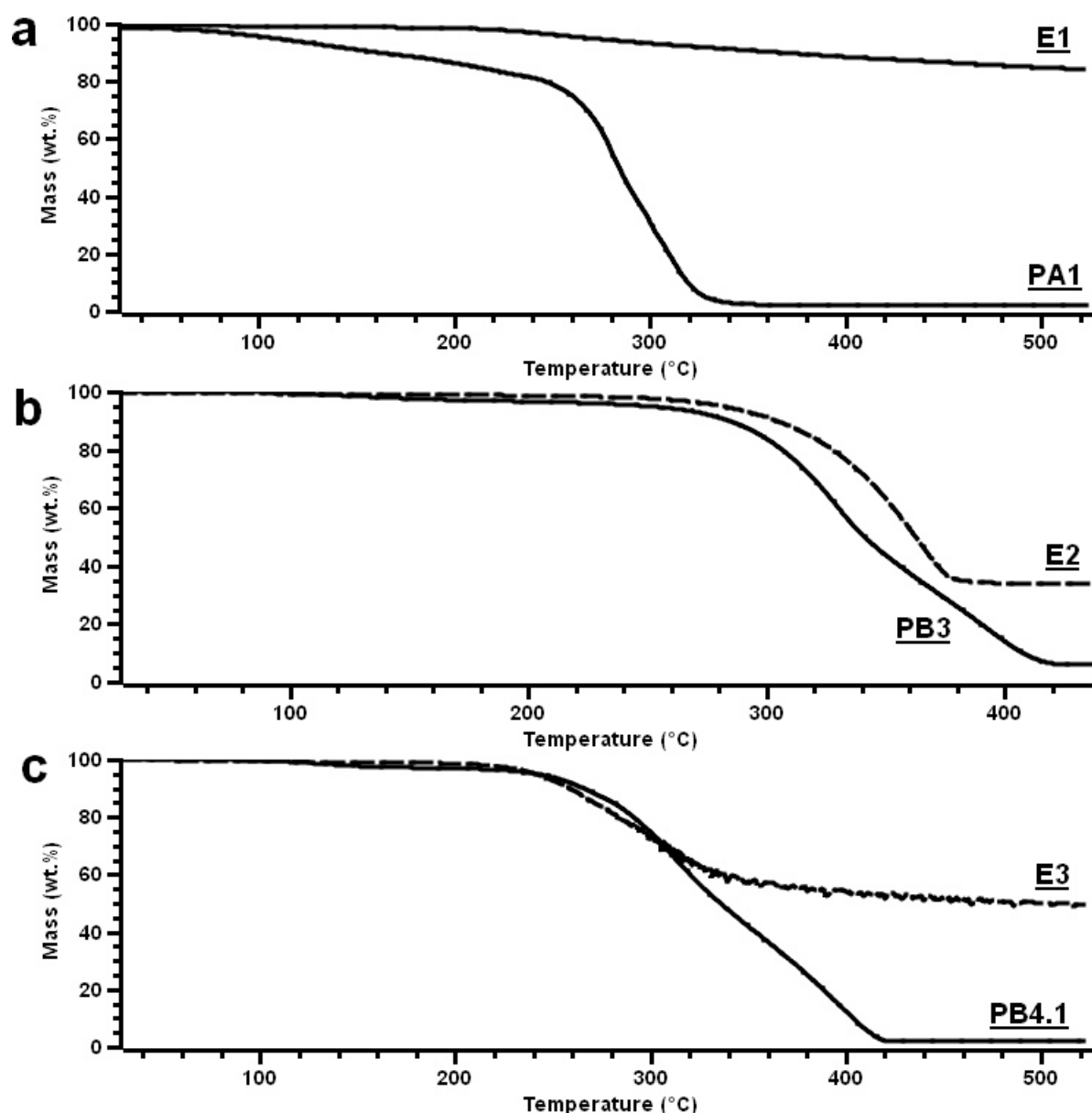


Figure 4.13: TGA thermograms of a) adduct **E1** and polymer **PA1**, b) adduct **E2** and polymer **PB3**, and c) adduct **E3** and polymer **PB4.1**, He atmosphere, $dT/dt = 10$ K/minute

Table 4.13: Decomposition temperature and polymer content of the adducts E1 - E3

Entry	Decomposition temperature [°C]	Polymer content (exp.) [wt.%]	Polymer content (theory) [wt.%]
<u>E1</u>	230	14.4	23.9
<u>E2</u>	240	66.3	49.2
<u>E3</u>	220	50.5	57.1

To obtain information about the functional groups present in the adducts, the substances were studied by infrared spectroscopy. Figure 4.14 compares the infrared spectra of a) polymer PA1, b) adduct E1, c) polymer PB4.1, and d) adduct E3. The spectra of polymer PA1 and polymer PB4.1 were discussed in Chapter 3.

The infrared spectrum of adduct E1 (Figure 4.14.b) showed polymer bands at similar positions as with polymer PA1 (Figure 4.14.a). In addition, an Al-OH stretching vibration band was detected at 3624 cm⁻¹. Compared to the non-modified bentonite (cf. Figure 4.8), the Si-O-Si stretching vibration bands shifted from 1117 to 1111 and from 980 to 998 cm⁻¹. The shift of the Si-O-Si bands indicates that the polymer interacts with the Si-O-Si moieties of the montmorillonite [11]. Deformation vibration bands of an Al-OH-Al function appeared at 913 cm⁻¹ and of an Al-O-Si group at 514 cm⁻¹. Additionally, an Al-OH-Mg deformation vibration band was measured at 843 cm⁻¹. The bands of the polymer exhibited a weak intensity which could be interpreted in that way that the polymer content of the adduct was very low which was also supported by the thermogravimetric measurement (cf. Figure 4.13.a).

With adduct E3 (Figure 4.14.d), bands corresponding to the polymer and the montmorillonite were also detected. While the bands of the polymer of the adduct were at similar positions as with the neat polymer (Figure 4.14.c), the Si-O-Si bands of the montmorillonite were shifted compared to the non-modified montmorillonite. As with adduct E1 (Figure 4.14.b), the shift of the Si-O-Si bands indicates an interaction between the polymer and the Si-O-Si group of the montmorillonite [11]. Different to adduct E1, the bands of the polymer of adduct E3 exhibited a stronger intensity which was caused by the higher polymer content of this adduct. Comparing the infrared spectrum of adduct E1 and adduct E3 with that of Na-bentonite B1 (cf. Figure 4.8) it was found that bands corresponding to water were missing, indicating that the workup procedures of the adducts were sufficient to remove most of the water. The position of the aliphatic C-H stretching vibration bands gave information whether a PEI(nkD)_{xQ} or a PEI(nkD)_{xQ}^{yR} polymer was used to modify the montmorillonite. The main change of neat (cf. Figure 4.8) to modified montmorillonite was the shift of the Si-O-Si bands. But since these shifts were monitored with all investigated adducts,

no statement about changes in the structure of the montmorillonite could be made.

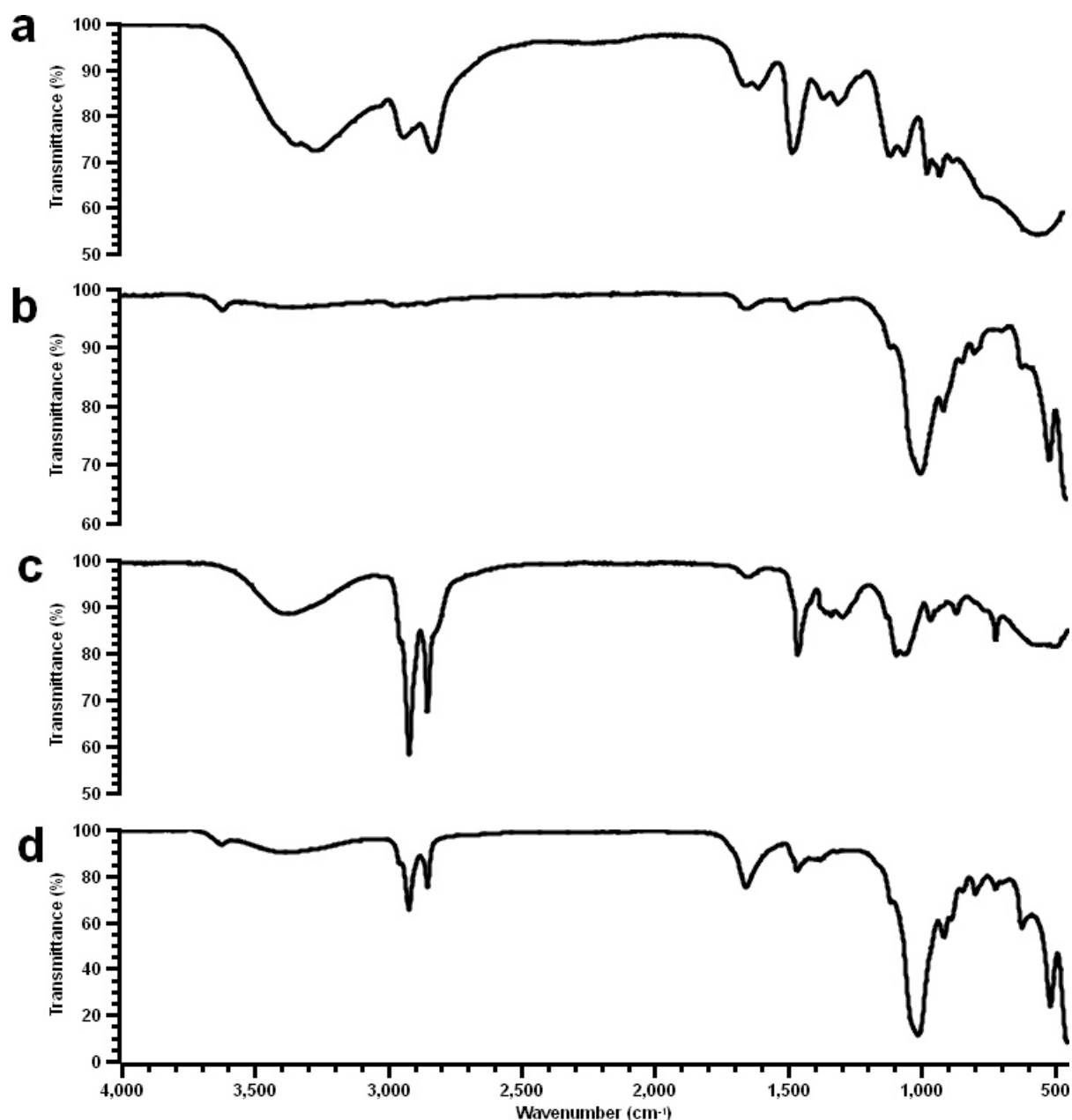


Figure 4.14: ATR-FT infrared spectra of a) polymer **PA1**, b) adduct **E1**, c) polymer **PB4.1**, and d) adduct **E3**

The elemental composition of adduct **E1** and adduct **E3** has been investigated by means of X-ray fluorescence. The measured elements are listed in Table 4.14 together with the sum formula of the montmorillonite of the adducts. The main elements found with both adducts were Si, Al, Fe, Mg, Ca, and Cl. As with Na-bentonite **B1** (cf. Table 4.8), the adducts contained also small amounts of sulphur and potassium. As

4 Preparation of [montmorillonite/PEI_xQyR] adducts

seen by the presence of sodium ions, the ammonium moieties of the polymer could not replace all cations. Adduct **E1** exhibited an Al:Mg ratio [mol/mol] of 7.49 and adduct **E3** of 7.27. Comparing the Al:Mg ratios of adduct **E1** and adduct **E3** with ratios of montmorillonites treated with an acid (Table 4.8 and [10]), it is concluded that the used bentonite **B1** was treated with an acid by the manufacturer beforehand.

Table 4.14: Elemental composition and sum formula of the montmorillonite of adduct **E1 and adduct **E3****

Element	E1 (wt.%)	E3 (wt.%)
Si	61.76	60.50
Al	18.78	17.40
Fe	11.83	13.60
Ca	2.33	1.30
Mg	2.26	2.16
Na	0.50	0.22
K	0.83	0.86
S	0.33	0.48
Cl	1.38	3.47
Sum formula of montmorillonite	$\text{Na}_{0.06}(\text{Al}_{1.76}\text{Mg}_{0.24})(\text{Si}_4\text{O}_{10})$ (OH) ₂	$\text{Na}_{0.03}(\text{Al}_{1.77}\text{Mg}_{0.23})(\text{Si}_4\text{O}_{10})$ (OH) ₂

Table 4.15: Mineral composition of the inorganic fraction of adduct **E1 and adduct **E3****

Entry	Na-Montmorillonite (wt.%)	Quartz/ cristobalite (wt.%)	CaCO ₃ (wt.%)	Other (wt.%)
E1	71.7	18.8	2.9	6.5
E3	69.1	21.4	1.7	7.8

Other = potassium, sulphur, iron

The mineral composition of the inorganic fraction of adduct **E1** and adduct **E3** is listed in Table 4.15. The bentonite of adduct **E1** consisted of 71.7 wt.% montmorillonite, 18.8 wt.% quartz/cristobalite (both SiO₂), 2.9 wt.% CaCO₃, and 6.5 wt.% of iron, potassium, and sulphur. The montmorillonite and CaCO₃ content of adduct **E3** were with 69.1 and 1.7 wt.% lower than in adduct **E1**. The diminishing of this materials indicated that both materials were partially dissolved by the hydrochloric acid added during the preparation of adduct **E3** as known for acid treated montmorillonites [10]. The bentonite of adduct **E3** consisted furthermore of 21.4 wt.% quartz/cristobalite and 7.8

4 Preparation of [montmorillonite/PEI_xQ_yR] adducts

wt.% iron, potassium, and sulphur.

In Table 4.16 the polymer content of adduct **E1** and **E3** calculated from XRF data and obtained from the TGA measurement as well as the theoretical value is listed. For the calculation of the polymer content, the amount of chlorine ions derived from the XRF data was used. Since the counter-ion of the trimethylammonium moiety of the PEI(nkD)_xQ^{YR} polymers was chlorine, the weight fraction of the polymers could be calculated since the composition of the polymers was known. It was found that adduct **E1** contained 9.5 – 15.4 wt.% less polymer than theoretically expected. With adduct **E3** the polymer content was determined to be 5.9 to 6.6 wt.% lower than expected. The stronger variations in the experimentally obtained polymer content of adduct **E1** compared to those of adduct **E3** indicates that the water-soluble PEI(1.2kD)_{13Q} polymer reacted less effective with the montmorillonite. With both adducts, the comparison of the polymer content obtained from two methods shows that the amount of chlorine obtained by the XRF measurement, in fact, can be used to calculate the polymer content of the adducts.

Table 4.16: Polymer content of the adducts **E1 - **E3****

Adduct	XRF (wt.%)	TGA (wt.%)	Theory (wt.%)
E1	8.5	14.4	23.9
E2	not determined	66.3	49.2
E3	51.2	50.5	57.1

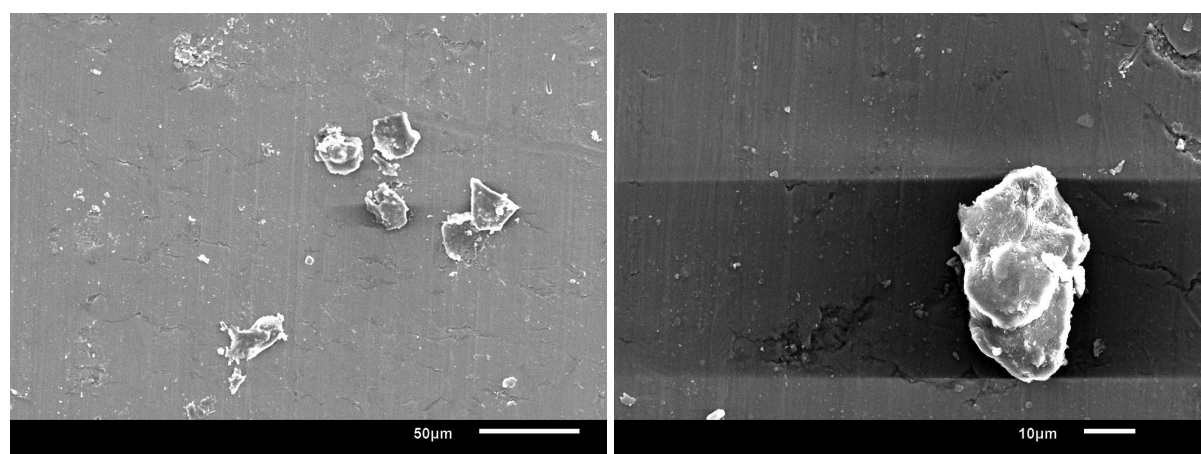


Figure 4.15: SEM pictures of Na-bentonite **B2**, dispersed in water (1.0 mg/mL)

In Figure 4.15 SEM pictures of Na-bentonite **B2** are shown. The sample was prepared by pouring one droplet of a dispersion (1 mg/mL water) onto an aluminium platelet, followed by spin-coating with 2200 rpm for one minute. Before the sample

4 Preparation of [montmorillonite/PEIxQyR] adducts

was observed by SEM, it was sputtered with gold for twenty seconds with a sputtering current of 8 mA. The sample was then examined at a voltage of 10 kV. Water was used as the solvent since it was hoped that the swelling property of the montmorillonite would be enough to separate the montmorillonite aggregates. The bentonite contained oval shaped aggregates which could be interpreted as stacked montmorillonite sheets. The diameters of the particles were in the range of 1 to 50 μm . The large aggregates show that the swelling of the montmorillonite in water is not sufficient to delaminate the montmorillonite platelets completely.

Figure 4.16 shows SEM pictures of adduct **E2**, obtained from an adduct/toluene dispersion. The preparation of the sample was performed analogously to the preparation of Na-bentonite **B2** (cf. Figure 4.15). Toluene was used as the solvent since it was able to dissolve the polymer (cf. Chapter 3) and should separate the montmorillonite platelets if the polymer was completely intercalated. Adduct **E2** contained, similar to the neat bentonite, oval shaped aggregates that resemble stacked montmorillonite sheets. The diameters of the particles ranged from 1 to 20 μm . In contrast to the neat bentonite **B2**, the number of particles with diameters below 10 μm was increased. It was concluded from the presence of smaller particles that the polymer surrounded the montmorillonite particles and was able to separate stacked montmorillonite sheets up to a certain degree which points to a partial exfoliation of the particles.

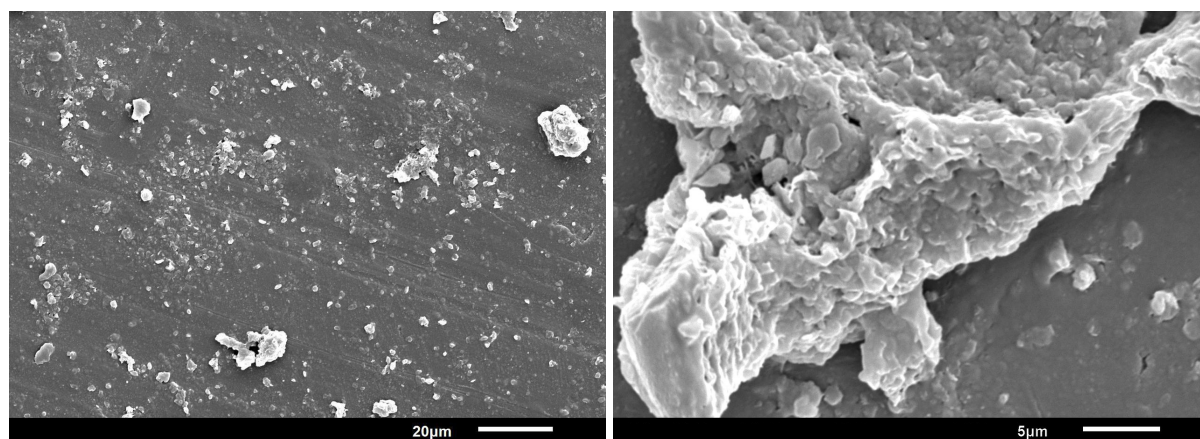


Figure 4.16: SEM pictures of adduct **E2**, dispersed in toluene (1.0 mg/mL)

In Figure 4.17 SEM pictures of adduct **E2**, obtained from an adduct/petroleum ether dispersion, are shown. The preparation of the sample was performed analogously to the preparation of Na-bentonite (cf. Figure 4.15). Petroleum ether was used as the solvent to investigate the influence of a more polar solvent than toluene on the delamination of the montmorillonite sheets. Besides montmorillonite stacks with diameters of about 8 μm the pictures also showed aggregates with diameters larger

than 100 μm . Although the right picture implies a partial delamination of the MMT sheets, the large aggregates show that the polymer was less soluble in petroleum ether than in toluene (cf. Figure 4.16).

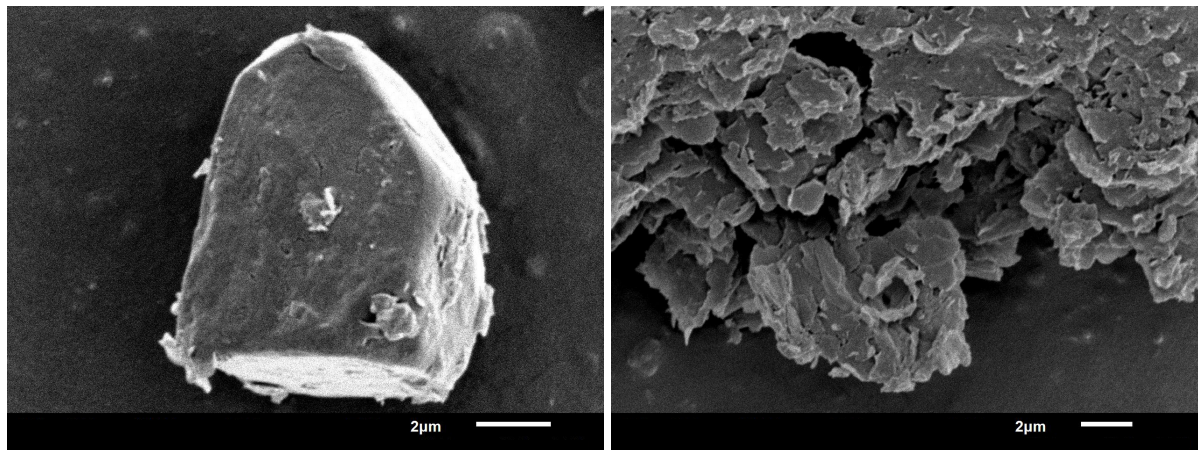


Figure 4.17: SEM pictures of adduct **E2**, dispersed in petroleum ether (1 mg/mL)

Discussion

In this paragraph, the “direct addition” of PEI(nkD)_{xQ}^{yR10} polymers to water pre-swollen Na-MMT is described. The degrees of intercalation of the polymers were determined from wide angle X-ray diffraction measurements. The adducts were further investigated by infrared spectroscopy to show the presence of the polymer and montmorillonite in the final product. With differential scanning calorimetry, changes of the thermal transitions of the polymer were studied. The polymer content of the adducts was measured by thermogravimetry and calculated from X-ray fluorescence data. Scanning electron microscopy enabled furthermore to examine the size of the particles when dispersed in a solvent that dissolves the polymer.

It was found that the reaction of a low molecular weight PEI(1.2kD)_{13Q} polymer with Na-MMT led to an adduct (**E1**) with an interlayer distance of 0.77 nm. The calculation of the degree of polymer intercalation showed that about 56 % of the polymer was intercalated into the montmorillonite platelets. This result shows that the polymer was only partially intercalated between montmorillonite platelets. The polymer content of the adduct was determined to be 14.4 wt.% (by thermogravimetry) and to be 8.4 wt.% (from X-ray fluorescence data). The differential scanning calorimetry measurement of the adduct revealed no glass transition of the polymer. The decrease or change of a glass transition temperature of a polymer confined in nanopores is not yet fully understood. Examples are given in the literature where the glass transition of a polymer either increased, decreased or didn't changed when confined in nanopores.

Different to the reaction of a low molecular weight PEI(1.2kD)_{13Q} with montmorillonite,

the reaction of a high molecular weight PEI(10kD)_{5Q}^{67R10} led to an adduct (**E2**) with a low degree of polymer intercalation of only 13 %. The lower degree of intercalation shows that the swelling of the montmorillonite by water was not sufficient to enlarge the gap between two platelets to that extent that the polymer could fully intercalate. SEM pictures of the in toluene dispersed adduct showed, similar to SEM pictures of the neat Na-bentonite, oval shaped aggregates which could be interpreted as stacked montmorillonite sheets. Different to the neat bentonite, the number of aggregates with diameters below 10 μm increased. The presence of the smaller particles points to a partial exfoliation of the particles.

When a high molecular weight PEI(10kD)_{10Q}^{80R10} was reacted with montmorillonite in the presence of hydrochloric acid, the degree of polymer intercalation increased to 37 % (adduct **E3**). The increase of the degree of intercalation shows that the addition of hydrochloric acid promotes the intercalation of the polymer. On the other hand, the hydrochloric acid also dissolves the montmorillonite partially which was demonstrated in the literature [10]. The adduct exhibited a lower glass transition temperature compared to the neat polymer as shown by a differential scanning calorimetry measurements. The polymer content of the adduct, obtained from a thermogravimetric measurement and calculated from X-ray fluorescence data, was found to 50.5 and 50.4 wt. % which was in good agreement to the theoretically expected polymer content of 57.1 wt.%. Generally, the decomposition temperatures of the polymers in the adducts were about 10°C lower than those of the neat polymers.

Summary

In conclusion, it was found that 56 % of a low molecular weight PEI(1.2kD)_{13Q} can be intercalated into montmorillonite by direct addition of the polymer to an aqueous Na-MMT solution. When a high molecular weight PEI(10kD)_{5Q}^{67R10} was used, the degree of intercalation decreased to 13 %. The low degree of intercalation shows that the swelling of the montmorillonite in water was not sufficient to provide the necessary enlargement of the gap between the platelets to enable the polymer to be completely intercalated. On the other hand, the addition of hydrochloric acid promoted the intercalation of a high molecular weight PEI(10kD)_{10Q}^{80R10} polymer which was shown by an increase of the degree of intercalation to 37 %. SEM pictures of the [MMT/PEI(10kD)_{5Q}^{67R10}] adduct showed that the adduct exhibited aggregates with diameters between 1 and 20 μm. An increase of particles with diameters below 10 μm in the adduct compared to the neat bentonite showed that the polymer coated montmorillonite nanoparticles were able to delaminate up to a certain degree. The mineral composition of the bentonite of the adducts showed that the bentonite contained be-

side montmorillonite also about 20 wt.% quartz/cristobalite which may be responsible for some of the particles with diameters above 10 μm measured. The low degrees of intercalation shows that the method of “direct addition” of PEI(nkD)_xQ^{yR10} polymers to Na-MMT cannot be applied to obtain [MMT/PEI(nkD)_xQ^{yR10}] adducts with completely intercalated polymers.

4.3.4 Characterisation of [MMT/CTAB] adducts

Adducts from montmorillonite and (1-hexadecyl)trimethylammonium bromide (= CTAB) were prepared and analysed for further studies. The analytical results of the prepared [MMT_{B1}/CTAB] adducts will be discussed in this paragraph. The adducts were prepared with the goal to obtain an adduct in which an organic molecule was intercalated into montmorillonite platelets and thus widen the interlayer gap between two montmorillonite platelets. The preparation of the adduct was performed as described in previous studies on the reaction of CTAB with Na-MMT [33 - 35]. The reaction of CTAB with Na-MMT is shown in Figure 4.18. The intercalation of CTAB into Na-MMT was achieved by adding CTAB to an in water swollen montmorillonite. The mixture was then stirred at elevated temperature for a certain time and the adduct was received after centrifugation and subsequent drying. Depending on the amount of CTAB used, mono-, double-, or pseudo trimolecular layers of CTAB between two montmorillonite sheets can be obtained [36, 37]. The adduct was investigated by wide-angle X-ray diffraction, IR, TGA, DSC, and solid-state NMR.

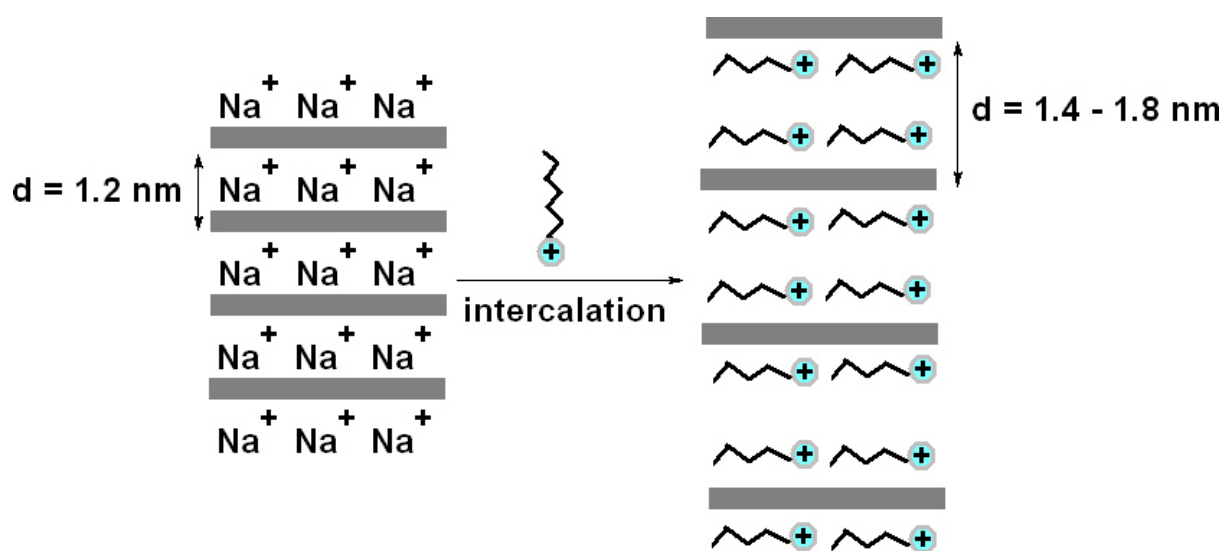


Figure 4.18: Model of the preparation of [MMT/CTAB]

4 Preparation of [montmorillonite/PEI_xQyR] adducts

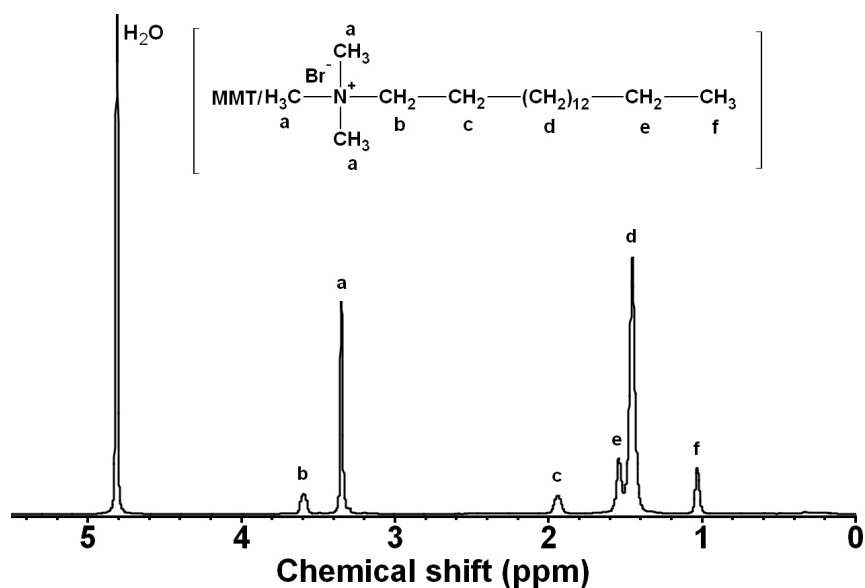


Figure 4.19: ¹H-MAS-NMR spectrum of adduct **E4.1**, 30°C, CDCl₃

Figure 4.19 shows the ¹H-MAS-NMR spectrum of adduct **E4.1**. The signal of the three methyl groups attached to the nitrogen was found at 3.59 ppm. The methyl groups of the alkyl chain gave signals at 3.35, 1.94, 1.54, 1.45 and 1.03 ppm, respectively.

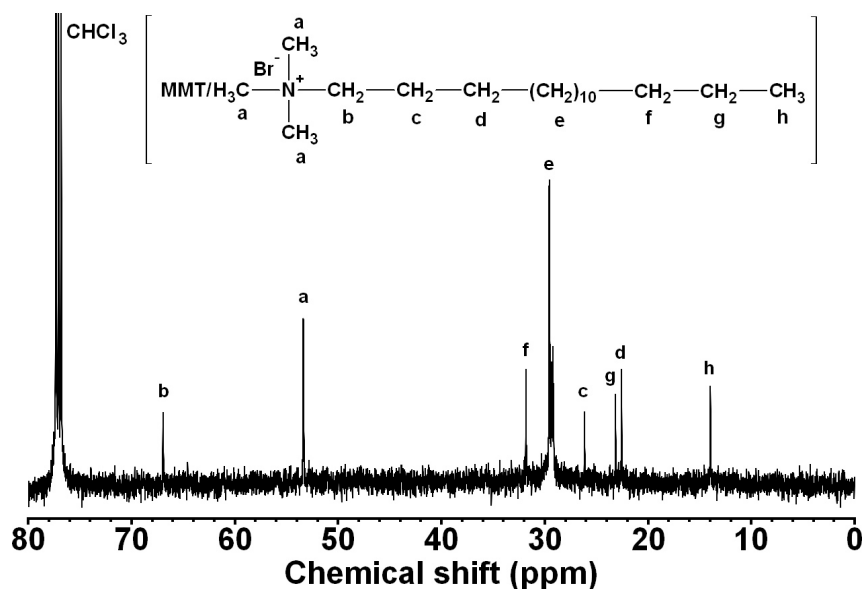


Figure 4.20: ¹³C-MAS-NMR spectrum of adduct **E4.10**, 30°C, CDCl₃

The ¹³C-MAS-NMR spectrum of adduct **E4.10** is shown in Figure 4.20. The signal of the three methyl groups attached to the nitrogen was measured at 53.3 ppm. The signals of the methyl groups of the alkyl chain were detected at 66.9, 31.8, 29.2, 26.1, 23.1, 22.5 and 13.9 ppm, respectively.

Figure 4.21 shows the wide-angle XRD diffractograms of a) Na-bentonite **B1** and b) adduct **E4.1**. The intensities of the diffractograms were normalised to the reflexes at $2\Theta = 19.7^\circ$. In the region between $2\Theta = 5$ and 20° the diffractogram of adduct **E4.1** (Figure 4.21.b) showed reflexes at $2\Theta = 6.8, 9.2, 13.7, 15.9, 17.0$ and 18.2° . The reflex at $2\Theta = 6^\circ$ corresponded to a $d_{001(1)}$ interlayer distance and was used to calculate the lattice constant $c_{(1)}$ of 1.32 nm. A second d_{001} interlayer distance ($= d_{001(2)}$) could be calculated by assigning the reflexes at $2\Theta = 9.2, 13.7$ and 18.2° to the Miller indices d_{002} to d_{004} . Extrapolation to d_{001} gave then the second d_{001} interlayer distance and a second lattice constant c of 1.96 nm. Subtracting the thickness of the montmorillonite platelets led to interlayer distances of 0.66 and 1.30 nm. As described in the literature [38], intercalated N-alkylammonium compounds are lying flat between the layers [38] which was confirmed by the small interlayer distances compared to the width of CTAB of about 2.5 nm. While the interlayer distance of 0.66 nm corresponded to a single layer of CTAB intercalated into MMT, the interlayer distance of 1.30 nm was attributed to a mixture of a double and a pseudo trimolecular layer of CTAB [39, 40]. The presence of three different arrangements of CTAB between two montmorillonite platelets shows that the adduct consisted of at least three different crystal structures.

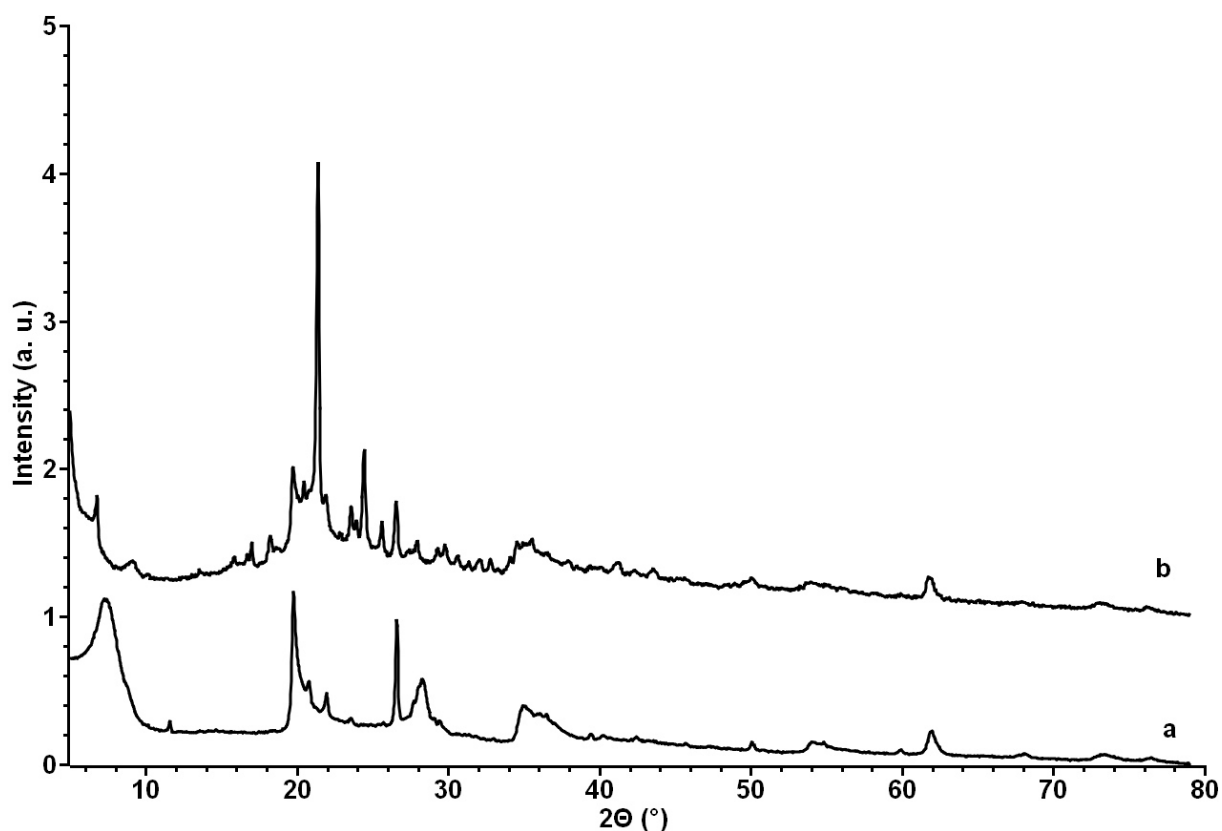


Figure 4.21: Wide-angle X-ray diffractograms of a) Na-bentonite **B1** and b) adduct **E4.1**

In Figure 4.22 the differential scanning calorimetry thermograms of a) CTAB, and b) adduct **E4.1** are shown. CTAB (Figure 4.22.a) exhibited a melting transition at 101.9°C which was attributed to the rearrangement from an ordered to a disordered state of the hydrocarbon chains of the 1-hexadecyltrimethylammonium bromide [41]. The enthalpy of the endothermic signal was determined to 169.9 J/g. Adduct **E4.1** (Figure 4.22.b) showed besides a melting transition at 98.2°C a second transition at 47.7°C. The enthalpy of the transition at 47.7°C was determined to be 7.9 J/g, the enthalpy of the transition at 98.2°C was found to be 24.8 J/g. The second transition was also detected in previous investigations on CTAB intercalated between montmorillonite platelets [42, 43]. It was found in previous studies that the melting transitions in a bulk material differ from that of the material confined in porous systems [31, 44 - 48]. The melting transition depression was successfully described [44 - 50] by the Gibbs–Thomson thermodynamic relationship [51 - 53].

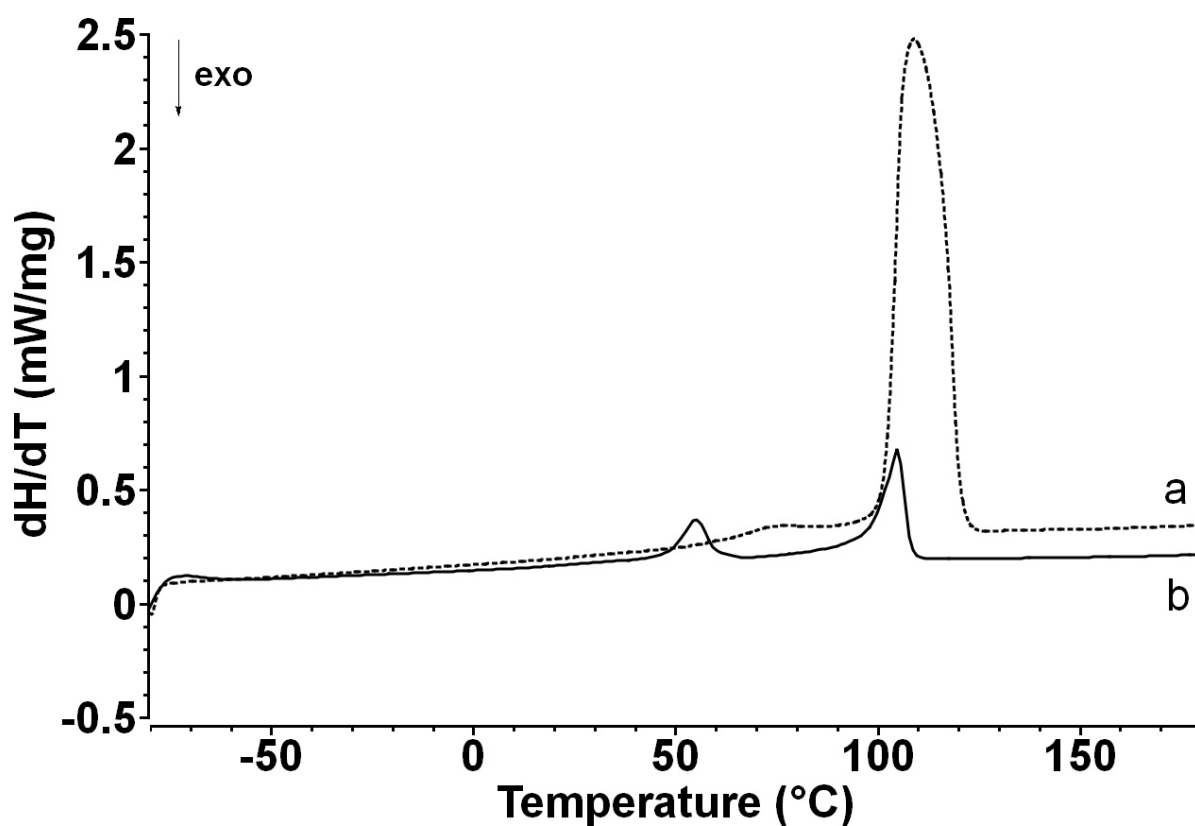


Figure 4.22: DSC thermograms of a) CTAB and b) adduct **E4.1**, 2. heating run, N_2 atmosphere, $dT/dt = 10$ K/minute

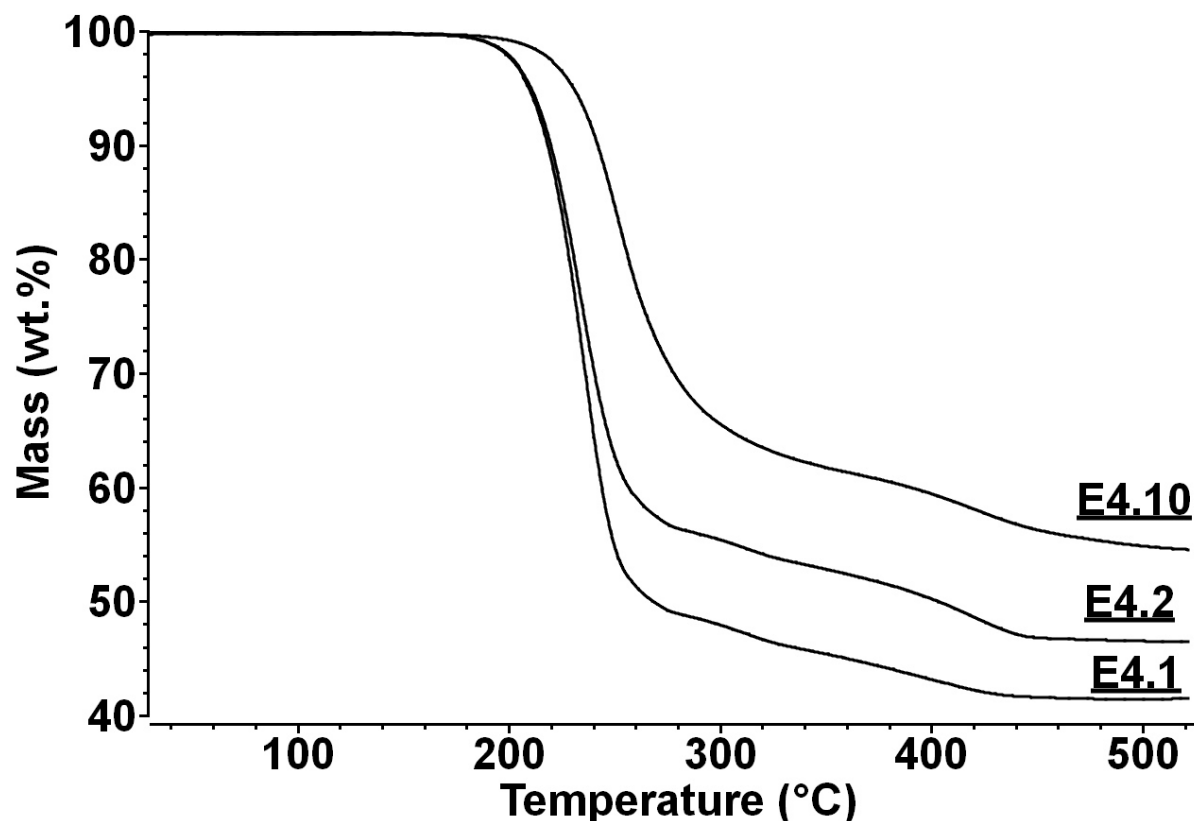


Figure 4.23: TGA thermograms of the adducts **E4.1** (a), **E4.2** (b), and **E4.10** (c), He atmosphere, $dT/dt = 10$ K/minute

Figure 4.23 compares the TGA thermograms of the adducts **E4.1** (a), **E4.2** (b), and **E4.10** (c). With all three samples, the CTAB exhibited a three step decomposition at 190 - 200, 300 and 390°C. From investigations described in the literature, the decomposition products were determined to be alkyl chains and alkyl amino fragments [54, 55]. The CTAB content was measured to be 53.6 wt.% with adduct **E4.1**, to be 58.5 wt.% with adduct **E4.2**, and to be 45.5 wt.% with adduct **E4.10**. Comparing the experimental obtained CTAB contents with the theoretical expected CTAB content of 60 wt.% it was found that the CTAB contents of the adducts were in the region of 52 ± 6.5 wt.%. Although the preparation procedures were virtually identical with all three adducts, the centrifugation force applied for the removal of the water after the reaction between the CTAB and the montmorillonite was finished was different. In detail, the raw solutions of the adducts **E4.1** and **E4.2** were centrifuged at 2817 g (2817 times the acceleration due to gravity) and the raw solution of adduct **E4.10** at 4472 g for 10 minutes each to remove the water. The low CTAB content of the adduct centrifuged with the higher centrifugation force (**E4.10**) as well as the different CTAB content of the adducts centrifuged at the same force (**E4.1** and **E4.2**) shows that the CTAB exhibited only a low adhesion to the montmorillonite and can be easily removed.

4 Preparation of [montmorillonite/PEI_xQyR] adducts

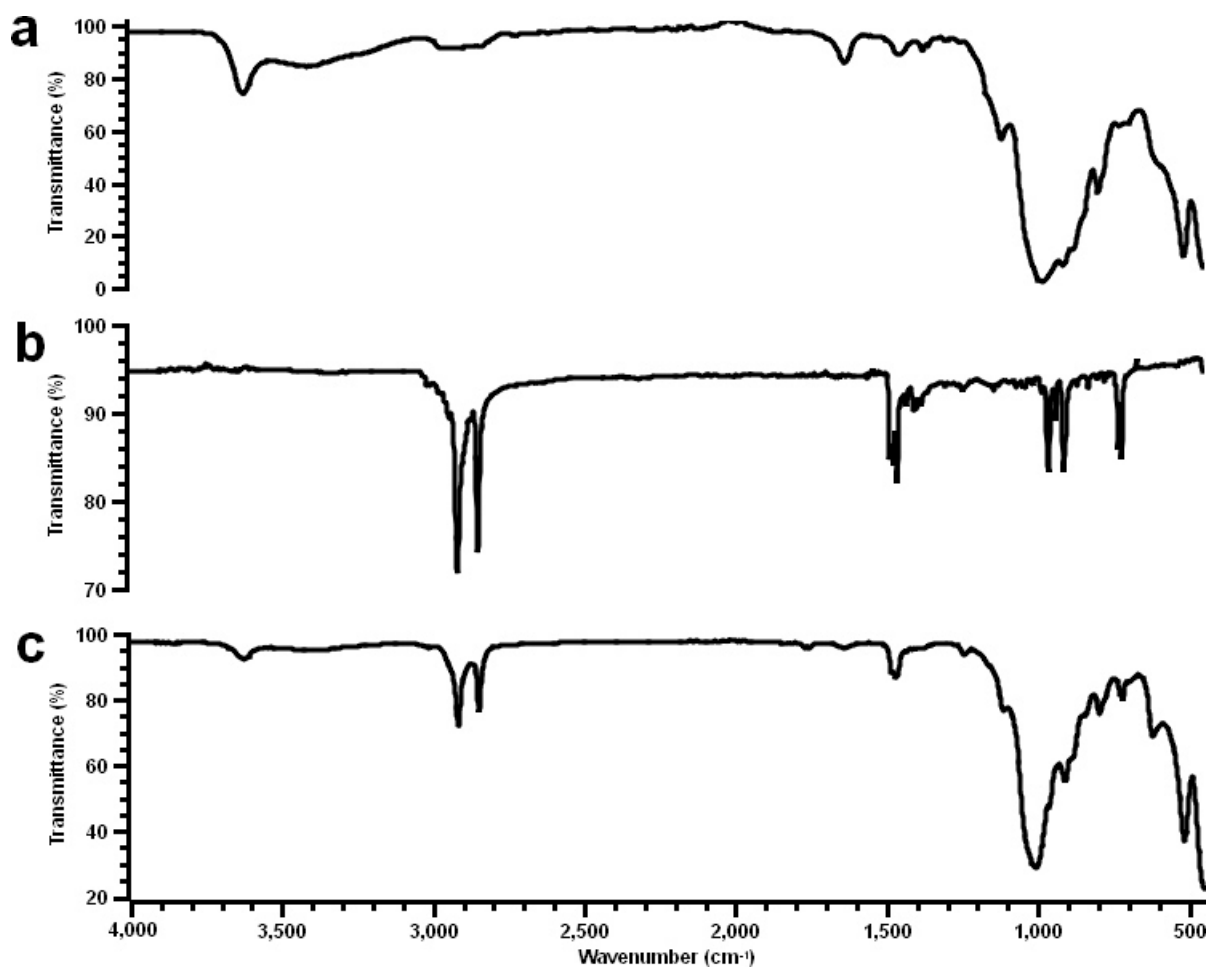


Figure 4.24: ATR-FT infrared spectra of Na-bentonite **B1**, b) CTAB, and c) adduct **E4.10**

In Figure 4.24 the infrared spectra of a) Na-bentonite **B1**, b) CTAB and c) adduct **E4.10** are compared. The analysis of the IR spectrum of Na-bentonite **B1** was done before (cf. Figure 4.8). The infrared spectrum of the CTAB (Figure 4.24.b) showed stretching vibration bands of aliphatic CH₂ groups at 2915 and 2848 cm⁻¹ as well as deformation vibration bands of aliphatic C-H moieties at 1472 and 1461 cm⁻¹. An N-CH₃ deformation vibration band was detected at 1486 cm⁻¹ and a C-N stretching vibration band at 910 cm⁻¹. Bands of the C-(CH₂)_n-C alkyl chains appeared at 729 and 718 cm⁻¹. The signals were assigned according to previous investigations [56]. In the infrared spectrum of adduct **E4.10** (Figure 4.24.c) bands corresponding to the MMT and CTAB were measured. Of the montmorillonite, the Al-OH stretching vibration band showed up at 3627 cm⁻¹ and the Si-O-Si stretching vibration bands at 1114 and 1007 cm⁻¹. An Al-OH-Al deformation vibration band was present at 911 cm⁻¹ and an Al-O-Si band at 515 cm⁻¹. Water O-H stretching and deformation vibration bands could be seen at 3395 and 1642 cm⁻¹, respectively. The bands of the CTAB appeared at similar positions as with the neat CTAB. The signals were assigned according to

4 Preparation of [montmorillonite/PEIxQyR] adducts

previous studies [57]. Comparing the spectrum of CTAB and the spectrum of adduct **E4.10** it was found that the Si-O-Si stretching vibration bands were shifted which points to an interaction between the ammonium groups of the CTAB and the Si-O-Si moiety of the montmorillonite [11].

Table 4.17: Elemental composition, mineral composition of the inorganic fraction and sum formula of the montmorillonite of adduct **E4.10**

Element	E4.10 (wt.%)
Si	47.53
Al	11.71
Fe	7.01
Ca	1.06
Mg	1.43
Na	0.28
K	0.64
S	0.25
Br	30.09
Sum formula of montmorillonite	$\text{Na}_{0.05}(\text{Al}_{1.76}\text{Mg}_{0.24})(\text{Si}_4\text{O}_{10})(\text{OH})_2$
Na-Montmorillonite	62.6
Quartz/ cristobalite	29.9
CaCO ₃	1.9
Other	5.6

Other = potassium, sulphur, iron

The elemental composition of adduct **E4.10** has been investigated by means of an XRF measurement and is listed in Table 4.17. The table lists also the sum formula of the montmorillonite and the mineral composition of the inorganic fraction of the adduct. The main elements detected were Si, Al, Fe, Mg, Ca, and Br. As with Na-bentonite **B1** (cf. Table 4.8), the adduct contained also small amounts of sulphur and potassium. As with the adducts **E1** and **E3** (cf. Table 4.14), the Al/Mg [mol/mol] ratio of adduct **E4.10** was with 7.37 higher than the previously reported Al:Mg ratio of neat montmorillonite of 4.56 [8, 9]. Comparing the Al:Mg ratio of adduct **E4.10** with ratios of montmorillonites treated with an acid (cf. Table 4.8 and [10]), it is, as mentioned before, concluded that the used bentonite **B1** was treated with an acid by the manufacturer beforehand. The bentonite consisted of 62.6 wt.% montmorillonite, 29.9 wt.% quartz/cristobalite (both SiO₂), 1.9 wt.% CaCO₃, and 5.6 wt.% of iron, potassium, and sulphur. Comparing the mineral composition of adduct **E4.10** with those of the ad-

4 Preparation of [montmorillonite/PEIxQyR] adducts

ducts **E1** and **E3** (cf. Table 4.15) it was found that adduct **E4.10** contained less montmorillonite. Since the adduct was centrifuged during the preparation it is assumed that fractions with low densities were removed.

In Table 4.18 the organic content of the adducts **E4.1**, **E4.2**, and **E4.10** obtained from XRF data and thermogravimetric measurements as well as the theoretical values are listed. Since the counter-ion of the trimethylammonium moiety of the CTAB was bromine, the weight fraction of the CTAB in the adduct could be calculated based on the bromine. With both methods, the organic content of adduct **E4.10** was about 15 wt.% lower than theoretically expected. Both methods could be used to determine the CTAB content in [MMT/CTAB] adducts.

Table 4.18: Organic content of the adducts **E4.1, **E4.2**, and **E4.10****

Entry	XRF (wt.%)	TGA (wt.%)	Theory (wt.%)	Δ_m (wt.%)
E4.1		53.6	60.0	6.4
E4.2		58.5	60.0	1.5
E4.10	49.2	45.5	60.0	14.5

Summary

In this paragraph, the results of the reaction of (1-hexadecyl)trimethylammonium bromide (= CTAB) with montmorillonite were described. The intercalation of CTAB into montmorillonite platelets was proved by the data obtained from a wide angle X-ray diffraction measurement. It was found that the [MMT/CTAB] adduct exhibited a lattice constant c of 0.66 and $c = 1.30$ nm (distance between the montmorillonite platelets after subtracting the thickness of the platelets) which corresponded to single and a pseudo trimolecular layers of CTAB and showed that the adduct consisted of at least two different crystal structures. By IR, ^1H -, and ^{13}C -MAS-NMR investigations the presence of the CTAB and the montmorillonite in the adduct was proven. The differential scanning calorimetry measurement revealed two melting transitions, one at 98.2 and one at 47.7°C. While the transition at 98.2°C corresponded to the re-arrangement from an ordered to a disordered state of the hydrocarbon chains of free 1-hexadecyltrimethylammonium bromide, the transition at 47.7°C was attributed to hydrocarbon chains confined between montmorillonite platelets. The CTAB content of the three adducts was measured by TGA and revealed that the average CTAB content was in the region of 52.5 ± 5.4 wt.% which was lower than the theoretical value of 60.0 wt.%. The difference between the highest and the lowest CTAB content was found to be $\Delta_m = 13$ wt.% which points to a low adhesion of the CTAB to the MMT.

Due to the low adhesion of the CTAB to the montmorillonite, it may be possible to displace the compound by other materials which bear ammonium groups.

4.3.5 “Replacement” of CTAB by addition of PEI(nkD)_xQ^{yR} polymers to [MMT/CTAB] adducts

The CTAB in [MMT/CTAB] adducts which were prepared by a known procedure [33 - 35] showed only a low adhesion to the montmorillonite. A displacement of the CTAB by the polymer is feasible since the cumulative electrostatic interaction between the ammonium moieties of the polymer and the montmorillonite leads to a stronger adhesion. The preparation of these [MMT/PEI(nkD)_xQ^{yR}] adducts was termed as the “replacement” procedure, which means the indirect intercalation of a PEI(nkD)_xQ^{yR} polymer into MMT. The procedure involved the reaction of a PEI(nkD)_xQ^{yR} polymer with an aqueous solution of an [MMT/CTAB] adduct under replacement of CTAB (cf. Figure 4.25). Since the ratio of MMT to CTAB varied in the prepared adducts (cf. Figure 4.23) the average MMT content was used to calculate the composition of the [MMT/CTAB] adducts used. The prepared [MMT/polymer] adducts were investigated by wide- and small-angle XRD, IR, TGA, DSC, and XRF.

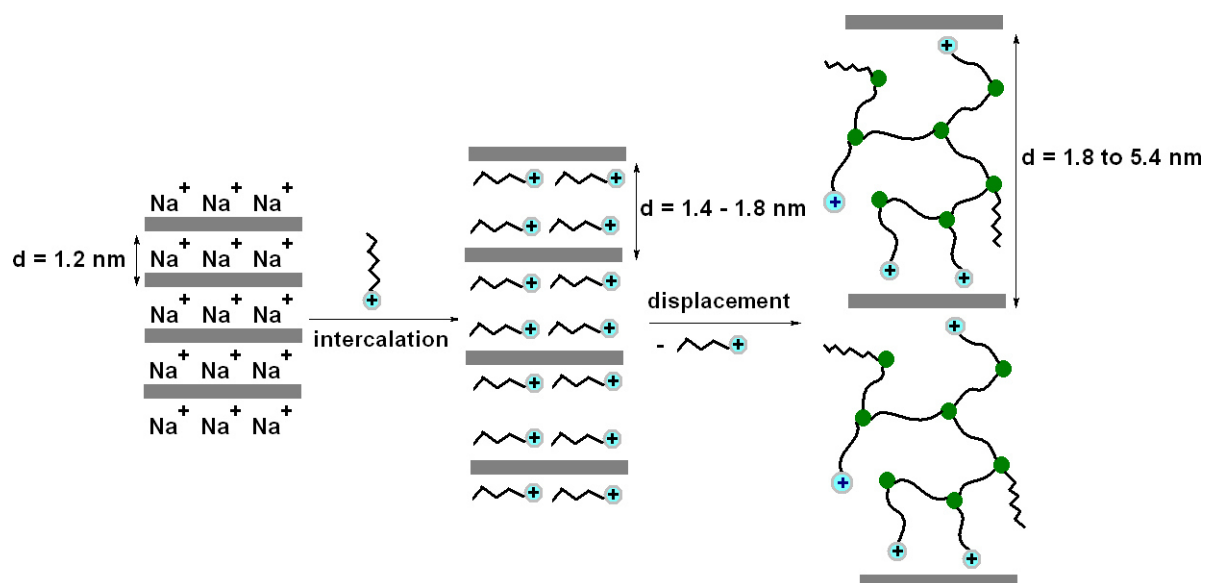


Figure 4.25: Model of the preparation of [MMT/PEI(nkD)_xQ^{yR}] adducts by the “replacement” method

The [MMT/PEI(nkD)_xQ^{yR10}] adducts discussed in this paragraph are listed in Table 4.19. While the polymer used to prepare adduct **E5** was soluble in water and methanol, the polymer used to prepare adduct **E6** only gave a dispersion in ethanol and was

4 Preparation of [montmorillonite/PEI_xQ_yR] adducts

non-soluble in water. During the work-up, adduct **E5** was purified with methanol in which both the polymer and the CTAB were soluble. Adduct **E6**, on the other hand, was purified with ethanol. While the CTAB was soluble in this solvent, only a dispersion was obtained with the polymer used.

Table 4.19: [MMT/PEI(nkD)_xQ^{yR10}] adducts prepared by the “replacement” method

Entry	Adduct composition	Sol. conc. (g/mL)	Preparation condition
E5	[MMT _{B1} /PEI(1.2kD) _{13Q}]	0.06	65°C, 72 h, 150 rpm, H ₂ O
E6	[MMT _{B1} /PEI(1.2kD) _{20Q} ^{80R10}]	0.10	70°C, 72 h, 150 rpm, H ₂ O/ethanol (V/V) = (7.3/ 1)

MMT_{B1} = Na-bentonite **B1** (cf. Table 4.2), PEI(1.2kD) = poly(ethylenimine) with M_n = 1,200 g/mol, M_w/M_n = 1.08, PEI(10kD) = poly(ethylenimine) with M_n = 10,000 g/mol, M_w/M_n = 2.5, xQ = mol% 2-hydroxypropyl-3-(N,N,N-trimethylammonium chloride), yR10 = mol% 2-hydroxydecane, Sol. conc. = solid concentration = MMT + polymer + CTAB

Figure 4.27 shows the ¹H-MAS-NMR spectra of a) adduct **E5** and b) adduct **E6**. With adduct **E5** (Figure 4.27.a) the signal of the poly(ethylenimine) ethyl hydrogen atoms was detected in the region 2.50 – 3.00 ppm (1 – 4), overlapping with two hydrogen atoms of the ammonium moiety (5). The signal of the four methyl groups attached to the ammonium moiety appeared at 3.27 ppm (7, 8). In addition, signals derived from CTAB were measured at 3.46, 3.23, 1.84, 1.44, 1.36, and 0.94 ppm. The presence of CTAB indicate that the intercalated CTAB was either trapped between the montmorillonite platelets (cf. Figure 4.26) or free on the outside of the adduct and the applied purification method was not sufficient to remove it completely.

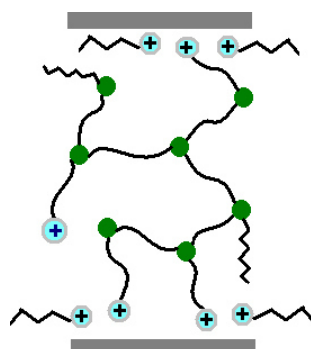


Figure 4.26: Model of [MMT/PEI(nkD)_xQ^{yR}] adducts with incorporated CTAB remainders

4 Preparation of [montmorillonite/PEI_xQyR] adducts

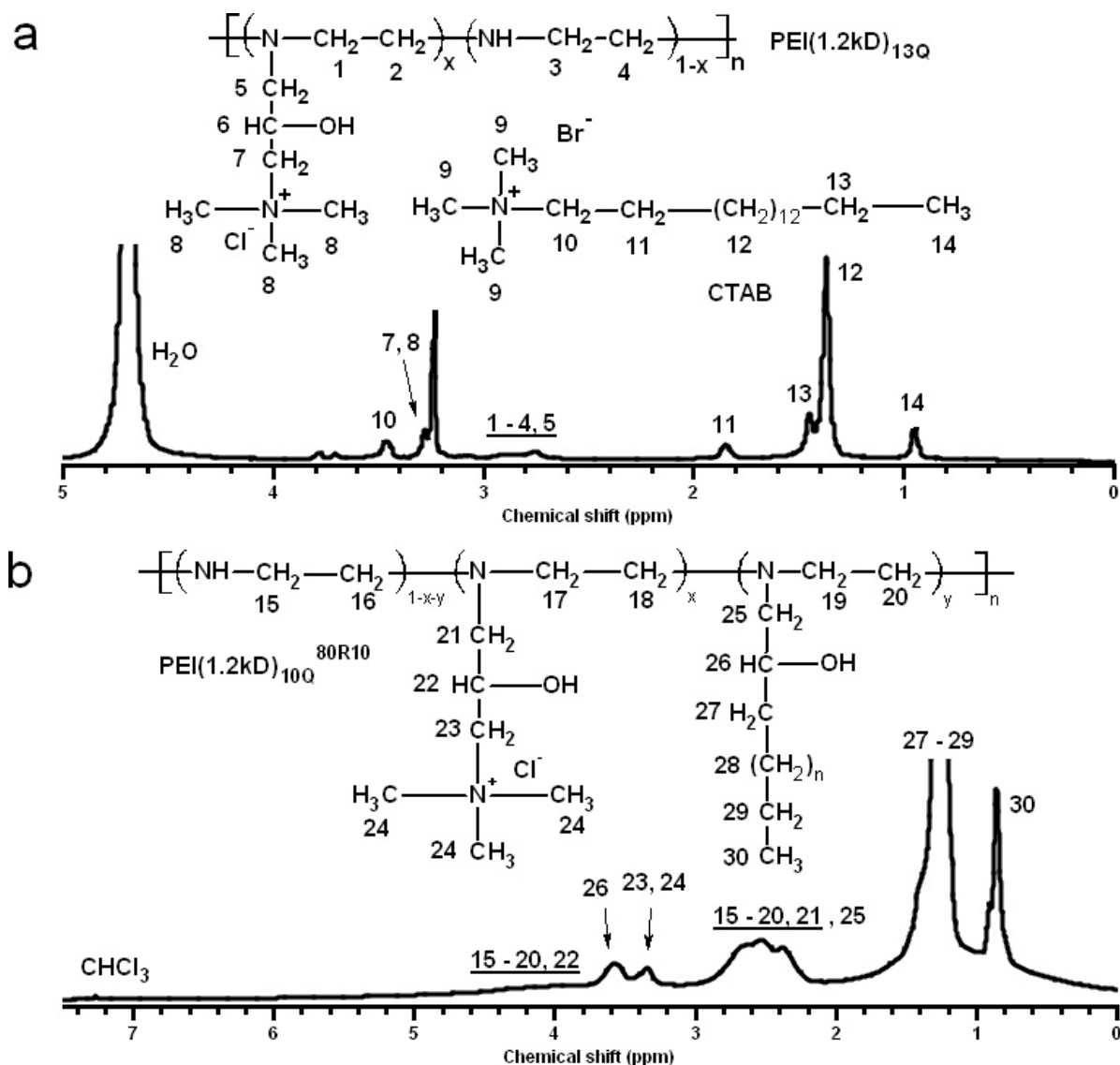


Figure 4.27: ^1H -MAS-NMR spectra of a) adduct **E5** (D_2O , 30°C) and b) adduct **E6** (CDCl_3 , 30°C)

The spectrum of adduct **E6** (Figure 4.27.b) showed a signal derived from the poly(ethylenimine) ethyl hydrogen atoms in the region 2.10 - 3.00 ppm (15 – 20) overlapping with the signal of four hydrogen atoms of methyl groups derived from the ammonium (21) and the alkyl moiety (25). Between 3.80 and 5.00 ppm, an additional signal of the polymer hydrogen atoms (15 – 20) and one hydrogen atom of the ammonium moiety (22) was detected. The signal of the four methyl groups attached to the ammonium moiety appeared between 3.25 - 3.45 ppm (23, 24). Between 3.45 - 3.80 ppm, the signal of the hydrogen atom on the carbon atom next to the hydroxyl group of the alkyl moiety (12) was measured. The methyl groups of the alkyl chains gave a signal between 0.90 – 2.00 ppm (27 - 29). The signal of the methyl group at

4 Preparation of [montmorillonite/PEIxQyR] adducts

the end of the alkyl chains showed up between 0.80 – 0.90 ppm (30). Signals corresponding to CTAB (cf. Figure 4.19) were not found, which shows that the CTAB content was below the NMR sensitivity. The missing CTAB signals demonstrate that the chosen combination of polymer and purification method led to an adduct with very low CTAB residues.

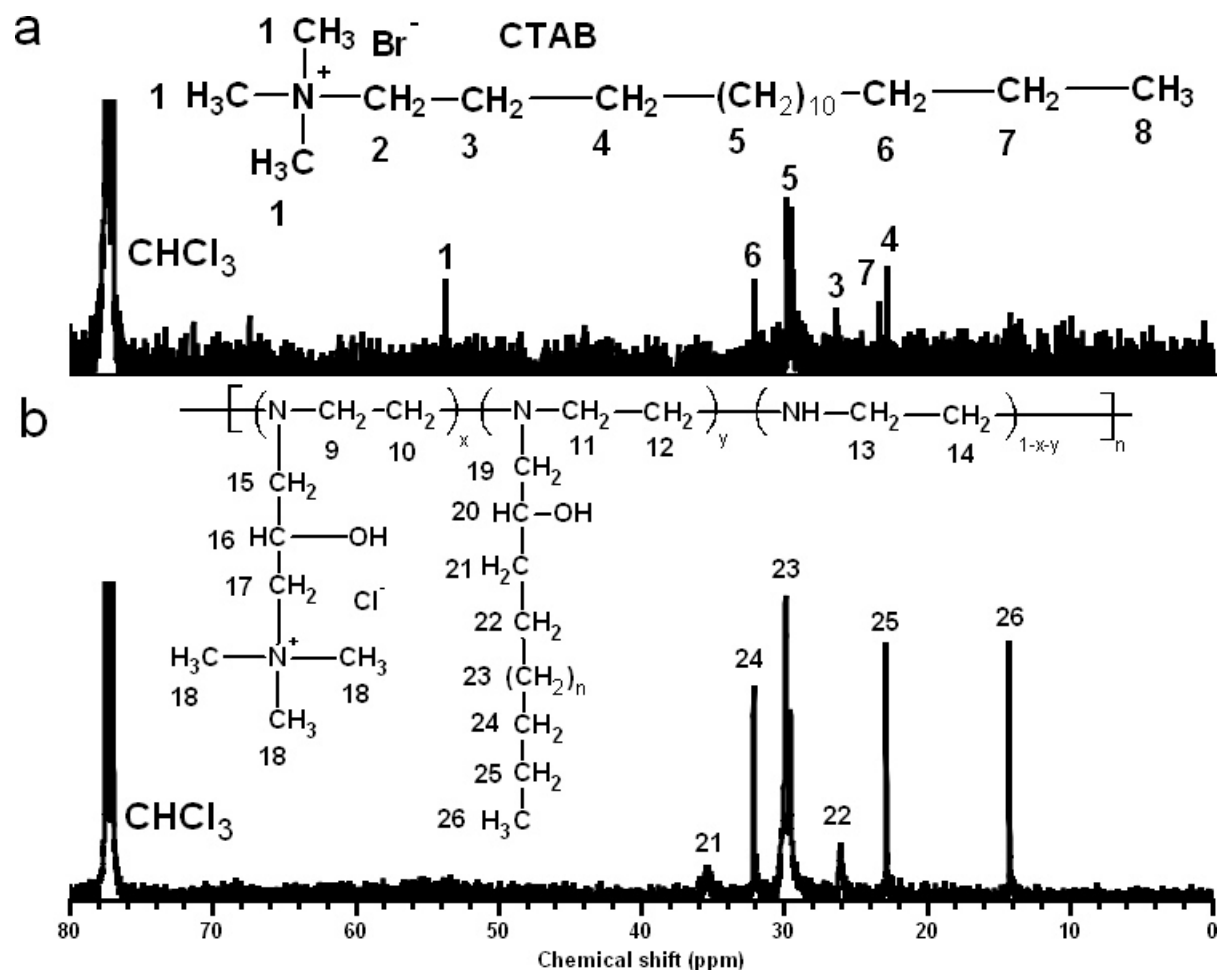


Figure 4.28: ¹³C-MAS-NMR spectra of a) adduct **E5** and b) adduct **E6**, 30°C, CDCl₃

In Figure 4.28 the ¹³C-MAS-NMR spectra of a) adduct **E5** and b) adduct **E6** are shown. The spectrum of adduct **E5** (Figure 4.28.a) showed signals corresponding to CTAB at 53.9, 32.1, 29.6, 27.0, 23.4, and 22.8 ppm (1- 8). Signals of the PEI(1.2kD)_{13Q} polymer were not detected. The spectrum of adduct **E6** (Figure 4.28.b), on the other hand, exhibited only signals corresponding to the alkyl chains attached to the poly(ethylenimine) at 35.4, 32.0, 29.8, 25.9, 22.8, and 14.2 ppm (21 – 26) but no signals of CTAB carbon atoms. The low signal intensity of the poly(ethylenimine) and the 2-hydroxypropyl-3-(N,N,N-trimethylammonium chloride) carbon atoms indicate a rapid spin-lattice relaxation process of the carbon atoms caused by a dipole-di-

pole interaction of the carbon atoms with directly attached or spatially neighbored atoms [58].

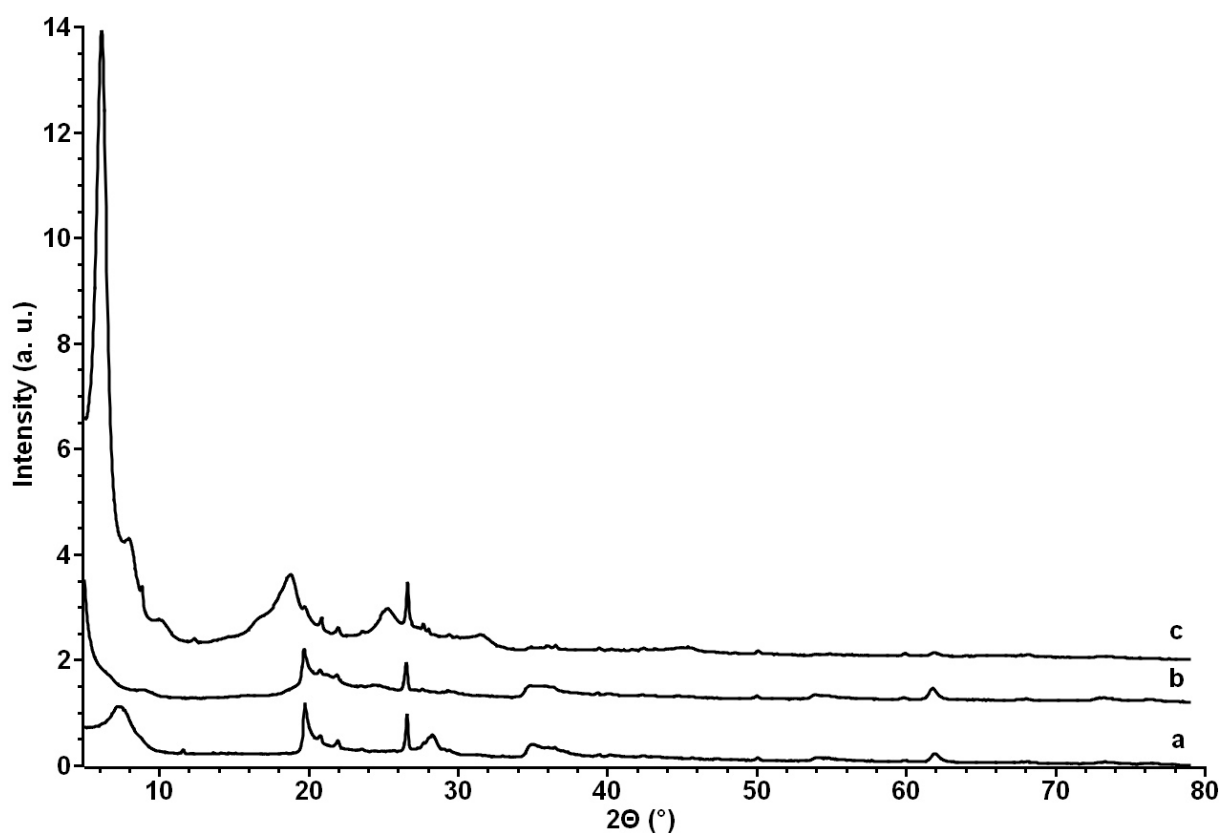


Figure 4.29: Wide-angle X-ray diffractograms of a) Na-bentonite **B1**, b) adduct **E5**, and c) adduct **E6**

Figure 4.29 compares the wide-angle XRD diffractograms of a) Na-bentonite **B1**, b) adduct **E5**, and c) adduct **E6**. The diffractograms were normalised to the reflexes at $2\Theta = 19.7^\circ$. An overview over the measured lattice constants c and the diameter of the polymers is given in Table 4.20. Apart from a broad reflex between $2\Theta = 18$ and 20° the diffractogram of adduct **E5** (Figure 4.29.b) showed also reflexes with maxima at $2\Theta = 8.7$ and 16.0° which were assigned to the Miller indices d_{002} and d_{004} . After extrapolation to the Miller index d_{001} , the lattice constant c was calculated to be 2.03 ± 0.20 nm. After subtraction of the thickness of one montmorillonite platelet from the lattice constant, the gap between the montmorillonite platelets was determined to be $d_m = 1.37$ nm. Comparing the interlayer distance with the calculated polymer diameter of 1.69 nm led to the conclusion that the polymer was completely intercalated although the differences between the measured and the predicted interlayer distance indicate a compressed polymer.

In addition to a broad reflex between $2\Theta = 14$ and 20° the diffractogram of adduct **E6**

(Figure 4.29.c) exhibited also reflexes with maxima at $2\Theta = 6.16, 8.00, 8.85, 10.10, 12.37, 16.90$ and 18.79° . Using the formula of a monoclinic crystal system for the determination of the Miller indices (cf. Chapter 2), the reflexes were attributed to the Miller indices d_{002} to d_{009} . After extrapolation to d_{001} , the lattice constant c was determined to be 4.44 ± 3.08 nm. Subtracting the thickness of one montmorillonite platelet, the interlayer distance d_m was determined to be 3.78 nm. The measured interlayer distance was higher than the expected interlayer distance of 2.58 nm, obtained from the calculation of the polymer diameter. Considering a compression of the polymer sandwiched between two MMT platelets it may be possible that a double layer of polymer molecules exist between the MMT platelets. Although the diffractograms of the adducts **E5** and **E6** were dominated by reflexes corresponding to an intercalated polymer, it could not be ruled out that small amounts of CTAB were still present.

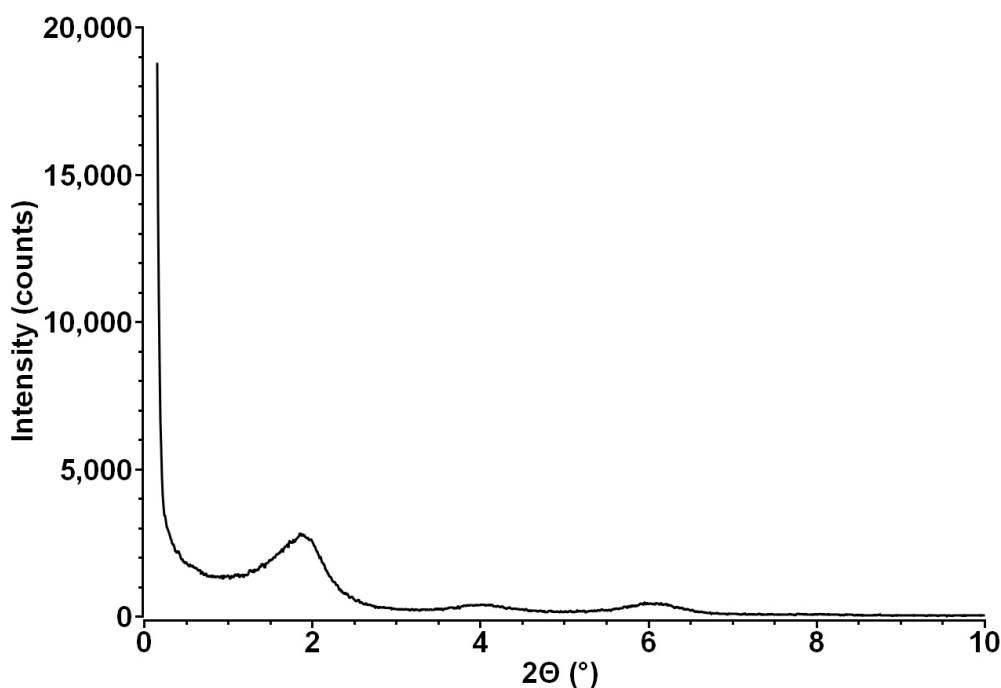


Figure 4.30: Small-angle X-ray diffractogram of adduct **E6**

By a small-angle XRD measurement of adduct **E6** (Figure 4.30), the fairly complete intercalation of the PEI(1.2kD)_{20Q}^{80R10} polymer into the MMT was confirmed. In the region of $2\Theta = 0.15$ to 10° reflexes with maxima at $2\Theta = 1.88, 4.00$ and 6.05° appeared. The reflexes were assigned to the Miller indices d_{001} to d_{003} . After calculating the full width at half maximum of the d_{001} reflex, the lattice constant c was determined to be 4.77 ± 0.70 nm. After subtracting the thickness of one MMT platelet, the gap between the MMT platelets was calculated to be 4.11 nm. Comparing the interlayer distances derived from the wide- (Figure 4.29.c) and the small-angle measurement it

4 Preparation of [montmorillonite/PEI_xQ_yR] adducts

was found that similar distances were obtained. This result shows that the calculation and the direct measurement of the interlayer distance lead to similar results which prove that wide-angle investigations can be used to determine the intercalation of polymers into the MMT.

Table 4.20: Lattice constant *c* and diameter of the polymers of the adducts **E5 and **E6****

Entry	Adduct composition	Lattice constant <i>c</i> (nm)	Calc. polymer diameter (nm)
E5	[MMT _{B1} /PEI(1.2kD) _{13Q}]	2.03 ± 0.20 (w)	1.69
E6	[MMT _{B1} /PEI(1.2kD) _{20Q} ^{80R10}]	4.44 ± 3.08 (w) 4.77 ± 0.70 (s)	2.58

MMT_{B1} = Na-bentonite **B1** (cf. Table 4.2), PEI(1.2kD) = poly(ethylenimine) with $M_n = 1,200$ g/mol, $M_w/M_n = 1.08$, PEI(10kD) = poly(ethylenimine) with $M_n = 10,000$ g/mol, $M_w/M_n = 2.5$, xQ = mol% 2-hydroxypropyl-3-(N,N,N-trimethylammonium chloride), yR10 = mol% 2-hydroxydecane, w = wide-angle XDR, s = small-angle XRD

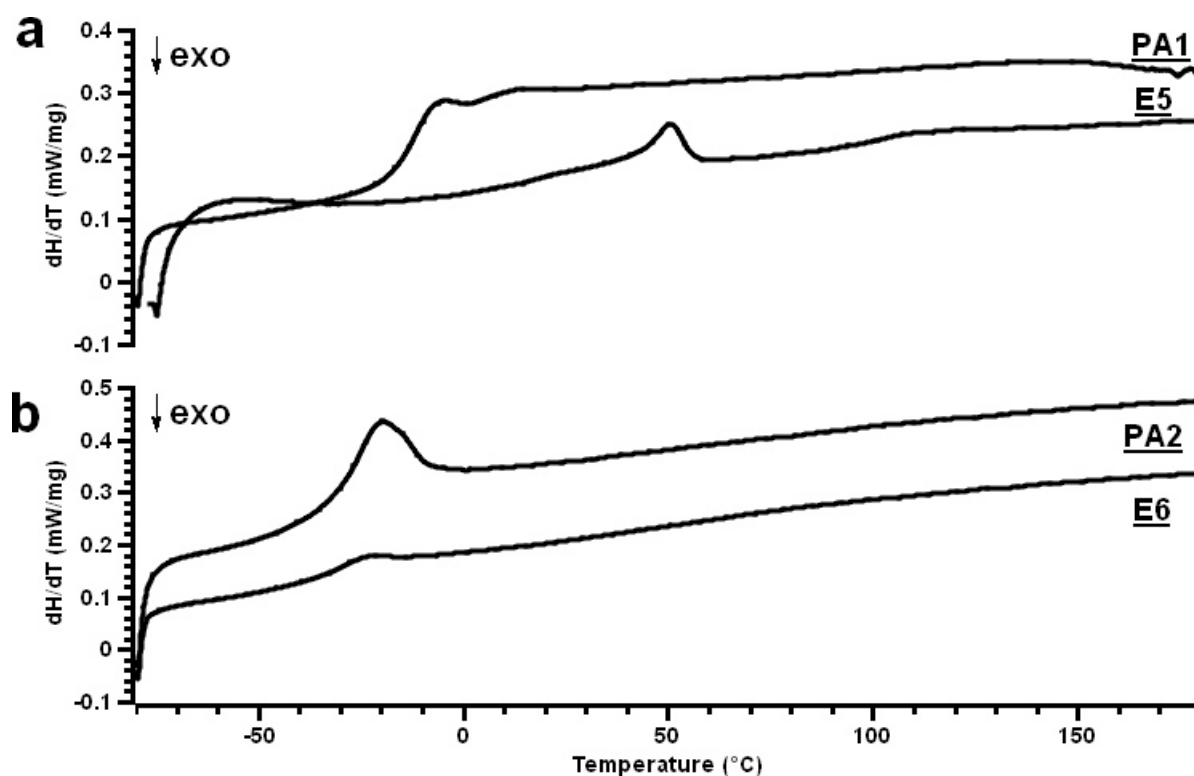


Figure 4.31: DSC thermograms of a) polymer **PA1** and adduct **E5** and b) polymer **PA2** and adduct **E6**, 2. heating run, N₂ atmosphere, dT/dt = 10 K/minute

To obtain information about the thermal behaviour of the polymers in the adducts, the adducts **E5** and **E6** were studied by differential scanning calorimetry. Figure 4.31

shows the differential scanning calorimetry thermograms of a) polymer **PA1** and adduct **E5**, and b) polymer **PA2** and adduct **E6**.

Polymer **PA1** (Figure 4.31.a) exhibited a glass transition at -10.6°C. The thermogram of adduct **E5** (also Figure 4.31.a) showed a melting transition at 45.9°C. Comparing the DSC thermogram of adduct **E5** and adduct **E4** (cf. Figure 4.22), the melting transition was interpreted as intercalated CTAB. Although the slope of the thermogram indicated a glass transition in the region -20 to 30°C, the intensity was too weak to be interpreted safely. With polymer **PA2** (Figure 4.31.b), a glass transition was measured at -24.5°C which was similar to the glass transition of adduct **E6** (Figure 4.31.b) of -28.1°C. Different to adduct **E5**, no signals corresponding to CTAB were detected with adduct **E6**.

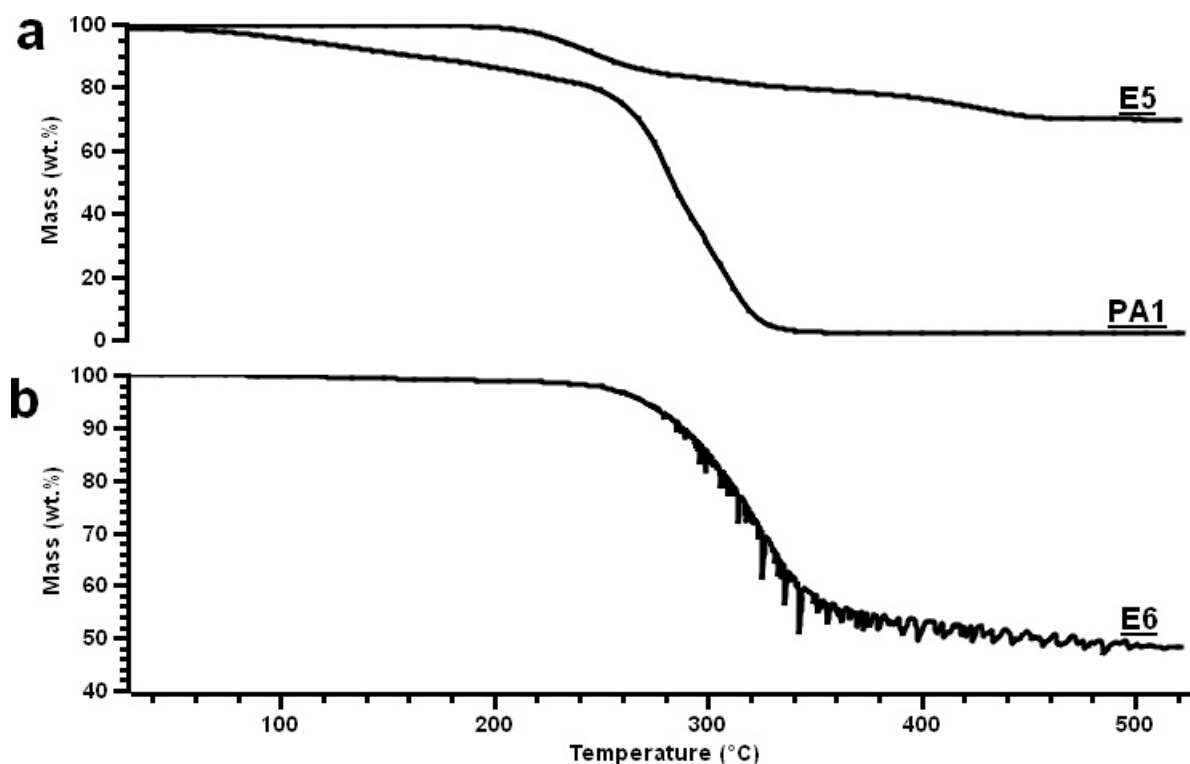


Figure 4.32: TGA thermograms of a) polymer **PA1** and adduct **E5**, and b) adduct **E6**, He atmosphere, $dT/dt = 10$ K/minute

To investigate the decomposition behaviour of the adducts **E5** and **E6**, thermogravimetric investigations were performed. In Figure 4.32 the TGA thermograms of a) adduct **E5** and polymer **PA1** and b) adduct **E6** are shown. The decomposition of polymer **PA1** (Figure 4.32.a) started at 240°C after losing about 20 wt.% water (the discussion can be found in Chapter 3). With adduct **E5** (Figure 4.32.a) the organic material showed the same decomposition behaviour as the adducts **E4** (Figure 4.23) which is a three step decomposition at 198, 300 and 380°C which showed again that

4 Preparation of [montmorillonite/PEIxQyR] adducts

CTAB was still present in the adduct. The organic content was determined to 30.3 wt.% which was 6.4 wt.% higher than theoretically expected and may be caused by the CTAB. Different to the neat polymer, adduct **E5** contained no moisture which indicates that the water shell around the ammonium groups was broken due to the proximity to the montmorillonite. Adduct **E6** (Figure 4.32.b) exhibited a decomposition temperature of 250°C. The noise of the thermogram was caused by a polluted valve. The polymer content was determined to be 51.8 wt.% which was in good agreement to the theoretically expected value of 50.0 wt.%. Furthermore, no moisture or CTAB impurities were detected.

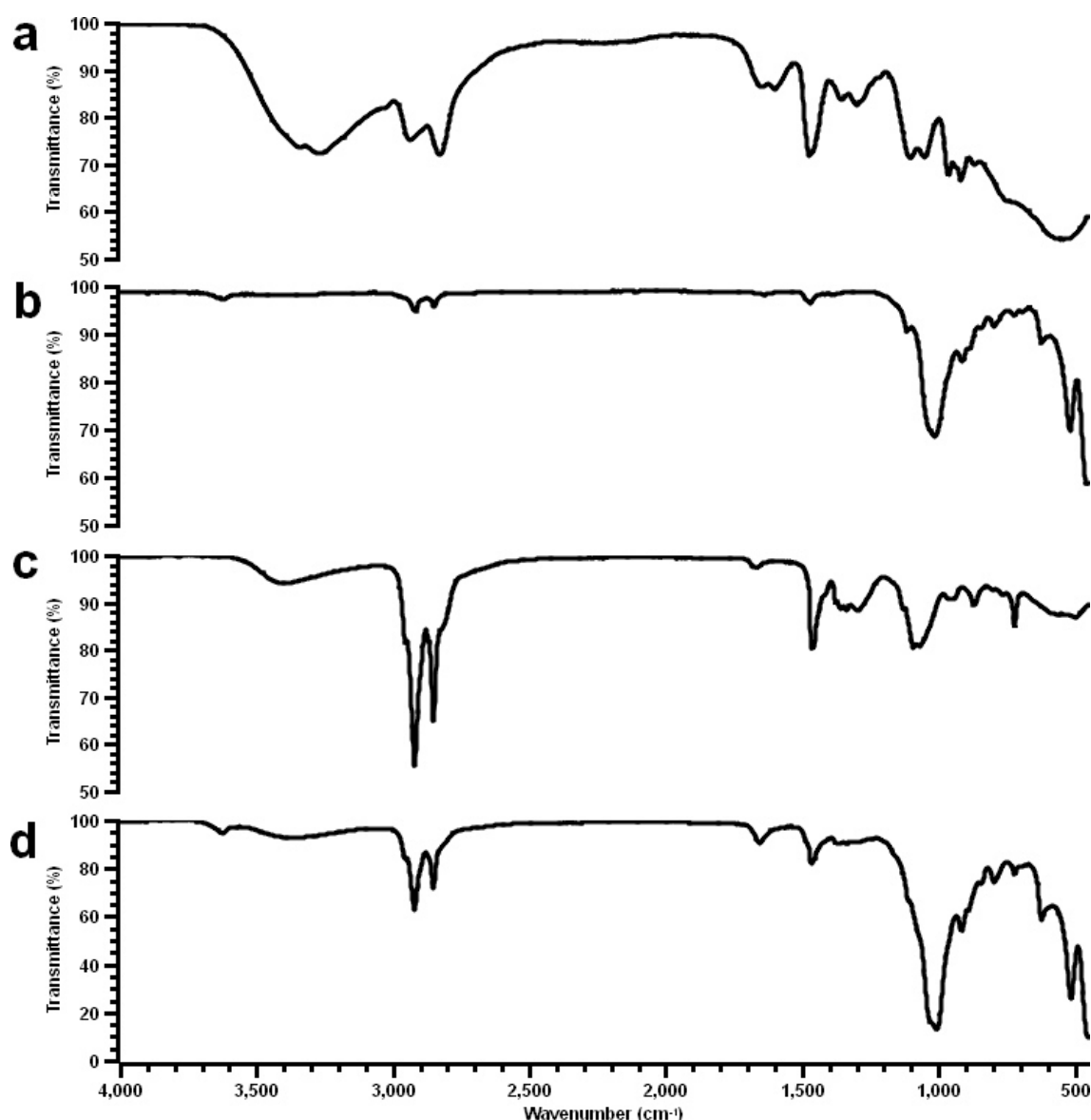


Figure 4.33: ATR-FT infrared spectra of a) polymer **PA1**, b) adduct **E5**, c) polymer **PA2**, and d) adduct **E6**

4 Preparation of [montmorillonite/PEIxQyR] adducts

With infrared spectroscopy studies, the functional groups present in the adducts **E5** and **E6** were determined. Figure 4.33 compares the infrared spectra of a) polymer **PA1**, b) adduct **E5**, c) polymer **PA2**, and d) adduct **E6**.

With adduct **E5** (Figure 4.33.b) bands corresponding to the polymer and the montmorillonite were detected. The bands of the polymer were very weak which points to a low polymer content. Bands of CTAB were not measured which indicates that the CTAB residues were very low. Also with adduct **E6** only bands of the polymer and the montmorillonite were measured. With both adducts, the Si-O-Si stretching vibration bands of the montmorillonite were shifted which points to an interaction between the ammonium groups of the polymers and the Si-O-Si moieties of the montmorillonite.

The elemental composition of the adducts **E5** and **E6** has been investigated by means of XRF measurements and is listed in Table 4.21. Also, the calculated sum formula of the montmorillonite of the adducts is given. The main elements detected with both adducts were Si, Al, Fe, Mg, Ca, Br, and Cl. The adducts contained also small amounts of sulphur and potassium. As shown by the presence of the sodium cations, the ammonium moieties of the polymers didn't replace this cation completely. Both adducts exhibited an Al:Mg [mol/mol] ratio of about 7.53 which points compared to the ratio of non-treated montmorillonite of 4.56 [8, 9] and montmorillonites treated with acids (cf. Table 4.8 and [10]) to a pretreatment of the montmorillonite with an acid by the manufacturer.

Table 4.21: Elemental composition of the adducts **E5 and **E6****

Element	E5 (wt.%)	E6 (wt.%)
Si	58.35	53.21
Al	15.33	13.29
Fe	8.70	11.63
Ca	1.12	1.33
Mg	1.83	1.59
Na	0.19	0.70
K	0.82	0.66
S	0.02	0.15
Cl	0.47	2.33
Br	13.16	15.10
Sum formula of montmorillonite	$\text{Na}_{0.03}(\text{Al}_{1.77}\text{Mg}_{0.23})(\text{Si}_4\text{O}_{10})$ (OH) ₂	$\text{Na}_{0.11}(\text{Al}_{1.77}\text{Mg}_{0.23})(\text{Si}_4\text{O}_{10})$ (OH) ₂

4 Preparation of [montmorillonite/PEI_xQyR] adducts

The mineral composition of the inorganic fraction of the adducts **E5** and **E6** is listed in Table 4.22. The bentonite of adduct **E5** consisted of 66.0 wt.% montmorillonite, 27.0 wt.% quartz/cristobalite (both SiO₂), 1.6 wt.% CaCO₃, and 5.4 wt.% of iron, potassium, and sulphur. The montmorillonite content of adduct **E6** was with 61.8 lower than with adduct **E5**, indicating that [MMT/PEI(1.2kD)_{20Q}^{80R10}] fractions with lower densities were removed during the purification of the adduct.

Table 4.22: Mineral composition of the inorganic fraction of the adducts **E5 and **E6****

Entry	Na-Montmorillonite (wt. %)	Quartz/ cristobalite (wt. %)	CaCO ₃ (wt. %)	Other (wt. %)
E5	66.0	27.0	1.6	5.4
E6	61.8	28.6	2.0	7.6

Other = potassium, sulphur, iron

It was tried to calculate the composition of the organic fraction of the adducts **E5** and **E6** by correlating the chlorine content with the polymer and the bromine content with the CTAB content of the adducts. The composition of the organic fraction of the adducts is listed in Table 4.23. While adduct **E5** contained CTAB as shown from the DSC and TGA data, neither the IR, DSC, TGA or XRD data of adduct **E6** showed the presence of CTAB impurities. With this background, it was assumed that the bromine and chlorine ions were exchanged between the trimethylammonium moiety of the quarternized poly(ethylenimine)s and the CTAB.

Table 4.23: Calculated composition of the organic fraction of the adducts **E5 and **E6****

Entry	CTAB (wt.%)	Polymer (wt.%)	Total organic material (wt.%)
E5	24.8	2.6	27.4
E6	22.6	23.8	46.4

CTAB = (1-hexadecyl)trimethylammonium bromide

To verify this assumption, after a reaction time of 20 h a sample of adduct **E8.22** was taken and purified as described in the experimental part of this Chapter. The liquid fraction was collected, dried at ambient temperature and atmosphere for 18 h and in vacuum at 80°C for 48 h. Afterwards, 2 g of the dried liquid fraction was dispersed in 3 mL toluene and precipitated in 30 mL methanol to remove most of the CTAB. The residue was washed with 20 mL methanol and dried under vacuum at 80°C for 74 h. The substance (= **E8.22.P**) was then investigated with ¹H-NMR and XRF. The ¹H-

4 Preparation of [montmorillonite/PEI_xQyR] adducts

NMR spectrum of **E8.22.P** is shown in Figure 4.34.

As shown by the presence of the signals at 1.7 ppm (18) and 3.4 ppm (17), the fraction **E8.22.P** contained beside the PEI(10kD)_{10Q}^{80R10} polymer **PB4.20** also CTAB. It was attempted to calculate the CTAB content of the fraction which included the correction of the integrated areas of the polymer and the CTAB and the determination of the molar ratio of polymer to CTAB. The applied procedures are described by the following equations. At $\delta = 3.30 - 3.50$ ppm the signal of the 11 hydrogen atoms of the methyl groups attached to the ammonium moieties of the polymer (9, 10) were overlapping with the signal of the 9 hydrogen atoms attached to the CTAB ammonium methyl groups (17). By fitting, the areas corresponding to the compounds were determined.

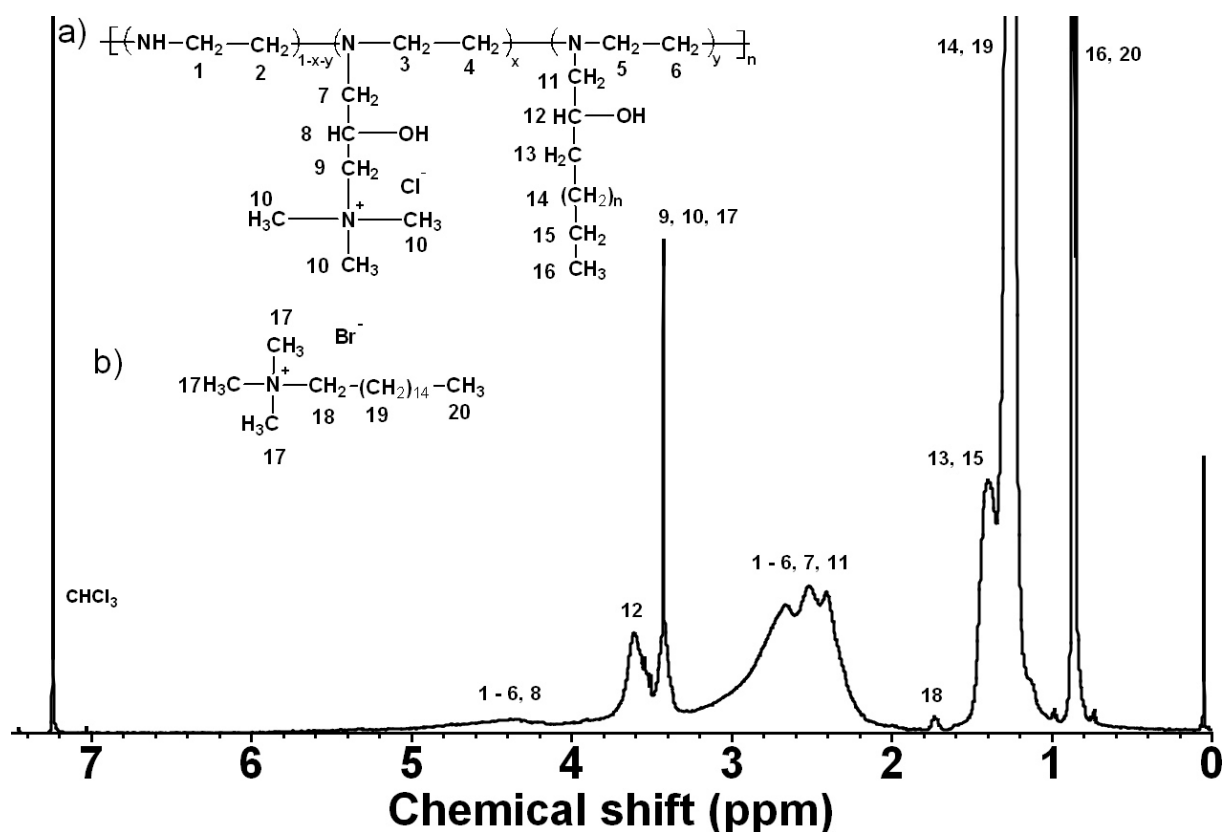


Figure 4.34: ¹H-NMR spectrum of **E8.22.P** with the structure units of a) PEI(nkD)_{xQ}^{yR}, and b) CTAB, CDCl₃, 30°C

At $\delta = 0.80 - 0.90$ ppm the signal corresponding to the alkyl methyl groups (16) and the signal corresponding to the CTAB methyl groups (20) were overlapping. The area corresponding to the alkyl groups was determined using the area of the CTAB methyl groups attached to the ammonium moiety at 1.70 – 1.80 ppm (17) as shown in Equation 4.6.

4 Preparation of [montmorillonite/PEI_xQyR] adducts

$$A'_{R10,CH3} = A_{R10,CH3} - \frac{A_{CTAB,CH2} \cdot 3}{2} \quad \text{Eq. 4.6}$$

(with $A'_{R10,CH3}$ = corrected area of the $^1\text{H-NMR}$ signal intensity at 0.80 – 0.90 ppm, $A_{R10,CH3}$ = integrated $^1\text{H-NMR}$ signal intensity at 0.80 – 0.90 ppm, $A_{CTAB,CH2}$ = integrated $^1\text{H-NMR}$ signal intensity at 1.70 – 1.80 ppm)

The signals of the polymer backbone at $\delta = 2.20 - 3.00$ ppm and $\delta = 4.20 - 5.20$ ppm (1 – 6) overlapped with signals of hydrogen atoms of the ammonium group at $\delta = 2.20 - 3.00$ ppm (7) and $\delta = 4.30$ ppm (8). Another overlap occurred between hydrogen atoms of the alkyl group and the polymer at $\delta = 2.90 - 2.20$ ppm (11). Thus, the area corresponding to the polymer hydrogen atoms was determined using Equation 4.7.

$$A'_{PEI,C2H4} = A_{PEI,C2H4} - \frac{2 \cdot A'_{R10,CH3}}{3} - \frac{3 \cdot A'_{Q,C4H11}}{11} \quad \text{Eq. 4.7}$$

(with $A_{PEI,C2H4}$ = corrected area of the $^1\text{H-NMR}$ signal intensity of the poly(ethylenimine) backbone from 2.20 - 3.00 and 4.20 - 5.20 ppm, $A_{PEI,C2H2}$ = integrated $^1\text{H-NMR}$ signal intensity of the poly(ethylenimine) backbone at 2.20 - 3.00 and 4.20 - 5.20 ppm, $A'_{R10,CH3}$ = corrected area of the integrated $^1\text{H-NMR}$ signal intensity of the alkyl methyl groups at 0.80 – 0.90 ppm, $A'_{Q,C4H11}$ = corrected area of the integrated $^1\text{H-NMR}$ signal intensity of the ammonium methyl groups from 3.30 – 3.50 ppm)

The molar ratio of CTAB to polymer was calculated using Equation 4.8. With the Equations 4.6 - 4.8, the CTAB content was determined to be 5.1 wt.%. The examination of the sample by X-ray fluorescence, on the other hand, showed that when all ions were assigned in that way that the chlorine ions belonged to the polymer and the bromine ions to the CTAB the mixture contained 28.2 wt.% CTAB. The high bromine content obtained by XRF is a sign for a matrix effect which leads to an overestimation of the bromine content in polymer/CTAB mixtures.

$$\frac{\text{CTAB}}{\text{PEI}} = \frac{A_{CTAB,CH2}}{A'_{PEI,C2H4}} \cdot \frac{4}{2} \quad \text{Eq. 4.8}$$

(with $A_{PEI,C2H4}$ = corrected area of the $^1\text{H-NMR}$ signal intensity of the poly(ethylenimine) backbone from 2.20 - 3.00 and 4.20 - 5.20 ppm, $A_{CTAB,CH2}$ = integrated $^1\text{H-NMR}$ signal intensity from 1.70 – 1.80 ppm)

To determine whether the chlorine and the bromine ions became equilibrated between polymer and CTAB during the preparation of the adduct, an elemental analysis of adduct **E8.2** (cf. Table 4.26) was performed.

4 Preparation of [montmorillonite/PEI_xQyR] adducts

The composition of the adduct is listed in Table 4.24. Since the adduct contained no CTAB (cf. Figure 4.37), the calculation of the polymer composition showed that both, the chlorine and the bromine ions, were attached to the polymer. The molar ratio of bromine to chlorine was determined to be 4.72 which was close to the ratio CTAB to 2-hydroxypropyl-3-(N,N,N-trimethylammonium chloride) during the preparation of adduct **E8.2** of 4.50. From the bromine to chlorine ratio it is concluded that the assumption was correct and the bromine and chlorine ions were indeed shared between CTAB and polymer during the preparation of the adducts. From XRF data, the molar ratio bromine to chlorine of adduct **E8.2** was determined to be 11.70. The high bromine content of the adduct implies that a matrix effect led to an enhancement of the bromine signal [59] which lead to false values of the bromine content of adducts prepared with the replacement procedure. Experiments which could correct the calibration were not successful because a suitable matrix was not found. In detail, XRF data of experiments in which KBr and NaCl were mixed with Na-bentonite and the ratios of the substances were varied led to much lower bromine and chlorine contents than theoretically expected. In conclusion, while the signals of the bromine and chlorine ions in Br/Cl/bentonite mixtures were lower than expected, with adducts prepared by the replacement procedure the signal of the bromine ions was enhanced. The polymer content obtained from XRF data is, therefore, prone to a high error. Nonetheless, it was tried to calculate the polymer content of the adducts **E5** and **E6** from XRF data by assigning the bromine and chlorine ions to the polymers.

Table 4.24: Elemental composition of adduct **E8.2**

Element	E8.2 [wt.%]
N	4.46
C	48.3
H	8.23
Cl	0.19
Br	2.02

Table 4.25: Polymer content of the adducts **E5 and **E6****

Entry	XRF (wt.%)	TGA (wt.%)	Theory (wt.%)
E5	34.4	30.3	23.9
E6	63.9	51.8	50.0

Table 4.25 lists the corrected polymer content of the adducts **E5** and **E6** calculated by using XRF data and obtained from thermogravimetric measurements. With adduct **E5**, the polymer content obtained from the two methods was about 10 wt.% higher

than theoretically expected which points to surplus CTAB in the adduct. Both methods exhibited a similar value which indicates that the polymer content influenced the enhancement of the signal intensity of the bromine. The thermogravimetric analysis of adduct **E6** revealed that the polymer content of the adduct was in good agreement to the theoretical expected value. The calculation of the polymer content based on XRF data, on the other hand, led to an about 12 wt.% higher polymer content than the content obtained from TGA. The higher value obtained from XRF data shows that a higher polymer content leads also to a higher error in the polymer calculation.

Discussion

In this paragraph [MMT/PEI(nkD)_xQ^{yR10}] adducts prepared by the “replacement” method were characterised. “Replacement” means that PEI(nkD)_xQ^{yR} polymers were reacted with pre-formed [MMT/CTAB] under replacement of CTAB. The degree of polymer intercalation of the adducts **E5** and **E6** was determined from wide- and small-angle X-ray diffraction measurements. The real gap between the montmorillonite platelets was calculated by subtracting the thickness of the platelets from the measured or calculated d_{001} interlayer distance. The reaction of a water-soluble PEI(1.2kD)_{13Q} polymer with [MMT/CTAB] led to an adduct with a gap between the montmorillonite platelets of 1.37 nm which was smaller than the calculated polymer diameter of 1.75 nm. The similar theoretical and experimental distances lead to the conclusion that the polymer was completely intercalated although the differences between the measured and the predicted interlayer distance indicate a compressed polymer. The reaction of a PEI(1.2kD)_{20Q}^{80R10} polymer with [MMT/CTAB], on the other hand, led to an adduct (= **E6**) in which a double layer of compressed polymer molecules existed between the MMT platelets. The presence of a double layer was indicated by the difference of the measured (4.11 nm, small-angle) and calculated (3.78 nm, wide-angle) interlayer distance to the calculated polymer diameter of 2.78 nm. Since similar interlayer distances were obtained from the wide-angle and the small-angle measurement it was concluded that the calculation and the direct measurement of the interlayer distance lead to similar results and wide-angle measurements can be applied to determine the intercalation of polymers into montmorillonite as long sufficient enough reflexes from higher order d_{001} distances are available.

While the ¹H-MAS-NMR and the ¹³C-MAS-NMR spectrum of adduct **E5** revealed the presence of CTAB in the adduct, no CTAB was detected with adduct **E6**. While the polymer used to prepare adduct **E5** was soluble in water, the polymer used to prepare adduct **E6** gave only a dispersion in the reaction mixture. It is assumed that CTAB molecules were trapped between the montmorillonite platelets and the purifica-

tion procedure didn't enlarge the gap enough for the CTAB to be removed. Furthermore, a melting transition derived from intercalated CTAB showed up in the differential scanning calorimetry thermogram of adduct **E5** and the TGA curve exhibited a similar profile as [MMT/CTAB]. With adduct **E6**, the polymer exhibited a slightly lower glass transition temperature compared to the neat polymer. No transitions corresponding to CTAB were measured. From the TGA investigations, the polymer content of adduct **E6** was determined to be 51.8 wt.% which was in good agreement to the theoretically expected value of 50.0 wt.%. Also, no moisture or CTAB impurities were detected showing that CTAB didn't exhibit a strong adhesion to the montmorillonite and can be, under the right conditions, removed completely. With adduct **E5**, the total organic content was measured to be 30.3 wt.% which was 6.4 wt.% higher than the theoretically expected value of 23.9 wt.%.

The elemental composition measured by XRF of both adducts showed that both adducts contained beside chlorine also bromine. Investigations on the origin of the bromine revealed that during the reaction of the polymers with [MMT/CTAB] the bromine and chlorine ions were shared between the CTAB and the polymers. The analysis of the XRF, ¹H-NMR and elemental analysis data on the molar ratio of bromine to chlorine of a polymer sample taken during the preparation of adduct **E8.2** showed that a matrix effect led to an enhancement of the bromine signal in adducts prepared by the "replacement" procedure and, therefore, to an overestimation of the polymer content of the adducts. The polymer content of adduct **E6** based on XRF data was about 12 wt.% higher than the content obtained from TGA. With adduct **E5**, on the other hand, the content from TGA and XRF differed only of about 4 wt.% which shows that the lower quantity of polymer in the adduct also lowered the matrix effect. With both adducts, only bands of the polymer and the montmorillonite were detected which indicate that the CTAB content of adduct **E5** was low. Also, the Si-O-Si bands of both adducts were shifted which points to an interaction between the ammonium groups of the polymers and the montmorillonite.

Summary

It was found that the reaction of low molecular PEI(1.2kD)_{13Q} and PEI(1.2kD)_{10Q}^{80R10} polymers with [MMT/CTAB] led to [MMT/PEI(nkD)_{xQ}^{yR10}] adducts with interlayer distances which were in good agreement to the calculated polymer diameters. The XRD data of the larger PEI(1.2kD)_{10Q}^{80R10} polymer indicated furthermore the formation of a polymer double layer. In addition, from ¹H- and ¹³C-MAS-NMR, TGA and DSC measurements the presence or absence of CTAB can be detected. XRF and elemental analysis of the polymer taken during the preparation an example adduct showed that

a matrix effect led to an enhancement of the bromine signal in the XRF and therefore to an overestimation of the bromine content. From the measured interlayer distances and the polymer content obtained from TGA measurements, it is concluded that the “replacement” procedure can be applied to obtain [MMT/PEI(nkD)_xQ^{yR}10] adducts with completely intercalated polymers and, under the right conditions, free of CTAB.

4.3.6 [MMT/PEI(nkD)_xQ^{yR}] adducts prepared by the “indirect replacement” method

Since the “replacement” procedure (Chapter 4.3.4) involved the reaction of PEI(nkD)_xQ^{yR} polymers with separately prepared and isolated [MMT/CTAB] adducts it was tried whether the intercalation of these polymers can also be achieved when the polymers are mixed with CTAB and montmorillonite in an aqueous solution. The investigated pathway is shown in Figure 4.35. In the mixture, the CTAB should intercalate firstly and then be displaced by the polymer due to the low adhesion of the CTAB to the montmorillonite (cf. Paragraph 4.3.4).

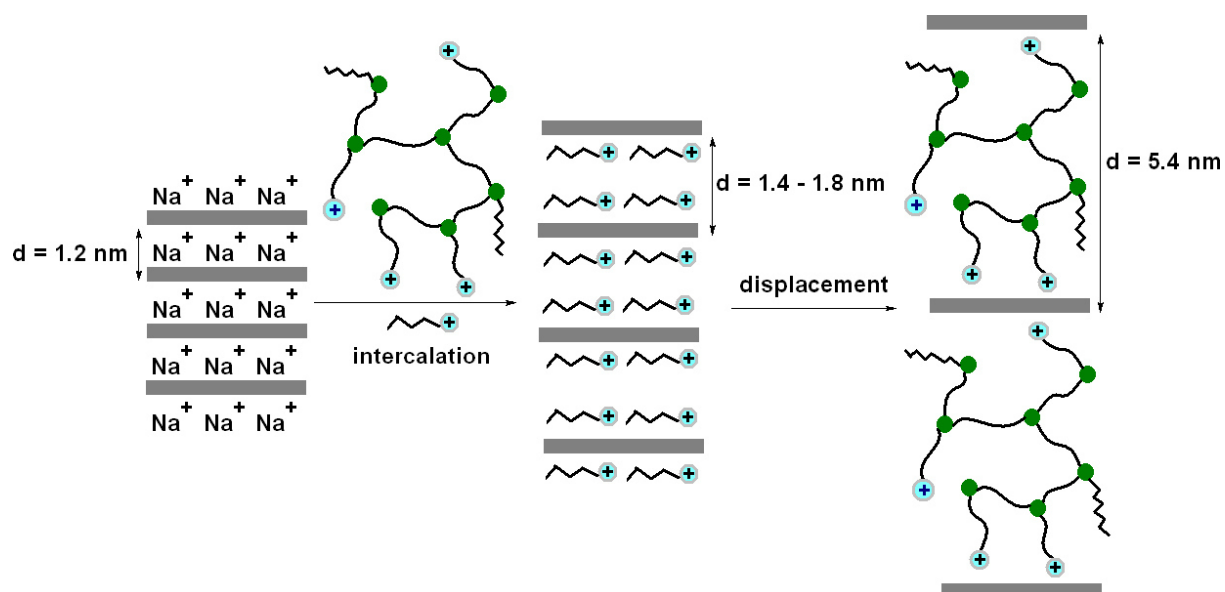


Figure 4.35: Model of the preparation of [MMT/PEI(nkD)_xQ^{yR}] adducts by the “indirect replacement” method

Table 4.26 lists the [MMT/PEI(nkD)_xQ^{yR}] adducts discussed in this paragraph. The adducts **E8** – **E15** were prepared using CTAB as the intercalation aid, with adduct **E7** 1-hexadecylamine was used for this purpose. While the alkyl groups of the polymers used to prepare the adducts **E7** - **E14** consisted of 2-hydroxydodecane moieties, the alkyl groups of the polymer used with adduct **E15** carried 2-hydroxyhexadecane moi-

4 Preparation of [montmorillonite/PEI_xQ_yR] adducts

eties. The prepared [MMT/polymer] adducts were investigated by wide- and small-angle X-ray diffraction, IR, TGA, DSC, XRF, as well as ¹H- and ¹³C-MAS-NMR.

Table 4.26: [MMT/PEI(nkD)_xQ^yR] adducts prepared by the “indirect replacement” method

Entry	Adduct composition	Sol. conc. (g/mL)	Additive	Preparation condition
E7	[MMT _{B1} /PEI(10kD) _{10Q} ^{80R10}]	0.05	1-H	35°C, 144 h, 150 rpm, H ₂ O/ ethanol/ HCl (37 %)/ NaOH (10 wt. % in water) (V/ V/ V/ V) = (141.7/ 18.8/ 1/ 4.4)
E8.1 – E8.22	[MMT _{B1,B2} /PEI(10kD) _{10Q} ^{80R10}]	0.07	CTAB	65°C, 122 h, 150 rpm, H ₂ O/ethanol (V/ V) = (6.3/ 1)
E9	[MMT _{B2} /PEI(10kD) _{10Q} ^{80R10}]	1.00	CTAB	65°C, 66 h, 150 rpm, H ₂ O/ethanol (V/ V) = (1.2/ 1)
E10	[MMT _{B1} /PEI(10kD) _{10Q} ^{80R10}]	0.04	CTAB	65°C, 93 h, 100 rpm, H ₂ O/ethanol (V/ V) = (11.7/ 1)
E11 – E14	[MMT _{B2} /PEI(10kD) _{10Q} ^{80R10}]	0.07	CTAB	as with the adducts E8.1 – E8.22
E15.5 – E15.13	[MMT _{B2} /PEI(10kD) _{10Q} ^{60R14}]	0.08	CTAB	65°C, 76 h, 110 rpm, H ₂ O/isopropanol (V/ V) = (16.5/ 1)

MMT_{B1} = Na-bentonite **B1** (cf. Table 4.2), MMT_{B2} = Na-bentonite **B2** (cf. Table 4.2), PEI(10kD) = poly(ethylenimine) with M_n = 10,000 g/mol, M_w/M_n = 2.5, xQ = mol% 2-hydroxypropyl-3-(N,N,N-trimethylammonium chloride), yR10 = mol% 2-hydroxydodecane, yR14 = mol% 2-hydroxyhexadecane, CTAB = 1-hexadecyltrimethylammonium bromide, 1-H = 1-hexadecylamine, Sol. conc. = solid concentration = MMT + polymer + CTAB

With adduct **E9** the solid concentration was increased to test whether the polymers were still able to intercalate in a concentrated solution. Although the adducts **E8.2** and **E8.21** were prepared in the same way, the adducts were prepared in different quantities and with different bentonites (234 g of adduct **E8.2** with bentonite **B1** and 161 g of adduct **E8.21** with bentonite **B2**). Na-bentonite **B1** was also used to prepare adduct **E7**. Na-bentonite **B2**, on the other hand, was used to prepare the adducts **E9** – **E15**. To determine the adhesion properties of the polymers, the adducts **E8.21** and **E15.8** were purified six times each and the adducts were indexed as **E8.21.1** – **E8.21.6** and **E15.8.1** – **E15.8.6** according to the purification runs performed. For further investigations, larger quantities of adduct **E8** (ca. 12.1 kg) and adduct **E15** (ca.

4 Preparation of [montmorillonite/PEIxQyR] adducts

3.2 kg) were prepared in several batches. While of adduct **E8** twenty batches with batch sizes of 234 g - 1254 g were prepared, only seven batches with batch sizes of 136 – 722 g were produced of adduct **E15**. The weighted average yield over all batches was calculated to be 96.3 % with adduct **E8** and 75.8 % with adduct **E15**.

Figure 4.36 shows the ¹H-MAS-NMR spectrum of adduct **E7**. Signals of the polymer hydrogen atoms (1 – 16) were detected at the same position as with adduct **E6** (cf. Figure 4.27). Additionally, the spectrum exhibited signals of the 1-hexadecylamine (17 - 21). From the presence of the 1-hexadecylamine, it is concluded that the purification of the adduct was not performed carefully enough to remove all 1-hexadecylamine residues.

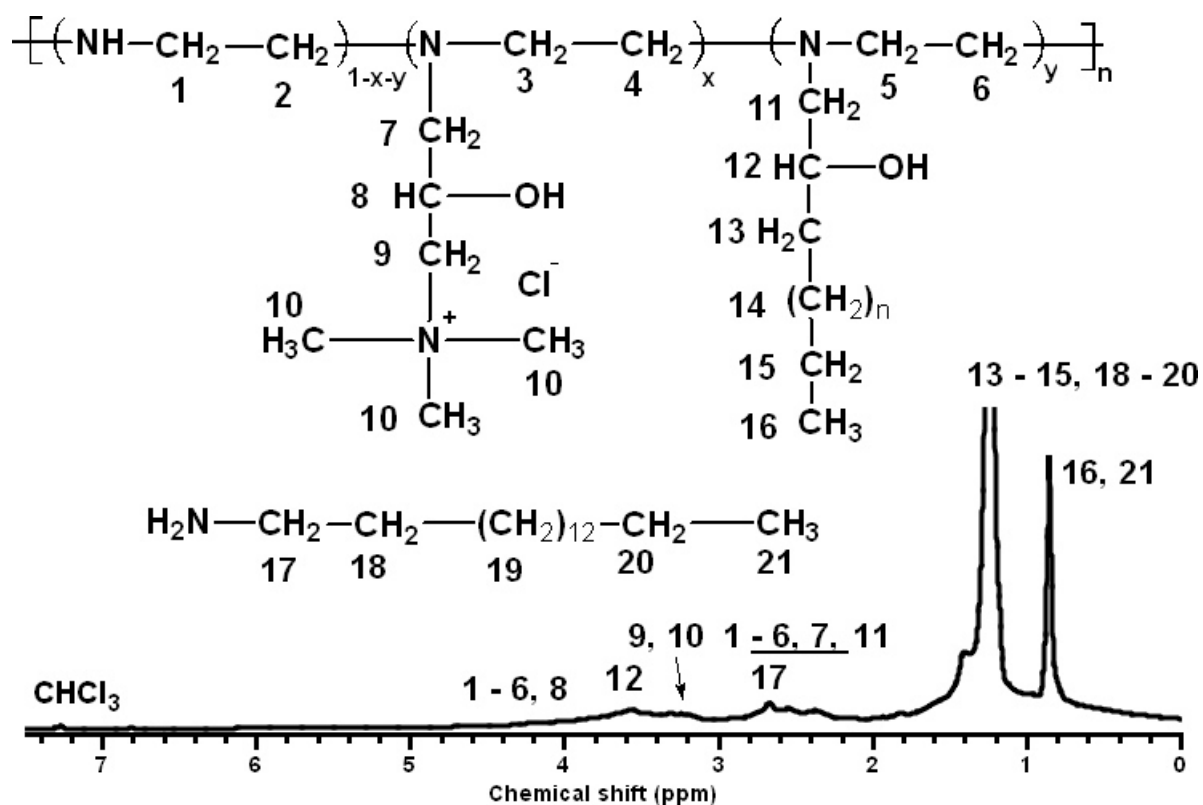


Figure 4.36: ¹H-MAS-NMR spectrum of adduct **E7**, CDCl₃, 30°C

Figure 4.37 compares the ¹H-MAS-NMR spectra of a) adduct **E8.2**, b) adduct **E9** and c) adduct **E15.8.2**. With all three adducts only signals of the polymers were detected but no signals of CTAB (cf. Figure 4.19). It is, therefore, concluded that the applied purification procedures were sufficient to remove most of the CTAB.

4 Preparation of [montmorillonite/PEIxQyR] adducts

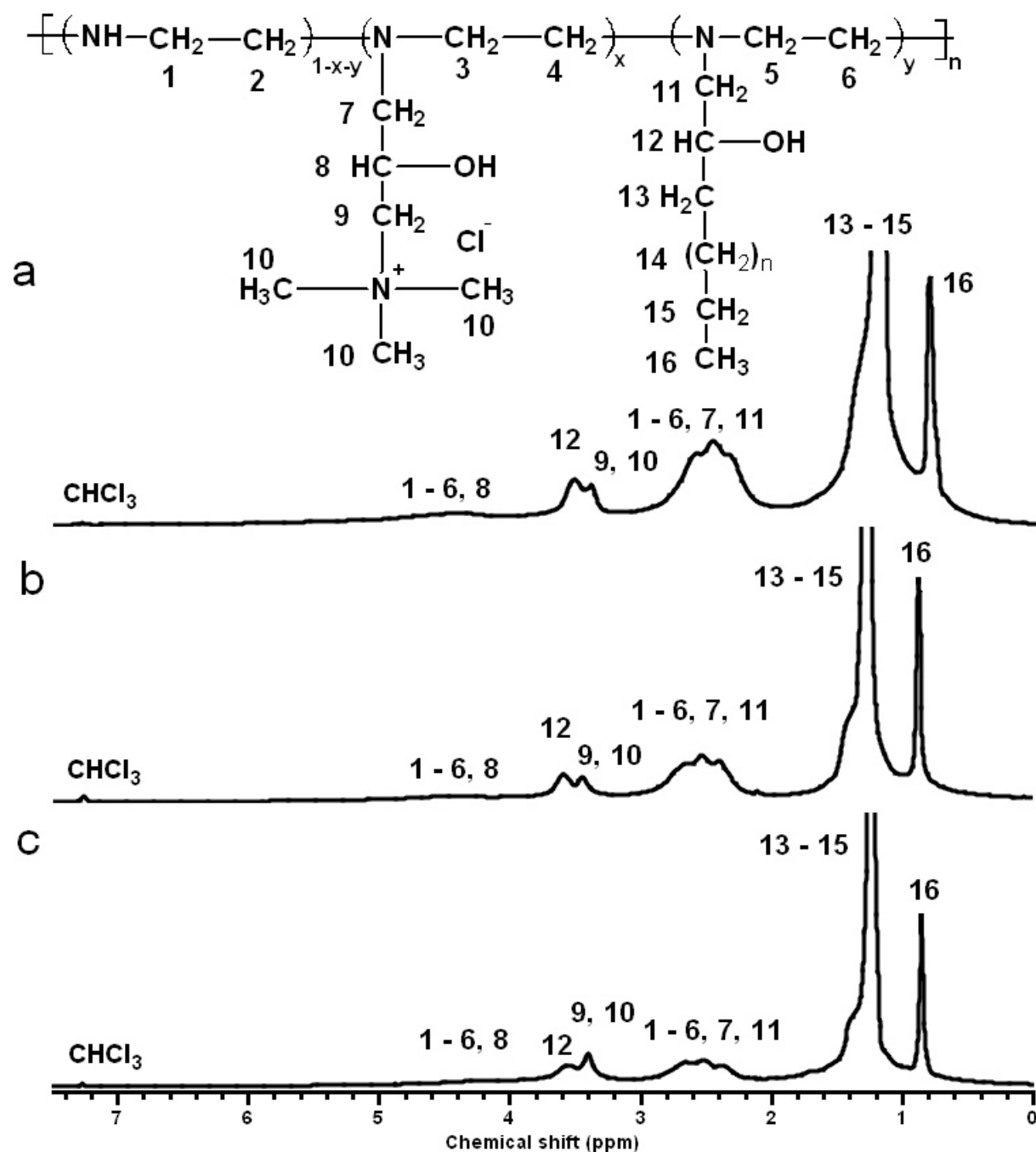


Figure 4.37: ¹H-MAS-NMR spectra of a) adduct **E8.2**, b) adduct **E9**, and c) adduct **E15.8.2**, CDCl₃, 30°C

In Figure 4.38 the ¹³C-MAS-NMR spectra of a) adduct **E8.2**, b) adduct **E9**, and c) adduct **E15.8.2** are compared. All three adducts exhibited only signals of the alkyl moieties around 35.2, 31.9, 29.7 – 29.3, 25.8, 22.6 and 14.0 ppm. Neither signals corresponding to the ammonium moiety or the poly(ethylenimine) were detected. With adduct **E7** also only signals corresponding to the alkyl chains were measured. With adduct **E15.8.2** (Figure 4.38.c), an additional signal was measured at 53.3 ppm which

points to the presence of CTAB residues (cf. Figure 4.20) and is a sign for an inhomogeneous adduct since the ^1H -MAS-NMR spectrum didn't show CTAB (cf. Figure 4.37.c).

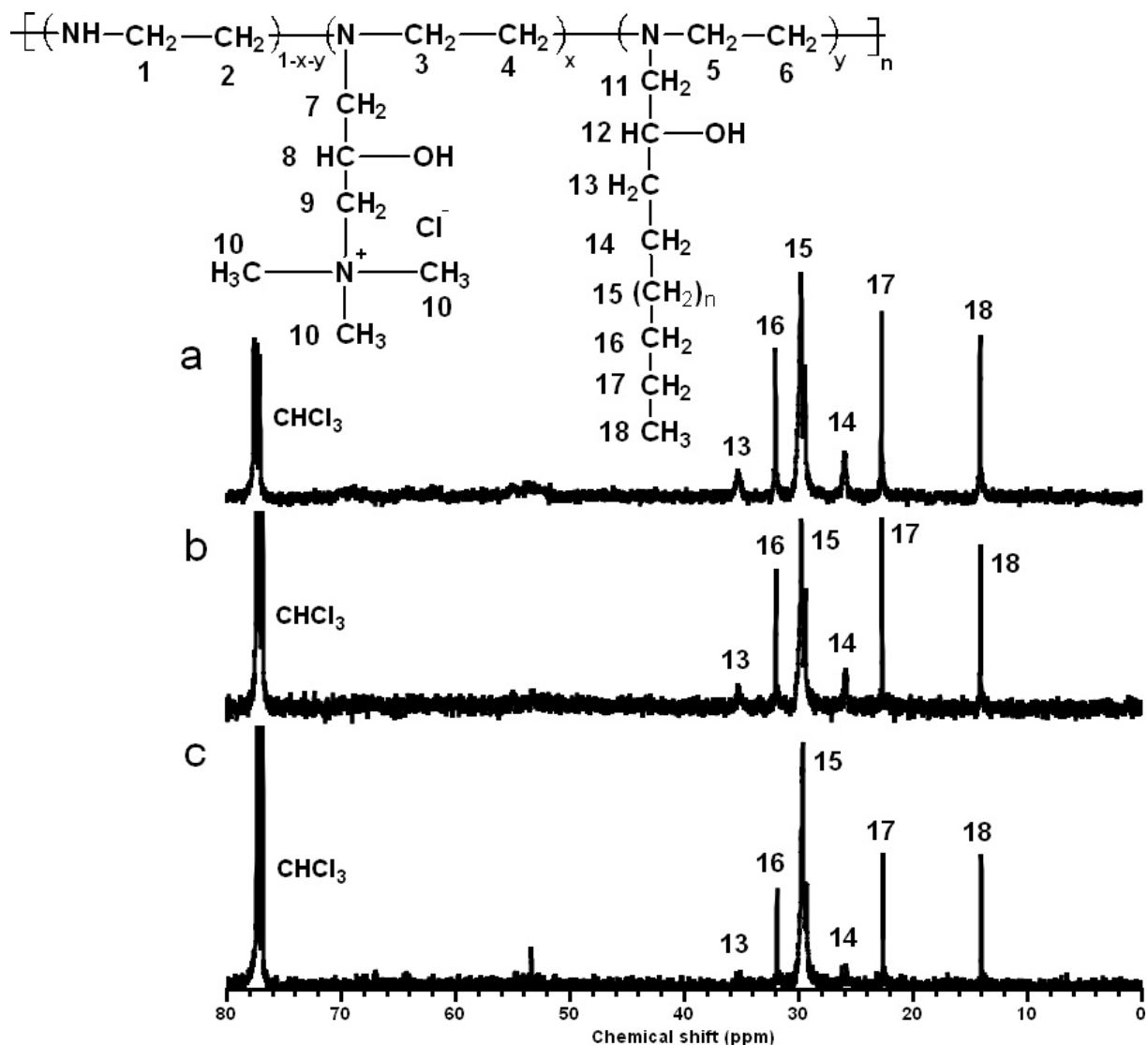


Figure 4.38: ^{13}C -MAS-NMR spectra of a) adduct **E8.2**, b) adduct **E9**, and c) adduct **E15.8.2**, CDCl_3 , 30°C

Figure 4.39 shows the small-angle X-ray diffractograms of a) adduct **E8.2** and b) adduct **E8.21.4**. While adduct **E8.2** was prepared as described in the experimental part of this Chapter, adduct **E8.21.4** was prepared in a smaller quantity and purified four times. Between $2\Theta = 0.15$ to 10° reflexes with maxima at $2\Theta = 1.30, 1.78, 3.35, 3.84, 5.80, 6.74$ and 7.50° were detected with adduct **E8.2** (Figure 4.39.a) and were assigned to the Miller indices d_{001} to d_{009} . After determination of the full width at half maximum of the d_{001} reflex, the lattice constant c was determined to be 6.89 ± 2.95

nm. The large width at half maximum agreed well with the broad size distribution of the used polymer. The gap d_m between the montmorillonite platelets in the adduct was calculated to be 6.23 nm which is in good agreement to the calculated polymer diameter of 5.28 nm and proves the successful intercalation of the polymer into the montmorillonite. With adduct **E8.21.4** (Figure 4.39.b), the lattice constant c was measured to be 6.89 ± 4.25 nm, the gap between the montmorillonite platelets was determined to be also 6.23 nm which proves the reproducibility of the preparation method.

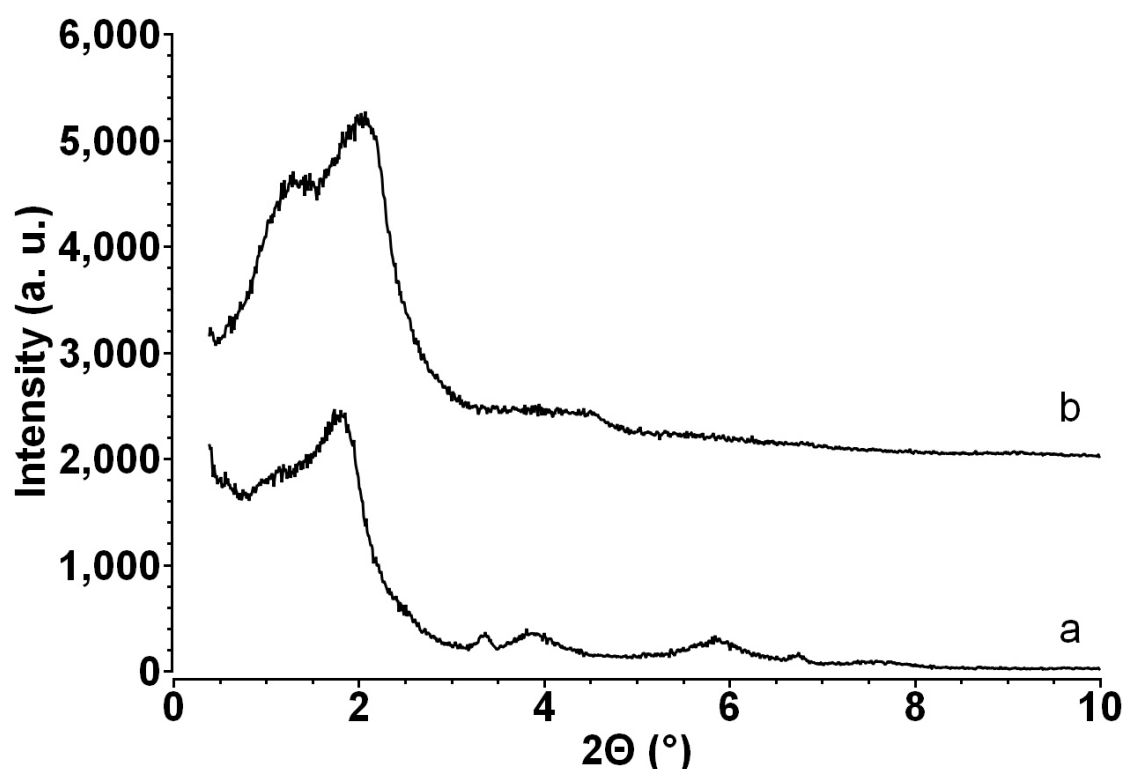


Figure 4.39: Small-angle X-ray diffractograms of a) adduct **E8.2** and b) adduct **E8.21.4**

Figure 4.40 compares the wide-angle XRD diffractogram of a) Na-bentonite **B2**, b) adduct **E7**, c) adduct **E8.2**, d) adduct **E9**, and e) adduct **E15.8.2**, with the intensities of the diffractograms normalised to the reflexes at $2\Theta = 19.7^\circ$. The diffractogram of adduct **E7** (Figure 4.40.b) showed between $2\Theta = 5$ and 14° only a broad band but no sharp reflexes. Although the slope of the diffractogram in the region $2\Theta = 5 - 10^\circ$ pointed to an interlayer distance larger than 1.80 nm, reflexes which could be used for the calculation are too broad to be assigned correctly. The adducts **E8.2**, **E9** and **E15.8.2**, on the other hand, exhibited sufficient enough reflexes in the region $2\Theta = 5 - 20^\circ$ to enable an extrapolation to the d_{001} interlayer distance and the calculation of the lattice constant c . With adduct **E8.2** (Figure 4.40.c) the lattice constant c was determined to be 4.66 ± 1.58 nm, the gap d_m was calculated to be 4.00 nm which cor-

responded, using Equation 4.1 and the value d_m obtained from the small-angle XRD diffractogram of adduct **E8.2** of 6.23 nm (cf. Figure 4.39.a), to a degree of polymer intercalation of 64 %.

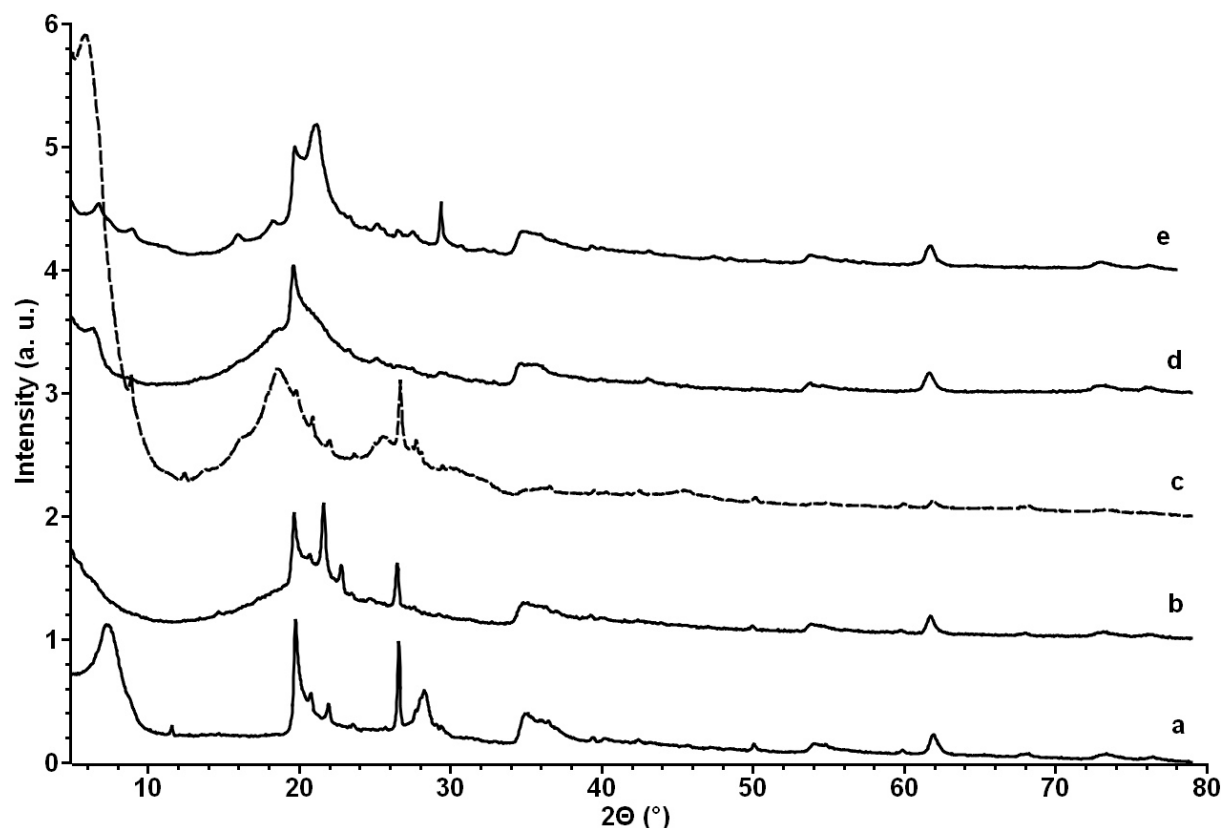


Figure 4.40: Wide-angle X-ray diffractograms of a) Na-bentonite **B2**, b) adduct **E7**, c) adduct **E8.2**, d) adduct **E9**, and e) adduct **E15.8.2**

Adduct **E9** (Figure 4.40.d) exhibited a lattice constant c of 4.29 ± 0.50 nm and a gap d_m of 3.63 nm and a degree of polymer intercalation of 58 % (using the d_m of adduct **E8.2**, shown in Figure 4.39.a). With adduct **E15.8.2** (Figure 4.40.e) the lattice constant c was calculated to be 4.04 ± 0.40 nm with a gap d_m of 3.38 nm. With the d_m value of adduct **E8.2** (cf. Figure 4.39.a), a degree of polymer intercalation of 54 % was calculated. The different degrees of polymer intercalation obtained from the small- and the wide-angle XRD were caused by that for the extrapolation to d_{001} only interlayer distances were available for which at least three higher order distances were known. The low degrees of intercalation obtained from wide-angle XRD implies that with the adducts **E8.2**, **E9**, and **E15.8.2** the polymers were only partially intercalated which is, at least with adduct **E8.2**, wrong and shows that wide-angle XRD can only be applied when the intercalation of materials with a diameter below a certain limit (about 4 nm) into montmorillonite is studied. The measured values of the lattice

4 Preparation of [montmorillonite/PEI_xQ_yR] adducts

constant *c*, the degrees of polymer intercalation and the calculated diameters of the used polymers are listed in Table 4.27.

Table 4.27: Lattice constant *c* and diameters of the polymers of the adducts **E7, **E8.2**, **E8.21.4**, **E9**, and **E15.8.2****

Entry	Adduct composition	Lattice constant <i>c</i> (nm)	Calculated polymer diameter (nm)	D _i (%)
E7	[MMT _{B1} /PEI(10kD) _{10Q} ^{80R10}]	not accessible from wide-angle XRD	5.28	-
E8.2	[MMT _{B1} /PEI(10kD) _{10Q} ^{80R10}]	4.66 ± 1.58 (w) 6.89 ± 2.95 (s)	5.28	64 (w) 100 (s)
E8.21.4	[MMT _{B2} /PEI(10kD) _{10Q} ^{80R10}]	6.89 ± 4.25 (s)	5.28	100
E9	[MMT _{B2} /PEI(10kD) _{10Q} ^{80R10}]	4.29 ± 0.50 (w)	5.28	58
E15.8.2	[MMT _{B2} /PEI(10kD) _{10Q} ^{60R14}]	4.04 ± 0.40 (w)	5.03	54

MMT_{B1} = Na-bentonite **B1** (cf. Table 4.2), MMT_{B2} = Na-bentonite **B2** (cf. Table 4.2), PEI(10kD) = poly(ethylenimine) with M_n = 10,000 g/mol, M_w/M_n = 2.5, xQ = mol% 2-hydroxypropyl-3-(N,N,N-trimethylammonium chloride), yR10 = mol% 2-hydroxydodecane, yR14 = mol% 2-hydroxyhexadecane, w = wide-angle XRD, s = small-angle XRD

To investigate whether the thermal behaviour of PEI(10kD)_{10Q}^{80R10} and PEI(10kD)_{10Q}^{60R14} polymers changed when attached to the montmorillonite, the adducts **E7**, **E8.2**, **E9**, and **E15.8.2** were investigated by differential scanning calorimetry (DSC). In Figure 4.41 the DSC thermograms of a) polymer **PB2** and adduct **E7**, b) polymer **PB4.1** and adduct **E8.2**, c) polymer **PB4.1** and adduct **E9**, and d) polymer **PC2.3** and adduct **E15.8.2** are shown. While the thermogram of polymer **PB2** (Figure 4.41.a) showed a glass transition at -25.8°C, adduct **E7** (Figure 4.41.a) exhibited a glass transition at -2.8°C. With adduct **E8.2** (Figure 4.41.b) a glass transition was detected at -23.2°C and with adduct **E9** (Figure 4.41.c) at -25.0°C. Both transitions were similar to that of polymer **PB4.1** (Figure 4.41.b and Figure 4.41.c) of -26.3°C. Although small and larger shifts of the transition temperatures were observed due to the unpredictable changes of the glass transitions of polymers in confinement no statements about the extent of the intercalation of polymers in nanopores can be made. In contrast to poly(ethylenimine)s with attached 2-hydroxydodecane groups (polymer **PB2** and polymer **PB4.1**), the PEI(10kD)_{10Q}^{60R14} polymer **PC2.3** (Figure 4.41.d) exhibited a melting transition of the alkyl chains at 26.5°C in addition to the glass transition of the poly(ethylenimine) which was indicated by the enthalpy change observed in the temperature region of -50°C - 26.5°C.

4 Preparation of [montmorillonite/PEI_xQyR] adducts

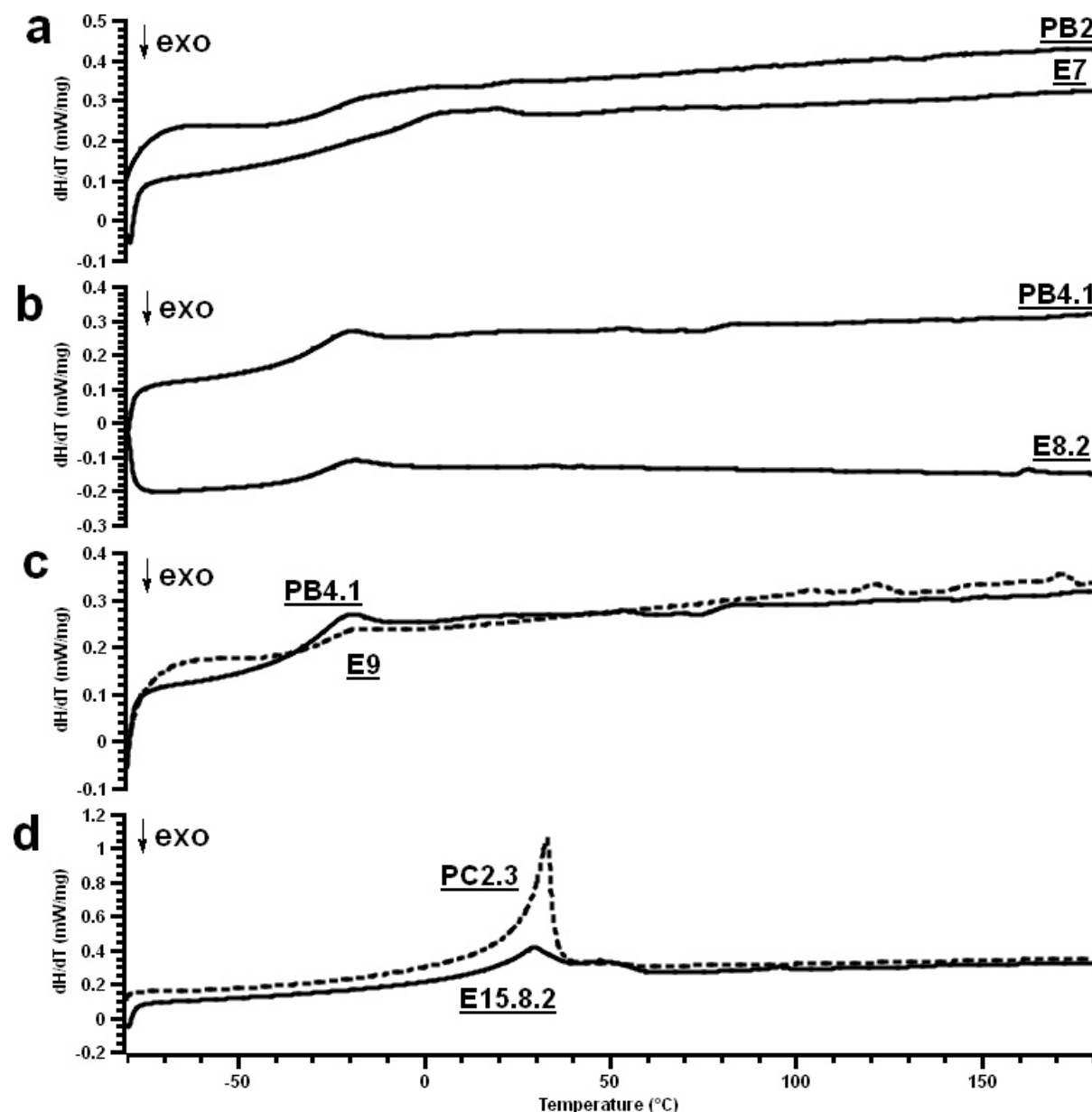


Figure 4.41: DSC thermogram of a) **PB2** and **E7**, b) **PB4.1** and **E8.2**, c) **PB4.1** and **E9**, and d) **PC2.3** and **E15.8.2**, 2. heating run, N_2 atmosphere, $dT/dt = 10$ K/minute

With adduct **E15.8.2** (Figure 4.41.d), the polymer showed two overlapping melting transitions. The first melting transition was measured at 16.9°C. As described by the Gibbs-Thomson thermodynamic relationship [51 - 53], the melting transitions of alkyl chains in confinement are found at lower temperatures. The melting transition at 16.9°C was therefore attributed to confined alkyl chains attached to the poly(ethylenimine) backbone. Of the total area below both the transitions, the first melting transition contributed 78 %, the second transition 22 % to the total area. To rule out the possibility that the melting transition at the higher temperature originated by CTAB

(cf. Figure 4.22), the adduct was purified four more times. It was found that the obtained adduct (= **E15.8.6**) exhibited also two overlapping melting transitions, starting at 2.8°C. The presence of the melting transition at a higher temperature was therefore attributed to a phase transition of the alkyl chains.

The DSC investigation of adduct **E8.2** showed that although the polymer was completely intercalated which was proven by the small-angle XRD measurement of the adduct (cf. Figure 4.39), the glass transition temperature of the intercalated polymer exhibited a similar value as with the neat polymer. On the other hand, the presence of the second melting transition found with adduct **E15.8.2** implies that alkyl chains attached to the polymer backbone were affected by the confinement of the polymer.

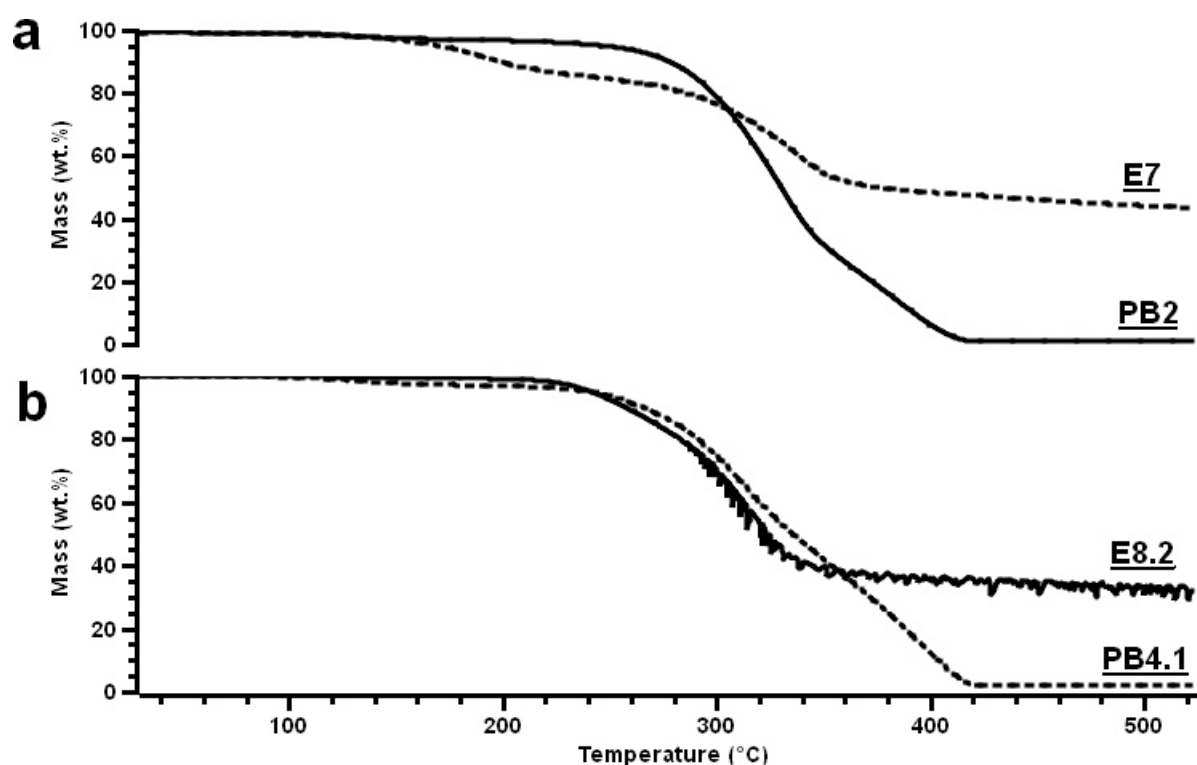


Figure 4.42: TGA thermogram of a) **PB2** and **E7**, and b) **PB4.1** and **E8.2**, He atmosphere, $dT/dt = 10$ K/minute

The decomposition temperature and the moisture content of adduct **E7** and adduct **E8.2** was also studied by thermogravimetry. Figure 4.42 shows the TGA thermograms of a) polymer **PB2** and adduct **E7**, and b) polymer **PB4.1** and adduct **E8.2**. The decomposition of polymer **PB2** (Figure 4.42.a) started at 240°C after losing about 2 wt.% moisture. Adduct **E7** (Figure 4.42.a) exhibited a two-step decomposition at 160 and 260°C. Comparing the TGA thermogram of adduct **E7** with the thermogram of adduct **E3** (cf. Figure 4.13) the decomposition at 240°C was attributed to the

decomposition of polymer **PB2**. In combination with the result from the infrared spectroscopy of adduct **E7** (cf. Figure 4.44.b), the decomposition at 160°C was attributed to 1-hexadecylamine residues. Although the organic content of the adduct was with 56.5 wt.% in good agreement to the theoretically expected value of 50.5 wt.%, the slope of the thermogram in the region 30 – 300°C indicated that the adduct contained about 20 wt.% 1-hexadecylamine. Comparing the DSC (cf. Figure 4.41) and TGA thermogram of adduct **E7** it was found that although the DSC thermogram didn't show the presence of 1-hexadecylamine due to the different decomposition behaviour of the amine and the polymer it was shown in the TGA thermogram.

The decomposition of polymer **PB4.1** (Figure 4.42.b) began at 230°C after losing about 5 wt.% moisture. With adduct **E8.2** (Figure 4.42.b), the polymer showed a decomposition at a similar temperature of 220°C. The noise of the thermogram was caused by a polluted valve. The polymer content of adduct **E8.2** was determined to be 67.9 wt.% which was in good agreement to the theoretically expected value of 65.4 wt.%. The low amount of moisture of the adducts **E7** and **E8.2** showed that the polymer in the adduct can be dried more effectively compared to the neat polymer.

To obtain information about the functional groups present in the adducts **E8.2** and **E9** infrared spectroscopy investigations on these adducts were performed. In Figure 4.43 the infrared spectra of a) polymer **PB4.1**, b) adduct **E8.2** and c) adduct **E9** are shown. With adduct **E8.2** (Figure 4.43.b) and adduct **E9** (Figure 4.43.c) the most distinctive bands of the polymer, which were the aliphatic C-H stretching vibration bands, the aliphatic C-H deformation vibration band, and the amine N-H deformation vibration band, were detected. Additionally, the adducts exhibited bands of montmorillonite. With both adducts, the Si-O-Si bands were shifted compared to the non-modified montmorillonite (cf. Figure 4.8) which point to an interaction between these groups with the ammonium moieties of the polymer.

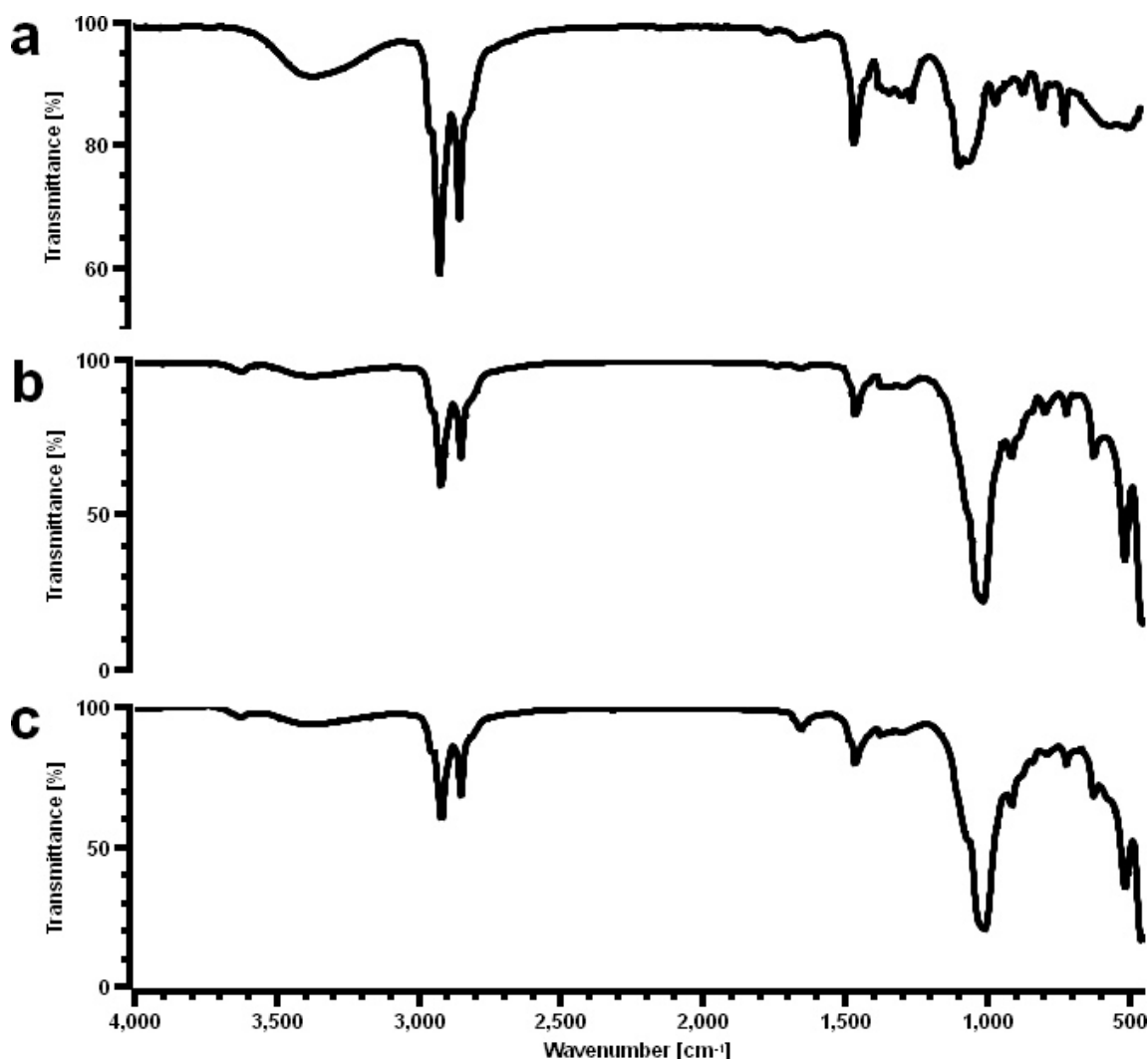


Figure 4.43: ATR-FT infrared spectra of a) polymer **PB4.1**, b) adduct **E8.2**, and c) adduct **E9**

Figure 4.44 shows the infrared spectra of a) polymer **PB2**, b) adduct **E7**, c) polymer **PC2.3**, and d) adduct **E15.8.2**. The infrared spectrum of adduct **E7** (Figure 4.44.b) exhibited beside bands corresponding to montmorillonite also bands of polymer **PB2** (Figure 4.44.a). In addition, at 1566 cm^{-1} an NH_3^+ deformation vibration band was detected which was attributed to 1-hexadecylamine since polymer **PB2** didn't show a signal in this region. In combination with the result obtained from ^1H -MAS-NMR (cf. Figure 4.36) and TGA (cf. Figure 4.42), it was concluded that the purification of the adduct was not sufficient enough to remove all 1-hexadecylamine. With adduct **E15.8.2** (Figure 4.44.d), on the other hand, only bands of the polymer and the montmorillonite were measured. Compared to the non-modified montmorillonites both adducts showed a shift of the Si-O-Si bands.

4 Preparation of [montmorillonite/PEIxQyR] adducts

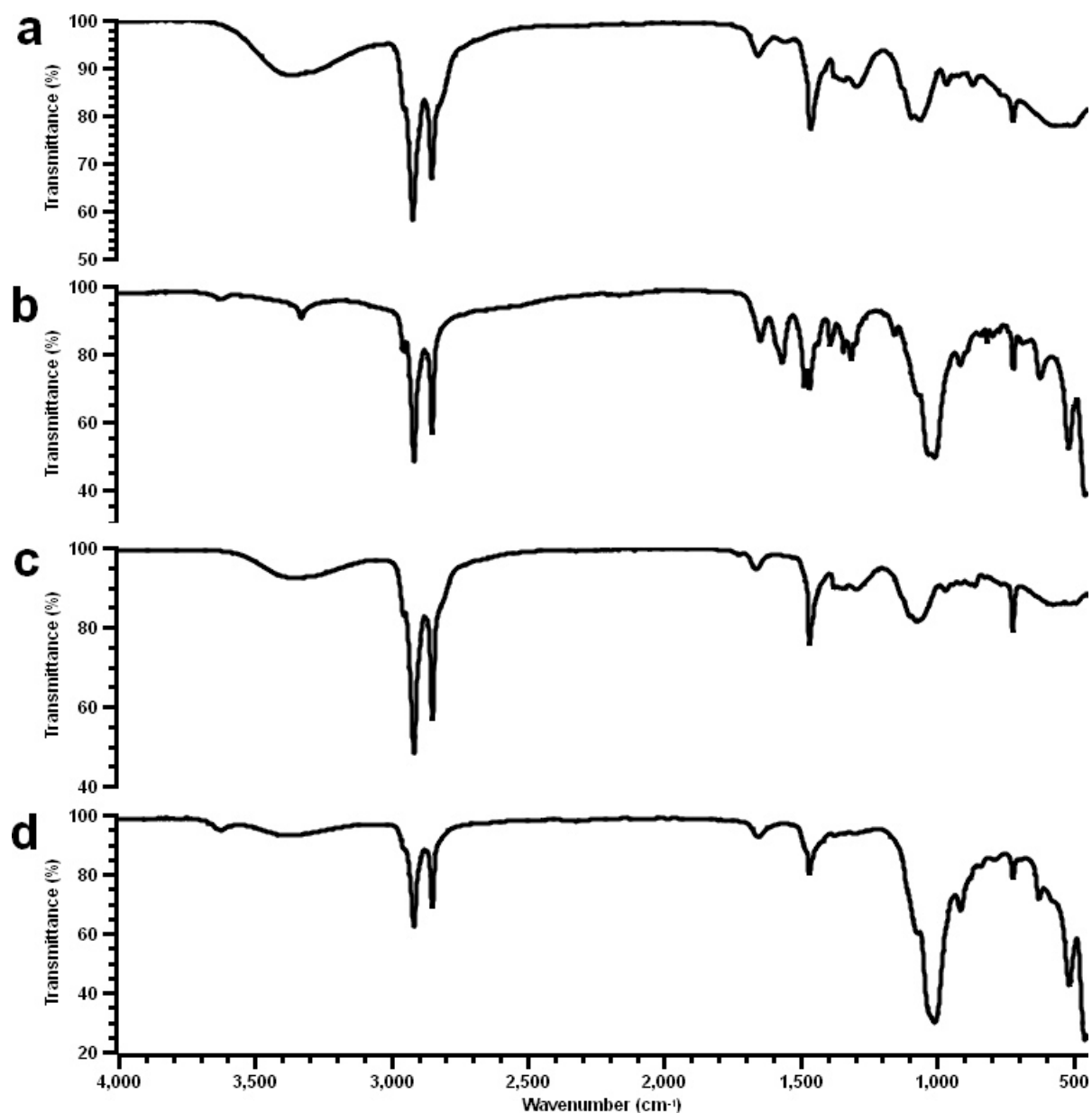


Figure 4.44: ATR-FT infrared spectrum of a) polymer **PB2**, b) adduct **E7**, c) polymer **PC2.3**, and d) adduct **E15.8.2**

The elemental composition of the adducts **E7**, **E8.2**, **E9**, and **E15.8.2** has been investigated by means of XRF and is listed in Table 4.28. The main elements detected with adduct **E7** were Si, Al, Fe, Ca, Mg, and Cl. In addition to these elements the adducts **E8.2**, **E9**, and **E15.8.2** contained also bromine. The lower quantity of calcium measured with adduct **E7** and adduct **E8.2** compared to the content detected with adduct **E9** and adduct **E15.8.2** indicated that Na-bentonite **B1** contained less Ca than Na-bentonite **B2**. The bromine of the adducts **E8.2**, **E9** and **E15.8.2** was attributed to the fact that during the preparation of the adducts bromine and chlorine ions were

4 Preparation of [montmorillonite/PEI_xQyR] adducts

shared by the polymer and the CTAB. The adducts **E7** and **E8.2** exhibited with an Al:Mg [mol/mol] ratio of about 8.09 a ratio which was similar to those of montmorillonites treated with an acid (cf. Table 4.8 and [10]). With the adducts **E9** and **E15.8.2**, the Al:Mg ratio was determined to be 4.88 which was similar to the Al:Mg ratio of the non-treated bentonite (cf. Table 4.8). Comparing the Al:Mg ratios of the adducts **E9** and **E15.8.2** with the Al:Mg ratio of previously investigated montmorillonites [8, 9] of 4.55 it was found that preparation of the adducts didn't change the composition of the montmorillonite.

Table 4.28: Elemental composition of adduct **E7, **E8.2**, **E9** and **E15.8.2****

Element	E7 [wt.%]	E8.2 [wt.%]	E9 [wt.%]	E15.8.2 [wt.%]
Si	56.08	50.68	44.97	41.99
Al	16.12	11.31	10.58	9.97
Fe	17.78	8.47	10.09	9.05
Ca	2.69	0.68	4.81	3.95
Mg	1.80	1.26	1.96	1.83
Na	0.36	0.11	0.30	0.08
K	1.21	0.61	1.33	1.14
S	0.31	0.25	0.42	0.40
Cl	3.64	0.97	1.45	1.67
Br		25.65	24.08	29.92
Sum formula of montmorillonite	Na _{0.05} (Al _{1.78} Mg _{0.22})(Si ₄ O ₁₀)(OH) ₂	Na _{0.02} (Al _{1.78} Mg _{0.22})(Si ₄ O ₁₀)(OH) ₂	Na _{0.06} (Al _{1.66} Mg _{0.34})(Si ₄ O ₁₀)(OH) ₂	Na _{0.02} (Al _{1.66} Mg _{0.34})(Si ₄ O ₁₀)(OH) ₂

The mineral composition of the inorganic fraction of the adducts **E7**, **E8.2**, **E8.21.1**, **E8.21.4**, **E9**, **E10**, and **E15.8.2** is listed in Table 4.29. Adduct **E7** consisted of 65.0 wt.% montmorillonite, 21.1 wt.% quartz (SiO₂), 3.6 wt.% CaCO₃, and 10.4 wt.% of iron, potassium, and sulphur. The montmorillonite content of the adducts **E8.2** - **E15.8.2** was lower than in the non-modified bentonite (cf. Table 4.9). The lower montmorillonite content indicates that [MMT/PEI(10kD)_xQ^{yR}] fractions with low densities were removed during the purification of the adducts due to the centrifugation of the adducts in the toluene/ methanol mixture.

Table 4.29: Mineral composition of the inorganic fraction of the adducts E7, E8.2, E8.21.1, E8.21.4, E9, and E15.2

Entry	Na-Montmorillonite [wt.%]	Quartz/ cristobalite [wt.%]	CaCO ₃ [wt.%]	Other [wt.%]
<u>E7</u>	65.0	21.1	3.6	10.4
<u>E8.2</u>	57.4	35.1	1.2	6.3
<u>E8.21.1</u>	54.7	29.5	7.7	8.1
<u>E8.21.4</u>	57.7	26.7	7.6	8.0
<u>E9</u>	57.4	26.5	8.1	8.0
<u>E10</u>	55.4	36.8	0.9	6.9
<u>E15.8.2</u>	58.5	26.6	7.2	7.7

Other = Potassium, sulphur, iron

In Table 4.30 the polymer content of the adducts E7, E8.2, E8.21.1, E8.21.4, E9, and E15.8.2, calculated from XRF data and obtained from TGA or calcination measurements as well as the theoretically expected values is listed. The polymer content of adduct E7 was calculated with the known sum formula of the polymer and the amount of chlorine ions derived from the XRF. The polymer content obtained with the two methods was in good agreement to the theoretically expected value. Although the matrix effect which led to an overestimation of the bromine content [59] shown from the analysis of the adducts E5 and E6 (cf. Table 4.25) could not be compensated, the organic content of the adducts E8.2, E9, and E15.8.2 was calculated based on XRF data by attributing both the bromine and chlorine ions to the polymers. It was found that while the polymer content of the adducts obtained by TGA and calcination experiments was in good agreement to the theoretically expected values the calculation of the polymer content based on the results from the XRF measurements led to values which were about 15 wt.% higher than those obtained by thermal decomposition methods. As described with adduct E6, the amount of polymer clearly influences the degree of enhancement of the bromine signal in the XRF. In conclusion, the determination of the polymer content of the adducts based on XRF data could be applied when only chlorine ions were attached to the polymer. When bromine and chlorine ions were attached to the polymers, a matrix effect led to an overestimation of the bromine content.

Table 4.30: Polymer content of the adducts E7, E8.2, E9, and E15.2

Entry	XRF [wt.%]	TGA or calcination [wt.%]	Theory [wt.%]
<u>E7</u>	53.1	56.5 (a)	50.5
<u>E8.2</u>	83.2	67.9 (a)	65.4
<u>E8.21.1</u>	90.4	68.9 (b)	65.2
<u>E8.21.4</u>	79.2	60.8 (b)	65.2
<u>E9</u>	82.8	65.9 (b)	65.8
<u>E10</u>	70.6	60.8 (a)	65.3
<u>E15.8.2</u>	86.4	60.6 (b)	53.5

(a) = TGA, (b) = calcination

In Figure 4.45 SEM pictures of adduct E8.2 are shown. The adduct was dispersed in toluene (2.5 mg/mL). The preparation of the sample was performed analogously to the preparation of Na-bentonite (Figure 4.15). Toluene was used as the solvent since it was able to dissolve the polymer (cf. Chapter 3) and should if the polymer was intercalated, separate the montmorillonite platelets. The pictures showed particles with diameters ranging from 1 to 20 μm . Given the mineral composition of the adduct (cf. Table 4.29), the particles with diameters of 10 – 20 μm may be attributed to quartz or cristobalite. As indicated by the particles with diameters below 1 μm , the stacks of montmorillonite platelets detected with the neat bentonite (cf. Figure 4.15) seems to be partially exfoliated. Given the number of particles with diameters below 10 μm , it was concluded that the polymer coated montmorillonite could be dispersed in the used solvent and exhibited a partially exfoliated structure.

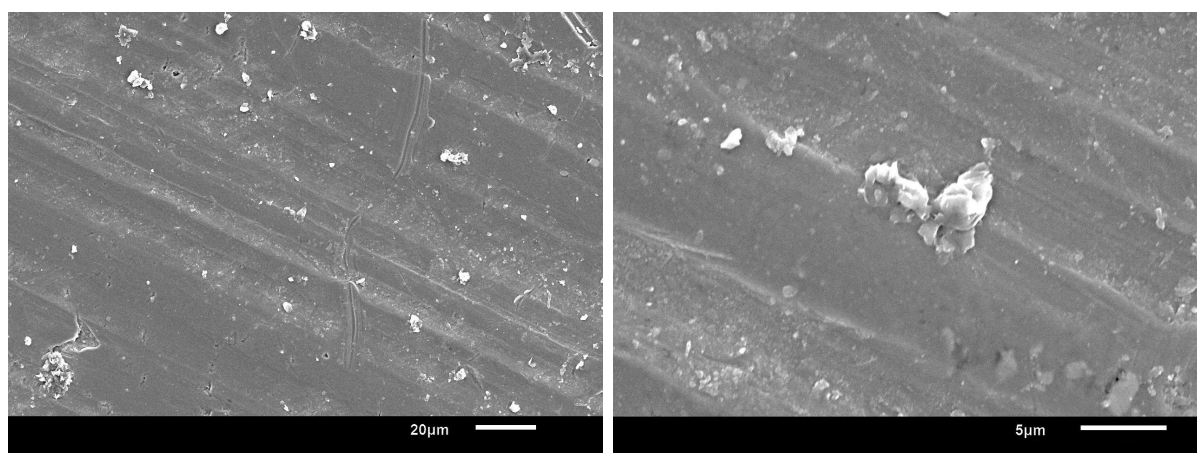


Figure 4.45: SEM pictures of adduct E8.2 dispersed in toluene (2.5 mg/mL)

Figure 4.46 shows SEM pictures of adduct **E15.8.2**. The adduct was dispersed in toluene (2.5 mg/mL). The preparation of the sample was performed analogously to the preparation of Na-bentonite (Figure 4.15). Since toluene was able to dissolve the polymer (cf. Chapter 3) the sample was prepared from a toluene/adduct dispersion. The adduct contained particles with diameters between 1 and 10 μm of which the oval shaped aggregates with diameters of 5 to 10 μm were most likely quartz. By the presence of particles with diameters below 1 μm it was concluded that this polymer was able to exfoliate the adduct up to a certain degree as the polymer used to prepare adduct **E8.2**. Comparing the SEM pictures of adduct **E8.2** (cf. Figure 4.45) with those of adduct **E15.8.2** it was found that adduct **E15.8.2** contained much more particles with diameters below 1 μm . The larger number of particles with diameters below 1 μm indicates that the used polymer was better soluble in the used solvent than that used to prepare adduct **E8.2**.

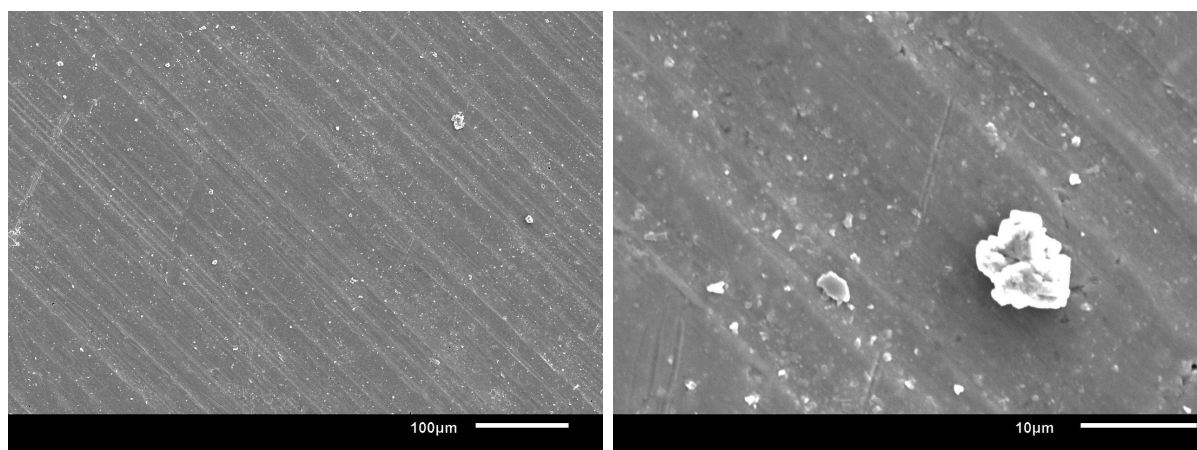


Figure 4.46: SEM pictures of adduct **E15.8.2** dispersed in toluene (2.5 mg/mL)

A sample of adduct **E8.21** and a sample of adduct **E15.8** was purified several times by dispersing the adducts in a toluene/methanol solution and removing the liquid fraction after each step. The solid fractions were dried and the organic content after each purification run was determined by calcination. Calcination experiments were performed by weighing 100 to 200 mg of the samples into 25 g porcelain crucibles. The samples were then heated from 30 to 530°C with a heating rate of 10 K/minute in an air atmosphere. After the samples were cooled down to 20°C, the residues were collected and weighed. Different to thermogravimetric measurements, the calcination experiments gave no information about the moisture content of the adducts. The obtained values from calcination are therefore the sum of the organic content and the moisture present in the adducts. The aim of this procedure was it to measure the stability of the attachment of PEI(nkD)_xQ^{yR} polymers to the montmorillonite.

4 Preparation of [montmorillonite/PEI_xQyR] adducts

The organic content of the adducts after each purification run is listed in Table 4.31. With adduct **E8.21**, the total loss of organic material after the sixth run was determined to be 8.8 wt.%. In the first four runs, 8.1 wt.% of the organic material could be removed. During the fifth and the sixth run, the adduct lost only 0.6 wt.% of the organic material.

With adduct **E15.8**, the total loss of organic material after the sixth purification run was found to be 8.2 wt.%. After the fourth run, the organic content of the adduct became almost constant. From the data obtained from the purification experiments, it is concluded that four purification runs were necessary with both adducts to remove all organic material with low adhesion which was assumed to be either CTAB or polymers with low quantities of ammonium groups attached to the montmorillonite. Different to adduct **E8.21**, at least two purification runs were necessary with adduct **E15.8** to remove most of the CTAB, independent of the prepared quantity. It was assumed that the longer alkyl chains of the polymer used to prepare adduct **E15.8** was the reason for the more difficult purification due to alkyl chain-alkyl chain attraction between the polymer and the CTAB by van der Waals forces [60]. The small losses of the polymers after the fourth purification run showed furthermore that the polymers were strongly attached to the montmorillonite.

Table 4.31: Organic content of adduct **E8.21 and adduct **E15.8** after several purification runs**

Entry	Purification runs	Organic content (th. wt.%)	Organic content (exp. wt.%)
E8.21.1	1	65.2	68.9
E8.21.2	2	65.2	66.0
E8.21.3	3	65.2	64.4
E8.21.4	4	65.2	60.8
E8.21.5	5	65.2	60.5
E8.21.6	6	65.2	60.1
E15.8.1	1	53.5	59.1
E15.8.2	2	53.5	60.6
E15.8.3	3	53.5	59.2
E15.8.4	4	53.5	51.0
E15.8.5	5	53.5	51.9
E15.8.6	6	53.5	50.9

The rate of adsorption of PEI(10kD)_{10Q}^{80R10} on montmorillonite was studied by taking samples during the preparation of adduct **E9**, as an example. The rate of adsorption

4 Preparation of [montmorillonite/PEI_xQyR] adducts

was measured from samples taken after a reaction time of 20, 44, 67 and 137 h. The samples were purified as described in the experimental part of this Chapter and the organic content was determined by calcination of the dried samples. The organic content of each sample is listed in Table 4.32. Of each sample, two measurements were performed to investigate the homogeneity of the samples.

Table 4.32: Rate of polymer adsorption during the preparation of adduct E9

Reaction time [h]	Organic content [wt.%]			
	Theory	1 st measurement	2 nd measurement	Arithmetic mean
20	65.8	54.3	58.7	56.5
44	65.8	58.5	63.9	61.2
67	65.8	61.6	65.2	63.4
137	65.8	67.4	67.1	67.3

In Figure 4.47 the rate of adsorption of PEI(10kD)_{10Q}^{80R10} on montmorillonite during the preparation of adduct E9 as well as the error bars is shown. After a reaction time of 20 h, about 86 wt.% of the polymer molecules were attached to the montmorillonite. After this time, the rate of adsorption became gradually slower. Also, the values of the standard deviations decreased with increasing reaction time which indicates that during the reaction the polymer displaced the CTAB gradually. With a polynomial fit the minimum reaction time for a complete conversion i. e. the time necessary to attach all polymer molecules to the montmorillonite was determined to be about 127 h.

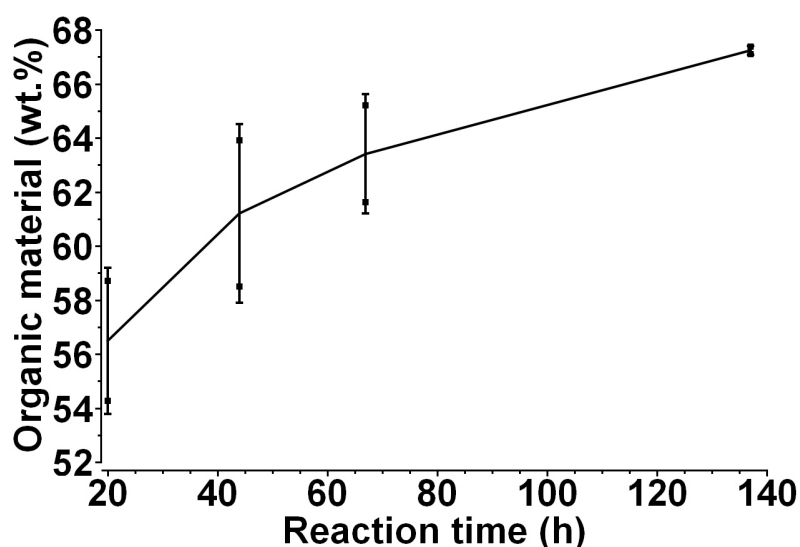


Figure 4.47: Adsorption of PEI(10kD)_{10Q}^{80R10} on montmorillonite during the preparation of adduct E9

Correlating the number of exchangeable cations of montmorillonite with the PEI(10kD)_{10Q}^{80R10} content of [MMT_{B2}/PEI_{10Q}^{80R10}] adducts

Since the polymer content of the [MMT_{B1,B2}/PEI_{10Q}^{80R10}] adducts **E2**, **E3**, and **E7 – E10** were chosen to be in the region of 50.5 – 67.9 wt.% it was of interest to determine the maximum amount of the PEI_{10Q}^{80R10} polymer **PB4** able to be attached to the montmorillonite. For this reason [MMT_{B2}/PEI_{10Q}^{80R10}] adducts with different polymer contents were prepared analogously to the preparation described with adduct **E8**. The yield as well as the polymer content of the adducts is listed in Table 4.33. The polymer content was determined by calcination experiments.

The neat montmorillonite contained 0.35 mol sodium ions per sum formula of montmorillonite (cf. Table 4.8) i. e. one mol of the mineral. The weight of one mol montmorillonite was calculated to be 367.34 g. With PEI_{10Q}^{80R10}, the molecular weight per formula unit was determined to be 205.67 g/mol, containing 0.1 mol 2-hydroxypropyl-3-(N,N,N-trimethylammonium chloride). With 0.35 mol of the ammonium units, the weight of the polymer was found to be 719.84 g. In theory, during the preparation of an [MMT_{B2}/PEI_{10Q}^{80R10}] adduct one sodium ion should be replaced by an ammonium unit which would lead to a maximum polymer content of 66.2 wt.%.

Table 4.33: Polymer content of the adducts **E11 - **E14****

Entry	Polymer content (theory wt.%)	Polymer content (exp. wt.%)	Yield (g)	Yield (wt.% of th.)
E11	54.1 (s)	66.2 (s)	25.1 (s)	93.7 (s)
E12	80.0 (s)	82.3 (s)	14.1 (s)	77.7 (s)
E13	90.0 (s)	58.7 (s)	0.4 (s)	2.5 (s)
		96.4 (l)	6.8 (l)	42.2 (l)
E14	99.9 (s)	77.4 (s)	0.1 (s)	0.8 (s)
		99.9 (l)	8.6 (l)	58.9 (l)

s = solid fraction, l = liquid fraction

With the adducts **E11** and **E12**, the main fraction obtained after centrifugation and purification consisted of [MMT_{B2}/PEI_{10Q}^{80R10}] adducts with a polymer content of 66.2 and 82.3 wt.%, respectively. On the other hand, with the adducts **E13** and **E14** the main fraction obtained were PEI_{10Q}^{80R10} with a low montmorillonite content. The polymer content of the minor fraction was measured to be 58.7 wt.% with adduct **E13** and 77.4 wt.% with adduct **E14**. Although the maximum polymer content was expected to be around 66 wt.%, the polymer content detected with the [MMT_{B2}/PEI_{10Q}^{80R10}] adduct fractions of the experiments **E11 – E14** was in the region of 58.7 – 83.2 wt.%. In addi-

4 Preparation of [montmorillonite/PEI_xQ_yR] adducts

tion, the used bentonite contained only about 72 wt.% montmorillonite which should reduce the maximum polymer content to a value around 57.8 wt.%. The high polymer contents could be explained in that way that although per polymer molecule a high number of ammonium groups were available to react with the montmorillonite, only a few groups were necessary to attach the polymer to the montmorillonite as shown in Figure 4.48.

Therefore, as long as the montmorillonite surface was not completely occupied polymer molecules could adhere to the montmorillonite. In conclusion, the maximum amount of polymer able to be attached to the montmorillonite couldn't be calculated from the number of sodium ions present in the montmorillonite. Instead, the available montmorillonite surface (ca. 700 m²/g for water molecules [61 - 65]) and the surface area which would be occupied by the polymer should be compared.

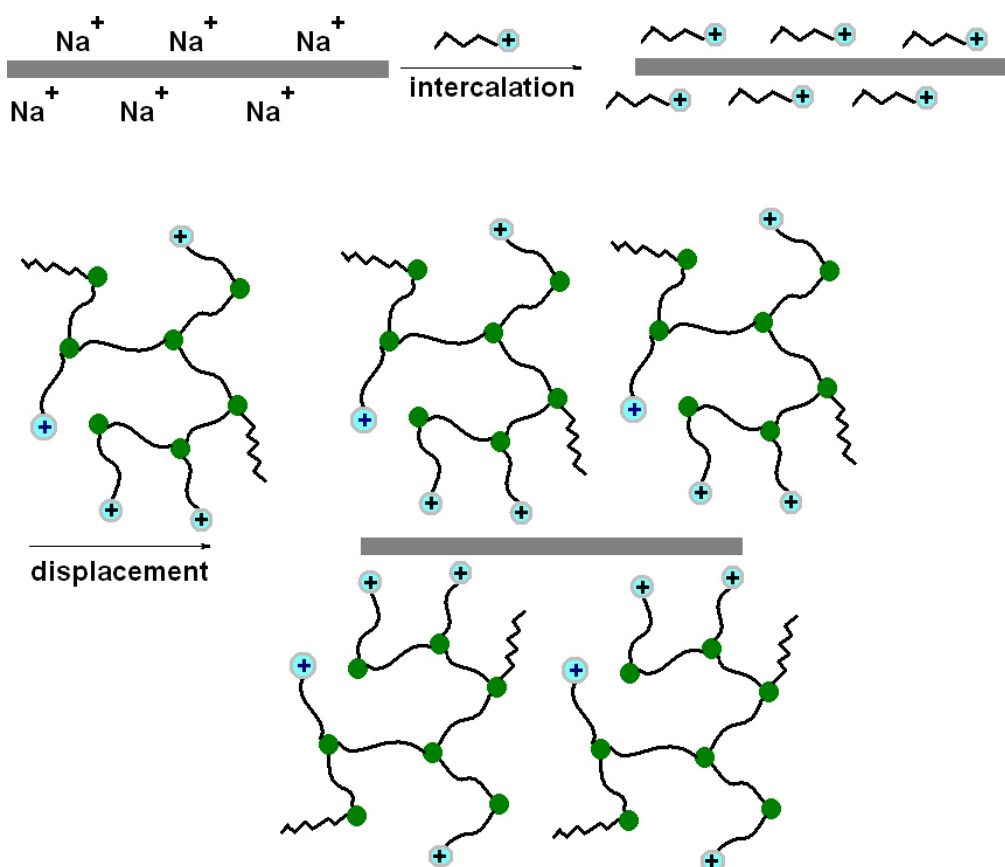


Figure 4.48: Model of the adhesion of PEI(10kD)_{10Q}^{80R10} to montmorillonite

Discussion

In this paragraph [MMT/PEI(nkD)_{xQ}^{yR}] adducts were discussed which were prepared by the “indirect replacement” procedure. The term “indirect replacement” means that

PEI(nkD)_xQ^{yR} polymers were mixed with CTAB and montmorillonite simultaneously and intercalated into the montmorillonite by displacing the CTAB in a formed [MMT/CTAB] intermediate adduct.

With small-angle XRD the gap between the montmorillonite platelets of adduct **E8.2** and adduct **E8.21.4** was measured to be 6.23 nm with both adducts which was in good agreement to the calculated polymer diameter of 5.42 and proved the intercalation of the polymer into the montmorillonite. From wide-angle XRD, on the other hand, only a gap of 4.0 nm was calculated with adduct **E8.2** since only reflexes in the region of $2\Theta = 5 - 20^\circ$ could be used. With the adducts **E9** and **E15.8.2**, wide-angle XRD investigations revealed that when the gap obtained from the small angle XRD study of adduct **E8.2** was used as the reference the degree of polymer intercalation was determined to be 58 % with adduct **E9** and 54 % with adduct **E15.8.2**. With adduct **E7** no gap could be obtained from wide-angle XRD due to the lack of reflexes in the region $2\Theta = 5$ and 14° .

It was found from the ¹H- and ¹³C-MAS-NMR investigations of the adducts **E7**, **E8.2**, **E9**, and **E15.8.2** that while the adducts **E8.2**, **E9** and **E15.8.2** contained only the polymers as the organic fraction, adduct **E7** contained in addition 1-hexadecylamine which was also detected in the TGA thermogram of the adduct. The organic content obtained from TGA or calcination experiments was determined to be in good agreement to the theoretically expected values with the adducts **E7**, **E8.2**, **E9**, and **E15.2**. The calculation of the polymer content based on XRF data, on the other hand, led with the adducts **E8.2**, **E9** and **E15.8.2** to about 15 wt.% higher contents compared to the values obtained from the thermal investigations but to a similar content with adduct **E7**. The overestimation of the polymer content from the XRF data was discussed in Chapter **4.3.4** and originated from a matrix effect which occurred when the polymer in the adduct had bromine and chlorine ions attached.

While the IR spectrum of adduct **E7** showed besides bands of the polymer and the montmorillonite also bands of 1-hexadecylamine, only bands of the polymers and the montmorillonite were detected with the adducts **E8.2**, **E9** and **E15.8.2**. The spectra of the adducts showed furthermore a shift of the Si-O-Si bands which points to an interaction between the ammonium groups of the PEI(nkD)_xQ^{yR} polymers with the montmorillonite. Differential scanning calorimetry studies on the adducts **E7**, **E8.2**, **E9**, and **E15.8.2** revealed that while the adducts **E8.2** and **E9** exhibited similar thermal behaviours as the neat polymers, the glass transition temperature of the polymer in adduct **E7** was shifted to a higher temperature which may be caused by the 1-hexadecylamine. In contrast, the thermogram of adduct **E15.8.2** showed the melting transitions of the alkyl chains attached to the polymer. Different to the neat polymer the polymer in the adduct exhibited two melting transitions which were attributed to free and alkyl

chains confined by the montmorillonite. SEM pictures of the adducts **E8.2** and **E15.8.2** showed besides quartz and calcite also partially exfoliated adduct particles which show that the adducts were able to delaminate in the used solvent toluene.

By washing adduct **E8.21** and adduct **E15.8** with toluene/methanol solutions several times the adhesion of the polymers on the montmorillonite was studied. In the first four steps 8 - 9 wt.% of the polymers could be removed. With both adducts, additional washing steps led only to a minor decrease of the polymer content which shows that after the materials with lower adhesion were removed the polymers appeared to be strongly attached to the montmorillonite. The rate of adsorption of PEI(nkD)_{xQ}^{yR10} on montmorillonite was studied by taking samples during the preparation of adduct **E9**. While in the first 20 h 86 % of the polymer could be attached to the montmorillonite, the rate became gradually slower until the full conversion was achieved after 137 h. From the polymer content obtained after 20, 44, and 67 h the minimum reaction time was calculated to be 127 h.

The number of exchangeable cations of the montmorillonite of bentonite **B2** was compared to the maximum amount of PEI(nkD)_{xQ}^{yR10} able to be attached to the montmorillonite. The calculation showed that according to the number of exchangeable cations the polymer content shouldn't exceed a value of 57.8 wt.%. Experiments in which the polymer was added in high excess to the montmorillonite showed that the polymer content can reach values up to 83.2 wt.%. The experiments showed that the number of exchangeable cations can't be used to calculate the maximum amount of PEI(nkD)_{xQ}^{yR10} able to be attached to the montmorillonite. Instead, the calculation should take the available montmorillonite surface and the surface area which would be occupied by the polymer into account.

Summary

Small-angle XRD investigation of an [MMT/PEI(10kD)_{10Q}^{80R10}] adduct, prepared by the "indirect replacement" procedure, showed that the polymer was completely intercalated into the montmorillonite. On the other hand, the extrapolation to the interlayer distance from higher order Miller indices from wide-angle XRD data showed that only interlayer distances up to about 4 nm were accessible. The reaction of a PEI(10kD)_{10Q}^{60R14} polymer with MMT and CTAB led to a partially intercalated polymer with a degree of intercalation of 54 %. Experiments to prove the stability of the attachment of PEI(nkD)_{xQ}^{yR} polymers on montmorillonite showed that after four purification runs the polymer content of the adducts became almost constant which prove the strong adhesion between the polymer and the montmorillonite. SEM pictures of an [MMT/PEI(10kD)_{10Q}^{80R10}] and an [MMT/PEI(10kD)_{10Q}^{60R14}] adduct showed a large

4 Preparation of [montmorillonite/PEI_xQ_yR] adducts

number of particles with diameters below 1 μm which were interpreted as partially or completely exfoliated adducts. While the polymer of [MMT/PEI(10kD)_{10Q}^{80R10}] adducts exhibited glass transition temperatures similar to that of the neat polymers, the polymer of [MMT/PEI(10kD)_{10Q}^{60R14}] adducts showed two melting transitions. While the transition at the lower temperature was attributed to the melting of confined alkyl chains, the transition at the higher temperature indicated a phase transition of the alkyl chains. From the measured interlayer distance and the polymer contents detected by TGA investigations it is concluded that the "indirect replacement" procedure can be applied to obtain [MMT/PEI(nkD)_{xQ}^{yR10}] adducts with completely intercalated polymers.

4.4 Conclusion

To prepare [MMT/PEI(nkD)_xQ^{yR}] adducts in which the polymer is completely intercalated into the montmorillonite platelets, three different preparation procedures were evaluated, namely: “direct addition”, “replacement”, and “indirect replacement”.

The “direct addition” procedure was carried out by reacting a PEI(nkD)_xQ^{yR} polymer with an in water swollen montmorillonite. Investigation of an [MMT/PEI(1.2kD)_{13Q}] adduct by wide-angle XRD revealed that 56 % of the small molecular weight PEI(1.2kD)_{13Q} polymer was able to be intercalated into the MMT. When a larger PEI(10kD)_{5Q}^{67R10} polymer was used, the degree of intercalation decreased to 13 % but reached a value of 37 % when hydrochloric acid was added to the reaction mixture. SEM pictures of an [MMT/PEI(10kD)_{5Q}^{67R10}] adduct showed aggregates with diameters between 1 and 20 μm. Comparing the number of particles with diameters below 10 μm of the adduct and the neat bentonite it was concluded that the polymer enabled the stacked montmorillonite platelets to exfoliate up to a certain degree. But as shown by the low degrees of polymer intercalation, the complete intercalation of polymers into the montmorillonite platelets could not be achieved with this method.

The “replacement” procedure was carried out by reacting PEI(nkD)_xQ^{yR} polymers with [MMT/CTAB] adducts. During the reaction, the polymer intercalated into the MMT by replacing the CTAB. It was found that the reaction of low molecular weight PEI(1.2kD)_{13Q} and PEI(1.2kD)_{10Q}^{80R10} polymers with [MMT/CTAB] led to [MMT/PEI(nkD)_xQ^{yR10}] adducts with interlayer distances which were in good agreement to the calculated polymer diameters. The XRD data of the larger PEI(1.2kD)_{10Q}^{80R10} polymer indicated furthermore the formation of a polymer double layer. The “replacement” procedure can, therefore, be applied to create [MMT/PEI(nkD)_xQ^{yR10}] adducts with fully intercalated polymers.

The “indirect replacement” procedure was carried out by mixing the polymer with CTAB and MMT simultaneously. During the reaction, the polymer displaced the CTAB of an intermediate formed [MMT/CTAB] adduct. Small-angle XRD investigation of an [MMT/PEI(10kD)_{10Q}^{80R10}] adduct revealed that the polymer was completely intercalated although a high molecular weight PEI(10kD)_{10Q}^{80R10} was used. The reaction of a PEI(10kD)_{10Q}^{60R14} polymer with MMT and CTAB led to a partially intercalated adduct with a degree of intercalation of 54 %. SEM pictures of an [MMT/PEI(10kD)_{10Q}^{80R10}] and an [MMT/PEI(10kD)_{10Q}^{60R14}] adduct showed large numbers of particles with diameters below 1 μm which were interpreted as exfoliated montmorillonite platelets. In any case, CTAB could be removed from the adducts by two washing steps with methanol/toluene fairly completely. In conclusion, the evaluation of the three tried procedures showed that the “direct addition” procedure led to adducts with only partially intercalated polymers. The “replacement” and the “indirect replacement” procedures, on the other hand, led under right conditions to adducts with completely intercalated polymers. Furthermore, only a low quantity of PEI(10kD)_{10Q}^{yR} polymers was removed from [MMT/PEI(10kD)_{10Q}^{yR}] adducts after six washing steps, demonstrating the strong adhesion of these polymers to montmorillonite.

References

- 1 Gao C., Yan D.; Hyperbranched polymers: from synthesis to applications; *Prog. Polym. Sci.* 29 (2004) 183 – 275
- 2 Seiler M.; Hyperbranched polymers: Phase behavior and new applications; *Fluid Phase Equilibria* 241 (2006) 155 – 174
- 3 Brandt M.; New quat-alkyl-primer polymers for use in montmorillonite-nanocomposites (2012)
- 4 Ray S. S., Okamoto M.; Polymer/layered silicate nanocomposites: a review from preparation to processing; *Progress in Polymer Science* 28 (2003) 1539 – 1641
- 5 Earley J. W., Osthaus B. B., Milne I. H.; Purification and properties of montmorillonite; *American Mineralogist* 38 (1953) 707 - 723
- 6 Earley J. W., Milne I. H., McVeagh W. J.; Thermal dehydration and x-ray studies on montmorillonite; *American Mineralogist* 38 (1953) 770 – 783
- 7 Schick P.; Purification of bentonite; US 3865240 A (1973)
- 8 Vogt K., Köster H. M.; Zur Mineralogie, Kristallchemie und Geochemie einiger Montmorillonite aus Bentoniten; *Clay Minerals* 13 (1978) 25 - 43
- 9 Lagaly G., Weiss A.; Neue Methoden zur Charakterisierung und Identifizierung quellungsfähiger Dreischichttonminerale; *Zeitschrift für Pflanzenernährung und Bodenkunde* 130 (1971) 9 – 24
- 10 Jovanović N., Janačković J.; Pore Structure and Adsorption Properties of an Acid Activated Bentonite; *Applied Clay Science* 6 (1991) 59 - 68
- 11 Iftiqar S. M.; Structural Studies on Semiconducting Hydrogenated Amorphous Silicon Oxide Films; *High temperature Material Processes* 6 (2002) 35 - 54
- 12 Farmer V. C., Russel J. D.; The infra-red spectra of layer silicates; *Spectrochimica Acta* 20 (1964) 1149 - 1173
- 13 Farmer V. C., Russel J. D.; Infrared absorption spectrometry in clay studies; *Clays and Clay Minerals* 15 (1967) 121 - 142
- 14 Vaia R. A., Ishii H., Giannelis E. P.; Synthesis and properties of two-dimensional nanostructures by direct intercalation of polymer melts in layered silicates; *Chemistry of Materials* 5 (1993) 1694 – 1696
- 15 Kooli F., Khimyak Y. Z., Alshahateet S. F., Fengxi Chen F.; Effect of the Acid Activation Levels of Montmorillonite Clay on the Cetyltrimethylammonium Cations Adsorption; *Langmuir* 21 (2005) 8717 - 8723
- 16 Hendricks S. B.; Base Exchange of the Clay Mineral Montmorillonite for Organic Cations and its Dependence upon Adsorption due to van der Waals Forces; *The Journal of Physical Chemistry* 45 (1941) 65 - 81
- 17 Jackson C. L., McKenna G. B.; The glass transition of organic liquids confined to

- pores; *Journal of Non-Crystalline Solids* 131 - 133 (1991) 221 - 224
- 18 Forrest J. A., Dalnoki-Veress K., Stevens J. R., Dutcher J. R.; Effect of free surfaces on the glass transition temperature of thin polymer films; *Physical Review Letters* 77 (1996) 2002 – 2005
- 19 Forrest J. A., Dalnoki-Veress K., Dutcher J. R.; Interface and chain confinement effects on the glass transition temperature of thin polymer films; *Physical Review E* 56 (1997) 5705 - 5716
- 20 Dalnoki-Veress K., Forrest J. A., Murray C., Gigault C., Dutcher J. R.; Molecular weight dependence of reductions in the glass transition temperature of thin freely standing polymer films; *Physical Review E* 63 (2001) 031801-1 - 031801-10
- 21 Keddie J. L., Jones R. A. L., Cory R. A.; Interface and surface effects on the glass-transition temperature in thin polymer films; *Faraday Discussions* 98 (1994) 219 – 230
- 22 Wallace W. E., Van Zanten J. H., Wu W. L.; Influence of an impenetrable interface on a polymer glass transition temperature; *Physical Review E* 52 (1995) R3329 – R3332
- 23 Jain T. S., de Pablo J. J.; Monte Carlo simulation of free-standing polymer films near the glass transition temperature; *Macromolecules* 35 (2002) 2167 – 2176
- 24 Zhang J., Liu G., Jonas J.; Effects of confinement on the glass transition temperature of molecular liquids; *The Journal of Physical Chemistry* 96 (1992) 3478 - 3480
- 25 Gibbs J. H., DiMarzio E. A.; Nature of the glass transition and the glassy state; *The Journal of Chemical Physics* 28 (1958) 373 - 383
- 26 DiMarzio E. A., Gibbs J. H.; Chain stiffness and the lattice theory of polymer phases; *The Journal of Chemical Physics* 28 (1958) 807 - 813
- 27 McKenna G. B.; Glass formation and glassy behavior; *Comprehensive Polymer Science (Vol 2 Polymer Properties)* (1989) pp 311 - 362
- 28 Simha R., Somcynsky T.; On the statistical thermodynamics of spherical and chain molecule fluids; *Macromolecules* 2 (1969) 342 - 350
- 29 Robertson R. E., Simha R., Curro J. G.; Effects of pressure on volume-recovery experiments; *Macromolecules* 18 (1985) 2239 - 2246
- 30 LaGasse Curro J. G., Simha R.; Diffusion-model for volume recovery in glasses; *Macromolecules* 15 (1982) 1621 - 1626
- 31 Alcoutlabi M., McKenna G. B.; Effects of confinement on material behaviour at the nanometre size scale; *Journal of Physics: Condensed Matter* 17 (2005) R461 – R524
- 32 Beckmann R.; “Quat – Primer” Polymers as Dispersants for Nanoparticles; *Dissertation* (2012)

- 33 Lagaly G., Weiss A.; Anordnung und Orientierung kationischer Tenside auf ebenen Silicatoberflächen I; *Kolloid-Zeitschrift und Zeitschrift für Polymere* 237 (1970) 266 – 273
- 34 He H., Ding Z., Zhu J., Yuan P., Xi Y., Yang D., Frost R. L.; Thermal Characterization of Surfactant-modified Montmorillonites; *Clays and Clay Minerals* 53 (2005) 287 - 293
- 35 Vishnu Mahesh K. R., Narasimha Murthy H. N., Kumaraswamy B. E., Raghavendra N., Sridhar R., Krishna M., Pattar N., Pal R., Sherigara B. S.; Synthesis and characterization of organomodified Na-MMT using cation and anion surfactants; *Frontiers of Chemistry in China* 6 (2011) 153 – 158
- 36 Lagaly G., Weiss A.; Anordnung und Orientierung kationischer Tenside auf Silicatoberflächen IV; *Kolloid-Zeitschrift und Zeitschrift für Polymere* 243 (1971) 48 – 55
- 37 Jordan J. W.; Organophilic Bentonites. I. Swelling in Organic Liquids; *The Journal of Physical Chemistry* 53 (1949) 294 - 306
- 38 Brindley G. W., Hoffmann R. W.; Orientation and packing of aliphatic chain molecules on montmorillonite: Clay-Organic studies-VI; *Clays and Clay Minerals* (1962) 546 - 556
- 39 Lagaly G., Weiss A.; Anordnung und Orientierung kationischer Tenside auf Silicatoberflächen; *Kolloid-Zeitschrift und Zeitschrift für Polymere* 243 (1971) 48 - 55
- 40 Chen G., Han B., Yan H.; attraction of Cationic Surfactants with Iron and Sodium Montmorillonite Suspensions; *Journal of Colloid and Interface Science* 201 (1998) 158 - 163
- 41 Iwamoto K., Ohnuki Y., Sawada K., Senō M.; Solid-Solid Phase Transitions of Long-Chain n-Alkyltrimethylammonium Halides; *Molecular Crystals and Liquid Crystals* 73 (1981) 95 - 103
- 42 Li Y., Ishida H.; A Differential Scanning Calorimetry Study of the Assembly of Hexadecylamine Molecules in the Nanoscale Confined Space of Silicate Galleries; *Chemistry of Materials* 14 (2002) 1398 - 1404
- 43 He H., Ding Z., Zhu J., Yuan P., Xi Y., Yang D., Frost R. L.; Thermal Characterization of Surfactant-modified Montmorillonites; *Clays and Clay Minerals* 53 (2005) 287 – 293
- 44 Jackson C. L., McKenna G. B.; The melting behavior of organic materials confined in porous solids; *The Journal of Chemical Physics* 93 (1990) 9002–9011
- 45 Jackson C. L., McKenna G. B.; Vitrification and crystallization of organic liquids confined to nanoscale pores; *Chemistry of Materials* 8 (1996) 2128 – 2137

- 46 Alba-Simionesco C., Dosseh G., Dumont E., Frick B., Geil B., Morineau D., Teboul V., Xia Y.; Confinement of molecular liquids: consequences on thermodynamic, static and dynamical properties of benzene and toluene; *The European Physical Journal E* 12 (2003) 19 – 28
- 47 Wallacher D., Ackermann R., Huber R., Enderle M., Knorr K.; Diffraction study of solid oxygen embedded in porous glasses; *Physical Review B* 64 (2001) 184203-1 – 184203-9
- 48 Knorr K., Wallacher D., Huber P., Soprunyuk V., Ackermann R.; Are solidified fillings of mesopores basically bulk-like except for the geometric confinement?; *The European Physical Journal E* 12 (2003) 51 – 56
- 49 Hung F. R., Dudziak G., Sliwiska-Bartkowiak M., Gubbins K. E.; Freezing/melting behaviour within carbon nanotubes; *Molecular Physics* 102 (2004) 223 – 234
- 50 Morishige K., Iwasaki H.; X-ray study of freezing and melting of water confined within SBA-15; *Langmuir* 19 (2003) 2808 – 2811
- 51 Gibbs J. W.; *Collected Works* (1928)
- 52 Thomson W.; On the equilibrium of vapour at a curved surface of liquid; *Philosophical Magazine Series* 42 (1871) 448 – 452
- 53 Defay R., Prigogine I., Bellemans A., Everett D. H.; *Surface Tension and Adsorption* (1966)
- 54 Gao Z., Xie W., Hwu J. M., Wells L., Pan W.-P.; The Characterization of Organic Modified Montmorillonite and Its Filled PMMA Nanocomposite; *Journal of Thermal Analysis and Calorimetry* 64 (2001) 467 - 475
- 55 Xie W., Gao Z., Liu K., Pan W.-P., Vaia R., Hunter D., Singh A.; Thermal characterization of organically modified montmorillonite; *Thermochimica Acta* 367 - 368 (2001) 339 – 350
- 56 Viana R. B., da Silva A. B. F., Pimentel A. S.; Infrared Spectroscopy of Anionic, Cationic, and Zwitterionic Surfactants; *Advances in Physical Chemistry* (2012), Article ID 903272, 14 pages
- 57 Hongping H., Ray F. L., Jianxi Z.; Infrared study of HDTMA⁺ intercalated montmorillonite; *Spectrochimica Acta Part A: Molecular and Biomolecular Spectroscopy* 60 (2004) 2853 - 2859
- 58 Silverstein R. M., Webster F. X., Kiemle D. J.; *Spectrometric identification of organic compounds seventh edition* (2006)
- 59 Kuczumow A., Rzačzyńska Z., Szewczak M.; Matrix Effects in the X-Ray Fluorescence Method; *X-Ray Spectrometry* 11 (2005) 135 – 139
- 60 Birdi K. S.; *Handbook of Surface and Colloid Chemistry, Fourth Edition* (2016)
- 61 Greenland D. J., Quirk J. P.; Determination of the total specific surface area of

4 Preparation of [montmorillonite/PEI_xQyR] adducts

- soils by adsorption of cetyl pyridinium bromide; *Journal of Soil Science* 15 (1964) 178 – 191
- 62 Macht F., Eusterhues K., Pronk G. J., Totsche K. U.; Specific surface area of clay minerals: Comparison between atomic force microscopy measurements and bulk-gas (N₂) and -liquid (EGME) adsorption methods; *Applied Clay Science* 53 (2011) 20 – 26
- 63 Blumstein A.; Polymerization of adsorbed monolayers. I. Preparation of the clay-polymer complex; *Journal of Polymer Science. A: Polymer Chemistry* 3 (1965) 2653 - 2664
- 64 Hendricks S. B., Nelson R. A., Alexander L. T.; Hydration Mechanism of the Clay Mineral Montmorillonite Saturated with Various Cations; *Journal of the American Chemical Society* 62 (1940) 1457 - 1464
- 65 Ammann L.; Cation exchange and adsorption on clays and clay minerals (2003)

5 Preparation of bitumen- [montmorillonite/PEI(nkD)_{xQ}^{yR}] composites

5.1 Introduction

This Chapter describes the preparation and characterization of bitumen-[MMT/PEI(nkD)_xQ^yR] nanocomposites. The aim of this work is to enhance the properties of bitumen by incorporating montmorillonite/alkyl-quat-primer adducts [MMT/PEI(nkD)_xQ^yR], that have been described in Chapter 4, into bitumen to obtain bitumen-[MMT/PEI_xQ^yR] composites.

[MMT/PEI(nkD)_xQ^yR] adducts were chosen for two reasons:

With diameters between 100 – 1000 nm, and a thickness of about 1 nm montmorillonite sheet particles exhibit high aspect ratios (diameter/thickness) of about $A_f = 100 - 1000$. The idea is therefore that the impermeable sheets of this clay mineral create a diffusion barrier (cf. Figure 5.1) which slows down the diffusion of oxygen and the loss of lubricating oils, and hence delays the oxidative ageing of the bitumen as well as its embrittlement. Furthermore, the alkyl-functionalized polymers, which surround the MMT platelets, enable the adducts to be compatible with the non-polar fractions of the bitumen.



Figure 5.1: Model for the path of a diffusing molecule through a polymer filled with circular or square plates [1]

Three kinds of organically modified montmorillonites (= MMT/organo adducts), namely adducts **A1** – **A3**, were incorporated into polymer modified and non-polymer modified bitumen. In this Chapter **A1** – **A3** denotes:

A1: An [MMT/CTAB] adduct in which the organic part consisted of an alkylammonium compound bearing a quaternary ammonium group and an alkyl chain build up of 16 carbon atoms (CTAB = (1-hexadecyl)trimethylammonium bromide).

A2: [MMT/PEI(10kD)_{10Q}^{80R10}] and [MMT/PEI(10kD)_{5Q}^{67R10}] adducts in which the organic part consisted of a hyperbranched poly(ethylenimine) (= PEI) macromolecule with covalently fixed quaternary ammonium groups (Q = glycidyltrimethylammonium chlor-

ide) and alkyl chains build up of 10 carbon atoms (R10 = 1,2-epoxydodecane).

A3: An [MMT/PEI(10kD)_{10Q}^{60R14}] adduct in which the organic part consisted of a hyper-branched poly(ethylenimine) (= PEI) macromolecule with covalently fixed quarternary ammonium groups (Q = glycidyltrimethylammonium chloride) and alkyl chains build up of 14 carbon atoms (R14 = 1,2-epoxyhexadecane).

Adduct type **A1** was chosen for comparison purposes as an example for a montmorillonite/alkylammonium adduct containing a low molecular alkylammonium salt as a mediator between the montmorillonite and the bitumen [2 - 4]. [MMT/PEI(10kD)_xQ^{yR10}] adducts (= type **A2**) were chosen because the used polymers exhibit a good solubility in non-polar solvents (cf. Chapter 3), while one [MMT/PEI(10kD)_xQ^{yR14}] adduct (= type **A3**) was used to investigate the influence of the length of the alkyl chain on the performance of the composites.

5.2 Experimental part

5.2.1 Materials

Table 5.1: Used bitumen

Bitumen	Supplier
70/100	AMO [5]
30/45	Shell
50/70	Nynas
Azalt 50/70	Total
Cariphalte 25/55-55	Shell
Olexobit 45	BP

5.2.2 Techniques

Bitumen-[MMT/PEI_{xQ}^{yR}] and bitumen-[MMT/CTAB] composites were prepared by mixing bitumen with [MMT/PEI_{xQ}^{yR}] or [MMT/CTAB] adducts in a Brabender Standalone KE 19 single screw extruder. The extruder could be operated in the temperature region of 40 – 450°C, at a maximum pressure of 700 bar, and with a rotational speed of the screw of 1 – 150 min⁻¹. The extruder was equipped with a dispersing screw of a diameter of 1.9 cm and a length of 47.5 cm. The extruder consisted of three zones, namely the feed zone (zone I), the compression zone (zone II), and the discharge zone (zone III). Each zone was equipped with a thermocouple with the aim to monitor the temperature of the zone. A strand nozzle head equipped with a nozzle was assembled at the end of zone III. The inside diameter of the discharge nozzle was chosen to be 1 mm. The strand nozzle head was equipped with a temperature and a pressure sensor and could be also heated. The bitumen and the adducts were introduced into the feed zone, mixed in the compression zone, and released in the discharge zone. Depending on the experiment, the rotational speed of the screw was operated in the range of 30 - 130 min⁻¹. In addition, the extruder was equipped with a heatable hopper which consisted of the hopper with a capacity of 4 L and a vertical screw. The screw exhibited a diameter of 2 cm and was powered by a 230 V (400 W) motor (obtained from Württembergische Elektromotoren GmbH) which could be operated at 5 – 150 min⁻¹. The heating of the hopper was ensured by a Julabo SE-6 thermostat which could be operated in the temperature region of 20 - 300°C. The extruder was computer controlled and operated via the program Brabender WinExt(Can) (version 4.3.4).

Microscopical investigations were done with a Zeiss Axio Imager.A1m microscope. The microscope was equipped with a Zeiss AxioCam Mrc camera and operated via the program Zeiss AxioVision Release 4.6.3. Two methods were used to investigate the size and distribution of the [MMT/organo] compounds in the bitumen. The first method was polarised light microscopy. For this method, the samples were prepared by putting the bitumen between two microscope slides. The sheets were pressed manually and examined at ambient temperature. The second method was dark field microscopy. For this method, the samples were prepared by putting the bitumen onto a microscope slide. Two 3.5 μm Pütz Mylar C polyester films were placed on the edges and the microscope slide was covered by a second microscope slide. A 10 kg weight was placed on the microscope slides and the samples were heated to 90 °C for 30 minutes. Afterwards, the microscope slides were cooled down to ambient temperature and examined in the dark field.

Rheological investigations were performed using a TA Instruments AR 2000ex dynamic shear rheometer. The measurement setup consisted of a parallel plate geometry using a TA Instruments Peltier plate assembly AR2000 plate which consisted of copper and was coated with chrome. The plate exhibited a diameter of 40 mm and could be operated in the temperature region of -20 – 200°C and at a heating rate up to 20°C/minute. The plate exhibited a temperature accuracy of $\pm 0.1^\circ\text{C}$. The samples were measured in the temperature region of 30 to 120°C, with a frequency $\omega = 6.28$ rad/s, and a stress $\delta = 30$ Pa. The gap was typically set to be $h = 1.0$ mm. The samples were poured onto the lower plate of the rheometer after heating the samples at 120°C for 1 minute with a heat gun. During the measurement, an environmental chamber was not used and the upper plate was not heated.

5.2.3 Preparation of Total Azalt 50/70-[MMT/CTAB] composites

(C1.1) Preparation of Total Azalt 50/70-[MMT_{B1}/CTAB]

20.1 g bitumen was heated to 90°C for 60 minutes in a closed tin can. 1.1 g [MMT_{B1}/CTAB] (adduct **E4.10**, cf. Chapter 4) was pre-ground at 20°C to 0.1 - 1 cm pieces and added to the bitumen. After the mixture was stirred manually, the mixture was introduced through a hopper into the extruder and extruded 1 time at 70°C and at a rotational speed of the extruder screw of 50 min⁻¹. The hopper was heated by a thermostat to 70°C and its “forced material supply device” was operated with a rotational speed of the screw of 45 min⁻¹.

Table 5.2: Prepared Total Azalt 50/70-[MMT/CTAB] composites with the adducts pre-ground at 20°C to 0.1 – 1 cm pieces

Entry	Bitumen	Adduct (Chapter 4)	Bitumen (g)	Adduct (g)	Extrusion con- ditions	Pretreatment be- fore extrusion
C1.1	T 50/70	E4.10	20.1	1.1	Extruder: 70°C, 50 min ⁻¹ , 1 ex- trusion run; hopper: 70°C, 45 min ⁻¹	Adduct was pre- ground at 20°C to 0.1 - 1 cm and pre- mixed with the bitu- men manually
C1.2	T 50/70	E4.10	18.3	2.0	as with C1.1	as with C1.1

T 50/70 = Total Azalt 50/70 bitumen

5.2.4 Preparation of 70/100-[MMT/PEI(10kD)_{5Q}^{67R10}] composites using adduct **E2**

(C2.1) Preparation of 70/100-[MMT_{B1}/PEI(10kD)_{5Q}^{67R10}]

693.4 g bitumen was heated to 90°C for 60 minutes in a closed tin can. 7.0 g [MMT_{B1}/PEI(10kD)_{5Q}^{67R10}] (adduct **E2**, cf. Chapter 4) was then added to the bitumen and the mixture was mixed manually. The mixture was then introduced through a hopper into the extruder and extruded 13 times with the zones exhibiting a temperature of 60, 80, 100, and 120°C, starting at the feeding zone. The rotational speed of the extruder screw was set to be 50 min⁻¹. The hopper was heated by a heat gun to 90°C.

Table 5.3: Bitumen-[MMT/PEI(10kD)_{5Q}^{67R10}] composites prepared with the non-pre-ground, “direct addition” adduct E2

Entry	Bitumen	Adduct (Chapter 4)	Bitumen (g)	Adduct (g)	Extrusion conditions	Pretreatment before extrusion
<u>C2.1</u>	70/100	<u>E2</u>	693.4	7.0	Extruder: 60, 80, 100, and 120°C, 50 min ⁻¹ , 13 extrusion runs; hopper was heated by a heat gun to 90°C	Adduct was pre-mixed with the bitumen manually
<u>C2.2</u>	70/100	<u>E2</u>	666.3	35.1	Extruder: 60, 80, 100, and 120°C, 50 min ⁻¹ , 24 extrusion runs; hopper was heated by a heat gun to 120°C	as with <u>C2.1</u>
<u>C2.3</u>	70/100	<u>E2</u>	630.0	70.0	Extruder: 60, 80, 100, and 120°C, 50 min ⁻¹ , 20 extrusion runs; hopper was heated by a heat gun to 120°C	as with <u>C2.1</u>

70/100 = 70/100 bitumen obtained from AMO [5]

5.2.5 Preparation of bitumen-[MMT/PEI(10kD)_{10Q}^{80R10}] and bitumen-[MMT/PEI(10kD)_{10Q}^{60R14}] composites with the adducts prepared by the “indirect replacement” method

(C3.1) Preparation of Nynas 50/70-[MMT_{B1}/PEI(10kD)_{10Q}^{80R10}]

448.4 g bitumen was heated to 90°C for 60 minutes in a closed tin can. 4.5 g [MMT_{B1}/PEI(10kD)_{10Q}^{80R10}] (adduct E7, cf. Chapter 4) was then added to the bitumen and the mixture was mixed manually. The mixture was introduced through a hopper into the extruder and extruded one time at 70°C and at a rotational speed of the extruder screw of 30 min⁻¹. The hopper was heated by a heat gun to 70°C.

Table 5.4: Bitumen-[MMT/PEI(10kD)_{10Q}^{80R10}] composites prepared with non-pre-ground adducts which were prepared by the “indirect replacement” method

Entry	Bitumen	Adduct (Chapter 4)	Bitumen (g)	Adduct (g)	Extrusion conditions	Pretreatment before extrusion
<u>C3.1</u>	N 50/70	<u>E7</u>	448.4	4.5	Extruder: 70°C, 30 min ⁻¹ , 1 extrusion run; hopper was heated by a heat gun to 70°C	Adduct was pre-mixed with the bitumen manually
<u>C3.2</u>	N 50/70	<u>E7</u>	321.5	35.7	as with <u>C3.2</u>	as with <u>C3.2</u>

N 50/70 = Nynas 50/70 bitumen

(C4.1.1) Preparation of Nynas 50/70-[MMT_{B1,B2}/PEI(10kD)_{10Q}^{80R10}]

730.5 g bitumen was heated to 90°C for 60 minutes in a closed tin can and put into the hopper (equipped with a screw and a heatable sheathing) afterwards. 38.4 g [MMT_{B1,B2}/PEI(10kD)_{10Q}^{80R10}] (adduct **E8.2**, cf. Chapter 4) was pre-ground at 20°C until the pieces reached a diameter of 1 – 3 cm and put also into the hopper. The mixture was then extruded one time at 70°C and at a rotational speed of the extruder screw of 50 min⁻¹. The hopper was heated by a thermostat to 70°C and its “forced material supply device” was operated with a rotational speed of the screw of 45 min⁻¹.

Table 5.5: Bitumen-[MMT/PEI(10kD)_{10Q}^{80R10}] composites with the adducts pre-ground at 20°C to 1 – 3 cm and prepared by the “indirect replacement” method

Entry	Bitumen	Adduct (Chapter 4)	Bitumen (g)	Adduct (g)	Extrusion conditions	Pretreatment before extrusion
<u>C4.1.1</u>	N 50/70	<u>E8.2</u>	730.5	38.4	Extruder: 70°C, 50 min ⁻¹ , 1 extrusion run; hopper: 70°C, 45 min ⁻¹	Adduct was pre-ground at 20°C to 1 - 3 cm
<u>C4.1.2</u>	N 50/70	<u>E8.2</u>	1313.4	68.6	as with <u>C4.1.1</u>	as with <u>C4.1.1</u>
<u>C4.2.1</u>	N 50/70	<u>E8.2</u>	900.7	100.0	as with <u>C4.1.1</u>	Adduct was pre-ground at 20°C to 1 - 3 cm and pre-mixed with the bitumen manually
<u>C4.2.2</u>	N 50/70	<u>E8.3</u>	1330.7	147.9	as with <u>C4.1.1</u>	as with <u>C4.2.1</u>

N 50/70 = Nynas 50/70 bitumen

(C5.1.1) Preparation of Shell 30/45-[MMT_{B1}/PEI(10kD)_{10Q}^{80R10}]

835.6 g bitumen was heated to 90°C for 60 minutes in a closed tin can. 44.0 g [MMT_{B1}/PEI(10kD)_{10Q}^{80R10}] (adduct **E8.9**, cf. Chapter 4) was frozen in liquid nitrogen and pre-ground until the pieces reached diameters between 0.1 and 1 cm. The adduct was then added to the bitumen and the mixture was mixed manually. The mixture was then introduced through a hopper (equipped with a screw and a heatable sheathing) into the extruder and extruded one time at 70°C and a rotational speed of the extruder screw of 50 min⁻¹. The hopper was heated by a thermostat to 70°C and its “forced material supply device” was operated with a rotational speed of the screw of 45 min⁻¹.

Table 5.6: BP Olexobit 45- and Shell 30/45-[MMT/PEI(10kD)_{10Q}^{80R10}] composites (the adducts **E8.n were prepared by the “indirect replacement” method, cf. Chapter 4, and were pre-ground under N₂^(l) to 0.1 – 1 cm pieces)**

Entry	Bitumen	Adduct (Chapter 4)	Bitumen (g)	Adduct (g)	Extrusion conditions	Pretreatment before extrusion
C5.1.1	S 30/45	E8.10	835.6	44.0	as with C4.1.1	Adduct was pre-ground under liquid nitrogen to 0.1 - 1 cm and pre-mixed with the bitumen manually
C5.1.2	S 30/45	E8.10	837.0	44.1	as with C4.1.1	as with C5.1.1
C5.1.3	S 30/45	E8.10	840.6	44.2	as with C4.1.1	as with C5.1.1
C5.2.1	S 30/45	E8.10	834.5	92.7	as with C4.1.1	as with C5.1.1
C5.2.2	S 30/45	E8.11	826.1	91.8	as with C4.1.1	as with C5.1.1
C5.2.3	S 30/45	E8.11	801.7	89.1	as with C4.1.1	as with C5.1.1
C6.1.1	B 45	E8.6	740.9	40.1	as with C4.1.1	as with C5.1.1
C6.1.2	B 45	E8.6	917.8	47.1	as with C4.1.1	as with C5.1.1
C6.1.3	B 45	E8.6	930.0	49.0	as with C4.1.1	as with C5.1.1
C6.1.4	B 45	E8.9	846.9	44.5	as with C4.1.1	as with C5.1.1
C6.1.5	B 45	E8.9	863.8	45.5	as with C4.1.1	as with C5.1.1
C6.2.1	B 45	E8.6	859.6	95.4	as with C4.1.1	as with C5.1.1
C6.2.2	B 45	E8.7	665.0	74.1	as with C4.1.1	as with C5.1.1
C6.2.3	B 45	E8.7	865.8	96.2	as with C4.1.1	as with C5.1.1
C6.2.4	B 45	E8.9	897.9	99.8	as with C4.1.1	as with C5.1.1
C6.2.5	B 45	E8.9	547.2	60.8	as with C4.1.1	as with C5.1.1

B 45 = BP Olexobit 45 bitumen, S 30/45 = Shell 30/45 bitumen

Table 5.7: Total Azalt 50/70- and Shell Cariphalte 25/55-55-[MMT/PEI(10kD)_{10Q}^{80R10}] composites (the adducts **E8 - **E10** were prepared by the “indirect replacement” method, cf. Chapter 4, and were pre-ground under N₂^(l) to 0.1 – 1 cm pieces)**

Entry	Bitumen	Adduct (Chapter 4)	Bitumen (g)	Adduct (g)	Extrusion conditions	Pretreatment before extrusion
C7.1.1	S Car	E8.4	308.4	16.2	as with C4.1.1	as with C5.1.1
C7.1.2	S Car	E8.4	482.5	25.3	as with C4.1.1	as with C5.1.1
C7.1.3	S Car	E8.4	481.4	25.4	as with C4.1.1	as with C5.1.1
C7.1.4	S Car	E8.5	482.6	25.2	as with C4.1.1	as with C5.1.1
C7.1.5	S Car	E8.5	481.8	25.4	as with C4.1.1	as with C5.1.1
C7.1.6	S Car	E8.5	467.5	24.4	as with C4.1.1	as with C5.1.1
C7.1.7	S Car	E8.7	926.5	48.8	as with C4.1.1	as with C5.1.1
C7.1.8	S Car	E8.8	842.6	44.4	as with C4.1.1	as with C5.1.1
C7.2.1	S Car	E8.5	468.6	52.1	as with C4.1.1	as with C5.1.1
C7.2.2	S Car	E8.5	462.2	51.4	as with C4.1.1	as with C5.1.1
C7.2.3	S Car	E8.5	454.2	50.5	as with C4.1.1	as with C5.1.1
C7.2.4	S Car	E8.6	447.4	49.7	as with C4.1.1	as with C5.1.1
C7.2.5	S Car	E8.6	448.0	49.8	as with C4.1.1	as with C5.1.1
C7.2.6	S Car	E8.8	875.7	97.4	as with C4.1.1	as with C5.1.1
C7.2.7	S Car	E8.8	826.4	90.9	as with C4.1.1	as with C5.1.1
C8.1	T50/70	E8.1	2660	140	as with C4.1.1	as with C5.1.1
C8.2.1	T50/70	E8.3	714.2	81.5	as with C4.1.1	as with C5.1.1
C8.2.2	T50/70	E8.4	873.4	94.9	as with C4.1.1	as with C5.1.1
C8.8.3	T50/70	E8.4	824.7	91.6	as with C4.1.1	as with C5.1.1
C9	T 50/70	E9	19.3	1.0	as with C4.1.1	as with C5.1.1
C10.1	T 50/70	E10	81.6	0.8	as with C4.1.1	as with C5.1.1
C10.2	T 50/70	E10	76.9	2.0	as with C4.1.1	as with C5.1.1
C10.3	T 50/70	E10	77.4	4.1	as with C4.1.1	as with C5.1.1
C10.4	T 50/70	E10	73.8	6.0	as with C4.1.1	as with C5.1.1
C10.5	T 50/70	E10	69.6	7.7	as with C4.1.1	as with C5.1.1

T 50/70 = Total Azalt 50/70 bitumen, S Car = Shell Cariphalte 25/55-55 bitumen

Table 5.8: Nynas 50/70- and Total Azalt 50/70-[MMT/PEI(10kD)_{10Q}^{60R14}] composites (the adducts E15.n were prepared by the “indirect replacement” method, cf. Chapter 4, and were pre-ground at 20°C to 0.1 – 1 cm pieces)

Entry	Bitumen	Adduct (Chapter 4)	Bitumen (g)	Adduct (g)	Extrusion con- ditions	Pretreatment be- fore extrusion
<u>C11.1</u>	N 50/70	<u>E15.8</u> , <u>E15.9</u>	477.4	53.0	as with <u>C4.1.1</u>	Adduct was pre-ground at 20°C to 0.1 - 1 cm and pre-mixed with the bitumen manually
<u>C11.2</u>	N 50/70	<u>E15.8</u> , <u>E15.9</u>	535.9	59.5	as with <u>C4.1.1</u>	as with <u>C11.1</u>
<u>C11.3</u>	N 50/70	<u>E15.8</u> , <u>E15.9</u>	610.3	67.8	as with <u>C4.1.1</u>	as with <u>C11.1</u>
<u>C11.4</u>	N 50/70	<u>E15.8</u> , <u>E15.9</u>	612.8	68.1	as with <u>C4.1.1</u>	as with <u>C11.1</u>
<u>C11.5</u>	N 50/70	<u>E15.8</u> , <u>E15.9</u>	135.0	15.0	as with <u>C4.1.1</u>	as with <u>C11.1</u>
<u>C12.1</u>	T 50/70	<u>E15.6</u>	20.1	0.2	as with <u>C4.1.1</u>	as with <u>C11.1</u>
<u>C12.2.1</u>	T 50/70	<u>E15.6</u>	795.3	41.9	as with <u>C4.1.1</u>	as with <u>C11.1</u>
<u>C12.2.2</u>	T 50/70	<u>E15.6</u>	717.9	37.8	as with <u>C4.1.1</u>	as with <u>C11.1</u>
<u>C12.2.3</u>	T 50/70	<u>E15.6</u>	628.7	33.1	as with <u>C4.1.1</u>	as with <u>C11.1</u>
<u>C12.2.4</u>	T 50/70	<u>E15.6</u>	449.4	23.7	as with <u>C4.1.1</u>	as with <u>C11.1</u>
<u>C12.3.1</u>	T 50/70	<u>E15.6</u>	721.9	80.2	as with <u>C4.1.1</u>	as with <u>C11.1</u>
<u>C12.3.2</u>	T 50/70	<u>E15.6</u>	746.4	83.0	as with <u>C4.1.1</u>	as with <u>C11.1</u>
<u>C12.3.3</u>	T 50/70	<u>E15.6</u>	191.7	21.3	as with <u>C4.1.1</u>	as with <u>C11.1</u>
<u>C12.3.4</u>	T 50/70	<u>E15.7</u>	690.1	76.7	as with <u>C4.1.1</u>	as with <u>C11.1</u>
<u>C12.4</u>	T 50/70	<u>E15.6</u>	16.2	4.1	as with <u>C4.1.1</u>	as with <u>C11.1</u>
<u>C12.5</u>	T 50/70	<u>E15.6</u>	14.0	6.0	as with <u>C4.1.1</u>	as with <u>C11.1</u>

N 50/70 = Nynas 50/70 bitumen, T 50/70 = Total Azalt 50/70 bitumen

5 Preparation of bitumen-[montmorillonite/PEI(nkD)xQyR] composites

Table 5.9: BP Olexobit 45-, Shell 30/45-, and Shell Cariphalte 25/55-55-[MMT/PEI(10kD)_{10Q}^{60R14}] composites (the adducts E15.n were prepared by the “indirect replacement” method, cf. Chapter 4, and were pre-ground at 20°C to 0.1 – 1 cm pieces)

Entry	Bitumen	Adduct (Chapter 4)	Bitumen (g)	Adduct (g)	Extrusion conditions	Pretreatment before extrusion
<u>C13.1</u>	S 30/45	<u>E15.8 – E15.11</u>	17.5	2.0	as with <u>C4.1.1</u>	as with <u>C11.1</u>
<u>C13.2</u>	S 30/45	<u>E15.8 – E15.11</u>	18.2	2.0	Extruder: 70°C, 130 min ⁻¹ , 1 extrusion run; hopper: 70°C, 45 min ⁻¹	as with <u>C11.1</u>
<u>C13.3.1</u>	S 30/45	<u>E15.8 – E15.11</u>	18.4	2.0	Extruder: 120°C, 130 min ⁻¹ , 1 extrusion run; hopper: 70°C, 45 min ⁻¹	as with <u>C11.1</u>
<u>C13.3.2.1</u>	S 30/45	<u>E15.8 – E15.11</u>	829.0	92.1	as with <u>C13.3.1</u>	as with <u>C11.1</u>
<u>C13.3.2.2</u>	S 30/45	<u>E15.8 – E15.11</u>	871.5	96.8	as with <u>C13.3.1</u>	as with <u>C11.1</u>
<u>C13.3.2.3</u>	S 30/45	<u>E15.8 – E15.11</u>	631.0	70.1	as with <u>C13.3.1</u>	as with <u>C11.1</u>
<u>C13.4</u>	S 30/45	<u>E15.8 – E15.11</u>	18.3	2.0	Extruder: 160°C, 130 min ⁻¹ , 1 extrusion run; hopper: 70°C, 45 min ⁻¹	as with <u>C11.1</u>
<u>C14.1</u>	B 45	<u>E15.8, E15.9</u>	800.1	88.9	as with <u>C4.1.1</u>	as with <u>C11.1</u>
<u>C14.2</u>	B 45	<u>E15.8, E15.9</u>	856.8	95.2	as with <u>C4.1.1</u>	as with <u>C11.1</u>
<u>C14.3</u>	B 45	<u>E15.8, E15.9</u>	728.3	80.9	as with <u>C4.1.1</u>	as with <u>C11.1</u>
<u>C15.1</u>	S Car	<u>E15.8, E15.9</u>	876.6	97.4	as with <u>C4.1.1</u>	as with <u>C11.1</u>
<u>C15.2</u>	S Car	<u>E15.8, E15.9</u>	439.7	48.9	as with <u>C4.1.1</u>	as with <u>C11.1</u>
<u>C15.3</u>	S Car	<u>E15.8, E15.9</u>	862.4	95.8	as with <u>C4.1.1</u>	as with <u>C11.1</u>
<u>C15.4</u>	S Car	<u>E15.8, E15.9</u>	201.3	22.4	as with <u>C4.1.1</u>	as with <u>C11.1</u>

B 45 = BP Olexobit 45 bitumen, S 30/45 = Shell 30/45 bitumen, S Car = Shell Cariphalte 25/55-55 bitumen

5.3 Results and Discussion

In this study [MMT/PEI(nkD)_{xQ}y^R] and [MMT/CTAB] adducts were incorporated into bitumen to create bitumen-[MMT/organo] nanocomposites. [MMT/PEI(nkD)_{xQ}y^R] adducts were prepared by reacting montmorillonite with a hyperbranched poly(ethylenimine) (= PEI) bearing glycidyltrimethylammonium chloride (= Q) moieties. Also, either 1,2-epoxydodecane (= R10) or 1,2-epoxyhexadecane (= R14) was attached to the poly(ethylenimine) to make the polymer soluble in non-polar solvents (cf. Chapter 4). The synthesis of the polymers used to make the adducts has been described in Chapter 3. The composition and the weight fraction of the organic material of the adducts are listed in Table 5.10. Note that adducts of different origin and preparation method, but of sufficient similar structure and composition will not be distinguished in this Chapter any more. “Like” adducts will be subsumed under a common identifier. Table 5.10 also gives a cross-reference to Chapter 4.

Table 5.10: [MMT/PEI(nkD)_{xQ}y^R] and [MMT/CTAB] adducts used to modify bitumen

Entry	Adduct composition	Adduct preparation method	Entry adduct (Chapter 4)	Organic content of the adduct (wt.%)
C1.1, C1.2	[MMT _{B1} /CTAB]	D	E4	45.5
C2.1 - C2.3	[MMT _{B1} /PEI(10kD) _{5Q} ^{67R10}]	D	E2	43.6
C3.1, C3.2	[MMT _{B1} /PEI(10kD) _{10Q} ^{80R10}]	I	E7	56.5
C4.1 – C8.2	[MMT _{B1} /PEI(10kD) _{10Q} ^{80R10}]	I	E8	67.9
C9	[MMT _{B2} /PEI(10kD) _{10Q} ^{80R10}]	I	E9	65.9
C10.1 - C10.5	[MMT _{B1} /PEI(10kD) _{10Q} ^{80R10}]	I	E10	60.8
C11 - C15	[MMT _{B2} /PEI(10kD) _{10Q} ^{60R14}]	I	E15	60.6

CTAB = (1-hexadecyl)trimethylammonium bromide, MMT_{B1} = Na-bentonite **B1** (cf. Chapter 4, Table 4.2), MMT_{B2} = Na-bentonite **B2** (cf. Chapter 4, Table 4.2), PEI(10kD) = poly(ethylenimine) with M_n = 10,000 g/mol, M_w/M_n = 2.5, xQ = mol% 2-hydroxypropyl-3-(N,N,N-trimethylammonium chloride), yR10 = mol% 2-hydroxydodecane, yR14 = mol% 2-hydroxyhexadecane, D = “direct addition” (cf. Chapter 4), I = “indirect replacement” (cf. Chapter 4)

The preparation of composites involved five parameters that may influence the size and distribution of the adduct particles in a bitumen-nanocomposite. The investigated parameters were (1) the used bitumen, (2) the adduct composition, (3) the preparation method of a respective adduct, (4) the applied compounding procedure including

(4a) the mixtures pretreatment, and (4b) the mixing procedure itself, as well as last but not least (5) the targeted weight concentration of the adduct in the bitumen matrix.

(1) The investigated bitumen were three non-polymer modified bitumen, namely: Nynas 50/70 bitumen, Total Azalt 50/70 bitumen, and Shell 30/45 bitumen, as well as two polymer-modified bitumen, namely: BP Olexobit 45 bitumen and Shell Cariphalte 25/55-55 bitumen.

(2) The studied adduct types were [MMT/PEI(10kD)_{5Q}^{67R10}], [MMT/PEI(10kD)_{10Q}^{80R10}], [MMT/PEI(10kD)_{10Q}^{60R14}], and [MMT/CTAB] adducts. While the [MMT/PEI(10kD)_{xQ}^{yR10}] and the [MMT/PEI(10kD)_{10Q}^{60R14}] adducts differed by the length of the alkyl chains (= R) used to modify the polymer, [MMT/CTAB] consisted of montmorillonite and (1-hexadecyl)trimethylammonium bromide (cf. Chapter 4).

(3) The [MMT/PEI(nkD)_{xQ}^{yR}] adducts were prepared by either the “direct addition” (adducts **E2** and **E4**) or the “indirect replacement” (adducts **E7** - **E15**) method (cf. Chapter 4).

(4a) It was tried whether the addition of adducts ground to particles of a smaller size to bitumen could lead to a more homogeneous distribution of the adducts in the bitumen. For this reason, [MMT/PEI(10kD)_{10Q}^{80R10}] adduct samples were used to prepare bitumen composites (i) without pre-ground adducts, (ii) adducts pre-ground at 20°C to 1 – 3 cm size, and (iii) adducts pre-ground under liquid nitrogen to small pieces of 0.1 – 1 cm. While with [MMT/CTAB] and [MMT/PEI(10kD)_{10Q}^{60R14}] adducts pieces with diameters of 0.1 – 1 cm could be obtained when the adducts were pre-ground at 20°C, [MMT/PEI(nkD)_{xQ}^{yR10}] adduct fractions adhered strongly to each other and could only be ground to pieces of 1 - 3 cm at this temperature. In addition, it was tried whether a pre-mixing of the adducts with the bitumen before the extrusion had an influence on the particle dispersion. The term pre-mixing means that the adducts were mixed manually into the bitumen melt until a homogeneous mixture was obtained.

(4b) The composites were prepared at extrusion temperatures in the region of 70 - 160°C and at rotational speeds of the extruder screw of 30 – 130 min⁻¹.

(5) The weight concentration of the adducts in the bitumen was chosen to be in the region of 1 to 30 wt.% with the aim to study whether agglomeration of the adducts occurred at higher concentrations.

5 Preparation of bitumen-[montmorillonite/PEI(nkD)xQyR] composites

The composites were prepared by mixing the adducts with the bitumen in a Brabender Standalone KE 19 single screw extruder (Figure 5.2). In addition, a heatable hopper equipped with a vertical screw powered by a 230 V (400 W) motor was placed on the injection opening of the extruder. The hopper was heated by a Julabo SE-6 thermostat. Via the program Brabender WinExt(Can) (version 4.3.4) the extruder was operated, i. e. its temperatures, and rotations were set, while the screw-torque was monitored. The extruder screw exhibited a diameter of 1.9 cm and a length of 47.5 cm, its zone structure (compression, mixing) is depicted in Figure 5.3.



Figure 5.2: Used Brabender Standalone KE 19 single screw extruder setup

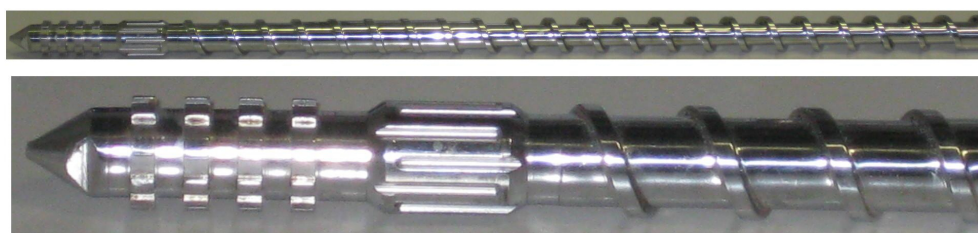


Figure 5.3: Used extruder screw

The bitumen-nanocomposites were investigated by dynamic shear rheology (DSR), polarized light and dark field microscopy. The DSR measurements yielded the storage modulus G' and the loss modulus G'' , describing the viscoelastic properties of the materials (cf. Chapter **2.5.5**, Rheology). The phase angle δ describes the viscoelastic character of the bitumen [6]. The dynamic viscosity η' gives the resistance

5 Preparation of bitumen-[montmorillonite/PEI(nkD)_xQyR] composites

of the composites to shearing. The loss factor $\tan \delta$ is defined as the ratio G''/G' and is a measure of the damping in a viscoelastic system. A material showing a high $\tan \delta$ behaves like a viscous liquid and a material exhibiting a low $\tan \delta$ like an elastic solid [7 - 9]. By means of microscopy, the size and distribution of the incorporated [MMT/organo] adduct particles in the bitumen matrix were visualized.

The composition of the investigated [MMT/PEI(nkD)_xQ^{yR}] and [MMT/CTAB] composites will be described in the following paragraphs and is listed in the corresponding tables. Two Total Azalt 50/70-[MMT_{B1}/CTAB] composites (**C1.1** and **C1.2**) were prepared with the concentration of the adduct chosen to be 5.2 wt.% with composite **C1.1** and 9.9 wt.% with composite **C1.2** to test whether agglomeration of the adducts occurred at higher adduct concentrations. The details of the prepared Total Azalt 50/70-[MMT_{B1}/CTAB] composites are listed in Table 5.11. The adduct was pre-ground at 20°C to 0.1 - 1 cm pieces and pre-mixed with the bitumen manually before extrusion. The extrusion temperature was set to be 70°C and the rotational speed of the extruder screw to be 50 min⁻¹. The bitumen/adduct mixtures were extruded one time each.

Table 5.11: Prepared Total Azalt 50/70-[MMT_{B1}/CTAB] composites

Entry	Bitumen	Adduct	Adduct preparation method	Adduct concentration (wt.%)	Extrusion runs	PG	PM
C1.1	T 50/70	[MMT _{B1} /CTAB]	D	5.2	1	20°C	√
C1.2	T 50/70	[MMT _{B1} /CTAB]	D	9.9	1	20°C	√

CTAB = (1-hexadecyl)trimethylammonium bromide, MMT_{B1} = Na-bentonite **B1** (cf. Chapter 4, Table 4.2), T 50/70 = Total Azalt 50/70 bitumen, D = “direct addition” (cf. Chapter 4), PG = pre-ground, PM = pre-mixed

Three composites consisting of 70/100 bitumen [5] and the [MMT_{B1}/PEI(10kD)_{5Q}^{67R10}] adduct **E2** (= **C2.1**, **C2.2**, and **C2.3**) were prepared with the aim to test whether an adduct prepared by the “direct addition” method could be fully exfoliated in a bitumen. The adduct concentration was set to be 1.0 wt.% with composite **C2.1**, **C2.2** contained 5.0 wt.% of the adduct and composite **C2.3** 10.0 wt.%. The studied 70/100-[MMT_{B1}/PEI(10kD)_{5Q}^{67R10}] composites are listed in Table 5.12. With all three composites, the adducts were pre-mixed with the bitumen before extrusion but not pre-ground. Furthermore, multiple extrusion runs were performed to test whether additional extrusion runs could reduce the size of the particles in the composites.

Table 5.12: Prepared bitumen-[MMT_{B1}/PEI(10kD)_{5Q}^{67R10}] composites with the adduct prepared by the “direct addition” method

Entry	Bitumen	Adduct	Adduct preparation method	Adduct concentration (wt.%)	Extrusion runs	PG	PM
C2.1	70/100	[MMT _{B1} /PEI(10kD) _{5Q} ^{67R10}]	D	1.0	13	-	√
C2.2	70/100	[MMT _{B1} /PEI(10kD) _{5Q} ^{67R10}]	D	5.0	24	-	√
C2.3	70/100	[MMT _{B1} /PEI(10kD) _{5Q} ^{67R10}]	D	10.0	20	-	√

70/100 = 70/100 bitumen obtained from AMO [5], MMT_{B1} = Na-bentonite **B1** (cf. Chapter 4, Table 4.2), PEI(10kD) = poly(ethylenimine) with M_n = 10,000 g/mol, M_w/M_n = 2.5, xQ = mol% 2-hydroxypropyl-3-(N,N,N-trimethylammonium chloride), yR10 = mol% 2-hydroxydodecane, D = “direct addition” (cf. Chapter 4), PG = pre-ground, PM = pre-mixed

It was further tested whether adducts prepared by the “indirect replacement” method (adducts **E7** – **E15**, composites **C3.1** – **C15**) gave more homogeneous dispersions of the adducts in bitumen matrices than composites containing adduct **E2** which was prepared by the “direct addition” method (**C2.1** – **C2.3**, cf. Table 5.12). With adduct **E7** (= [MMT_{B1}/PEI(10kD)_{10Q}^{80R10}]), two composites were prepared using Nynas 50/70 bitumen as the base bitumen and with the adduct concentration set to be 1.0 wt.% (**C3.1**) and 10.0 wt.% (**C3.2**) (Table 5.13). As with the composites **C2.1** – **C2.3** the composites were prepared by pre-mixing non-pre-ground adducts with the bitumen before extrusion, but different to the composites **C2.1** – **C2.3** the mixtures were extruded only one time.

Table 5.13: Prepared bitumen-[MMT_{B1}/PEI(10kD)_{10Q}^{80R10}] composites with the adducts prepared by the “indirect replacement” method and without the use of pre-ground adducts

Entry	Bitumen	Adduct	Adduct preparation method	Adduct concentration (wt.%)	Extrusion runs	PG	PM
C3.1	N 50/70	[MMT _{B1} /PEI(10kD) _{10Q} ^{80R10}]	I	1.0	1	-	√
C3.2	N 50/70	[MMT _{B1} /PEI(10kD) _{10Q} ^{80R10}]	I	10.0	1	-	√

N 50/70 = Nynas 50/70 bitumen, MMT_{B1} = Na-bentonite **B1** (cf. Chapter 4, Table 4.2), PEI(10kD) = poly(ethylenimine) with M_n = 10,000 g/mol, M_w/M_n = 2.5, xQ = mol% 2-hydroxypropyl-3-(N,N,N-trimethylammonium chloride), yR10 = mol% 2-hydroxydodecane, I = “indirect replacement” (cf. Chapter 4)

5 Preparation of bitumen-[montmorillonite/PEI(nkD)xQyR] composites

With composite **C4.1** it was tested whether a composite prepared by the direct mixing of bitumen with an adduct which was pre-ground at 20°C to 1 – 3 cm pieces in an extruder would lead to a composite with a more homogeneous dispersion compared to the composites **C3.1** and **C3.2** (cf. Table 5.13). During the preparation of composite **C4.2**, the adduct was pre-mixed with the bitumen before extrusion to test the influence of a pre-mixing step. The described composites are listed in Table 5.14, the used adduct was the $[\text{MMT}_{\text{B1}}/\text{PEI}(10\text{kD})_{10\text{Q}}^{80\text{R}10}]$ adduct **E8** (cf. Chapter 4). The adduct concentration was set to be 5.0 wt.% (**C4.1**) and 10.0 wt.% (**C4.2**).

Table 5.14: Prepared bitumen- $[\text{MMT}_{\text{B1}}/\text{PEI}(10\text{kD})_{10\text{Q}}^{80\text{R}10}]$ composites with the adducts prepared by the “indirect replacement” method and pre-ground at 20°C to 1 – 3 cm pieces

Entry	Bitumen	Adduct	Adduct preparation method	Adduct concentration (wt.%)	Extrusion runs	PG	PM
C4.1	N 50/70	$[\text{MMT}_{\text{B1}}/\text{PEI}(10\text{kD})_{10\text{Q}}^{80\text{R}10}]$	I	5.0	1	20°C	-
C4.2	N 50/70	$[\text{MMT}_{\text{B1}}/\text{PEI}(10\text{kD})_{10\text{Q}}^{80\text{R}10}]$	I	10.0	1	20°C	√

N 50/70 = Nynas 50/70 bitumen, MMT_{B1} = Na-bentonite **B1** (cf. Chapter 4, Table 4.2), PEI(10kD) = poly(ethylenimine) with $M_n = 10,000$ g/mol, $M_w/M_n = 2.5$, xQ = mol% 2-hydroxypropyl-3-(N,N,N-trimethylammonium chloride), yR10 = mol% 2-hydroxydodecane, I = “indirect replacement” (cf. Chapter 4)

In contrast to the composites prepared by using adducts which were pre-ground at 20°C to 1 – 3 cm pieces (**C4.1** and **C4.2**, cf. Table 5.14) several composites (**C5.1** – **C10.5**, cf. Table 5.15) were prepared using $[\text{MMT}_{\text{B1,B2}}/\text{PEI}(10\text{kD})_{10\text{Q}}^{80\text{R}10}]$ adducts which were pre-ground under liquid nitrogen to pieces with diameters of 0.1 – 1 cm. As with composite **C4.2**, these adducts were pre-mixed with the bitumen before extrusion. Using Shell 30/45 bitumen as the base bitumen two composites, namely composite **C5.1** and **C5.2** were prepared. The adduct concentration was set to be 5.0 wt.% with composite **C5.1** and 10.0 wt.% with composite **C5.2**. Two composites were prepared using BP Olexobit 45 bitumen as the base bitumen (**C6.1** and **C6.2**) and contained 5.0 and 10.0 wt.% of adduct **E8**, respectively. Using Shell Cariphalte 25/55-55 bitumen as the base bitumen, two composites, indexed as **C7.1** and **C7.2**, were prepared. The composites contained 5.0 wt.% (**C7.1**) and 10.0 wt.% (**C7.2**) of the adduct. With Total Azalt 50/70 bitumen as the base bitumen two composites, namely: **C8.1** and **C8.2** were prepared. The adduct concentration was set to be 5.0 wt.% with composite **C8.1** and 10.0 wt.% with composite **C8.2**.

With adduct **E9** (= $[\text{MMT}_{\text{B2}}/\text{PEI}(10\text{kD})_{10\text{Q}}^{80\text{R}10}]$) one composite containing 4.9 wt.% of

5 Preparation of bitumen-[montmorillonite/PEI(nkD)xQyR] composites

the adduct was prepared (= composite **C9**). The base bitumen used to prepare this composite was Total Azalt 50/70 bitumen. With adduct **E10** (= [MMT_{B1}/PEI(10kD)_{10Q}^{80R10}]), five composites (**C10.1** – **C10.5**) were prepared using also Total Azalt 50/70 bitumen as the base bitumen. With composite **C10.1**, the adduct concentration was set to be 1.0 wt.%. Composite **C10.2** contained 2.5 wt.% of the adduct and composite **C10.3** 5.0 wt.%. With the composites **C10.4** and **C10.5** the adduct concentrations were chosen to be 7.5 wt.% (**C10.4**) and 10.0 wt.% (**C10.5**).

Table 5.15: Prepared bitumen-[MMT_{B1}/PEI(10kD)_{10Q}^{80R10}] composites with the adducts prepared by the “indirect replacement” method and pre-ground under liquid nitrogen to 0.1 – 1 cm pieces

Entry	Bitumen	Adduct	Adduct preparation method	Adduct concentration (wt.%)	Extrusion runs	PG	PM
C5.1	S 30/45	[MMT _{B1} /PEI(10kD) _{10Q} ^{80R10}]	I	5.0	1	N ₂ ^(l)	√
C5.2	S 30/45	[MMT _{B1} /PEI(10kD) _{10Q} ^{80R10}]	I	10.0	1	N ₂ ^(l)	√
C6.1	B 45	[MMT _{B1} /PEI(10kD) _{10Q} ^{80R10}]	I	5.0	1	N ₂ ^(l)	√
C6.2	B 45	[MMT _{B1} /PEI(10kD) _{10Q} ^{80R10}]	I	10.0	1	N ₂ ^(l)	√
C7.1	S Car	[MMT _{B1} /PEI(10kD) _{10Q} ^{80R10}]	I	5.0	1	N ₂ ^(l)	√
C7.2	S Car	[MMT _{B1} /PEI(10kD) _{10Q} ^{80R10}]	I	10.0	1	N ₂ ^(l)	√
C8.1	T 50/70	[MMT _{B1} /PEI(10kD) _{10Q} ^{80R10}]	I	5.0	1	N ₂ ^(l)	√
C8.2	T 50/70	[MMT _{B1} /PEI(10kD) _{10Q} ^{80R10}]	I	10.0	1	N ₂ ^(l)	√
C9	T 50/70	[MMT _{B2} /PEI(10kD) _{10Q} ^{80R10}]	I	4.9	1	N ₂ ^(l)	√
C10.1	T 50/70	[MMT _{B1} /PEI(10kD) _{10Q} ^{80R10}]	I	1.0	1	N ₂ ^(l)	√
C10.2	T 50/70	[MMT _{B1} /PEI(10kD) _{10Q} ^{80R10}]	I	2.5	1	N ₂ ^(l)	√
C10.3	T 50/70	[MMT _{B1} /PEI(10kD) _{10Q} ^{80R10}]	I	5.0	1	N ₂ ^(l)	√
C10.4	T 50/70	[MMT _{B1} /PEI(10kD) _{10Q} ^{80R10}]	I	7.5	1	N ₂ ^(l)	√
C10.5	T 50/70	[MMT _{B1} /PEI(10kD) _{10Q} ^{80R10}]	I	10.0	1	N ₂ ^(l)	√

S 30/45 = Shell 30/45 bitumen, B 45 = BP Olexobit 45 bitumen, S Car = Shell Cariphalte 25/55-55 bitumen, T 50/70 = Total Azalt 50/70 bitumen, MMT_{B1} = Na-bentonite **B1** (cf. Chapter 4, Table 4.2), PEI(10kD) = poly(ethylenimine) with M_n = 10,000 g/mol, M_w/M_n = 2.5, xQ = mol% 2-hydroxypropyl-3-(N,N,N-trimethylammonium chloride), yR10 = mol% 2-hydroxydodecane, I = “indirect replacement” (cf. Chapter 4)

With alkyl-quat-primer polymers bearing 1,2-epoxyhexadecane as the alkyl groups (= PEI(nkD)_{xQ}^{yR14}, cf. Chapter 3), 13 bitumen-[MMT/PEI(10kD)_{10Q}^{60R14}] composites were prepared using the [MMT/PEI(10kD)_{10Q}^{60R14}] adduct **E15**. The prepared bitumen-

5 Preparation of bitumen-[montmorillonite/PEI(nkD)xQyR] composites

[MMT/PEI(10kD)_{10Q}^{60R14}] composites are listed in Table 5.16. One composite with an adduct concentration of 10.0 wt.% was prepared using Nynas 50/70 bitumen as the base bitumen (**C11**). Five composites were prepared using Total Azalt 50/70 bitumen as the base bitumen (**C12.1** to **C12.5**) and contained 1.0, 5.0, 10.0, 20.2, and 30.0 wt.% of the adduct, respectively. Four composites were prepared at different temperatures and rotational speeds of the extruder screw each using Shell 30/45 bitumen as the base bitumen and with adduct concentrations of about 10 wt.% (**C13.1** - **C13.4**). Using BP Olexobit 45 bitumen as the base bitumen one composite with an adduct concentration of 10.0 wt.% was prepared (**C14**). Using Shell Cariphalte 25/55-55 bitumen as the base bitumen, one composite was prepared (**C15**) with the adduct concentration set to be 10.0 wt.%. With all composites the adducts were pre-ground at 20°C to 0.1 – 1 cm pieces and pre-mixed with the bitumen before extrusion.

Table 5.16: Prepared bitumen-[MMT/PEI(10kD)_{10Q}^{60R14}] composites with the adducts prepared by the “indirect replacement” method and pre-ground at 20°C to 0.1 – 1 cm pieces

Entry	Bitumen	Adduct	Adduct preparation method	Adduct concentration (wt.%)	Extrusion runs	PG	PM
C11	N 50/70	[MMT _{B2} /PEI(10kD) _{10Q} ^{60R14}]	I	10.0	1	20°C	√
C12.1	T 50/70	[MMT _{B2} /PEI(10kD) _{10Q} ^{60R14}]	I	1.0	1	20°C	√
C12.2	T 50/70	[MMT _{B2} /PEI(10kD) _{10Q} ^{60R14}]	I	5.0	1	20°C	√
C12.3	T 50/70	[MMT _{B2} /PEI(10kD) _{10Q} ^{60R14}]	I	10.0	1	20°C	√
C12.4	T 50/70	[MMT _{B2} /PEI(10kD) _{10Q} ^{60R14}]	I	20.2	1	20°C	√
C12.5	T 50/70	[MMT _{B2} /PEI(10kD) _{10Q} ^{60R14}]	I	30.0	1	20°C	√
C13.1	S 30/45	[MMT _{B2} /PEI(10kD) _{10Q} ^{60R14}]	I	10.3	1	20°C	√
C13.2	S 30/45	[MMT _{B2} /PEI(10kD) _{10Q} ^{60R14}]	I	9.9	1	20°C	√
C13.3.1	S 30/45	[MMT _{B2} /PEI(10kD) _{10Q} ^{60R14}]	I	9.8	1	20°C	√
C13.3.2	S 30/45	[MMT _{B2} /PEI(10kD) _{10Q} ^{60R14}]	I	10.0	1	20°C	√
C13.4	S 30/45	[MMT _{B2} /PEI(10kD) _{10Q} ^{60R14}]	I	9.9	1	20°C	√
C14	B 45	[MMT _{B2} /PEI(10kD) _{10Q} ^{60R14}]	I	10.0	1	20°C	√
C15	S Car	[MMT _{B2} /PEI(10kD) _{10Q} ^{60R14}]	I	10.0	1	20°C	√

N 50/70 = Nynas 50/70 bitumen, T 50/70 = Total Azalt 50/70 bitumen, S 30/45 = Shell 30/45 bitumen, B 45 = BP Olexobit 45 bitumen, S Car = Shell Cariphalte 25/55-55 bitumen, MMT_{B2} = Na-bentonite **B2** (cf. Chapter 4, Table 4.2), PEI(10kD) = poly(ethylenimine) with M_n = 10,000 g/mol, M_w/M_n = 2.5, xQ = mol% 2-hydroxypropyl-3-(N,N,N-trimethylammonium chloride), yR14 = mol% 2-hydroxyhexadecane, I = “indirect replacement” (cf. Chapter 4)

5.3.1 Microscopical investigation of bitumen-[MMT/PEI(nkD)_xQ^{yR}] and bitumen-[MMT/CTAB] composites

Polarised light and dark field microscopy investigations of bitumen-[MMT/CTAB] and bitumen-[MMT/PEI(nkD)_xQ^{yR}] composites were performed to visualise the size and distribution of the adduct particles in the bitumen. Particles with diameters below the wavelength of the used light cannot be resolved, but in the dark field their Airy-diffraction disc can be seen (cf. Chapter 2.5.4 “Polarised light” and “dark field” microscopy). If, however, the average distance of the particles falls short of about $\lambda/2$, these discs mutually overlap and the presence of nanoparticles is revealed by a brightening of the background.

To test whether the adduct preparation method influenced the size and distribution of the adduct particles in bitumen, three 70/100-[MMT_{B1}/PEI(10kD)_{5Q}^{67R10}] composites (**C2.1** - **C2.3**) which contained an adduct prepared by the “direct addition” method (**E2**) were compared to two Nynas 50/70-[MMT_{B1}/PEI(10kD)_{10Q}^{80R10}] composites (**C3.1** and **C3.2**) containing an adduct prepared by the “indirect replacement” method (**E7**). The adduct concentration was set to be 1.0 wt.% with the composites **C2.1** and **C3.1**, 5.0 wt.% with composite **C2.2**, and 10.0 wt.% with the composites **C2.3** and **C3.2**. The adducts were pre-mixed with the bitumen before the extrusion. With the composites **C3.1** and **C3.2**, the preparation procedure was the same as that used to prepare the composites **C2.1** – **C2.3** except from the fact that only one single extrusion run was performed.

In Figure 5.4 the polarised light microscopy pictures of a) composite **C2.1**, b) composite **C2.2**, c) composite **C2.3**, d) Nynas 50/70 bitumen, e) composite **C3.1**, and f) composite **C3.2** are compared. The investigation of the composites **C2.1** – **C2.3** (Figure 5.4.a - Figure 5.4.c) revealed that all three compounds contained particles with diameters up to 50 μm . From SEM investigations of the adducts **E8** and **E15** (cf. Chapter 4), it was known that the used bentonites contained mineral particles with diameters up to 20 μm . All particles larger than 20 μm were therefore attributed to adduct agglomerates. Although 13 (**C2.1**), 24 (**C2.2**), and 20 (**C2.3**) extrusion runs were performed, the size of the particles was similar with all three composites. Since macroscopic adduct pieces of diameters beyond 3 cm were added it may be possible that the rotational speed of the screw of 50 min^{-1} was not sufficiently high enough to break down adduct agglomerates. The Nynas 50/70 bitumen (Figure 5.4.d) contained non-uniform distributed particles with diameters between 1 and 10 μm . The objects observed in composites **C3.1** (Figure 5.4.e) and **C3.2** (Figure 5.4.f) exhibited similar diameters as seen in the composites **C2.1** – **C2.3** (Figure 5.4.a - Figure 5.4.c), i. e.

5 Preparation of bitumen-[montmorillonite/PEI(nkD)xQyR] composites

adduct particles with diameters up to 50 μm . The presence of the large particles showed that with the used preparation conditions the size and distribution of the adduct particles in the bitumen did not depend on the adduct preparation procedure, i. e. “direct addition” versus “indirect replacement”.

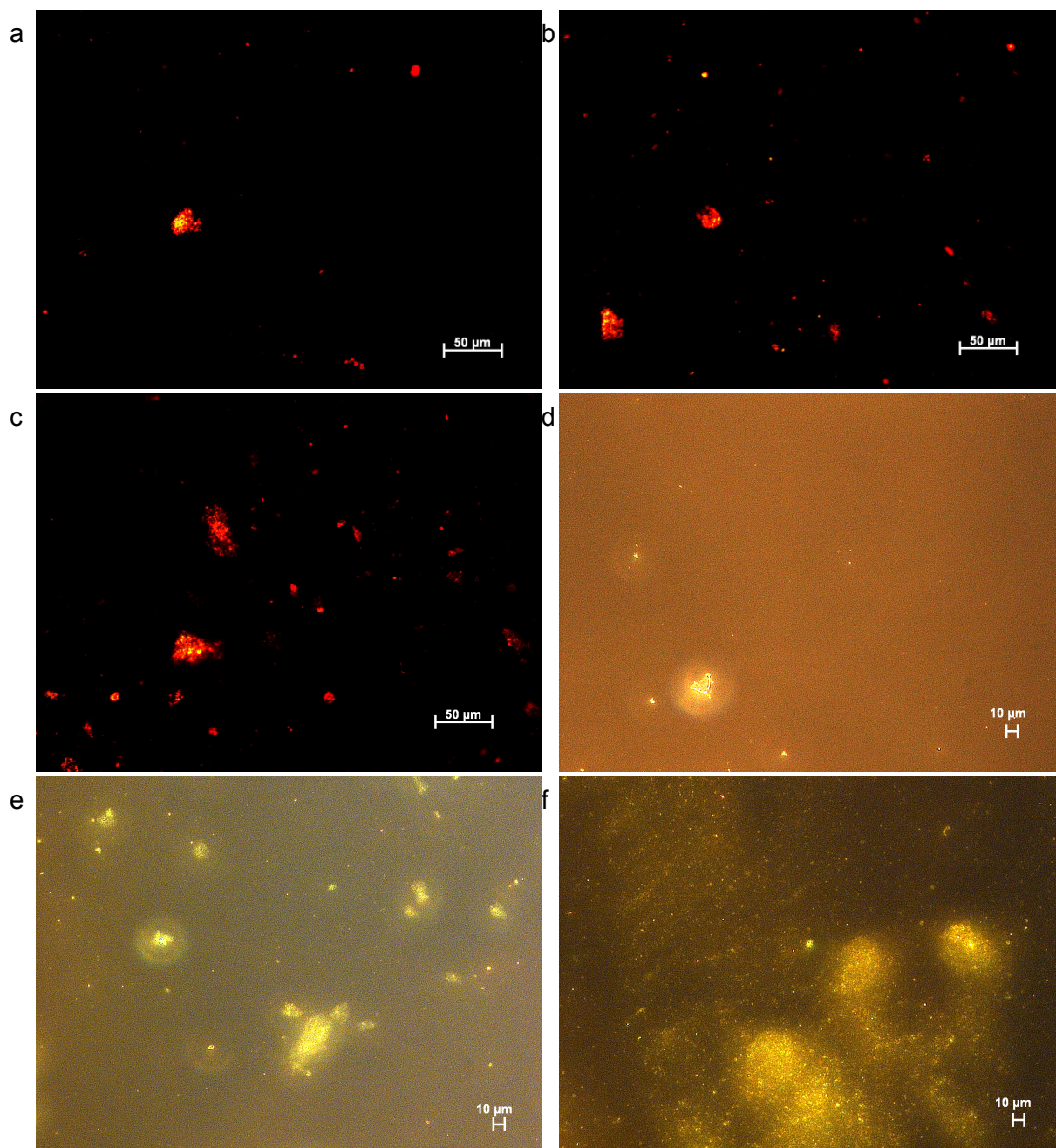


Figure 5.4: Polarized light microscopy pictures of the 70/100 bitumen-**E2** composites a) **C2.1** (1.0 wt.% **E2**), b) **C2.2** (5.0 wt.% **E2**), and c) **C2.3** (10.0 wt.% **E2**), d) Nynas 50/70 bitumen, and the Nynas 50/70-**E7** composites e) **C3.1** (1.0 wt.% **E7**), and f) composite **C3.2** (10.0 wt.% **E7**), **E2** = [MMT_{B1}/PEI(10kD)_{5Q}^{67R10}], **E7** = [MMT_{B1}/PEI(10kD)_{10Q}^{80R10}]

5 Preparation of bitumen-[montmorillonite/PEI(nkD)xQyR] composites

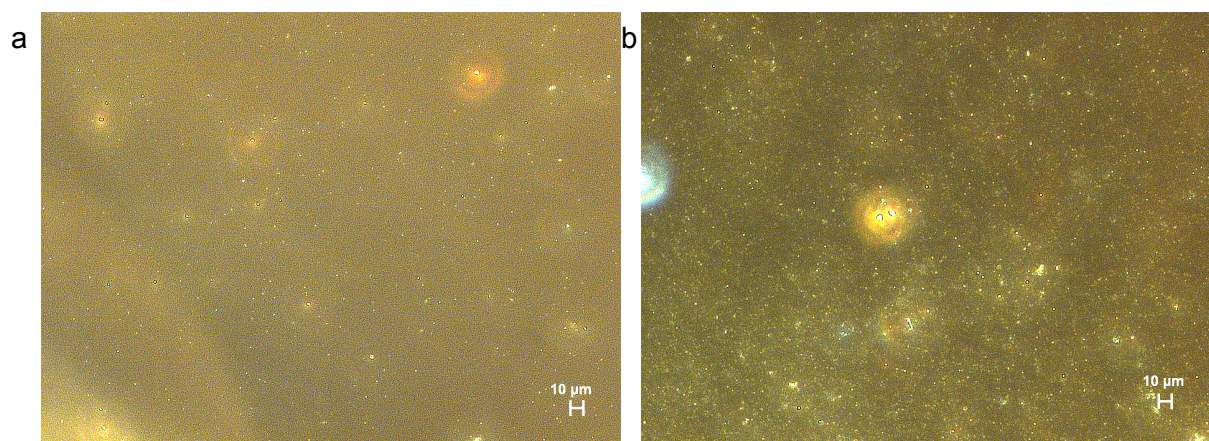


Figure 5.5: Dark field microscopy pictures of the Nynas 50/70-**E8** composites a) **C4.1.2** (5.0 wt.% **E8**), and b) **C4.2.2** (10.0 wt.% **E8**), **E8** = [MMT_{B1}/PEI(10kD)_{10Q}^{80R10}]

In the next step it was tested whether the addition of adducts pre-ground to pieces of 1- 3 cm and a pre-mixing of the pre-ground adducts with the bitumen prior to the extrusion would be sufficient to lower the size of the adducts in the resulting Nynas 50/70-[MMT_{B1}/PEI(10kD)_{10Q}^{80R10}] composites **C4.1** and **C4.2**. While composite **C4.1** was prepared by simply mixing the adduct and the bitumen in the extruder (both components were added separately into the hopper), with composite **C4.2** a pre-mixing step was added in which the adduct was mixed with the bitumen manually before the further mixing of the mixture in the extruder. The adduct concentration was set to be 5.0 wt.% with composite **C4.1**, and to be 10.0 wt.% with composite **C4.2**.

In Figure 5.5, the dark field microscopy pictures of a) composite **C4.1.2**, and c) composite **C4.2.2** are shown. With composite **C4.1.2** (Figure 5.5.b), the number of particles with diameters of 1 – 5 µm increased compared to the non-modified bitumen (cf. Figure 5.4.d) but no particles larger than 20 µm were detected any more in contrast to the composites **C2.1** – **C3.2** (cf. Figure 5.4.a - Figure 5.4.f). A further increase of the number of particles with diameters of 1 – 5 µm was detected with composite **C4.2.2** (Figure 5.5.c) which was in good agreement to the higher adduct concentration in the composite. At the same time, a higher number of particles with diameters of about 10 µm were measured which points to the presence of a higher number of adduct agglomerates in the composite.

In conclusion, it was found that the addition of pre-ground adducts led to smaller particles in the bitumen. Most likely the pre-grinding may have compensated low shear rates due to a slow extrusion rate applied during the preparation of the composites. But as shown by the presence of particles with diameters around 10 µm in composite **C4.2.2** some of the added particles were still too large to be broken down completely during the extrusion. The pre-mixing of the adducts with the bitumen before extrusion led to a composite with a more homogeneous distribution of the adduct

particles in the bitumen.

Since the disintegration step was of importance, subsequently composites will be discussed that were prepared by using adducts that were pre-ground to small pieces of 0.1 – 1 cm in size. The grinding was either performed at 20°C (using [MMT_{B2}/PEI(10kD)_{10Q}^{60R14}]), or under cooling with liquid nitrogen (using [MMT_{B1,B2}/PEI(10kD)_{10Q}^{80R10}]). In all cases the adduct-pieces were manually pre-mixed with the bitumen in the tin can prior to extrusion. Total Azalt was used as the bitumen matrix, the adduct concentrations of the respective composites **C10.1** – **C10.5** were 1.0 wt.% (**C10.1**), 2.5 wt.% (**C10.2**), 5.0 (**C10.3**), 7.5 (**C10.4**), and 10.0 wt.% (**C10.5**) of the [MMT_{B1}/PEI(10kD)_{10Q}^{80R10}] adduct **E10**.

Figure 5.6 shows the dark field microscopy pictures of a) Total Azalt 50/70 bitumen, b) composite **C10.1**, c) composite **C10.2**, d) composite **C10.3**, e) composite **C10.4**, and f) composite **C10.5**. The picture of the non-modified Total Azalt 50/70 bitumen (Figure 5.6.a) showed a large number of particles with diameters between 1 and 10 µm. Most of the particles exhibited a diameter of about 1 µm. Compared to the neat Total Azalt 50/70 bitumen, the composites **C10.1** – **C10.5** exhibited a higher number of particles with diameters ranging from 1 – 10 µm with most of the particles exhibited diameters in the region of 1 µm. While with an adduct concentration of 1.0 wt.% (**C10.1**, Figure 5.6.b) and 2.5 wt.% (**C10.2**, Figure 5.6.c) the adduct particles appeared as single particles.

Starting with an adduct concentration of 5.0 wt.% (**C10.3**, Figure 5.6.d) the background became brighter, indicating the presence of numerous light-scattering particles with lateral distances below $\lambda/2$. Hence, the adducts seemed to form a superstructure across the bitumen which became more distinct with increasing adduct concentration as shown in the pictures of the adducts **C10.4** (Figure 5.6.e) and **C10.5** (Figure 5.6.f). Comparing the composites **C4.1.2** (Figure 5.5.b) and **C10.3** (Figure 5.6.d), and the composites **C4.2.2** (Figure 5.5.c) and **C10.5** (Figure 5.6.f) it was found that the composites **C10.3** and **C10.5** exhibited a more homogeneous distribution of the adduct particles in the bitumen matrices. Although the diameters of the adduct particles of the four composites were similar, no superstructure was detected with the composites **C4.1.2** and **C4.2.2**. In conclusion, using adducts that were pre-ground under liquid nitrogen to 0.1 – 1 cm led to a more homogeneous distribution and to smaller adduct particles in the bitumen.

5 Preparation of bitumen-[montmorillonite/PEI(nkD)xQyR] composites

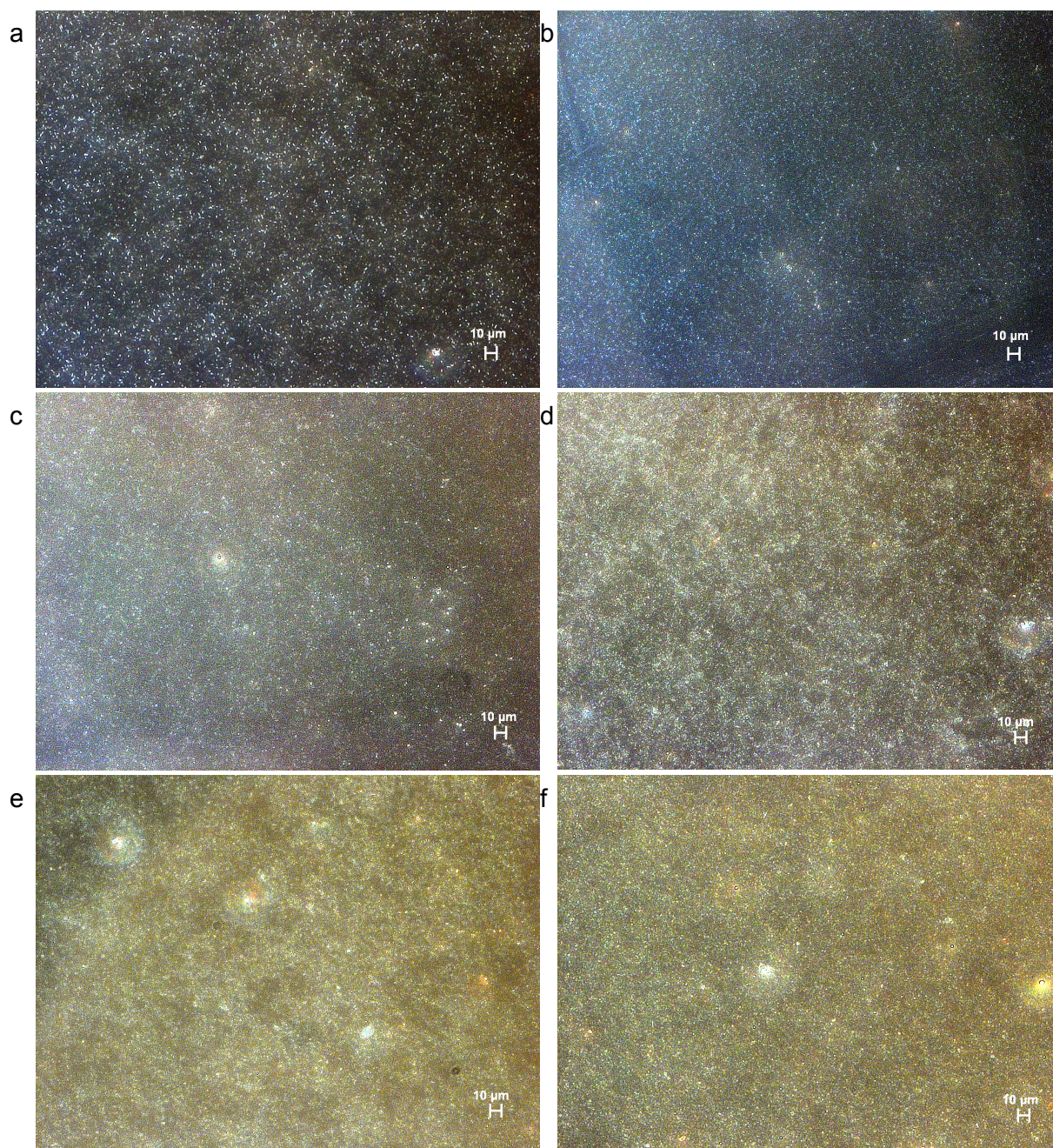


Figure 5.6: Dark field microscopy pictures of a) Total Azalt 50/70 bitumen, and the Total Azalt 50/70-**E10** composites b) **C10.1** (1.0 wt.% **E10**), c) **C10.2** (2.5 wt.% **E10**), d) **C10.3** (5.0 wt.% **E10**), e) **C10.4** (7.5 wt.% **E10**), and f) **C10.5** (10.0 wt.% **E10**), **E10** = [MMT-B₁/PEI(10kD)_{10Q}^{80R10}]

Composite **C9** was prepared to investigate whether an adduct prepared with a higher mass/solvent ratio (= adduct **E9**, cf. Chapter 4) would lead to a composite with a similar distribution and size of the adduct particles in bitumen as composites prepared with an adduct prepared from a lower mass/solvent ratio (= adduct **E10**, composites

C10.1 – C10.5). With composite **C9**, the adduct concentration was set to be 4.9 wt.%. In Figure 5.7 the dark field microscopy pictures of a) Total Azalt 50/70 bitumen and b) composite **C9** are compared. Composite **C9** (Figure 5.7.b) contained adduct particles with diameters in the region of 1 – 10 μm with most of the particles exhibiting diameters around 1 μm . Compared to composite **C10.3** (Figure 5.6.d) it was found that both composites exhibited similar particle sizes and particle distributions. In addition, from the bright background it must be concluded that the adduct of composite **C9** was also able to form a superstructure across the bitumen.

In conclusion the data demonstrate no significant dependency of the composites morphology on the mass/solvent ratio used to generate adducts via the “indirect replacement” method. As long as sufficient pre-grinding, and mixing takes place homogeneous composites containing highly exfoliated adduct particles can be made also from adducts prepared under “high concentration” conditions.

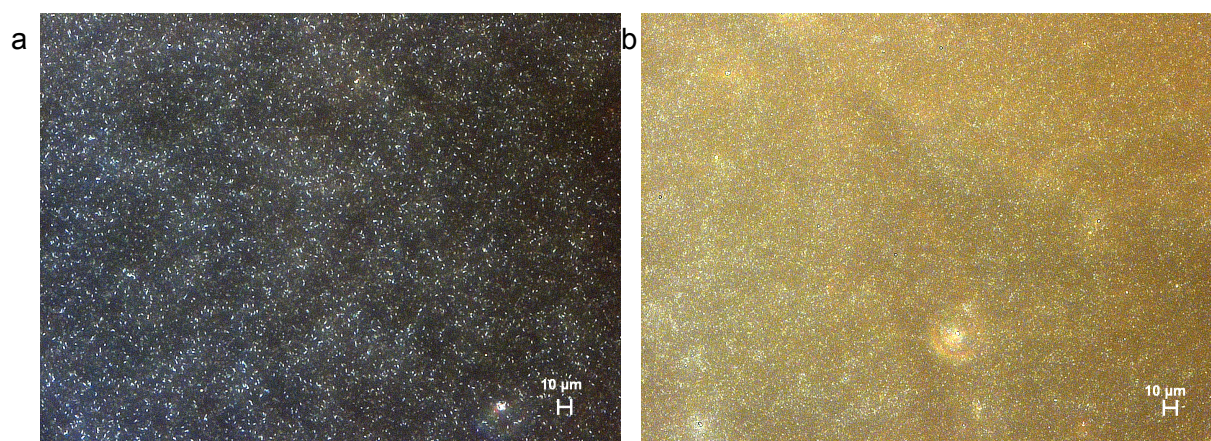


Figure 5.7: Dark field microscopy pictures of a) Total Azalt 50/70 bitumen and b) the Total Azalt 50/70-**E9** composite **C9** (4.9 wt.% **E9**), **E9** = $[\text{MMT}_{\text{B2}}/\text{PEI}(10\text{kD})_{10\text{Q}}^{80\text{R}10}]$

To investigate the influence of the polymer shell surrounding the MMT, five Total Azalt 50/70- $[\text{MMT}_{\text{B2}}/\text{PEI}(10\text{kD})_{10\text{Q}}^{60\text{R}14}]$ composites (**C12.1 – C12.5**) were prepared, and compared to the Total Azalt 50/70- $[\text{MMT}_{\text{B1,B2}}/\text{PEI}(10\text{kD})_{10\text{Q}}^{80\text{R}10}]$ composites **C9** (Figure 5.7.b) and **C10.1 – C10.5** (Figure 5.6.b - Figure 5.6.f). The adduct concentration was set to be 1.0 wt.% with composite **C12.1**, 5.0 wt.% with composite **C12.2**, 10.0 wt.% with composite **C12.3**, 20.2 wt.% with composite **C12.4**, and 30.0 wt.% with composite **C12.5**. The high adduct concentrations of 20.2 and 30.0 wt.% were chosen with the aim to determine if agglomeration of the adduct particles occurred at elevated adduct volume fractions.

Figure 5.8 compares the dark field microscopy pictures of a) Total Azalt 50/70 bitumen, b) composite **C12.1**, c) composite **C12.2.1**, d) composite **C12.3.1**, e) composite **C12.4**, and f) composite **C12.5**. Composite **C12.1** (Figure 5.8.b) exhibited a high

number of homogeneously distributed particles with diameters between 1 and 5 μm with most of the particles showing a diameter around 1 μm .

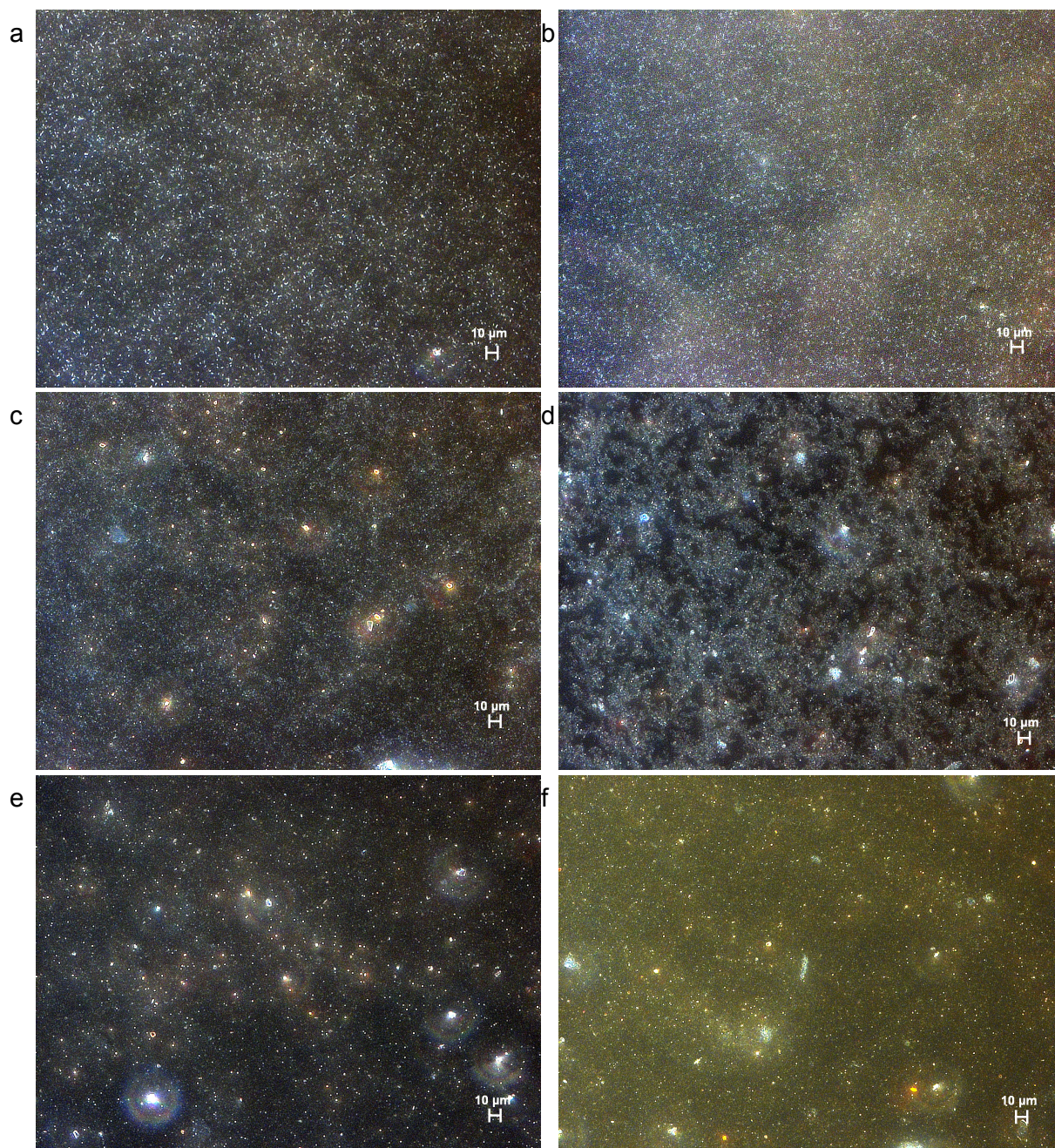


Figure 5.8: Dark field microscopy pictures of a) Total Azalt 50/70 bitumen, and the Total Azalt 50/70-**E15** composites b) **C12.1** (1.0 wt.% **E15**), c) **C12.2.1** (5.0 wt.% **E15**), d) **C12.3.1** (10.0 wt.% **E15**), e) **C12.4** (20.2 wt.% **E15**), and f) **C12.5** (30.0 wt.% **E15**), **E15** = [MMT-_{B2}/PEI(10kD)_{10Q}^{60R14}]

The pictures of the composites **C12.2.1** (Figure 5.8.c) and **C12.3.1** (Figure 5.8.d)

showed beside a high number of particles with diameters around 1 μm also agglomerates with a diameter of about 10 μm . At the same time, the adducts formed a superstructure in the bitumen which became more distinct with increasing concentration as shown in the picture of composite **C12.3.1**.

With the composites **C12.4** (Figure 5.8.e) and **C12.5** (Figure 5.8.f), a high number of adduct agglomerates with diameters of about 10 μm were detected. Hence, with adduct concentrations of 1.0 – 10.0 wt.% small adduct particles were found forming a superstructure in the bitumen on exceeding about 5.0 wt.%. With adduct concentrations above 20 wt.% the presence of a high number of adduct agglomerates was detected. Comparing the morphology of composites made from [MMT_{B1}/PEI(10kD)_{10Q}^{80R10}] (**C10.1**, cf. Figure 5.6.b), and [MMT_{B2}/PEI(10kD)_{10Q}^{60R14}] (**C12.1**, cf. Figure 5.8.b) adducts, no significant difference in particle size, and -distribution was detected at an adduct concentration of 1.0 wt.%. However, at larger adduct concentrations the pictures demonstrate PEI(10kD)_{10Q}^{80R10} coatings to be superior to PEI(10kD)_{10Q}^{60R14} layers, because the respective composites **C9** and **C10** (Figure 5.6.d - Figure 5.6.f and Figure 5.7.b) contained less, and smaller particulate structures than the **C12** compounds (see Figure 5.8.c and Figure 5.8.d).

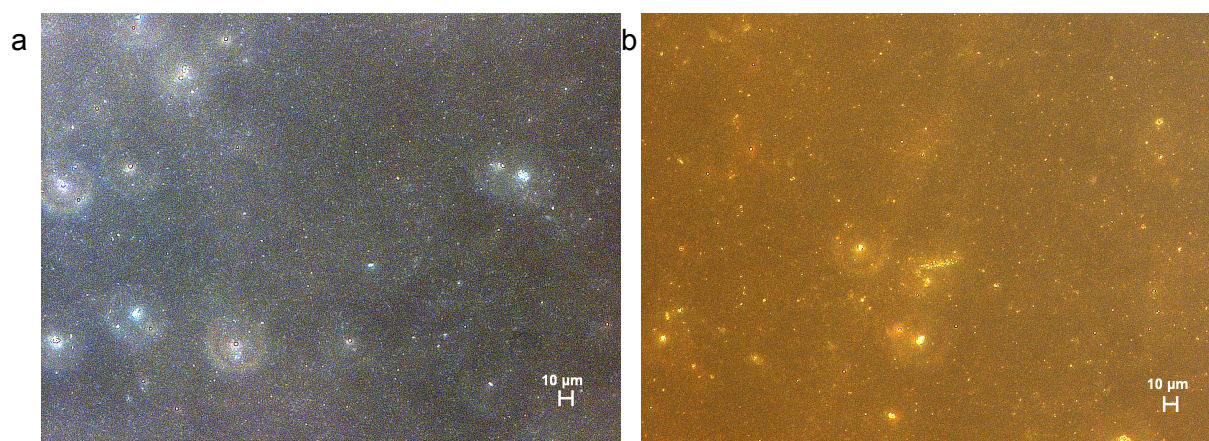


Figure 5.9: Dark field microscopy pictures of the Total Azalt 50/70-**E4** composites a) **C1.1** (5.2 wt.% **E4**) and b) **C1.2** (9.9 wt.% **E4**), **E4** = [MMT_{B1}/CTAB]

In comparison to the Total Azalt 50/70-[MMT_{B1}/PEI(10kD)_{10Q}^{80R10}] composites **C10.1** – **C10.5** (Figure 5.6.b - Figure 5.6.f) and the Total Azalt 50/70-[MMT_{B2}/PEI(10kD)_{10Q}^{60R14}] composites **C12.1** to **C12.5** (Figure 5.11.b - Figure 5.11.f) the dark field microscopy pictures of two Total Azalt 50/70-[MMT_{B1}/CTAB] composites with adduct concentrations of 5.2 wt.% (**C1.1**) and 9.9 wt.% (**C1.2**) were evaluated. Figure 5.9 shows the dark field microscopy pictures of a) composite **C1.1** and b) composite **C1.2**. With both composites, the number of particles with diameters around 10 μm was higher than in the non-modified bitumen (Figure 5.8.a) which lead to the conclusion that the

5 Preparation of bitumen-[montmorillonite/PEI(nkD)xQyR] composites

adducts formed agglomerates in the bitumen. Furthermore, the adduct didn't form a superstructure in the bitumen which indicates that the $[\text{MMT}_{\text{B1}}/\text{CTAB}]$ adduct was inferior to the $[\text{MMT}_{\text{B1,B2}}/\text{PEI}(10\text{kD})_{10\text{Q}}^{60\text{R}10}]$ and the $[\text{MMT}_{\text{B2}}/\text{PEI}(10\text{kD})_{10\text{Q}}^{60\text{R}14}]$ adducts.

To investigate if the origin, i. e., the manufacturer of the bitumen matrix is of influence on the bitumen morphology, 10.0 wt.% of adduct **E15** ($= [\text{MMT}_{\text{B2}}/\text{PEI}(10\text{kD})_{10\text{Q}}^{60\text{R}14}]$) were compounded with Nynas 50/70 bitumen to yield composite **C11.3**. Its morphology was compared to that of the analogous Total Azalt 50/70-bitumen based composite **C12.3**. In Figure 5.10 the dark field microscopy pictures of a) Nynas 50/70 bitumen and b) composite **C11.3** are shown. Composite **C11.3** (Figure 5.10.b) contained particles with diameters of about 1, 5, and 10 μm which were homogeneously distributed in the bitumen matrix. While the size and distribution of the particles of composite **C11.3** was similar to that of composite **C12.3.1** (Figure 5.11.d), no adduct superstructure was detected with composite **C11.3** which points to larger particles in composite **C11.3** and therefore to a lower compatibility of the $[\text{MMT}_{\text{B2}}/\text{PEI}(10\text{kD})_{10\text{Q}}^{60\text{R}14}]$ adduct **E15** with the Nynas 50/70 bitumen.

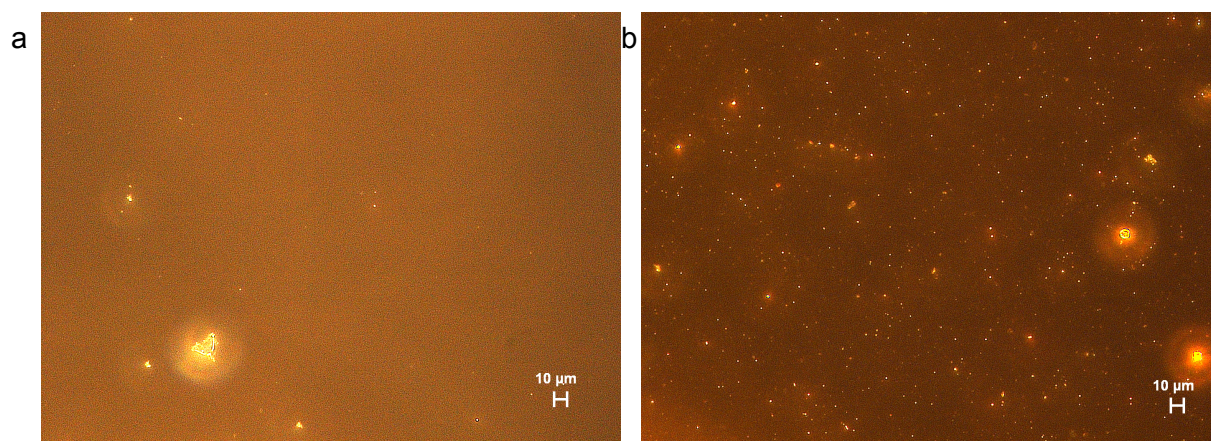


Figure 5.10: Dark field microscopy pictures of a) Nynas 50/70 bitumen and b) the Nynas 50/70-**E15** composite **C11.3** (10.0 wt.% **E15**), **E15** = $[\text{MMT}_{\text{B2}}/\text{PEI}(10\text{kD})_{10\text{Q}}^{60\text{R}14}]$

To determine the influence of the rotational speed of the extruder screw and the extrusion temperature on the size and distribution of $[\text{MMT}_{\text{B2}}/\text{PEI}(10\text{kD})_{10\text{Q}}^{60\text{R}14}]$ adduct particles in the composites, four Shell 30/45- $[\text{MMT}_{\text{B2}}/\text{PEI}(10\text{kD})_{10\text{Q}}^{60\text{R}14}]$ composites (**C13.1** – **C13.4**) were prepared. For comparison the parameters of composite **C13.1** were chosen to be identical to those of composite **C5.1**. With composite **C13.2**, the rotational speed of the extruder screw was raised to 130 min^{-1} . The extrusion temperature was the same as with composite **C13.1**. With composite **C13.3**, the extrusion temperature was raised to 120°C . The rotational speed of the screw was set to be 130 min^{-1} . Composite **C13.4** was prepared with an extrusion temperature of 160°C

and a rotational speed of the screw of 130 min^{-1} . The adduct concentration was set to be 10 wt.% with all four composites. Figure 5.11 shows the dark field microscopy pictures of a) Shell 30/45 bitumen, b) composite **C13.1**, c) composite **C13.2**, d) composite **C13.3.1**, and e) composite **C13.4**.

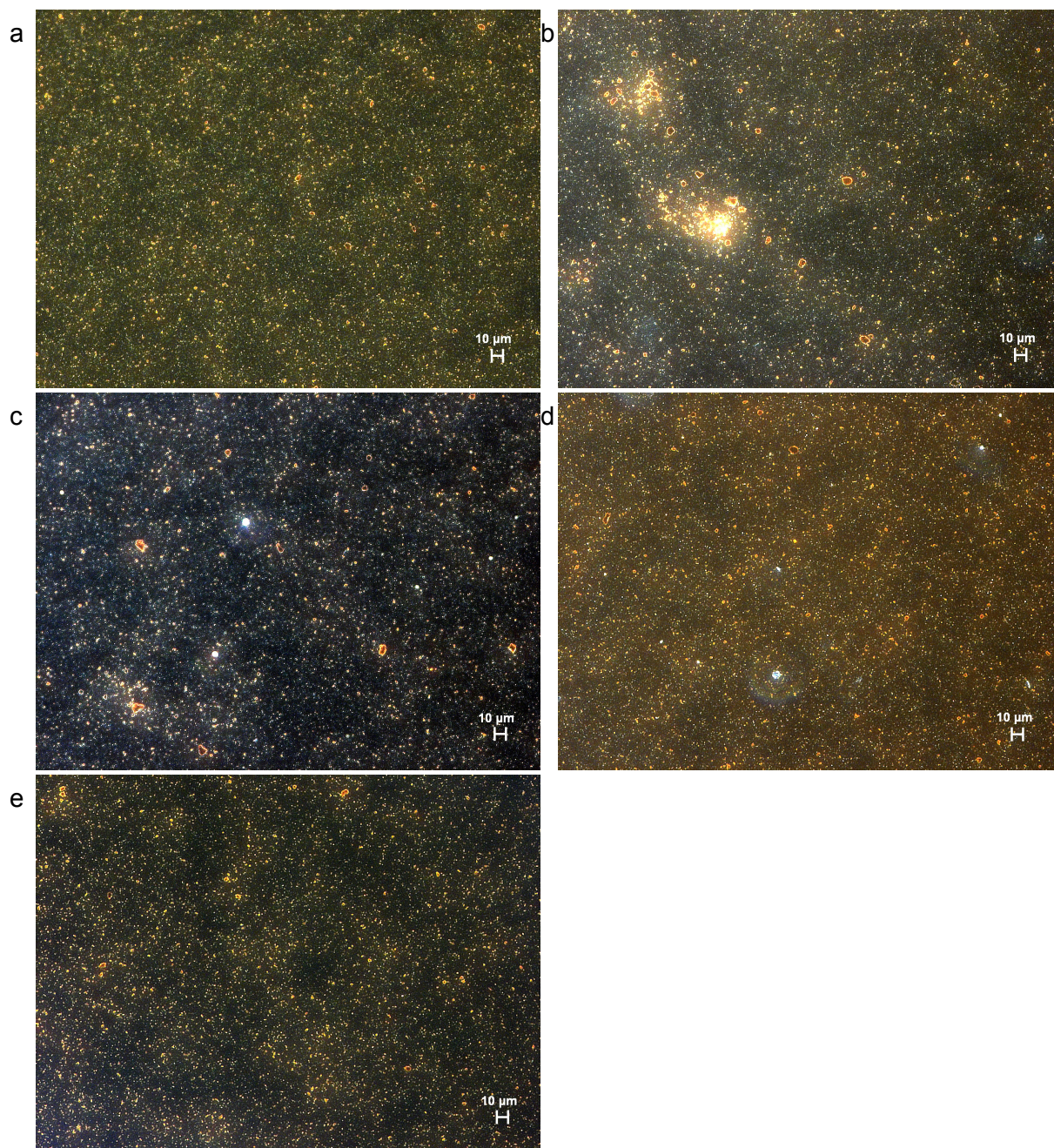


Figure 5.11: Dark field microscopy pictures of a) Shell 30/45 bitumen, and the Shell 30/45-**E15** composites b) **C13.1** (10.0 wt.% **E15**, 50 min^{-1} , 70°C), c) **C13.2** (10.0 wt.% **E15**, 130 min^{-1} , 70°C), d) **C13.3.1** (10.0 wt.% **E15**, 130 min^{-1} , 120°C), and e) composite **C13.4** (10.0 wt.% **E15**, 130 min^{-1} , 160°C), **E15** = $[\text{MMT}_{\text{B2}}/\text{PEI}(10\text{kD})_{10\text{Q}}^{60\text{R}14}]$

The Shell 30/45 bitumen (Figure 5.11.a) contained a high number of particles with diameters between 1 and 10 μm which were homogeneous distributed across the bitumen. While with composite **C13.1** (Figure 5.11.b) the adduct particles were inhomogeneously distributed and formed agglomerates with diameters up to 20 μm , the distribution became more homogeneous with the composites **C13.2** – **C13.4** (Figure 5.11.c - Figure 5.11.e). Furthermore, the size of the particles decreased to diameters of 1 – 10 μm which were similar to those of the non-modified bitumen.

To summarise the results, the extrusion temperature and the rotational speed of the extruder screw strongly influenced the size and distribution of the adduct particles in the bitumen. While with a rotational speed of the extruder screw of 50 min^{-1} and an extrusion temperature of 70°C particles with diameters up to 20 μm were detected, the increase of the extrusion temperature and the rotational speed of the extruder screw lowered the size of the particles to 1- 10 μm . The lower size of the particle shows that larger adduct agglomerates were broken down by the higher shear force at higher shear rates.

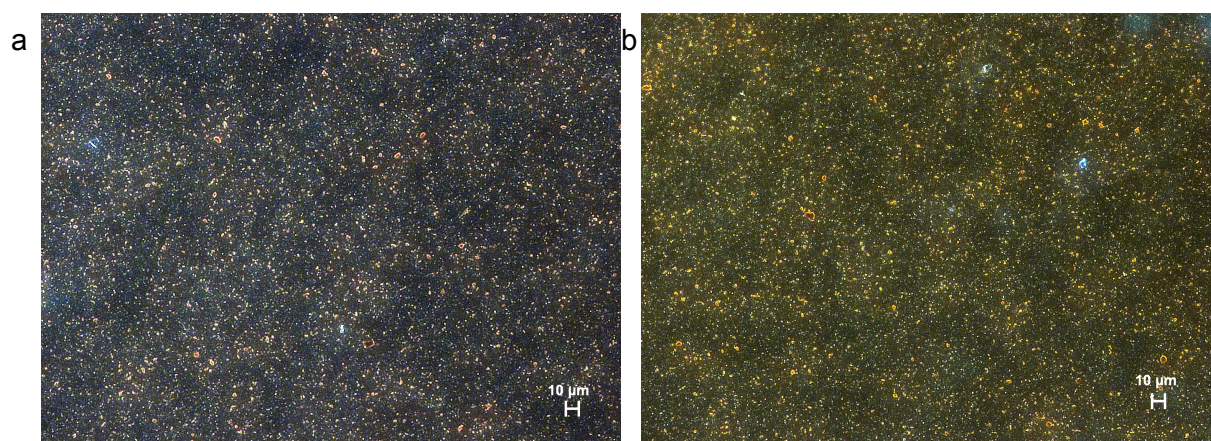


Figure 5.12: Dark field microscopy pictures of the Shell 30/45-**E8** composites a) **C5.1.3** (5.0 wt.% **E8**) and b) **C5.2.1** (10.0 wt.% **E8**), **E8** = $[\text{MMT}_{\text{B1}}/\text{PEI}(10\text{kD})_{10\text{Q}}^{80\text{R}10}]$

With the extrusion parameters of the Shell 30/45- $[\text{MMT}_{\text{B2}}/\text{PEI}(10\text{kD})_{10\text{Q}}^{60\text{R}14}]$ composite **C13.1** (Figure 5.11.b) two Shell 30/45- $[\text{MMT}_{\text{B1}}/\text{PEI}(10\text{kD})_{10\text{Q}}^{80\text{R}10}]$ composites (**C5.1** and **C5.2**) were prepared for comparison purposes. The adduct concentration was set to be 5.0 wt.% with composite **C5.1** and 10.0 wt.% with composite **C5.2**. In Figure 5.12 the dark field microscopy pictures of a) composite **C5.1.3** and b) composite **C5.2.1** are compared. With both composites, adduct particles with diameters in the region of 1 – 10 μm were detected but no adduct agglomerates as with composite **C13.1**. It was therefore concluded that with the used preparation conditions the $[\text{MMT}_{\text{B1}}/\text{PEI}(10\text{kD})_{10\text{Q}}^{80\text{R}10}]$ adduct was more compatible with the Shell 30/45 bitumen than $[\text{MMT}_{\text{B2}}/\text{PEI}(10\text{kD})_{10\text{Q}}^{60\text{R}14}]$ adduct.

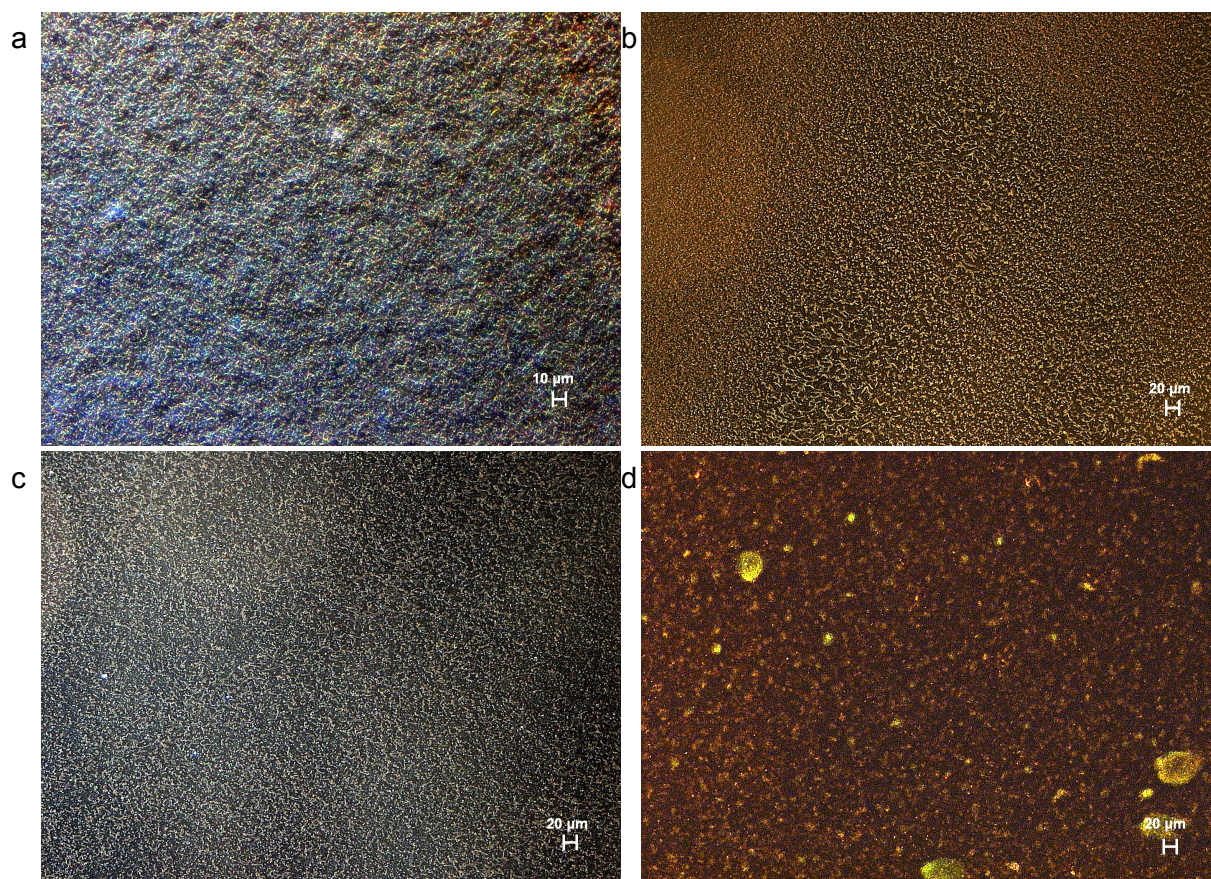


Figure 5.13: Dark field microscopy pictures of a) BP Olexobit 45 bitumen, and the BP Olexobit 45-**E8** composites b) **C6.1.1** (5.0 wt.% **E8**) and c) **C6.2.3** (10.0 wt.% **E8**), and d) the BP Olexobit 45-**E15** composite **C14.2** (10.0 wt.% **E15**), **E8** = $[\text{MMT}_{\text{B1}}/\text{PEI}(10\text{kD})_{10\text{Q}}^{80\text{R}10}]$, **E15** = $[\text{MMT}_{\text{B2}}/\text{PEI}(10\text{kD})_{10\text{Q}}^{60\text{R}14}]$

Polymer modified bitumina (= PmBs) differ in many respects from non-modified bitumina (cf. Chapter 2). The two PmBs Olexobit 45 and Cariphalte 25/55-55 were hence used as composite matrices to investigate the effect of mixed-in polymers on composite formation and morphology. In a first series of experiments, three composites based on BP Olexobit 45 have been prepared. The composites **C6.1**, and **C6.2** contained 5.0 wt.%, and 10.0 wt.% of adduct **E8** (= $[\text{MMT}_{\text{B1}}/\text{PEI}(10\text{kD})_{10\text{Q}}^{80\text{R}10}]$), while compound **C14** was made with 10.0 wt.% of the $\text{PEI}(10\text{kD})_{10\text{Q}}^{60\text{R}14}$ coated adduct **E15** (= $[\text{MMT}_{\text{B2}}/\text{PEI}(10\text{kD})_{10\text{Q}}^{60\text{R}14}]$). The three composites were prepared using adducts pre-ground to 0.1 – 1 cm pieces. Before extrusion, the adducts were added to the bitumen melt in the tin cans and pre-mixed manually. The extrusion temperature was set to be 70°C and the rotation speed of the extruder screw to be 50 min⁻¹.

Figure 5.13 compares the dark field microscopy pictures of a) BP Olexobit 45 bitumen, b) composite **C6.1.1**, c) composite **C6.2.3**, and d) composite **C14.2**. The BP Olexobit 45 bitumen (Figure 5.13.a) formed inside a phase-segregation a superstruc-

ture with a characteristic length-scale of ca. 20 μm across the bitumen. The superstructure could be attributed to a polymer network which was observed in styrene-butadiene-styrene (SBS) and ethylenevinylacetate (EVA) modified bitumen in previous studies [13, 12]. With the composites **C6.1.1** (Figure 5.13.b) and **C6.2.3** (Figure 5.13.c), the polymer network was partially fragmented which indicates an interaction between the polymer and the adduct particles. The size of the adduct particles was measured with both composites to be in the region of 1 – 10 μm . Compared to the composites **C6.1.1** and **C6.2.3** composite **C14.2** (Figure 5.13.d) showed a higher number of particles with diameters around 10 μm . At the same time, the polymer network was strongly fragmented and the polymers seemed to form micelles with diameters up to 50 μm which were similar to those observed in ethylene vinyl acetate modified bitumen [12].

In a second series of PmB-experiments Shell Cariphalte 25/55-55 was used as the composites matrix. Three composites (**C7.1**, **C7.2**, and **C15**) were prepared in a similar way as the Olexobit composites **C6.1**, **C6.2**, and **C14**. While **C7.1** and **C7.2** contained 5.0 wt.% (**C7.1**) and 10.0 wt.% (**C7.2**) of adduct **E8** (= [MMT_{B1}/PEI(10kD)_{10Q}^{80R10}]), **C15** contained 10.0 wt.% of the [MMT_{B2}/PEI(10kD)_{10Q}^{60R14}] adduct **E15**.

In Figure 5.14 the dark field microscopy pictures of a) Shell Cariphalte 25/55-55 bitumen, b) composite **C7.1.3**, c) composite **C7.2.1**, and d) composite **C15.3** are shown. As with the BP Olexobit 45 bitumen (Figure 5.13.a) the Shell Cariphalte 25/55-55 bitumen (Figure 5.14.a) contained also a polymer network. With the composites **C7.1.3** (Figure 5.14.b), **C7.2.1** (Figure 5.14.c), and **C15.3** (Figure 5.14.d), particles with diameters between 1 and 10 μm were measured. Furthermore, although the original polymer network was fragmented by the adducts the adduct particles interacted with each other and formed a network in the bitumen. The base bitumen consisted of polymer-rich and polymer-poor phases which were non-uniform distributed across the bitumen. Because of this, it was not clear whether the detected adduct network could only be measured in polymer-poor phases but also in polymer-rich phases. In conclusion, both adduct types were not compatible with the bitumen and induced the fragmentation of the polymer network of the base bitumen.

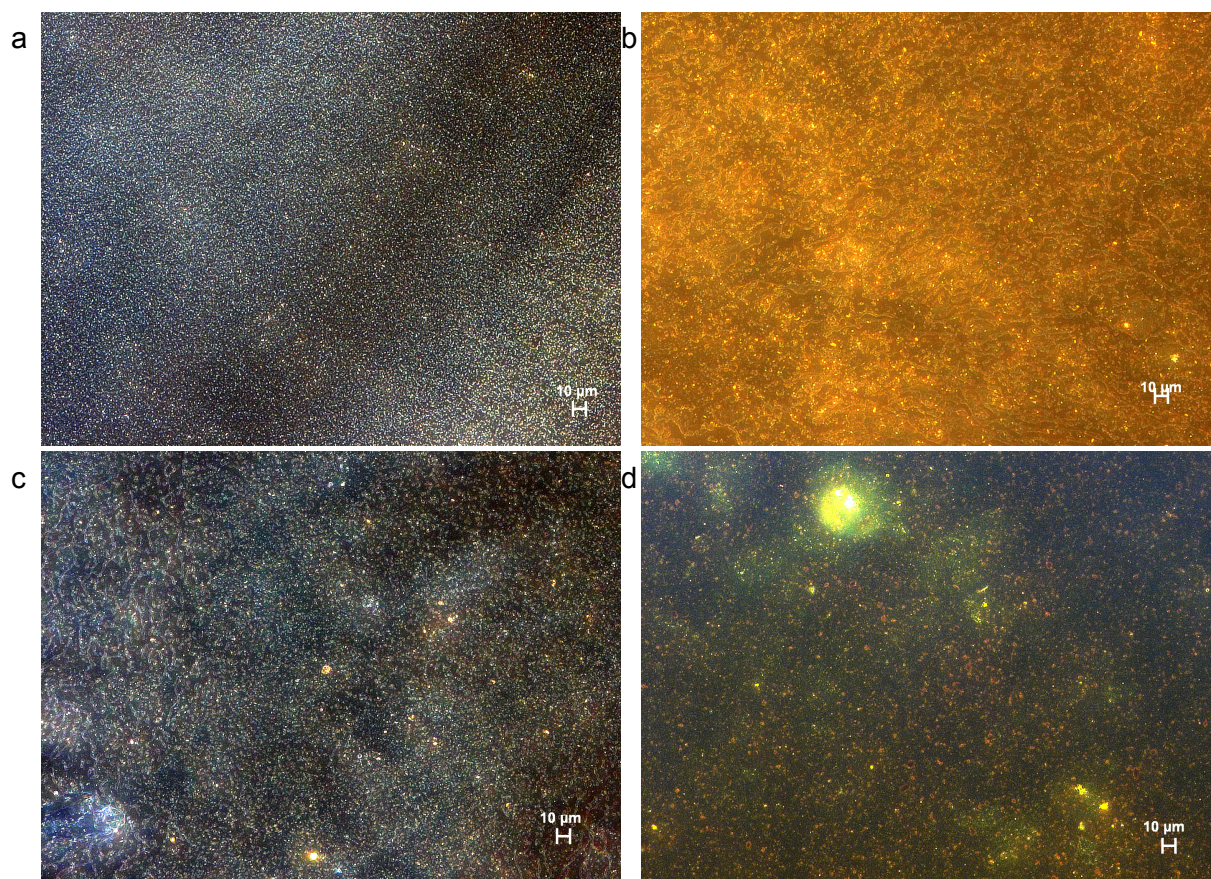


Figure 5.14: Dark field microscopy pictures of a) Shell Cariphalte 25/55-55 bitumen, and the Shell Cariphalte 25/55-55-**E8** composites b) **C7.1.3** (5.0 wt.% **E8**) and c) composite **C7.2.1** (10.0 wt.% **E8**), and d) the Shell Cariphalte 25/55-55-**E15** composite **C15.3** (10.0 wt.% **E15**), **E8** = [MMT_{B1}/PEI(10kD)_{10Q}^{80R10}], **E15** = [MMT_{B2}/PEI(10kD)_{10Q}^{60R14}]

Discussion

In this study organic modified montmorillonite was mixed with bitumen to create bitumen-nanocomposites. The investigated adducts consisted of montmorillonite modified with (i) CTAB (= [MMT/CTAB]), (ii) [MMT_{B1}/PEI(10kD)_{5Q}^{67R10}] prepared by the “direct addition” method, (iii) [MMT_{B1,B2}/PEI(10kD)_{10Q}^{80R10}] and (iv) [MMT_{B2}/PEI(10kD)_{10Q}^{60R14}], the latter types prepared by the “indirect replacement” method. Each composite was prepared with a set of specific parameters to investigate the influence of the used bitumen, the adduct composition, the preparation method of the adduct, the applied compounding procedure, and the weight concentration of the adduct in the bitumen on the size and distribution of the adduct particles in the composites.

To test the influence of the adducts preparation method, composites containing an

[MMT_{B1}/PEI(10kD)_{5Q}^{67R10}] adduct prepared by the “direct addition” method were compared to composites containing an [MMT_{B1}/PEI(10kD)_{10Q}^{80R10}] adduct prepared by the “indirect replacement” method. The comparison of the polarised light microscopy pictures of 70/100-[MMT_{B1}/PEI(10kD)_{5Q}^{67R10}] composites with adduct concentrations of 1.0 wt.% (**C2.1**), 5.0 wt.% (**C2.2**), and 10.0 wt.% (**C2.3**) with the dark field microscopy pictures of Nynas 50/70-[MMT_{B1}/PEI(10kD)_{10Q}^{80R10}] composites containing adduct concentrations of 1.0 wt.% (**C3.1**) and 10.0 wt.% (**C3.2**) revealed that the used compounding conditions resulted in adduct particles of similar size and distribution in the bitumen. Although this result implied that the adduct preparation method was of little influence, the compounding procedure was definitely not optimised.

To optimise the compounding procedure composites containing [MMT_{B1}/PEI(10kD)_{10Q}^{80R10}] adducts pre-ground either at 20°C to pieces of 1 - 3 cm or under liquid nitrogen to 0.1 – 1 cm, and composites containing [MMT_{B2}/PEI(10kD)_{10Q}^{60R14}] adducts pre-ground at 20°C to pieces of 0.1 – 1 cm were evaluated. In addition, the effect of the pre-mixing of the adducts with the bitumen before extrusion was evaluated. It was found that Nynas-[MMT_{B1}/PEI(10kD)_{10Q}^{80R10}] composites containing 5.0 wt.% (**C4.1**) and 10.0 wt.% (**C4.2**) of an adduct pre-ground at 20°C to 1 - 3 cm exhibited a high number of particles with diameters of 1 – 5 µm, but also particles with diameters around 10 µm. While the addition of pre-ground adducts led to smaller particles in the bitumen compared to composites containing non-pre-ground adducts the presence of particles with diameters around 10 µm showed that during the extrusion not all adduct agglomerates were broken down. The pre-mixing of the adducts with the bitumen before extrusion led to a more homogeneous distribution of the adduct particles in the bitumen.

To determine the influence of the extrusion temperature and the shear rate, Shell-30/45-[MMT_{B2}/PEI(10kD)_{10Q}^{60R14}] composites (**C13.1** - **C13.4**) with a combination of a specific extrusion temperature and a specific rotational speed of the extruder screw with each composite were prepared. While at 70°C and 50 min⁻¹ adduct particles with diameters up to 20 µm were observed, the diameters decreased to values between 1 and 10 µm after the rotational speed of the extruder screw was raised to 130 min⁻¹ at temperatures in the region of 70 - 160°C. Higher extrusion rates are, therefore, able to break down larger adduct agglomerates.

The optimised preparation method of a bitumen nanocomposite hence involves three subsequent steps:

- 1) grind the adduct to a fine powder,
- 2) disperse the adduct-powder in molten bitumen to a macroscopically homogeneous

state,

3) break up aggregates, and form a microhomogeneous dispersion by means of a single extrusion step at 70 - 160°C and 130 min⁻¹.

The effect of the MMTs organic coatings on the composites morphology was investigated with [MMT_{B1}/CTAB], [MMT_{B1,B2}/PEI(10kD)_{10Q}^{80R10}] and [MMT_{B2}/PEI(10kD)_{10Q}^{60R14}] adducts. Composites, prepared under use of the optimised preparation technique were evaluated and contained, when [MMT_{B1,B2}/PEI(10kD)_{10Q}^{80R10}] or [MMT_{B2}/PEI(10kD)_{10Q}^{60R14}] adducts were used (composites **C9**, **C10.1** – **C10.5**, and **C12.1** – **C12.5**), small particles with diameters in the range of 1 – 10 µm when the adduct concentration was set to be in the region of 1.0 – 30.0 wt.%. In addition, most of the particles exhibited diameters around 1 µm and the adducts formed a superstructure across the bitumen with adduct concentrations above 5 wt.%. The direct comparison of composites containing 5 and 10 wt.% of the respective adduct showed that composites containing an [MMT_{B2}/PEI(10kD)_{10Q}^{60R14}] adduct exhibited a higher number of particles with diameters around 10 µm which points to that this adduct type was less compatible with the bitumen. Although Total Azalt 50/70-[MMT_{B1}/CTAB] composites (**C1.1** and **C1.2**) contained also a high number of particles with diameters between 1 and 10 µm, the number of particles with diameters around 10 µm was higher than with Total Azalt 50/70-[MMT_{B1}/PEI(10kD)_{10Q}^{80R10}] and Total Azalt 50/70-[MMT_{B2}/PEI(10kD)_{10Q}^{60R14}] composites which shows that the [MMT_{B1}/CTAB] adduct was inferior to the other two adduct types.

The comparison of the morphology of a Total Azalt 50/70-[MMT_{B2}/PEI(10kD)_{10Q}^{60R14}] composite (**C12.3**) with that of a Nynas 50/70-[MMT_{B2}/PEI(10kD)_{10Q}^{60R14}] compound (**C11.3**) showed that the adduct formed a superstructure with the Total Azalt 50/70 based composite only which shows that although both bitumina had a pen-grade of 50/70 the different origin of the bitumen influenced the compatibility of the adduct with the bitumen. Furthermore, while the [MMT_{B1,B2}/PEI(10kD)_{10Q}^{80R10}] and the [MMT_{B2}/PEI(10kD)_{10Q}^{60R14}] adducts were generally well compatible with the non-polymer-modified bitumen Nynas 50/70, Total Azalt 50/70, and Shell 30/45, the addition of these adducts to the polymer-modified bitumen BP Olexobit 45 and Shell Cariphalte 25/55-55 led to composites with phase segregated structures which show that both adduct types were not compatible with the polymers used to modify the bitumen.

Summary

In this investigation polymer- and non-polymer-modified bitumen were mixed with organically modified montmorillonite to create bitumen-nanocomposites. It was found that composites containing a non-pre-ground [MMT_{B1}/PEI(10kD)_{5Q}^{67R10}] adduct prepared by the “direct addition” method exhibited adduct particles with diameters of 1 – 50 μm which were similar to the size of the particles detected with composites containing a non-pre-ground [MMT_{B1}/PEI(10kD)_{10Q}^{80R10}] adduct prepared by the “indirect replacement” method and shows that the extrusion rate was too low to break down larger adduct particles. Modification of non-polymer-modified bitumen with [MMT_{B1,B2}/PEI(10kD)_{10Q}^{80R10}] and [MMT_{B2}/PEI(10kD)_{10Q}^{60R14}] adducts which were both prepared by the “indirect replacement” method and pre-ground to 0.1 – 1 cm led to composites with diameters in the region of 1 – 10 μm, with most of the particles exhibiting diameters around 1 μm, when the adduct concentration was set to be in the region of 1.0 – 30.0 wt.%. In addition, composites containing 5 – 10 wt.% of the adducts formed a superstructure across the bitumen similar to the polymer networks of polymer-modified bitumen. On the other hand, although bitumen-[MMT_{B1}/CTAB] composites contained also particles with diameters of 1 – 10 μm, the number of particles with a diameter around 10 μm was higher than with bitumen-[MMT_{B1,B2}/PEI(10kD)_{10Q}^{80R10}] and bitumen-[MMT_{B2}/PEI(10kD)_{10Q}^{60R14}] composites. Furthermore, bitumen-[MMT/CTAB] composites showed no superstructure with adduct concentrations of 5 and 10 wt.%. When [MMT_{B1,B2}/PEI(10kD)_{10Q}^{80R10}] and [MMT_{B2}/PEI(10kD)_{10Q}^{60R14}] adducts were mixed with polymer-modified bitumen the polymer networks of the bitumen were broken which shows that the polymers used to modify the bitumen were not compatible with the used adducts.

5.3.2 Rheological investigation of bitumen-[MMT/PEI(nkD)_{xQ}^{yR}] and bitumen-[MMT/CTAB] composites

The rheological investigation of the five base bitumen Nynas 50/70, Total Azalt 50/70, Shell 30/45, BP Olexobit 45, and Shell Cariphalte 25/55-55 bitumen, the Total Azalt 50/70-[MMT/CTAB] composites **C1.1** and **C1.2** and the bitumen-[MMT/PEI(nkD)_{xQ}^{yR}] composites **C3.1** – **C15** were performed with the aim to characterise the viscoelastic behaviour of those composites in the temperature region of 30 - 120°C. With the dynamic viscosity η' , the degree of delamination of the montmorillonite platelets was calculated according to the procedure developed by Bicerano, Douglas and Brune [10].

It was found that the same bitumen exhibited a different viscoelastic behaviour when the gap was varied which will be shown in the following paragraph. The reason was that thermal gradients occurred across the thickness and radius of the sample since no environmental chamber was used and the upper plate was not heated [6].

Figure 5.15 compares the storage modulus G' (a), the loss modulus G'' (b), and the phase angle δ (c) of the Nynas 50/70 bitumen measured at two different gaps. The measurements were performed with a gap h of 1.0 mm (= **N1**) and $h = 1.7$ mm (= **N2**).

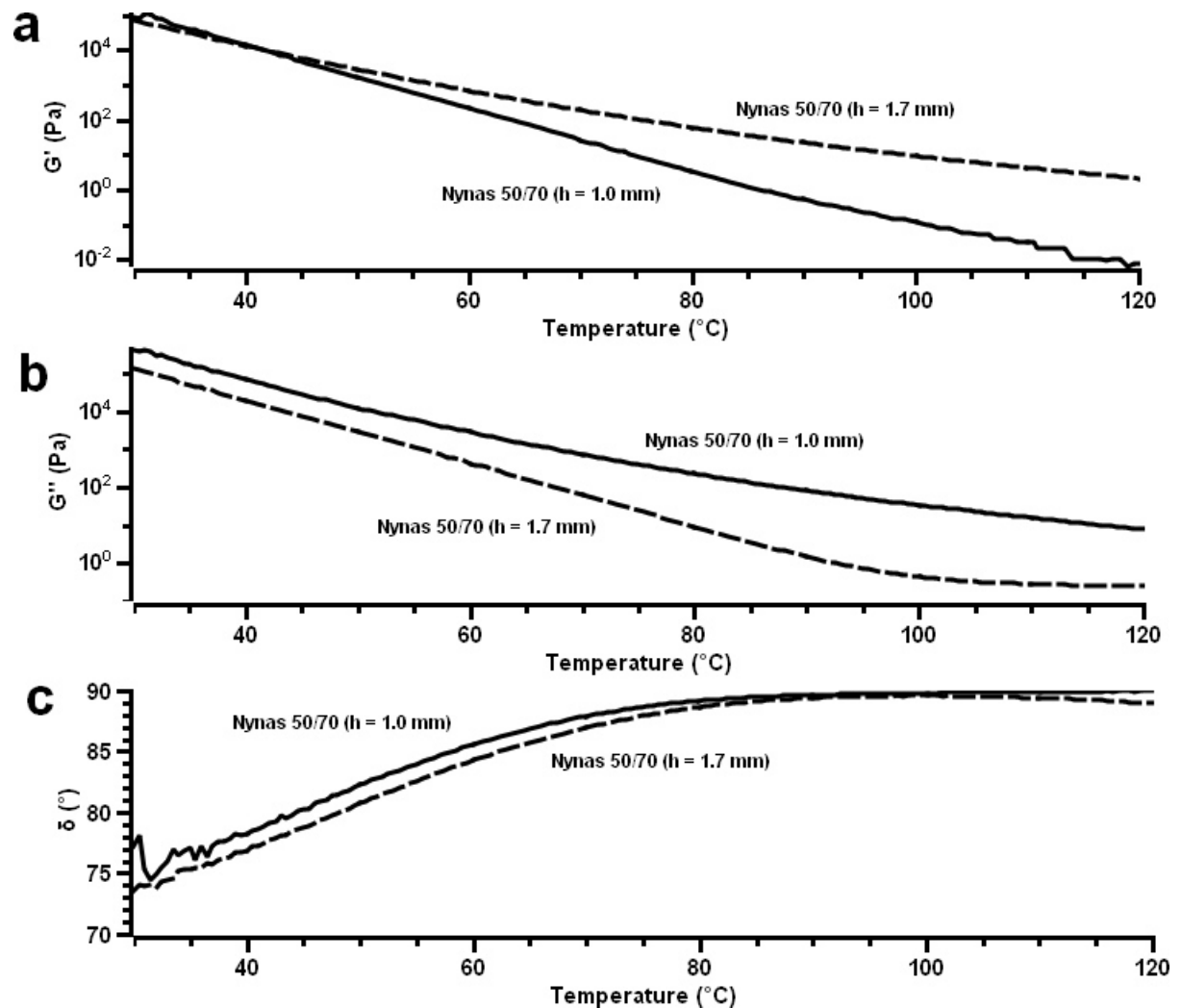


Figure 5.15: Rheology plots of a) G' , b) G'' , and c) phase angle δ of Nynas 50/70 bitumen measured at a gap of $h = 1.0$ mm (= **N1**) and $h = 1.7$ mm (= **N2**), $\omega = 6.28$ rad/s, $\sigma = 30$ Pa

With both bitumina, the storage modulus (Figure 5.15.a) and the loss modulus (Figure 5.15.b) decreased steadily with increasing temperature. On the other hand, differences between **N1** and **N2** appeared when the phase angle δ at a given temperature was compared. With bitumen **N1**, the phase angle δ (Figure 5.15.c) increased

strongly from about 74° at 30°C to 89.2° at 80°. In the temperature region of 80 – 120°C, the phase angle increased slowly up to 89.9° at 120°C. For comparative purposes this characteristic temperature dependence of the phase angle will be named as a “steady growth” δ -system in future descriptions. At 56°C, the phase angle exhibited a value of 84.4°. The bitumen exhibited viscoelastic properties over the whole temperature range but behaved mainly like a viscous liquid above a temperature of 56°C. On the other hand, with bitumen **N2** the values of the phase angle δ were shifted to lower values in the temperature region of 30 – 80°C compared to bitumen **N1** showing that at lower temperatures bitumen **N2** was more elastic than bitumen **N1**. Above 80°C, bitumen **N2** behaved, as bitumen **N1**, like a viscous liquid.

In conclusion, the different viscoelastic behaviour of bitumen **N1** and **N2** shown by the values of the phase angle at a given temperature demonstrate that the gap had a huge influence on the viscoelastic response of the bitumen. When the gap was too wide (bitumen **N2**) the heat transport through the sample was slower and the upper part of the sample was cooler than it should be which led to a higher elasticity of the sample. On the other hand, comparing bitumen of the same type measured at gap $h = 1$ mm, the storage, the loss modulus, and the phase angle exhibited almost the same value at a given temperature. Samples measured at a gap $h = 1$ mm could be, therefore, used for the calculation of the aspect ratio of the montmorillonite in the composites. Measurements at larger gaps served mainly to describe a trend when the viscoelastic behaviour of the modified bitumen with the applied preparation procedures was correlated.

To investigate the influence of the adduct preparation method on the viscoelastic behaviour of bitumen one 70/100-[MMT_{B1}/PEI(10kD)_{5Q}^{67R10}] composite containing 10.0 wt.% of the by the “direct addition” method prepared adduct **E2** (= **C2.3**) was studied by rheology. The adduct was not pre-ground but pre-mixed with the bitumen which means that adduct pieces with diameters larger 3 μm were added to the bitumen melt in the tin can and the dispersion was pre-mixed manually before extrusion. Furthermore, 20 extrusion runs were performed to ensure the thorough mixing of the components.

In Figure 5.16 the storage modulus G' (a), the loss modulus G'' (b), and the phase angle δ (c) of the non-modified 70/100 bitumen and composite **C2.3** is compared. With the neat 70/100 bitumen, the phase angle δ increased steadily from about 78° at 30°C up to 90° at 102.5°C and became constant in the temperature region of 102.5 – 120°C which shows that the bitumen behaves like a viscous liquid above 102.5°C. With composite **C2.3** the phase angle exhibited an almost constant angle of about 65° in the temperature region of 30 - 44°C and decreased then steadily up to

an angle of 30.6° at 120°C . This “steady decline” of the phase angle with growing temperature is the second archetype of rheological behaviour we want to mark in this investigation. Although composite was more elastic in the studied temperature region than the non-modified bitumen the steady growth of the elasticity with increasing temperature indicates that during the measurement adduct particles may have accumulated on the upper plate of the rheometer which led to the enhancement of the elasticity at higher temperatures and points to the presence of large adduct particles in the composite.

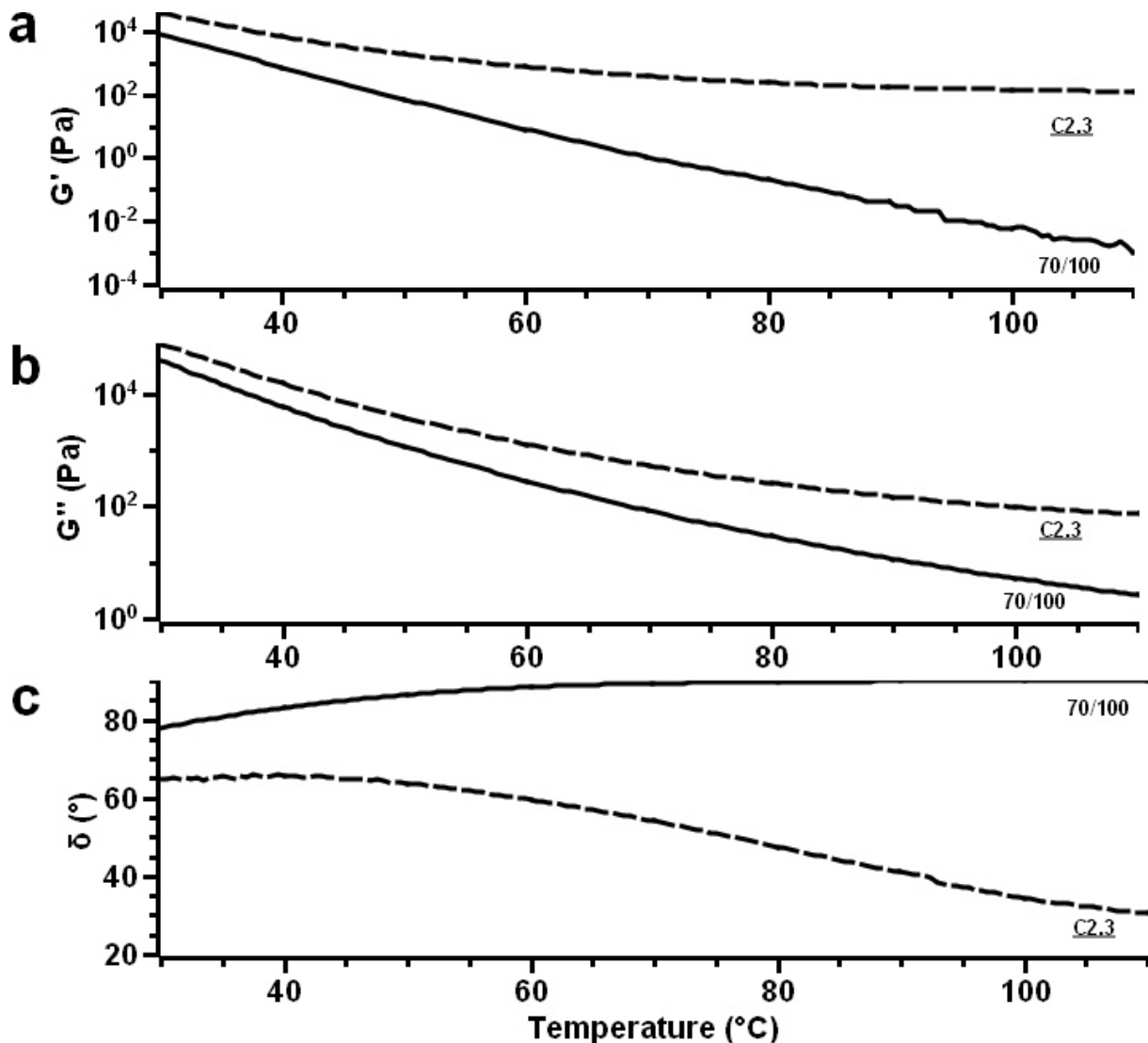


Figure 5.16: Rheology plots of a) G' , b) G'' , and c) phase angle δ of 70/100 bitumen ($h = 2.2$ mm, $\omega = 0.82$ rad/s, $\sigma = 30$ Pa), and the 70/100-**E2** composite **C2.3** ($h = 1.2$ mm, 10.0 wt.% **E2**, $\omega = 0.82$ rad/s, $\sigma = 30$ Pa), **E2** = [MMT_{B1}/PEI(10kD)_{5Q}^{67R10}]

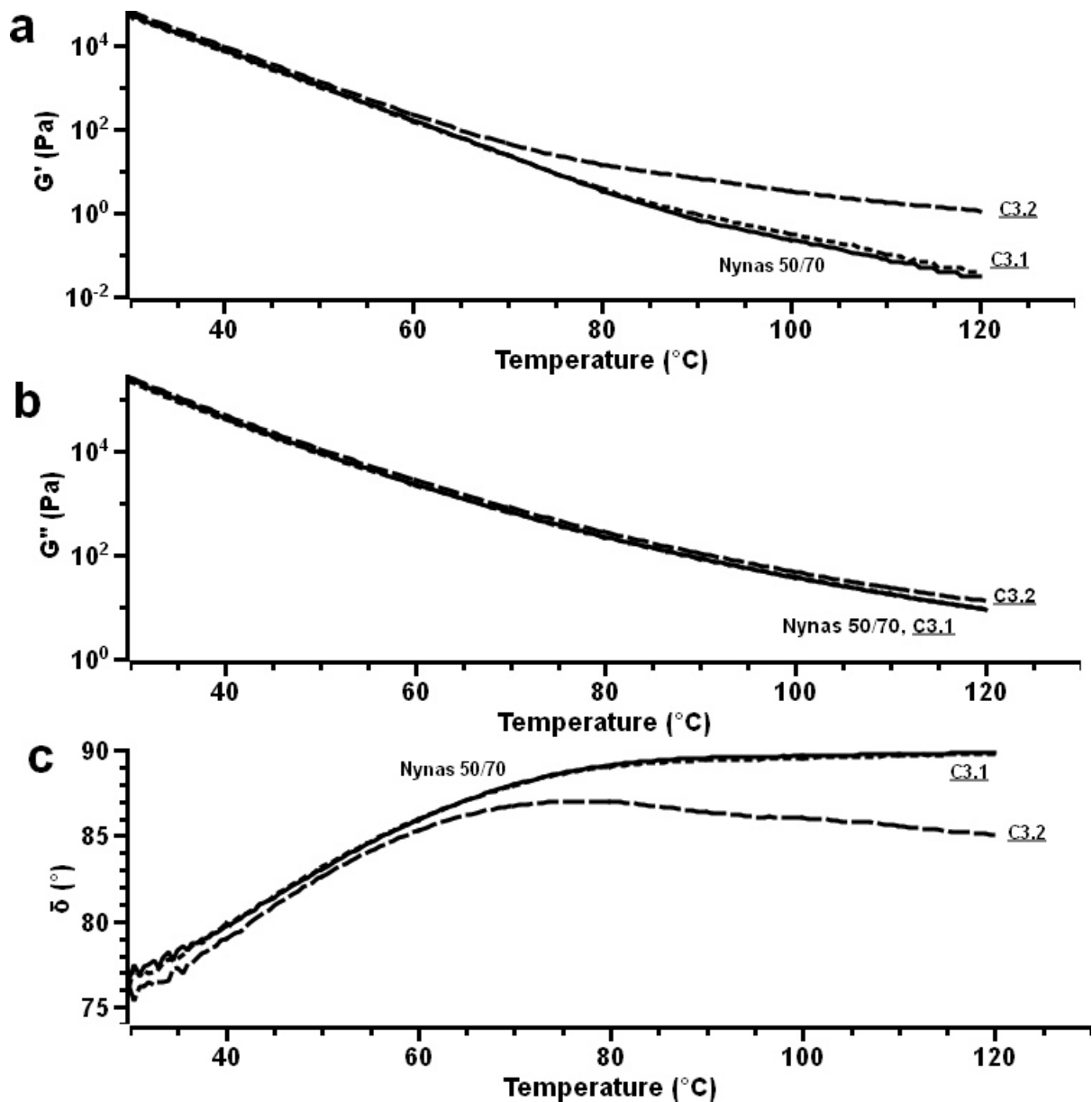


Figure 5.17: Rheology plots of a) G' , b) G'' , and c) phase angle δ of Nynas 50/70 bitumen ($h = 1.1$ mm), and the Nynas 50/70-**E7** composites **C3.1** ($h = 1.3$ mm, 1.0 wt.% **E7**) and **C3.2** ($h = 1.3$ mm, 10.0 wt.% **E7**), **E7** = $[\text{MMT}_{\text{B1}}/\text{PEI}(10\text{kD})_{10\text{Q}}^{80\text{R}10}]$, $\omega = 6.28$ rad/s, $\sigma = 30$ Pa

The viscoelastic properties of two Nynas 50/70- $[\text{MMT}_{\text{B1}}/\text{PEI}(10\text{kD})_{10\text{Q}}^{80\text{R}10}]$ composites (**C3.1** and **C3.2**) containing an adduct prepared by the “indirect replacement” method (= **E7**) were compared to that of the 70/100- $[\text{MMT}_{\text{B1}}/\text{PEI}(10\text{kD})_{5\text{Q}}^{67\text{R}10}]$ composite **C2.3**. The composites preparation procedure was the same with the three compounds except that with the composites **C3.1** and **C3.2** only one single extrusion run was performed. The adduct concentrations were set to be 1.0 wt.% (**C3.1**) and 10.0 wt.% (**C3.2**). Figure 5.17 compares the storage modulus G' (a), the loss modulus G''

(b), and the phase angle δ (c) of the non-modified Nynas 50/70 bitumen, and the composites **C3.1** and **C3.2**.

With the Nynas 50/70 bitumen the phase angle δ rose strongly from about 77° at 30°C to 89.2° at 81.5°C followed by a slow increase up to 89.8° at 120°C. With composite **C3.1** the value of the phase angle δ at a given temperature was similar to that of the non-modified bitumen which implies that the adduct concentration of 1.0 wt.% was not sufficiently high enough to show a measurable influence on the bitumen. With composite **C3.2**, the phase angle δ increased strongly from about 76° at 30°C to 87° at 75°C. Above 75°C, the phase angle decreased slowly up to 85° at 120°C. As with composite **C2.3** (cf. Figure 5.16), the steady decrease of the phase angle above 75°C may be caused by the segregation of large particles.

In conclusion, while the addition of 1.0 wt.% of the adduct (= composite **C3.1**) didn't influence the viscoelastic behaviour of the base bitumen, with an adduct concentration of 10.0 wt.% (= composite **C3.2**), the bitumen became more elastic but large adduct particles were present in the composite. This clearly proved that the simple pre-mixing of non-pre-ground adducts and bitumen before extrusion was not sufficient to obtain a composite with small adduct particles. Compared to composite **C2.3** (cf. Figure 5.16) the enhancement of the elasticity started at a higher temperature which may be a sign for a better compatibility of adduct **E7** with non-polymer modified bitumen. Note that the presence of large agglomerations impeded the calculation of the particles aspect ratio.

The composites discussed in the next paragraphs were all prepared using adducts made by the "indirect addition" method but the preparation conditions were varied. To test the influence of the adduct pre-treatment the next composites evaluated contained an adduct which was pre-ground at 20°C to diameters of 1 – 3 μ m before mixing with the bitumen in the extruder (= composites **C4.1** and **C4.2**). The adduct concentration was set to be 5.0 wt.% with composite **C4.1** and 10.0 wt.% with composite **C4.2**. In Figure 5.18, the storage modulus G' (a), the loss modulus G'' (b), and the phase angle δ (c) of the Nynas 50/70 bitumen, composite **C4.1.1**, and composite **C4.2.1** is shown. The characteristics of the Nynas 50/70 bitumen measured with a gap h of 1.7 mm (= **N2**) was described during the discussion of the influence of the gap on the viscoelastic behaviour of the bitumen (cf. Figure 5.15). When the adduct concentration was set to be 5.0 wt.% but no pre-mixing of the adduct with the bitumen was done before extrusion (= composite **C4.1.1**) the values of the phase angle δ were measured to be similar to those of the non-modified bitumen which indicates that the size of the adducts was still too large and no sufficient delamination was achieved to affect the characteristics of the base bitumen.

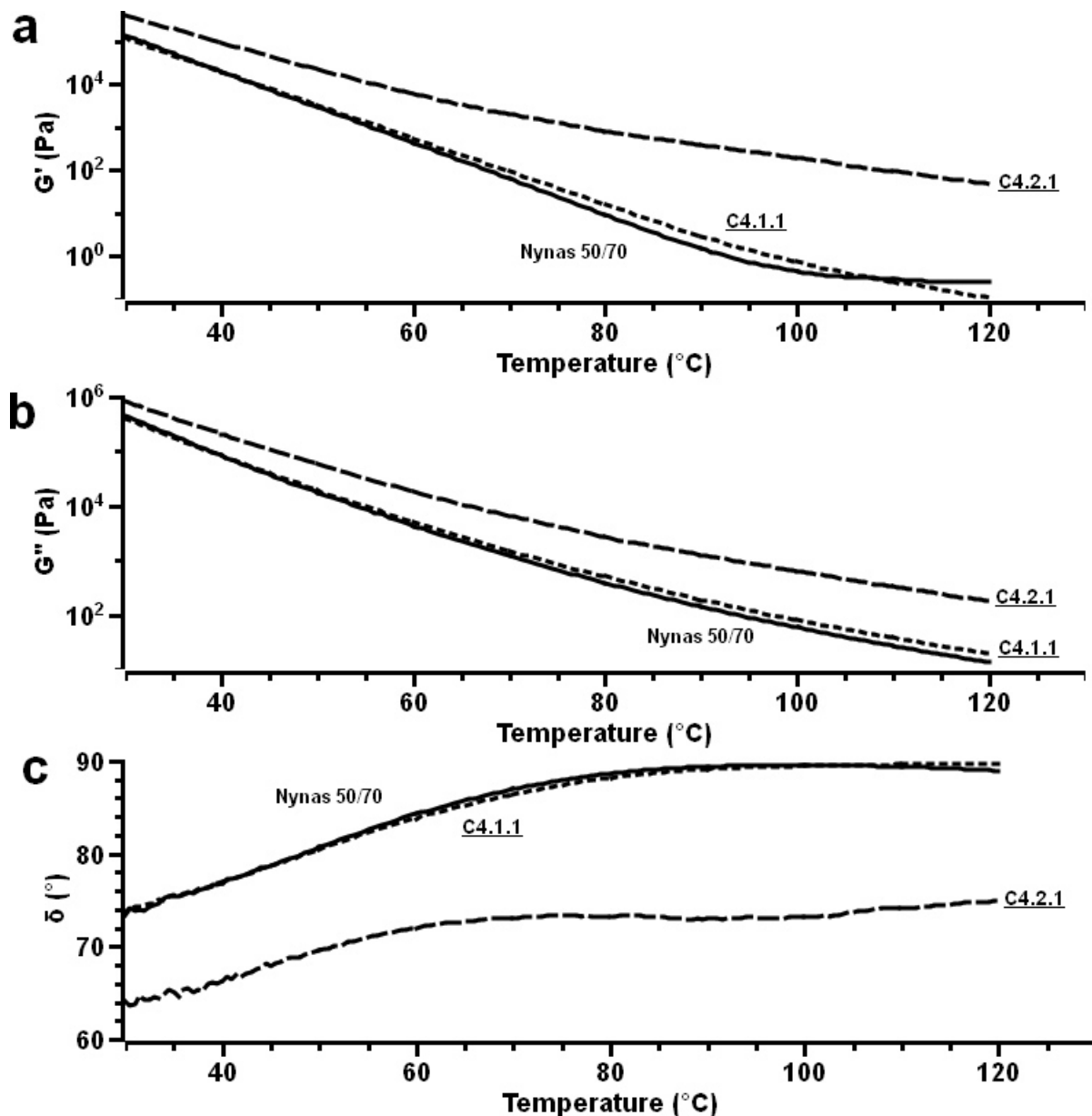


Figure 5.18: Rheology plots of a) G' , b) G'' , and c) δ of Nynas 50/70 bitumen ($h = 1.7$ mm), and the Nynas 50/70-**E8** composites **C4.1.1** ($h = 2.3$ mm, 5.0 wt.% **E8**) and **C4.2.1** ($h = 2.0$ mm, 10.0 wt.% **E8**), **E8** = [MMT_{B1}/PEI(10kD)_{10Q}^{80R10}], $\omega = 6.28$ rad/s, $\sigma = 30$ Pa

With an adduct concentration of 10.0 wt.% and when the adduct was premixed with the bitumen before extrusion (composite **C4.2.1**) the phase angle showed an increase from about 64° at 30°C to 73.3° at 74.5°C . Between 74.5°C and 88.0°C , the phase angle decreased slowly until it reached an angle of 72.9° and increased above 88°C again up to a value of 75.0° at 120.0°C . The values of the phase angle δ between 30 and 120°C show that the composite behaved mainly like a viscous liquid, while the elasticity didn't decrease much with increasing temperature.

The higher elasticity of the composite compared to that of the non-modified bitumen could not be explained by the wrong measurement setup alone, i. e. the large gap. Instead, the high elasticity of the composite indicates the presence of an adduct network in the bitumen, similar to the behaviour of styrene-butadiene-styrene (SBS) modified bitumen [13]. The presence of the network is characterised by a typical “maximum/minimum” behaviour: on increasing temperature the phase angle first increases steadily until it reaches a maximum (73.3° at 74.5°C with **C4.2.1**), followed by a decrease towards a minimum value (72.9° at 88.0°C with **C4.2.1**). Increasing the temperature further the phase angle continuously grows. With polymer modified bitumen the behaviour of the bitumen is explained by the fact that bitumen behaves like a Newtonian liquid at higher temperatures and allows the elastic network of the polymer to rule the mechanical properties of the bitumen [13]. The minimum of the phase angle correspond to a plateau region of the storage modulus and is indicative for polymer networks or continuous polymer phases in the modified bitumen [13].

In conclusion, while the phase angle of the composite containing 5.0 wt.% of adduct **E8 (C4.1.1)** exhibited a “steady growth” behaviour typical for non-polymer modified bitumina, a “maximum/minimum” behaviour was observed after the concentration was raised to 10.0 wt.% (**C4.2.1**) which points to the presence of an adduct network in the composite. Therefore the pre-mixing of the bitumen and the adduct, as well as the pre-grinding of the adducts, was necessary. But since the addition of 5.0 wt.% of the adduct didn't influence the bitumen much it was concluded that the added pieces were still too large. The reduction of the particle size in the composites could be achieved by either a higher shear rate or by an addition of smaller primer-pieces. A calculation of the aspect ratio of the montmorillonite in these composites was not performed since the compounds were measured with different gaps each.

In comparison to the viscoelastic behaviour measured with composites prepared with non-pre-ground adducts (**C3.1** and **C3.2**) and adducts pre-ground at 20°C to 1 - 3 cm pieces (**C4.1** and **C4.2**), Total Azalt 50/70-[MMT_{B2}/PEI(10kD)_{10Q}^{80R10}] composites were investigated using adducts which were pre-ground under liquid nitrogen to 0.1 – 1 cm pieces (**C9**, and **C10.1** – **C10.5**). The composites **C10.1** to **C10.5** contained the [MMT_{B1}/PEI(10kD)_{10Q}^{80R10}] adduct **E10** in adduct concentrations of 1.0 wt.% (**C10.1**), 2.5 wt.% (**C10.2**), 5.0 wt.% (**C10.3**), 7.5 wt.% (**C10.4**), and 10.0 wt.% (**C10.5**). Composite **C9** contained 4.9 wt.% of the [MMT_{B2}/PEI(10kD)_{10Q}^{80R10}] adduct **E9** which was prepared in a “high concentration” solution to test the influence of the adduct preparation method. Figure 5.19 compares the storage modulus G' (a) and the loss modulus G'' (b), and the phase angle δ (c) of the non-modified Total Azalt 50/70 bitumen, the composites **C10.1** – **C10.5**, and composite **C9**.

5 Preparation of bitumen-[montmorillonite/PEI(nkD)xQyR] composites

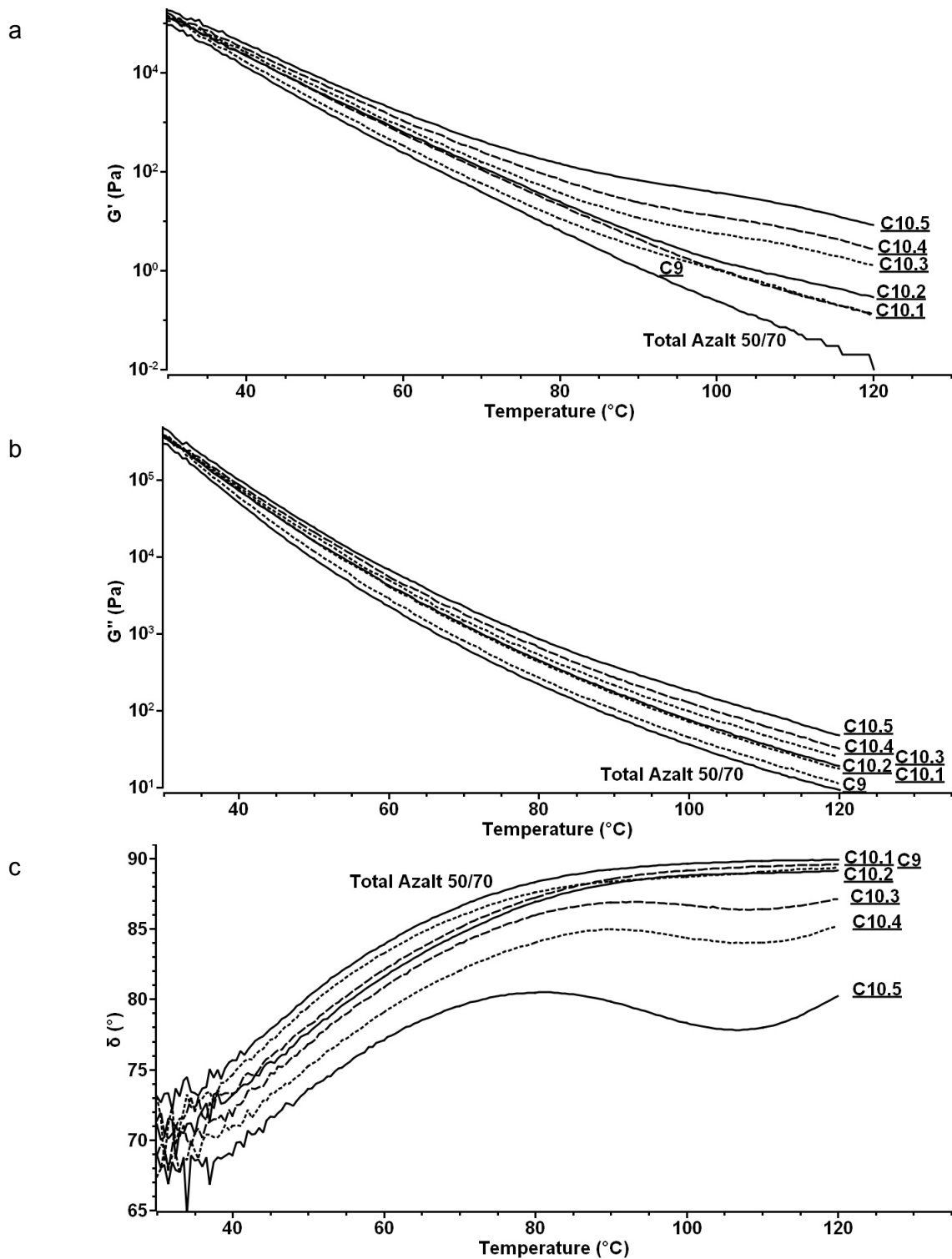


Figure 5.19: Rheology plots of a) G' and b) G'' , and c) the phase angle δ of Total Azalt 50/70 bitumen, the Total Azalt 50/70-**E10** composites **C10.1** – **C10.5** (1.0 wt.%, 2.5 wt.%, 5.0 wt.%, 7.5 wt.%, and 10.0 wt.% **E10**), and the Total Azalt 50/70-**E9** composite **C9** (4.9 wt.% **E9**), **E9** = $[\text{MMT}_{\text{B2}}/\text{PEI}(10\text{kD})_{10\text{Q}}^{80\text{R}10}]$, **E10** = $[\text{MMT}_{\text{B1}}/\text{PEI}(10\text{kD})_{10\text{Q}}^{80\text{R}10}]$, $\omega = 6.28 \text{ rad/s}$, $\sigma = 30 \text{ Pa}$, $h = 1.0 \text{ mm}$

With the Total Azalt 50/70 bitumen, the temperature dependence of the phase angle δ exhibited the typical “steady growth” behaviour measured with non-polymer-modified bitumina. The phase angle rose strongly from a value of about 71° at 30°C up to a value of 88.3° at 80°C followed by a slow increase up to 89.9° at 120°C .

With the composites **C10.1** and **C10.2**, the temperature dependence of the phase angle δ was similar as with the non-modified bitumen, i. e. a “steady growth” behaviour, but the angle at a given temperature was shifted to a lower value which shows that with increasing adduct concentration the bitumen became increasingly more elastic.

With adduct concentrations of 5.0 – 10.0 wt.% (**C10.3** – **C10.5**) the phase angle exhibited a “maximum/minimum” temperature dependence as observed with polymer-modified bitumen [13]. In detail, with composite **C10.3** the phase angle reached a maximum at 94°C of 86.9° . With increasing temperature the phase angle decreased until a minimum of 86.4° at 108°C and rose again up to 87.1° at 120°C . Furthermore, with increasing adduct concentration the maximum (85.0° at 90.5°C with **C10.4** and 80.5° at 80.5°C with **C10.5**) and minimum (84.0° at 107.5°C with **C10.4** and 77.8° at 106.5°C with **C10.5**) shifted to lower temperatures which shows that with increasing adduct concentration the influence of the adduct on the viscoelastic properties of the bitumen became more distinct. At the same time, with increasing adduct concentration the value of the phase angle at a given temperature decreased which shows that with increasing concentration the bitumen became more elastic. It was therefore concluded that the $[\text{MMT}_{\text{B1}}/\text{PEI}(10\text{kD})_{10\text{Q}}^{80\text{R}10}]$ adduct formed also a network in the bitumen. On the other hand, composite **C9** was only slightly more elastic than the non-modified bitumen and showed the same temperature dependence of the phase angle which showed that the composite contained no adduct-network which may be caused by the lower montmorillonite concentration of the adduct (cf. Table 5.17).

It was of interest to study to which degree the added adducts were delaminated into single montmorillonite platelets in the bitumen. To enable such a delamination the polymers which coated the montmorillonite has to be compatible with the bitumen. Furthermore, the adduct preparation played an important role since adducts which consisted of montmorillonite stacks coated by a polymer film would not be able to give single montmorillonite platelets in the bitumen. As described in Chapter 2, montmorillonite platelets exhibited a length of about 10 to 1000 μm and a thickness of about 1 nm. From the data obtained from atomic force microscopy (AFM) studies, the aspect ratios of montmorillonite platelets were calculated to be 60 – 500, with most of the platelets exhibiting aspect ratios between 80 and 300 [11]. In this work, the aspect ra-

tio of the montmorillonite in the bitumen was calculated using the relationships developed by Bicerano, Douglas, and Brune [10], who proposed a model for the calculation of the aspect ratio of platelets and fibres in polymer matrices by using the relative viscosity $\eta(\text{dispersion})/\eta(\text{polymer})$, and the relative volume fraction Φ of the dispersed particles. The procedure was described in detail in Chapter 2 (Eq. 2.5 - Eq. 2.9).

The volume fraction of the dispersed montmorillonite particles in the composites was calculated from the known masses of the components, and their densities using Equation 5.1. Since only the volume fraction of the montmorillonite in the composites was of interest, the volume fraction of the organic material used to modify the montmorillonite was assigned to be a part of the bitumen. The volumes of the CTAB and the polymers could be added to the volume of the bitumen since they served only the purpose of making the montmorillonite compatible with the bitumen. Inorganic components of the used bentonites (cf. Chapter 4) were assigned to be part of the montmorillonite since not all components could be qualified and quantified.

$$\Phi_M = \frac{V_M}{V_B + V_M + V_O} = \frac{\frac{m_M}{\rho_M}}{\frac{m_B}{\rho_B} + \frac{m_M}{\rho_M} + \frac{m_O}{\rho_O}} \quad \text{Eq. 5.1}$$

(with Φ_M = volume fraction of montmorillonite, V_M = volume of montmorillonite [cm^3], V_B = volume of bitumen [cm^3], V_O = volume of the organic fraction of the adduct [cm^3], m_M = mass of montmorillonite [g], m_B = mass of bitumen [g], m_O = mass of the organic fraction of the adducts [g], ρ_M = density of montmorillonite [= 2.86 g/cm^3], ρ_B = density of bitumen [= 0.95 g/cm^3], ρ_O = density of the organic fraction of the adducts [g/cm^3])

The mass fraction of the montmorillonite (in this case the mass fraction of the bentonite was used) as obtained from TGA and calcination experiments, cf. Chapter 4, of the adducts was calculated using Equation 5.2.

$$m_M = m_T - m_O \quad \text{Eq. 5.2}$$

(with m_M = mass of montmorillonite [g], m_T = sum of the montmorillonite mass and the mass of the organic fraction [g], m_O = mass of the organic fraction [g])

In Table 5.17 the volume fraction Φ_M of the montmorillonite obtained from Equation 5.1, the dynamic viscosity η' , the relative viscosity η/η_0 , the critical volume fraction Φ^* of the montmorillonite at which the viscosity of the dispersion approaches infinity, and the aspect ratios A_f of the montmorillonite of the non-modified Total Azalt 50/70 bitu-

men, the composites **C10.1** - **C10.5**, and composite **C9** are listed.

Table 5.17: Aspect ratio of the montmorillonite of the composites **C9, and **C10.1** - **C10.5****

T [°C]	Entry	Adduct [wt.%]	Φ_M	η' [Pa·s]	η/η_0	Φ^*	A_f
61.5	T 50/70	0	-	295.7	1	-	-
	C9	4.9	0.0056	368.0	1.24	0.0026	975
	C10.1	1.0	0.0013	546.9	1.85	0.0044	572
	C10.2	2.5	0.0033	571.1	1.93	0.0105	238
	C10.3	5.0	0.0066	663.8	2.24	0.0037	675
	C10.4	7.5	0.0100	730.2	2.47	0.0058	432
	C10.5	10.0	0.0134	911.9	3.08	0.0082	303
106.5	T 50/70	0	-	3.55	1	-	-
	C9	4.9	0.0056	4.44	1.25	0.0026	971
	C10.1	1.0	0.0013	6.93	1.95	0.0041	609
	C10.2	2.5	0.0033	7.37	2.08	0.0096	259
	C10.3	5.0	0.0066	9.82	2.77	0.0039	637
	C10.4	7.5	0.0100	12.92	3.64	0.0063	393
	C10.5	10.0	0.0134	18.67	5.26	0.0092	271
120.0	T 50/70	0	-	1.47	1	-	-
	C9	4.9	0.0056	1.81	1.23	0.0026	979
	C10.1	1.0	0.0013	2.76	1.88	0.0043	582
	C10.2	2.5	0.0033	3.02	2.05	0.0098	255
	C10.3	5.0	0.0066	4.02	2.73	0.0039	639
	C10.4	7.5	0.0100	5.12	3.48	0.0063	398
	C10.5	10.0	0.0134	7.61	5.18	0.0091	272

T = temperature [°C], T 50/70 = Total Azalt 50/70 bitumen, Φ_M = volume fraction of montmorillonite, η' = dynamic viscosity [Pa·s], η/η_0 = relative viscosity, Φ^* = critical volume fraction of the dispersed particles, A_f = aspect ratio of the montmorillonite

The values were calculated for the temperatures of 61.5, 106.5, and 120°C. The temperature of 61.5°C was chosen since the non-modified bitumen behaved mainly like a viscous liquid at this temperature (cf. Figure 5.19.c). As shown from the phase angles of the composites **C10.3** - **C10.5** (cf. Figure 5.19.c), the system undergoes structural changes around 106.5°C. It was therefore of interest whether the aspect ratio of the montmorillonite at this temperature was different to that obtained at

61.5°C. To check whether an agglomeration of the montmorillonite platelets occurred at higher temperatures, the aspect ratio of the montmorillonite at 120°C was also calculated.

The montmorillonite of composite **C10.1** exhibited an average aspect ratio of the three temperatures of 588 ± 16 . With composite **C10.2**, the montmorillonite showed an aspect ratio of 251 ± 9 and with composite **C10.3** of 650 ± 17 . With the composites **C10.4** and **C10.5**, aspect ratios of 400 ± 17 and 282 ± 15 were calculated. The montmorillonite of composite **C9** exhibited an even higher aspect ratio of 975 ± 3 . With all six composites, the relative error was calculated to be equal or lower than 5 % which was interpreted as a sign for very stable particle dispersions.

The high aspect ratio of the montmorillonite of the composites **C10.1** and **C10.3** indicates that the montmorillonite consisted mainly as single platelets in the bitumen. The even higher aspect ratio of the montmorillonite of composite **C9** point to the conclusion that almost all montmorillonite platelets were dispersed to single platelets. The lower aspect ratio of the montmorillonite of composite **C10.2** may be caused by inhomogeneous pre-ground adduct particles. When the adduct concentration was raised (= composites **C10.4** and **C10.5**), the aspect ratio of the montmorillonite became gradually lower. The decrease of the aspect ratios point to that montmorillonite platelets attracted each other and formed stacks when the concentration exceeded a certain limit.

Compared to the montmorillonite aspect ratios calculated with the composites **C1.1** and **C1.2** (cf. Table 5.19) with **C9** A_f was larger for a factor of 29, and the aspect ratio of composite **C10.3** was 19 times higher than that found with composite **C1.1**. The aspect ratio found with composite **C10.5** was 7 times higher than the ratio of composite **C1.2** which shows that composites prepared with the $[MMT_{B1,B2}/PEI(10kD)_{10Q}^{80R10}]$ adducts **E9** and **E10** contained much smaller montmorillonite stacks than composites prepared with the $[MMT_{B1}/CTAB]$ adduct **E4**. To sum up, the addition of the $[MMT_{B2}/PEI(10kD)_{10Q}^{80R10}]$ adducts **E9** and **E10** to bitumen led to composites with a high number of exfoliated montmorillonite single platelets, i. e. a higher effective degree of exfoliation.

Five Total Azalt 50/70- $[MMT_{B2}/PEI(10kD)_{10Q}^{60R14}]$ composites (**C12.1** - **C12.5**) with adduct concentrations of 1.0 wt.% (**C12.1**), 5.0 wt.% (**C12.2**), 10.0 wt.% (**C12.3**), 20.2 wt.% (**C12.4**), and 30.0 wt.% (**C12.5**) were rheologically investigated with the aim to study the influence of the polymers used to prepare the adducts. Different to the $PEI(10kD)_{10Q}^{80R10}$ polymer of the $[MMT_{B1,B2}/PEI(10kD)_{10Q}^{80R10}]$ adducts used to prepare the composites **C9** and **C10.1** – **C10.5**, the $PEI(10kD)_{10Q}^{60R14}$ polymer used for the preparation of the $[MMT_{B2}/PEI(10kD)_{10Q}^{60R14}]$ adduct exhibited a longer alkyl chain.

In Figure 5.20 the storage modulus G' (a), the loss modulus G'' (b), and the phase angle δ (c) of the Total Azalt 50/70 bitumen, and the composites **C12.1** – **C12.5** is shown. The viscoelastic behaviour of the Total Azalt 50/70 bitumen was described as part of the discussion of the composites **C10.1** and **C10.5** (cf. Figure 5.19).

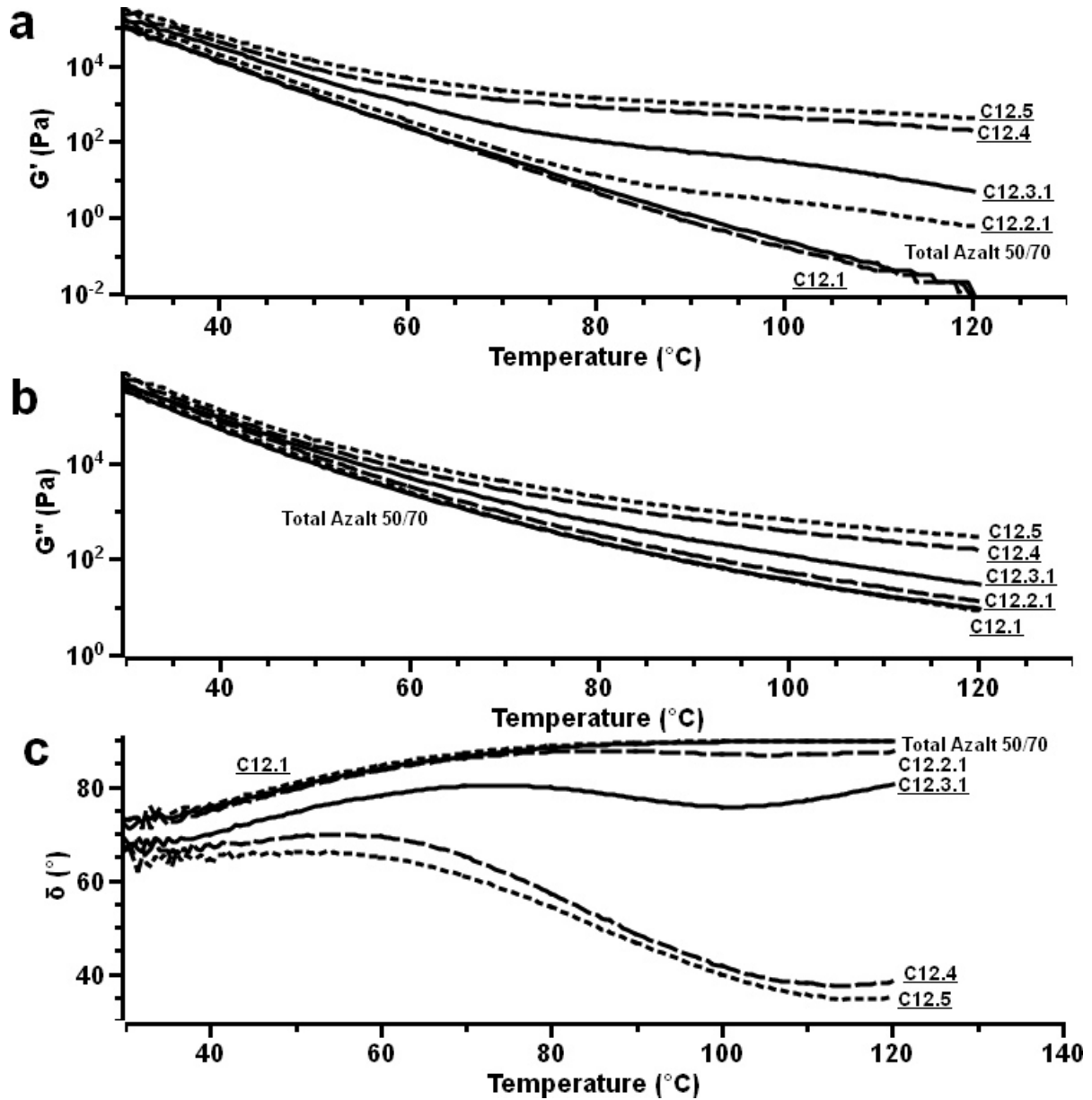


Figure 5.20: Rheology plots of a) G' , b) G'' , and c) δ of Total Azalt 50/70 bitumen, and the Total Azalt 50/70-**E15** composites **C12.1** – **C12.5** (1.0, 5.0, 10.0, 20.2, and 30.0 wt.% **E15**), **E15** = [MMT_{B2}/PEI(10kD)_{10Q}^{60R14}], $\omega = 6.28$ rad/s, $\sigma = 30$ Pa, $h = 1.0$ mm

With composite **C12.1**, the phase angle exhibited the same characteristic as the non-modified bitumen shown by the strong increase of the angle from about 73° at 30°C

to 88.8° at 80°C followed by a slow increase up to 89.9° at 120°C. The values of the phase angle at a given temperature was similar to that of the base bitumen which shows that the adduct concentration of 1.0 wt.% was not sufficiently high enough to influence the viscoelastic behaviour of the bitumen.

Starting with an adduct concentration of 5.0 wt.% (composite **C12.2.1**) the phase angle exhibited the same “maximum/minimum” behaviour as measured with the composites **C10.3** – **C10.5** (cf. Figure 5.19.c) which is indicative of the presence of an adduct network in the bitumen as described in the literature [13]. With composite **C12.2.1** a maximum of 87.7° was reached at 86.4°C followed by a decrease up to a minimum of 86.8° at 106.9°C. Then the phase angle rose again until it reached a value of 87.5° at 120°C. The angles of the maximum and minimum measured with composite **C12.2.1** were similar to those of composite **C10.3** (max = 87.7° at 86.4°C and min = 86.4° at 108°C) which shows that the elasticity of both compounds was similar and points to the conclusion that the [MMT_{B2}/PEI(10kD)_{10Q}^{60R14}] adduct **E15** was equally compatible with the Total Azalt 50/70 bitumen as the [MMT_{B1}/PEI(10kD)_{10Q}^{80R10}] adduct **E10**.

With composite **C12.3.1**, the maximum of 80.3° was reached at a lower temperature of 74.9°C compared to composite **C12.2.1**. The following minimum was also measured at a lower temperature of 101.5°C and exhibited an angle of 75.7°. The higher adduct concentration led, therefore, to a more elastic bitumen. While the angle at the maximum was the same as with composite **C10.5** (max = 80.5° at 80.5°C and min = 77.8° at 106.5°C) the angle at the minimum was 2° lower which shows that at higher temperatures composite **C12.3.1** was more elastic than composite **C10.5**. But different to composite **C10.5** the maximum of composite **C12.3.1** was found at a 5.5°C and the minimum at a 5.0°C lower temperature which indicates that the used polymer interacted also with the bitumen matrix.

When the adduct concentration was raised to 20.2 wt.% (= composite **C12.4**) the maximum of 69.8° was reached at 56°C and declined then strongly until it reached a minimum of 37.4° at 114.5°C. Between 114.5 and 120°C, the phase angle rose slowly until a value of 38.3° at 120°C. With an adduct concentration of 30.0 wt.% (= composite **C12.5**), the maximum of 66.2° was reached at an even lower temperature of 51°C followed by a strong decrease of the angle up to a minimum of 34.4° at 114.1°C. The low value of the minimum shows that the adduct formed an even stronger network within the bitumen as with composite **C12.4**. Also as shown by the values of the phase angle the composites **C12.4** and **C12.5** behaved like an elastic solid in the temperature region of 30 – 120°C.

In conclusion, the viscoelastic behaviour of the composite modified with 1.0 wt.% of the [MMT_{B2}/PEI(10kD)_{10Q}^{60R14}] adduct **E15** (= composite **C12.1**) was similar to that of

the non-modified bitumen, i. e. a “steady growth” behaviour of the phase angle, which indicates that the used adduct concentration was not high enough to influence the properties of the bitumen. On the other hand, the elasticity of the bitumen was strongly enhanced when the adduct concentration was set to be in the region of 5.0 – 30 wt.%. Furthermore as shown by the “maximum/minimum” behaviour of the phase angles the adduct formed a network in the bitumen which became stronger with increasing adduct concentration. The formation of an adduct network in the bitumen depended, therefore, strongly on the montmorillonite concentration. Compared to the Total Azalt 50/70-[MMT_{B1}/PEI(10kD)_{10Q}^{80R10}] composites **C10.3** and **C10.5** the phase angle exhibited similar values at the maximum and the minimum but the temperatures were lower with the composites **C12.2.1** and **C12.3.1** which points to the conclusion that the melt and glass transition of the used polymers (cf. Chapter 3) decided at which temperatures the adduct network enhanced the elasticity of the modified bitumen.

Table 5.18 lists the aspect ratio of the montmorillonite of the composites **C12.1** - **C12.5** as obtained at the temperatures of 61.5, 114.1, and 120.0°C. These temperatures were selected for the same reasons as explained with the composites **C9** – **C10**, cf. Table 5.17.

With a concentration of 1.0 wt.% of the [MMT_{B2}/PEI(10kD)_{10Q}^{60R14}] adduct **E15** (= composite **C12.1**) the relative viscosity η/η_0 was slightly lower than one, indicating that the montmorillonite concentration was too low to affect the viscosity of the bitumen. When the adduct concentration was set to be 5.0 wt.% (= composite **C12.2.1**), the montmorillonite exhibited similar aspect ratios at the three studied temperatures combined to an average aspect ratio of 71 ± 3 with the low relative error of about 4 % pointing to a stable dispersion. With composite **C12.3.1** the average aspect ratio was calculated to be 78 ± 10 . The average aspect ratios obtained with the composites **C12.4** and **C12.5** were with 56 ± 11 and 53 ± 17 lower than those of the composites **C12.2.1** and **C12.3.1** which indicates that the adduct formed agglomerates with concentrations of 20.2 and 30.0 wt.%.

Starting with an adduct concentration of 10.0 wt.% (**C12.3.1**) the aspect ratios were found to be higher at 114.1 and 120.0°C compared to those obtained at 61.5°C which causes high relative errors up to 32 % and points to that higher temperatures may promote the delamination of the montmorillonite platelets. Compared to the aspect ratios calculated with the composites **C10.1** - **C10.5** and composite **C9** (cf. Table 5.17), the ratios found with the composites **C12.1** - **C12.5** were much lower, which implies that the [MMT_{B2}/PEI(10kD)_{10Q}^{60R14}] adduct **E15** could not be used to obtain composites with exfoliated montmorillonite platelets.

Table 5.18: Aspect ratio of montmorillonite of the composites C12.1 - C12.5

T [°C]	Entry	Adduct [wt.%]	Φ_M	η' [Pa·s]	η/η_0	Φ^*	A_f
61.5	T 50/70	0	-	295.7	1	-	-
	C12.1	1.0	0.0013	320.5	1.08	-	-
	C12.2.1	5.0	0.0067	419.6	1.42	0.0354	68
	C12.3.1	10.0	0.0136	645.1	2.18	0.0380	64
	C12.4	20.2	0.0286	963.9	3.26	0.0598	40
	C12.5	30.0	0.0443	1382.0	4.67	0.0783	29
114.1	T 50/70	0	-	4.21	1	-	-
	C12.1	1.0	0.0013	4.10	0.97	-	-
	C12.2.1	5.0	0.0067	6.17	1.47	0.0326	75
	C12.3.1	10.0	0.0136	14.04	3.33	0.0281	87
	C12.4	20.2	0.0286	49.43	11.74	0.0395	62
	C12.5	30.0	0.0443	85.45	20.30	0.0362	67
120.0	T 50/70	0	-	1.47	1	-	-
	C12.1	1.0	0.0013	1.34	0.91	-	-
	C12.2.1	5.0	0.0067	2.10	1.43	0.0350	69
	C12.3.1	10.0	0.0136	4.61	3.14	0.0291	84
	C12.4	20.2	0.0286	25.15	17.11	0.0371	65
	C12.5	30.0	0.0443	45.13	30.7	0.0375	64

T = temperature [°C], T 50/70 = Total Azalt 50/70 bitumen, Φ_M = volume fraction of montmorillonite, η' = dynamic viscosity [Pa·s], η/η_0 = relative viscosity, Φ^* = critical volume fraction of the dispersed particles, A_f = aspect ratio of the montmorillonite

The Total Azalt 50/70-[MMT_{B1}/CTAB] composites **C1.1** (5.2 wt.% [MMT_{B1}/CTAB]) and **C1.2** (9.9 wt.% [MMT_{B1}/CTAB]) were studied with the purpose to determine whether an adduct consisting of montmorillonite modified by an alkylammonium compound would influence the Total Azalt 50/70 bitumen in the same way as the adducts consisting of montmorillonite modified by polymers (**C9**, **C10.3**, and **C10.5**, cf. Figure 5.19, and **C12.2** and **C12.3**, cf. Figure 5.20) did.

In Figure 5.21 the default rheology data (G' , G'' , and δ) of the Total Azalt 50/70 bitumen, composite **C1.1**, and composite **C1.2** are shown. The temperature dependence of the phase angle δ of the non-modified Total Azalt 50/70 bitumen belongs to the “steady growth” type as described during the discussion of the composites **C10.1** and **C10.5** (cf. Figure 5.19.c).

With the composites **C1.1** and **C1.2**, the temperature dependence of the phase angle was also of the “steady growth” type, but different to the non-modified bitumen the

angles exhibited a lower value at a given temperature which shows the higher elasticity of the composites and points to an interaction between the montmorillonite platelets and the bitumen matrix. In comparison to the composites **C10.3**, **C10.5**, **C12.2**, and **C12.3** no adduct network was detected in the composites **C1.1** and **C1.2** which indicates that a network could only be formed with adducts coated by a polymer, but not with adducts consisting of low molecular alkyl ammonium units attached to montmorillonite.

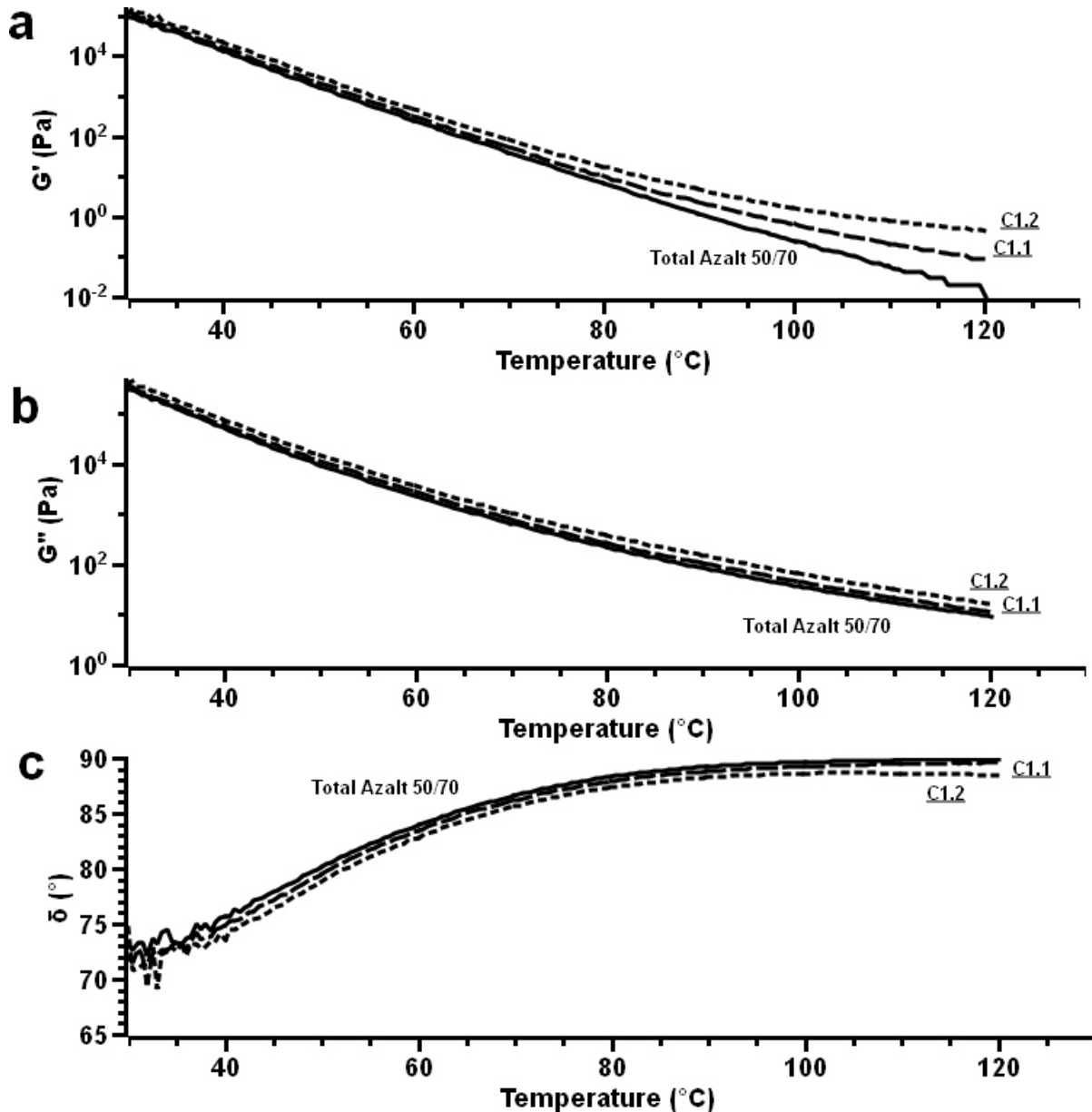


Figure 5.21: Rheology plots of a) G' , b) G'' , and c) phase angle δ of Total Azalt 50/70 bitumen, and the Total Azalt 50/70-**E4** composites **C1.1** (5.2 wt.% **E4**) and **C1.2** (9.9 wt.% **E4**), **E4** = [MMT_{B1}/CTAB], $\omega = 6.28$ rad/s, $\sigma = 30$ Pa, $h = 1.0$ mm

Table 5.19 lists the aspect ratios of the montmorillonite of the composites **C1.1** and **C1.2**. The values were calculated for the temperatures of 61.5°C and 120°C. With composite **C1.1** the aspect ratio was calculated to be 34 ± 3 , the montmorillonite of composite **C1.2** exhibited an aspect ratio of 39 ± 4 . The relative error was found to be 7 % with composite **C1.1** and 10 % with composite **C1.2** which points to a certain temperature dependence of the degree of particle dispersion. Given the aspect ratio of one montmorillonite platelet of 10 to 1000, it was concluded that both composites contained stacks of montmorillonite platelets which shows that the [MMT_{B1}/CTAB] adduct could not be delaminated in single montmorillonite platelets.

Table 5.19: Aspect ratio of the montmorillonite of the composites C1.1 and C1.2

T [°C]	Entry	Adduct [wt.%]	Φ_M	η' [Pa·s]	η/η_0	Φ^*	A_r
61.5	T 50/70	0	-	295.7	1	-	-
	C1.1	5	0.0081	366.5	1.24	0.066	36
	C1.2	10	0.0154	461.7	1.56	0.067	35
120.0	T 50/70	0	-	1.47	1	-	-
	C1.1	5	0.0081	1.78	1.21	0.074	31
	C1.2	10	0.0154	2.58	1.75	0.0555	43

T = temperature [°C], T 50/70 = Total Azalt 50/70 bitumen, Φ_M = volume fraction of montmorillonite, η' = dynamic viscosity [Pa·s], η/η_0 = relative viscosity, Φ^* = critical volume fraction of the dispersed particles, A_r = aspect ratio of the montmorillonite

In the following paragraph the viscoelastic properties of a Nynas 50/70-[MMT_{B2}/PEI(10kD)_{10Q}^{60R14}] composite with an adduct concentration of 10.0 wt.%. (= **C11**) will be discussed. The composite was prepared with the aim to test whether bitumen of different origin but with the same pen-grade would exhibit similar viscoelastic properties when modified by an [MMT_{B2}/PEI(10kD)_{10Q}^{60R14}] adduct (cf. Figure 5.20, composite **C12.3.1**).

Figure 5.22 compares the storage modulus G' (a), the loss modulus G'' (b), and the phase angle δ (c) of the Nynas 50/70 bitumen and composite **C11.2**. With composite **C11.2** the temperature dependence of the phase angle δ showed a weak “maximum/minimum” behaviour, similar to composite **C12.3.1** (cf. Figure 5.20). After a steady increase the phase angle reached a maximum of 79.7° at 71.4°C and decreased then until it reached a minimum of 79.5° at 80.5°C. Between 80.5 and 120°C, the phase angle increased again steadily up to 84.9° at 120°C. Although composite **C11.2** exhibited a higher elasticity than the non-modified bitumen, the elasticity was lower than with composite **C12.3.1** (max = 80.3° at 74.9°C, min = 75.7° at 101.5°C) which shows that the pen-grade alone is not sufficient to predict the effect

of adduct addition on the composites rheology. Obviously the rheological properties depend on the details of bitumen compositions, which are yet unknown, but seem to be different in both used bitumen matrices.

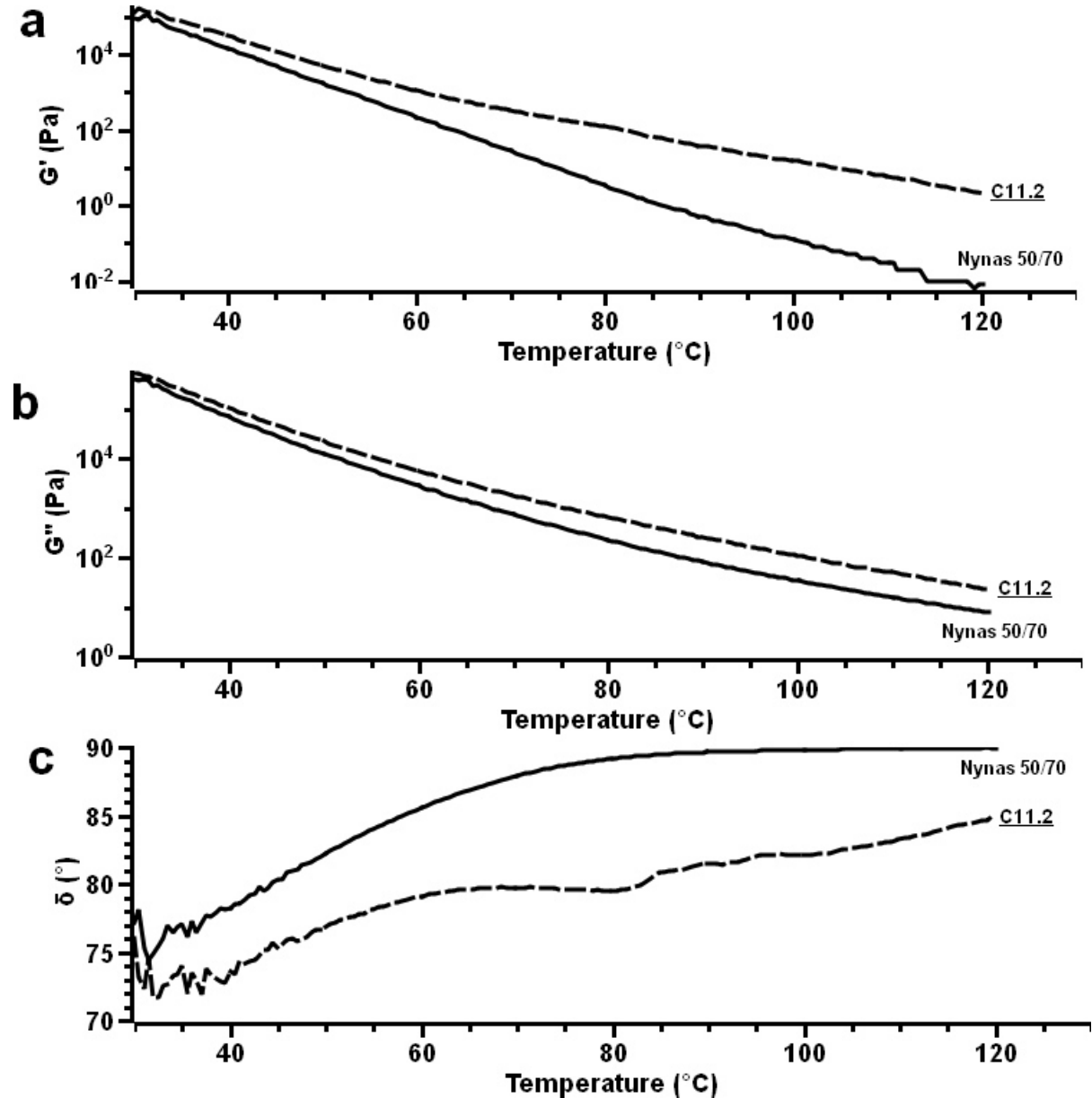


Figure 5.22: Rheology plots of a) G' , b) G'' , and c) δ of Nynas 50/70 bitumen and the Total Azalt 50/70-E15 composite **C11.2** (10.0 wt.% **E15**), **E15** = [MMT_{B2}/PEI(10kD)_{10Q}^{60R14}], ω = 6.28 rad/s, σ = 30 Pa, h = 1.0 mm

In Table 5.20 the aspect ratio of the montmorillonite of composite **C11.2** at 56°C and 120°C is listed. It was found that the montmorillonite exhibited an average aspect ratio of 67 ± 12 and a relative error of 18 %. The aspect ratio was slightly lower than the ratio calculated with composite **C12.3.1** of 78 ± 10 which shows that composite **C11.2** contained montmorillonite stacks build up of a higher number of montmorillonite platelets and points to a lower compatibility of the Nynas 50/70 bitumen with the [MMT_{B2}/PEI(10kD)_{10Q}^{60R14}] adduct than the Total Azalt 50/70 bitumen.

Table 5.20: Aspect ratio of the montmorillonite of the composite C11.2

T [°C]	Entry	Adduct [wt.%]	Φ_M	η' [Pa · s]	η/η_0	Φ^*	A_f
56	N 50/70	0	-	799.5	1	-	-
	C11.2	10	0.0135	1530.0	1.91	0.0437	55
120	N 50/70	0	-	1.26	1	-	-
	C11.2	10	0.0135	3.59	2.85	0.0308	79

T = temperature [°C], N 50/70 = Nynas 50/70 bitumen, Φ_M = volume fraction of montmorillonite, η' = dynamic viscosity [Pa·s], η/η_0 = relative viscosity, Φ^* = critical volume fraction of the dispersed particles, A_f = aspect ratio of the montmorillonite

To determine how the extrusion rate and the extrusion temperature used to prepare bitumen-[MMT/PEI(10kD)_{10Q}^{60R14}] composites influences the viscoelastic properties of the bitumen, four Shell 30/45-[MMT_{B2}/PEI(10kD)_{10Q}^{60R14}] composites with adduct concentrations of ≈ 10.0 wt.% were prepared using a different set of extrusion rate and the extrusion temperature each.

In Figure 5.23 the phase angle δ (a), the storage modulus G' (b), and the loss modulus G'' (c) of the Shell 30/45 bitumen and the composites **C13.1** – **C13.4** is shown. With the Shell 30/45 bitumen, the phase angle exhibited a “steady growth” temperature dependence typical for non-modified bitumen which was a strong increase from about 76° at 40°C to 88.7° at 80°C followed by a slow increase up to an angle of 89.9° at 120°C. With the composite prepared at an extrusion temperature of 70°C and a rotational speed of the extruder screw of 50 min⁻¹ (**C13.1**), the phase angle was of the same “steady growth” type as the non-modified bitumen, but the angle was shifted to a lower value above the temperature of 50°C which shows that the composite was more elastic than the neat bitumen at higher temperatures.

5 Preparation of bitumen-[montmorillonite/PEI(nkD)xQyR] composites

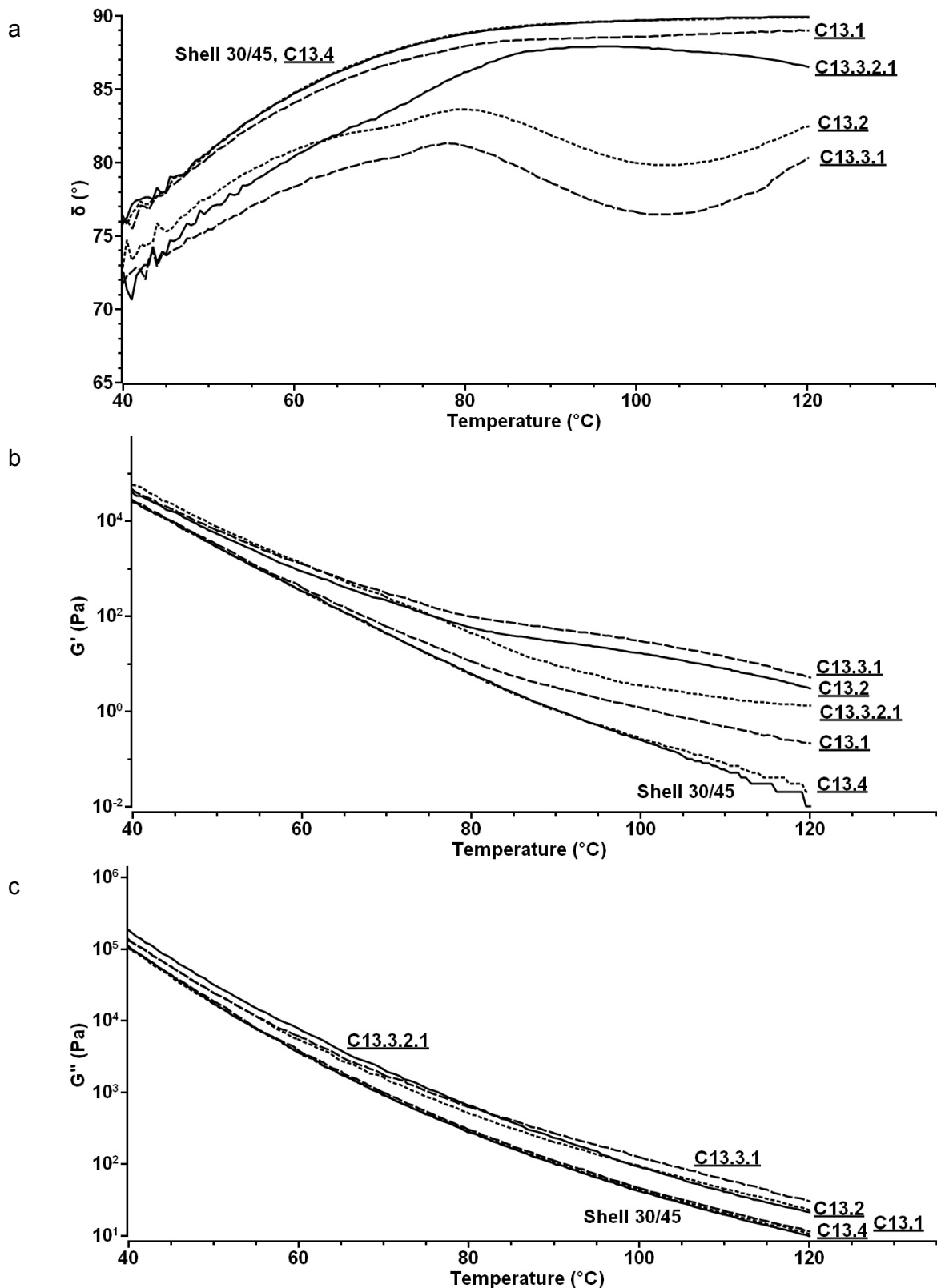


Figure 5.23: Rheology plots of a) the phase angle δ , b) G' and c) G'' of Shell 30/45 bitumen, and the Shell 30/45-**E15** composites **C13.1** – **C13.4** (≈ 10.0 wt.% **E15**), **E15** = $[\text{MMT}_{\text{B2}}/\text{PEI}(10\text{kD})_{10\text{Q}}^{60\text{R}14}]$, $\omega = 6.28$ rad/s, $\sigma = 30$ Pa, $h = 1.0$ mm

With the composite prepared at an extrusion temperature of 70°C and a rotational speed of the extruder screw of 130 min⁻¹ (**C13.2**) and the composite prepared at an extrusion temperature of 120°C and a rotational speed of the extruder screw of 130 min⁻¹ (**C13.3.1**), on the other hand, the temperature dependence of the phase angle showed clearly a “maximum/minimum” behaviour showing that an adduct network was present in both composites. With composite **C13.2**, the maximum of 83.6° was reached at 79.4°C and the minimum of 79.8° at 102.5°C. With composite **C13.3.1**, the position of the maximum of 81.3° was shifted to 77.9°C and the minimum of 76.3° to 101.5°C. Furthermore, since no network was present in composite **C13.1** it was concluded that due to the higher shear rate of 130 min⁻¹ larger adduct particles were broken down which created smaller particles with a larger surface which could interact with the bitumen.

The higher elasticity of composite **C13.3.1** compared to that of composite **C13.2** indicates that the higher processing temperature enhanced the delamination process of the adduct pieces in the bitumen during the extrusion. With composite **C13.3.2.1**, the temperature dependence of the phase angle was determined to be of the “steady decline” type as observed with composite **C3.2** (cf. Figure 5.17). The phase angle rose strongly from about 76° at 40°C to 87.2° at 84.9°C followed by a slow increase up to 87.9° at 97.9°C and a steady decrease until it reached a value of 86.5° at 120°C. The increase in the elasticity between 97.9°C and 120°C indicates that during the measurement adduct particles may accumulated in the upper part of the sample which points to the presence of larger adduct particles in the composite and shows the need thoroughly pre-ground adducts which could not always be ensured with experiments that demanded larger quantities of the adducts because of equipment limitations. On the other hand, in comparison to the non-modified bitumen the lower values of the phase angle in the temperature region of 40 to 97.5°C shows that the adduct was still able to enhance the elasticity of the bitumen to a certain degree.

When the extrusion temperature was raised to 160°C (= composite **C13.4**) the value of the phase angle at a given temperature of the composite was found to be almost the same as with the non-modified bitumen. The reason may be that due to the high processing temperature the viscosity of the bitumen became too low and, in combination with the high rotational speed of the extruder screw, the bitumen flowed past the particles. This led to a composite with a very low adduct content.

To summarize the results from the investigation of the composites **C13.1** – **C13.4**, the preparation of a composite at an extrusion temperature of 70°C and a rotational speed of the extruder screw of 50 min⁻¹ led to a composite that was more elastic than the neat bitumen in the temperature region of 50 – 120°C shown by the shift of the phase angle to a lower value at a given temperature. When the shear rate was raised

to 130 min^{-1} and the temperature was chosen to be either 70°C or 120°C , composites were created with the phase angle exhibiting a “maximum/minimum” behaviour. This behaviour shows that the higher shear broke down adduct pieces which led to smaller particles which were able to form an adduct network in the bitumen. The composite prepared with a shear rate of 130 min^{-1} and a processing temperature of 120°C exhibited the highest elasticity which indicates that the higher temperature may support the miscibility of the adduct with the bitumen. On the other hand, when the temperature was raised to 160°C the viscoelastic behaviour of the composite was the same as with the non-modified bitumen which points to a very low adduct concentration in the bitumen that may be caused by the bitumen flowing past the adduct particles due to the low viscosity of the bitumen at this temperature. The best preparation condition found was an extrusion temperature of 120°C and a rotational speed of the extruder screw of 130 min^{-1} .

Table 5.21 lists the aspect ratios of the montmorillonite of the composites **C13.1** - **C13.4**. The values were calculated for the temperatures 59.0 , 102.5 and 120.0°C . While with composite **C13.1** the montmorillonite exhibited a very low average aspect ratio of 9 ± 3 , the average aspect ratio increased to 56 ± 16 with composite **C13.2** and to 70 ± 19 with composite **C13.3.1**. With composite **C13.3.2.1**, a lower average aspect ratio of 62 ± 1 was found which could be attributed to the non-uniform adduct pretreatment. Composite **C13.4** exhibited a relative viscosity η/η_0 of about 1 at all three temperatures which indicate that the adduct content of the composite was very low. With the composites **C13.1**, **C13.2**, and **C13.3.1**, the relative error was calculated to be $\approx 28 \%$. Composite **C13.3.2.1** exhibited a relative error of $\approx 2 \%$. The higher aspect ratios measured with the composites **C13.2**, **C13.3.1**, and **C13.3.2.1** compared to that of composite **C13.1** shows clearly that due to the higher shear rate the delamination of the montmorillonite platelets in the bitumen was promoted.

Table 5.21: Aspect ratio of the montmorillonite of the composites C13.1 - C13.4

T [°C]	Entry	Adduct [wt.%]	Φ_M	η' [Pa·s]	η/η_0	Φ^*	A_f
59.0	S 30/45	0	-	671.7	1	-	-
	C13.1	10.3	0.0139	731.1	1.09	0.2700	7
	C13.2	9.9	0.0133	975.7	1.45	0.0680	34
	C13.3.1	9.8	0.0132	1077.0	1.60	0.0552	43
	C13.3.2.1	10.0	0.0135	1407.0	2.09	0.0397	61
	C13.4	9.9	0.0133	661.9	0.99	-	-
102.5	S 30/45	0	-	5.45	1	-	-
	C13.1	10.3	0.0139	6.00	1.10	0.2400	8
	C13.2	9.9	0.0133	12.37	2.27	0.0363	67
	C13.3.1	9.8	0.0132	16.45	3.02	0.0291	84
	C13.3.2.1	10.0	0.0135	11.85	2.17	0.0382	63
	C13.4	9.9	0.0133	5.76	1.06	-	-
120.0	S 30/45	0	-	1.58	1	-	-
	C13.1	10.3	0.0139	1.83	1.16	0.1600	13
	C13.2	9.9	0.0133	3.62	2.29	0.0360	67
	C13.3.1	9.8	0.0132	4.77	3.02	0.0291	84
	C13.3.2.1	10.0	0.0135	3.39	2.15	0.0386	63
	C13.4	9.9	0.0133	1.68	1.06	-	-

T = temperature [°C], S 30/45 = Shell 30/45 bitumen, Φ_M = volume fraction of montmorillonite, η' = dynamic viscosity [Pa·s], η/η_0 = relative viscosity, Φ^* = critical volume fraction of the dispersed particles, A_f = aspect ratio of the montmorillonite

The viscoelastic behaviour of two Shell 30/45-[MMT_{B1}/PEI(10kD)_{10Q}^{80R10}] composites (**C5.1** and **C5.2**) was studied in comparison to the Shell 30/45-[MMT_{B2}/PEI(10kD)_{10Q}^{60R14}] composite **C13.1** with the aim to evaluate the influence of the composition of the used polymers. While the composites **C13.1** and **C5.2** contained 10.0 wt.% of the corresponding adduct, the adduct concentration was set to be 5.0 wt.% with composite **C5.1**.

Figure 5.24 shows the storage modulus G' (a), the loss modulus G'' (b), and the phase angle δ (c) of the Shell 30/45 bitumen, composite **C5.1.2**, and composite **C5.2.1**. With composite **C5.1.2** the phase angle δ exhibited the same temperature dependence as the non-modified bitumen, i. e. a “steady growth”, but the value at a given temperature was shifted to a lower angle showing the higher elasticity of the composite in the temperature region of 40 – 120°C.

With composite **C5.2.1**, on the other hand, the temperature dependence of the phase

angle δ exhibited a “maximum/minimum” behaviour with max = 84° at 87°C and min = 81.6° at 112.5°C which implies that an adduct network was present in the composite which enhanced the elasticity of the bitumen at higher temperatures.

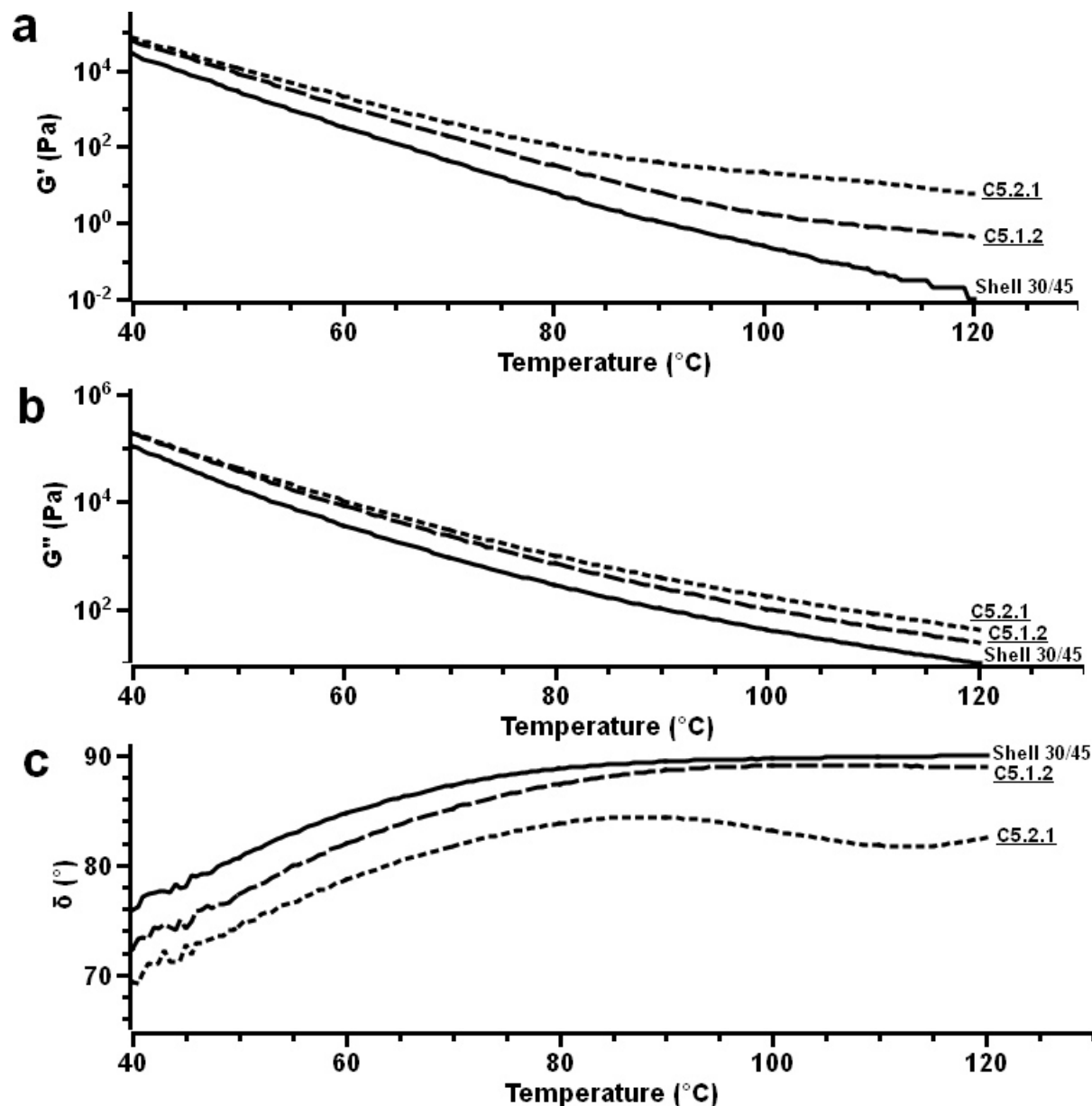


Figure 5.24: Rheology plots a) G' , b) G'' , and c) phase angle δ of Shell 30/45 bitumen, and the Shell 30/45-**E8** composites **C5.1.2** (5.0 wt.% **E8**) and **C5.2.1** (10.0 wt.% **E8**), **E8** = [MMT- B_1 /PEI(10kD) $_{10Q}^{80R10}$], $\omega = 6.28$ rad/s, $\sigma = 30$ Pa, $h = 1.0$ mm

Comparing the viscoelastic behaviour of composite **C5.2.1** with that of composite **C13.1** (cf. Figure 5.23) it was found that the [MMT- B_1 /PEI(10kD) $_{10Q}^{80R10}$] adduct used to prepare composite **C5.2.1** was able to enhance the elasticity of the bitumen much

more than the $[\text{MMT}_{\text{B2}}/\text{PEI}(10\text{kD})_{10\text{Q}}^{60\text{R}14}]$ adduct used to prepare composite **C13.1**. On the other hand, composite **C5.2.1** exhibited a lower maximum and minimum value compared to those of the composites **C13.2** and **C13.3.1** (max = 83.6° at 79.4°C, min = 79.8° at 102.5°C with **C13.2**, and max = 81.3° at 77.9°C, min = 76.3° at 101.5°C with **C13.3.1**, cf. Figure 5.23) which shows the lower elasticity of composite **C5.2.1** and points to that the preparation conditions were not optimised. But since composite **C5.2.1** exhibited a higher elasticity than composite **C13.1** it was concluded that the $[\text{MMT}_{\text{B1}}/\text{PEI}(10\text{kD})_{10\text{Q}}^{80\text{R}10}]$ adduct was more compatible with the Shell 30/45 bitumen.

Table 5.22: Aspect ratio of the montmorillonite of the composites **C5.1.2 and **C5.2.1****

T [°C]	Entry	Adduct [wt.%]	Φ_{M}	η' [Pa·s]	η/η_0	Φ^*	A_{r}
59.0	S 30/45	0	-	671.7	1	-	-
	C5.1.2	5.0	0.0066	1516.0	2.26	0.0037	673
	C5.2.1	10.0	0.0134	1925.0	2.87	0.0081	310
112.5	S 30/45	0	0	2.60	1	-	-
	C5.1.2	5.0	0.0066	6.22	2.39	0.0038	663
	C5.2.1	10.0	0.0134	11.06	4.25	0.0088	283
120.0	S 30/45	0	-	1.58	1	-	-
	C5.1.2	5.0		3.83	2.42	0.0038	660
	C5.2.1	10.0		6.74	4.27	0.0088	283

T = temperature [°C], S 30/45 = Shell 30/45 bitumen, Φ_{M} = volume fraction of montmorillonite, η' = dynamic viscosity [Pa·s], η/η_0 = relative viscosity, Φ^* = critical volume fraction of the dispersed particles, A_{r} = aspect ratio of the montmorillonite

In Table 5.22, the aspect ratios of the montmorillonite of the composites **C5.1.2** and **C5.2.1** are listed. The values were calculated for the temperatures of 59.0, 112.5°C and 120°C. With composite **C5.1.2** the montmorillonite exhibited an average aspect ratio of 665 ± 6 and with composite **C5.2.1** of 292 ± 13 . The relative error was found to be below 5 % with both composites which show that the adduct dispersions were stable in the temperature region of 59 – 120°C. The high aspect ratio of the montmorillonite of composite **C5.1.2** shows that the montmorillonite was mainly dispersed as single platelets. As shown from the ratio of the montmorillonite of composite **C5.2.1**, agglomeration of the montmorillonite occurred when the adduct concentration was raised to 10.0 wt.%. Compared to the average aspect ratio of the montmorillonite of composite **C13.3.1** ($A_{\text{r}} = 71$, cf. Table 5.21), the aspect ratio of composite **C5.2.1** was 4 times higher which shows that the used polymer promoted the exfoliation of the montmorillonite platelets in the bitumen strongly.

5 Preparation of bitumen-[montmorillonite/PEI(nkD)xQyR] composites

To investigate to which extent the [MMT/PEI(10kD)_{10Q}^{80R10}] and the [MMT/PEI(10kD)_{10Q}^{60R14}] adduct influenced the viscoelastic behaviour of polymer-modified bitumen (BP Olexobit 45 and Shell Cariphalte 25/55-55), composites containing 10.0 wt.% of the respective adduct were prepared. Figure 5.25 shows the storage modulus G' (a), the loss modulus G'' (b), and the phase angle δ (c) of the BP Olexobit 45 bitumen, composite **C6.2.2**, and composite **C14.1**.

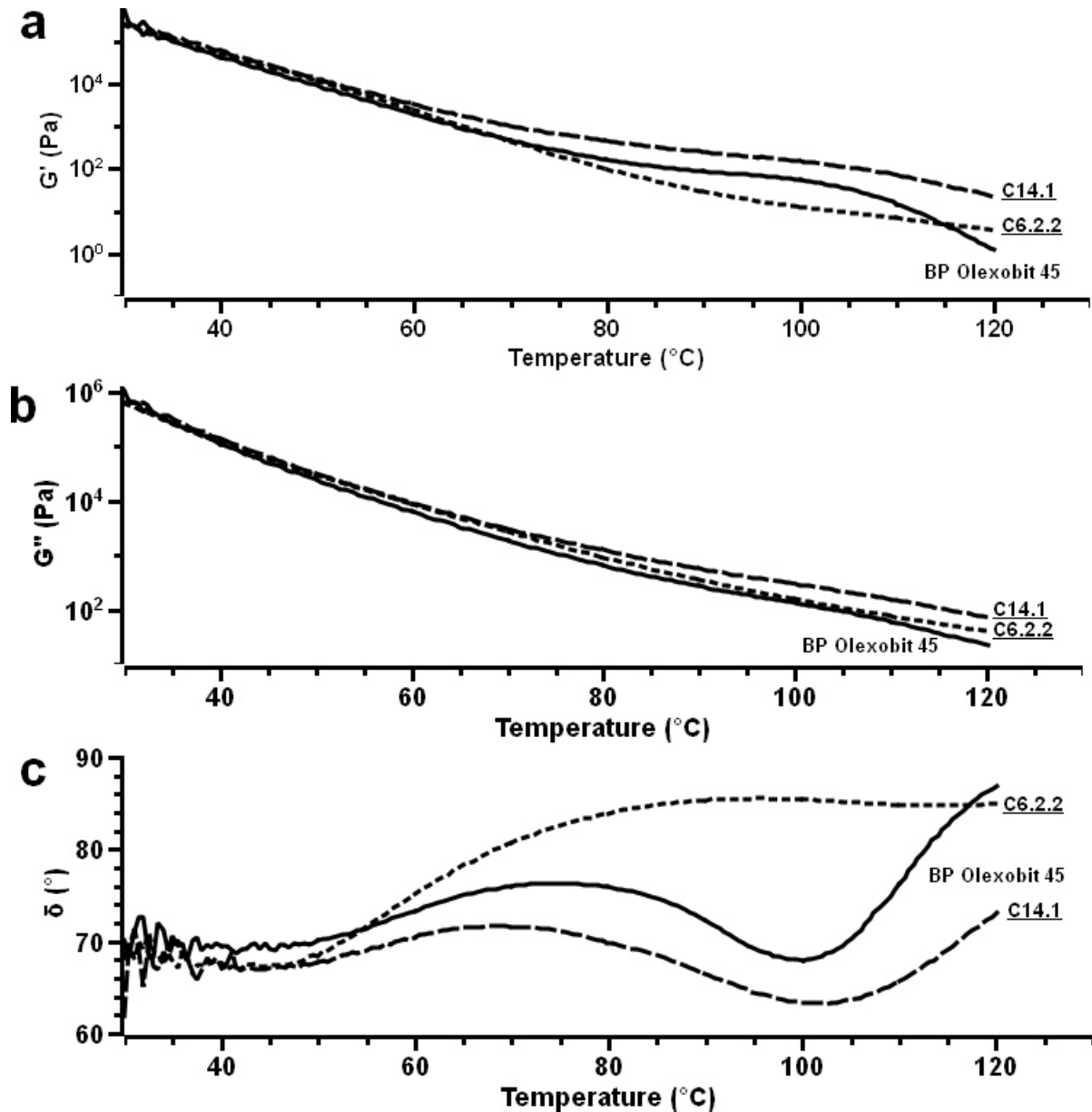


Figure 5.25: Rheology plots of a) G' , b) G'' , and c) phase angle δ of BP Olexobit 45 bitumen, the BP Olexobit 45-**E8** composite **C6.2.2** (10.0 wt.% **E8**), and the BP Olexobit 45-**E15** composite **C14.1** (10.0 wt.% **E15**), **E8** = [MMT_{B1}/PEI(10kD)_{10Q}^{80R10}], **E15** = [MMT_{B2}/PEI(10kD)_{10Q}^{60R14}], $\omega = 6.28$ rad/s, $\sigma = 30$ Pa, $h = 1.0$ mm

With the BP Olexobit 45 bitumen, the phase angle δ showed an almost constant value of 70° between 30 and 51°C . With increasing temperature, the temperature dependence of the phase angle showed the typical “maximum/minimum” behaviour of polymer-modified bitumina shown by that the angle rose up to a maximum of 76.3° at 73.4°C and declined then steadily up to a minimum of 68.0° at 100.1°C . Between 100.1 and 120°C , the angle increased again steadily and reached a value of 86.9° at 120°C . Besides the enhancement of the elasticity at higher temperatures due to the polymer network inside the bitumen, the almost constant value of the phase angle in the temperature region of 30 and 51°C shows that the added polymer enhanced the elasticity of the bitumen also at lower temperatures.

With the composites **C6.2.2** and **C14.1**, the phase angle δ exhibited also an almost constant value of about 68° in the temperature region of 30 to 50°C which shows that both adduct types have only little influence on the bitumen at low temperatures. At higher temperatures, on the other hand, the temperature dependence of the phase angle was different with each composite. While with composite **C6.2.2** the phase angle exhibited a weak “maximum/minimum” behaviour at high angles of $\text{max} = 85.5^\circ$ at 96°C and $\text{min} = 84.8^\circ$ at 115.5°C which shows the low elasticity of this composite, the maximum and minimum value was considerably lower with composite **C14.1** ($\text{max} = 71.8^\circ$ at 68.9°C , $\text{min} = 63.2^\circ$ at 102.5°C). The different values of the maximum and minimum of the composites show that while the $[\text{MMT}_{\text{B1}}/\text{PEI}(10\text{kD})_{10\text{Q}}^{80\text{R}10}]$ adduct lowered the elasticity of the base bitumen, the addition of the $[\text{MMT}_{\text{B2}}/\text{PEI}(10\text{kD})_{10\text{Q}}^{60\text{R}14}]$ adduct had an enhancement effect. This result points to that while the $[\text{MMT}_{\text{B1}}/\text{PEI}(10\text{kD})_{10\text{Q}}^{80\text{R}10}]$ adduct exhibited only a poor compatibility with the BP Olexobit 45 bitumen, the $[\text{MMT}_{\text{B2}}/\text{PEI}(10\text{kD})_{10\text{Q}}^{60\text{R}14}]$ adduct was well compatible with it.

Table 5.23 lists the aspect ratios of the montmorillonite of the composites **C6.2.2** and **C14.1**. The values are calculated for the temperatures of 49.0 , 73.5 , 100.0 , and 120.0°C . These temperatures were chosen to take the viscoelastic behaviour of the non-modified bitumen at these temperatures into account (cf. Figure 5.25).

It was found that the average aspect ratios of the montmorillonite were similar with both composites. Composite **C6.2.2** exhibited an average aspect ratio of 37 ± 20 , and composite **C14.1** of 55 ± 23 . The relative error was calculated to be 55% with composite **C6.2.2** and 41% with composite **C14.1** which shows that the delamination of the montmorillonite stacks may depend on the temperature. The average aspect ratio obtained by using the values of the three temperatures 73.5 , 100.0 , and 120.0°C was with **C14.1** determined to be 65 ± 15 with a relative error of 23% . But as shown from the low aspect ratios both composites contained montmorillonite stacks build up of

several montmorillonite platelets and no exfoliated montmorillonite platelets.

Table 5.23: Aspect ratio of the montmorillonite of the composites C6.2.2 and C14.1

T [°C]	Entry	Adduct [wt.%]	Φ_M	η' [Pa·s]	η/η_0	Φ^*	A_f
49.0	B 45	0	-	4392	1	-	-
	<u>C6.2.2</u>	10	0.0109	5413	1.23	0.0930	24
	<u>C14.1</u>	10	0.0135	5609	1.28	0.0980	23
73.5	B 45	0	-	202.6	1	-	-
	<u>C6.2.2</u>	10	0.0109	286.1	1.41	0.0590	40
	<u>C14.1</u>	10	0.0135	348.6	1.72	0.0505	47
100.0	B 45	0	-	20.99	1	-	-
	<u>C6.2.2</u>	10	0.0109	24.86	1.18	0.1150	19
	<u>C14.1</u>	10	0.0135	46.74	2.23	0.0373	65
120.0	B 45	0	-	3.57	1	-	-
	<u>C6.2.2</u>	10	0.0109	6.42	1.80	0.0380	64
	<u>C14.1</u>	10	0.0135	11.19	3.13	0.0291	84

T = temperature [°C], B 45 = BP Olexobit 45 bitumen, Φ_M = volume fraction of montmorillonite, η' = dynamic viscosity [Pa·s], η/η_0 = relative viscosity, Φ^* = critical volume fraction of the dispersed particles, A_f = aspect ratio of the montmorillonite

The second polymer-modified bitumen modified with 10.0 wt.% of the [MMT_{B2}/PEI(10kD)_{10Q}^{60R14}] adduct **E15** was the Shell Cariphalte 25/55-55 bitumen. Figure 5.26 compares the storage modulus G' (a), the loss modulus G'' (b), and the phase angle δ (c) of the Shell Cariphalte 25/55-55 bitumen and composite **C15.1**.

The temperature dependence of the phase angle δ of the Shell Cariphalte 25/55-55 bitumen exhibited the same “steady growth” behaviour as known from non-polymer modified bitumen (cf. Figure 5.15) shown by a strong increase from 67° at 40°C up to 88.3° at 89°C and a slow increase up to a value of 89.6° at 120°C. Since no polymer network was detected it was concluded that the base bitumen and the polymer were not compatible which led to a non-uniform distribution of the polymer in the bitumen and the measured fraction contained possibly only a small amount of polymer.

With composite **C15.1**, on the other hand, a “maximum/minimum” behaviour typical for a polymer-modified bitumen was detected. The phase angle δ increased from about 63° at 40°C up to a maximum of 78° at 81°C and declined then until it reached a minimum of 74.9° at 104.6°C. Between 104.6 and 120°C, the phase angle increased again slowly until a value of 76.3° at 120°C. As shown by the increase of the

elasticity between 81 and 104.6°C, an adduct network was present in the bitumen which shows that the adduct was at least compatible with the base bitumen. But the lower elasticity of composite **C15.1** compared to that of composite **C14.1** (max = 71.8° at 68.9°C, min = 63.2° at 102.5°C) shows that the adduct was less compatible with the Shell Cariphalte 25/55-55 bitumen than it was with the BP Olexobit 45 bitumen.

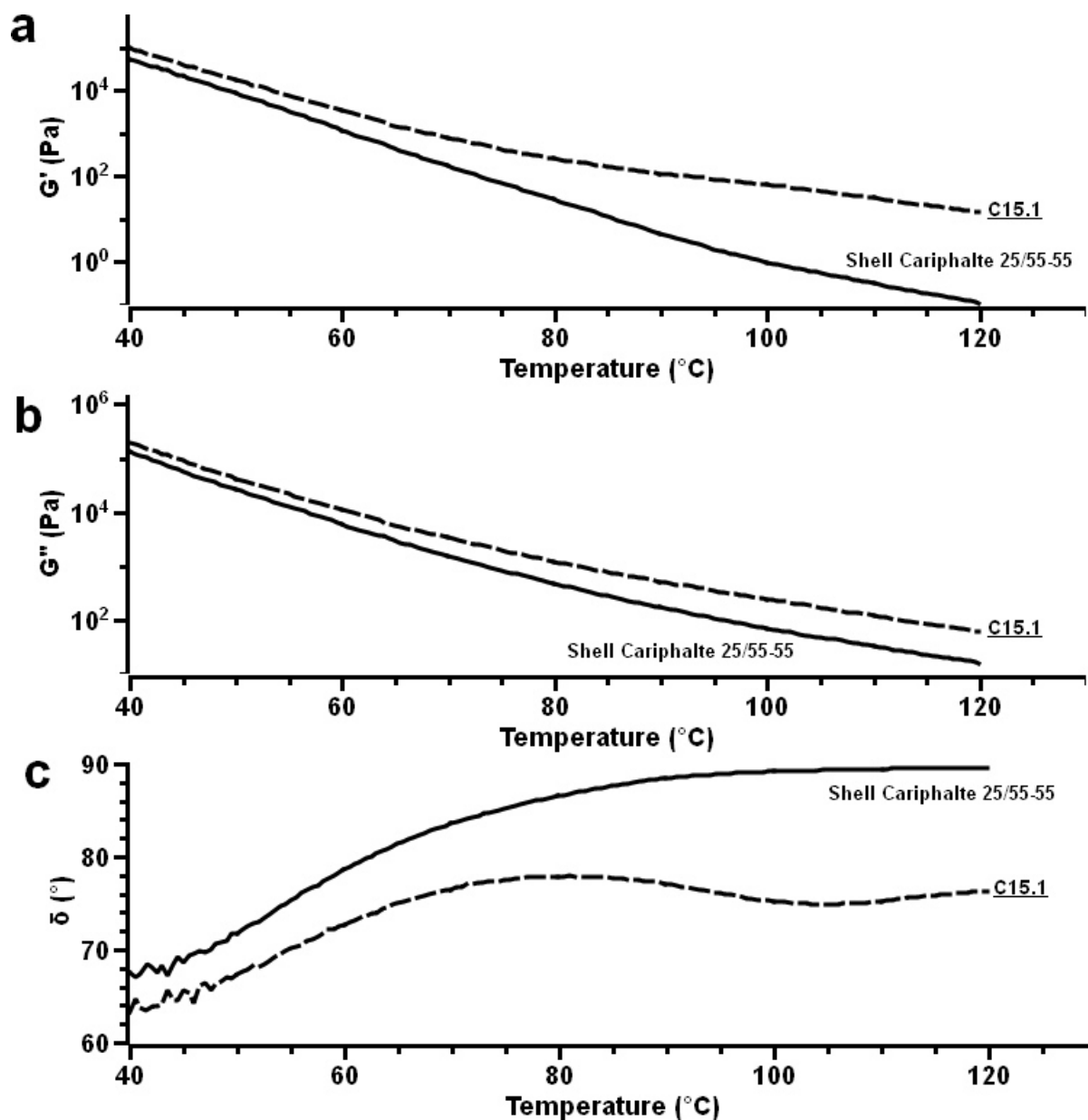


Figure 5.26: Rheology plots of a) G' , b) G'' , and c) phase angle δ of Shell Cariphalte 25/55-55 bitumen and the Shell Cariphalte 25/55-55-**E15** composite **C15.1** (10.0 wt.% **E15**), **E15** = [MMT_{B2}/PEI(10kD)_{10Q}^{60R14}], $\omega = 6.28$ rad/s, $\sigma = 30$ Pa, $h = 1.0$ mm

In Table 5.24 the aspect ratio of the montmorillonite in composite **C15.1** at 72.5, 104.6, and 120°C is listed. The average aspect ratio was found to be 83 ± 12 with a relative error of 15 %. The aspect ratio was higher than with composite **C14.1** of 65 ± 15 (cf. Table 5.23) showing that the montmorillonite stacks exhibited a higher degree of delamination.

Table 5.24: Aspect ratio of the montmorillonite of composite C15.1

T [°C]	Entry	Adduct [wt.%]	Φ_M	η' [Pa·s]	η/η_0	Φ^*	A_f
72.5	S Car	0	-	178.7	1	-	-
	C15.1	10	0.0135	404.4	2.26	0.0365	66
104.6	S Car	0	-	7.68	1	-	-
	C15.1	10	0.0135	27.48	3.58	0.0268	90
120.0	S Car	0	-	2.53	1	-	-
	C15.1	10	0.0135	9.56	3.78	0.0261	93

T = temperature [°C], S Car = Shell Cariphalte 25/55-55 bitumen, Φ_M = volume fraction of montmorillonite, η' = dynamic viscosity [Pa·s], η/η_0 = relative viscosity, Φ^* = critical volume fraction of the dispersed particles, A_f = aspect ratio of the montmorillonite

Discussion

In this study bitumen-[montmorillonite/organo] nanocomposites prepared under different conditions were characterised by rheology. The investigated parameters which could influence the viscoelastic behaviour of the composites were the adduct preparation method, the applied compounding procedure, the weight concentration of the adduct, the adduct composition, and the used bitumen. Samples prepared under systematic variations of these parameters have been measured from 30 – 120°C with oscillation rheology to determine $G'(T)$, $G''(T)$, and $\delta(T)$. The rheology data were used to estimate the aspect ratio A_f of the montmorillonite in the composites according to the procedure described by Bicerano, Douglas and Brune [10].

The comparison of a composite containing 10.0 wt.% of an [MMT_{B1}/PEI(10kD)_{5Q}^{67R10}] adduct prepared by the “direct addition” (= **C2.3**) with a composite containing 10.0 wt.% of an [MMT_{B1}/PEI(10kD)_{10Q}^{80R10}] adduct prepared by the “indirect replacement” method (= **C3.2**) showed that when non-pre-ground adducts were used composites containing large adduct agglomerates were obtained independently of the adduct preparation method as indicated by a steady increase of the composites elasticity with increasing temperatures. Different to composite **C2.3**, composite **C3.2** showed no enhancement effect at lower temperatures which was interpreted as a sign for a

higher stability of the adduct dispersion in the composite and, therefore, for a better compatibility of adducts prepared by the “indirect replacement” method with bitumina.

To test the influence of the compounding conditions on the viscoelastic behaviour of bitumen-[MMT_{B1}/PEI(10kD)_{10Q}^{80R10}] composites, adducts pre-ground either at 20°C to 1 – 3 cm pieces or under liquid nitrogen to fragments with diameters of 0.1 – 1 cm were added to 50/70 bitumina. While the viscoelastic behaviour of a composite which contained 5.0 wt.% of an at 20°C pre-ground adduct was similar to that of the neat bitumen, the phase angle exhibited a temperature dependence as known from styrene-butadiene-styrene (SBS) modified bitumen [13] which was characterised by that with increasing temperature the phase angle increased up to a maximum, decreased then until it reached a minimum and rose again after the adduct concentration was raised to 10.0 wt.%. This temperature dependence indicates that an adduct network was present in the bitumen which shows that the pre-grinding step supported the delamination of the adduct particles. On the other hand, with adducts pre-ground to 0.1 – 1 cm pieces the presence of an adduct network was already detectable with an adduct concentration of 5.0 wt.% showing that the smaller the added adduct pieces were the easier they could be dispersed in a bitumen, i. e. the smaller pieces could be broken down more easily by the applied shear force which created a high number of small adduct particles which were, due to their large surface, able to interact with the bitumen matrix more effectively.

The evaluation of Shell 30/45-[MMT_{B2}/PEI(10kD)_{10Q}^{60R14}] composites prepared with different extrusion temperatures and shear rates showed that high shear rates caused composites with a high elasticity, i. e. an adduct network in the composites to form, which points to the conclusion that larger adduct particles were broken down to smaller sizes which created small particles with a large surface. The best preparation condition found was an extrusion temperature of 120°C and a rotational speed of the extruder screw of 130 min⁻¹. On the other hand, when the extrusion temperature was raised to 160°C the viscoelastic behaviour of the prepared composite was identical to that of the non-modified bitumen which indicates that the viscosity of the base bitumen was too low at this temperature to enable an interaction between the bitumen and the adduct.

The influence of the adduct concentration was tested by adding either an [MMT_{B1}/PEI(10kD)_{10Q}^{80R10}] adduct (= **E10**) or an [MMT_{B2}/PEI(10kD)_{10Q}^{60R14}] adduct (= **E15**) to a Total Azalt 50/70 bitumen. Both adduct types were pre-ground to 0.1 – 1 cm pieces before added to the bitumen. It was found that when 1.0 - 2.5 wt.% of adduct **E10** were added to the bitumen the elasticity of the composites increased with

increasing concentration, but no adduct network was measured. When 1.0 wt.% of adduct **E15** was added, on the other hand, the viscoelastic behaviour of the composite was the same as the non-modified bitumen, the adduct concentration was, therefore, too low to have an influence on the bitumen. But when the adduct concentration of the adducts **E10** and **E15** exceeded 5.0 wt.% the phase angle exhibited a temperature dependence which indicated the presence of an adduct network in the bitumen. On the other hand, the Total Azalt 50/70-[MMT_{B2}/PEI(10kD)_{10Q}^{80R10}] composite which contained 4.9 wt.% of adduct **E9** didn't show the presence of a network. The adduct exhibited a lower montmorillonite content compared to those of the adducts **E10** and **E15** which indicates that the ratio polymer to montmorillonite plays an important role in the formation of an adduct network in the bitumen.

The influence of the adduct composition on the viscoelastic behaviour of a Total Azalt 50/70 bitumen and the aspect ratio of the montmorillonite in the composites was studied by comparing composites which contained either 5.0 wt.% or 10.0 wt.% of the [MMT_{B1}/PEI(10kD)_{10Q}^{80R10}] adduct **E10**, the [MMT_{B2}/PEI(10kD)_{10Q}^{60R14}] adduct **E15**, or the [MMT_{B1}/CTAB] adduct **E4**. While the composites containing either adduct **E10** or adduct **E15** showed the presence of an adduct network in the bitumen, no network was detected with composites containing adduct **E4**. It was, therefore, concluded that an adduct network was formed only when a polymer was attached to the montmorillonite. Furthermore, with composites prepared with adduct **E15** the network was detected at lower temperatures compared to composites containing adduct **E10** which indicates that the melt and glass transition of the used polymers influenced at which temperature the adduct network enhanced the elasticity of the bitumen.

The calculation of the aspect ratio of the montmorillonite in Total Azalt 50/70-[MMT/organo] composites at three temperatures showed that the montmorillonite exhibited in composites containing the [MMT_{B1}/PEI(10kD)_{10Q}^{80R10}] adduct **E10** average aspect ratios of 651 ± 17 (5.0 wt.% **E10**) and 284 ± 15 (10.0 wt.% **E10**) and in the composite containing 4.9 wt.% of the [MMT_{B2}/PEI(10kD)_{10Q}^{80R10}] adduct **E9** an aspect ratio of 977 ± 2 . The high aspect ratios of the montmorillonite in the composites containing ≈ 5 wt.% of the [MMT_{B1,B2}/PEI(10kD)_{10Q}^{80R10}] adducts indicates that the composites contained a high number of exfoliated montmorillonite platelets but with a concentration of 10.0 wt.% montmorillonite stacks consisting of several montmorillonite platelets were present probably by that when the adduct concentration exceeded a certain limit the platelets were attracted to each other. The small relative errors of 0.2 - 5 % show furthermore that the particle dispersions were stable in the temperature region of 30 – 120°C.

On the other hand, the average aspect ratios from three temperatures of Total Azalt 50/70-[MMT_{B2}/PEI(10kD)_{10Q}^{60R14}] composites prepared with the adduct **E15** were lower than those of the Total Azalt 50/70-[MMT_{B1,B2}/PEI(10kD)_{10Q}^{80R10}] composites and exhibited a ratio of 71 ± 3 (5.0 wt.% **E15**) and 79 ± 11 (10.0 wt.% **E15**). The lower aspect ratios show that the adducts consisted of montmorillonite stacks with several montmorillonite platelets which lead to the conclusion that adduct **E15** could not be used to obtain composites with exfoliated montmorillonite platelets. Composites containing the [MMT_{B1}/CTAB] adduct **E4** exhibited even lower average aspect ratios of 34 ± 3 (5.0 wt.% **E4**) and 39 ± 4 (10.0 wt.% **E4**) which shows that the montmorillonite stacks consisted of even more montmorillonite platelets than with the Total Azalt 50/70-[MMT_{B2}/PEI(10kD)_{10Q}^{60R14}] composites which point to a very low compatibility of the [MMT_{B1}/CTAB] adduct with the Total Azalt 50/70 bitumen.

It was further tested how the [MMT_{B1}/PEI(10kD)_{10Q}^{80R10}] adducts **E8** and **E10** and the [MMT_{B2}/PEI(10kD)_{10Q}^{60R14}] adduct **E15** influenced bitumina with the same pen-grade but of different origin (Total Azalt 50/70 and Nynas 50/70), bitumen of a higher pen-grade (Shell 30/45) and polymer-modified bitumina (BP Olexobit 45 and Shell Cariphalte 25/55-55).

The comparison of the elasticity and the particles aspect ratios of a Nynas 50/70-[MMT_{B2}/PEI(10kD)_{10Q}^{60R14}] and a Total Azalt 50/70-[MMT_{B2}/PEI(10kD)_{10Q}^{60R14}] composite, both modified with 10.0 wt.% of adduct **E15** showed that the Nynas 50/70-[MMT_{B2}/PEI(10kD)_{10Q}^{60R14}] composite exhibited a lower elasticity and a lower aspect ratio of the montmorillonite than the values measured with the Total Azalt 50/70-[MMT_{B2}/PEI(10kD)_{10Q}^{60R14}] composite. Hence, the origin of the bitumen had, in fact, an influence of the compatibility of the adduct with the bitumen.

The comparison of the viscoelastic properties of Shell 30/45-[MMT_{B1}/PEI(10kD)_{10Q}^{80R10}] and Shell 30/45-[MMT_{B2}/PEI(10kD)_{10Q}^{60R14}] composites, and the aspect ratios of the montmorillonite in the composites showed that with an adduct concentration of 10.0 wt.% and with the same preparation condition the 30/45-[MMT_{B1}/PEI(10kD)_{10Q}^{80R10}] composite exhibited a higher elasticity and a higher average aspect ratio which shows that the [MMT_{B1}/PEI(10kD)_{10Q}^{80R10}] adduct **E8** was more compatible with the Shell 30/45 bitumen than the [MMT_{B2}/PEI(10kD)_{10Q}^{60R14}] adduct **E15**. Although the Shell 30/45-[MMT_{B2}/PEI(10kD)_{10Q}^{60R14}] composite, prepared under optimised preparation conditions, exhibited a higher elasticity than a Shell 30/45-[MMT_{B1}/PEI(10kD)_{10Q}^{80R10}] composite, prepared under poor conditions, the average aspect ratio of the montmorillonite was still lower by a factor of four. This demonstrates that the addition of both adduct types leads to composites with a high elasticity but the used polymer influenced the exfoliation of the montmorillonite

platelets in the bitumen. With both adduct types, an adduct concentration of 10.0 wt. % was necessary for the formation of an adduct network.

The investigation of composites consisting of a polymer-modified BP Olexobit 45 bitumen and either a the $[\text{MMT}_{\text{B1}}/\text{PEI}(10\text{kD})_{10\text{Q}}^{80\text{R}10}]$ adduct **E8** or the $[\text{MMT}_{\text{B2}}/\text{PEI}(10\text{kD})_{10\text{Q}}^{60\text{R}14}]$ adduct **E15** (modified with 10.0 wt.% of the respective adduct) revealed that both adduct types only slightly influenced the viscoelastic behaviour of the bitumen at low temperatures. At higher temperatures, on the other hand, the elasticity of the composite containing adduct **E15** was higher and the elasticity of the composite containing adduct **E8** lower compared to that of the base bitumen which indicates that in contrast to the polymer used to prepare adduct **E8** the polymer used to prepare adduct **E15** was well compatible with the bitumen.

The comparison of the viscoelastic behaviour of neat Shell Cariphalte 25/55-55 bitumen and a Shell Cariphalte 25/55-55- $[\text{MMT}_{\text{B2}}/\text{PEI}(10\text{kD})_{10\text{Q}}^{60\text{R}14}]$ composite containing 10.0 wt.% of adduct **E15** revealed that the composite exhibited a higher elasticity at a given temperature which shows that the polymer used to prepare adduct **E15** was also well compatible with the Shell Cariphalte 25/55-55 bitumen. On the other hand, the low average aspect ratios of the montmorillonite of 36 ± 20 (BP Olexobit 45- $[\text{MMT}_{\text{B1}}/\text{PEI}(10\text{kD})_{10\text{Q}}^{80\text{R}10}]$), 43 ± 15 (BP Olexobit 45- $[\text{MMT}_{\text{B2}}/\text{PEI}(10\text{kD})_{10\text{Q}}^{60\text{R}14}]$), and 84 ± 13 (Shell Cariphalte 25/55-55- $[\text{MMT}_{\text{B2}}/\text{PEI}(10\text{kD})_{10\text{Q}}^{60\text{R}14}]$) shows that all three composites contained montmorillonite stacks build up of several montmorillonite platelets which point to the conclusion that with both adduct types composites with exfoliated montmorillonite platelets could not be obtained.

Summary

Bitumen-[montmorillonite/organo] nanocomposites were investigated with oscillation rheology to determine the influence of the adduct preparation method, the applied compounding procedure, the weight concentration of the adduct in the respective composite, the adduct composition, and the used bitumen on the viscoelastic behaviour of the composites. The aspect ratio A_f of the montmorillonite in the composites was estimated from rheological data to semi-quantitatively judge the degree of exfoliation.

Comparing the viscoelastic behaviour of composites containing either an $[\text{MMT}_{\text{B1}}/\text{PEI}(10\text{kD})_{5\text{Q}}^{67\text{R}10}]$ adduct prepared by the “direct addition” or an $[\text{MMT}_{\text{B1}}/\text{PEI}(10\text{kD})_{10\text{Q}}^{80\text{R}10}]$ adduct prepared by the “indirect replacement” method it was found that composites consisting of non-polymer-modified bitumen and an adduct prepared by the “indirect replacement” method exhibited a more stable

particle dispersion which points to a better compatibility of these adducts with bitumen.

The evaluation of composites prepared under different conditions showed that composites with high elasticity were obtained when the adducts were pre-ground to 0.1 – 1 nm pieces and the adducts were pre-mixed with the bitumen before extrusion. Furthermore, with high shear rates larger adduct pieces were broken down which led to a further increase of the elasticity. Of the studied extrusion temperatures and shear rates, the extrusion temperature of 120°C with the shear rate of 130 min⁻¹ was found to be the most suitable for the preparation of the composites.

Depending on the applied compounding procedure, the composites composition, and the weight concentration of the adduct in the respective composite the temperature dependence of the phase angle δ exhibited one of three different behaviours.

A “steady growth” (of the angles δ) behaviour was measured with neat non-polymer-modified bitumina, as well as with composites containing very small quantities of [MMT_{B1,B2}/PEI(10kD)_{10Q}^{YR}] adducts (≤ 2.5 wt.%), and with composites prepared by using [MMT_{B1}/CTAB] adducts. This behaviour was characterised by a continuous rising of δ on increasing temperature, approaching 90° at a certain temperature. Hence, with increasing temperature, the bitumen became increasingly more liquid indicating that at low adduct concentrations the adducts were not able to influence the temperature dependence of the base bitumina.

A “steady decline” of δ behaviour was detected with composites prepared by using non- and poorly pre-ground adducts. In this case, the phase angle declined steadily with increasing temperature, i. e. the bitumen became increasingly more elastic, which points to a segregation of the adducts from the bitumen.

With polymer-modified bitumina and composites prepared under optimised conditions, i. e. adducts pre-ground to a fine powder and the adducts pre-mixed with the bitumen before extrusion, and with adduct concentrations ≥ 5.0 wt.% the temperature dependence of the phase angle exhibited a “maximum/minimum” behaviour which points to the presence of a polymer and an adduct network in the bitumina. The formation of an adduct network was desired since such a network enhanced the mechanical properties of the bitumen at higher temperatures.

The aspect ratio A_f of the montmorillonite in the studied bitumen-nanocomposites is shown in Figure 5.27. It was found that the aspect ratio depended on the adduct composition, the weight concentration of the adduct in the respective composite, and the bitumen type. While very high aspect ratios were obtained when a Total Azalt 50/70 bitumen was modified with 5 wt.% of an [MMT_{B1,B2}/PEI(10kD)_{10Q}^{80R10}] adduct (= R10), the aspect ratio decreased when the concentration was raised to 10 wt.%

which indicates that the adduct formed agglomerates at higher concentrations. But the aspect ratio was similar to that measured with the composite using Shell 30/45 bitumen as the base bitumen which shows that the pen-grade of the bitumen played only a minor role. The aspect ratios measured with Total Azalt 50/70-[MMT_{B2}/PEI(10kD)_{10Q}^{60R14}] composites were found to be lower compared to those containing an [MMT_{B1,B2}/PEI(10kD)_{10Q}^{80R10}] adduct which points to a lower compatibility of this adduct type with the bitumen. On the other hand, Total Azalt 50/70-[MMT_{B1}/CTAB] composites exhibited even lower aspect ratios showing that the compatibility of the adducts with non-polymer-modified bitumina increased from [MMT_{B1}/CTAB] < [MMT_{B2}/PEI(10kD)_{10Q}^{60R14}] < [MMT_{B1,B2}/PEI(10kD)_{10Q}^{80R10}]. The modification of the polymer-modified BP-Olexobit 45 bitumen with R10 and R14 adducts led to composites with very low aspect ratios which show the very low compatibility of this adduct types with this bitumen.

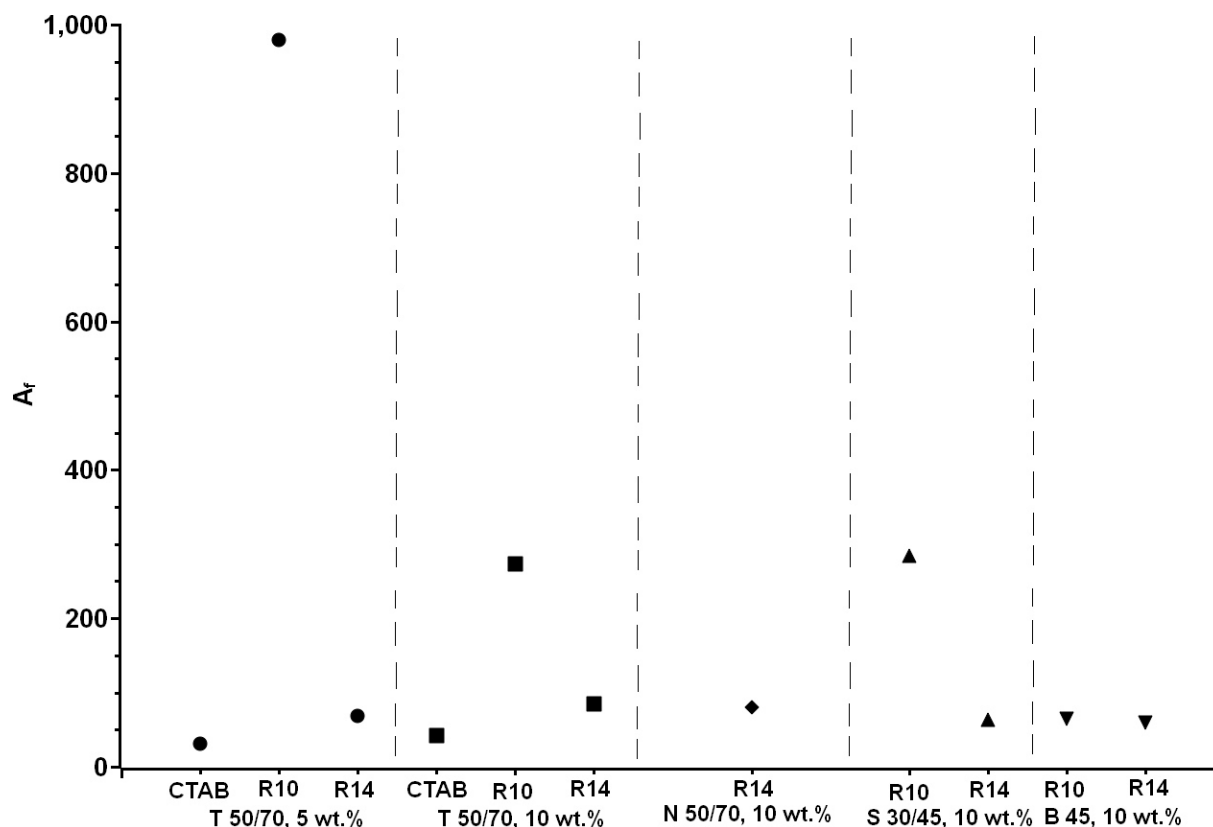


Figure 5.27: Aspect ratio A_r of montmorillonite in bitumen-nanocomposites (N 50/70 = Nynas 50/70 bitumen, T 50/70 = Total Azalt 50/70 bitumen, S 30/45 = Shell 30/45 bitumen, B 45 = BP Olexobit 45 bitumen, CTAB = [MMT_{B1}/CTAB], R10 = [MMT_{B1,B2}/PEI(10kD)_{10Q}^{80R10}], R14 = [MMT_{B2}/PEI(10kD)_{10Q}^{60R14}])

5.4 Conclusion

In this study bitumen-[montmorillonite/organo] nanocomposites were characterised by polarised light and dark field microscopy, as well as with oscillation rheology to investigate their morphology and viscoelastic behaviour. In addition, the aspect ratio A_f of the montmorillonite in the composites was estimated from rheological data. The composites were prepared by adding [montmorillonite/organo] adducts consisting of (i) montmorillonite modified with CTAB (= [MMT/CTAB]), (ii) [MMT/PEI(10kD)_{5Q}^{67R10}] prepared by the “direct addition” method, (iii) [MMT/PEI(10kD)_{10Q}^{80R10}], and (iv) [MMT/PEI(10kD)_{10Q}^{60R14}], the last two types prepared by the “indirect replacement” method to polymer- and non-polymer-modified bitumina with the aim to test the influence of (i) the adduct preparation method, (ii) the applied compounding procedure, (iii) the weight concentration of the adduct, (iv) the adduct composition, and (iv) the used bitumen. Comparing the viscoelastic behaviour of composites containing an adduct prepared by the “direct addition” method with that of composites containing an adduct prepared by the “indirect replacement” method revealed that with the latter adduct type the particle dispersion in the composite was more stable which indicates a higher compatibility of these adducts with bitumina. Through optimising the compounding procedure it was found that by using adducts which were pre-ground to a powder and by pre-mixing the adducts with the bitumen before extrusion composites exhibiting a high number of particles with diameters around 1 μm were obtained when non-polymer-modified bitumina were modified. Furthermore, the rheological investigation of composites prepared under optimised conditions revealed that starting with an adduct concentration of 5 wt.% an adduct network was present in the bitumina which enhanced their elasticity at higher temperatures. The aspect ratios of the montmorillonite in bitumen-[MMT/PEI(10kD)_{10Q}^{80R10}] composites were very high which points to the presence of mainly exfoliated montmorillonite platelets in the bitumina and shows the good compatibility of these adduct type with non-polymer modified bitumina. The aspect ratios measured with composites containing either [MMT/PEI(10kD)_{10Q}^{60R14}] or [MMT/CTAB] adducts were much lower which points to the presence of montmorillonite stacks consisting of several montmorillonite platelets in the bitumina. Nonetheless, the aspect ratios were higher with [MMT/PEI(10kD)_{10Q}^{60R14}] adducts showing that the [MMT/CTAB] adduct was inferior to the other two adduct types. The modification of polymer-modified bitumina with either [MMT/PEI(10kD)_{10Q}^{80R10}] or [MMT/PEI(10kD)_{10Q}^{60R14}] adducts, on the other hand, led to composites with phase segregated structures and very low aspect ratios which show the incompatibility of these adduct types with polymer-modified bitumina. By testing the influence of the extrusion temperature and the shear rate it was found that at higher shear rates larger adduct agglomerates were broken down into smaller pieces which were able to interact with the bitumen matrix more efficiently due to their larger surface. In further attempts, it should be tested whether the time-consuming steps pre-grinding of the adducts and pre-mixing of the adducts with the bitumen could be avoided by mixing both compounds in a high-shear mixer. Since the chain length of the alkyl moieties of the polymers had an influence on the viscoelastic behaviour of the bitumina other groups which have an even higher compatibility should also be tried.

References

- 1 Nielsen, L.; Models for the Permeability of Filled Polymer Systems; *Journal of Macromolecular Science: Part A - Chemistry* 1 (1967) 929 – 942
- 2 Zhang H.L., Yu J. Y., Xue L. H., Li Z. C.; Effect of montmorillonite organic modification on microstructures and ultraviolet aging properties of bitumen; *Journal of Microscopy* 244 (2011) 85 - 92
- 3 Mahdi L. M. J., Muniandy R., Yunus R. B., Hasham S., Aburkaba E.; Effect of Short Term Aging on Organic Montmorillonite Nanoclay Modified Asphalt; *Indian Journal of Science and Technology* 6 (2013) 5434 - 5442
- 4 You Z., Mills-Beale J., Foley J. M., Roy S., Odegard G. M., Dai Q., Goh S. W.; Nanoclay-modified asphalt materials: Preparation and characterization; *Construction and Building Materials* 25 (2011) 1072 - 1078
- 5 AMO - Asphalt-Mischwerke Osnabrück GmbH & Co. KG, Mischwerk Osnabrück-Piesberg, Süberweg 60, 49090 Osnabrück, Germany
- 6 Petersen J.C., Robertson R. E., Branthaver J. F., Harnsberger P. M., Duvall J. J., Kim S. S., Anderson D. A., Christiansen D. W., Bahia H. U., Dongre R., Antle C. E., Sharma M. G., Button J., Glover J. C.; SHRP-A-370 Binder Characterization and Evaluation Volume 4 (1994)
- 7 ISO 6721-1:2011
- 8 Macosko C. W.; *Rheology: principles, measurements and applications* (1994)
- 9 Mezger T. G.; *The rheology handbook: for users of rotational and oscillatory rheometers* 2nd Edition (2006)
- 10 Bicerano J., Douglas J. F., Brune D. A.; Model for the Viscosity of Particle Dispersions; *Journal of Macromolecular Science, Part C* 39 (1999) 561 – 642
- 11 Ploehn H. J., Liu C.; Quantitative Analysis of Montmorillonite Platelet Size by Atomic Force Microscopy; *Industrial Engineering Chemistry Research* 45 (2006) 7025 - 7034
- 12 Polacco G., Stastna J., Vlachovicova Z., Biondi D., Zanzotto L.; Temporary Networks in Polymer-Modified Asphalts; *Polymer Engineering & Science* 44 (2004) 2185 – 2193
- 13 Lu X., Soenen H., Redelius P.; Rheological Characterization of Polymer Modified Bitumens; *Annual Transactions of the Nordic Rheology Society* 19 (2011)

6 Preparation of [montmorillonite/PEI(nkD)_xQ^yPS(nkD)]

6.1 Introduction

The aim of this work was it to prepare a polystyrene-quat-primer polymer and react this polymer with montmorillonite with the purpose of creating a [montmorillonite/polystyrene-quat-primer] adduct.

Hyperbranched poly(ethylenimine) (PEI) with a number average molecular weight of 10,000 g/mol was used as the architectural scaffold because of its commercial availability, and the high reactivity of the amine groups [1, 2]. Through the addition of glycidyltrimethylammonium chloride (quat = Q) to poly(ethylenimine), polymers termed as “quat-primer” polymers [3] are obtained which contains positively charged ammonium units. “Polystyrene-quat-primer” polymers are obtained by adding polystyrene units to quat-primer polymers. Polystyrene was chosen since the aromatic moieties were assumed to have a good compatibility with the asphaltene fraction of the bitumen (cf. Chapter 2).

By reacting a polystyrene-quat-primer polymer with montmorillonite it was tested whether an adduct with a completely intercalated polymer could be obtained when prepared by the “indirect replacement” method as described previously with [MMT/PEI(nkD)_xQ^{yR}] adducts (cf. Chapter 4).

6.2 Experimental Part

6.2.1 Materials

Table 6.1: Used chemicals

Reagent	Purity	Supplier
2-Aminoethanol	99 %	Sigma-Aldrich
Ammonium chloride	99.5 %	J. T. Baker
Na-Bentonite batch <u>2</u> (= B2)	Main impurities: Quartz, calcite, iron; montmorillonite content \approx 72.0 wt. %	Alfa Aesar
2-Bromo-2-methylpropionic acid	98 %	Sigma-Aldrich
Copper(I) bromide	98 %	Alfa Aesar
N,N'-Dicyclohexylcarbodiimide	99 %	Alfa Aesar
4-Dimethylaminopyridine	99 %	Fluka
Glycidyltrimethylammonium chloride	90 wt. % (calc. based on dry substance), containing 20 – 25 wt. % water; calculated purity 67 wt. %	Sigma-Aldrich
(1-Hexadecyl)trimethylammonium bromide	98 %	Alfa Aesar
N-Hydroxysuccinimide (Novabio- chem HOSu)	98 %	Merck
N,N,N',N',N''-Pentamethyldiethylen- etriamine	98 %	Merck
Poly(ethylenimine), branched	Average Mn \sim 10,000 g/mol by GPC, average Mw \sim 25,000 g/mol by LS	Sigma-Aldrich
Styrene (stabilized)	99 %	Merck

Purification of copper(I) bromide:

The purification of copper(I) bromide was performed analogously to the procedure described in the literature before [4]. In an example experiment, 74.9 g copper(I) bromide was stirred in 700 mL glacial acetic acid for 24 h at ambient temperature. The acid was then removed under reduced pressure and washed three times with 210 mL ethanol and six times with 105 mL diethyl ether. The copper(I) bromide was then dried at 60°C for 23 h in vacuum. After drying, 66.1 g (= 88.3 % of theory) of a green-white powder was obtained.

Purification of styrene:

The stabilised styrene was distilled at 90 – 100°C under reduced pressure to remove the inhibitor. The first 20 mL of the distillate were removed and the rest collected. Afterwards, the destabilised styrene was stored in the refrigerator at 4°C.

Table 6.2: Used solvents

Solvent	Purity	Supplier
Chloroform	Technical	VWR Chemicals
Diethyl ether	p. a.	Fluka
Ethanol	Technical	Berkel
Methanol	Technical	Stockmeiner Chemie GmbH
Tetrahydrofuran	99.7 %	VWR
Toluene	Technical	VWR Chemicals
Water	Deionized	

6.2.2 Techniques

¹H-NMR (500 MHz), ¹H-DOSY-NMR (500 MHz), and ¹³C-NMR (125 MHz) experiments were recorded on a Bruker Avance III 500 spectrometer at 30°C. The concentration was set to be 20 mg/mL with ¹H measurements and to be 200 mg/mL with ¹³C measurements. The chemical shifts were given in parts per million (ppm). ¹H-DOSY-NMR measurements were performed using a Bruker 5 mm PABBO BB-1H/D Z-GRD z110902/0001 probe. **Solid-state magic angle spinning nuclear magnetic resonance spectroscopy (MAS-NMR) ¹H-NMR (500 MHz) and ¹³C-NMR (125 MHz)** measurements were also recorded on a Bruker Avance III 500 spectrometer. The temperature was set to be 30°C and the samples were rotated at a frequency of 8 kHz at an angle of 54.7° oriented to the applied magnetic field. About 17 mg of the sample was weighed in 50 µL ZrO₂ holder. 3 to 4 drops CDCl₃ were added to lower the viscosity. The chemical shifts were given in parts per million (ppm). The measurements were performed using a high-resolution magic angle spinning (HR-MAS) probe with the label: 4 mm HRMAS 1H/2H/13C/31P Z-GRD B3175/0476. With both methods, the software used to acquire the data was called Bruker Topspin 2.1.

ATR-FT-IR investigations were performed using a Perkin Elmer Spectrum Two spectrometer equipped with a Perkin Elmer Spectrum Two universal diamond/ZnSe-ATR crystal. The samples were pressed on the ATR unit and measured in reflection. The scan resolution was set to be 4 cm⁻¹, each sample was scanned four times and an average spectrum was created.

Calcination experiments were performed with a Naber N 11 industrial oven. The samples were heated from 30 to 530°C with a heating rate of 10 K/minute. All experiments were performed in an air atmosphere without a lid. 25 g porcelain crucibles were used in which 100 to 200 mg of a sample was weighed.

Differential scanning calorimetry (DSC) measurements were performed with a Netzsch 204 F1 Phoenix thermal analyzer, equipped with a T-sensor and a Netzsch Intracooler. The DSC was calibrated against Bi, Hg, In, Sn and Zn standards. 5 to 15 mg samples were weighed in 25 μ L aluminium pans. The pans were sealed with a perforated lid. The samples were measured under an N₂ stream over a temperature range of -80 to 180°C and at a heating and cooling rate of 10 K/minute.

Elemental analysis was performed with an Elementar vario MICRO cube to determine the carbon, hydrogen, and nitrogen content. 2.5 mg of a sample was measured and the experiment was performed three times to get an average.

The size-exclusion chromatography (SEC) setup consisted of four main devices. The pumping device was a Waters 2695 alliance autosampler. The column was a styrene-divinylbenzene copolymer (SDV) network, received from PSS Polymer Standards Service GmbH. The diameter of the particles were 5 μ m and the nominal pore sizes were 10³, 10⁵ and 10⁶ Å, respectively. For low molecular samples, the particles with the pore size of 10³ Å were replaced by particles with a pore size of 10² Å. Light scattering was measured with a multi-angle light scattering (MALS) Wyatt Dawn Heleos II detector and the refractive index (RI) with a Wyatt Optilab rEX detector. The wavelength of the laser of both detectors was 658 nm. Tetrahydrofuran was used as the eluent. Typically, the samples were measured at a concentration of 4 mg/mL. The molecular weight of the polymers was calculated using linear polystyrene standards with weight average molecular weights ranging from 1,920 to 524,000 g/mol.

The solubility of the polymers was tested by weighing 5 mg of the sample into a glass vial, adding 0.5 mL of the respective solvent, closing the lid and allowing the mixture to stand for half an hour at 20°C. When the substance didn't dissolve, the vial was shaken for 2 minutes. The solubility was qualitative judged by optical inspection, distinguishing between soluble (no visible substance particles in the solution), dispersion (visible substance particles in the solution), and insoluble (no dissolved substance).

X-ray diffraction (XRD) measurements were performed with a Panalytical X'Pert Pro Diffractometer, equipped with a copper cathode and a Bragg-Brentano geometry. Measurements were done with a voltage of 40 kV and a current of 40 mA. About 100 mg of a sample was measured between $2\theta = 5 - 79^\circ$ with a step width of $0.033423^\circ/\text{s}$.

6.2.3 Synthesis of 2-bromo-2-methyl-propionic acid 2,5-dioxopyrrolidin-1-yl ester

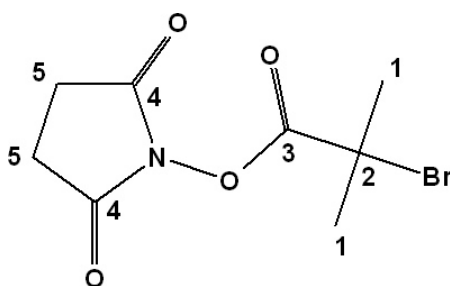


Figure 6.1: Structure of 2-bromo-2-methyl-propionic acid 2,5-dioxopyrrolidin-1-yl ester

(I1) Synthesis of 2-bromo-2-methyl-propionic acid 2,5-dioxopyrrolidin-1-yl ester

56.0 g (0.335 mol) 2-bromo-2-methylpropionic acid was dissolved in 57 mL tetrahydrofuran. 0.4 g (0.003 mol) 4-dimethylaminopyridine was then added and the solution was stirred at 20°C for five minutes. Afterwards, 42.9 g (0.373 mol) N-hydroxysuccinimide, dissolved in 224 mL tetrahydrofuran, was added and the solution was cooled down to 0°C . 76.9 g (0.373 mol) N,N'-dicyclohexylcarbodiimide dissolved in 170 mL tetrahydrofuran was then added and the reaction was stirred for 216 hours at 20°C . Afterwards, the solution was filtered under reduced pressure and the liquid fraction was collected. Most of the solvent was then removed under reduced pressure at 30°C and the product was obtained by precipitation the slurry in 1 L demineralised water. The liquid fraction was removed, 120 mL diethyl ether was added to the residue and the mixture was stirred for one hour at 20°C . Then the solvents were removed under reduced pressure and the product was dried at 40°C for 19 h in vacuum. After drying 55.4 g (= 62.5 % of theory) of a white powder was obtained.

$^1\text{H-NMR}$ (CDCl_3 , δ [ppm]): 2.83 (H-5), 2.06 (H-1); $^{13}\text{C-NMR}$ (CDCl_3 , δ [ppm]): 168.7 (C-4), 167.6 (C-3), 51.4 (C-2), 30.8 (C-1), 25.7 (C-5); Elemental analysis: found (calculated for $\text{C}_8\text{H}_{10}\text{N}_1\text{O}_4\text{Br}_1$): C: 35.99 (37.36), H: 3.98 (3.92), N: 5.45 (5.45); IR (ATR; ν [cm^{-1}]): 2943, 2851, 1807, 1776, 1730, 1574, 1464, 1455, 1424, 1370, 1254, 1203, 1074, 989, 923, 856, 808, 734, 641, 598

6.2.4 Synthesis of polystyrenes with active ester chain ends

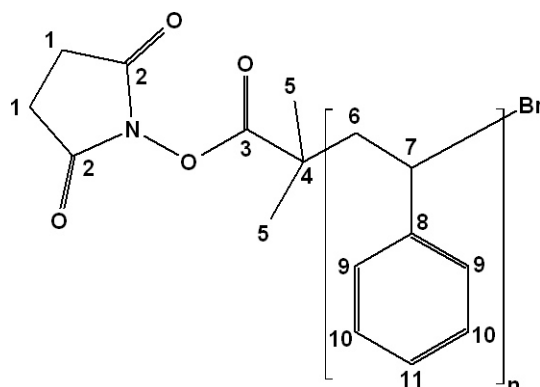


Figure 6.2: Structure of polystyrenes with active ester chain ends

(PSA1) Synthesis of PS(2.3kD)

14.1 g (0.135 mol) de-stabilised styrene was degassed by means of three freeze-thaw cycles before flushing with nitrogen gas. 0.5 g (0.003 mol) copper(I) bromide and 0.5 g (0.003 mol) N,N,N',N',N''-pentamethyldiethylenetriamine were then added to the styrene in a nitrogen countercurrent and the mixture was stirred another 10 minutes under a steady nitrogen flow. 0.8 g (0.003 mol) 2-bromo-2-methyl-propionic acid 2,5-dioxopyrrolidin-1-yl ester was then added, the mixture was heated to 60°C and stirred for 8 hours under a nitrogen atmosphere which was ensured by enclosing the polymerization device by a balloon. Afterwards, the slurry was cooled down to 20°C and poured into a solution of 14 mL NH₄Cl (20 wt.% in water) and 28 mL methanol. The mixture was poured then into a separation funnel, the lower part was removed, diluted with 2 mL toluene and precipitated in 28 mL methanol. The slurry fraction was collected, washed with another 10 mL of methanol, and the non-crystalline fraction was removed by filtration. The product was then dried at 60°C for 21 h in vacuum. After drying, 2.17 g (= 14.6 % of theory) of a yellow-white powder was obtained.

¹H-NMR (CDCl₃, δ [ppm]): 7.20 - 6.85 (H-9, H-11), 6.85 – 6.30 (H-10), 2.80 – 2.70 (H-1), 2.10 – 1.70 (H-5, H-7), 1.70 – 1.20 (H-6); ¹³C-NMR (CDCl₃, δ [ppm]): 170.0 (C-3), 169.0 (C-2), 147.0 – 145.0 (C-8), 129.0 – 127.0 (C-9, C-10), 127.0 – 125.0 (C-11), 48.0 – 41.5 (C-6), 41.5 – 39.5 (C-7), 27.7 (C-4), 25.7 (C-1), 21.6 (C-5); DSC: T_G = 82.4°C; IR (ATR; ν [cm⁻¹]): 3081, 3058, 3024, 2921, 2847, 1807, 1781, 1740, 1600, 1582, 1492, 1451, 1363, 1203, 1153, 1063, 1028, 907, 845, 755, 696, 538; **Molecular weight:** ¹H-NMR: M_n = 1,277 ± 128 g/mol; Elemental analysis (average): C: 84.7, H: 7.01, N: 0.48, corresponding to M_n = 2,758 ± 176 g/mol; SEC: M_n = 2,330 ± 466 g/mol, M_w/M_n = 1.078

(PSA2) Synthesis of PS(6.4kD)

1035.4 g (9.941 mol) de-stabilised styrene was stirred at 20°C for 20 minutes under a steady nitrogen flow. 32.9 g (0.229 mol) copper(I) bromide and 39.8 g (0.229 mol) N,N,N',N',N''-pentamethyldiethylenetriamine were then added to the styrene in a nitrogen countercurrent. Afterwards, the mixture was stirred another 10 minutes under a steady nitrogen flow. 52.7 g (0.199 mol) 2-bromo-2-methyl-propionic acid 2,5-dioxopyrrolidin-1-yl ester was then added and the mixture was stirred for another 10 minutes under a steady nitrogen flow. The mixture was then heated to 60°C and stirred for 8 hours also under a steady nitrogen flow. Afterwards, the mixture was allowed to stay at 20°C and on the air overnight. The product was received by pouring the slurry into a solution of 1 L NH₄Cl (20 wt.% in water) and 7 L methanol and stirring the mixture for 72 hours. The liquid fraction was then removed by filtration under reduced pressure, the polymer was collected and dissolved in 1.7 L toluene. The polymer was then poured into a mixture of 1.5 L NH₄Cl (10 wt.% in water) and 2.6 L methanol. The liquid fraction was removed and the polymer poured into 10.6 L methanol. The liquid fraction was again removed and the polymer collected. The polymer was then stirred two times for 30 minutes and one time for 17 hours with 0.5 L methanol using fresh solvent each run. The solvent was then removed under reduced pressure and the product was dried at 60°C for 24 h in vacuum. After drying, 505.4 g (= 46.5 % of theory) of a white powder was obtained.

¹H-NMR (CDCl₃, δ [ppm]): 7.20 - 6.85 (H-9, H-11), 6.85 – 6.30 (H-10), 2.80 – 2.70 (H-1), 2.10 – 1.70 (H-5, H-7), 1.70 – 1.20 (H-6); ¹³C-NMR (CDCl₃, δ [ppm]): 170.0 (C-3), 169.0 (C-2), 147.0 – 145.0 (C-8), 129.0 – 127.0 (C-9, C-10), 127.0 – 125.0 (C-11), 48.0 – 41.5 (C-6), 41.5 – 39.5 (C-7), 27.7 (C-4), 25.7 (C-1), 21.6 (C-5); DSC: T_G = 82.4°C; IR (ATR; ν [cm⁻¹]): 3082, 3059, 3025, 2920, 2848, 1807, 1782, 1742, 1600, 1583, 1492, 1451, 1367, 1203, 1154, 1065, 1028, 906, 842, 755, 695, 538; **Molecular weight:** ¹H-NMR: M_n = 5,612 ± 561 g/mol; Elemental analysis (average): C: 88.73, H: 7.39, N: 0.08, corresponding to M_n = 30,473 ± 40,726 g/mol; SEC: M_n = 6,407 ± 1281 g/mol, M_w/M_n = 1.036

Table 6.3: Prepared polystyrenes

Entry	Description	Synthesis condition	Prepared quantity (g)	Yield (wt.%)
PSA1	PS-NHS-ester	60°C, 8 h, b, N ₂ ^(g) atmosphere	2.17	14.6
PSA2	PS-NHS-ester	60°C, 8 h, b, N ₂ ^(g) flow	505.4	46.5

PS-NHS-ester = polystyrene-g-(2-methyl-propionic acid 2,5-dioxopyrrolidin-1-yl ester), b = bulk reaction, N₂^(g) = gaseous nitrogen

6.2.5 Synthesis of polystyrene-quat-primer polymers bearing ammonium moieties and polystyrene groups

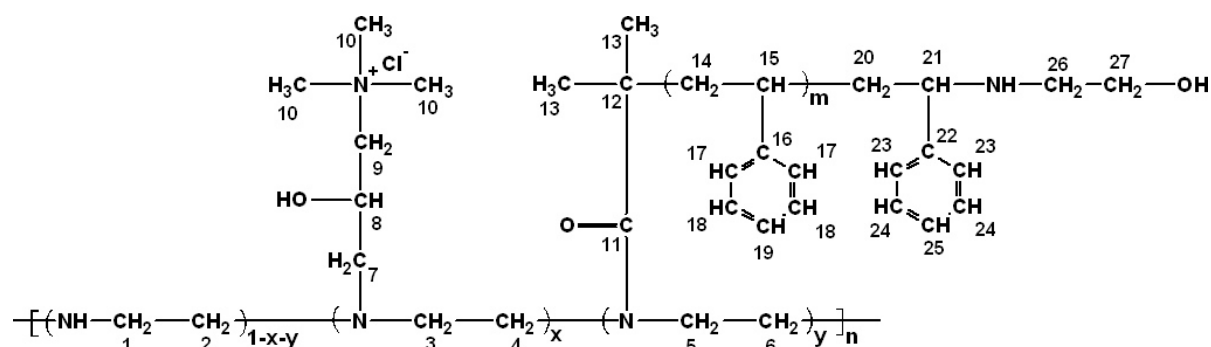


Figure 6.3: Structure of polystyrene-quat-primer polymers bearing ammonium moieties and polystyrene groups (= PEI(nkD)_xQ^yPS(nkD))

(PPS1) Synthesis of PEI(10kD)_{10Q}^{6.1PS(2.3kD)}

0.5 g (10.5 mmol) poly(ethylenimine) was dissolved in 9 mL chloroform. 0.2 g (1.1 mmol) glycidyltrimethylammonium chloride as well as 1.5 g (0.6 mmol) polystyrene (**PSA1**, $M_n = 2,330$ g/mol (SEC), $M_w/M_n = 1.078$ (SEC)) which was dissolved in 3.8 mL chloroform were added and the solution was stirred for 23 hours at 60°C. Afterwards, 2.3 g (37.2 mmol) 2-aminoethanol was added and the solution was stirred for another 66 hours. Then the solvent was removed under reduced pressure and the polymer was poured into 15 mL demineralised water. Afterwards, the liquid fraction was removed by centrifugation at 2817 g (2817 times the acceleration due to gravity) for 10 minutes and the residue was dried at 60°C for 19 hours in vacuum. After drying, 1.2 g (= 51.2 % of theory) of a yellow and waxy, solid polymer was obtained.

¹H-NMR (CDCl₃, δ [ppm]): 7.20 - 6.85 (H-17, H-19, H-23, H-25), 6.85 - 6.30 (H-18, H-24), 4.50 - 3.10 (H-8, H-21), 3.80 - 3.60 (H-26), 3.50 - 3.30 (H-4, H-5), 3.40 - 3.20 (H-9, H-10), 3.00 - 2.80 (H-27), 3.00 - 2.40 (H-1 - H-3, H-6, H-7), 2.20 - 1.70 (H-15), 1.70 - 1.20 (H-14, H-20), 1.24 (H-13); ¹³C-NMR (CDCl₃, δ [ppm]): 147.0 - 144.0 (C-16, C-20), 129.0 - 126.5 (C-17, C-18, C-23, C-24), 126.5 - 124.5 (C-19, C-25), 62.0 - 60.0 (C-27), 55.0 - 54.0 (C-26), 54.0 - 50.0 (C-1 - C-6), 48.9 (C-10), 48.9 - 41.5 (C-14, C-20), 41.5 - 39.5 (C-15, C-21), 28.0 - 24.5 (C-13); DSC: T_G = 60.2°C; Elemental analysis: C: 65.11, H: 7.90, N: 7.93; IR (ATR; ν [cm⁻¹]): 3281, 3081, 3058, 3025, 2959, 2920, 2848, 1651, 1600, 1583, 1492, 1451, 1362, 1260, 1069, 1026, 907, 866, 798, 756, 696, 538

The synthesis of two PEI(10kD)_{10Q}^{2.2PS(6.4kD)} polymers (= **PPS2** and **PPS3**) was performed analogously to the preparation described with polymer **PPS1**. Only a small

6 Preparation of [montmorillonite/PEI(nkD)xQyPS(nkD)]

fraction of polymer **PPS2** was purified, dried, and used to analyse the composition of the polymer. After most of the solvent was removed by centrifugation the main fractions of the polymers **PPS2** and **PPS3** were used directly for the preparation of adduct **EP1**.

Table 6.4: Prepared PEI(10kD)_{xQ}^{yPS(nkD)} polymers

Entry	Description	Polystyrene	Synthesis condition	Prepared quantity (g)	Yield (wt. %)
		M _{n,SEC} (g/mol)			
PPS1	PEI(10kD) _{10Q} ^{6.1PS(2.3kD)}	2,330	60°C, 89 h, CHCl ₃	1.2	51.2
PPS2	PEI(10kD) _{10Q} ^{2.2PS(6.4kD)}	6,407	60°C, 89 h, CHCl ₃	128.2	not determined
PPS3	PEI(10kD) _{10Q} ^{2.2PS(6.4kD)}	6,407	60°C, 89 h, CHCl ₃	577.1	not determined

PEI(10kD) = poly(ethylenimine) with M_n = 10,000 g/mol, M_w/M_n = 2.5, xQ = mol% 2-hydroxypropyl-3-(N,N,N-trimethylammonium) chloride, yPS = mol% polystyrene-g-2-aminoethanol, M_{n,SEC} = number average molecular weight obtained from size exclusion chromatography [g/mol]

6.2.6 Preparation of [MMT_{B2}/PEI(10kD)_{10Q}^{2.2PS(6.4kD)}]

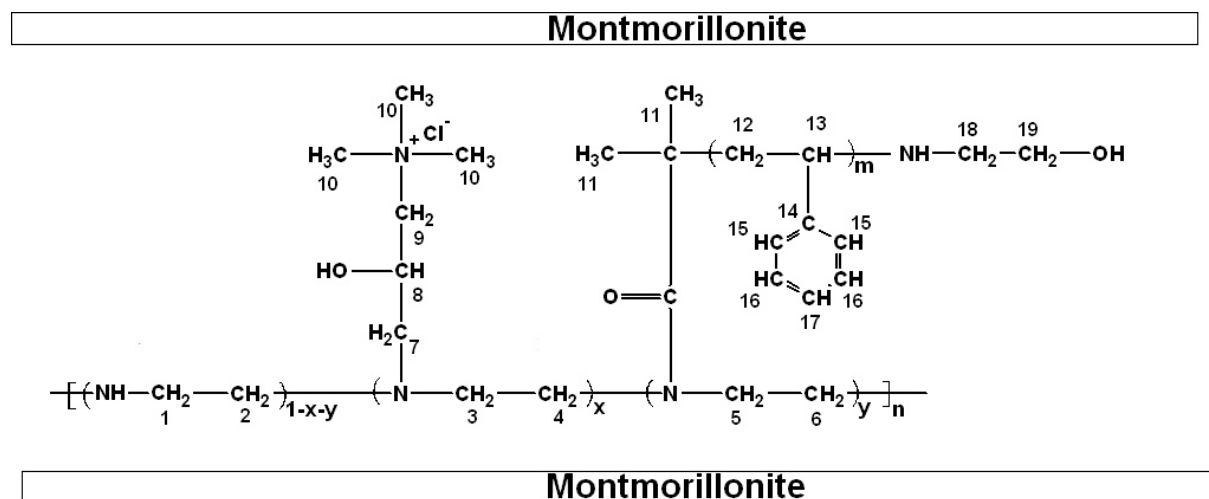


Figure 6.4: Structure of [MMT/PEI(nkD)_{xQ}^{yPS(nkD)}]

(EP1) Preparation of [MMT_{B2}/PEI(10kD)_{10Q}^{2.2PS(6.4kD)}]

298.8 g Na-bentonite was stirred with a mechanical stirrer (KPG, 110 min⁻¹) in 10.6 L demineralised water for 3 h at 20°C. Afterwards, 447.9 g (1.229 mol) (1-hexadecyl)trimethylammonium bromide (CTAB) was added and the mixture was stirred for another 72 h. The temperature was then raised to 60°C and 960 mL of a **PPS2/PPS3** mix-

6 Preparation of [montmorillonite/PEI(nkD)xQyPS(nkD)]

ture which was dispersed in 470 mL demineralised water (theoretical polymer content \approx 337.7 g) was added in the period of 28 hours. Then, the mixture was stirred for another 47 h at 60°C and 24 h at 20°C. Afterwards, the mixture was centrifuged at 4472 g (4472 times the acceleration due to gravity) for 10 minutes. The sediment was collected, slurried in 225 mL methanol for 30 minutes at 20°C and centrifuged for 20 minutes. This procedure was repeated two more times and the residue was dried afterwards at 80°C for 94 h in vacuum. After drying, 661.3 g (= 103.9 % of theory) of a brown coloured solid substance was obtained.

^1H -MAS-NMR (CDCl_3 , δ [ppm]): 7.20 - 6.85 (H-15, H17), 6.85 – 6.30 (H-16), 3.44 (H-18), 2.78 (H-19), 2.70 – 2.20 (H-1 – H-7), 1.59 (H-13), 1.20 (H-11), 1.10 (H-12); ^{13}C -MAS-NMR (CDCl_3 , δ [ppm]): 129.9 (C-15, C-16), 125.7 (C-17), 40.4 (C-18); Calcination: Organic material: 67.8 wt.% (theory: 53.1 wt.%); DSC: $T_g = 14.6^\circ\text{C}$, $T_{m(1)} = 27.2$, $T_{m(2)} = 33.2$, $T_{m(3)} = 60.0$, $T_{m(4)} = 82.4$; IR (ATR; ν [cm^{-1}]): 3622, 3281, 3029, 3017, 2943, 2916, 2848, 1636, 1600, 1577, 1486, 1472, 1461, 1010, 960, 911, 730, 718, 697, 623, 515; XRD (wide-angle): Lattice constant $c_{(1)} = 1.34 \pm 0.02$ nm (single layer CTAB) and lattice constant $c_{(2)} = 4.5 \pm 0.03$ nm

6.3 Results and Discussion

Within this Chapter the preparation and characterisation of (i) an N-hydroxysuccinimide active ester, (ii) polystyrenes bearing an active ester group (= poly(N-hydroxysuccinimide styrene)), (iii) hyperbranched poly(ethylenimine)s modified by glycidyltrimethylammonium chloride (= quat) and polystyrenes-g-2-aminoethanol (= PEI(nkD)_xQ^yPS(nkD)), and (iv) a montmorillonite modified by a PEI(nkD)_xQ^yPS(nkD) polymer (= [montmorillonite/polystyrene-quat-primer] adduct) will be described. The evaluated synthesis route of the preparation of a [montmorillonite/polystyrene-quat-primer] adduct is shown in Figure 6.5 and an overview over the synthesised compounds is given in Table 6.5. The adduct was prepared by the “indirect replacement” method which means that the polystyrene-quat-primer polymer was reacted with a priorly formed [MMT/CTAB] intermediate and replaced the CTAB moieties.

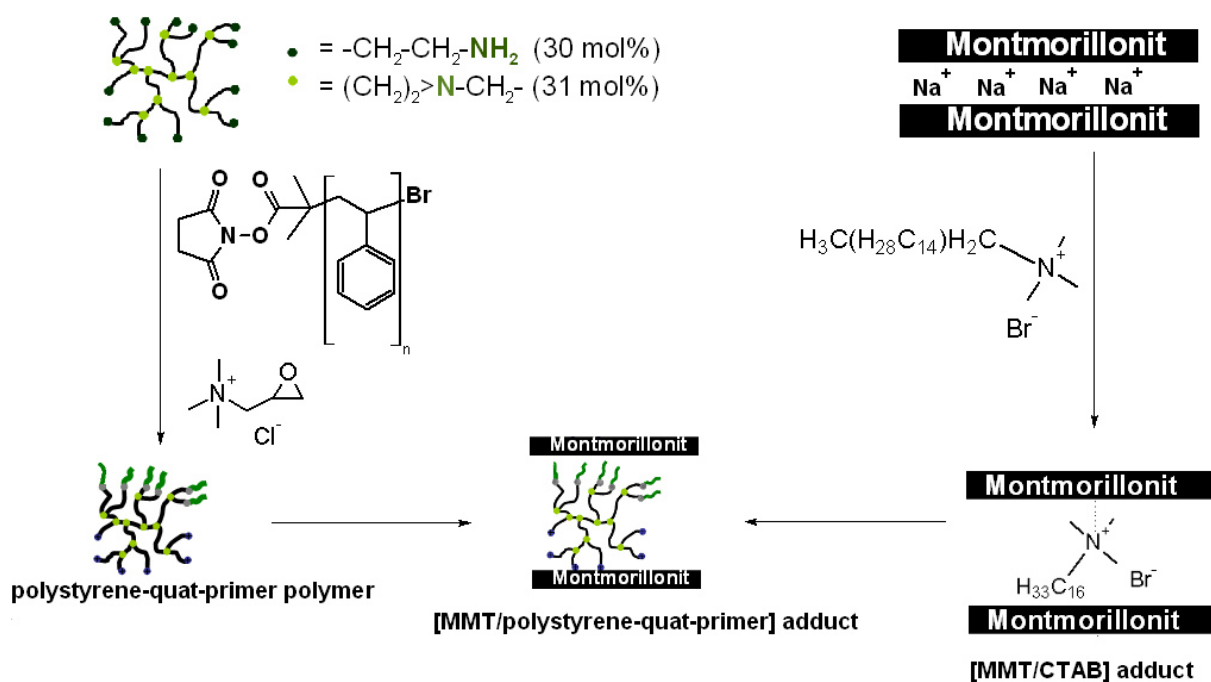


Figure 6.5: Synthesis route of the preparation of [montmorillonite/polystyrene-quat-primer] adducts

Table 6.5: Prepared compounds

Entry	Description	M _{n,SEC} [g/mol]	Synthesis condition	Yield (wt.%)
I1	NHS-ester		20°C, 216 h, THF	62.5
PSA1	PS-NHS-ester	2,330	60°C, 8 h, b, N ₂ ^(g) atmosphere	14.6
PSA2	PS-NHS-ester	6,407	60°C, 8 h, b, N ₂ ^(g) flow	46.5
PPS1	PEI(10kD) _{10Q} ^{6.1PS(2.3kD)}		60°C, 89 h, CHCl ₃	51.2
PPS2, PPS3	PEI(10kD) _{10Q} ^{2.2PS(6.4kD)}		60°C, 89 h, CHCl ₃	-
EP1	[MMT/PEI(10kD) _{10Q} ^{2.2PS(6.4kD)}]		60°C, 174, h H ₂ O	103.9

NHS-ester = 2-bromo-2-methyl-propionic acid 2,5-dioxopyrrolidin-1-yl ester, PS-NHS-ester = polystyrene-g-(2-methyl-propionic acid 2,5-dioxopyrrolidin-1-yl ester), PEI(10kD) = poly(ethylenimine) with M_n = 10,000 g/mol, M_w/M_n = 2.5, xQ = mol% 2-hydroxypropyl-3-(N,N,N-trimethylammonium chloride), yPS = mol% polystyrene-g-2-aminoethanol, M_{n,SEC} = number average molecular weight obtained from size exclusion chromatography [g/mol], b = bulk reaction, N₂^(g) = gaseous nitrogen

Synthesis of initiator **I1**

In this work, polystyrenes were prepared via an ATRP polymerization (Atom Transfer Radical Polymerization) initiated with 2-bromo-2-methyl-propionic acid 2,5-dioxopyrrolidin-1-yl ester (= initiator **I1**). **I1** was prepared through a Steglich esterification [5] in analogy to the procedure reported in a previous investigation [3] with the difference that the purification step was optimised. To prepare larger quantities of a polystyrene active ester 55.4 g of initiator **I1** was prepared in total. The spectra of the initiator were in good agreement to those found in the literature [3] and will be shown together with the spectra of the polystyrene active esters in the following paragraphs.

6.3.1 Preparation of polystyrenes with active ester chain ends

Since the polystyrene don't exhibit functional groups which are able to react with the amino groups of the poly(ethylenimine) on its own, a modification of the polystyrene was necessary. Functional groups that are able to react with amines are for example epoxides [6 - 12], anhydrides [13] and N-hydroxysuccinimide active esters [3, 14 - 16]. The reaction of amino groups with epoxides, anhydrides, and N-hydroxysuccinimide active esters is shown in Figure 6.6. To obtain an epoxide-functionalized polystyrene, poly(styryl)lithium (PSLi) was reacted with either epichlorohydrin [17] or epibromohydrin [18]. An anhydride functionalized polystyrene was prepared by reacting maleic anhydride with polystyrene [19, 20]. The grafting of poly(methyl methacrylate)

on poly(ethylenimine) was accomplished by reacting a poly(methyl methacrylate)-N-hydroxysuccinimide ester with the amine [3, 21].

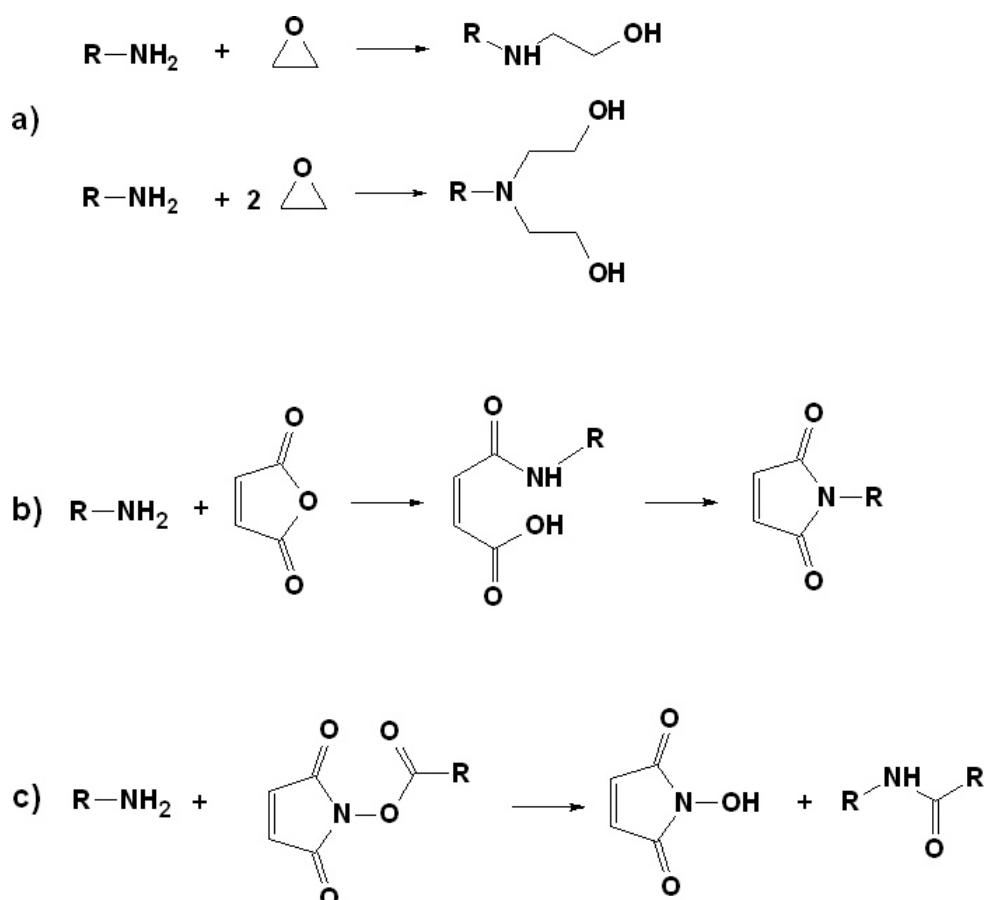


Figure 6.6: Reaction of amino groups with a) epoxides [6], b) anhydrides [13] and c) N-hydroxysuccinimide active esters [14]

In this study the polymerization of styrene was initiated by 2-bromo-2-methyl-propionic acid 2,5-dioxopyrrolidin-1-yl ester (= initiator **11**) and catalysed by a Cu(I)Br/PMDTA complex (PMDTA = N,N,N',N',N''-pentamethyldiethylenetriamine) according to the mechanism of an ATRP polymerization described in the literature [22, 23] (cf. Figure 6.7). During the polymerization, styrene monomer units reacted with initiator radical molecules and formed polystyrene by repetitive atom transfer radical additions [22, 23].

6 Preparation of [montmorillonite/PEI(nkD)xQyPS(nkD)]

Initiation

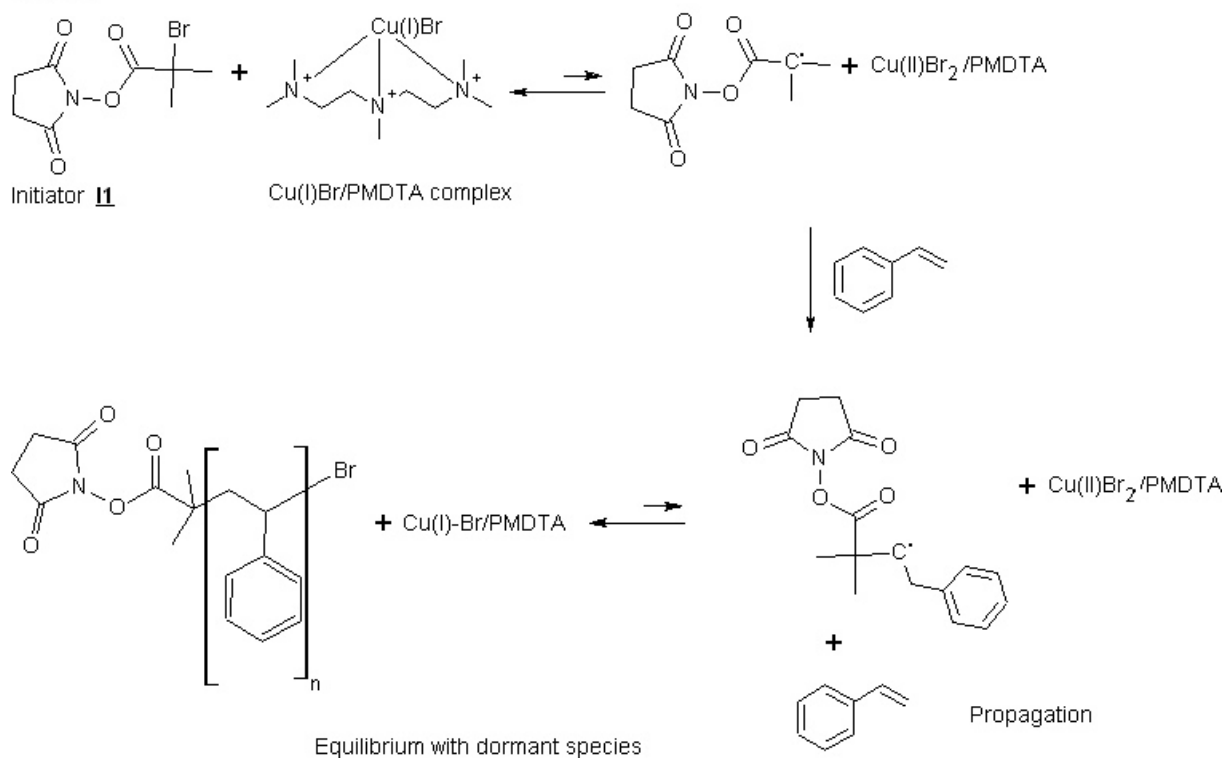


Figure 6.7: Preparation of polystyrenes bearing active ester chain ends by an “ATRP” polymerization (polymerization mechanism according to literature data [22, 23])

The studied polystyrenes are listed in Table 6.6. Polystyrene **PSA1** was prepared in a smaller quantity to scope the purification conditions necessary to obtain a styrene monomer free polymer. The polymer was obtained by pouring the reaction mixture into a solution of NH₄Cl/ methanol. The polymer was then diluted with toluene and precipitated in methanol. After removal of the liquid fraction, the residue was washed with methanol, the solvent was removed by filtration and the polymer dried under vacuum at elevated temperature. With polystyrene **PSA2**, on the other hand, the polymer was precipitated in NH₄Cl/methanol, dissolved in toluene afterwards and poured a second time into a NH₄Cl/methanol solution. Then the polymer was washed three times with methanol.

Table 6.6: Prepared polystyrenes

Entry	Description	Synthesis condition	Prepared quantity (g)	Yield (wt.%)
PSA1	PS-NHS-ester	60°C, 8 h, b, N ₂ ^(g) atmosphere	2.17	14.6
PSA2	PS-NHS-ester	60°C, 8 h, b, N ₂ ^(g) flow	505.4	46.5

PS-NHS-ester = polystyrene-g-(2-methyl-propionic acid 2,5-dioxopyrrolidin-1-yl ester), b = bulk reaction, N₂^(g) = gaseous nitrogen

6 Preparation of [montmorillonite/PEI(nkD)xQyPS(nkD)]

The presence of the polystyrene and the active ester in the product was verified by $^1\text{H-NMR}$ spectroscopy. In Figure 6.8, the $^1\text{H-NMR}$ spectrum of a) initiator **I1**, b) polystyrene **PSA1**, and c) polystyrene **PSA2** is shown. With initiator **I1** (Figure 6.8.a), the four hydrogen atoms of the succinimide ring gave a signal at 2.83 ppm (1) and the signal of the six hydrogen atoms of the ester was found at 2.06 ppm (2). The position of the signals was in good agreement to the predicted positions calculated based on an increment system.

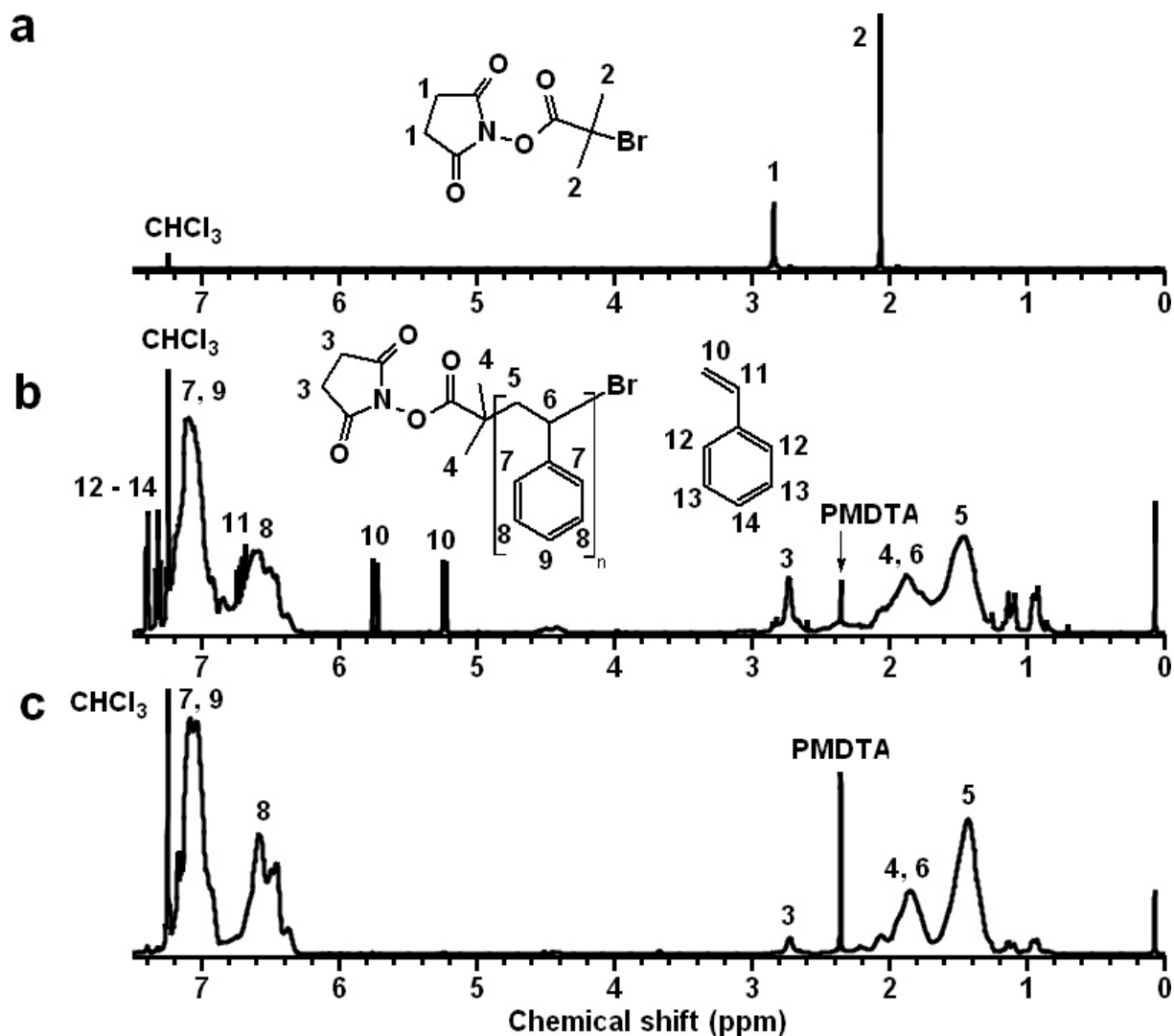


Figure 6.8: $^1\text{H-NMR}$ spectra of a) initiator **I1**, b) polystyrene **PSA1**, and c) polystyrene **PSA2**, CDCl_3 , 30°C

The ratio of hydrogen atoms of the succinimide ring to the hydrogen atoms of the methyl groups was calculated with Equation 6.1 to be 0.98 which was in reasonable good agreement to the theoretical value of 1 which was the second prove of the successful synthesis of the initiator.

6 Preparation of [montmorillonite/PEI(nkD)xQyPS(nkD)]

$$\frac{N_{\text{Su}}}{N_{\text{E}}} = \frac{A_{\text{Su}(\text{CH}_2)_2}}{A_{\text{E}(\text{CH}_3)_2}} \cdot \frac{6}{4} \quad \text{Eq. 6.1}$$

(with N_{Su} = number of succinimide groups, N_{E} = number of ester groups, $A_{\text{Su}(\text{CH}_2)_2}$ = integrated $^1\text{H-NMR}$ signal intensity of the succinimide hydrogen atoms at 2.83 ppm, $A_{\text{E}(\text{CH}_3)_2}$ = integrated $^1\text{H-NMR}$ signal intensity of the ester hydrogen atoms at 2.06 ppm)

The spectrum of polystyrene **PSA1** (Figure 6.8.b) and the spectrum of polystyrene **PSA2** (Figure 6.8.c) showed signals corresponding to the hydrogen atoms of the aromatic rings at 6.30 - 6.85 ppm (8) and 6.85 - 7.20 ppm (7, 9). Signals corresponding to the aliphatic C-H groups appeared between 1.70 - 2.10 ppm (6) and 1.20 - 1.70 ppm (5). Compared to initiator **I1**, the signal of the hydrogen atoms of the succinimide ring shifted to 2.70 - 2.80 ppm (3) and became broader. The signal of the methyl groups attached to the carbon atom next to the ester shifted also and overlapped with the aliphatic C-H groups of the polystyrenes at 1.70 - 2.10 ppm (4). The spectra revealed furthermore that the polymers were not pure but contained N,N,N',N',N''-pentamethyldiethylenetriamine (= PMDTA) impurities shown by a signal at 2.34 ppm which corresponded to the hydrogen atoms of the methylene groups and the methyl moiety attached to the tertiary nitrogen atom.

The spectrum of polystyrene **PSA1** furthermore revealed the presence of non-reacted styrene (10 - 14) which shows that the purification procedure had to be optimised to obtain pure polymers which was successfully accomplished with polystyrene **PSA2** (cf. Figure 6.8.c) and shows that the more complex purification was necessary to remove non-reacted styrene. The molar ratio of non-reacted styrene to polystyrene of **PSA1** was calculated with Equation 6.2 to be 0.07 to 1 which corresponded to a weight concentration of styrene in the mixture of 0.6 wt.%. The calculation was performed using the corrected integrated signal intensity of the polystyrene hydrogen atoms at 1.70 - 2.10 ppm (5, 6) and the integrated signal intensity of the styrene hydrogen atoms of the vinyl group at 5.24 and 5.75 ppm (10).

$$\frac{N_{\text{S}}}{N_{\text{PS}}} = \frac{A_{\text{S}(\text{CH}_2)}}{A_{\text{PS}(\text{C}_2\text{H}_3)}} \cdot \frac{3}{2} \quad \text{Eq. 6.2}$$

(with N_{S} = number of styrene molecules [mol], N_{PS} = number of polystyrene molecules [mol], $A_{\text{S}(\text{CH}_2)}$ = integrated $^1\text{H-NMR}$ signal intensity of the styrene hydrogen atoms at 5.24 and 5.75 ppm, $A_{\text{PS}(\text{C}_2\text{H}_3)}$ = integrated $^1\text{H-NMR}$ signal intensity of the polystyrene hydrogen atoms at 1.70 - 2.10 ppm)

To calculate the number average molecular weights of the polystyrenes **PSA1** and **PSA2** based on $^1\text{H-NMR}$ data, the ratio of the signal intensities of the hydrogen

atoms of the aliphatic CH groups of the polystyrene at 1.70 - 2.10 ppm (5, 6, cf. Figure 6.8.b) to the CH₂ hydrogen atoms of the succinimide ester at 2.70 - 2.80 ppm (3, cf. Figure 6.8.b) was calculated using Equation 6.3. With **PSA2** the ratio was calculated to be 52.21, polystyrene **PSA1** exhibited a polystyrene to NHS-ester ratio of 10.59.

$$\frac{N_{PS}}{N_E} = \frac{A_{PS(C2H3)}}{A_{E(C2H4)}} \cdot \frac{4}{3} \quad \text{Eq. 6.3}$$

(with N_{PS} = number of polystyrene molecules [mol], N_E = number of succinimide ester molecules [mol], A_{PS(C2H3)} = integrated ¹H-NMR signal intensity of the polystyrene hydrogen atoms at 1.70 - 2.10 ppm, A_{E(C2H4)} = integrated ¹H-NMR signal intensity of the succinimide ester hydrogen atoms at 2.70 - 2.80 ppm)

With the ratio obtained from Equation 6.3, the number average molecular weight of the polymers was calculated to be M_n = 1,277 ± 128 g/mol (**PSA1**), and M_n = 5,612 ± 561 g/mol (**PSA2**), respectively, with the error of the molecular weight derived from the integration of the area of around 10 %.

$$M_n = \frac{N_{PS}}{N_E} \cdot M_S + M_I \quad \text{Eq. 6.4}$$

(with M_n = number average molecular weight of polystyrene [g/mol], N_{PS} = number of polystyrene molecules [mol], N_E = number of succinimide ester molecules [mol], M_S = molecular weight of styrene [g/mol], M_I = molecular weight of the succinimide ester [g/mol])

In conclusion, both polystyrenes, **PSA1** and **PSA2**, contained a succinimide moiety which indicates that polystyrene active esters were successfully prepared. Furthermore, while the polystyrene synthesised under a constant nitrogen stream (= **PSA2**) exhibited a number average molecular weight M_n of 5,612 ± 561 g/mol, the molecular weight of the polystyrene synthesised under a nitrogen atmosphere but enclosed by a balloon (= **PSA1**) reached only a value of M_n = 1,277 ± 128 g/mol. In addition, the spectrum of **PSA1** showed the presence of non-reacted styrene which points in combination with the low molecular weight to the conclusion that during the reaction oxygen diffused into the solution which stopped the conversion of the styrene at some point. The inactivation of the radical molecules may be caused by that during the reaction the sealing around the used balloon came off and oxygen diffused into the reaction mixture which reacted with the radical species. From the number average molecular weight of **PSA2** and the reaction time of 8 h, the growing rate of the polymer chains was calculated to be about 700 g/mol per hour.

The covalent attachment of the succinimide esters to the polystyrenes was confirmed by ¹H-DOSY NMR investigations. Figure 6.9 shows the ¹H-DOSY NMR spectra of **PSA1** and **PSA2**. In both spectra, the signals of styrene and initiator groups appeared at a single diffusion coefficient which shows that the succinimide units were covalently attached to the respective polystyrene. Polymer **PSA1** exhibited a diffusion coefficient of $-\log D = 8.93 \text{ m}^2/\text{s}$, corresponding to a hydrodynamic radius of 0.37 nm. With polystyrene **PSA2**, the diffusion coefficient exhibited a value of $-\log D = 9.05 \text{ m}^2/\text{s}$ which corresponded, using the dynamic viscosity of chloroform at 303.15 K of $0.507 \text{ mPa}\cdot\text{s}$ [24], to a hydrodynamic radius of 0.49 nm. While the diffusion coefficient of PMDTA was measured to be $-\log D = 8.5 \text{ m}^2/\text{s}$ with **PSA2**, corresponding to a hydrodynamic radius of 0.139 nm, the PMDTA concentration of **PSA1** was too low and could not be attributed correctly.

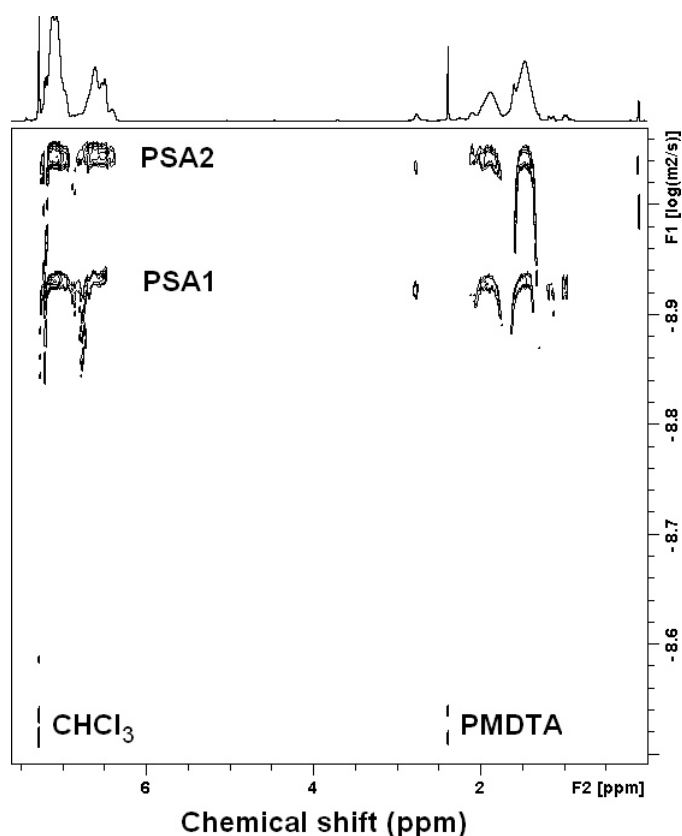


Figure 6.9: ¹H-DOSY-NMR spectra of **PSA1** and **PSA2**, CDCl₃, 30°C

The neat CHCl₃ exhibited a diffusion coefficient of $D = 3.02 \cdot 10^{-9} \text{ m}^2/\text{s}$ ($-\log D = 8.52 \text{ m}^2/\text{s}$) with both polymers which corresponded to a hydrodynamic radius of 0.145 nm. The measured diffusion coefficient of the neat chloroform was in good agreement to the reported diffusion coefficient of chloroform of $D = 2.56 \cdot 10^{-9} \text{ m}^2/\text{s}$ of a chloroform methyl acrylate solution measured at 30°C [25] and measurements of PEI(nkD)_xQ^{YR}

polymers (cf. Chapter 3) showing the reliability of the method. The slightly higher diffusion coefficient D measured with the polymers **PSA1** and **PSA2** may be attributed to an interaction between the solvent and the polymers [26].

The diffusion coefficient of dissolved molecules is described by the Stokes–Einstein Equation 6.5 and was used to calculate the hydrodynamic radii of the polystyrenes **PSA1** and **PSA2**. An overview over the measured diffusion coefficients and hydrodynamic radii is given in Table 6.7.

$$R_0 = K_B \cdot \frac{T}{6 \cdot \pi \cdot \eta \cdot D} \quad \text{Eq. 6.5}$$

(with R_0 = hydrodynamic radius of the diffusing particles [m], K_B = Boltzmann constant [$1.3806485279 \cdot 10^{-23} \text{ kg} \cdot \text{m}^2 \cdot \text{s}^{-2} \cdot \text{K}^{-1}$], T = temperature [K], η = dynamic viscosity of the solvent [$\text{kg} \cdot \text{m}^{-1} \cdot \text{s}^{-1}$], D = logarithmic diffusion coefficient [$\text{m}^2 \cdot \text{s}^{-1}$])

Table 6.7: Diffusion coefficients of the polystyrenes **PSA2 and **PSA1****

Entry	Solvent	Diffusion coefficient (-log D m ² /s)	R ₀ (nm)
PSA1	CDCl ₃	8.93	0.37
PSA2	CDCl ₃	9.05	0.49

R_0 = hydrodynamic radius [nm]

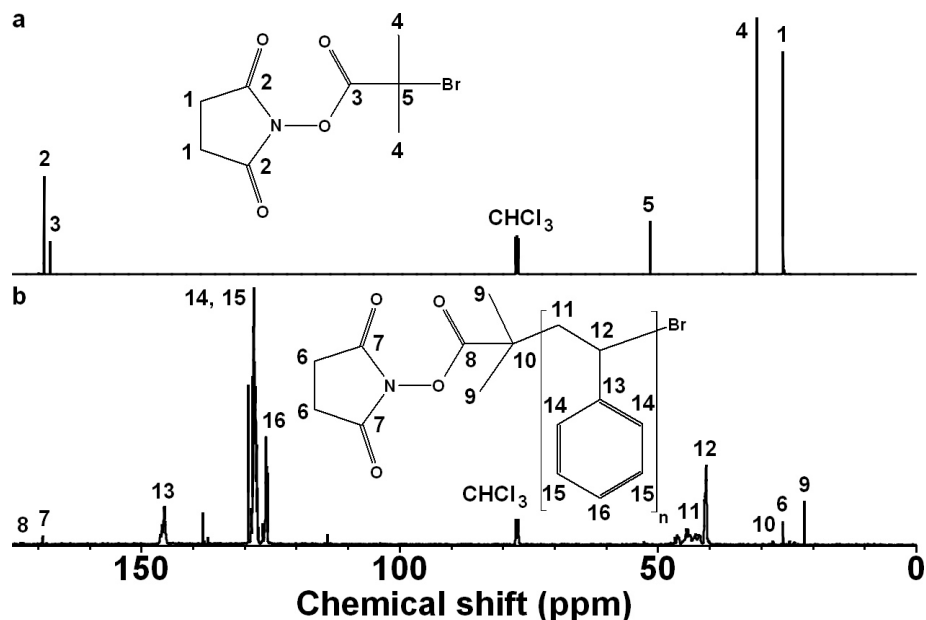


Figure 6.10: ¹³C-NMR spectra of a) initiator **1** and b) polystyrene **PSA2**, CDCl₃, 30°C

To obtain information about the structure of initiator **1** and the polystyrenes **PSA1** and **PSA2**, the compounds were studied by ¹³C-NMR. In Figure 6.10, the ¹³C-NMR spectra of a) initiator **1** and b) polystyrene **PSA2** are shown. With initiator **1** (Figure

6.10.a) signals of the carbon atoms of the succinimide ring were detected at 25.7 ppm (1) and 168.7 ppm (2). The carbonyl carbon atom of the ester moiety gave a peak at 167.6 ppm (3), and the carbon atoms of the two methyl groups at 30.8 ppm (4). The signal of the quaternary carbon atom appeared at 51.4 ppm (5).

With polystyrene **PSA2** (Figure 6.10.b), carbon atoms corresponding to the aromatic ring could be identified by peaks at 147.0 – 145.0 ppm (13), 129.0 – 127.0 ppm (14, 15) and 127.0 - 125.0 ppm (16). Signals of the carbon atoms of the aliphatic C-H groups of the styrene moieties showed up at 48.0 – 41.5 ppm (11) and 41.5 - 39.5 ppm (12). The positions of the carbon atoms of the succinimide group were found to be similar to those of the neat initiator **I1** of 25.7 ppm (6) and 168.7 - 169 ppm (7). The signal of the two methyl groups attached to the quaternary carbon atom was shifted from 25.7 ppm (4) with initiator **I1** to 21.6 ppm (9) with polystyrene **PSA2**. The signal of the quaternary carbon atom of the ester also shifted from 51.4 ppm (5) with initiator **I1** to 27.7 ppm (10) with polystyrene **PSA2**. The ester carbonyl group gave a very weak peak at 170.0 ppm (8).

The carbon atoms of polystyrene **PSA1** gave signals at the same position as with polystyrene **PSA2** showing that the composition of both polymers was the same. But different to **PSA2** the spectrum of polystyrene **PSA1** exhibited additional signals at 137.0, 126.6, and 113.9 ppm which could be attributed to non-polymerised styrene. In conclusion, the spectra of both polystyrenes exhibited signals of the polystyrene and the succinimide ester which shows that the ester was present in the respective polymer.

IR investigations on the polystyrenes and the initiator were performed to obtain information about the functional groups present in the polymers. The infrared spectra of a) initiator **I1**, b) polystyrene **PSA1**, and c) polystyrene **PSA2** are shown in Figure 6.11. The spectrum of initiator **I1** (Figure 6.11.a) exhibited C-H stretching vibration bands at 2943 and 2851 cm^{-1} as well as C-H deformation vibration bands at 1464, 1455, 1424, and 1370 cm^{-1} . Anhydride C=O stretching vibration bands were detected at 1807 cm^{-1} and 1776 cm^{-1} . The ester C=O stretching vibration band appeared at 1730 cm^{-1} . The ester C-O stretching vibration bands were measured at 1203 cm^{-1} and 1074 cm^{-1} . In the fingerprint region ($= <1000 \text{ cm}^{-1}$), bands were found at 989, 923, 856, 808, 734, 641, and 598 cm^{-1} .

With polymer **PSA1** (Figure 6.11.b), C-C stretching vibration bands corresponding to the aromatic rings showed up at 3081, 3058, 3024, 1600, 1492, and 1451 cm^{-1} . Stretching vibration bands of aliphatic C-H groups were measured at 2921, 2847, and 1363 cm^{-1} . The anhydride C=O stretching vibration bands appeared at 1807 cm^{-1} and 1781 cm^{-1} . The ester C=O stretching vibration band was found to be shifted from

1730 cm^{-1} with initiator **I1** to 1740 cm^{-1} with polystyrene **PSA1**. The ester C-O stretching vibration bands were detected at 1203 and 1063 cm^{-1} . Further bands showed up at 907, 845, 755, 696, and 538 cm^{-1} in the region of 450 - 1000 cm^{-1} . Polystyrene **PSA2** (Figure 6.11.c) contained the same functional groups as polystyrene **PSA1** shown by the presence of the corresponding bands at similar positions. The bands in the fingerprint region were also at similar positions showing that the composition of the polymers was virtually the same. From the presence of the anhydride C=O stretching vibration bands, and the ester C=O stretching vibration band it was concluded that both polystyrenes contained an active ester functionality.

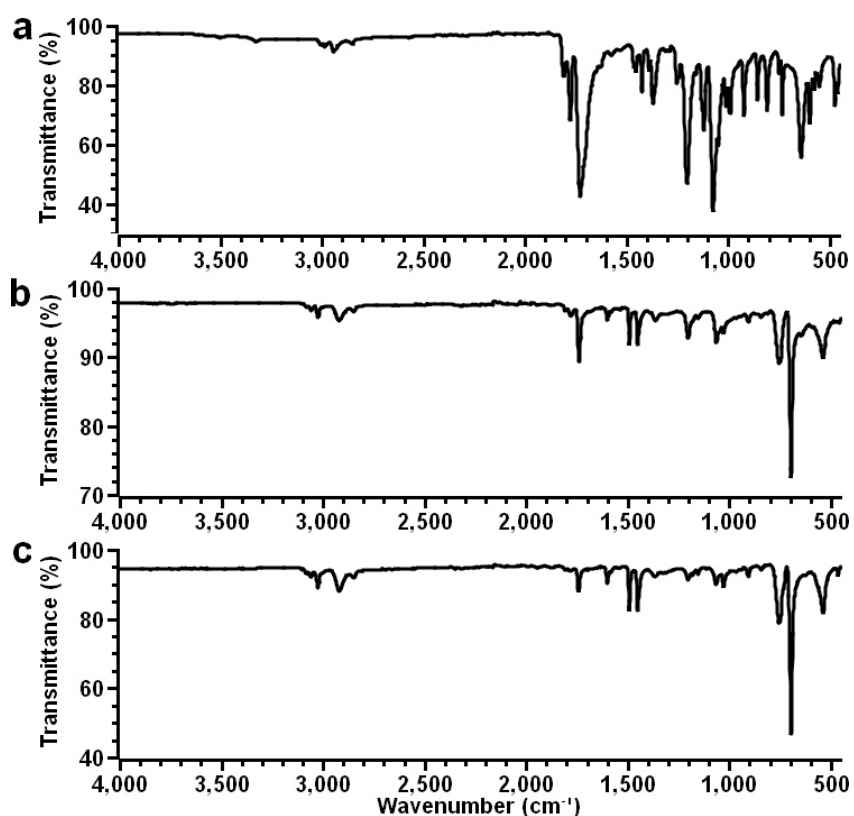


Figure 6.11: ATR-FT infrared spectra of a) initiator **I1**, b) polystyrene **PSA1**, and c) polystyrene **PSA2**

As a comparison to the calculated number average molecular weights of **PSA1** and **PSA2** based on $^1\text{H-NMR}$ data, the molecular weights of the two polystyrenes were determined using size-exclusion chromatography (SEC). Figure 6.12 shows the refractive index (RI, straight lines) and the multi-angle light scattering (MALS, dotted lines) detector signals of the elution-diagrams of a) linear polystyrene standards with weight average molecular weights (with increasing elution volume) of 524,000, 120,000, 27,500, 5,610, 1,920 g/mol, b) polymer **PSA1**, and c) polymer **PSA2** obtained from size exclusion chromatography. From the data derived from the light scat-

tering detector and with the refractive index increment (dn/dc) value of linear polystyrene ($= 0.184 \text{ mg/mL}$) the absolute molecular weight of a fraction at a given elution volume was calculated. The RI signal is proportional to the weight fraction of the eluted polymer and thus, the molecular weight distribution of the measured polymer is obtained [27 - 31].

With polystyrene **PSA1** (Figure 6.12.b), a number average molecular weight of $M_n = 2,330 \pm 466 \text{ g/mol}$ was measured assuming the error of the obtained molecular weight being within 20 %. The dispersity was found to be $M_w/M_n = 1.078$. Polystyrene **PSA2** (Figure 6.12.c) exhibited a number average molecular weight of $M_n = 6,407 \pm 1281 \text{ g/mol}$, with a dispersity of $M_w/M_n = 1.036$. The elution diagrams revealed that the peaks of both polymers were monomodal without fronting and tailing which shows that during the polymerisation no side reactions i. e. formation of dimers [17] or self-initiation and polymerization of the styrene [32] took place.

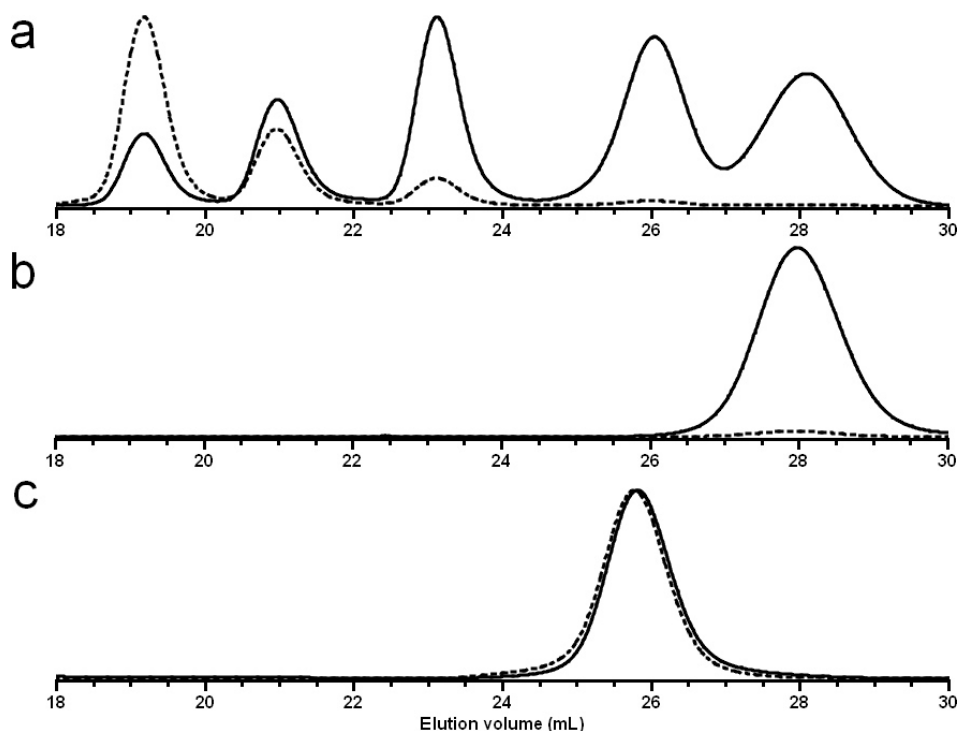


Figure 6.12: SEC elution diagrams (light scattering (dotted lines) and refractive index (straight lines)) of a) linear polystyrene standards, b) **PSA1**, and c) **PSA2**

With elemental analysis, an additional method besides $^1\text{H-NMR}$ and SEC was used to determine the number average molecular weights of the polystyrenes **PSA1** and **PSA2**. An overview over the measured and calculated number average molecular weights is given in Table 6.8. The composition of the polymers was calculated using the ratio nitrogen to carbon. It was found that **PSA1** exhibited a number average mo-

molecular weight of $M_n = 2,758 \pm 176$ g/mol and **PSA2** of $M_n = 30,473 \pm 40,726$ g/mol calculated based on the data of three measurements performed.

Table 6.8: Number average molecular weights M_n of the polystyrenes **PSA1 and **PSA2** based on $^1\text{H-NMR}$, SEC, and elemental analysis data**

	$^1\text{H-NMR}$	SEC	Elemental analysis
Entry	M_n (g/mol)	M_n (g/mol)	M_n (g/mol)
PSA1	$1,277 \pm 128$	$2,330 \pm 466$	$2,758 \pm 176$
PSA2	$5,612 \pm 561$	$6,407 \pm 1281$	$30,473 \pm 40,726$

SEC = size exclusion chromatography, M_n = number average molecular weight [g/mol]

Using the molecular weights obtained from the three methods the average molecular weight was calculated to be $M_n = 2121$ g/mol with **PSA1**. With **PSA2** the average molecular weight was determined to be $M_n = 6009$ g/mol using the molecular weights of the $^1\text{H-NMR}$ and SEC measurement since the molecular weight obtained from the elemental analysis was clearly too high. The error was calculated using the Gaussian error propagation law to be ± 772 g/mol. The measured and calculated molecular weights of **PSA1** and **PSA2** were within the scope of the error limits except the molecular weight obtained from the elemental analysis of **PSA2**.

By differential scanning calorimetry, the thermal behaviour of the polystyrenes **PSA1** and **PSA2** in the temperature region of -80 to 180°C was investigated to determine the temperatures at which melt and glass transitions occurs. In Figure 6.13, the differential scanning calorimetry thermograms of a) polystyrene **PSA1** and b) polystyrene **PSA2** are shown.

Polystyrene **PSA1** (Figure 6.13.a) exhibited a glass transition T_g at 57.7°C , while polystyrene **PSA2** (Figure 6.13.b) showed a glass transition at a lower temperature of $T_g = 82.4^\circ\text{C}$. The heat capacity change was determined to be $\Delta C_p = 0.27$ J/(g·K) with **PSA1** and 0.32 J/(g·K) with **PSA2**. The transition was reversible with both polymers. The higher glass transition temperature of **PSA2** was caused by that the number of repeating groups influencing the density of the configurational structure of the polymer at a given temperature in proportion to $1/M_n$ [33, 34] as shown in Equation 6.5.

$$T_{G,n} = T_{G,\infty} - \frac{K}{X_n} \quad \text{Eq. 6.6}$$

(with $T_{G,n}$ = glass transition temperature (T_G) of polymers exhibiting a chain length n , X_n = number average chain length, K = polymer-specific constant, $T_{G,\infty}$ = asymptotic value toward which T_G tends as molecular weight increases)

With the reported glass transition temperatures of polystyrenes ($M_n = 1940 - 5200$ g/mol) [35], a calibration curve was created and the glass transition temperatures of **PSA1** and **PSA2** were calculated using the number average molecular weights obtained from SEC. The expected temperatures were 63.8°C with **PSA1** and 90.3°C with **PSA2**. The lower glass transition temperatures measured were most likely caused by the impurities present in the polymers which were styrene and PMDTA with **PSA1** and PMDTA with **PSA2**.

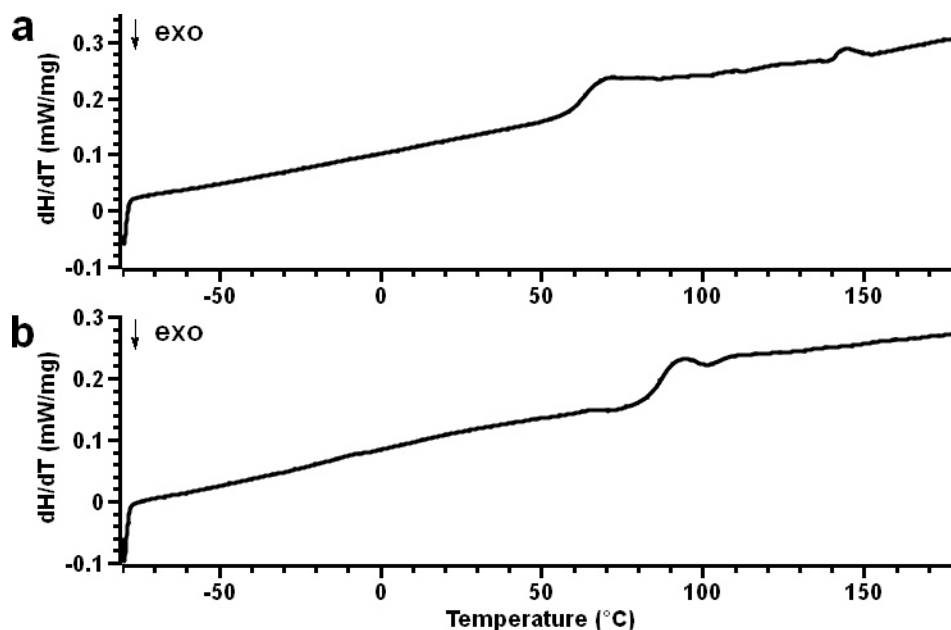


Figure 6.13: Differential scanning calorimetry thermograms of a) polystyrene **PSA1** and b) polystyrene **PSA2**, 2. heating run, N_2 atmosphere, $dT/dt = 10$ K/minute

The solubility of initiator **I1** and the polystyrenes **PSA2** and **PSA1** in common solvents was investigated. The results are listed in Table 6.9 and the solvents are arranged from the most polar to the most non-polar solvent in descending order using the empirical parameter of the solvent polarity $E_s(30)$ [36, 37]. While initiator **I1** was soluble in polar to semi-polar solvents ranging from methanol to tetrahydrofuran, both polystyrenes were soluble in semi-polar to non-polar solvents ranging from dimethylformamide to cyclohexane. The reaction of poly(ethylenimine) with these polystyrenes should, therefore, lead to polymers which are soluble in semi-polar to non-polar solvents.

Table 6.9: Solubility of initiator I1, and the polystyrenes PSA1 and PSA2

Solvent	<u>I1</u>	<u>PSA1</u>	<u>PSA2</u>
Water	x	x	x
Methanol	o	x	x
Dimethylformamide	o	o	o
Acetone	o	o	o
Dichloromethane	o	o	o
Chloroform	o	o	o
Ethyl acetate	o	o	o
Tetrahydrofuran	o	o	o
Diethyl ether	x	o	o
Toluene	x	o	o
Cyclohexane	x	o	o
Heptane	x	x	x

o = soluble, - = dispersion, x = insoluble

Discussion

Two polystyrenes were prepared by an ATRP polymerization of styrene using 2-bromo-2-methyl-propionic acid 2,5-dioxopyrrolidin-1-yl ester (= I1) as the initiator to create polystyrenes bearing an active ester moiety (PSA2 and PSA1).

The ¹H-NMR and ¹³C-NMR spectrum of initiator I1 exhibited signals of the succinimide and the ester hydrogen and carbon atoms at positions which were in good agreement to the theoretical values showing that the initiator was successfully prepared. The spectra of PSA1 and PSA2 showed besides signals of the succinimide and the ester hydrogen and carbon atoms also signals of the polystyrene aromatic and aliphatic groups. It was found that while the spectra of PSA1 exhibited traces of non-polymerised styrene and PMDTA, PSA2 contained only PMDTA impurities but no non-reacted styrene which shows that the more complex purification performed with PSA2 was necessary to remove non-reacted styrene.

The functional groups present in initiator I1 and the polystyrenes PSA2 and PSA1 were determined by IR spectrometry. While the spectrum of initiator I1 exhibited only bands of the succinimide and the ester moiety, both polymers showed additionally the characteristic bands of polystyrene which indicates that both polystyrenes contained an active ester group.

The investigation of the polystyrenes by ^1H -DOSY NMR revealed that both polystyrenes exhibited only one diffusion coefficient at positions at which the signals of the polystyrene and the active ester appeared which show that each polystyrene had an active ester covalently attached to it.

The number average molecular weight of polystyrene **PSA2** was determined to be $M_n = 5,612 \pm 561$ g/mol with ^1H -NMR, $M_n = 6,407 \pm 1281$ g/mol with size exclusion chromatography (SEC), and $M_n = 30,473 \pm 40,726$ g/mol with elemental analysis. The values obtained from ^1H -NMR and SEC were within the scope of the error limits which shows that both methods could be used to determine the molecular of the polymer. Since the calculation of the molecular weight based on elemental analysis data was performed by using the ratio carbon to nitrogen atoms the higher molecular weight obtained indicates that a matrix effect caused a diminishing of the nitrogen signal intensity and, therefore, to the detection of a lower number of nitrogen atoms than it should be. Polystyrene **PSA1** exhibited lower molecular weights of $M_n = 1,277 \pm 128$ g/mol (^1H -NMR), $M_n = 2,330 \pm 466$ g/mol (SEC), and $M_n = 2,758 \pm 176$ g/mol (elemental analysis) compared to those obtained with polystyrene **PSA2** which shows, taking into account that both polymers were prepared at the same temperature and reaction time, that the polymerization of the styrene stopped at some point most likely due to the diffusion of oxygen into the reaction mixture. Furthermore, since the three molecular weights were within the scope of the error limits it was concluded that with very small polymers the matrix effect was not as drastic and elemental analysis could be used for the determination of the molecular weight.

The analysis of the elution diagrams of the polymers revealed that both polymers exhibited monomodal peaks without fronting and tailing which shows that during the polymerisation no side reactions such as the formation of dimers or self-initiation and polymerization of the styrene occurred. The polymers exhibited small dispersities of $M_w/M_n = 1.078$ (**PSA1**) and $M_w/M_n = 1.036$ (**PSA2**) which shows a well-controlled ATRP polymerization.

The investigation of the polystyrenes **PSA2** and **PSA1** by differential scanning calorimetry showed that the temperature at which the glass transition occurred depended on the length of the polymer chain. The low molecular weight polymer **PSA1** exhibited a glass transition at 57.7°C . Polymer **PSA2**, on the other hand, showed a glass transition at 82.4°C . The reason for this behaviour was that the number of segments influenced the density of the configurational structure of the polymer at a given temperature in proportion to $1/M_n$ [33, 34]. Both transitions were lower than the theoretical values which could be attributed to styrene and PMDTA (**PSA1**) and PMDTA (**PSA2**) impurities present in the polymers.

Solubility studies of initiator **I1** and the polystyrenes **PSA2** and **PSA1** revealed that

while **I1** was soluble in polar to semi-polar solvents ranging from methanol to tetrahydrofuran, the polystyrenes were soluble in semi-polar to non-polar solvents ranging from dimethylformamide to cyclohexane making them suitable for the preparation of poly(ethylenimine)s which could be dissolved in semi-polar to non-polar solvents.

6.3.2 Preparation of “polystyrene-quat-primer” polymers bearing ammonium moieties and polystyrene groups (= PEI(nkD)_xQ^{yPS(nkD)})

Poly(ethylenimine)s bearing simultaneously ammonium and polystyrene moieties were prepared by reacting hyperbranched poly(ethylenimine) with glycidyltrimethylammonium chloride and polystyrene-N-hydroxysuccinimide esters to create PEI(nkD)_xQ^{yPS(nkD)} polymers (cf. Figure 6.14).

It was found that crosslinked polymers were obtained after workup and drying which could not be re-dissolved in any solvents. Most likely the crosslinking was caused by the reaction of the amine groups of the poly(ethylenimine) with the halogenoalkane-termini of the polystyrene side-chains. To bypass this problem literature reports to react propylene oxide with the non-occupied amine groups to prevent them from reacting with the halogenoalkanes [38]. Since this procedure added about 200 (i. e. one OH group per monomer unit) of polar alcohol groups to the poly(ethylenimine) which may lower the solubility of the polymer in semi-polar or non-polar solvents it has been decided to react the halogenoalkanes of the polystyrenes with 2-aminoethanol instead. Although polar alcohol moieties will also be added by this procedure, the molar ratio of hydroxyl groups to poly(ethylenimine) would be the same as the molar ratio of polystyrene chains to poly(ethylenimine), i. e. about 2.2 – 6.1 mol% (i. e. \approx 5 – 14 OH groups per polymer unit). Hence, blocking the PS-termini with 2-aminoethanol introduces by far less OH groups than reacting all amino groups with propylene oxide.

Three polymers namely **PPS1** – **PPS3** were prepared by stirring the compounds in chloroform for 23 hours at 60°C. Afterwards, 2-aminoethanol was added and the mixture was stirred another 66 h at 60°C. The solvent was then removed under reduced pressure and the polymer was precipitated in water. The liquid fraction was removed by centrifugation and the polymers were dried at 60°C for 19 hours in vacuum. Polymer **PPS1** was prepared in a smaller quantity to test the preparation conditions. The yield after drying was determined to be 1.2 g (51.2 wt.% of theory).

PPS1 was scaled up (**PPS2**, 128.2 g and **PPS3**, 577.1 g) and used directly for the preparation of adduct **EP1** after the reactions were finished and most of the solvents were removed. A small amount of **PPS2** was purified as described with **PPS1** and characterised with the aim to verify that this type of polymer could be synthesised in

6 Preparation of [montmorillonite/PEI(nkD)xQyPS(nkD)]

a larger quantity.

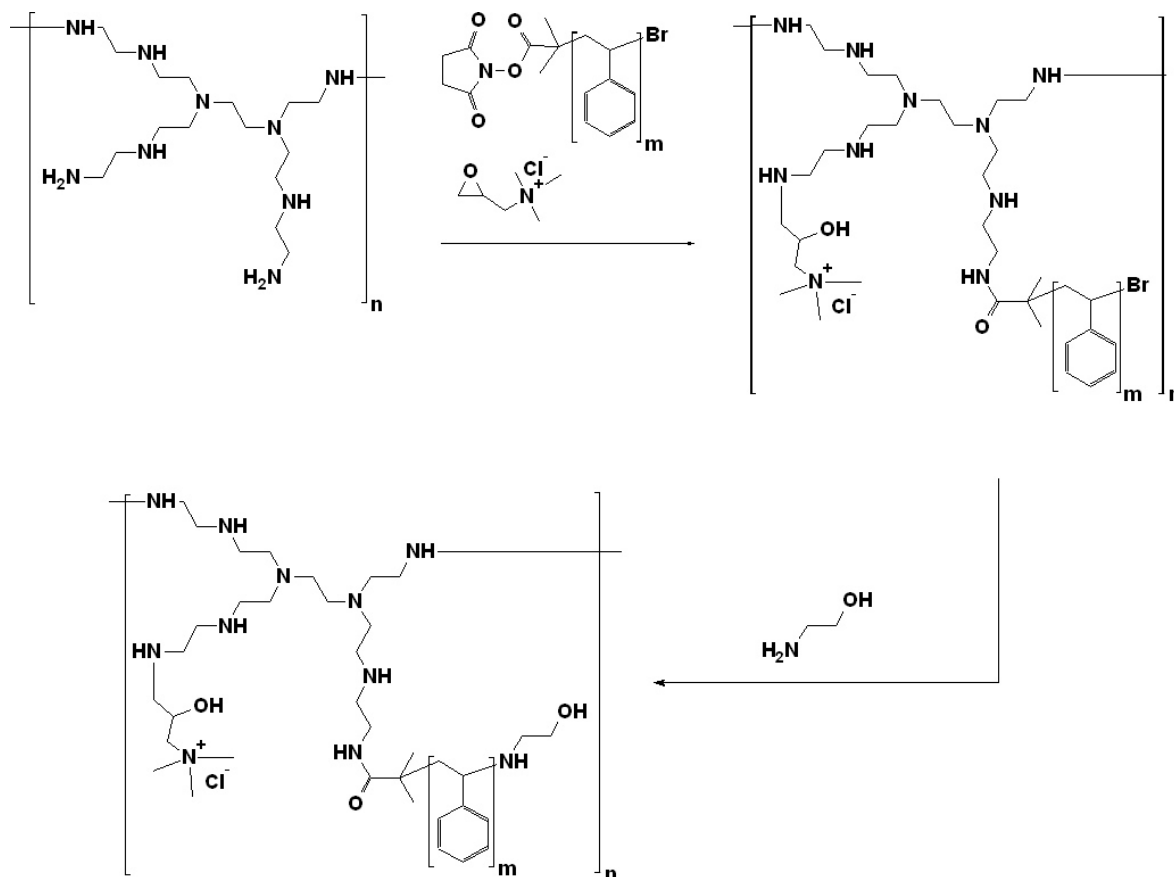


Figure 6.14: Preparation of "polystyrene-quat-primer" polymers bearing ammonium moieties and polystyrene groups (= PEI(nkD)_{xQ}^{yPS(nkD)})

Table 6.10 lists the PEI(10kD)_{10Q}^{yPS(nkD)} polymers which will be discussed in the following paragraphs. The used polystyrenes **PSA1** and **PSA2** exhibited two different molecular weights which enabled the study of the influence of the polystyrene chain length on the solubility properties of the respective PEI(10kD)_{10Q}^{yPS(nkD)} polymer.

Table 6.10: PEI(10kD)_{10Q}^{yPS(nkD)} polymers discussed in the following paragraphs

Entry	Description	Polystyrene M _{n,SEC} (g/mol)	Synthesis condition	Yield (wt.%)
PPS1	PEI(10kD) _{10Q} ^{6.1PS(2.3kD)}	2,330	60°C, 89 h, CHCl ₃	51.2
PPS2	PEI(10kD) _{10Q} ^{2.2PS(6.4kD)}	6,407	60°C, 89 h, CHCl ₃	not determined

PEI(10kD) = poly(ethyleneimine) with M_n = 10,000 g/mol, M_w/M_n = 2.5, xQ = mol% 2-hydroxypropyl-3-(N,N,N-trimethylammonium chloride), yPS = mol% polystyrene-g-2-aminoethanol, M_{n,SEC} = number average molecular weight obtained from size exclusion chromatography [g/mol]

6 Preparation of [montmorillonite/PEI(nkD)_xQyPS(nkD)]

The presence of polystyrene and 2-hydroxypropyl-3-(N,N,N-trimethylammonium chloride) groups in the PEI(10kD)_{10Q}^{yPS(nkD)} polymers **PPS1** and **PPS2** was verified by ¹H-NMR spectroscopy. In Figure 6.15, the ¹H-NMR spectrum of polymer **PPS1** is shown.

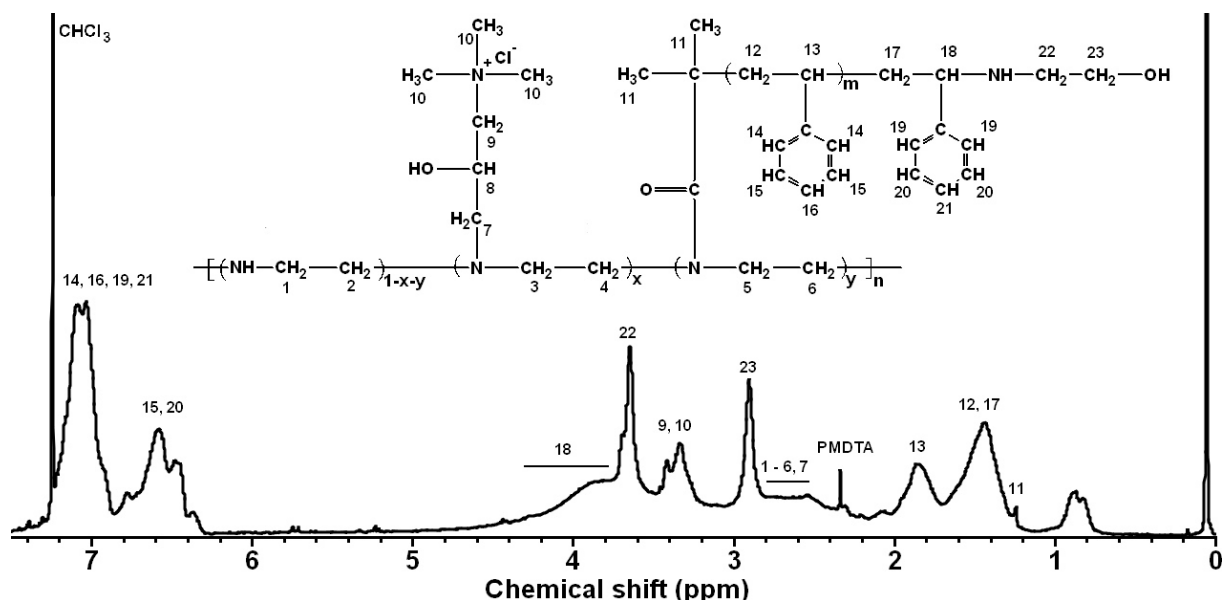


Figure 6.15: ¹H-NMR spectrum of polymer **PPS1**, CDCl₃, 30°C

The signal belonging to the poly(ethylenimine) methylene hydrogen atoms was measured at 2.40 - 3.00 ppm (1 - 6), overlapping with the signal of the methylene group (7) of the 2-hydroxypropyl-3-(N,N,N-trimethylammonium chloride) attached to the polymer. The methylene group of the ammonium moieties was detected at 3.20 - 3.40 ppm (9, 10). The hydrogen atoms of the polystyrene methylene group in the direct vicinity of the 2-aminoethanol were found at 3.10 - 4.50 ppm (18). Different to the PEI(10kD)_{xQ}^{yR} polymers discussed in Chapter 3 no peak of the hydrogen atom of the methylene group (8) attached to the hydroxyl moiety was detected at 3.50 - 3.70 ppm, probably due to the strong signal intensity of the hydrogen atom of the polystyrene methylene group in the direct vicinity of the 2-aminoethanol at 3.10 - 4.50 ppm (18).

The six hydrogen atoms of the methyl groups (11) sandwiched by the amide moiety and the polystyrene were measured at 1.24 ppm. The two hydrogen atoms of the methylene group of the polystyrene appeared at 1.20 - 1.70 ppm (12, 17). The hydrogen atom of the methylene group of the polystyrene in the direct vicinity of the aromatic ring was located at 1.70 - 2.20 ppm (13). The hydrogen atoms of the aromatic ring of the polystyrene gave signals at 6.85 - 7.20 ppm (14, 16, 19, 21) and 6.30 - 6.85 ppm (15, 20). The four hydrogen atoms of the methylene groups of the 2-amino-

ethanol were found at 3.64 ppm (22) and 2.90 ppm (23). Furthermore, the presence of N,N,N',N',N''-pentamethyldiethylenetriamine (= PMDTA) was shown by the peak at 2.34 ppm showing that the purification procedure had to be optimised to remove all impurities.

With polymer **PPS2**, the location of the signals of the hydrogen atoms was the same as with polymer **PPS1** with the difference that the hydrogen atom of the polystyrene methylene group (18) attached to the 2-aminoethanol showed a distinct peak with a maximum at 4.07 ppm. Since many signals were overlapping with each other, a calculation of the ratio poly(ethylenimine) to the compounds was very difficult to accomplish. Nonetheless, the spectra of **PPS1** and **PPS2** revealed the presence of poly(ethylenimine), polystyrene and the attached 2-aminoethanol, and 2-hydroxypropyl-3-(N,N,N-trimethylammonium chloride) in the polymers but no succinimide groups which indicates that the replacement of these moieties by the poly(ethylenimine)s was successful.

The covalent attachment of the 2-hydroxypropyl-3-(N,N,N-trimethylammonium chloride) and the polystyrenes to the poly(ethylenimine)s was checked by ^1H -DOSY NMR studies. Figure 6.16 shows the ^1H -DOSY NMR spectra of a) polymer **PPS1** and b) polymer **PPS2**. The diffusion coefficients and hydrodynamic radii are also listed in Table 6.11.

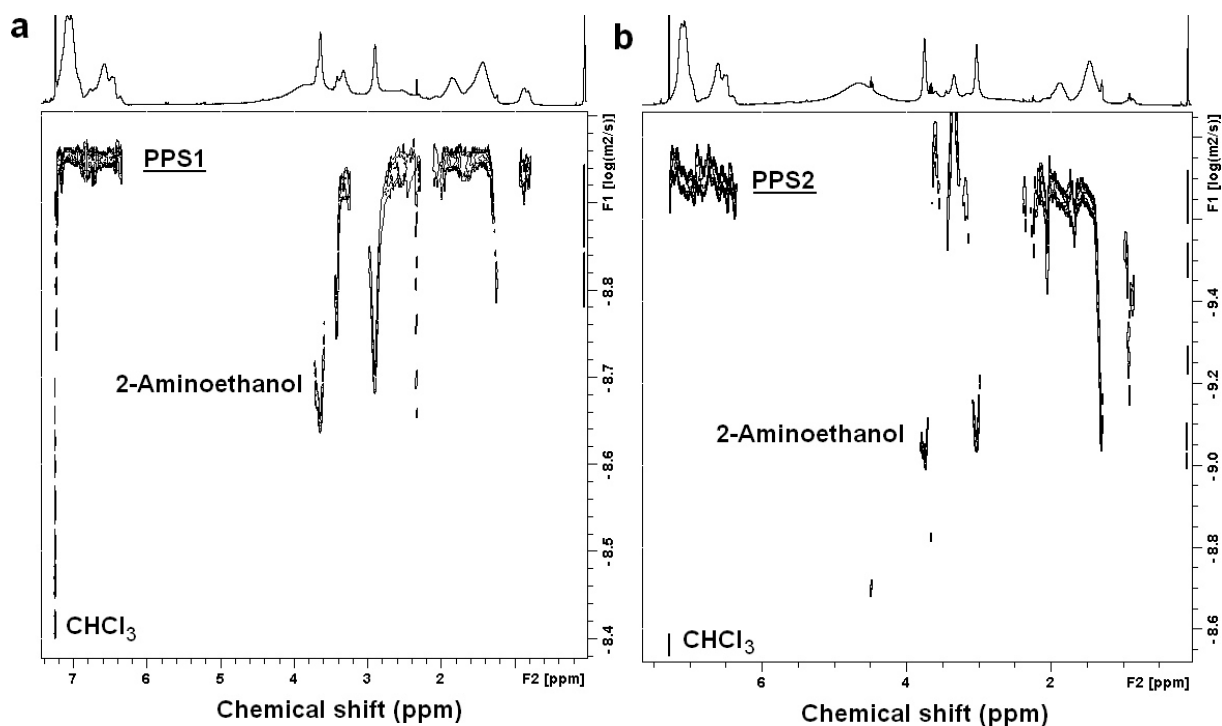


Figure 6.16: ^1H -DOSY NMR spectra of a) polymer **PPS1** and b) polymer **PPS2**, CDCl_3 , 30°C

Table 6.11: Diffusion coefficients of the PEI(10kD)_{10Q}^{yPS(nkD)} polymers **PPS1 and **PPS2****

Entry	Composition	Solvent	Diffusion coefficient (-log D m ² /s)	R ₀ (nm)
PPS1	PEI(10kD) _{10Q} ^{6.1PS(2.3kD)}	CDCl ₃	8.95	0.39
PPS2	PEI(10kD) _{10Q} ^{2.2PS(6.4kD)}	CDCl ₃	9.60	1.74

PEI(10kD) = poly(ethylenimine) with M_n = 10,000 g/mol, M_w/M_n = 2.5, xQ = mol% 2-hydroxypropyl-3-(N,N,N-trimethylammonium chloride), yPS = mol% polystyrene-g-2-aminoethanol, R₀ = hydrodynamic radius [nm]

The diffusion coefficient of dissolved molecules is described by the Stokes–Einstein Equation shown earlier (cf. Eq. 6.4), revealing diffusion coefficients of -log D = 8.95 m²/s (**PPS1**, Figure 6.16.a) and -log D = 9.60 m²/s (**PPS2**, Figure 6.16.b) as well as hydrodynamic radii of 0.39 nm (**PPS1**) and 1.74 nm (**PPS2**), respectively.

The spectra showed furthermore that both compounds contained besides aminoethanol units attached to the polymers also free 2-aminoethanol moieties. With polymer **PPS1**, the free 2-aminoethanol exhibited two diffusion coefficients of (i) -log D = 8.64 m²/s and (ii) -log D = 8.68 m²/s which corresponded to hydrodynamic radii of 0.19 nm and 0.21 nm. Diffusion coefficients of free 2-aminoethanol of (i) -log D = 9.025 m²/s (R₀ = 0.46 nm) and (ii) -log D = 9.05 m²/s (R₀ = 0.49 nm) were detected with **PPS2**. The higher diffusion coefficients of the non-reacted 2-aminoethanol shows that the mobility of free 2-aminoethanol was higher than those of 2-aminoethanol groups attached to the PEI(10kD)_{10Q}^{yPS(nkD)} polymers proving the successful addition of this groups to the polymers.

The diffusion coefficient of the chloroform in the **PPS1** solution was measured to be D = 3.89·10⁻⁹ m²/s (-log D = 8.41 m²/s), corresponding to a hydrodynamic radius of 0.11 nm. The chloroform in the **PPS2** solution, on the other hand, exhibited with a diffusion coefficient of D = 2.82·10⁻⁹ m²/s (-log D = 8.55 m²/s) a hydrodynamic radius of 0.16 nm. The diffusion coefficients of the chloroform were in reasonable good agreement to the coefficients measured with the polystyrenes **PSA2** and **PSA1** (cf. Figure 6.9) as well as the values obtained with PEI(nkD)_{xQ}^{yR} polymers (cf. Chapter 3), and those reported in a previous study [25].

Comparing the hydrodynamic radius of polymer **PPS1** of 0.39 nm with that of the corresponding polystyrene **PSA1** of 0.37 nm (cf. Figure 6.9) it was found that the addition of the short polystyrene chains only led to a small increase of the hydrodynamic radius. The hydrodynamic radius of polymer **PPS2** of 1.74 nm, on the other hand, was much higher than that of the corresponding polystyrene **PSA2** (cf. Figure 6.9) of 0.49 nm. In conclusion, since both polymers showed only one diffusion coefficient of the poly(ethylenimine) and the attached compounds the covalent attachment of the

6 Preparation of [montmorillonite/PEI(nkD)xQyPS(nkD)]

components to the poly(ethylenimine)s was confirmed.

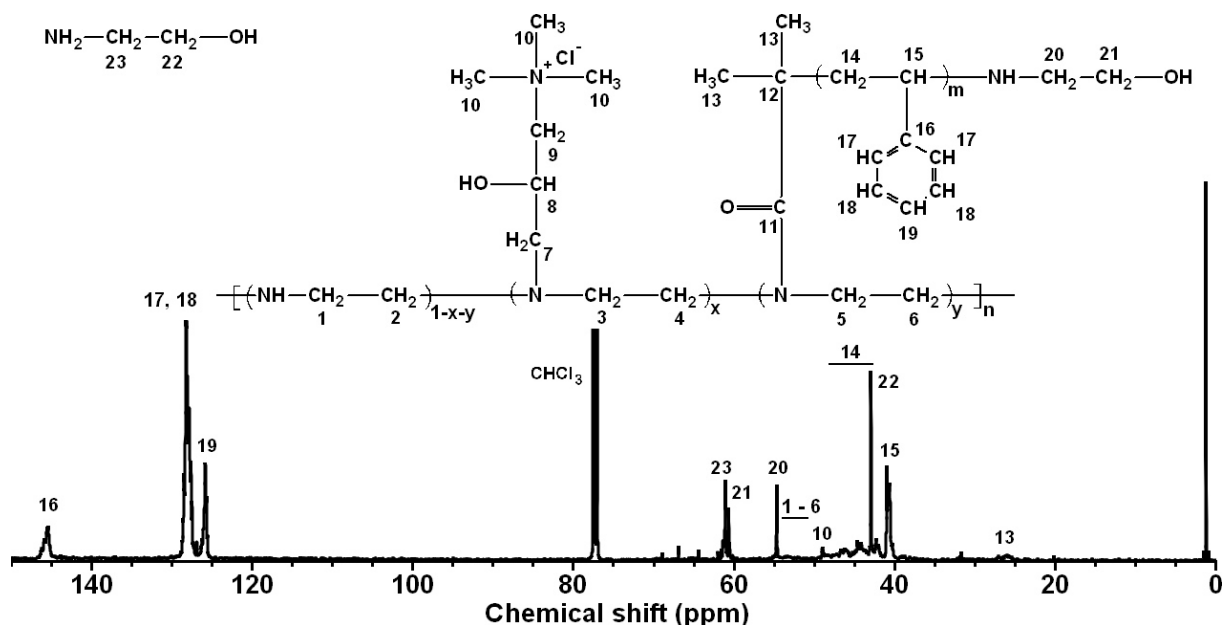


Figure 6.17: ^{13}C -NMR spectrum of polymer **PPS1**, CDCl_3 , 30°C

The structures of the polymers **PPS1** and **PPS2** were further investigated by ^{13}C -NMR. The spectrum of polymer **PPS1** is shown in Figure 6.17. With both polymers, the poly(ethylenimine) methylene carbon atoms were detected at 50.0 - 54.0 ppm (1 - 6). The methyl carbon atoms attached to the ammonium moiety of the 2-hydroxypropyl-3-(N,N,N-trimethylammonium chloride) appeared at 48.9 ppm (10). Signals of the other carbon atoms of the ammonium moieties were too weak to be correctly assigned. The polystyrene methylene carbon atoms were measured at 41.5 - 48.9 ppm (14), and 39.5 - 41.5 ppm (15). The carbon atoms of the aromatic rings were found at 144.0 - 147.0 ppm (16), 126.5 - 129.0 ppm (17, 18), and 124.5 - 126.5 ppm (19). The carbon atoms (13) of the methyl groups located between the amide moiety and the polystyrene units appeared at 24.5 - 28.0 ppm.

The 2-aminoethanol units attached to the polystyrenes showed up at 60.5 ppm (21) and 54.6 ppm (20), and signals of non-reacted 2-aminoethanol were detected at 61.0 ppm (23) and 42.8 ppm (22) which shows that a) both polymers contained attached 2-aminoethanol units which prove the successful addition of this groups to the polystyrenes, and b) that the purification procedure had to be optimised to remove excess 2-aminoethanol. By integration of the area of the peaks at 60.5 ppm and 61.0 ppm, the molar ratio of free 2-aminoethanol units to 2-aminoethanol groups attached to polymer **PPS1** was determined to be 1.4 to 1 which corresponded with the theoretical composition of the polymer of $\text{PEI}(10\text{kD})_{10\text{Q}}^{6.1\text{PS}(2.3\text{kD})}$ to a free 2-aminoethanol concentration in the mixture of 2.5 wt.%.

6 Preparation of [montmorillonite/PEI(nkD)xQyPS(nkD)]

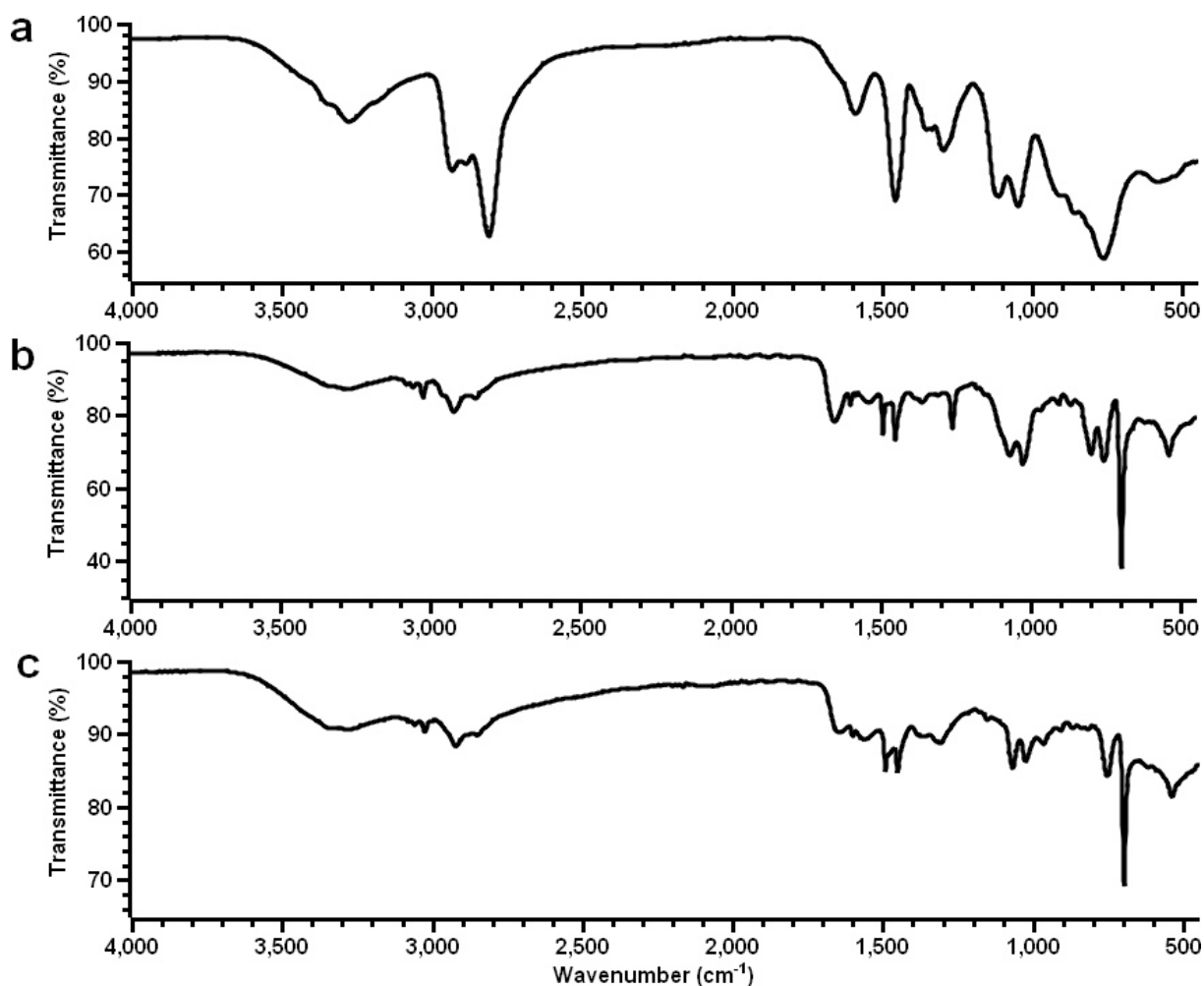


Figure 6.18: ATR-FT infrared spectra of a) poly(ethylenimine), b) polymer **PPS1**, and c) polymer **PPS2**

IR investigations on the polymers **PPS1** and **PPS2** were performed to obtain information about the functional groups present in the polymers. In Figure 6.18 the infrared spectra of a) poly(ethylenimine), b) polymer **PPS1**, and c) polymer **PPS2** are compared.

The spectrum of the neat poly(ethylenimine) (Figure 6.18.a) showed an amine N-H stretching band at 3277 cm^{-1} and an amine N-H deformation vibration band at 1587 cm^{-1} . Amine C-N deformation vibration bands were measured at 1333, 1295, 1111, and 1045 cm^{-1} . Alkane C-H stretching bands appeared at 2932, 2885, and 2810 cm^{-1} . An alkane C-H deformation vibration band was detected at 1455 cm^{-1} . In the fingerprint region ($= <1000\text{ cm}^{-1}$), bands were measured at 762 and 575 cm^{-1} .

With polymer **PPS1** (Figure 6.18.b), the N-H stretching vibration band of the poly(ethylenimine) amine groups and the O-H stretching vibration bands of the alcohol moieties of the 2-hydroxypropyl-3-(N,N,N-trimethylammonium chloride), free 2-

aminoethanol, and 2-aminoethanol groups attached to the polymer were found at 3281 cm^{-1} . The stretching vibration band of the secondary CH-OH alcohol derived from the ammonium groups was detected at 1069 cm^{-1} . A band corresponding to the O-H stretching vibration band of free 2-aminoethanol groups, and attached 2-aminoethanol moieties was measured at 1026 cm^{-1} . The amide (I) C=O stretching vibration band was located at 1651 cm^{-1} , and the amide (II) C=O stretching vibration band at 1538 cm^{-1} . C-C stretching vibration bands corresponding to the aromatic ring showed up at 3081 , 3058 , 3025 , 1600 , 1492 , and 1451 cm^{-1} . Stretching vibration bands of aliphatic C-H groups were measured at 2959 , 2920 , 2848 , and 1362 cm^{-1} . In the fingerprint region ($= <1000\text{ cm}^{-1}$), bands were found at 907 , 866 , 798 , 756 , 696 , and 538 cm^{-1} .

The spectrum of polymer **PPS2** (Figure 6.18.c) showed bands at similar positions as detected with polymer **PPS1** with the differences that the band at 2959 was too weak to be assigned correctly, and the band at 756 cm^{-1} was missing. Both polymers contained no bands corresponding to succinimide moieties or ester carbonyl groups as measured with the polystyrenes (cf. Figure 6.11). Instead, bands of an amide moiety were observed which shows that the poly(ethylenimine)s reacted with the active ester and replaced the succinimide groups.

The thermal behaviour of the polymers **PPS1** and **PPS2** in the temperature region of $-80 - 180^\circ\text{C}$ was investigated by differential scanning calorimetry to obtain information about the transitions of the polymers at this temperatures. In Figure 6.19 the differential scanning calorimetry thermograms of a) poly(ethylenimine), b) polymer **PPS1**, and c) polymer **PPS2** are shown.

The neat poly(ethylenimine) (Figure 6.19.a) exhibited a glass transition T_g at -49.5°C and a heat capacity change of $\Delta C_p = 0.84\text{ J/(g}\cdot\text{K)}$. With polymer **PPS1** (Figure 6.19.b) the glass transition of the poly(ethylenimine) backbone was detected at $T_g = -47.4^\circ\text{C}$ ($\Delta C_p = 0.07\text{ J/(g}\cdot\text{K)}$) and the transition of the polystyrene chains at $T_g = 60.2^\circ\text{C}$ ($\Delta C_p = 0.12\text{ J/(g}\cdot\text{K)}$). In the thermogram of polymer **PPS2** (Figure 6.19.c), on the other hand, only the glass transition of the polystyrene chains was observed at $T_g = 80.2^\circ\text{C}$ ($\Delta C_p = 0.13\text{ J/(g}\cdot\text{K)}$). The higher glass transition temperature of the polystyrene of polymer **PPS2** was caused by the dependence of the glass transition on the number of segments in the chain in proportion $1/M_n$ [33, 34] (cf. Equation 6.5). The transition was reversible with the three polymers. The glass transition temperatures were similar to those of the polystyrenes **PSA2** and **PSA1** (cf. Figure 6.13) which shows that the thermal transitions of the polystyrenes were influenced only little by the poly(ethylenimine)s most likely due to the distance of the polystyrene chains to the poly(ethylenimine) backbone created by the amide spacers. The similar

glass transition temperatures of the free and attached polystyrenes point to that block-copolymers were created in which a microphase-segregation occurred.

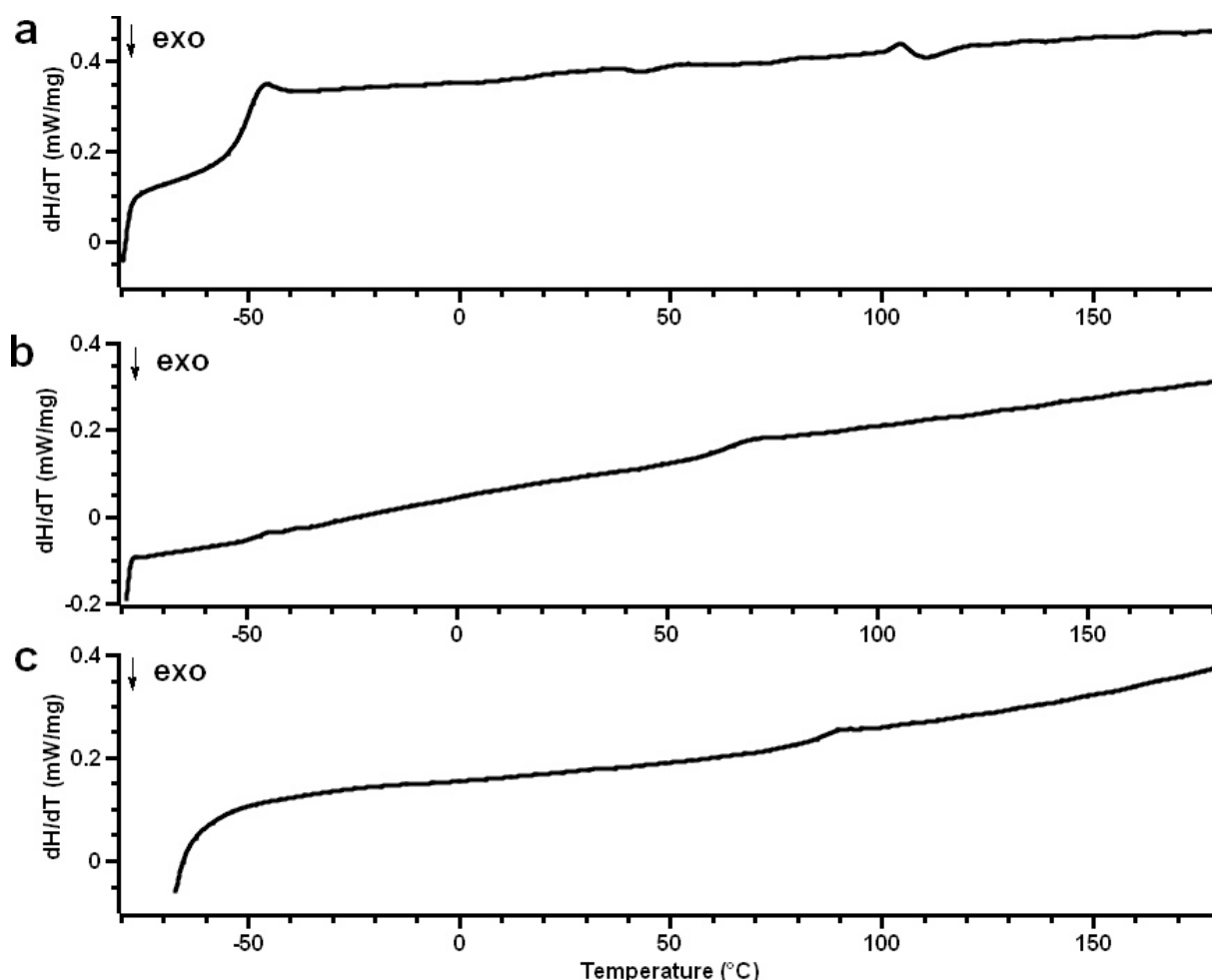


Figure 6.19: Differential scanning calorimetry thermograms of a) poly(ethylenimine), b) polymer **PPS1**, and c) polymer **PPS2**, 2. heating run, N_2 atmosphere, $dT/dt = 10$ K/minute

With the data obtained from the elemental analysis of the polymers **PPS1** and **PPS2**, the polystyrene and 2-hydroxypropyl-3-(N,N,N-trimethylammonium chloride) content of the polymers was calculated. The calculation was performed by using the number average molecular weights obtained from elemental analysis of the polystyrenes **PSA2** and **PSA1** which are $M_n = 12,975$ g/mol (**PSA2**) and $M_n = 2,758$ g/mol (**PSA1**). The obtained values of the polymers **PPS1** and **PPS2** are listed in Table 6.12.

With polymer **PPS1**, the molar ratio polystyrene to poly(ethylenimine) was calculated to be 0.042 to 1 which corresponded to a degree of polystyrene modification of 4.2 mol%. Polymer **PPS2** exhibited a degree of polystyrene modification of 0.7 mol%. The 2-hydroxypropyl-3-(N,N,N-trimethylammonium chloride) content was found to be 11 mol% with both polymers which was in good agreement to the theoretical ammoni-

um content of 10 mol%. Although the calculated degrees of polystyrene modification were only 1.9 mol% (**PPS1**) and 1.5 mol% (**PPS3.2**) lower than the theoretical ones the high uncertainty of this method for the determination of polymer compositions was illustrated during the discussion of the polystyrene polymers **PSA1** and **PSA2** before (cf. Table 6.8).

Table 6.12: Polystyrene and “quat” content of the PEI(10kD)_xQ_yPS(nkD) polymers **PPS1 and **PPS2** based on elemental analysis data**

Entry	Composition	PS (mol%)			Q (mol%)		
		exp.	th.	Δ	exp.	th.	Δ
PPS1	PEI(10kD) _{10Q} ^{6.1PS(2.3kD)}	4.2	6.1	1.9	11	10	1
PPS2	PEI(10kD) _{10Q} ^{2.2PS(6.4kD)}	0.7	2.2	1.5	11	10	1

PEI(10kD) = poly(ethylenimine) with $M_n = 10,000$ g/mol, $M_w/M_n = 2.5$, $xQ = \text{mol\% 2-hydroxypropyl-3-(N,N,N-trimethylammonium chloride)}$, $yPS = \text{mol\% polystyrene-g-2-aminoethanol}$

The solubility of the polymers **PPS1** and **PPS2** in common solvents was investigated to check how the chain length of the added polystyrenes influenced the solubility. Mixtures of 10 mg polymer per mL solvent were qualitatively judged by optical inspection after a standing time of 30 minutes at $T = 20^\circ\text{C}$. The respective polymer was regarded to be soluble when no substance particles were visible in the solution. Blurry solutions or solutions containing visible substance particles in the solution were called a dispersion. When the polymer didn't dissolve in a solvent it was judged as insoluble. Table 6.13 lists the solubility of the polymers with the solvents arranged from the most polar to the most non-polar solvent in descending order using the empirical parameter of the solvent polarity $E_T(30)$ [36, 37].

While the neat poly(ethylenimine) was soluble in water and polar to semi-polar solvents ranging from methanol to chloroform, polymer **PPS1** was soluble in some semi-polar solvents such as dimethylformamide, dichloromethane, chloroform, and tetrahydrofuran but not in acetone. On the other hand, the polymer was soluble in the non-polar solvent toluene. Only a dispersion was obtained when ethyl acetate was used as the solvent. Different to the solubility of polystyrene **PSA1** (cf. Table 6.9) the solubility was narrowed to a smaller window centred around the semi-polar solvent chloroform. Polymer **PPS2**, on the other hand, formed dispersions in dimethylformamide, dichloromethane, and chloroform and was insoluble in all other solvents tested.

Table 6.13: Solubility of poly(ethylenimine) and the polymers PPS1 and PPS2

	PEI(10kD)	PPS1	PPS2
xQ		10	10
yPS		6.1 ($M_{n,SEC} = 2,330$ g/mol)	2.2 ($M_{n,SEC} = 6,407$ g/mol)
Solvent			
Water	o	x	x
Methanol	o	x	x
Dimethylformamide	o	o	-
Acetone	o	x	x
Dichloromethane	o	o	-
Chloroform	o	o	-
Ethyl acetate	-	-	x
Tetrahydrofuran	-	o	x
Diethyl ether	x	x	x
Toluene	x	o	x
Cyclohexane	x	x	x
Heptane	x	x	x

o = soluble, - = dispersion, x = insoluble, PEI(10kD) = poly(ethylenimine) with $M_n = 10,000$ g/mol, $M_w/M_n = 2.5$, xQ = mol% 2-hydroxypropyl-3-(N,N,N-trimethylammonium) chloride, yPS = mol% polystyrene-g-2-aminoethanol, $M_{n,SEC}$ = number average molecular weight obtained from size exclusion chromatography [g/mol]

To compare the number average molecular weight of the polymers **PPS1** and **PPS2** with their solubility's, the number average molecular weight M_n of the polymers was calculated using Equation 6.6.

$$M_{n,Pol} = X_{n,PEI} \cdot (M_{PEI} + M_{n,PS} \cdot N_{PS} + M_Q \cdot N_Q + M_{2-A} \cdot N_{2-A}) \quad \text{Eq. 6.7}$$

(with $M_{n,Pol}$ = number average molecular weight of the whole polymer [g/mol], $X_{n,PEI(10kD)}$ = degree of polymerization, M_{PEI} = molecular weight of the repeating unit of poly(ethylenimine) [g/mol], $M_{n,PS}$ = number average molecular weight of the respective polystyrene [g/mol], M_Q = molecular weight of 2-hydroxypropyl-3-(N,N,N-trimethylammonium chloride) [g/mol], M_{2-A} = molecular weight of 2-aminoethanol, N_{PS} , N_Q , and N_{2-A} = mole fraction of 2-aminoethanol, 2-hydroxypropyl-3-(N,N,N-trimethylammonium chloride), and polystyrene)

Polymer **PPS1** exhibited a theoretical number average molecular weight of $M_n = 47,402$ g/mol and polymer **PPS2** of $M_n = 46,576$ g/mol. Although the number average molecular weights of both polymers were similar, the addition of larger quantities of a polystyrene with a lower number average molecular weight led to a polymer which

was soluble in semi-polar solvents, the addition of lower quantities of higher molecular weight polystyrene, on the other hand, created a polymer with very poor solubility properties. Poly(ethylenimine) should be therefore modified by a polystyrene with a molecular weight around 2,000 g/mol to obtain a polymer with a solubility suitable for the modification of bitumen.

Discussion

In this investigation two PEI(10kD)_{10Q}^{yPS(nkD)} polymers bearing simultaneously ammonium and polystyrene moieties (**PPS1** and **PPS2**) were prepared by reacting hyperbranched poly(ethylenimine) with glycidyltrimethylammonium chloride and polystyrene-N-hydroxysuccinimide esters of two different molecular weights. It was found that the amine groups of the poly(ethylenimine) reacted with the halogenoalkane group at the end of the polystyrene chains which led to crosslinked polymers upon drying. Therefore the halogenoalkane moieties were reacted with 2-aminoethanol to prevent the crosslinking of the PEI(10kD)_{10Q}^{yPS(nkD)} polymers.

The ¹H-NMR spectra of both polymers exhibited peaks corresponding to the poly(ethylenimine), the polystyrene-g-2-aminoethanol, and the 2-hydroxypropyl-3-(N,N,N-trimethylammonium chloride) which shows these compounds were present in the polymers. The spectra revealed furthermore the presence of PMDTA residues derived from the preparation of the polystyrenes which shows that the purification procedure had to be optimised. No signals corresponding to succinimide groups were measured which indicates that these groups were successfully replaced by the poly(ethylenimine)s.

The ¹³C-NMR spectra of the polymers **PPS1** and **PPS2** showed sharp signals with high intensities of the carbon atoms of the polystyrene and the 2-aminoethanol moieties but broad signals with weak intensities of the poly(ethylenimine) and the 2-hydroxypropyl-3-(N,N,N-trimethylammonium chloride) groups. On the other hand, both spectra revealed the presence on non-reacted 2-aminoethanol moieties showing again the need of a thorough purification of the polymers.

The investigation of the polymers **PPS1** and **PPS2** by IR showed that both polymers contained poly(ethylenimine) and the polystyrene groups. The successful formation of an amide linkage between the poly(ethylenimine)s and the polystyrenes was proven by the presence C=O amide (I) and amide (II) bands around 1651 and 1538 cm⁻¹. Both polymers exhibited no bands of the NHS-ester which shows that the succinimide groups were successfully replaced by the poly(ethylenimine)s.

The attachment of the reactants to the poly(ethylenimine)s was confirmed from the diffusion coefficient of the polymers **PPS1** and **PPS2** obtained from ¹H-DOSY NMR

measurements. With both polymers, only one diffusion coefficient was measured of the poly(ethylenimine), the polystyrene, and the 2-hydroxypropyl-3-(N,N,N-trimethylammonium chloride) moieties which prove the covalent attachment of the reactants to the poly(ethylenimine)s. While polymer **PPS1** exhibited a diffusion coefficient of $-\log D = 8.95 \text{ m}^2/\text{s}$, corresponding to a hydrodynamic radius of 0.39 nm, the diffusion coefficient of polymer **PPS2** was lower with $-\log D = 9.60 \text{ m}^2/\text{s}$ and corresponded to a hydrodynamic radius 1.74 nm. It was found further that the diffusion coefficients of the free 2-aminoethanol moieties in the samples were higher than those of the 2-aminoethanol units attached to the polymers which prove the successful addition of this moieties to the polystyrenes.

Investigations of the thermal behaviour of the polymers **PPS1** and **PPS3** by differential scanning calorimetry showed that polymer **PPS1** exhibited glass transitions of the poly(ethylenimine) at $T_G = -47.4^\circ\text{C}$ and of the polystyrene at $T_G = 60.2^\circ\text{C}$. With polymer **PPS2**, the glass transition was measured at $T_G = 80.2^\circ\text{C}$ but the signal of the poly(ethylenimine) backbone was too weak to be assigned accordingly. The glass transition temperatures of the free and attached polystyrenes were found to be similar which indicates that block-copolymers were created in which a micro-phase-segregation of the compounds took place.

Based on elemental analysis data the molar ratio poly(ethylenimine) to polystyrene was calculated. The calculated degrees of polystyrene modification were found to be with 4.2 mol% with polymer **PPS1** and 0.7 mol% with polymer **PPS2** in reasonable good agreement to the theoretical ones of 6.1 mol% (**PPS1**) and 2.2 mol% (**PPS2**). But as shown from previous investigations, this method bears a high uncertainty due to a matrix effect which caused the detection of a lower number of nitrogen atoms in the samples as it should be.

Comparing the solubility of the polymers **PPS1** and **PPS2** in common solvents it was found that while polymer **PPS1** was soluble in dimethylformamide, dichloromethane, chloroform, tetrahydrofuran, and toluene, polymer **PPS2** gave only dispersions in dimethylformamide, dichloromethane, and chloroform. Although both polymers exhibited similar number average molecular weights, the differences in the solubility shows that the solubility of the modified poly(ethylenimine) depended strongly on the polystyrenes chain length, i. e. the addition of a larger number of smaller polystyrene polymers created a modified poly(ethylenimine) which was soluble in non-polar solvents.

6.3.3 Preparation of the [MMT_{B2}/PEI(10kD)_{10Q}^{2.2PS(6.4kD)}] adduct **EP1**

The polymers **PPS2** and **PPS3** were selected for the modification of the montmoril-

lonite with the aim to test whether this polymer type could be used to prepare an [MMT_{B2}/PEI(10kD)_{10Q}^{2.2PS(6.4kD)}] adduct with fully intercalated polymers and to test the influence of the polymer fraction after the adduct was incorporated into bitumen.

The adduct was prepared by mixing the PEI(10kD)_{10Q}^{2.2PS(6.4kD)} polymers **PPS2** and **PPS3** with an aqueous solution of montmorillonite and 1-hexadecyltrimethylammonium bromide (= "indirect replacement" method, cf. Figure 4.25, Chapter 4) at an elevated temperature. After the reaction was complete, the liquid fraction was removed by centrifugation and the residue was washed three times with methanol. After removal of the solvent by centrifugation the adduct was dried under vacuum at elevated temperature. After drying, the adduct appeared as a brown coloured solid substance, the yield was determined to be 103.9 % of theory.

To determine the interlayer distance between the montmorillonite platelets, adduct **EP1** was examined by wide-angle X-ray diffraction. Figure 6.20 compares the XRD diffractograms of a) Na-bentonite **B2** and b) adduct **EP1**, with the intensities of the diffractograms normalised to the reflexes at $2\Theta = 19.7^\circ$.

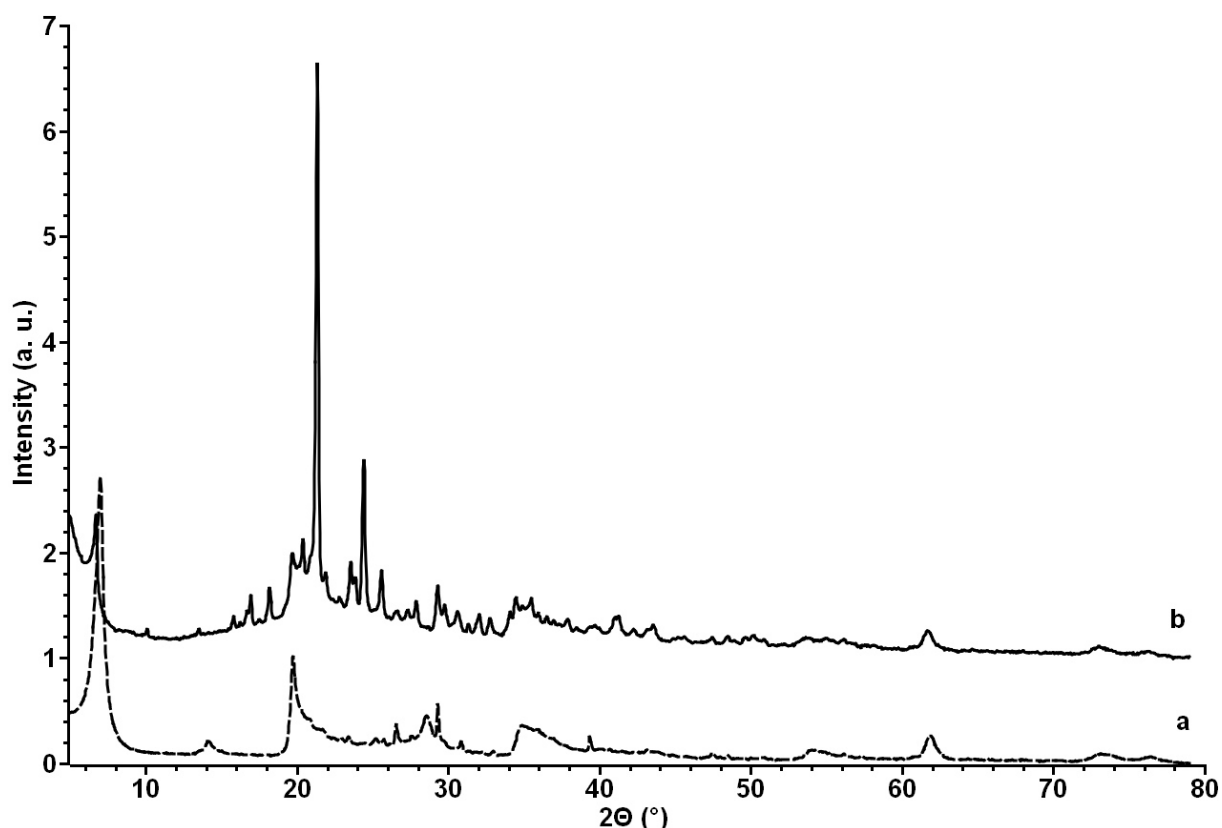


Figure 6.20: Wide-angle X-ray diffractograms of a) Na-bentonite **B2** and b) adduct **EP1**

In the region of $2\Theta (^\circ) = 5$ to 20° adduct **EP1** (Figure 6.20.b) showed reflexes at $2\Theta =$

6.7, 10.1, 13.5, 15.8, 16.3, 16.7, 17.0 and 18.2°. The reflexes at $2\Theta = 6.7, 15.8, 16.7, 17.0$ and 18.2° were attributed to intercalated 1-hexadecyltrimethylammonium bromide with an interlayer distance $d_{001(1)}$ of 1.32 ± 0.02 nm. On the other hand, using the formula of a monoclinic crystal system (cf. Chapter 2), the reflexes at $2\Theta = 10.1, 13.5$ and 16.3° could be assigned to the Miller indices $d_{005}, d_{007},$ and d_{008} which led after extrapolation to an interlayer distance $d_{001(2)}$ of 4.44 ± 0.03 nm, corresponding to a lattice constant c of $4.5 \text{ nm} \pm 0.03 \text{ nm}$. The gap d_m between the montmorillonite platelets was calculated by subtracting the thickness of one montmorillonite platelet (0.66 nm [39]) from the value of the lattice constant c and was found to be $d_m = 3.84 \text{ nm}$.

Since two distinct d_{001} interlayer distances were measured it is clear that the adduct consisted of a mixture of montmorillonite with intercalated CTAB and montmorillonite containing a mixture of PEI(10kD)_{10Q}^{2.2PS(6.4kD)} and CTAB as shown in Figure 4.26, Chapter 4. The “degree of polymer intercalation”, D_i , was calculated using Equation 4.1 of Chapter 4, the theoretical diameter of the polymer of 5.17 nm (Eq. 4.2 – 4.5, Chapter 4), and the gap of a sample with a fully intercalated polymer of a similar polymer diameter of $d_i = 6.23 \text{ nm}$ (adduct **E8.2**, cf. Figure 4.39) to be $D_i = 62 \%$. This means that 62 % of the total area of one polymer molecule was intercalated between the montmorillonite platelets while 38 % remained outside. In conclusion, although the main part of the polymer was successfully intercalated as shown from the high value of the degree of polymer intercalation no complete intercalation was achieved showing that the preparation method had to be improved further.

To determine the purity and composition of adduct **EP1** the compound was studied by ¹H-MAS-NMR and the corresponding spectrum is shown in Figure 6.21. The spectrum showed signals of the five hydrogen atoms in the aromatic rings of the polystyrene in the region of 6.10 - 7.20 ppm (14 -16). The hydrogen atoms of the aliphatic groups were measured at 1.59 ppm (13) and 1.10 ppm (12). Both signals were overlapping with signals derived from 1-hexadecyltrimethylammonium bromide (21, 22). The 2-aminoethanol groups attached to the polystyrene moieties were detected at 3.44 ppm (17) and 2.78 ppm (18), overlapping with the signal of two hydrogen atoms of the 1-hexadecyltrimethylammonium bromide (20).

The poly(ethylenimine) methyl groups (1 – 6) and the methyl moiety (7) of the 2-hydroxypropyl-3-(N,N,N-trimethylammonium chloride) attached to the polymer appeared between 2.70 – 2.20 ppm. The assignment of the 2-hydroxypropyl-3-(N,N,N-trimethylammonium chloride) methyl groups was performed by using the spectrum of a neat PEI(10kD)_{10Q}^{yPS(nkD)} polymer (cf. Figure 6.15) because the strong signal intensities of the CTAB hydrogen atoms at 3.30 ppm (19) made the correct assignment impossible. The methyl groups (11) located between by the amide and the polystyrene

6 Preparation of [montmorillonite/PEI(nkD)xQyPS(nkD)]

aliphatic groups were found at 1.20 ppm, also overlapping with the signal of one CTAB methyl moiety (23). The methyl group (24) at the end of the CTAB alkyl chain was detected at 0.72 ppm.

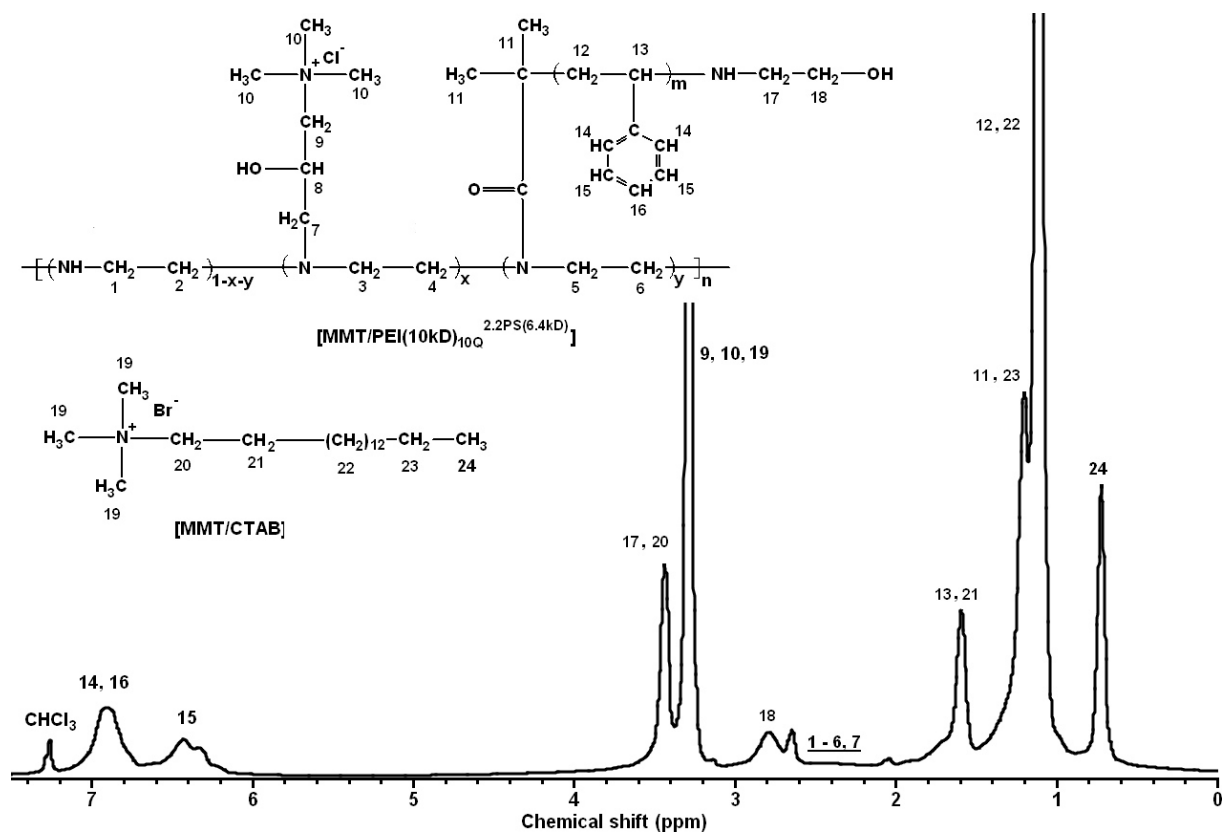


Figure 6.21: ¹H-MAS-NMR spectrum of adduct **EP1**, CDCl₃, 30°C

The ratio of polystyrene to CTAB was calculated by using the integrated area of the hydrogen atoms of the polystyrene ring (14 – 16) and the integrated area of the hydrogen atoms of the methyl group (24) at the end of the CTAB alkyl chain as shown in Equation 6.8 to be 0.8 to 1. With the theoretical composition of the polymer, the weight concentration of CTAB in the polymer/CTAB mixture was determined to be 4.8 wt.%.

$$\frac{N_{\text{PS}}}{N_{\text{CTAB}}} = \frac{A_{\text{PS(C5H5)}}}{A_{\text{CTAB(CH3)}}} \cdot \frac{3}{5} \quad \text{Eq. 6.8}$$

(with N_{PS} = number of polystyrene molecules [mol], N_{CTAB} = number of CTAB molecules [mol], $A_{\text{PS(C5H5)}}$ = integrated ¹H-NMR signal intensity of the polystyrene hydrogen atoms at 6.10 - 7.20 ppm, $A_{\text{CTAB(CH3)}}$ = integrated ¹H-NMR signal intensity of the CTAB hydrogen atoms at 0.72 ppm)

To sum up, although signals of the poly(ethylenimine), and the polystyrene were

6 Preparation of [montmorillonite/PEI(nkD)xQyPS(nkD)]

found in the spectrum, the strong intensities derived from the 1-hexadecyltrimethylammonium bromide methyl groups made the verification of the presence of 2-hydroxypropyl-3-(N,N,N-trimethylammonium chloride) impossible.

To further investigate the structure of adduct **EP1** the compound was studied by ^{13}C -MAS-NMR. The corresponding spectrum is shown in Figure 6.22.

Signals of the five carbon atoms of the aromatic ring of the polystyrene showed up at 127.9 ppm (15, 16) and 125.7 ppm (17). The signal of the carbon atom of the aliphatic C-H group attached to the ring was detected at 40.4 ppm (13). Signals of 1-hexadecyltrimethylammonium bromide appeared at 66.6, 53.2, 31.6, 29.4, 26.0, 23.0, 22.4 and 13.8 ppm (20 - 27). Furthermore, signals of the 2-aminoethanol groups attached to the polystyrene moieties were measured at 63.3 ppm (19) and 43.8 ppm (18). Signals of the poly(ethylenimine) and the 2-hydroxypropyl-3-(N,N,N-trimethylammonium chloride) carbon atoms were too weak to be assigned correctly.

In conclusion, while the ^1H -MAS-NMR spectrum revealed the presence of polystyrene in the adduct, the ^{13}C -MAS-NMR spectrum proved that the 2-aminoethanol moieties were attached to the polystyrene groups. The presence of CTAB shows again that with the used preparation procedure no pure $[\text{MMT}_{\text{B2}}/\text{PEI}(10\text{kD})_{10\text{Q}}]^{2.2\text{PS}(6.4\text{kD})}$ adduct was obtained.

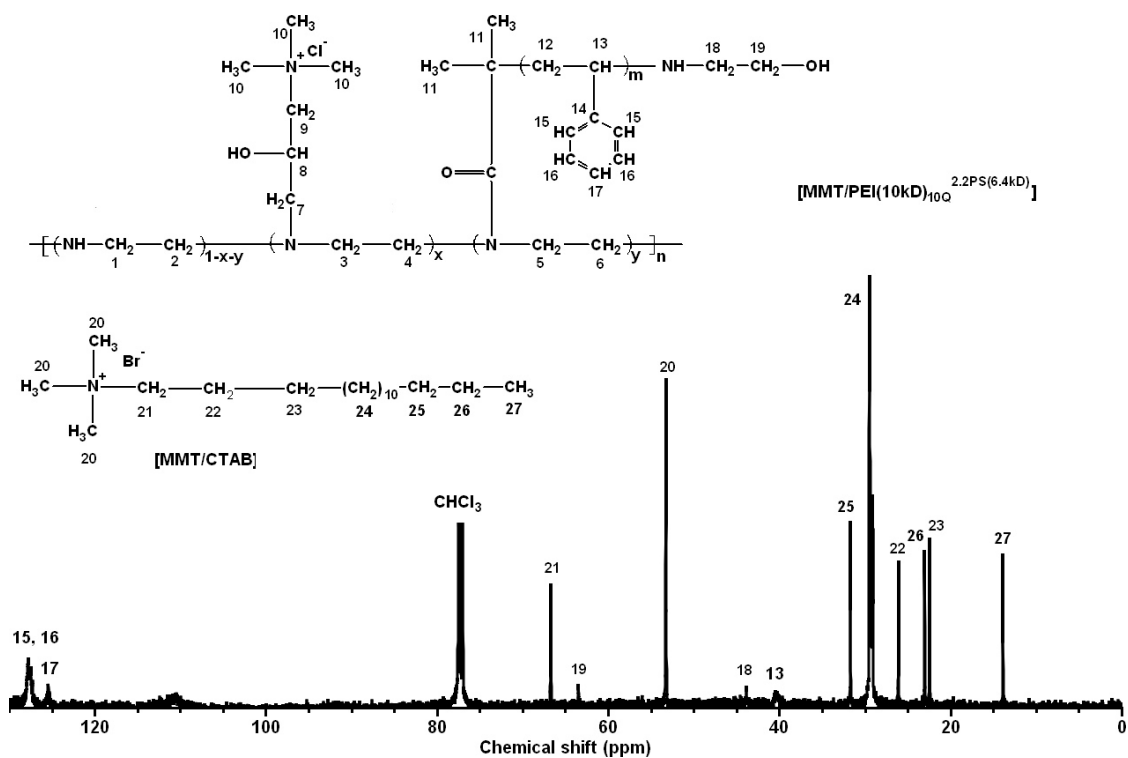


Figure 6.22: ^{13}C -MAS-NMR spectrum of adduct **EP1**, CDCl_3 , 30°C

To determine the functional groups present in adduct **EP1**, the adduct was investigated by infrared spectroscopy. In Figure 6.23, the infrared spectra of a) Na-bentonite **B2** and b) adduct **EP1** are compared. The neat Na-bentonite (Figure 6.23.a) exhibited an Al-OH stretching vibration band at 3625 cm^{-1} and Si-O stretching vibration bands at 1113 and 994 cm^{-1} . Deformation vibration bands of Al-OH-Al and Al-OH-Mg moieties and an Al-O-Si function were found at 915 , 841 , and 514 cm^{-1} . Water O-H stretching and deformation vibration bands were detected at 3402 and 1633 cm^{-1} [40, 41].

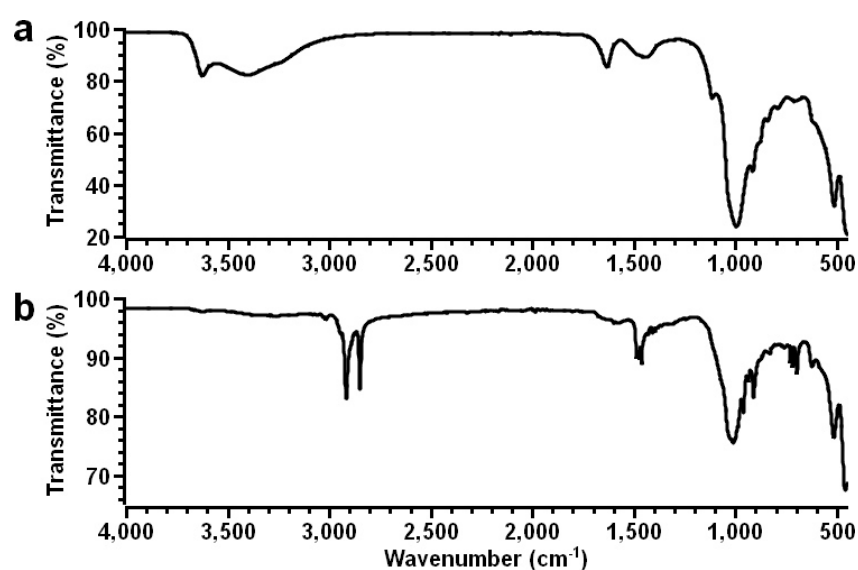


Figure 6.23: ATR-FT infrared spectra of a) Na-bentonite **B2** and b) adduct **EP1**

With adduct **EP1** (Figure 6.23.b), a shift of the Al-OH stretching vibration band to a smaller wavelength of 3622 cm^{-1} was observed. Of the two Si-O stretching vibration bands which appeared in the spectrum of the neat bentonite, only one band showed up which was also shifted from 994 to 1010 cm^{-1} which point to an interaction between the organic compounds with the Si-O-Si groups of the montmorillonite. Deformation vibration bands of an Al-OH-Al group and an Al-O-Si function were detected at 911 and 515 cm^{-1} . The presence of 1-hexadecyltrimethylammonium bromide was shown by aliphatic C-H stretching vibration bands at 2916 and 2848 cm^{-1} as well as C-H deformation vibration bands at 1472 and 1461 cm^{-1} . An N-CH₃ deformation vibration band was measured at 1486 cm^{-1} . Bands derived from the alkyl chain C-(CH₂)_n-C were present at 730 and 718 cm^{-1} [42, 43]. The presence of polystyrene was shown by C-C stretching vibration bands, derived from the aromatic ring, at 3029 , 3017 and 1600 cm^{-1} . The N-H stretching vibration band of the poly(ethylenimine) amine groups and the O-H stretching vibration bands of the alcohol groups of the 2-hydroxypropyl-3-(N,N,N-trimethylammonium chloride) and the 2-aminoethanol moiety-

ies attached to the polystyrene groups gave a very weak signal in the region of 3550 to 3050 cm^{-1} with a maximum similar to that of the neat polymer (cf. Figure 6.18.c) at 3281 cm^{-1} . The amide (I) C=O stretching vibration band was found to be shifted from 1647 cm^{-1} with polymer **PPS2** to at 1636 cm^{-1} with adduct **EP1** and the amide (II) C=O stretching vibration band from 1561 cm^{-1} to 1577 cm^{-1} . Other bands in the fingerprint region ($= < 1000 \text{ cm}^{-1}$) were detected at 960, 697, and 623 cm^{-1} .

Due to the strong intensity of the Si-O-Si stretching vibration band of the montmorillonite at 1010 cm^{-1} stretching vibration bands of the $\text{CH}_n\text{-OH}$ hydroxyl groups of the 2-hydroxypropyl-3-(N,N,N-trimethylammonium chloride) and the 2-aminoethanol moieties in this region could not be assigned. The spectrum of adduct **EP1** showed again that the adduct contained besides montmorillonite and the $\text{PEI}(10\text{kD})_{10\text{Q}}^{2.2\text{PS}(6.4\text{kD})}$ polymer also CTAB. The shift of the Si-O-Si stretching vibration band indicates that the ammonium groups of the CTAB and the polymer interacted with the montmorillonite.

The thermal behaviour of adduct **EP1** in the temperature region of -80 to 180°C was investigated by differential scanning calorimetry to obtain information about the transitions of the polymer in the adduct. Since the $^1\text{H-MAS-NMR}$, the $^{13}\text{C-MAS-NMR}$, and the IR investigation of the adduct revealed the presence of CTAB the differential scanning calorimetry thermograms of a) polymer **PPS2**, b) adduct **E4.1** and c) adduct **EP1** are compared in Figure 6.24.

The thermogram of adduct **EP1** (Figure 6.24.c) exhibited a glass transition T_g at 14.6°C with a heat capacity change of $\Delta C_p = 0.22 \text{ J}/(\text{g} \cdot \text{K})$. The origin of this transition was not clear since the neat poly(ethylenimine) exhibited a glass transition at a much lower temperature of $T_g = -49.5^\circ\text{C}$ (cf. Figure 6.19.a). The thermogram exhibited another two melting transitions at $T_m = 27.2^\circ\text{C}$ and 60.0°C . While the melting transition T_m at 27.2°C (enthalpy = 2.8 J/g) was attributed to 2-aminoethanol groups confined between the montmorillonite platelets, the transition at 60.0°C (enthalpy = 9.2 J/g) could be caused by the polystyrene attached to the poly(ethylenimine) but due to the strong intensity of the CTAB the assignment of this transition was not sure. The melting transition of free CTAB was detected at $T_m = 82.4^\circ\text{C}$ with the enthalpy of the transition measured to be 26.4 J/g. One melting transition of intercalated CTAB appeared at $T_m = 33.2^\circ\text{C}$ [44]. The enthalpy of the transition was determined to be 2.3 J/g. With the enthalpies the molar ratio of free to intercalated CTAB was calculated to be 11.5 to 1 which means that only 8 wt.% of the CTAB was intercalated into the montmorillonite platelets. All mentioned transition were reversible indicating that the transitions which could not be attributed to CTAB had to be caused by the intercalated polymer.

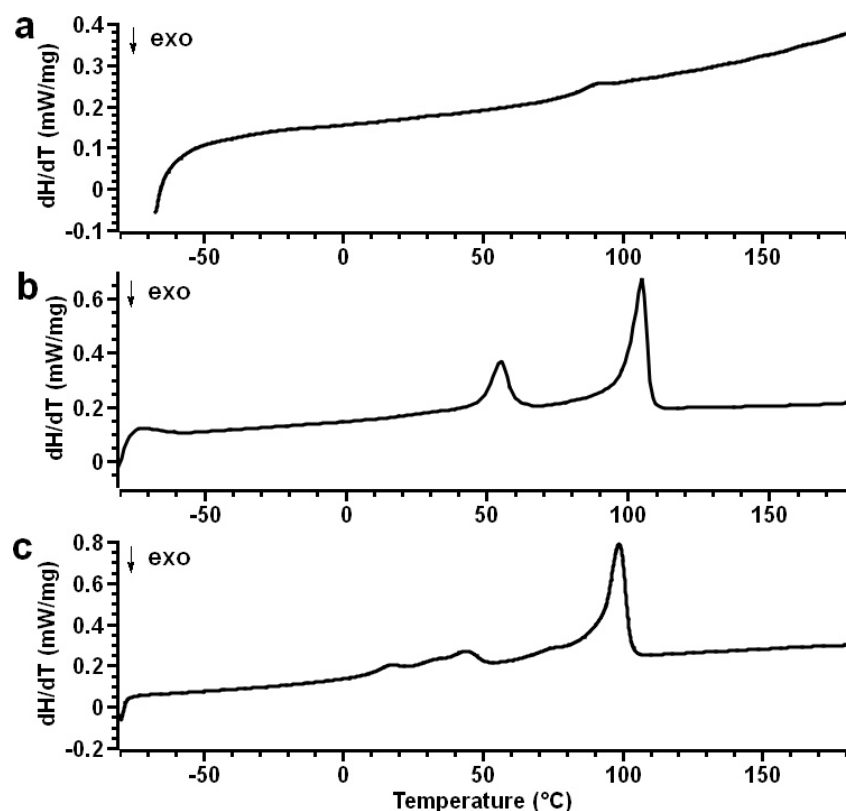


Figure 6.24: Differential scanning calorimetry thermograms of a) polymer **PPS2**, b) adduct **E4.1**, and c) adduct **EP1**, 2. heating run, N_2 atmosphere, $dT/dt = 10$ K/minute

The organic content of adduct **EP1** was determined by a calcination experiment (cf. experimental part for details). It was found that the adduct contained 67.8 wt.% of the organic material, which was 14.7 wt.% higher than theoretically expected. With the weight concentration of CTAB in the polymer/CTAB mixture of 4.8 wt.% (cf. Equation 6.7), the weight concentration of CTAB in the adduct was determined to be 3.2 wt.%.

Discussion

In this work, an $[MMT_{B2}/PEI(10kD)_{10Q}^{2.2PS(6.4kD)}]$ adduct (= **EP1**) was prepared by reacting a $PEI(10kD)_{10Q}^{2.2PS(6.4kD)}$ polymer with montmorillonite by simultaneous replacement of 1-hexadecyltrimethylammonium bromide in an [MMT/CTAB] intermediate.

The interlayer distance between the montmorillonite platelets in the adduct was calculated from the data obtained by a wide-angle X-ray diffraction measurement. It was found that the adduct exhibited two d_{001} interlayer distances of $d_{001(1)} = 1.32 \pm 0.02$ nm and $d_{001(2)} = 4.44 \pm 0.03$ nm. While the $d_{001(1)}$ distance was attributed to a montmorillonite with intercalated CTAB, the $d_{001(2)}$ distance could be assigned to a montmorillonite containing a mixture of $PEI(10kD)_{10Q}^{2.2PS(6.4kD)}$ and CTAB. With the lattice constant c of the $d_{001(2)}$ distance the gap d_m between the montmorillonite platelets was de-

terminated to be 3.84 nm which was smaller than the theoretical diameter of the polymer of 5.17 nm and shows that the polymer was not completely intercalated. The calculation of the degree of polymer intercalation revealed that 62 % of the total area of one polymer molecule was intercalated between the montmorillonite platelets while 38 % remained outside.

Through the investigation of the adduct by ^1H - and ^{13}C -MAS-NMR the presence of polystyrene, poly(ethylenimine), and CTAB moieties in the adduct was confirmed showing that not a pure $[\text{MMT}_{\text{B2}}/\text{PEI}(10\text{kD})_{10\text{Q}}^{2.2\text{PS}(6.4\text{kD})}]$ adduct was obtained. Furthermore, due to the strong intensities of the CTAB methyl groups the presence of the 2-hydroxypropyl-3-(N,N,N-trimethylammonium chloride) groups attached to the poly(ethylenimine) could not be determined. The IR study of the adduct showed that the ammonium groups of the polymer and the CTAB interacted with the Si-O-Si moieties of the montmorillonite shown by a shift of the band corresponding to the montmorillonite Si-O-Si moieties.

The investigation of the adduct by differential scanning calorimetry revealed that the adduct exhibited one glass transition T_g at 14.6°C and four melting transitions T_m at 27.2, 33.2, 60.0, and 82.4. While the melting transitions at 33.2 and 82.4°C were attributed to free CTAB and CTAB intercalated into the montmorillonite platelets, the transition at $T_m = 33.2^\circ\text{C}$ was attributed to confined 2-aminoethanol and the transition at $T_m = 60.0^\circ\text{C}$ to polystyrene groups. By a calcination experiment, the organic content of the adduct was determined to be 67.8 wt.% which was 14.7 wt.% higher than theoretically expected. The weight concentration of CTAB in the adduct was determined by ^1H -MAS-NMR to be 3.2 wt.%. Due to the non-uniform distributed CTAB in the adduct, the determination of the correct polymer content was difficult which could explain the high organic content measured with the sample.

Summary

In this study two polystyrenes, **PSA1** and **PSA2** which contained both active ester chain ends were prepared by polymerising styrene via an ATRP polymerization. The covalent attachment of a succinimide active ester moiety to the polystyrenes was verified by means of a combination of ^1H -, ^1H -DOSY, ^{13}C -NMR and IR spectroscopy. The substances contained, however, small quantities of non-converted styrene monomers, and PMDTA. The number average molecular weights and dispersities of the polystyrenes determined by size exclusion chromatography (SEC) were $M_n = 2,330$ g/mol ($M_w/M_n = 1.078$) (**PSA1**), and $M_n = 6,407$ g/mol ($M_w/M_n = 1.036$) (**PSA2**). The low dispersities demonstrates a well controlled ATRP polymerization. The elution diagrams of the polymers revealed both polystyrenes to be monomodal without indic-

ators of side reactions. The glass transition temperatures of the polymers were 57.7°C (**PSA1**) and 82.4 °C (**PSA2**), lower than the theoretical temperatures which could be attributed to the impurities present in the samples. The evaluation of solubility investigations revealed that both polystyrenes were soluble in a broad range of semi-polar to non-polar solvents ranging from dimethylformamide to cyclohexane which indicates that both polymers could be suitable to graft to poly(ethylenimine)s.

The polystyrenes were grafted on poly(ethylenimine) to create polymers bearing aromatic chains. The poly(ethylenimine)-g-polystyrene polymers **PPS1** and **PPS2** were further reacted with glycidyltrimethylammonium chloride with the aim to add permanently positive charge to the poly(ethylenimine). The polystyrene groups were end-capped by 2-aminoethanol moieties afterwards to prevent a reaction of the poly(ethylenimine) amino groups with the halogenoalkane moiety at the end of the polystyrene chains. Through the characterization of the polymers by ¹H-NMR, ¹H-DOSY-NMR, ¹³C-NMR, and IR spectroscopy the covalent attachment of the polystyrene-g-2-aminoethanol, and the 2-hydroxypropyl-3-(N,N,N-trimethylammonium chloride) to the poly(ethylenimine)s was confirmed. The spectra further revealed the presence of non-reacted 2-aminoethanol moieties which shows that the purification procedure was not yet optimised. It was found that the temperatures of the thermal transitions of the modified poly(ethylenimine)s were similar to those of the pure substances which shows that due to the distance between the poly(ethylenimine)s and the polystyrenes, created by the amide linkage, the transitions of the single compounds was not hindered, i. e. block-copolymers were created which exhibited a microphase-segregation. The calculation of the molar ratio of poly(ethylenimine) to polystyrene based on elemental analysis data showed that the experimentally obtained values were in fairly good agreement to the theoretically expected values. The solubility investigation of the polymers showed that the addition of a higher quantity of a low molecular weight polystyrene (with $M_n = 2,330$ g/mol) to poly(ethylenimine) created a polymer which was soluble in semi-polar to non-polar solvents. The addition of a lower quantity of a higher molecular weight polystyrene (with $M_n = 6,407$ g/mol), on the other hand, resulted in a polymer which could only be dispersed in semi-polar solvents. For the modification of poly(ethylenimine) polystyrenes with number average molecular weights around 2,000 g/mol should be therefore used to ensure the compatibility of the modified poly(ethylenimine) with bitumen.

The [MMT_{B2}/PEI(10kD)_{10Q}^{2.2PS(6.4kD)}] adduct **EP1** was prepared in a larger quantity of 661.3 g (yield = 103.9 % of theory) by the “indirect replacement” method. Investigations of the adduct revealed that the adduct was a mixture of two adduct types consisting of montmorillonite with intercalated CTAB, and montmorillonite containing PEI(10kD)_{10Q}^{2.2PS(6.4kD)}/CTAB. The degree of polymer intercalation was found to be only

6 Preparation of [montmorillonite/PEI(nkD)xQyPS(nkD)]

62 %. Hence, no complete intercalation of the polymer was achieved. The presence of polystyrene and CTAB in the adduct was further confirmed with ^1H - and ^{13}C -MAS-NMR and the investigation of the adduct by IR showed that the ammonium groups of the CTAB and the polymer interacted with the montmorillonite Si-O-Si moieties. The organic content of the adduct was found to be with 67.8 wt.% about 15 wt.% higher than theoretically expected which was most likely caused by non-uniformly distributed CTAB impurities. But the impurities were with 3.2 wt.% only low which points to that with a better purification this adduct can be obtained CTAB free.

6.4 Conclusion

In this work, styrene was polymerised via an ATRP polymerization with the aim to create polystyrenes bearing active ester chain ends. Two polymers were prepared, their polymerizations being initiated by 2-bromo-2-methyl-propionic acid 2,5-dioxopyrrolidin-1-yl ester. The polystyrenes active esters were of low molecular weights ($M_n = 2,330$ g/mol, $M_n = 6,407$ g/mol) and low dispersities ($M_w/M_n = 1.036$, $M_w/M_n = 1.078$). The succinimide active ester moiety was covalently attached to the respective polystyrene. The purification of the polymers appeared to be difficult since both polymers contained PMDTA, and the lower molecular weight polymer was contaminated with small quantities of non-reacted styrene. Although the non-reacted styrene and PMDTA can be removed by a more extensive purification [45], this was not tried due to the large quantity of the polystyrene active ester (≈ 505 g) prepared. PEI(10kD)_{10Q}^{yPS(nkD)} polymers were prepared by reacting poly(ethylenimine) with (i) glycidyltrimethylammonium chloride and (ii) polystyrene active esters ($M_n = 2,330$ g/mol, and $M_n = 6,407$ g/mol) with the aim to create polystyrene-quat-primer polymers which contains positively charged ammonium groups and polystyrene chains. The polystyrenes were end-capped by 2-aminoethanol to prevent a reaction of the poly(ethylenimine) amino groups with the halogenoalkanes of the polystyrenes. The covalent attachment of the polystyrene-g-2-aminoethanol and the 2-hydroxypropyl-3-(N,N,N-trimethylammonium chloride) groups to the poly(ethylenimine)s was confirmed by ¹H-, ¹H-DOSY, ¹³C-NMR, and IR spectroscopy. It was found that the polymers contained non-reacted 2-aminoethanol impurities which were not removed in this study due to the high effort necessary to purify the large quantities of the polymers prepared (≈ 128 and 577 g). In further studies, the removal of this impurities could be tried by dissolving the polymers in a suitable solvent and precipitating the solution in water. Depending on the length of the polystyrene chains the polymers were found to be either soluble in semi-polar to non-polar solvents (with $M_{n,PS} = 2,330$ g/mol) or to give only dispersions in semi-polar solvents (with $M_{n,PS} = 6,407$ g/mol). The modification of poly(ethylenimine) with low molecular weight polystyrenes of $M_n \approx 2,000$ g/mol should lead to polymers with a good compatibility with bitumen. To test the influence of an [montmorillonite/polystyrene-quat-primer] adduct on bitumen about 661 g of an [MMT_{B2}/PEI(10kD)_{10Q}^{2.2PS(6.4kD)}] adduct was prepared by the "indirect replacement" method. It was found that the polymer was not completely intercalated shown by that the degree of polymer intercalation was measured to be only 62 %. The organic content of the adduct was measured to be about 15 wt.% higher than theoretically expected which was caused by non-uniformly distributed CTAB impurities (= 3.2 wt.%). Since a CTAB free adduct with a completely intercalated polymer was obtained with the [MMT/PEI(10kD)_{10Q}^{80R10}] adduct **E8** discussed earlier in Chapter **4** the optimisation of the preparation procedure should be performed in further studies.

References

- 1 Gao C., Yan D.; Hyperbranched polymers: from synthesis to applications; *Prog. Polym. Sci.* 29 (2004) 183 – 275
- 2 Seiler M.; Hyperbranched polymers: Phase behavior and new applications; *Fluid Phase Equilibria* 241 (2006) 155 – 174
- 3 Beckmann R.; “Quat – Primer” Polymers as Dispersants for Nanoparticles; Dissertation (2012)
- 4 Keller R. N., Wycoff H. D.; *Inorganic Synthesis Volume II* (1946) 1 - 4
- 5 Neises B., Steglich W.; Simple Method for the Esterification of Carboxylic Acids; *Angewandte Chemie International Edition* 17 (1978) 522 – 524
- 6 Möller F.; *Houben-Weyl Methods of Organic Chemistry Vol. XI/1, 4th Edition: Amines I* (1967) 311 - 326
- 7 McManus S. P., Larson C. A., Hearn R. A.; The Synthesis of Aminoalcohols from Epoxides and Ammonia; *Synthetic Communications* 3 (1973) 177 - 180
- 8 Fujiwara M., Imada M., Baba A., Matsuda H.; Tetraphenylstibonium triflate as a regio- and chemoselective catalyst in the reaction of oxiranes with amines; *Tetrahedron Letters* 30 (1989) 739 – 742
- 9 Iqbal J., Pandey A.; An unusual chemoselectivity in cobalt(II) chloride catalysed cleavage of oxiranes with anilines: A highly regioselective synthesis of β -amino alcohols; *Tetrahedron Letters* , 31 (1990) 575 – 576
- 10 Chini M., Crotti P., Macchia F.; Metal salts as new catalysts for mild and efficient aminolysis of oxiranes; *Tetrahedron Letters* 31 (1990) 4661 – 4664
- 11 Carre M. C., Houmounou J. P., Caubere P.; A convenient preparation of β -amino alcohols from epoxides and halomagnesium alkylamides; *Tetrahedron Letters* 26 (1985) 3107 - 3110
- 12 Yamada J., Yumoto M., Yamamoto Y.; Aminolead compounds as a new reagent for regioselective ring opening of epoxides; *Tetrahedron Letters* , 30 (1989) 4255 - 4258
- 13 Cava M. P., Deana A. A., Muth K., Mitchell M. J.; N-Phenylmaleimide; *Organic Syntheses Coll.* 5 (1973) 944- 946
- 14 Lapidot Y., Rappoport S., Wolman Y.; Use of esters of N-hydroxysuccinimide in the synthesis of N-acylamino acids; *Journal of Lipid Research* 8 (1967) 142 - 145
- 15 Anderson G. W., Zimmerman J. E., Callahan F. M.; N-Hydroxysuccinimide Esters in Peptide Synthesis; *Journal of the American Chemical Society* 85 (1963) 3039 – 3039
- 16 Anderson G. W., Zimmerman J. E., Callahan F. M.; The Use of Esters of N-Hydroxysuccinimide in Peptide Synthesis; *Journal of the American Chemical Soci-*

- ety 86 (1964) 1839 – 1842
- 17 Quirk R. P., Zhuo Q.; Anionic Synthesis of Epoxide-Functionalized Macromonomers by Reaction of Epichlorohydrin with Polymeric Organolithium Compounds; *Macromolecules* 30 (1997) 1531 – 1539
 - 18 Ji H., Farmer B. S., Nonidez W. K., Advincula R. C., Smith G. D., Kilbey S. M., Dadmun M. D., Mays J. W.; Anionic Synthesis of Epoxy End-Capped Polymers; *Macromolecular Chemistry and Physics* 208 (2007) 807 – 814
 - 19 Buchak B. E., Ramey K. C.; Monomer sequence distribution in styrene-maleic anhydride copolymers; *Journal of Polymer Science: Polymer Letters Edition* 14 (1976) 401 – 405
 - 20 Roth H., Arnold M., Rätzsch M.; ¹³C-NMR-Untersuchungen an Styren-Maleinsäureanhydrid-Copolymeren; *Acta Polymerica* 32 (1981) 277 – 280
 - 21 Beckmann R., Beginn U.; Synthesis and Characterization of New Poly(ethyleneimine)-*g*-Poly(methylmethacrylate) Star-Block Copolymers with Hyperbranched Cationic Core; *Journal of Polymer Science Part A: Polymer Chemistry* 51 (2013) 3700 – 3715
 - 22 Wang J.-S., Matyjaszewski K.; Controlled/"living" radical polymerization. atom transfer radical polymerization in the presence of transition-metal complexes; *Journal of the American Chemical Society* 117 (1995) 5614 - 5615
 - 23 Matyjaszewski K., Xia J.; Atom Transfer Radical Polymerization; *Chemical Reviews* 101 (2001) 2921 - 2990
 - 24 Oswal S. L., Phalak R. P.; Viscosities of nonelectrolyte liquid mixtures. I. binary mixtures containing p-dioxane; *International Journal of Thermophysics* 13 (1992) 251 - 267
 - 25 Haase R., Engels W.; Diffusion in the Liquid System Chloroform + Methyl Acetate; *Zeitschrift für Naturforschung* 41a (1986) 1337 – 1338
 - 26 Masaro L., Zhu X. X.; Physical models of diffusion for polymer solutions, gels and solids; *Progress in Polymer Science* 24 (1999) 731 – 775
 - 27 Lord Rayleigh F. R. S.; X. On the electromagnetic theory of light; *Philosophical Magazine* 12 (1881) 81 - 101
 - 28 Lord Rayleigh F. R. S.; XXXIV. On the transmission of light through an atmosphere containing small particles in suspension, and on the origin of the blue of the sky; *Philosophical Magazine* 47 (1899) 375 - 384
 - 29 Lechner M. D., Gehrke K., Nordmeier E. H.; *Makromolekulare Chemie* 3rd Edition (2003)
 - 30 Debye P.; Light Scattering in Solutions; *Journal of Applied Physics* 15 (1944) 338 - 342
 - 31 Debye P.; Molecular-weight Determination by Light Scattering; *The Journal of*

- Physical and Colloid Chemistry 51 (1947) 18 – 32
- 32 Khuong K. S., Jones W. H., Pryor W. A., Houk K. N.; The Mechanism of the Self-Initiated Thermal Polymerization of Styrene. Theoretical Solution of a Classic Problem; Journal of the American Chemical Society 127 (2005) 1265 – 1277
- 33 Fox T. G., Flory P. J.; Second-Order Transition Temperatures and Related Properties of Polystyrene. I. Influence of Molecular Weight; Journal of Applied Physics 21 (1950) 581 – 591
- 34 O'Driscoll K., Amin Sanayei R.; Chain-length dependence of the glass transition temperature; Macromolecules 24 (1991) 4479 – 4480
- 35 DSC measurements of polystyrene; TA 68 (1995) 1 – 4; http://www.hitachi-hightech.com/file/global/pdf/products/science/appli/ana/thermal/application_TA_068e.pdf (23.01.2017)
- 36 Dimroth K., Reichardt C., Siepmann T., Bohlmann F.; Über Pyridinium-N-phenol-betaine und ihre Verwendung zur Charakterisierung der Polarität von Lösungsmitteln; Justus Liebigs Annalen der Chemie 661 (1963) 1 – 37
- 37 Reichardt C.; Solvatochromic Dyes as Solvent Polarity Indicators; Chemical Reviews 94 (1994) 2319 – 2358
- 38 Jin M., Liu H., Pu H., Wan D.; Kinetic Topology-Selective Encapsulation and Mixture Separation by a Nanocapsule with Hyperbranched Polyethylenimine as Core and Polystyrene as Shell; Journal of Polymer Science Part B: Polymer Physics 51 (2013) 1273 – 1281
- 39 Hendricks S. B.; Base Exchange of the Clay Mineral Montmorillonite for Organic Cations and its Dependence upon Adsorption due to van der Waals Forces; The Journal of Physical Chemistry 45 (1941) 65 - 81
- 40 Farmer V. C., Russel J. D.; The infra-red spectra of layer silicates; Spectrochimica Acta 20 (1964) 1149 - 1173
- 41 Farmer V. C., Russel J. D.; Infrared absorption spectrometry in clay studies; Clays and Clay Minerals 15 (1967) 121 – 142
- 42 Viana R. B., da Silva A. B. F., Pimentel A. S.; Infrared Spectroscopy of Anionic, Cationic, and Zwitterionic Surfactants; Advances in Physical Chemistry (2012), Article ID 903272, 14 pages
- 43 Hongping H., Ray F. L., Jianxi Z.; Infrared study of HDTMA⁺ intercalated montmorillonite; Spectrochimica Acta Part A: Molecular and Biomolecular Spectroscopy 60 (2004) 2853 – 2859
- 44 Iwamoto K., Ohnuki Y., Sawada K., Senō M.; Solid-Solid Phase Transitions of Long-Chain n-Alkyltrimethylammonium Halides; Molecular Crystals and Liquid Crystals 73 (1981) 95 – 103
- 45 Matyjaszewski K., Coca S., Gaynor S. G., Greszta D., Patten T. E., Wang J.-S.,

6 Preparation of [montmorillonite/PEI(nkD)xQyPS(nkD)]

Xia J.; Improved processes based on atom (or group) transfer radical polymerization and novel (co)polymers having useful structures and properties; Patent WO1997018247A1 (1997)

7 Summary

7 Summary

In this thesis the synthesis of poly(ethylenimine)s simultaneously bearing ammonium groups and either (i) alkyl chain groups of 10 or 14 carbon atoms in the chains, so-called “alkyl-quat-primer” polymers, or (ii) polystyrene moieties, termed as “polystyrene-quat-primer” polymers, is described. With these polymers, [montmorillonite/polymer] adducts were prepared by either (i) adding the polymers directly to an in water swollen montmorillonite (= “direct addition” method), (ii) replacing CTAB by reacting the polymers with an aqueous solution of [MMT/CTAB] (= “replacement” method), or (iii) mixing the polymers with montmorillonite and CTAB in an aqueous solution and replacing the CTAB of an intermediate formed [MMT/CTAB] adduct (= “indirect replacement” method). The [montmorillonite/polymer] adducts were further incorporated into polymer- and non-polymer-modified bitumina to create bitumen-nanocomposites.

In Chapter **3** the reaction of poly(ethylenimine) with (i) glycidyltrimethylammonium chloride (Q) and either (ii) 1,2-epoxydodecane (R10) or (iii) 1,2-epoxyhexadecane (R14) in solution and in bulk is described. Due to the ammonium groups, these alkyl-quat-primer polymers (= PEI(nkD)_{xQ}^{yR}) are able to adsorb on negatively charged surfaces. Furthermore, by varying the number of attached alkyl groups the solubility of these polymers can be adjusted. The study of these polymers by ¹H-, ¹³C-NMR, and infrared spectroscopy (IR) revealed that polymers prepared in bulk exhibited comparable chemical and physical characteristics as those prepared in solution. Based on ¹H-NMR data and elemental analysis the parameters R and Q were calculated with the aim to determine the degree of alkylation and quarternization. The parameters were defined as the ratio of the number of modified repeating units per polymer molecule and the degree of polymerization. The investigation of PEI(nkD)_{xQ}^{yR} polymers by differential scanning calorimetry (DSC) revealed that PEI(nkD)_{xQ}^{yR10} polymers exhibited a glass transition which depended on the parameters R and Q, while PEI(nkD)_{xQ}^{yR14} polymers showed one glass transition derived from the quat-primer fraction, and a melting transition caused by the alkyl chain moieties. The thermogravimetric analysis (TGA) of PEI(nkD)_{xQ}^{yR} polymers revealed the polymers to decompose at 230 – 240 °C. On the other hand, heating these polymers to 180 °C for a prolonged time resulted in the complete fragmentation of the polymers, showing that these polymers can only be exposed to temperatures above 180 °C for a short time.

In Chapter **4** three pathways of the preparation of [MMT/alkyl-quat-primer] adducts (= [MMT/PEI(nkD)_{xQ}^{yR}]), namely: “direct addition”, “replacement”, and “indirect replace-

ment”, were evaluated. The degree of polymer intercalation was determined by small-, and wide-angle X-ray diffraction (XRD) and the size of the adduct particles was measured by scanning electron microscopy (SEM). Adducts prepared by the “direct addition” method exhibited only low degrees of polymer intercalation and formed aggregates with diameters between 1 and 20 μm which shows that this method can not be used to prepare adducts with completely intercalated polymers. Adducts with fully intercalated polymers were obtained by the “replacement” and “indirect replacement” methods in the case when $\text{PEI}(\text{nkD})_{\text{xQ}}^{\text{yR}10}$ polymers were used. With $\text{PEI}(\text{nkD})_{\text{xQ}}^{\text{yR}14}$ polymers, on the other hand, the degree of polymer intercalation decreased to about 54 %. The organic content of the adducts, as determined by TGA, calcination experiments, ^1H -MAS-NMR, ^{13}C -MAS-NMR, and IR, was in good agreement to the theoretically expected composition of the respective adduct with well-purified adducts, but exhibited higher values when CTAB impurities were present. But in all cases, the CTAB could be removed from the adducts by two washing steps with methanol/toluene fairly completely. The strong adhesion of $\text{PEI}(10\text{kD})_{10\text{Q}}^{\text{yR}}$ polymers to montmorillonite was demonstrated by a low quantity of polymeric material lost after washing [MMT/ $\text{PEI}(10\text{kD})_{10\text{Q}}^{\text{yR}}$] adducts several times with methanol/toluene. In further studies the conditions necessary to obtain adducts with fully intercalated polymers should be investigated.

In Chapter 5 the morphology and viscoelastic properties of bitumen-[MMT/alkyl-quat-primer] and bitumen-[MMT/CTAB] composites were investigated by polarised light and dark field microscopy, as well as with oscillation rheology. Furthermore, the rheological data were used to estimate the aspect ratio A_f of the montmorillonite particles in the composites. The composites were prepared using a Brabender Standalone KE 19 single screw extruder. The investigation of the influence of the preparation method of [MMT/alkyl-quat-primer] adducts revealed that adducts prepared by the “indirect replacement” method exhibited a higher compatibility with non-polymer modified bitumina than adducts prepared by the “direct addition” method. Adducts prepared by the “indirect replacement” method were used to determine the extrusion conditions necessary to obtain composites containing homogeneously distributed adduct particles as well as a high number of particles with high aspect ratios. Composites containing a high number of particles around 1 μm were obtained when the adducts were pre-ground to a powder, and pre-mixed with the bitumen before extrusion. Furthermore, at higher shear rates larger adduct agglomerates were broken down into smaller pieces which were able to interact with the bitumen matrix more efficiently due to their larger surface as shown by the increase of the composites elasticity with increasing higher shear rate. Composites prepared under optimised conditions exhib-

ited, starting with an adduct concentration of 5 wt.%, an adduct network in the bitumina which enhanced the elasticity of the bitumina at higher temperatures. The aspect ratios of the montmorillonite in composites containing [MMT/PEI(10kD)_{10Q}^{80R10}] adducts were very high (~ 300 - 1000) showing the presence of mainly exfoliated montmorillonite platelets in the bitumina. Lower aspect ratios (~ 30 - 90) were found with [MMT/PEI(10kD)_{10Q}^{60R14}] and [MMT/CTAB] adducts which point to a lower compatibility with this adduct types with the used bitumina. But all three adduct types exhibited only a low compatibility with polymer-modified bitumina.

In Chapter 6 the preparation of polystyrene active esters, polystyrene-quat-primer polymers, and an [MMT/polystyrene-quat-primer] adduct is described. Low molecular polystyrene active esters ($M_n = 2,330$ g/mol, $M_n = 6,407$ g/mol) were prepared by an ATRP polymerization initiated by 2-bromo-2-methyl-propionic acid 2,5-dioxopyrrolidin-1-yl ester. The prepared polymers contained besides polystyrene and 2-methyl-propionic acid 2,5-dioxopyrrolidin-1-yl ester groups also PMDTA impurities which lowered the glass transition temperature of the polymers. Polystyrene-quat-primer polymers were prepared by reacting poly(ethylenimine) with glycidyltrimethylammonium chloride and polystyrene active esters with the purpose of creating polymers which contain positively charged ammonium groups and polystyrene chains. Afterwards, the polystyrenes were end-capped by 2-aminoethanol to prevent a reaction of the poly(ethylenimine) amino groups with the halogenoalkanes of the polystyrenes. The solubility of these polymers depended strongly on the length of the polystyrene chains added. The polymers were soluble in semi-polar to non-polar solvents with $M_{n,PS} = 2,330$ g/mol and gave only dispersions in semi-polar solvents with $M_{n,PS} = 6,407$ g/mol. The compounds were prepared in higher quantities which made their purification difficult. The [MMT/polystyrene-quat-primer] adduct was prepared by the "indirect replacement" method with the aim to investigate the influence of a [montmorillonite/polystyrene-quat-primer] adduct on bitumen by adding a polystyrene-quat-primer polymer to an aqueous solution of CTAB and montmorillonite. The degree of polymer intercalation was measured to be 62 % and the adduct contained about 3.2 wt.% CTAB impurities which shows that the preparation and purification procedure has to be optimised in further studies.